



University
of Glasgow

Ashton, Miranda Jane (2020) *Advances towards the use of radical radiotherapy in malignant pleural mesothelioma*. PhD thesis.

<http://theses.gla.ac.uk/81491/>

Copyright and moral rights for this work are retained by the author

A copy can be downloaded for personal non-commercial research or study, without prior permission or charge

This work cannot be reproduced or quoted extensively from without first obtaining permission in writing from the author

The content must not be changed in any way or sold commercially in any format or medium without the formal permission of the author

When referring to this work, full bibliographic details including the author, title, awarding institution and date of the thesis must be given

Enlighten: Theses

<https://theses.gla.ac.uk/>
research-enlighten@glasgow.ac.uk

Advances towards the use of radical radiotherapy in malignant pleural mesothelioma

Miranda Jane Ashton

BSc, MB ChB, MRCP

This thesis is submitted in fulfilment of the requirements for the
Degree of Doctor of Philosophy

Institute of Cancer Sciences

College of Medical, Veterinary and Life Sciences

University of Glasgow

June 2020

Abstract

Background

The complex shape of the pleural cavity and the close proximity of normal radiosensitive structures render the delivery of radical radiotherapy in malignant pleural mesothelioma (MPM) challenging. However, the advent of conformal, intensity modulated radiotherapy (IMRT), where dose is selectively delivered to the tumour whilst sparing normal tissues, can facilitate safe dose escalation. SYSTEMS-2 is the only randomised controlled trial of radiotherapy dose escalation to be attempted in MPM and is comparing the palliative efficacy of two hypofractionated radiotherapy regimes to sites of pain using conformal techniques.

Although traditionally associated with unacceptable late normal tissue toxicity, the success of stereotactic radiotherapy (SABR) and the discovery that two common malignancies exhibit low α/β ratios, has enhanced the popularity of hypofractionated regimes. While the radiobiology of MPM is not well understood, its slow growth and apparent radioresistance suggests that it may exhibit a low α/β ratio and therefore that it may respond more favourably to dose hypofractionation.

Aims of thesis

To investigate the possibility of further radiotherapy dose escalation in MPM, beyond that delivered in the SYSTEMS-2 study.

Methods

- I. Novel radiotherapy dose constraints were generated for use in the SYSTEMS-2 study and tested on five patients from the SYSTEMS study.
- II. Multi criteria optimisation (MCO) software was used to assess whether the original dose escalated radiotherapy plans for the

Glasgow cohort of SYSTEMS-2 could be improved, without compromising target volume coverage.

- III. A clinically relevant 3D *in vitro* spheroid model was used to investigate the radiobiology of two independent MPM cell lines (H2052 and 211H). Spheroids were established and exposed to the same total dose of ionising radiation (IR) delivered in different doses per fraction. Data was used to investigate response to dose fractionation and to estimate the α/β ratio of this tumour.
- IV. The response of H2052 and 211H spheroids to two radiosensitising agents was investigated in combination with fractionated radiotherapy. Spheroids were incubated with increasing concentrations of either NU7441 (a DNA-PKcs inhibitor) or A1331852 (a BH3 mimetic) before being exposed to fractionated IR. The immunohistochemical (IHC) expression of DNA-PKcs and Bcl-xL was explored in diagnostic biopsies obtained from MPM patients to investigate clinical validity of the targets.
- V. IHC expression of nine proteins, selected for their potential to impact on radioresponse, was analysed in diagnostic tumour tissue collected from SYSTEMS and SYSTEMS-2 patients. Expression data was correlated with baseline clinical trial data in all patients, and with clinical trial outcome data from SYSTEMS patients.

Results

- I. Initial planning studies showed that none of the five SYSTEMS patients met all of the SYSTEMS-2 dose constraints, but the plans were deemed to be potentially clinically acceptable and the constraints were taken forward in the trial. The value of familiarity with a planning technique was evidenced by the fact that all constraints were achieved when the cases were re-planned by the same staff member in April 2019.

- II. MCO re-planning of dose escalated SYSTEMS-2 plans achieved clinically significant dose reductions to organs at risk (OAR) without compromising target volume coverage in 13/20 cases. Plans which did not meet OAR constraints or conform to the prescribed target volume coverage may still have been clinically acceptable.
- III. *In vitro* studies confirmed that growth of MPM spheroids can be delayed by IR. Spheroids demonstrated sensitivity to changes in dose per fraction, with the greatest volume reductions observed in hypofractionated radiotherapy regimes. This data implies that these MPM cell lines may exhibit a low α/β ratio, a suggestion which was further supported by *in vitro* multi-fraction IR studies.
- IV. Data suggest that NU7441 and A1331852 are potent radiosensitisers of MPM spheroids and that both are valid clinical targets in MPM. The supposition that a BH3 mimetic may offer tumour specific radiosensitisation, combined with the observation that A1331852 demonstrated greatest efficacy with hypofractionated IR, suggests that this agent may be clinically valuable in the radiosensitisation of MPM.
- V. No statistically significant correlations were found between baseline clinical characteristics and expression of the proteins of interest and no potential biomarkers of radiosensitisation were identified in the SYSTEMS cohort.

Conclusions

Novel dose constraints are being used to facilitate the delivery of hypofractionated, dose escalated palliative radiotherapy in the SYSTEMS-2 study. Results from this trial may guide future dose escalation in this disease and data from MCO planning studies suggest that further dose escalation to the target volume may be feasible without breaching OAR limits. *In vitro* studies suggest that MPM is sensitive to IR, responds more effectively to dose hypofractionation and may have a low α/β ratio. This

data may be helpful in determining dose and fractionation regimes in future MPM radiotherapy trials. Combination of BH3 mimetics with IR may provide MPM specific radiosensitisation, achieving greatest efficacy with dose hypofractionation. Ongoing IHC analysis of tumour samples from the SYSTEMS-2 study may identify a biomarker of radiotherapy response which would be helpful in guiding radiotherapy treatment decisions for future patients.

In summary, this thesis has investigated ways in which radiotherapy could be delivered with radical intent in MPM. Practical aspects of radiotherapy planning and delivery have been considered and are presented in conjunction with laboratory data to demonstrate how technical advances can be combined with an appreciation of disease radiobiology to facilitate radical treatment.

Acknowledgements

The research within this thesis has been performed under the supervision and expert guidance of Professor Anthony Chalmers, to whom I am extremely grateful. Further supervision has also been kindly provided by Dr Kevin Blyth.

I would like to thank the Chalmers' lab for their support and guidance. In particular, I would like to acknowledge the help and mentorship of Dr Mark Jackson, both in terms of the *in vitro* studies, and also for his endless patience and endurance in proof reading various versions of this work. Advice on the isoeffective *in vitro* work was kindly provided by Dr Charles Deehan. Thanks to Dr Craig Dick for expediting the retrieval of tumour blocks from the Glasgow Biorepository and to Dr Colin Nixon, for processing the tissue and performing the automated IHC analyses. Guidance on statistical analyses was provided by Jamie Stobo, to whom I will be eternally grateful, given my allergy to stats.

I would like to thank Laura Alexander and all the members of the SYSTEMS-2 TMG for their hard work in running this important study. Furthermore, thank you to the June Hancock Mesothelioma Research Fund and the Beatson Cancer Charity for their continued financial and moral support and to Slater and Gordon for co-funding the sample collection.

I would like to acknowledge the hard work and kindness of Suzanne Currie and Ronan Valentine, who performed much of the original radiotherapy planning presented and whose guidance and advice throughout this research has been invaluable. I would also like to acknowledge the help provided by Dr Stephen Harrow and Dr Kevin Franks in the generation of the SYSTEMS-2 dose constraints.

I would like to thank my husband, Stuart for providing endless coffee and for being so patient with me when I was '2 weeks off finishing' for about 3 months. Thanks also to my parents and to my sister, for helping with many of the figures. Finally, but most importantly, I would like to thank all of the SYSTEMS-2 patients, whose willingness to engage in research has made this project possible.

Author's Declaration

I declare that I am the sole author of this thesis. The work presented here is my own, unless otherwise acknowledged. This thesis has not been submitted for consideration of another degree in this or any other university.

Table of contents

| | |
|---|---------------|
| Abstract | - 2 - |
| Background | - 2 - |
| Aims of thesis | - 2 - |
| Methods | - 2 - |
| Results | - 3 - |
| Conclusions | - 4 - |
| Acknowledgements..... | - 6 - |
| Author’s Declaration | - 7 - |
| Table of contents | - 8 - |
| Tables and figures | - 15 - |
| Publications relating to this thesis | - 20 - |
| Presentations to Learned Societies | - 21 - |
| List of abbreviations | - 22 - |
| Chapter 1: Introduction | - 27 - |
| 1.1 Malignant Pleural Mesothelioma | - 27 - |
| 1.1.1 Incidence and epidemiology | - 27 - |
| 1.1.2 Pathogenesis | - 28 - |
| 1.1.3 Diagnosis and staging..... | - 30 - |
| 1.1.4 Prognostication | - 35 - |
| 1.1.5 Management of MPM..... | - 36 - |
| 1.2 The changing role of radiotherapy in MPM | - 39 - |
| 1.2.1 Palliative radiotherapy | - 39 - |
| 1.2.2 Prophylactic radiotherapy..... | - 41 - |
| 1.2.3 Adjuvant radiotherapy | - 42 - |
| 1.2.4 Neo-adjuvant radiotherapy..... | - 45 - |
| 1.3 Advances in radiotherapy delivery | - 46 - |
| 1.3.1 Fixed-field IMRT | - 46 - |
| 1.3.2 VMAT/HT..... | - 47 - |
| 1.3.3 RapidPlan | - 49 - |
| 1.3.4 Multi-criteria optimisation..... | - 49 - |
| 1.4 Radiobiological considerations impacting radiotherapy delivery..... | - 51 - |
| 1.4.1 The lethality of ionising radiation | - 51 - |
| 1.4.2 Normal tissue radiation toxicity..... | - 52 - |

| | |
|--|---------------|
| 1.4.3 The linear quadratic model of cell survival | - 53 - |
| 1.4.4 The rationale of dose fractionation | - 55 - |
| 1.4.5 The application of hypofractionation | - 58 - |
| 1.4.6 Radiobiological modelling | - 60 - |
| 1.5 <i>In vitro</i> studies of MPM..... | - 62 - |
| 1.5.1 <i>In vitro</i> tumour models | - 62 - |
| 1.5.2 Cell lines | - 63 - |
| 1.5.3 <i>In vitro</i> 3D Spheroid Models | - 63 - |
| 1.5.4 Studies of radiosensitivity | - 66 - |
| 1.6 Apoptosis | - 70 - |
| 1.6.1 Background | - 70 - |
| 1.6.2 The intrinsic pathway..... | - 71 - |
| 1.6.3 The Bcl-2 family..... | - 72 - |
| 1.6.4 The final common pathway of apoptosis..... | - 73 - |
| 1.6.5 Mesothelioma and apoptosis | - 74 - |
| 1.6.6 Dysregulation of Bcl-2 family in MPM | - 75 - |
| 1.6.7 Single agent Bcl-xL inhibition | - 76 - |
| 1.6.8 Bcl-2 protein downregulation in combination with IR..... | - 77 - |
| 1.7 DNA damage responses | - 79 - |
| 1.7.1 DNA damage and cell cycle arrest | - 79 - |
| 1.7.2 Repair of DNA-DSB | - 79 - |
| 1.7.3 DNA-DSB Repair and MPM | - 81 - |
| 1.7.4 DNA-dependent protein kinase catalytic subunit..... | - 82 - |
| 1.7.5 Inhibition of DNA-PKcs..... | - 84 - |
| 1.8 Aims of thesis | - 85 - |
| Chapter 2: Materials and Methods..... | - 88 - |
| 2.1 Methods used to determine dose constraints for SYSTEMS-2 | - 88 - |
| 2.1.1 Dose constraints..... | - 88 - |
| 2.1.2 PTV constraints | - 89 - |
| 2.1.3 Radiotherapy feasibility planning studies | - 89 - |
| 2.2 Methods used for MCO analysis of SYSTEMS-2 radiotherapy plans..... | - 90 - |
| 2.2.1 Dose escalated radiotherapy plans (Glasgow cohort) | - 90 - |
| 2.2.2 Planning information | - 90 - |
| 2.2.3 MCO of the original 36Gy in 6 fraction plan | - 91 - |
| 2.2.4 Setting optimisation objectives | - 91 - |
| 2.2.5 Trade-off selection | - 91 - |

| | |
|---|----------------|
| 2.2.6 Plan generation | - 92 - |
| 2.2.7 Plan Trade-off..... | - 92 - |
| 2.2.8 Generating a deliverable VMAT plan | - 93 - |
| 2.2.9 Plan comparison..... | - 93 - |
| 2.2.10 Statistical analysis | - 93 - |
| 2.3 Methods used for 3D <i>in vitro</i> spheroid model..... | - 94 - |
| 2.3.1 Cell culture | - 94 - |
| 2.3.2 Cell culture procedures for radiation only experiments..... | - 96 - |
| 2.3.3 Cell culture procedures for radiation and drug combination experiments..... | - 97 - |
| 2.3.4 Irradiation of spheroids..... | - 99 - |
| 2.3.5 Spheroid imaging | - 100 - |
| 2.3.6 Image processing and spheroid quantification..... | - 101 - |
| 2.3.7 Statistical analysis | - 105 - |
| 2.3.8 Method used to estimate the α/β ratio of MPM spheroids | - 107 - |
| 2.4 Methods used for immunohistochemical studies | - 109 - |
| 2.4.1 Tissue Acquisition..... | - 109 - |
| 2.4.2 Sectioning and mounting of tissue..... | - 109 - |
| 2.4.3 Antibody optimisation | - 109 - |
| 2.4.4 Manual immunohistochemical procedures | - 113 - |
| 2.4.5 Automated immunohistochemical procedures | - 114 - |
| 2.4.6 Data interpretation | - 114 - |
| Chapter 3: SYSTEMS-2 | - 117 - |
| 3.1 Introduction | - 117 - |
| 3.2 Methods..... | - 119 - |
| 3.2.1 Regulatory processes | - 119 - |
| 3.2.2 Study design..... | - 120 - |
| 3.2.3 Study population..... | - 120 - |
| 3.2.4 Inclusion criteria..... | - 120 - |
| 3.2.5 Exclusion criteria | - 121 - |
| 3.2.6 Schedule of assessment | - 121 - |
| 3.2.7 Study procedures | - 125 - |
| 3.2.8 Trial endpoints and objectives | - 127 - |
| 3.2.9 Protocol development | - 128 - |
| 3.2.10 Site selection and opening process..... | - 130 - |
| 3.2.11 Central radiology review process..... | - 130 - |
| 3.2.12 Safety reporting | - 131 - |

| | |
|---|----------------|
| 3.2.13 Statistical analysis | - 132 - |
| 3.2.14 Translational research..... | - 132 - |
| 3.2.15 No-cost extension | - 134 - |
| 3.3 Results..... | - 135 - |
| 3.3.1 Site set up and recruitment | - 135 - |
| 3.3.2 Radiotherapy delivery technique..... | - 145 - |
| 3.3.3 Glasgow Screening Cohort..... | - 147 - |
| 3.3.4 Collaborations..... | - 155 - |
| 3.4 Discussion..... | - 155 - |
| 3.4.1 Challenges of site set up | - 156 - |
| 3.4.2 Challenges of patient recruitment..... | - 158 - |
| 3.4.3 Measures taken to enhance trial recruitment..... | - 160 - |
| 3.4.4 Issues of analgesia optimisation | - 162 - |
| 3.4.5 Challenges of pain assessments..... | - 164 - |
| 3.5 Summary | - 164 - |
| Chapter 4: Development of dose constraints for SYSTEMS-2 | - 166 - |
| Chapter aim..... | - 166 - |
| 4.1 Introduction | - 166 - |
| 4.1.1 Selection of hypofractionated radiotherapy regime for SYSTEMS-2 | - 166 - |
| 4.1.2 Established dose constraints for lung radiotherapy | - 167 - |
| 4.1.3 Developing dose constraints for SYSTEMS-2 | - 168 - |
| 4.2 Results..... | - 169 - |
| 4.2.1 Typical PTV sizes for SYSTEMS-2 are an order of magnitude greater than those for SABR-169 | - 169 - |
| 4.2.2 Radiobiological analysis of local SABR dose constraints has guided the development of constraints for a 6 fraction regime within SYSTEMS-2..... | - 170 - |
| 4.2.3 VMAT planning studies highlight the challenge of achieving adequate PTV coverage without breaching OAR dose constraints..... | - 178 - |
| 4.2.4 Planner experience impacts on the quality of a SYSTEMS-2 radiotherapy plan..... | - 180 - |
| 4.3 Discussion..... | - 184 - |
| 4.3.1 Clinical considerations of the SYSTEMS-2 dose constraints | - 184 - |
| 4.3.2 A planning study of five cases suggests that the SYSTEMS-2 PTV constraints are challenging to meet without breaching OAR constraints | - 189 - |
| 4.3.3 The quality of the radiotherapy plan is influenced by the familiarity of the planner with SYSTEMS-2 planning..... | - 190 - |
| 4.4 Summary | - 191 - |

Chapter 5: Assessing the impact of MCO on SYSTEMS-2 dose escalated VMAT plans - 192 -

Chapter aim..... - 192 -

5.1 Introduction - 192 -

5.2 Results..... - 193 -

5.2.1. MCO generated clinically superior radiotherapy plans for the majority of SYSTEMS-2 patients..... - 193 -

5.2.2 No predictive pattern was identified between PTV location and MCO dose sparing- 194

5.2.3 MCO achieved clinically significant reductions in multiple OAR doses without compromising PTV coverage..... - 206 -

5.2.4 Plans which failed this planning study were predominantly left sided, but were not associated with significantly larger PTV sizes - 211 -

5.3 Discussion..... - 215 -

5.3.1 MCO can significantly reduce dose to organs which are associated with problematic acute toxicities..... - 216 -

5.3.2 Plans generated by MCO may be clinically acceptable despite breaching dose constraints..... - 217 -

5.3.3 The future role of MCO in SYSTEMS-2 radiotherapy planning - 218 -

5.3.4 The potential for further dose escalation with MCO - 219 -

5.3.5 Physician led radiotherapy planning using MCO - 220 -

5.4 Summary - 220 -

Chapter 6: Characterising the radiosensitivity of mesothelioma using an *in vitro* 3D model - 221 -

Chapter aim..... - 221 -

6.1 Introduction - 221 -

6.1.1 Clinical assessment of radiosensitivity in MPM - 221 -

6.1.2 *In vivo* studies of MPM radiosensitivity - 222 -

6.1.3 *In vitro* studies of MPM radiosensitivity - 223 -

6.1.4 Validation of a 3D *in vitro* model of MPM - 225 -

6.2 Results..... - 226 -

6.2.1 MPM cells exhibit radiosensitivity to IR in a dose dependent manner - 226 -

6.2.2 Hypofractionated radiotherapy regimens delay MPM spheroid growth with improved efficacy..... - 233 -

6.2.3 Estimation of isoeffective radiation doses suggest MPM spheroids exhibit a low α/β ratio..... - 237 -

6.3 Discussion..... - 250 -

6.3.1 Cell line considerations - 251 -

6.3.2 The radiation dose-dependent response of MPM to IR - 252 -

| | |
|---|----------------|
| 6.3.3 The response of MPM to hypofractionated IR | - 253 - |
| 6.3.4 Estimating the α/β ratio of MPM..... | - 254 - |
| 6.3.5 Clinical translation of data | - 259 - |
| 6.4 Summary | - 260 - |
| Chapter 7: Assessing the impact of novel radiosensitising drugs with fractionated radiotherapy on MPM spheroids | - 261 - |
| Chapter aim..... | - 261 - |
| 7.1 Introduction | - 261 - |
| 7.1.1 The rationale for using radiosensitisers..... | - 261 - |
| 7.1.2 Rationale for investigating the radiosensitising properties of DNA damage repair proteins..... | - 262 - |
| 7.1.3 Rationale for investigating the radiosensitising properties of BH-3 mimetics | - 264 - |
| 7.1.4 Selection of radiosensitisers for investigation in MPM | - 265 - |
| 7.1.5 Selection of an appropriate platform to investigate radiosensitisation of MPM..... | - 265 - |
| 7.1.6 Confirming target proteins in experimental and clinical samples | - 265 - |
| 7.2 Results..... | - 266 - |
| 7.2.1 Fractionation determines efficacy of IR in delaying MPM spheroid growth | - 266 - |
| 7.2.2 NU7441 did not exert any single agent activity in MPM cell lines | - 267 - |
| 7.2.3 Combination of NU7441 with IR exhibits a therapeutic interaction | - 268 - |
| 7.2.4 An enhanced radiosensitising effect of NU7441 was detected with hypofractionated IR at low drug concentrations..... | - 270 - |
| 7.2.5 A1331852 exhibits single agent activity in H2052 cells | - 273 - |
| 7.2.6 The combination of A1331852 with IR exhibits a therapeutic interaction..... | - 275 - |
| 7.2.7 The radiosensitising effects of A1331852 is enhanced with hypofractionated IR | - 276 - |
| 7.2.8 MPM spheroids strongly express Bcl-xL and DNA-PKcs, but Bcl-2 and Mcl-1 are differentially expressed between H2052 and 211H cell lines..... | - 280 - |
| 7.2.9 DNA-PKcs is robustly expressed in MPM tissue..... | - 283 - |
| 7.2.10 Anti-apoptotic Bcl-2 proteins are expressed with differential intensities in MPM tissue- | 286 - |
| 7.3 Discussion..... | - 291 - |
| 7.3.1 The growth of MPM spheroids is delayed by ionising radiation and A1331852, but unaffected by NU7441..... | - 291 - |
| 7.3.2 Both NU7441 and A1331852 exert a radiosensitising effect on MPM cells when delivered with a single fraction of IR..... | - 293 - |
| 7.3.3 Optimal radiosensitisation with hypofractionated IR is more consistently demonstrated with A1331852 than with NU7441..... | - 298 - |
| 7.3.4 DNA-PKcs and Bcl-xL are clinically relevant targets of radiosensitisation | - 300 - |
| 7.3.5 Clinical application of data | - 301 - |

7.4 Summary - 302 -

Chapter 8: Assessment of potential biomarkers of radiotherapy response in MPM - 304 -

8.1 Introduction - 304 -

8.1.1 Predictive biomarkers of radiotherapy response - 304 -

8.1.2 Selection of proteins for investigation..... - 305 -

8.2 Results..... - 309 -

8.2.1 IHC validity in MPM samples is enhanced by the generation of reliable positive controls..... - 309 -

8.2.2 MPM tissue exhibits heterogeneity in protein expression - 313 -

8.2.3 Protein expression is not significantly different between histological subtypes of MPM..... - 314 -

8.2.4 No correlation was found between baseline clinical parameters and protein expression in MPM tissue..... - 314 -

8.3 Discussion..... - 319 -

8.3.1 Proteins of interest were expressed in MPM tissue - 319 -

8.3.2 Protein expression in MPM tissue could not be correlated with baseline clinical parameters in this limited dataset..... - 321 -

8.3.3 Study limitations - 322 -

8.4 Summary - 323 -

Chapter 9: Final discussion - 324 -

9.1 The changing landscape of MPM research - 324 -

9.2 Dose constraints..... - 325 -

9.3. Dose delivery..... - 326 -

9.4 Radiobiological considerations of MPM - 329 -

9.5 The potential for radiosensitisation in MPM - 330 -

9.6 Biomarkers of MPM radiosensitivity..... - 331 -

9.7 Summary - 333 -

Appendix 1: Isoeffective data - 334 -

Appendix 2: Volume data for radiosensitising drug experiments - 344 -

Appendix 3: γ H2Ax expression - 346 -

Appendix 4: IHC Correlation data - 347 -

References - 356 -

Tables and figures

| | |
|---|---------|
| Figure 1.1 Cell survival curves for densely and sparsely ionising radiation, illustrating the linear quadratic model..... | 54 |
| Figure 1.2 Cell survival curves for late-responding normal tissue and tumour effects associated with low and high α/B ratios, respectively..... | 56 |
| Figure 1.3 Fractionation-associated straightening of the survival curves, illustrating the radiobiological basis of the improved therapeutic ratio achieved with fractionated radiotherapy..... | 57 |
| Figure 1.4 Tumour control probability (TCP) for target volumes exhibiting different α/B ratios, receiving a homogenous dose over 1-50 fractions..... | 62 |
| Figure 1.5 A schematic outlining the apoptotic pathway..... | 74 |
| Figure 1.6 A schematic outlining the process of NHEJ..... | 83 |
| Table 2.1 Dose rate (in Gy/minute) delivered by the Xstrahl cabinet irradiator..... | 100 |
| Figure 2.1 Spheroid imaging using GelCount™ and Spyder software..... | 101 |
| Figure 2.2 Analysis of 2D images using Cell Profiler determined the area of each spheroid..... | 103 |
| Figure 2.3 Generation of 3D volume data using 2D images..... | 105 |
| Table 2.2 Parameters investigated in the process of antibody optimisation for Bcl-xL, Bcl-2 and Mcl-1 antibodies..... | 110 |
| Table 2.3 Final conditions selected for antigen retrieval and antibody dilution..... | 111-112 |
| Figure 3.1 Outline of the study visits for SYSTEMS-2..... | 122 |
| Table 3.1 Schedule of assessment for SYSTEMS-2..... | 123-124 |
| Table 3.2 Summary of the SYSTEMS-2 sample collection..... | 133 |
| Figure 3.2 Predicted recruitment to the SYSTEMS-2 study..... | 136 |
| Table 3.3 Outcome data for sites invited to enter SYSTEMS-2..... | 137-144 |
| Table 3.4 Planning methods employed by current SYSTEMS-2 sites..... | 145-147 |
| Figure 3.3 Summary of screening outcomes in patients who were not registered for SYSTEMS-2..... | 148 |
| Table 3.5 Screening outcomes for patients who did not enter SYSTEMS-2 immediately..... | 149-154 |
| Table 4.1 Comparative values for planning target volumes in SABR and SYSTEMS-2..... | 169 |

| | |
|---|---------|
| Table 4.2 BED and EQD2 for a 55Gy/5 fraction thoracic SABR regime and 36Gy/6 fraction SYSTEMS-2 regime..... | 170 |
| Table 4.3 Comparison of maximum SABR OAR dose constraints delivered in 5 or 6 fractions, expressed as EQD2 and BED..... | 171-172 |
| Table 4.4 Initial dose constraints for SYSTEMS-2 presented as EQD2 and BED (SABR constraints presented for radiobiological comparison)..... | 174-175 |
| Table 4.5 Dose constraints submitted to Beatson West of Scotland Cancer Centre radiotherapy planning department for planning feasibility studies..... | 176-177 |
| Table 4.6 Expected PTV coverage..... | 177 |
| Table 4.7 Dosimetry data from VMAT planning studies undertaken on 5 patients from the original SYSTEMS trial..... | 178-179 |
| Table 4.8 Dosimetry data from VMAT planning studies undertaken in March 2019..... | 180-181 |
| Figure 4.1 DVH illustrating the improvement in PTV coverage achieved for Patient 1 | 182 |
| Figure 4.2 DVH showing improvements in oesophageal dose for Patient 5..... | 183 |
| Figure 4.3 Plan showing distribution of dose to 5Gy..... | 183 |
| Table 5.1 Changes to OAR doses achieved with MCO in left sided MPM..... | 196-199 |
| Table 5.2 Changes to OAR doses achieved with MCO in right sided MPM... | 200-203 |
| Figure 5.1 Changes in dosimetry achieved with MCO compared to clinical VMAT plans in patients with left sided MPM..... | 204 |
| Figure 5.2 Changes in dosimetry achieved with MCO compared to clinical VMAT plans in patients with right sided MPM..... | 205 |
| Figure 5.3 Dose volume histogram comparing OARs doses from the clinical VMAT plan (triangle markers) with the MCO generated plan (square markers) for patient 5..... | 207 |
| Figure 5.4 Dose volume histogram showing PTV coverage in the clinical VMAT plan (triangle markers) and MCO plan (square markers) for patient 5..... | 207 |
| Figure 5.5 Comparison of the 30% isodose distribution between the clinical VMAT plan (A) and the MCO plan (B) for patient 5..... | 208 |
| Figure 5.6 Dose volume histograms comparing OARs doses from the clinical VMAT plan (triangle markers) with the MCO generated plan (square markers) for patient 7..... | 208 |
| Figure 5.7 Dose volume histogram showing PTV coverage in the clinical VMAT plan (triangle markers) and MCO plan (square markers) for patient 7..... | 209 |
| Figure 5.8 Comparison of the 500cGy isodose distribution between the clinical VMAT plan (A) and the MCO plan (B) for patient 7..... | 209 |

Figure 5.9 Dose volume histograms comparing OARs doses from the clinical VMAT plan (triangle markers) with the MCO generated plan (square markers) for patient 11.....210

Figure 5.10 Dose volume histogram showing PTV coverage in the clinical VMAT plan (triangle markers) and MCO plan (square markers) for patient 11.....211

Figure 5.11 Comparison of the 50% isodose distribution between the clinical VMAT plan (A) and the MCO plan (B) for patient 11.....211

Table 5.3 Comparison of plan parameters.....212-213

Table 5.4 PTV and OAR parameters achieved in plans which failed the planning study.....214-215

Figure 6.1 H2052 spheroid volumes following exposure to single fractions of IR.....228

Figure 6.2 Representative H2052 spheroids at day 0 and day 21 following irradiation with increasing doses of IR.....228

Figure 6.3 211H spheroid volumes following exposure to single fractions of IR.....229

Figure 6.4 Representative 211H spheroids sizes at day 0 and day 21 following irradiation with increasing doses of IR.....229

Figure 6.5 H2052 spheroid volumes following exposure to single fractions of IR.....230

Figure 6.6 211H spheroid volumes following exposure to single fractions of IR.....231

Figure 6.7 H2052 spheroid volumes following exposure to single fractions of IR.....232

Figure 6.8 211H spheroid volumes following exposure to single fractions of IR..232

Table 6.1 Fractionated radiotherapy regimes.....234

Figure 6.9 The effect of 6Gy on H2052 (A) and 211H (B) spheroid volumes day at 21..... 235

Figure 6.10 The effect of 8Gy on H2052 (A) and 211H (B) spheroid volumes day at 21.....236

Table 6.2 Radiation schedules delivered to MPM spheroids to investigate tumour α/β ratio.....238

Figure 6.11 H2052 spheroid growth curves following exposure to IR.....239-242

Figure 6.12 211H spheroid growth curves following exposure to IR.....242-245

Table 6.3 H2052 spheroid volume reduction caused by each IR regime at day 14.....246

| | |
|--|---------|
| Figure 6.13 Dose effect curves illustrating the impact of different fractionation schedules on H2052 spheroid damage at day 14..... | 247 |
| Table 6.4 Dosimetry information on the IR regimes required to reduce H2052 spheroid volume by 0.2mm ³ from the sham irradiated control at day 14..... | 247 |
| Figure 6.14 Estimate of the α/β ratio of H2052 spheroids..... | 248 |
| Table 6.5 Estimated α/β ratios from H2052 spheroids..... | 249 |
| Table 6.6 Estimated α/β ratios from 211H spheroids..... | 250 |
| Figure 7.1 The effect of radiation alone on MPM spheroid volume at day 21... | 267 |
| Figure 7.2 The effect of NU7441 alone on MPM spheroid volume at day 21..... | 268 |
| Figure 7.3 The effect of combination therapy with NU7441 and IR on relative MPM spheroid volume at day 21..... | 270 |
| Figure 7.4 The effect of NU7441 on relative MPM spheroid volume at day 21, normalised for the effect of fractionation regime..... | 272-273 |
| Figure 7.5 The effect of A1331852 alone on MPM spheroid volume at day 21..... | 274 |
| Figure 7.6 The effect of combination therapy with A1331852 and IR on relative MPM spheroid volume at day 21..... | 276 |
| Figure 7.7 The effect of A1331852 on relative MPM spheroid volume at day 21, normalised for the effect of fractionation regime..... | 278-279 |
| Figure 7.8 Relative expression of DNA-PKcs in H2052 and 211H spheroids..... | 281 |
| Figure 7.9 Percentage of cellular expression of DNA-PKcs in H2052 and 211H cells..... | 281 |
| Figure 7.10 Relative expression of Bcl-xL, Bcl-2 and Mcl-1 in H2052 and 211H spheroids..... | 282 |
| Figure 7.11 MPM expression of anti-apoptotic Bcl-2 proteins..... | 283 |
| Figure 7.12 Expression of DNA-PKcs in MPM tissue selected as positive and negative controls..... | 284 |
| Figure 7.13 Expression of DNA-PKcs in MPM tissue..... | 285 |
| Table 7.1 Levels of DNA-PKcs expression in MPM cells..... | 285 |
| Figure 7.14 Expression of Bcl-xL, Bcl-2 and Mcl-1 in positive and negative controls and in clinical samples..... | 287 |
| Figure 7.15 Expression of Bcl-xL, Bcl-2 and Mcl-1 in MPM tissue..... | 288 |
| Table 7.2 Expression of Bcl-xL, Bcl-2 and Mcl-1 in MPM cells..... | 289 |
| Figure 7.16 Expression of Bcl-xL, Bcl-2 and Mcl-1 in MPM tissue..... | 290 |
| Figure 8.1 Representative expression profiles of selected proteins in MPM biopsy tissue and positive controls..... | 311-312 |

Figure 8.2 Negative controls determining binding specificity of rabbit and mouse primary antibodies.....312

Figure 8.3 Expression of selected proteins in MPM tissue samples.....313

Figure 8.4 A-R Correlation of protein H-scores in tissue samples taken from SYSTEMS patients with pain outcomes at week 5 and 12 after radiotherapy....315

Table 8.1 Statistical significance of correlation analyses between protein expression in patient biopsy samples and clinical trial data.....318-319

Publications relating to this thesis

1. The role of radical radiotherapy in the management of malignant pleural mesothelioma: A systematic review
Ashton M, O'Rourke N, Currie S, Rimner A and Chalmers A.
Radiotherapy & Oncology. 2017 Oct; 125 (1):1-12
2. SYSTEMS-2: A randomised phase II study of radiotherapy dose escalation for pain control in malignant pleural mesothelioma
Ashton M, O'Rourke N, Macleod N, Laird B, Stobo J, Kelly C, Alexander L, Franks K, Moore K, Currie S, Valentine R and Chalmers A
Clin Transl Radiat Oncol. 2017; 8: 45-49
3. Pain management in patients with malignant mesothelioma: challenges and solutions
Saunders J, Ashton M, Hall C, Laird B, MacLeod N
Lung Cancer (Auckl). 2019 Apr 2;10: 37-46
4. The role of radiation treatment in pleural mesothelioma: Highlights of the 14th International Conference of the International mesothelioma interest group
MacRae RM, Ashton M, Lauk O, Wilson W, O'Rourke N, Simone CB 2nd, Rimner A
Lung Cancer. 2019 Jun;132: 24-27
5. Mesothelioma cells depend on the anti-apoptotic protein Bcl-xL for survival and are sensitized to ionizing radiation by BH-3 mimetics
Jackson MR, Ashton M, Koessinger AL, Dick C, Verheij M, Chalmers AJ
International Journal of Radiation Oncology, Biology, Physics, 106(4): 867-877

Presentations to Learned Societies

1. 'SYSTEMS-2'
International Mesothelioma Interest Group, Birmingham (May 2016)
2. 'The future of radiotherapy in mesothelioma'
House of Lords, London (November 2016)
3. 'Radiotherapy in mesothelioma'
Scottish Oncology Conference, Stirling (September 2017)
4. 'Development of dose constraints for a hypofractionated, dose escalated radiotherapy regime for malignant pleural mesothelioma'
European Society for Radiotherapy and Oncology, Barcelona (April 2018)
5. 'SYSTEMS-2: A phase II randomised study of radiotherapy dose escalation for pain control in malignant pleural mesothelioma'
International Mesothelioma Interest Group, Ottawa (May 2018)
6. 'Growth of mesothelioma spheroids is optimally controlled by hypofractionated radiotherapy in conjunction with radiosensitising drugs'
Scottish Radiotherapy Research Forum, Stirling (Nov 2018)
7. 'Utilising multicriteria optimisation in radiotherapy planning for malignant pleural mesothelioma'
Scottish Radiotherapy Research Forum, Stirling (March 2020)

List of abbreviations

| | |
|----------|---|
| 2D | Two dimensional |
| 3DCRT | 3D conformal radiotherapy |
| AAA | Anisotropic analytical algorithm |
| AE | Adverse events |
| ANOVA | Analysis of variance |
| ATM | Ataxia-telangiectasia mutated |
| ATR | Ataxia-telangiectasia and rad-3 related |
| BAP-1 | BRCA1 Associated Protein-1 |
| Bcl-2 | B cell lymphoma protein 2 |
| BED | Biologically equivalent dose |
| BH | Bcl-2 homology |
| CAD | Caspase-Activated-DNase |
| CALGB | Cancer and leukaemia group B |
| CHHIP | Conventional or hypofractionated high dose intensity modulated radiotherapy for prostate cancer |
| CHK1/2 | Checkpoint effector kinases |
| CT | Computed tomography |
| CTV | Clinical target volume |
| CV | Coefficient of variance |
| DAB | 3,3'-diaminobenzidine tetrahydrochloride |
| DDR | DNA damage response |
| Dmax | Maximum dose |
| DNA-PKcs | DNA-dependent protein kinase catalytic subunit |

| | |
|---------|--|
| DSB | Double strand breaks |
| DVH | Dose volume histogram |
| EORTC | European Organisation for Research and Treatment of Cancer |
| EPP | Extrapleural pneumonectomy |
| FFPE | Formalin fixed paraffin embedded |
| FISH | Fluorescent in situ hybridisation |
| GTV | Gross tumour volume |
| Gy | Gray |
| H Score | Weighted Histology-score |
| HRP | Horseradish peroxidase |
| HRR | Homologous recombination repair |
| IAP | Inhibitor of apoptosis family of proteins |
| IASLC | International Association for the Study of Lung Cancer |
| IDO | Indoleamine 2,3-dioxygenase |
| IHC | Immunohistochemical/ immunohistochemistry |
| IMIG | International Mesothelioma Interest Group |
| IMRT | Intensity modulated radiotherapy |
| IR | Ionising radiation |
| LET | Linear energy transfer |
| LQ | Linear quadratic |
| MAPS | Mesothelioma Avastin Cisplatin Pemetrexed Study |
| MARS | Mesothelioma and Radical Surgery |
| MCO | Multi-criteria optimisation |
| MCR | Macroscopic complete resection |

| | |
|--------|--|
| MDT | Multidisciplinary team |
| MID | Mean inactivation dose |
| MLC | Multileaf collimator |
| MLD | Mean lung dose |
| MOMP | Mitochondrial outer membrane permeabilisation |
| MPF | Megakaryocyte-potentiating factor |
| MPM | Malignant pleural mesothelioma |
| MRI | Magnetic resonance imaging |
| MTT | 3-(4,5-dimethylthiazole-2-yl) -2,5-diphenyltetrazolium bromide |
| MU | Monitor units |
| NHEJ | Non-homologous end joining |
| NSCLC | Non-small cell lung cancer |
| NTCP | Normal tissue complication probability |
| NU7026 | 2-(morpholin-4-yl)-benzo-h-chromen-4-one |
| NU7441 | 2-N-morpholino-8-dibenzothiophenyl-chromen-4-one |
| OAR | Organ at risk |
| OS | Overall survival |
| PD | Pleurectomy decortication |
| PET-CT | Positron emission tomography-computer tomography |
| PI3K | Phosphatidylinositol 3-kinase |
| PIS | Patient information sheet |
| PNK | Polynucleotide kinase |
| PS | Performance status |
| PTV | Planning target volume |

| | |
|---------|--|
| QoL | Quality of life |
| QUANTEC | Quantitative Analysis of Normal Tissue Effects in the Clinic |
| R&D | Research and development |
| RCT | Randomised controlled trial |
| REC | Research ethics committee |
| RECIST | Response evaluation criteria in solid tumours |
| ReVISP | Reconstruction and visualisation from a single projection |
| RTOG | Radiation Therapy Oncology Group |
| RTTQA | Radiotherapy trials quality assurance team |
| $s(D)$ | Survival probability |
| SABR | Stereotactic ablative radiotherapy |
| SAE | Serious adverse event |
| SCLC | Small cell lung cancer |
| SF | Surviving fraction |
| SF2Gy | Survival fraction after delivery of 2Gy of IR |
| SLD | Sub lethal damage |
| Spyder | Scientific PYthon Development EnviRonment |
| SSB | Single strand breaks |
| SUVmax | Maximal standardised uptake value |
| SV40 | Simian virus 40 |
| SYSTEMS | Symptoms study of radiotherapy in mesothelioma |
| TBS-T | Tris-buffered saline with tween |
| TCP | Tumour control probability |
| TMG | Trial Management Group |

| | |
|------|------------------------------|
| TNM | Tumour, nodes, metastases |
| VATS | Video assisted thoracoscopy |
| VIM | Vinorelbine in mesothelioma |
| Vx | Volume of lung receiving xGy |

Chapter 1: Introduction

1.1 Malignant Pleural Mesothelioma

1.1.1 Incidence and epidemiology

Malignant pleural mesothelioma (MPM) is an aggressive malignancy which affects the lining of the lung. Therapeutic options are limited and the prognosis is dismal, with a median overall survival of 8 to 14 months (Wiggins, 2007) and survival rates at one and three years of just 41% and 12% respectively. (Beckett et al., 2015)

The incidence of MPM in the UK is amongst the highest worldwide, with numbers of disease-related deaths rising dramatically since 1968, when the British Mesothelioma Register was established. (McElvenny et al., 2005) Asbestos exposure is widely documented as the common aetiological factor and studies suggest that up to 85% of cases in the UK are directly attributable to this material. (Yates et al., 1997, Howel et al., 1997) High-risk occupations for exposure include production of brake and clutch linings, construction/demolition work, electricians, plumbers and shipyard workers. (Aguilar-Madrid et al., 2010) The use of asbestos was banned in the UK in 1999, but the incidence of the disease is expected to increase for the remainder of this decade, reflecting the long latency period of 30 to 40 years (McElvenny et al., 2005) and the heavy industrial use of asbestos in the 1970's and 80's. The National Lung Cancer Audit report suggests that 8740 cases of MPM were seen in England and Wales between 2008 and 2012. (Beckett et al., 2015) The vast majority (83%) of these patients were male and the median age at diagnosis was 73 years. The recently published British Thoracic Society guidelines into the investigation and management of MPM state that 2535 mesothelioma deaths were reported in the UK in 2015 (Woolhouse and Maskell, 2018) and it is estimated that 1/170 of men born in Britain in the 1940s will die of MPM. (McElvenny et al., 2005)

Asbestos continues to be mined and exported from several countries and is still used without adequate protection in much of the world. Therefore, it can be

expected that the MPM-epidemic which is currently affecting westernised countries may develop in more recently industrialised areas in the near future. (Rudd, 2010) This epidemiological trend will present both diagnostic and clinical challenges as more effective treatment options are sought for these patients.

1.1.2 Pathogenesis

The link between MPM and asbestos was first made in an epidemiological study published in 1960, (Wagner et al., 1960) but the pathogenic mechanisms through which asbestos causes neoplastic transformation of mesothelial cells is not fully understood.

The type of asbestos fibre to which exposure occurs appears to have a dramatic effect on the risk of developing MPM. Evidence suggests that amphiboles, of which the most commonly used types industrially, are crocidolite (blue asbestos) and amosite (brown asbestos), are much more potent inducers of MPM than chrysotile (white asbestos). Chrysotile appears to be cleared from the lungs more rapidly than amphiboles which may at least partly explain its lower carcinogenic capacity. (Rudd, 2010) Hodgson suggests that the potency of each type of fibre to induce carcinogenic changes is in the ratio of 1:100:500 for chrysotile, amosite and crocidolite respectively. (Hodgson and Darnton, 2000) By far the most commonly used type of asbestos in the UK was chrysotile, but amosite and crocidolite were both used to some degree and therefore many exposures are likely to have involved a mixture of fibre types. (Shuker et al., 1997)

Data suggests that asbestos fibres interact with mesothelial cells through direct and indirect mechanisms. Direct effects occur after inhaled fibres, which are deposited in the lungs, translocate to the pleura and cause irritation. Morphological studies have confirmed that contact between the fibres and mesothelial cells results in phagocytosis of the fibre, (Jaurand et al., 1979) which in turn is associated with intracellular oxidation and free radical production. (Liu et al., 2000) The interaction between reactive oxygen species

and cellular molecules induces DNA damage and alters the expression of proteins important in the control of cell proliferation and apoptosis. (Jaurand and Fleury-Feith, 2005) Asbestos fibres can also directly penetrate mesothelial cells where they disrupt the mitotic process, inducing structural chromosomal alterations and aneuploidy. (Wang et al., 1987, Yegles et al., 1993)

Indirect effects of asbestos on mesothelial cells are mediated through the release of inflammatory and growth factors in the pleural cavity, creating an environment which favours tumour growth. (Sekido, 2013) Furthermore, asbestos has been linked with activation of the mitogen activated protein kinase pathway, inducing the phosphorylation of proteins which drive the transcription of inflammatory proteins which facilitate tumorigenesis. (Zanella et al., 1996)

Although asbestos accounts for the majority of MPM, around 20% of cases have no history of asbestos exposure, suggesting that alternative aetiological factors may be important. DNA sequencing of MPM tissue has detected simian virus 40 (SV40) in some cases of MPM, suggesting that this virus may trigger neoplastic transformation within the pleura. (Carbone et al., 1994) Nevertheless, reports of false positives associated with contaminants from common laboratory plasmids containing SV40 should be taken into consideration. (Lopez-Rios et al., 2004) A role for ionizing radiation (IR) has been suggested, (Cavazza et al., 1996) as has exposure to chemicals such as nitrosamine or nitrosurea derivatives. (Peterson et al., 1984, Katada et al., 1983) Furthermore, fibres other than asbestos have been linked with MPM. An epidemiological study investigating the high incidence of MPM amongst inhabitants from villages in Turkey has suggested that erionite fibres from the volcanic region of Cappadocia represent the local carcinogenic agent. (Baris et al., 1987)

Clustering of MPM cases within families suggest that there may be a genetic component to the disease. Genetic profiling has identified a number of mutations which are commonly seen in MPM, although recently published studies

suggests that MPM has a relatively low mutational burden compared to many tumours. (Guo et al., 2015, Bueno et al., 2016)

Whilst studies have failed to identify any persisting oncogenic mutations, (Papp et al., 2001, Ni et al., 2000, Kitamura et al., 2002) research into tumour suppressor gene activity has been more successful. While *TP53* is relatively preserved, (Murthy and Testa, 1999, Vivo et al., 2003) common tumour suppressor gene mutations have been identified in *p16/CDKN2A* and the *NF2* gene, which appears to confer susceptibility to MPM in patients with a history of asbestos exposure. (Baser et al., 2002, Murthy and Testa, 1999, Deguen et al., 1998, De Rienzo and Testa, 2000) More recently, the loss of the tumour suppressor gene BRCA1 Associated Protein-1 (*BAP-1*) has been identified as an important driver mutation in MPM. (Bott et al., 2011, Testa et al., 2011) Germline mutations in *BAP-1* are known to be associated with an increased susceptibility to a number of malignancies, including MPM, uveal melanoma and cutaneous melanoma. (Cheung and Testa, 2017)

1.1.3 Diagnosis and staging

The diagnosis of MPM can be challenging and relies on a combination of clinical history, physical examination, radiology and pathology. For this reason, it is recommended that all suspected cases of MPM should be discussed by a regional MPM multidisciplinary team. (Woolhouse et al., 2018)

1.1.3.1 Clinical presentation

The clinical signs and symptoms of MPM are insidious and non-specific, leading to a high rate of misdiagnosis in the early stages. Chest pain and breathlessness are the most common presenting symptoms. (Macleod et al., 2014) Less frequently, patients may present with cough, weight loss, fatigue or fevers. (Wiggins, 2007) The pain of MPM is typically dull and diffuse and characteristically gets worse throughout the course of the disease. Its aetiology can be multifactorial: infiltration of the intercostal nerves or brachial plexus by the tumour can cause

a neuropathic component while invasion of ribs and vertebrae results in bone pain. (Saunders et al., 2019) Furthermore, in addition to tumour infiltration, pain can also result from the investigation and management of the disease. (Baas et al., 2015) MPM-associated pain is typically difficult to control, even with a combination of analgesics and patients often require non-pharmacological interventions to achieve symptom relief. (Saunders et al., 2019) The dyspnoea of early disease is typically caused by pleural effusions, but as the disease progresses, a restrictive effect is exerted on the chest wall due to pleural thickening.

1.1.3.2 Imaging

Several imaging modalities are employed in the diagnosis and staging of MPM. A contrast-enhanced computed tomography (CT) is usually the first cross-sectional imaging to be undertaken. Pleural disease (malignant or inflammatory) enhances strongly and the contrast can help distinguish between the thickened pleura, effusion and underlying collapsed or aerated lung. (Wiggins, 2007) Features may be present which suggest malignancy rather than benign pleural disease, including circumferential pleural thickening, pleural nodularity, parietal pleural thickening >1cm, chest wall invasion and mediastinal pleural involvement. (Leung et al., 1990) While many of these features have a high specificity, their sensitivity is less accurate and their absence does not exclude MPM. There may be other radiological features of asbestos exposure to support a diagnosis of MPM (e.g. pleural plaques), but CT cannot definitively differentiate between benign pleural disease and MPM. Furthermore, CT is poor at assessing soft tissue involvement and in detecting nodal disease.

Where a surgical approach is being considered, magnetic resonance imaging (MRI) can be used to highlight morphological and anatomical features of the disease and in particular, to clarify the tumour stage by delineating the extent of diaphragmatic involvement, as well as that of the chest wall and mediastinum. (Stewart et al., 2003) Studies suggest that gadolinium-based contrast MRI can distinguish between malignant pleural thickening and benign disease, with sensitivity of 100% and specificity of 95% reported by Boraschi *et*

al. (Boraschi et al., 1999) Furthermore, diffusion-weighted MRI has been reported to distinguish between epithelioid and non-epithelioid subtypes of MPM, (Gill et al., 2010) but these data are yet to be robustly validated in a prospective manner. (Woolhouse et al., 2018)

Positron emission tomography-computer tomography (PET-CT) may have additional value in distinguishing benign pleural disease from MPM, through differentiating the maximal standardised uptake value (SUVmax) detected in pleural thickening. (Treglia et al., 2014) Furthermore, this imaging modality may aid in the choice of biopsy site and is helpful in the staging of nodal disease and distant metastases. (Wilcox et al., 2009) Despite having a high sensitivity and specificity for malignant disease, PET-CT can be associated with false positives, particularly following talc pleurodesis which is associated with a large inflammatory response. (Coolen et al., 2012) False negatives can also occur, especially in small volume disease and where the malignancy has a low proliferative index. (Woolhouse et al., 2018)

1.1.3.3 Staging

MPM is staged using the tumour, nodes and metastases (TNM) system, as proposed by the International Mesothelioma Interest Group (IMIG) in 1995. (Aisner et al., 1995) This system was originally developed as an assessment tool for surgical intervention and can be difficult to reliably apply with CT or MRI imaging, both of which can under-stage the tumour. (Heelan et al., 1999) Information is often required from thoracoscopy with regard to the degree of visceral and parietal involvement. The diagnosis of mediastinal nodal disease is also difficult to accurately assess on imaging and mediastinoscopy may be required to determine nodal stage. In 2016, an update to the staging system was proposed by the International Association for the Study of Lung Cancer (IASLC), which allowed categories to be modified according to prognostic performance in surgically and non-surgically managed patients. (Rusch et al., 2016) This eighth edition of the TNM system is currently in clinical use, although data from the 2016 National Mesothelioma Audit suggests that stage is not recorded in the majority of patients. (2016)

1.1.3.4 Response assessment

Tumour response to treatment is traditionally graded according to the response evaluation criteria in solid tumours (RECIST). These criteria are based on the assumption that tumours are spherical and that the maximal uni-dimension measurement is sufficient to determine the degree of response. (Therasse et al., 2000) MPM does not conform to these assumptions because it grows circumferentially around the pleural cavity and response to treatment is therefore more accurately assessed by measuring the thickness of the pleural disease perpendicular to the chest wall. The RECIST criteria have now been amended to reflect this and validated with reference to MPM. (Byrne and Nowak, 2004a) Caution needs to be applied when patients have undergone talc pleurodesis since this can make the pleural lining appear thicker.

1.1.3.5 Pathology

Securing a pathological diagnosis of MPM can be difficult because MPM mimics a number of other malignancies of epithelioid or sarcomatoid origin. Pleural fluid can be obtained for analysis if an effusion is present, but making an accurate cytological diagnosis is challenging, as immunocytochemistry does not clearly distinguish highly reactive mesothelial cells from malignant ones. The British Thoracic Society guidelines advise against relying on cytology alone to make a diagnosis of MPM. (Woolhouse et al., 2018)

A pleural biopsy provides a more robust diagnostic sample and can be obtained through an image guided procedure or thoracoscopy. Studies have shown that a CT-guided percutaneous pleural biopsy is more effective for diagnosing the cause of pleural thickening than a blind Abram's punch biopsy (Maskell et al., 2003) and therefore this is the preferred technique. In cases which are clearly malignant on initial imaging, thoracoscopy is a useful technique for evaluating the pleural space and draining pleural effusions prior to talc pleurodesis. (Waller et al., 1995) This procedure is associated with a diagnostic sensitivity of >90% and a 10% complication rate. (Pistolesi and Rusthoven, 2004)

There are three different histological subtypes of MPM: epithelioid, sarcomatoid and mixed/biphasic. Accurate histological subtyping is important for prognostication and guiding treatment, since non-epithelioid subtypes are associated with significantly shorter overall survival (2016) and tend to be more refractory to treatment. Morphologically, epithelioid mesothelioma is associated with several patterns which can look microscopically similar to adenocarcinoma. Sarcomatoid mesothelioma often displays a spindle-cell pattern, which can look very similar to benign pleural fibrosis and can also be difficult to distinguish from sarcomas. Mixed/biphasic tumours exhibit a combination of epithelioid and sarcomatoid patterns and are the easiest to distinguish from other malignancies morphologically. (Inai, 2008)

Due to the non-specific morphological appearance of these subtypes, a range of immunohistochemical (IHC) markers are used to differentiate MPM from other pathologies. Commonly expressed mesothelial markers include calretinin, thrombomodulin, CK5/6, CAM5.2, EMA, vimentin, GLUT-1, HBME-1, WT-1 and p53. Negative markers include Ber-Ep4, CEA, Leu-1, CD15 and TTF-1. It is recommended that a combination of at least two positive mesothelial IHC markers and at least two negative adenocarcinoma IHC markers should be used to support a diagnosis of MPM. (Woolhouse et al., 2018)

Unfortunately, it is not uncommon for the definitive pathology to remain uncertain, even after detailed immunohistochemical analysis. Furthermore, IHC profiling cannot reliably distinguish malignant disease from benign mesothelial proliferations; nevertheless, clinically useful information can be obtained from expression analysis of *p16* and *BAP1* genes. In a study by Wu *et al*, hemizygous or homozygous deletion of *p16*, assessed by fluorescent in situ hybridisation (FISH), was predictive of MPM over benign fibrous pleurisy, demonstrating 100% positivity in cases of sarcomatoid MPM. (Wu et al., 2013) This trend was repeated in a study by Hida *et al*, which also suggested a role for *BAP1* deletion in differentiating MPM from benign mesothelial proliferation. (Hida et al., 2015)

1.1.3.6 Biomarkers

Extensive research efforts have been directed towards finding an MPM biomarker to aid screening, diagnosis, guide prognostication and assess response to treatment. Sources include serum, plasma or pleural fluid and amongst promising candidates are mesothelin, fibulin-3, megakaryocyte-potentiating factor (MPF), soluble mesothelin related peptide and osteopontin.

Unfortunately, the sensitivity and specificity of these markers are too low to permit their use in clinical diagnosis, even when combined together. (Creaney et al., 2008) Fibulin-3 was proposed as a soluble diagnostic biomarker by Pass *et al* in 2012, who demonstrated encouraging results in retrospective analysis. (Pass, 2012) More recent data has suggested that this marker may be useful in prognostication, but is of limited value in the diagnosis of MPM. (Kirschner et al., 2015) Soluble mesothelin related peptide has demonstrated a positive correlation with tumour bulk and falls following surgical resection of disease, but cannot predict stage of disease at baseline. (Creaney et al., 2011) The current British Thoracic Society guidelines suggest that biomarkers should not be used to screen for MPM, nor should they be used to predict treatment response or survival. They may be helpful at diagnosis in patients with suspicious cytology who are not fit enough for more invasive tests. (Woolhouse et al., 2018)

1.1.4 Prognostication

Whilst the overall outlook following an MPM diagnosis is poor, a number of independent factors have been studied in an attempt to identify outcome predictors. These include patient factors, disease variables and symptom burden.

Three large retrospective studies identified an association between worse overall survival and the presence of increasing age, male sex, advanced stage and non-epithelioid histology. (Gemba et al., 2013, Milano and Zhang, 2010, Taioli et al., 2014) The presence of chest wall pain has also been identified as an independent predictor of poor outcome in three retrospective case series. (Meniawy et al., 2013, Herndon et al., 1998, Bottomley et al., 2007)

A number of validated MPM prognostication scores are available, including the European Organisation for Research and Treatment of Cancer (EORTC) prognostic score, the Cancer and leukaemia group B (CALGB) score and the modified Glasgow Prognostic Score. (Woolhouse et al., 2018)

1.1.5 Management of MPM

1.1.5.1 Surgery

Surgical resection, in conjunction with chemotherapy and radiotherapy, is the most aggressive therapy offered to a highly selected cohort of patients with MPM, although its role is controversial. The traditional surgical approach of extrapleural pneumonectomy (EPP) is an extensive and technically challenging operation which aims to remove all macroscopic disease, including the underlying lung. This approach seemed encouraging in 1996, when Sugarbaker *et al* reported a 22% five year survival in 120 patients treated with multimodality therapy, (Sugarbaker et al., 1996) however, EPP has fallen out of favour in recent years due to safety concerns. Peri-operative mortality rates of 3-9% have been reported (Treasure and Sedrakyan, 2004) and significant post-operative complications have been observed in up to 60% of cases. (Sugarbaker et al., 2004) A number of non-randomised studies suggest that combination treatment may be associated with better overall survival, (Weder et al., 2007, Federico et al., 2013, Van Schil et al., 2010, Krug et al., 2009) but the first and only randomised study to assess the role of EPP in multimodality treatment of MPM was the Mesothelioma and Radical Surgery (MARS) study. This feasibility study enrolled 50 patients and concluded that a larger study would not be possible due to the high mortality associated with EPP. (Treasure et al., 2011) This outcome was largely contested in the oncological and surgical communities because MARS had been neither designed nor powered to assess the outcome of surgery versus no surgery, but EPP has largely been abandoned since the publication of this data.

The less aggressive surgical approach of pleurectomy decortication (PD) may be a more suitable option for patients with operable disease. This procedure, which

leaves the underlying lung intact has been shown to be effective in preventing the re-accumulation of fluid in MPM. (Soysal et al., 1997) It appears to be associated with lower rates of intraoperative mortality (Flores et al., 2008) and better quality of life post-operatively. (Mollberg et al., 2012) The MARS-2 trial is currently underway in the UK to assess the feasibility of recruiting to a large randomised controlled study of PD versus no surgery in association with neoadjuvant chemotherapy. (Lim, 2016)

1.1.5.2 Systemic anti-cancer treatment

1.1.5.2.1 First line treatment

Chemotherapy is the only treatment modality for which there is randomised controlled evidence of survival benefit in MPM. The Vogelzang study, published in 2003, is the largest randomised controlled trial (RCT) of chemotherapy in MPM. (Vogelzang et al., 2003) The study recruited 456 patients and compared a combination of 3 weekly Pemetrexed and Cisplatin to Cisplatin alone. Results suggested that dual administration of Pemetrexed and Cisplatin was associated with a significant survival benefit compared to Cisplatin alone (12.1 months versus 9.3 months: $p=0.02$). Patients who received full vitamin supplementation had a further survival advantage (median survival of 13.2 months). Similar benefits were seen in a smaller randomised study of 250 patients, assessing Raltitrexed with Cisplatin, or Cisplatin alone. (van Meerbeeck et al., 2005) Median overall survival was 11.4 months in the combined arm and 8.8 months in the Cisplatin only arm, supporting the efficacy of antifolates in MPM.

Guidelines suggest that all patients who are PS 0-1 should be considered for palliative chemotherapy. (Woolhouse et al., 2018) The optimal timing for this is uncertain, but studies suggest that early chemotherapy offers a better survival advantage than delayed. (O'Brien et al., 2006)

The Mesothelioma Avastin Cisplatin Pemetrexed Study (MAPS) recently reported a significant survival advantage associated with the addition of Bevacizumab to

Cisplatin/Pemetrexed chemotherapy in MPM. This randomised phase III trial randomised 448 patients and delivered 3 weekly cycles of either Cisplatin/Pemetrexed alone or in combination with Bevacizumab. A median overall survival of 18.8 months was reported in the group treated with Cisplatin/Pemetrexed/ Bevacizumab compared to 16.1 months in those treated with Cisplatin and Pemetrexed only ($p=0.0167$). The addition of Bevacizumab was associated with higher rates of hypertension and thromboses and more grade 3 events. (Zalcman et al., 2015) Bevacizumab is not currently licenced in the UK for use in MPM and is not available on the NHS; current UK British Thoracic Society guidelines recommend the use of Cisplatin/Pemetrexed in the first line setting. (Woolhouse et al., 2018)

1.1.5.2.2 Second line treatment

Studies investigating second line chemotherapy in MPM report no survival advantage of Pemetrexed (Jassem et al., 2008) or Vorinostat (Krug et al., 2015). Whilst single agent Vinorelbine is offered to patients of good performance status (PS) who relapse following first line platinum-containing chemotherapy, a systematic review of the literature concluded that fit patients should be referred for clinical trials, since the reported activity of second line chemotherapeutic agents is low. (Buikhuisen et al., 2015) The Vinorelbine in mesothelioma (VIM) study is a randomised controlled phase II trial of Vinorelbine versus best supportive care in the second line setting. This study, which has now completed recruitment in the UK, aims to establish whether Vinorelbine confers a survival advantage in MPM and whether underlying molecular changes may predict drug efficacy.

1.1.5.2.3 Ongoing clinical trials of systemic therapy

Despite a relative stagnation in the development of systemic treatment options for MPM in the years following publication of the Vogelzang study, the research climate in this disease has progressed dramatically in more recent years. Some of the most promising early phase data has been generated using molecularly targeted agents, such as Nintedanib (Grosso et al., 2017) and immunotherapy,

with drugs such as Pembrolizumab. (Alley et al., 2017) Anti-mesothelin agents have shown promise in the epithelioid subtype, (Hassan et al., 2014) whilst arginine deprivation has been shown to have activity alongside standard chemotherapy in patients with sarcomatoid and biphasic MPM. (Beddowes et al., 2017)

A large number of clinical trials of systemic therapies are ongoing in the first, second and third line MPM settings, using a variety of these systemic approaches. A comprehensive summary of these studies has been recently published in The Clinical Respiratory Journal. (Bibby and Maskell, 2018)

1.2 The changing role of radiotherapy in MPM

Radiotherapy delivery in MPM is challenging because of the complex shape of the pleural cavity and the close proximity of critical radiosensitive structures to the planning target volume (PTV). Attempts to deliver radical radiotherapy to the hemithorax using parallel opposed beams have been associated with severe radiation lung injuries (Maasilta, 1991, Linden et al., 1996, Ball and Cruickshank, 1990, Mattson et al., 1992, Law et al., 1984) and changes in spirometry compatible with total loss of ipsilateral lung function. (Maasilta, 1991) For this reason, radiotherapy in MPM has traditionally been limited to modest doses delivered using standard 2-dimensional (2D) techniques, for prophylactic or palliative purposes. Nevertheless, recent developments in radiotherapy planning and delivery technologies have revolutionised our ability to dose escalate treatment to the pleura, whilst keeping doses to normal tissues at an acceptable level.

1.2.1 Palliative radiotherapy

To date, the only robust evidence supporting the use of radiotherapy in MPM is in the palliation of pain. (MacLeod et al., 2015a) One of the first studies addressing this was performed in Glasgow by Bissett *et al* with a cohort of 19 patients. (Bissett et al., 1991) A radiation dose of 30Gy in 10 fractions was

delivered over 2 weeks to the whole hemithorax using parallel opposed pairs, with pain assessments before and after the treatment. This regimen was reported to be well tolerated, with results suggesting an improvement in pain control for about 70% of patients, but the response was short lived, displaying a median duration of 2 months.

A number of case reports and studies detailing the use of radiotherapy for pain control in MPM have subsequently been published (Ball and Cruickshank, 1990, Linden et al., 1996, Jenkins et al., 2011, de Graaf-Strukowska et al., 1999) and a systematic review of the available literature was carried out by MacLeod *et al* in 2014. (Macleod et al., 2014) It was noted that there were large variations in the total radiotherapy doses and fractionation regimes employed and in response rates, which varied from 0% to 69%. Eight papers were identified which fulfilled the inclusion criteria but due to a combination of poor study design and small patient numbers, only Level 2 to 3 evidence was identified, rendering it impossible to draw firm conclusions regarding the use of radiotherapy for pain control in MPM. This review exposed the fact that radiotherapy was being utilised as the key analgesic modality in MPM, recommended by both the British Thoracic Society and the European Respiratory Society, (Scherpereel et al., 2010) despite there being no consensus on dose, fractionation or optimal mode of delivery and with very little efficacy data. The need for a robust prospective study to address this practise was identified. (Macleod et al., 2014)

The symptoms study of radiotherapy in mesothelioma (SYSTEMS) was the first prospective study to use validated outcome measures to assess pain response to radiotherapy in MPM. (MacLeod et al., 2015a) This multicentre, single arm phase II trial recruited forty patients from three centres over eighteen months and delivered a standard radiotherapy dose of 20 Gray (Gy) in 5 fractions to sites of pain using parallel opposed pairs. Analgesia was optimised prior to study entry and pain was assessed using the brief pain inventory, a validated assessment tool for cancer pain, (Cleeland and Ryan, 1994) at baseline and at five weeks after the radiotherapy. Radio-opaque wire markers were applied at the time of CT planning scan acquisition to demarcate painful areas and aid radiotherapy

planning. A clinically significant response was deemed as a $\geq 30\%$ reduction in pain score from baseline to week 5. (Farrar et al., 2000) Complete case analysis revealed a clinically significant improvement in pain in 47% of the 30 patients assessable at week 5 (confidence intervals 28.3 to 65.7), with minimal toxicity. Although a variety of secondary endpoints were assessed, radiotherapy was not found to be useful in the palliation of any other symptoms.

This study provided the first robust evidence for using radiotherapy for pain control in MPM. The value of dose-escalated radiotherapy for MPM-associated pain is now being assessed in the SYSTEMS-2 study. (Ashton et al., 2018) This prospective, multicentre, randomised, Phase II study is comparing standard palliative radiotherapy (20Gy in 5 fractions delivered over 1 week) with a dose-escalated regime (36Gy in 6 fractions delivered over 2 weeks) and aims to recruit 112 patients from 20 UK centres. To facilitate safe dose escalation to the PTV without incurring unacceptable toxicities to organs at risk (OARs), radiotherapy is planned using either 3D conformal radiotherapy (3DCRT) or intensity modulated radiotherapy (IMRT). The primary outcome of this trial is pain control at week 5, assessed using the brief pain inventory. Secondary endpoints include acute toxicity, duration of pain response, radiological response and overall survival. The set up and progress of SYSTEMS-2 is discussed in more detail in Chapter 2.

1.2.2 Prophylactic radiotherapy

The value of prophylactic radiotherapy in preventing subcutaneous MPM tumour deposits at intervention sites has been investigated in a number of studies. Low *et al* published retrospective data on 20 patients irradiated prophylactically at a single centre between 1990 and 1994 and concluded that prophylactic radiation is highly effective in preventing tumour seeding following chest wall intervention in MPM. (Low et al., 1995) Findings of a French study, using a dose of 21Gy in 3 fractions, supported this conclusion, (Boutin et al., 1995) although subsequent studies using 21Gy in 3 fractions and a 10Gy single fraction failed to find any benefit of prophylactic radiotherapy and concluded that drain site radiotherapy in MPM is a wasted resource. (O'Rourke et al., 2007, Bydder et al., 2004) Practise

changing studies in this field were published in 2016 and 2019. (Clive et al., 2016, Bayman et al., 2019) The SMART study, a multicentre, open-label, Phase III, randomised controlled trial recruited 203 patients, from 22 UK hospitals, who had undergone large-bore pleural intervention in the 35 days prior to recruitment. Patients were randomised to receive immediate radiotherapy (21Gy in 3 fractions) or the same dose only at diagnosis of tract site metastases. No significant difference was seen in the incidence of tract site metastases in the immediate and deferred radiotherapy groups and the authors concluded that routine use of prophylactic radiotherapy is not justified. (Clive et al., 2016) This conclusion was supported by the results of the prophylactic irradiation of tracts (PIT) study in 2019, which recruited 375 patients from 54 centres and delivered 21Gy in 3 fractions to intervention sites. (Bayman et al., 2019)

1.2.3 Adjuvant radiotherapy

Tri-modality treatment with chemotherapy, surgery and radiotherapy is the most aggressive and radical option available to patients with MPM, although a change in the surgical landscape means that this is not currently offered in the UK. The aim of surgery is to achieve a macroscopic complete resection (MCR), although the infiltrative growth pattern of MPM renders this objective very challenging. Neoadjuvant chemotherapy is given with the intent of down staging the tumour prior to surgery, but local recurrence remains a problem, even after complete MCR. (Baldini et al., 1997, Stewart et al., 2004, Yan et al., 2009) Hemithoracic adjuvant radiotherapy has been an integral component of this treatment approach for decades, (Vaeth and Purcell, 1964) aiming to prevent recurrent local disease. The practise is supported by prospective data collected from 59 patients, suggesting that radiotherapy is associated with improved disease control: local recurrence occurred in 51% of the overall cohort compared to 29% of those who received adjuvant radiotherapy. (Yan et al., 2009)

Despite the relative advantage conveyed by removal of the ipsilateral underlying lung during EPP, the post-operative volume is large and complex, with a number of dose-limiting structures remaining in close proximity to the PTV. The inability to dose escalate without selectively protecting radiosensitive OARs has rendered

traditional radiotherapy techniques largely obsolete in this setting, (Ashton et al., 2017) although a number of solutions have been described which facilitate dose escalation to target volumes using a 2D or 3D approach. (Baldini et al., 1997, Rusch et al., 2001, Mychalezak et al., 1989) Nevertheless, high rates of local failure have been reported (Yajnik et al., 2003), substantiating concerns regarding target dose inhomogeneity with these techniques. (Gupta et al., 2009)

Advanced radiotherapy planning techniques, such as IMRT, increase dose conformity, facilitating dose escalation to the target volume, while keeping doses delivered to OARs at a safe level. In MPM, IMRT has been demonstrated to achieve a more uniform pleural dose than could be accomplished with traditional techniques, (Tobler et al., 2002) although the popularity of this modality in the post-operative setting has fluctuated. Encouraging initial data from MD Anderson suggested that IMRT could deliver 45-50Gy to the post-operative volume, with boosts to 60Gy in areas of clinical concern, and reported 100% local control rates within treated volumes at 9 months. (Ahamad et al., 2003) Enthusiasm for IMRT declined however, following the publication of toxicity data from three centres of excellence between 2006 and 2008. (Allen et al., 2006, Miles et al., 2008, Rice et al., 2007a) High incidences of fatal pneumonitis were reported and were found to correlate with dosimetric parameters received by the contralateral (intact) lung. While the volume of lung receiving 5Gy (V5) and the mean lung dose (MLD) were both linked with pneumonitis, only the volume receiving 20Gy (V20) has been found to have a predictive association. (Rice et al., 2007a) Generation of dose constraints informed by these studies, combined with modifications to the delivery of IMRT (Allen et al., 2007) and significant advances in patient imaging which increases the accuracy of treatment delivery, has led to the re-emergence of IMRT in the post-EPP setting. Encouraging rates of local control associated with improved median survival have been reported (14.2 months in irradiated patients versus 10.2 months in non-irradiated cohort). This survival advantage was extended to 28 months in patients with favourable clinical features (node negative disease and epithelioid histology). (Rice et al., 2007b)

The change in surgical management of MPM from EPP to PD has rendered the role of the clinical oncologist even more challenging, since radical doses now need to be delivered to the pleura in the context of two intact radiosensitive lungs. Furthermore, the incomplete resection associated with PD brings with it a stronger indication for adjuvant radiotherapy. (Ashton et al., 2017) A prospective phase II study by Rimner *et al* demonstrated the feasibility of delivering hemithoracic IMRT to the pleura to a dose of 50.4Gy in 28 fractions following PD. In conjunction with chemotherapy, this technique was not associated with any incidences of grade 3 or 4 pneumonitis. (Rimner et al., 2016b) Nevertheless, increasingly sophisticated methods of radiotherapy delivery, such as volumetric arc radiotherapy (VMAT) and helical tomotherapy (HT) have been used in MPM to achieve greater dose conformity in the context of two intact lungs than can be achieved with IMRT. (Dumane et al., 2016, Minatel et al., 2012, Minatel et al., 2014, Giraud et al., 2011, Helou et al., 2013) Recently published retrospective data from Parisi *et al* has demonstrated that hypofractionated radiotherapy can be safely delivered to the hemithorax after PD or biopsy using HT. A dose of 25Gy was delivered in 5 fractions to 36 patients with MPM, with acceptable levels of toxicity. (Parisi et al., 2017)

There are several difficulties in drawing robust conclusions regarding the efficacy of adjuvant radiotherapy from the available data, primarily due to the lack of control groups and randomisation. (Ashton et al., 2017) Many of the studies are retrospective and report results from small numbers of patients at single centres. Between studies there is variation in the radiotherapy technique employed, dose delivered to the PTV and in the reporting of achieved dosimetry. Furthermore, the inherent selection bias associated with studies in which patients have been selected for surgery (Hasani et al., 2009) makes the accurate interpretation of survival data even more challenging.

The only RCT to specifically address the role of radiotherapy in the tri-modality treatment of MPM was published in 2015. (Stahel et al., 2015) Patients received neo-adjuvant chemotherapy and those who achieved MCR after EPP were randomised to receive hemithoracic radiotherapy or not. A dose of 45Gy to 46Gy

(in 1.75Gy, 1.8Gy or 2Gy fractions) was delivered to the post-operative volume with boosts of 55.9Gy to 57.6Gy to areas of clinical concern using either IMRT or 3DCRT. A total of 54 patients were eligible for randomisation; 27 patients started radiotherapy and 25 patients completed the treatment. No statistically significant difference in relapse-free survival was found between those who received adjuvant radiotherapy and those who did not (9.4 months and 7.6 months respectively) and the study concluded that there was inadequate support for the routine use of hemithoracic radiotherapy in the post-operative setting. (Stahel et al., 2015) This conclusion has been challenged by the oncological community, particularly given the lack of statistical power, the heterogenous nature of the radiotherapy planning, the absence of central review and the failure to publish any dosimetry data. (Rimner et al., 2016a)

1.2.4 Neo-adjuvant radiotherapy

A novel approach using pre-operative radiotherapy has been reported from Princess Margaret Hospital, Toronto, with encouraging results. (de Perrot et al., 2016, Cho et al., 2014) In this technique, the aim of which is to sterilise the tumour bed and prevent tumour seeding during surgery, 25Gy in 5 fractions is delivered to the pre-operative hemithorax using IMRT, with a concomitant boost of 5Gy to areas of gross tumour volume (GTV) and tract sites. Patients proceed to EPP within one week of the radiotherapy, the timing of which is crucial in preventing the development of fatal pneumonitis. Adjuvant chemotherapy is offered to any patient found to have mediastinal node involvement post operatively. Findings from a non-randomised, phase I/II feasibility study of 25 patients with T1-T3 disease were encouraging, with a peri-operative mortality rate of zero and no grade 3-5 radiation toxicities. Post-operatively, 96% of the cohort was confirmed to have had stage III or IV disease and cumulative overall survival was reported as 58% at 3 years. Dichotomising these data by histological subtype revealed that patients with epithelioid disease survived significantly longer (84% at 3 years) than their biphasic counterparts. (Cho et al., 2014) Further phase II data from 62 patients, 94% of whom had stage III or IV disease, supported a prognostic advantage for the epithelioid subtype, reporting a median overall survival of 51 months and disease free survival of 47 months in this cohort. (de Perrot et al., 2016)

1.3 Advances in radiotherapy delivery

Many of the changes seen in MPM-associated radiotherapy over recent years have been driven by accumulating data which suggest that delivery of an increased radiation dose to the tumour may be associated with better local control. (Rusch et al., 2001, Rosenzweig et al., 2012, Buduhan et al., 2009, Krayenbuehl et al., 2014) Furthermore, encouraging data from the SYSTEMS study has prompted the question of whether dose escalated radiotherapy may be of additional benefit in palliation of MPM-associated pain. (MacLeod et al., 2015a)

In order to safely dose escalate treatment to the PTV, increasingly sophisticated methods of radiotherapy delivery have been utilised which can better manage the compromise between adequate tumour irradiation and sparing of healthy tissue. These techniques vary from fixed-field IMRT, to increasingly complex rotational techniques (VMAT and HT).

1.3.1 Fixed-field IMRT

In fixed-field IMRT, dose conformity is enhanced by dividing the radiation beam into multiple small beamlets, which are delivered from a number of angles. The intensity of the beams are modulated through the presence of a multileaf collimator (MLC), using either a segmental-based or dynamic-based approach. In the segmental (or step-and-shoot) approach, the MLC aperture is set to discrete shapes and the beam is only delivered when the leaves are stationary at each position. In the dynamic (or sliding-windows) approach, the leaves move continuously, modulating the beam as the radiotherapy is delivered. In addition to achieving a more uniform dose distribution and greater conformity to the target, IMRT allows boosts to be incorporated into the plan so areas at high risk of disease relapse can be further dose escalated throughout the course of the treatment, rather than at the end. Furthermore, challenges to dose delivery resulting from the large field sizes associated with MPM and the constraints of the MLC leaves have been addressed using a leaf-sequencing algorithm. (Xia et al., 2002)

A significant disadvantage of any technique that dose escalates through the use of multiple beams delivered from different angles is the ‘dose bathing effect’. This refers to the low radiation dose which is necessarily deposited in normal tissue by the increased number of beams to achieve dose escalation at the target. Planning studies comparing post-operative radiotherapy delivered with IMRT and conventional techniques have highlighted the potential impact of this issue in MPM. (Cho et al., 2010, Hill-Kayser et al., 2009, Krayenbuehl et al., 2007) Although IMRT was associated with improved clinical target volume (CTV) coverage and the achieved dosimetry was more homogenous across the target, this technique consistently delivered larger doses to OARs than conventional 2D or 3D techniques. Worryingly, one study identified that IMRT was associated with a statistically significant increase of 7.2% in the contralateral lung V20. (Krayenbuehl et al., 2007) The clinical impact of this dose bathing effect in mesothelioma patients was highlighted in 2006-2008, when toxicity data from three large institutions was published. (Allen et al., 2006, Miles et al., 2008, Rice et al., 2007a) A correlation was noted between the dose delivered to the single remaining lung and poor patient outcomes. In particular, the volume of lung receiving 20Gy was demonstrated to have a statistically significant predictive association with pneumonitis. (Rice et al., 2007a) This data has been crucial in informing appropriate dose constraints to OARs in both the post-EPP and non-surgical setting.

1.3.2 VMAT/HT

VMAT and HT are progressively more advanced methods of IMRT. They theoretically facilitate safer dose escalation by further enhancing dose conformity. Both are rotational techniques, in which the gantry rotates around the patient, delivering continuous radiotherapy beams, as opposed to the ‘fixed-field’, static gantry technique associated with traditional IMRT. VMAT is able to achieve highly conformal radiation doses by allowing simultaneous variations in rotation of the gantry, dose rate and MLC position. This facilitates delivery of radiotherapy to the entire tumour in a 360° rotation using single or multiple arcs. (Rana, 2013) HT permits further conformity through continuous rotation of the gantry around the patient, delivering a fan-beam of radiotherapy which is modulated by a pneumatically powered multileaf collimator. Additional

manipulation of the treatment couch position as it moves through the gantry facilitates the delivery of a very precise radiotherapy shape and dose to the target. Treatment verification with on-board CT imaging also helps to ensure accurate treatment delivery and increases the feasibility of dose escalation. (Welsh et al., 2002)

A planning study comparing Varian's Rapid Arc VMAT with conventional dynamic-based IMRT in 6 MPM patients reported equivalent target coverage and homogeneity but observed that VMAT was associated with improved OAR sparing and also required fewer monitor units (MU) and less time to deliver the treatment. (Scorsetti et al., 2010) A similar study comparing Philips' Smart Arc VMAT with segmental-based IMRT found very little difference in the dose indices achieved, but reported consistently shorter delivery times and more efficient MU use with VMAT. (Kawashima et al., 2013) Such data imply that this technique may be more suited to the treatment of MPM patients, in whom target volumes may be large and where reduced intra-fraction patient motion and variability would help ensure that dose is delivered within the intended target margins. (Rana, 2013)

Sterzing *et al* compared the dosimetry achieved with HT to segmental-based IMRT. They reported that HT significantly improved dose homogeneity and target coverage (average PTV receiving more than 95% of the prescribed dose: 96.42% for HT compared to 87.10% for IMRT) and that the contralateral MLD could be reduced to less than 5Gy with HT. (Sterzing et al., 2008) Clinical studies have confirmed this dosimetric superiority. (Sylvestre et al., 2010) In a pilot study, performed on a single patient post-pleurectomy, Rapid Arc VMAT was compared with HT. While homogenous PTV coverage and acceptable OAR doses were achieved with both techniques, HT was associated with improved dosimetry in the contralateral lung (V20, V10, V5: 0%, 2.3%, 17.1% for HT compared to 0%, 14.8%, 65.8% for VMAT), while VMAT required fewer MUs and could deliver treatment significantly faster than HT. (Yip et al., 2011)

1.3.3 RapidPlan

In order to reduce planning time and streamline workflow, knowledge-based radiotherapy planning has been incorporated into clinical practise. Within Eclipse (v15.5), a database of previously created IMRT or VMAT plans are accumulated for a particular anatomical area to create a 'training cohort'. The RapidPlan model learns from these plans by exploiting anatomical correlations of dose volume distributions, specifically the geometrical arrangement of OARs with respect to the PTV and the previously achieved doses to OARs and PTVs. The system is then able to automatically generate dose volume histogram (DVH) estimates for a new patient and translate these into suggested optimal IMRT or VMAT plan objectives. (Appenzoller et al., 2012, Chanyavanich et al., 2011, Zarepisheh et al., 2014) RapidPlan has been demonstrated to reduce planner interaction time and improve plan quality and consistency, (Tol et al., 2015, Fogliata et al., 2017) but the quality of the plans produced is heavily dependent on the quality and robustness of those in the training database. (Hussein et al., 2016)

1.3.4 Multi-criteria optimisation

Common to these advanced radiotherapy techniques is the inverse planning process, in which the desired dose to the PTV is prescribed and acceptable dose limits for the surrounding radiosensitive structures are set. An iterative optimisation process is then undertaken, whereby the cost-function associated with the stated objectives is minimised to create the 'optimal' plan. This approach is time consuming and is often associated with sub-optimal plans, in which, for example, the compromise made between the planning goals may not be clinically acceptable. (Miguel-Chumacero et al., 2018) Radiotherapy planning is therefore a multi-criteria problem, in which the risk of under dose in the PTV is balanced against the risk of overdose in the OARs. (Teichert et al., 2019)

To address this, a multi-criteria optimisation (MCO) approach has been suggested. (Craft et al., 2006, Craft et al., 2012a, Craft et al., 2012b, Kierkels et al., 2015, Wala et al., 2013, Kamran et al., 2016, Thieke et al., 2007, Muller

et al., 2017) This system finds multiple solutions to the problem, all of which prioritise a specific optimisation objective over all others. By combining these solutions in a mathematical construct, trade-offs can be made between two or more conflicting objectives, allowing the 'best-compromise' solution to be found. This method brings the plan closer to the Pareto surface, which represents the optimal solution from which it is impossible to reallocate to make any one preference criterion better off, without making at least one preference criterion worse off. A comprehensive review of the mathematical modelling which underpins this technology is presented by Katrin *et al.* (Teichert et al., 2019)

In practise, MCO generates $3n+1$ alternate plans for each objective. The first plan targets the selected objective and optimises it as much as possible along the Pareto surface, while letting some of the other objectives vary. The second plan allows the chosen objective to deteriorate in a controlled manner, while letting the others improve. The final plan is a combination of the first two plans. This process is repeated for each of the objectives and an 'optimal' plan is selected for trade-off taking into account all of the parameters. Possible solutions with the resulting trade-offs can be explored to find the plan that best fulfils the treatment goals. Choice of initial plan is critical, since this influences the subsequent approximation of the Pareto front. It is therefore advisable to begin trade-off exploration using a plan which is already clinically acceptable. (Teichert et al., 2019)

The value of MCO has been explored in a number of tumour sites, including pancreatic cancer, glioblastoma, non-small cell lung cancer and prostate cancer. (Wala et al., 2013, Muller et al., 2017, Kamran et al., 2016) MCO has consistently demonstrated the ability to reduce planning time and increase plan quality compared to standard planning techniques. (Craft et al., 2012b, Wala et al., 2013, Kamran et al., 2016, Teichert et al., 2019) Paramount to the success of MCO is the ability to trade off small variations in PTV coverage, which do not compromise clinically stipulated requirements, while significantly sparing OAR doses. (Teichert et al., 2019)

Miguel-Chumacero *et al* explored the combination of MCO with RapidPlan in head and neck cancer and reported that combination of these techniques could improve the balance between OAR doses and PTV coverage. It was observed that plans generated through a RapidPlan model provide an optimal starting point for MCO; plan quality was maximally enhanced by the MCO optimisation of a plan generated via the RapidPlan model which had been trained using MCO-optimised plans. Compared to the original clinical plan, these plans were associated with a mean parotid dose of 15 ± 4.6 Gy versus 22.9 ± 5.5 Gy (left) and 17.1 ± 5 Gy versus 24.8 ± 5.8 Gy (right). (Miguel-Chumacero et al., 2018)

Despite the potential benefits associated with MCO, no studies have been published in which radiotherapy plans for MPM have been optimised using this technology.

1.4 Radiobiological considerations impacting radiotherapy delivery

1.4.1 The lethality of ionising radiation

The consequences of cell exposure to ionising radiation (IR) are mediated through its interaction with DNA and include cell death, carcinogenesis and genomic mutation. Both direct ionisations and free radical production can result in DNA-lesions including base damage, DNA-protein crosslinks, single strand breaks (SSB) and double strand breaks (DSB). A 2Gy dose of radiation will produce on average around 2000 SSB and 80 DSB. An intricate series of pathways exist through which the cell can sense and repair each type of lesion prior to undergoing mitosis. (Thacker and Zdzienicka, 2003) Checkpoints within the cell cycle block the progression of the cell into the subsequent stage until the damage has been repaired, or until cell death is triggered. (Sancar et al., 2004) SSB are generally repaired readily by the cell and do not directly contribute to the cytotoxicity of IR. DSB, by contrast, are difficult for the cell to repair and are the most toxic form of radiation-induced DNA damage. Failure to accurately repair DSB leads to the development of genomic aberrations. Where these involve two chromosome breaks, asymmetric exchange-type aberrations can occur, forming di-centrics and rings, culminating in the loss of reproductive

integrity and death, either by apoptosis, mitotic catastrophe or an alternative cell death pathway. Cells deficient in the DSB-DNA repair pathways have been demonstrated to have an increased number of chromosomal aberrations and are very sensitive to radiation-induced cell death, (Willers et al., 2009, Abbott et al., 1998) supporting the proposal that DSB is the principle cytotoxic lesion for IR. Mechanisms of DSB repair will be discussed further in section 1.7.

1.4.2 Normal tissue radiation toxicity

The toxicity associated with radiotherapy can be explained by the radiation-induced death of normal cells and are generally categorised into ‘acute’ and ‘late’ effects. Although the DNA damage is inflicted at the time of radiotherapy, cell death and therefore side effects may not become apparent until cell division is attempted. (Fowler, 1992) Acute/early side effects typically occur in rapidly proliferating tissues which are actively renewing and tend to occur during or shortly after radiotherapy. Such effects tend to cause inflammatory reactions in exposed epithelial surfaces and mucosa. These are usually manageable with supportive treatment and tend to be temporary due to proliferation and repopulation by surviving stem cells. (Timmerman, 2008, Fowler, 1992)

Late side effects, conversely, occur in slowly, or non-proliferating tissues and become apparent months to years after the completion of radiotherapy. Unlike acute reactions which can be reversed, the slow growing nature of these cells means that the effects tend to be permanent. Late effects can be destructive and are often associated with underlying vascular injury and chronic inflammation. This can lead to devascularisation and denervation of tissue and consequential fibrosis, stenosis and ulceration. These events can have devastating implications for patients, heavily impacting on quality of life with considerable morbidity and mortality. For this reason, late normal tissue effects are the dose limiting factor in radiotherapy delivery. (Timmerman, 2008)

1.4.3 The linear quadratic model of cell survival

Depending on the situation, cell survival is defined in several ways. In differentiated tissues where cells do not proliferate, cell survival can be defined as the retention of function or viability, whereas in actively dividing tissues (e.g. intestinal epithelium), ‘survivors’ are those cells which have maintained their reproductive integrity. Cells able to proliferate indefinitely are said to have retained clonogenic capacity. The relationship between a delivered radiation dose and the proportion of cells that retain their ability to reproduce is described by a cell survival curve and can be demonstrated experimentally in an *in vitro* clonogenic assay. In clonogenic assays, the proportion of cells that have retained clonogenic capacity can be calculated and expressed as the surviving fraction of cells. The shape of the curve depends on the type of radiation delivered. For densely ionising radiation with a high linear energy transfer (LET), e.g. α particles, the response follows an approximately linear relationship (i.e. survival is approximated by an exponential function of dose). Conversely, for sparsely ionizing radiation (e.g. x- or γ -rays), the curve has an initial linear slope, but exhibits curvature at higher radiation doses, reflecting a quadratic relationship between dose and surviving fraction. This characteristic cell survival curve, shown in Figure 1.1, illustrates the linear quadratic (LQ) model, which has become the cornerstone of radiobiological modelling to predict cellular survival following exposure to a given dose of IR. (Hall, 1973) Whilst a number of models have been proposed to predict radiobiological response, the LQ model is the most robustly validated by both experimental and clinical data. (van Leeuwen et al., 2018) It is used clinically to account for missed treatments and to compare different dose/fractionation regimes, and several extensions to the basic model have been suggested, to compensate for factors of incomplete DNA repair (Dale, 1985) and tumour repopulation. (Dale, 1989)

The linear quadratic model has been derived to describe experimental cell survival data, in which the coefficients α and β relate dose to surviving fraction. Although the parameters α and β have no mechanistic basis, attempts have been made to link them with biological processes, including DNA damage repair. (Goodhead, 1994, Chapman, 2003, Chapman et al., 1999) A lack of dose rate dependence for α inactivation suggests that this coefficient may represent

irreparable damage, leading to instant cell death. Conversely, β does seem to be affected by a change in dose-rate, suggesting time as a factor and leading to this parameter being linked to the accumulation of repairable damage eventually causing death. (Chapman, 2003)

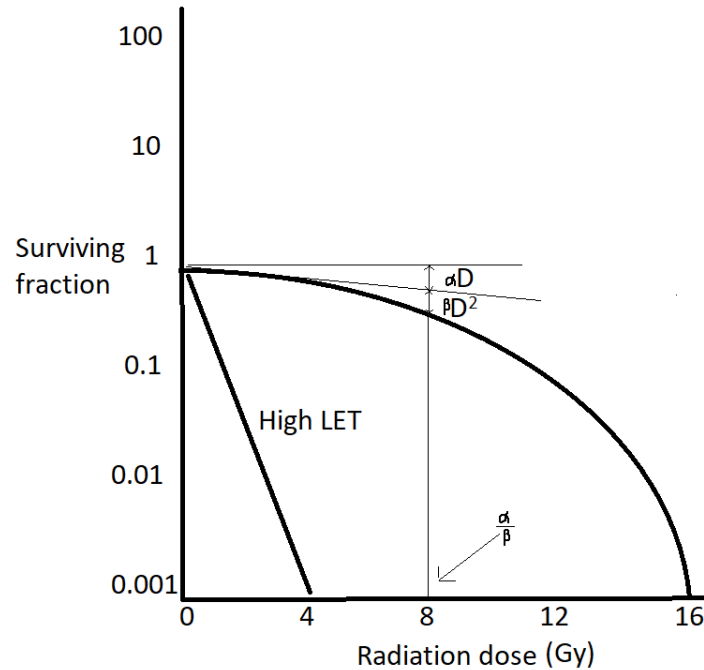


Figure 1.1 Cell survival curves for densely and sparsely ionising radiation, illustrating the linear quadratic model. Adapted from Joiner and van der Kogel. (Joiner and van der Kogel, 2009)

The linear quadratic model of cell killing can be expressed as:

$$SF = \frac{N_s}{N_0} = \exp\{-\alpha d - \beta d^2\}$$

where N_0 is the initial number of clonogens, N_s is the mean number of surviving clonogens after a radiation dose (d) and SF is the surviving fraction. (Nahum, 2015)

The ratio of α to β provides a convenient way of expressing the shape of the survival curve in a single parameter and the shape of the survival curve, specifically, its shoulder or 'bendiness', determines the effect of dose fractionation.

1.4.4 The rationale of dose fractionation

When given with curative intent, external beam radiotherapy is almost always delivered in a large number of small fractions, usually of the order of 2Gy. The rationale for this practice can initially seem confusing, since radiobiologically, a given dose of IR is almost always less effective at cell killing if given in divided doses compared to one single exposure. (Chapman, 2003) Nevertheless, radiotherapy dose fractionation is biologically advantageous to normal tissue over tumour, due to subtle differences between them, as defined by the 5R's of radiobiology: repopulation, re-distribution, re-oxygenation, radiosensitivity and repair. (Withers, 1975, Steel and Peacock, 1989) In order to be effective, a radiotherapy regime should deliver a sufficient dose per fraction to ensure that more tumour cells are killed per day than are added in the process of repopulation. Cells which are undergoing mitosis (tumour cells and rapidly proliferating normal tissues) will be preferentially killed, allowing other cells time to redistribute into a radiosensitive part of the cell cycle prior to the next dose. Tumours are usually more hypoxic than normal tissue and cell killing in oxygenated parts of the tumour may, over time, result in improved perfusion of hypoxic areas, thereby increasing radiosensitivity by re-oxygenation. Repair of sublethal radiation damage between fractions occurs in both tumour and in normal tissue and although fractionation reduces the amount of tumour kill, it permits the restoration of late normal tissues. (Chapman, 2014)

Of these radiobiological concepts, it is repair of sublethal DNA damage which is the most important factor in the success of dose fractionation. The biological advantage conveyed to late normal tissues over tumour can be explained by the

differences in the shape of their relative cell survival curves (and therefore α/β ratios).

The α/β ratio varies between normal tissue effects and clonogen kill for most tumours. Classically, it has been taught that tumours and rapidly proliferating normal tissues (e.g. gastric mucosa) have 'high' α/β ratios, in the order of 8Gy-10Gy (with a linear cell survival curve), whereas well differentiated normal tissue effects have 'lower' α/β ratios of between 1Gy and 3Gy (displaying a broad shoulder on the cell survival curve).

When exposed to low doses of radiation, late normal tissues are more proficient at repairing DNA damage than cancer cells. Therefore, within this part of the cell survival curve exists a window of opportunity for selectively killing greater numbers of tumour cells than normal tissue. This therapeutic benefit is illustrated in Figure 1.2.

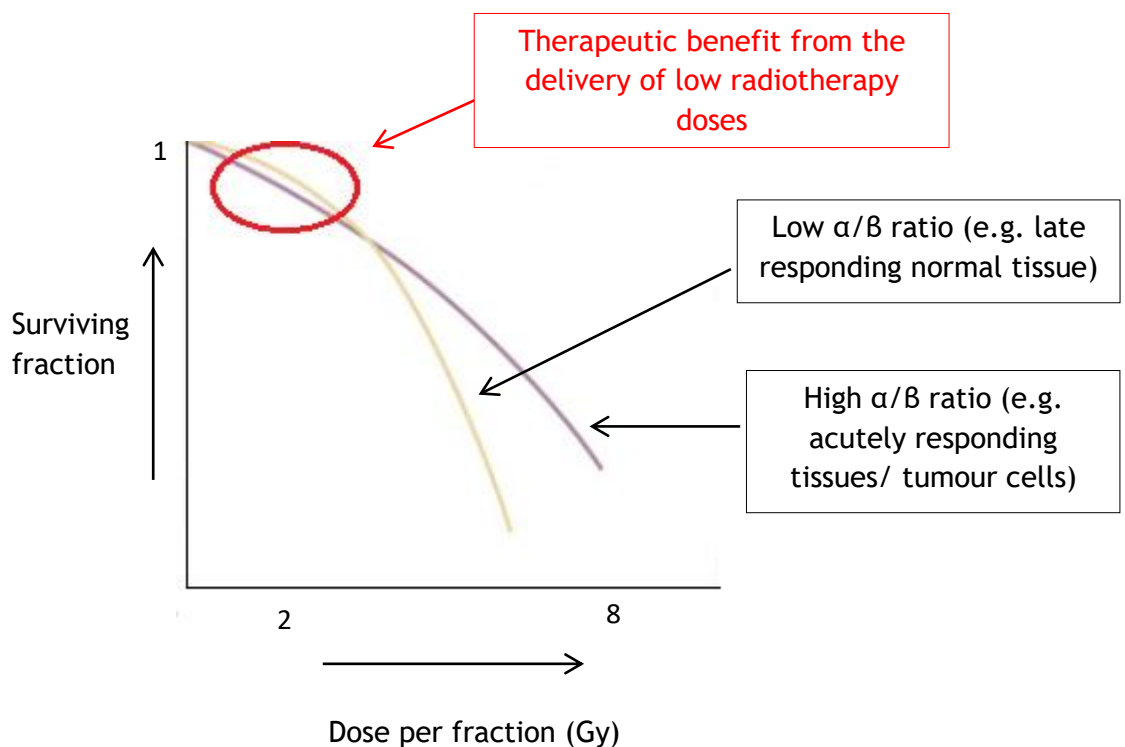


Figure 1.2 Cell survival curves for late-responding normal tissue and tumour effects associated with low and high α/β ratios, respectively

When radiotherapy is delivered in a large number of small fractions, the initial linear part of the cell survival curve is repeated as the total dose accumulates. This leads to a straightening of the curves for both tumour and late normal tissue effects, but the sparing effect is much greater in tissues with a high β value (low α/β ratio) than in those with a low β (high α/β ratio). If the time between dose delivery is sufficient, fractionation allows for almost complete repair to occur in late normal tissues, thereby negating the influence of β . In this manner, tissues with a greater shoulder on their survival curve are preferentially spared over tissues that typically have straighter curves. This important radiobiological phenomenon is illustrated in Figure 1.3 and is the fundamental basis for dose fractionation and the sparing of late normal tissue toxicity.

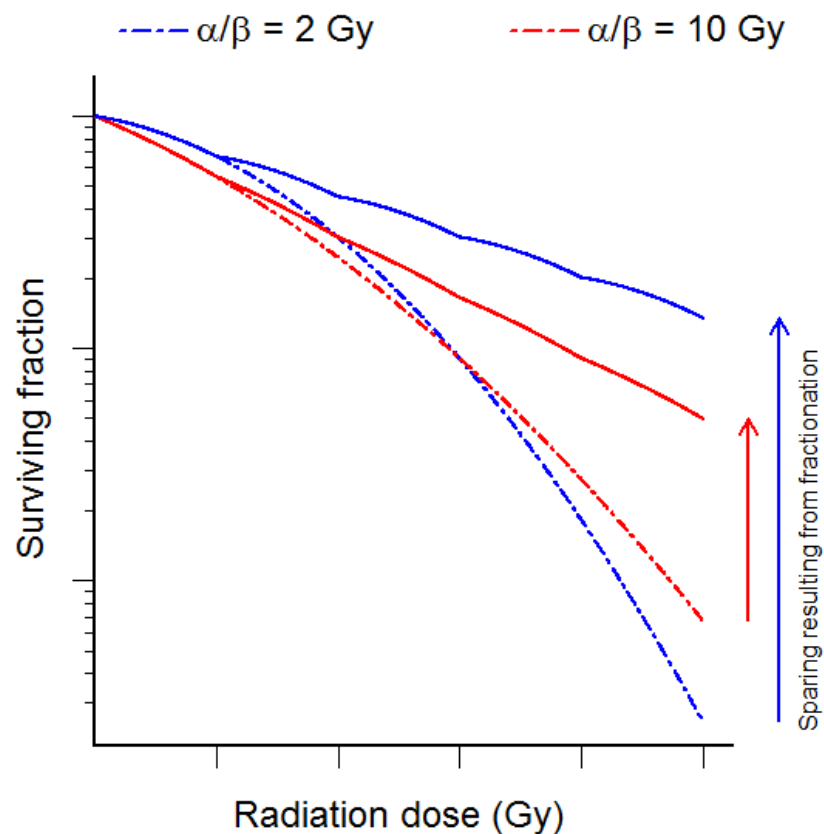


Figure 1.3 Fractionation-associated straightening of the survival curves, illustrating the radiobiological basis of improved therapeutic ratio achieved with fractionated radiotherapy

Despite the firmly held concept that all tumours exhibit a generically high α/β ratio, recent data suggests that α/β ratios of two common tumour types (breast and prostate) may be significantly lower than originally assumed. (Yarnold et al., 2011, Miralbell et al., 2012) Furthermore, work by Chapman *et al* which summarised the *in vitro* and *in vivo* radiosensitivity of a number of human tumour cell lines demonstrates that the α/β ratios are mostly lower than the generic value of 10Gy. (Chapman, 2014) Clinically, this is extremely relevant, since the α/β ratio is used to predict tissue sensitivity to a change in the delivered dose per fraction. Therefore, whilst fractionating the prescribed dose spares late normal tissue toxicity, if the tumour has a low α/β ratio then it is also spared to a similar extent, negating much of the advantage of fractionation. In this situation, the optimal therapeutic ratio is likely achieved from hypofractionated dose delivery since this would maximise tumour kill. There is currently a paucity of data on which to estimate the α/β ratio of MPM, although the slow growth and mesenchymal origin of this tumour suggests that the α/β ratio may be low therefore that hypofractionated radiotherapy may be more efficacious in this malignancy.

1.4.5 The application of hypofractionation

The first radiotherapy regimes used soon after the discovery of x-rays in 1895 were hypofractionated (i.e. delivered $>2\text{Gy}/\text{fraction}$). Although techniques were fairly crude and dose deposition in-homogenous, hypofractionated regimes were employed during surgical interventions and in the treatment of skin cancer. (Williams, 1901, Forssell, 1910) Treatment over a short timeframe was convenient for the patient and afforded the radiobiological advantage of a reduced overall treatment time, which could often produce dramatic tumour responses. Nevertheless, the appearance of late normal tissue toxicity meant that hypofractionation was abandoned for curative regimes and reserved for palliation.

The successful and safe application of large doses of radiotherapy in a single fraction during neurosurgery was pioneered in the 1950s by Lars Leksell. His work, subsequently termed stereotactic radiosurgery, identified that damage to

normal tissue and therefore late toxicity, could be minimised if the areas receiving a large dose were of small volume or noneloquent. (Leksell, 1951) Likewise, the intraoperative delivery of 1 or 2 hypofractionated doses of radiotherapy safely continued during the 1960s under the same premise, i.e. that late effects could be avoided if radiosensitive structures could be physically moved out of the radiotherapy beam or that only very small volumes of nearby critical structures were irradiated. (Timmerman, 2008)

As discussed in section 1.3, recent advances in radiotherapy planning and delivery have facilitated our ability to conform radiotherapy beams to the target lesion more precisely, permitting much steeper margins of dose fall-off than traditional techniques can offer. Not only has this facilitated dose escalation of conventionally fractionated regimes, but it has presented a mechanism through which hypofractionated treatments, such as stereotactic ablative radiotherapy (SABR) could be safely delivered. Initially used to treat lung cancer, this technique can deliver ablative, hypofractionated regimes (in the order of 11Gy per fraction) without incurring an unacceptable late toxicity profile because the volume of critical tissue treated is a very small proportion of the total tissue volume (usually $<1\text{cm}^3$ for lung cancer with minimal margins). Patient set-up is very precise to avoid a geographical miss in the precarious moving lung and the application of sophisticated delivery regimes permit rapid dose fall-off beyond the target volume. The success of this approach in lung cancer has led to its use for other primary cancer sites and in oligometastatic disease.

In addition to treating tumours with high α/β ratios, through careful management of normal tissue volume effects, hypofractionated radiotherapy has now become the standard of care in breast and prostate cancer. Radiobiological data estimate that prostate cancer has an α/β ratio of 1.4Gy to 1.9Gy, (Brenner et al., 2002, Fowler et al., 2001) which is lower than the estimated α/β ratio of 3Gy for late normal bowel effects. (Thames et al., 1990) In this situation, hypofractionation of dose could potentially improve tumour control, without disproportionately increasing side effects. This hypothesis was tested in the conventional or hypofractionated high dose intensity modulated radiotherapy for

prostate cancer (CHHIP) trial. (Dearnaley et al., 2016) This randomised controlled phase III trial compared conventional radiotherapy (74Gy delivered in 37 fractions over 7.4 weeks) with one of two hypofractionated schedules (60Gy in 20 fractions over 4 weeks or 57Gy in 19 fractions over 3.8 weeks). Data suggested that the hypofractionated regime utilising 3Gy per fraction to a total dose of 60Gy was equally effective as the conventional 2Gy per fraction regime, with no clinically apparent increase in toxicity. This suggests that in tumours with a low α/β ratio, where the rationale for dose fractionation is lost, hypofractionated radiotherapy can improve the therapeutic ratio, safely improving the probability of disease control with a lower total dose of radiation than is required for conventional fractionation. This study has now defined the standard of care in localised prostate cancer.

1.4.6 Radiobiological modelling

Fundamental to the prediction of the likely clinical outcome of a given radiation regime is the accurate determination of the radiobiological parameters of the LQ model, α , β and so α/β ratio. These values are most commonly established through clonogenic survival assays using cancer cell lines, which will be discussed in sections 1.5 and 6.1.

Following the generation of reliable radiobiological data, a number of approaches are used to predict radiotherapy response and to guide optimal dose and fractionation schedules. Classically, the concept of a biologically equivalent dose (BED) is used in the clinical setting to illustrate the dependence of the therapeutic ratio on the number of fractions. If delivered in an infinite number of tiny fractions, a total dose equivalent to the BED would be radiobiologically equal to the dose/fractionation regime in question. (Nahum, 2015) BED for late normal tissue effects is typically calculated assuming α/β ratio of 3Gy and for early responding normal tissue and tumour effects with an α/β of 10Gy. Conventionally fractionated radical schedules usually have a BED for late effects of between 100 Gy_3 and 117 Gy_3 and between 72 Gy_{10} and 84 Gy_{10} for tumour effects. (Fowler, 1992) As the number of fractions increases, the $\text{BED}_{\alpha/\beta=3}$ decreases steadily, so the highest therapeutic ratio is obtained at the smallest

fraction sizes. (Nahum, 2015) Our understanding of the likely effects of a change in dose/fractionation schedule can also be facilitated by the concept of relative effectiveness, which is used to express the radiobiological impact of any schedule in terms of a number of 2Gy fractions. (Yaes et al., 1991) Although BED continues to be a valid and useful tool, the analysis has to assume a single uniform dose per structure, which isn't a realistic reflection of radiotherapy delivery in current practice.

More recently, a greater appreciation of volume effects for late normal tissue complications have permitted the development of macroscopic models of radiobiological modelling, which are beginning to supersede traditional methods. Tumour control probability (TCP) and normal tissue complication probability (NTCP) models are advantageous in that they can account for heterogeneous dose distributions throughout the tumour and normal tissue as well as their volume effects. Using these methods, we can simulate the effect in both the tumour and normal tissue of changing the number of fractions in a given regime. (Nahum, 2015)

These models eloquently demonstrate the influence of fractionation on therapeutic ratio. Plotting the TCP of target volumes exhibiting different α/β ratios over a range of fraction numbers illustrates how, for a fixed NTCP, the therapeutic ratio will depend on fraction number. This is shown in Figure 1.4, where the complication of rectal bleeding (α/β ratio = 3Gy) is modelled. For a tumour clonogen displaying an α/β ratio of 10Gy, treating with a high number of fractions clearly results in an enhanced therapeutic ratio. As the α/β ratio of the tumour is reduced however, the benefit of increased fraction number declines, and where the α/β ratio of the tumour clonogens is equivalent to the α/β ratio of the modelled complication (i.e. 3Gy), the dependence on fractionation is completely lost. When the tumour α/β ratio is reduced to below that of the critical tissue complication, the effect of fractionation is reversed, with the greatest therapeutic ratio being achieved with a single fraction.

Although the optimal dose and fraction size for hypofractionated regimes will eventually be established through the outcomes achieved in clinical trials employing hypofractionated radiotherapy regimes, such as SYSTEMS-2, TCP/NTCP models are advantageous in guiding the protocols for such studies.

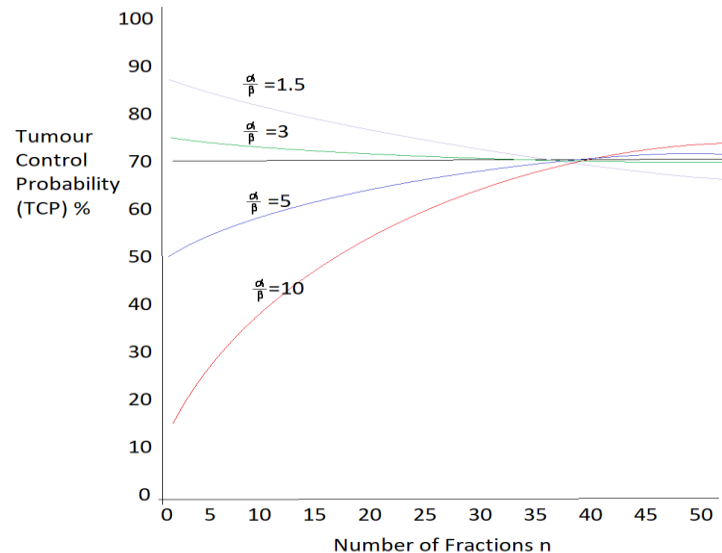


Figure 1.4 Tumour control probability (TCP) for target volumes exhibiting different α/β ratios, receiving a homogenous dose over 1-50 fractions

All curves are isotoxic for the same normal tissue late complication of rectal bleeding (4.3%), for which α/β ratio of 3Gy has been applied. (No account has been taken of re-oxygenation between fractions and clonogen proliferation assumed to be negligible). Adapted from: Nahum AE. The radiobiology of hypofractionation. (Nahum, 2015)

1.5 *In vitro* studies of MPM

1.5.1 *In vitro* tumour models

The ability to study cancer using *in vitro* models has advanced our understanding of specific tumour biology, as well as aiding the selection and development of the most efficacious anticancer strategies to employ. A chronic lack of investment in mesothelioma research, however, has meant that this disease has not been studied as intensively as many other types of cancer. Although the link with asbestos exposure is well established (Yates et al., 1997, McElvenny et al., 2005), there is an ongoing hiatus in our understanding of the basic biology of this disease and how it can be effectively treated. This is illustrated by the fact that

first line chemotherapy option carries with it a survival benefit of just 3 months (Vogelzang et al., 2003) and further reflected in the dismal prognosis of 9-12 months. (Beckett et al., 2015) There is a desperate need for the development of relevant pre-clinical models of MPM, with which to explore basic tumour biology and facilitate the development of novel therapeutic interventions.

1.5.2 Cell lines

Immortal cell lines are frequently used to study tumour characteristics in place of primary cells. The advantages of this approach include cost effectiveness, ease of attainment and the ability to bypass ethical considerations associated with use of human tissue. Furthermore, many cell lines exist as a relatively homogenous population, which can provide a consistent sample and reproducible behaviour. (Kaur and Dufour, 2012) Primary cells are also difficult to maintain in culture or to store successfully, as has been the experience of our own laboratory with primary MPM cells and lends further weight to the case for utilising cell lines in the research of this disease. Despite the benefits of using established cell lines, the genetic manipulation often required for their creation, in addition to the genetic drift associated with sequential passaging has led to controversy surrounding the extent to which they reflect the phenotype and behavioural characteristics of the original tumour. (Kaur and Dufour, 2012) Furthermore, contamination with *Mycoplasma* or other cell lines has been demonstrated to be a substantial problem surrounding the integrity of cell lines in the past, (Nelson-Rees et al., 1981) necessitating regular monitoring with cell line authentication and *Mycoplasma* testing.

1.5.3 *In vitro* 3D Spheroid Models

Traditional *in vitro* models consist of cell lines grown as 2D monolayers. (Zanoni et al., 2016) Although this approach has many advantages, the use of 3D *in vitro* models has recently become an attractive alternative to 2D systems for a number of reasons. Firstly, a 3D tumour model is able to mimic more closely the complexities of cellular organisation, architecture and cell to cell communication seen in clinical tumours. It is this structure and cell to cell

interaction that is thought to be in part responsible for the increased resistance of cancer cells cultured as spheroids to anticancer therapies compared to their 2D counterparts. (Kobayashi et al., 1993) This property, which may contribute to the chemo and radioresistance of solid tumours, is known as 'multicellular resistance' (Desoize and Jardillier, 2000) and suggests that a 3D spheroid system would provide a more clinically-relevant model for studies of radioresistance or drug screening than a 2D system. (Thoma et al., 2014) Mesothelioma cells have been demonstrated to display enhanced resistance to chemo and radiotherapy when they are grown as multi-cellular spheroids rather than in monolayer culture, which matches the resistance to therapies observed in the clinic. (Barbone et al., 2008)

In addition to multicellular resistance, 3D spheroid models can adequately represent other inherent properties of solid tumours, which can affect treatment outcomes, such as hypoxia (Wartenberg et al., 2003), sub lethal damage (SLD) repair (Dubessy et al., 2000) and the presence of chemical gradients (oxygen, nutrients, catabolites). (Zanoni et al., 2016) Low penetration into solid tumours may limit drug efficacy, which can also be better modelled by spheroid systems (Minchinton and Tannock, 2006) and a dynamic response can be monitored in terms of spheroid growth or shrinkage. Furthermore, large spheroids (diameter exceeding 500µm) exhibit the spatial heterogeneity often seen in solid tumours, with peripheral proliferative cells, an internal quiescent zone with limited oxygen availability and a necrotic core. (Mueller-Klieser, 1987, Vinci et al., 2012) For studies of radiosensitivity, a hypoxic environment is particularly relevant, in light of the oxygen fixation hypothesis. This hypothesis states that DNA damage caused by radiation in the presence of oxygen is more difficult to repair, leading to increased cytotoxicity in oxygenated cells. (Gray et al., 1953) Oxygen therefore acts as a radiosensitiser, increasing the lethality of any given dose of radiation. Conversely, hypoxia renders IR less effective at cell killing and contributes to the radioresistance exhibited by many solid tumours. Cancer cells cultured in parallel in 2D and 3D conditions frequently exhibit different gene expression profiles, with 3D culture more closely aligning with the clinical specimens. (Kim et al., 2012, Sakai et al., 2010) Furthermore, analysis of the gene expression profile of spheroids has identified tumour-relevant genes

associated with survival. (Ernst et al., 2009) The use of *in vitro* 3D tumour models is now commonplace and this valuable resource appears to be bridging the gap between conventional *in vitro* 2D systems and animal models. (Yamada and Cukierman, 2007)

There are many general 3D culture systems, but two of the commonly used 3D *in vitro* tumour spheroid models are multicellular spheroids and tumour fragment spheroids. Multicellular spheroids are generated from cell lines that have been allowed to grow into 3D structures. (Mueller-Klieser, 1997) Whilst they are particularly useful for studying resistance to radiotherapy (Santini et al., 1999), they remain a highly artificial model, generated from selected clonal subpopulations, which lacks the complexity of the primary tumour and its associated microenvironment. (Kim et al., 2005) Tumour fragment spheroids by contrast, are small pieces of the original tumour, cultivated to form a 3D structure. This model is more representative of the original tumour, the heterogeneity of which is preserved with the expression of the actual (rather than selected) tumour cells, non-malignant tumour-associated cells and the tumour extracellular matrix. The interaction between these cell types is known to be important in determining the growth, migration and differentiation of tumour cells as well as survival and resistance to apoptosis. (Chrenek et al., 2001, Fracasso and Colombatti, 2000)

Within this thesis, 3D spheroid models will be used to study not only the radiosensitivity of MPM cell lines, but also to investigate the impact of various radiosensitisers on MPM response to single dose and fractionated IR. These radiosensitisers target important pathways that determine cell survival after exposure to IR, including apoptosis and DNA damage repair.

1.5.4 Studies of radiosensitivity

1.5.4.1 2D techniques

Radiosensitivity measures generated from a clonogenic survival assay include the survival fraction after delivery of 2Gy of IR (SF2Gy), in addition to the individual values of α and β . Mean inactivation dose (MID) is commonly quoted as a measure of radiosensitivity in human cell lines. This approach has several advantages over other parameters in that it is representative of the whole cell population and minimises variation in survival data of a given cell line quoted by different authors, (Fertil et al., 1984) a phenomenon which has been observed in a number of established cancer cell lines. (Brock et al., 1990, Kelland and Bingle, 1988, Rofstad et al., 1987) The concept of MID was first introduced by Kellerer and Hug (Kellerer and Hug, 1972) and its application is based on the assumption that the survival curve is regarded as a probability distribution of dose. More accurately: 'the survival probability $s(D)$ can be considered as an integral probability distribution; this is so because $s(D)$ is the probability that a dose larger than D is necessary to inactivate a cell which has been randomly selected from the population'; where s =surviving fraction and D =dose. (Kellerer and Hug, 1972) The differential probability distribution $s(D)$ can be characterised by its average dose, the 'mean inactivation dose'. (Fertil et al., 1984)

Despite the well-established role of the clonogenic assay in radiobiology, this technique is laborious and time consuming and the advance of automated cell survival assays has allowed the rapid assessment of cell viability in microtitre plates following exposure to drugs or IR. The MTT assay, for example, detects the enzymatic reduction of 3-(4,5-dimethylthiazole-2-yl) -2,5-diphenyltetrazolium bromide (MTT) to MTT-formazan, in the presence of mitochondrial respiration. The reaction produces a colour change which can be easily detected from cell monolayers and used to produce dose response curves from which SF2Gy and other measures of radiosensitivity can be determined. A similar approach is taken with the fluorescence based assay, using the DNA specific dye Hoechst 33258 to determine the number of viable cells per well. (Begg and Mooren, 1989) Whilst these assays may be more rapid, they are less

robust than a clonogenic approach, since they cannot distinguish between viable but sterilized cells and true surviving cells.

1.5.4.2 3D techniques

Common to both the clonogenic and cell viability assays is the requirement for cells to be grown as monolayers prior to irradiation. The advantages of 3D culture systems in representing tumour behaviour and complexity has been discussed in section 1.5.3, and several studies have shown that cells grown in 3D better model the clinical response to drugs and radiation. (Gomez-Roman et al., 2017, Hehlhans et al., 2008, Zschenker et al., 2012) A number of studies assessing the impact of IR alone have used 3D spheroid models. Culture of neuroblastoma (Wheldon et al., 1985, Deacon et al., 1985) and melanoma cells (Rofstad et al., 1986) as multicellular tumour spheroids demonstrated a good correlation of the behaviour of both cell types to the original clinical tumour following single doses of IR. Furthermore, Schwachofer *et al* demonstrated that following single doses of IR, parameters of growth delay and cell survival analysis could be used to determine the relative radiosensitivity of five different human tumour cell lines grown as multi-cellular tumour spheroids and that these sensitivities paralleled the behaviour of the original tumour. (Schwachofer et al., 1989) Spheroids have also been used to study brachytherapy regimes (Fritz et al., 1996) and dose fractionation, where they have been found to be superior to monolayers in assessing hypofractionated protocols in glioblastoma cells. (Kaaijk et al., 1997) Their role in assessing response to multi-fractionation radiation schedules has been reported by Sham *et al* (1988), where cellular growth kinetics and repopulation rates of irradiated spheroids were determined by flow cytometry. Results importantly highlighted that tumour repopulation began earlier during the fractionation regime than had been assumed from clinical data and the authors concluded that spheroid models are a valuable tool in the evaluation of fractionation regimes, yielding results which are closer to the clinical picture than observed with monolayers. (Sham and Durand, 1998)

Despite the improved representation of clinical tumours, determining parameters of radiosensitivity from 3D systems may be more difficult than in 2D

experiments. Nevertheless, suggested techniques have been published (Stuschke et al., 1995) and approaches used to determine α/β ratio from *in vivo* models provide useful guidance. (Stewart et al., 1984, Douglas and Fowler, 1976)

1.5.4.3 *In vivo techniques*

Mouse models are essential tools in cancer research, advancing understanding of basic tumour biology and allowing the assessment of responses to anti cancer therapies. Furthermore, the study of radiobiology has greatly benefitted from the use of animal models, pioneered by work by Regaud and Nogier in 1911, in which the ability of fractionation to spare normal tissues was investigated in rams. (Regaud, 1911) The outcome from this work formed the biological basis of fractionation, which has subsequently guided radiotherapy delivery. Recent developments in small animal irradiators have significantly improved techniques for studying radioresponse, allowing more advanced radiotherapy delivery to be studied in the laboratory.

While *in vivo* models are useful for studying objective cancer responses and normal tissue toxicity to radiotherapy, the ability to extrapolate accurate radiobiological parameters in this setting is more difficult than in the traditional clonogenic assay. Derivation of such data assumes that endpoints such as tumour control or normal tissue response are driven by cell death, and the magnitude of effect is directly related to the fraction of surviving target cells. (Butterworth, 2019) Accurate application of the LQ model from *in vivo* endpoints is therefore challenging, since the proportion of surviving cells is difficult to determine.

This issue was noted in a review of the literature conducted by van Leeuwen *et al* in 2018. This work provides a summary of α and β parameters derived from clinical radiotherapy studies of a number of different tumours, although no data were provided for MPM. (van Leeuwen et al., 2018) Investigated outcomes included local and local regional tumour control, patient survival and biochemical data. A combination of radiobiological approaches were used to generate measures of α and β , including the standard LQ model in addition to

versions modified to consider repair and repopulation. In studies not quoting individual values for α and β , α/β ratio was often estimated based on iso-effective treatment schedules. (van Leeuwen et al., 2018) Considerable variation was noted in reported α/β ratios for the same tumour type, attributed to inter-study heterogeneity rather than expected statistical uncertainty. Discrepancies were attributed to differences in patient populations and radiotherapy techniques, in addition to the models used to predict response and calculate the α/β ratio. This work highlights the importance of considering underlying assumptions when applying radiobiological models as well as the inherent difficulties of quantifying radiation response in the clinical or *in vivo* setting. (McMahon, 2018)

Despite these difficulties, a seminal paper investigating radioresponse *in vivo* was published by Stewart *et al* in 1984. In this study, a mouse model was used to determine the repair capacity of kidneys exposed to hyperfractionated radiotherapy and subsequently used to establish the α/β ratio of murine renal tissue. Radiation schedules employed 1 to 64 fractions, using 240kVp X-rays, delivering a dose of between 0.9Gy and 16Gy per fraction. The treatment time was limited to three weeks to ensure that there was limited cell proliferation during treatment, and a minimum of five hours was left between fractions, a delay which had previously been shown to provide adequate time for SLD repair in irradiated mouse skin. (Douglas and Fowler, 1976) Three non-destructive, functional endpoints (isotope clearance, urine output and haematocrit) were assessed 19 to 48 weeks post irradiation and used to generate steep dose effect curves. Isoeffective doses between the differing radiation schedules could be estimated by determining equivalent levels of damage inflicted by each regime. Using this information, 'equivalent single dose' response curves for an isoeffect could be constructed, in which the 100% effect is attributed to that achieved by a single dose, the 50% effect is the dose per fraction given in two equal fractions and the 25% effect is the dose per fraction given in four fractions. Plotting data in this manner generated a continuously bending curve, which fitted the LQ model. It has been suggested that data expressed in this fashion may be considered 'quasi-survival' if the assumption is made that the endpoint is the direct result of cell death and that each fraction contributes equally to total cell

kill. (Hornsey, 1970, Fowler, 1983) Nevertheless, Fowler *et al* state that it is more accurate to consider these curves as dose effect curves for function rather than cell survival, unless a direct link between clonogenic survival and function has been confirmed. (Fowler, 1983)

While dose effect curves illustrate the effect of radiation dose fractionation and allow isoeffective dose levels to be established, they cannot be used to determine absolute radiosensitivity. This is because the surviving fraction of cells corresponding to the measured effect (e.g. spheroid volume) is unknown. (Stewart et al., 1984) Nevertheless, by using the ' F_e ' technique, described by Douglas and Fowler, such data can be used to establish the dose at which α and β components of cell kill become equally effective. (Douglas and Fowler, 1976) For data which conform to the LQ equation, plotting the reciprocal of the total isoeffective dose (F_e) against the corresponding dose per fraction exhibits a linear relationship, with gradient proportional to the value of β and y-intercept corresponding to the value of α . (Douglas and Fowler, 1976)

1.6 Apoptosis

1.6.1 Background

Cells that are experiencing extensive stress, for example, that following damage induced by IR, often activate pathways of cell death, including the apoptotic pathway. Apoptosis is the carefully controlled process of programmed cell death, characterised by distinct morphological cellular changes and energy dependent biochemical mechanisms. It is crucial in maintaining the homeostatic balance of cell populations in tissues and is responsible for the healthy functioning of a number of processes, including normal cell turnover, embryonic development and immune regulation and function. (Elmore, 2007) Disruption of the pathways that control apoptosis can lead to various disease states. Excessive activation can cause autoimmune and neurodegenerative conditions, whereas apoptotic resistance is considered to be a critical step in the development of cancer (Hanahan and Weinberg, 2000) and may underpin the mechanism by

which some tumours are resistant to chemo and radiotherapy. (Johnstone et al., 2002)

Initiation of apoptosis results in the activation of a complex and coordinated series of cysteine proteases, known as caspases, leading to the final demise of the cell. (Elmore, 2007) The stimuli that initiate apoptosis are varied, but there are two principal mechanisms through which apoptosis can be triggered: the extrinsic pathway and the intrinsic pathway. The extrinsic pathway involves interaction between extracellular ligands and their transmembrane receptors to produce an intracellular cascade of events leading to the activation of caspase 8 and ultimately cell death. A full review of this pathway can be found in 'Apoptosis: a review of programmed cell death' by Susan Elmore, (Elmore, 2007) but will not be considered further here.

1.6.2 The intrinsic pathway

The intrinsic pathway is a non-receptor driven pathway of apoptosis in which mitochondria are of central importance. Intracellular signals are generated which act on targets to affect apoptosis. Signals such as DNA damage result from exposure to cellular stresses (toxins, IR, viruses and free radicals) and promote apoptosis. (Elmore, 2007) Loss of cell survival proteins, such as hormones or growth factors, result in a lack of apoptotic suppression and tips the cell towards death. However the stimulus is generated, the intrinsic pathway is initiated as a result of mitochondrial outer membrane permeabilisation (MOMP). In this process, the formation of pores in the mitochondrial outer membrane release proapoptotic proteins from the mitochondrial intermembrane space into the cytosol. (Saelens et al., 2004) These include Cytochrome C, Smac/DIABLO and HtrA2/omi. Cytochrome C binds to the adaptor protein (APAF1) and procaspase 9, forming an apoptosome which activates caspase 9 by proteolytic cleavage. (Hill et al., 2004, Chinnaiyan, 1999) Smac/DIABLO and HtrA2/omi antagonise the inhibitor of apoptosis family of proteins (IAP), which inhibit the function of activated caspases. Inhibition of IAPs liberates active caspases to drive the cell towards death. (van Loo et al., 2002)

1.6.3 The Bcl-2 family

Critical to the control and regulation of the mitochondrial pathway of apoptosis, is the B cell lymphoma protein 2 (Bcl-2) family of proteins. This family of structurally related proteins consists of both promoters and inhibitors of apoptosis, which interact to create a delicate intracellular equilibrium, the balance of which will ultimately determine whether a cell will undergo apoptosis. (Cory and Adams, 2002) More than 25 members of the Bcl-2 family have been identified to date, characterised by the presence of a conserved sequence, known as the Bcl-2 homology (BH) domain. Those proteins acting as apoptotic inhibitors share all 4 BH domains and include Bcl-2, Bcl-xL, Bcl-W, A1/BFL-1 and Mcl-1. Pro-apoptotic family members express either BH1-3 domains or BH3 only and are classified as either 'activator', 'effector' or 'sensitiser' proteins. Activator BH3-only proteins (Bid, Bim, Puma) bind to the effector proteins (Bax and Bak) which, once activated, oligomerise in the mitochondrial outer membrane to produce pores, leading to MOMP. Anti-apoptotic proteins can bind directly to the BH3 motifs of activator proteins, inhibiting their function and promoting cell survival. The sensitiser BH3-only pro-apoptotic subset (Bad, Bik, HRK) do not directly activate effector proteins, but compete with activators binding with anti-apoptotic proteins, thereby releasing the brake exerted on the pro-death signal. (Chipuk et al., 2010, Czabotar et al., 2014, Letai, 2008) The role of Bcl-2 proteins in the regulation of apoptosis is illustrated in Figure 1.5.

The expression of the Bcl-2 family of proteins is in turn carefully regulated by the tumour suppressor gene *TP53*. (Schuler and Green, 2001) The product of the *TP53* gene, p53, is critical for regulating the cell cycle and maintaining the integrity of the genome. On the detection of DNA damage, genomic repair proteins are activated and cell cycle arrest is induced, allowing time for DNA repair to occur. If the damage is too extensive to be repaired, p53 induces apoptosis by a number of mechanisms, including interaction with the Bcl-2 family. (Pietenpol and Stewart, 2002) Although the exact mechanism of this interaction is not fully understood, data suggest that p53 may promote Bcl-2 phosphorylation and inactivation via Cdc42. (Thomas et al., 2000) Further data suggest that p53 related manipulation of the pro-apoptotic proteins PUMA and

Noxa may also contribute to release of Cytochrome C from the mitochondria, pushing the damaged cell into apoptosis. (Oda et al., 2000, Nakano and Vousden, 2001)

1.6.4 The final common pathway of apoptosis

Both the extrinsic and intrinsic pathway of apoptosis converge on a final common apoptotic pathway, involving the executioner caspases, caspase 3, 6 and 7. Activation of these proteases leads to the degradation of nuclear and cytoskeletal proteins, resulting in the morphological and biochemical changes that are characteristic of apoptosis. (Slee et al., 2001) Of the effector caspases, caspase 3 is critical and can be activated by any of the initiator caspases (8, 9 or 10). Active caspase 3 cleaves and inactivates the CAD (Caspase-Activated-DNase) inhibitor. CAD is an endonuclease which in its active form degrades chromosomal DNA and causes chromatin condensation. (Sakahira et al., 1998) Activated caspase 3 also causes the reorganisation of the cytoskeleton and promotes cell disintegration into apoptotic bodies. Expression of phosphatidylserine on apoptotic bodies leads to early phagocytic recognition and efficient uptake without the release of any intracellular material; thereby ensuring that apoptosis is a non-immunogenic process. (Fadok et al., 2001) An illustration of the mechanisms involved in the apoptotic pathway are shown in Figure 1.5.

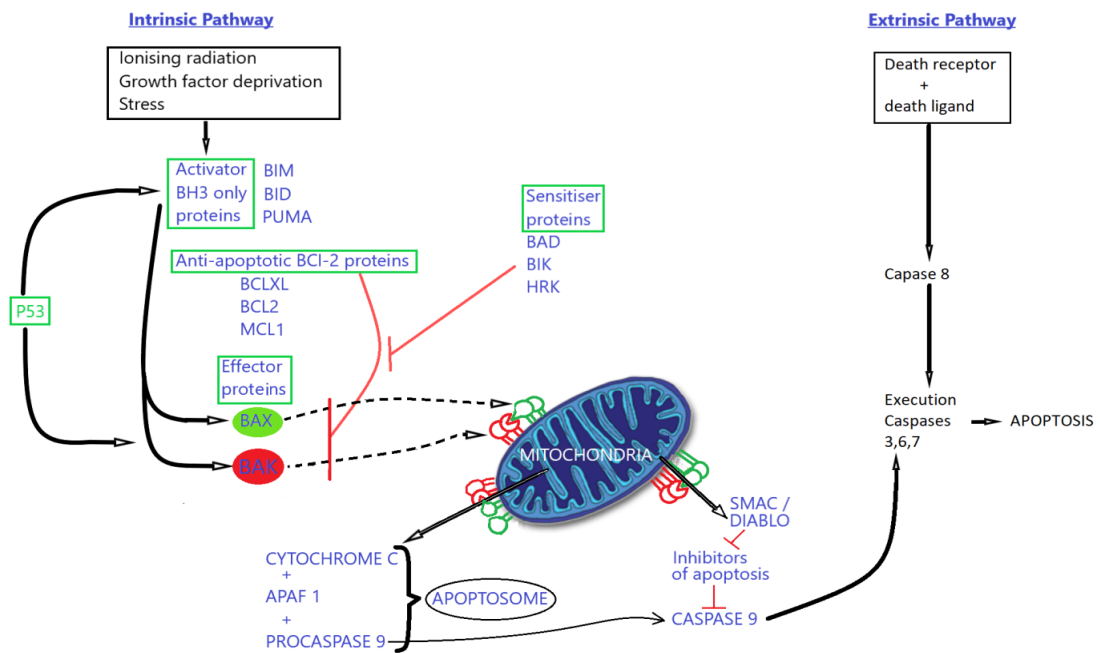


Figure 1.5 A schematic outlining the apoptotic pathway

The induction of MOMP is the pivotal event which drives the intrinsic apoptotic pathway. This process is carefully regulated by the interaction of the Bcl-2 family of proteins following cellular stress. Following the induction of MOMP, pro-apoptotic proteins are released into the cytoplasm and drive a sequence of caspase activation which pushes the cell towards the final common pathway of apoptosis. This final common pathway critically utilises caspase 3 to induce the morphological and biochemical changes that are characteristic of apoptosis.

1.6.5 Mesothelioma and apoptosis

Mesothelioma is highly resistant to the activation of apoptosis, (Fennell and Rudd, 2004, Narasimhan et al., 1998) a property which is likely to confer much of the resistance to therapy that is seen in this aggressive tumour. Apoptosis is a highly complex process and disruption to any one of its integrative pathways can have an impact on its regulation and result in a treatment-resistant phenotype. Understanding the molecular mechanisms by which mesothelioma avoids apoptosis is advancing, bringing with it developments in therapeutic strategies to overcome resistance. (Villanova et al., 2008) Dysregulation of a number of pathways has been implicated in MPM, including TNF death receptor activation pathways (Liu et al., 2001, Broaddus et al., 2005) and the PI3/Akt mTOR survival pathway (Ramos-Nino et al., 2005, Mohiuddin et al., 2002). However, the central role played by the Bcl-2 family of proteins in controlling intrinsic apoptosis and

the potential consequences of protein misregulation, has generated great interest in this area and makes this family a very attractive target for the development of novel anti-cancer therapies.

1.6.6 Dysregulation of Bcl-2 family in MPM

Over-expression of anti-apoptotic Bcl-2 proteins is a common strategy used by cancer cells to increase the threshold for activation of apoptosis. (Inoue-Yamauchi et al., 2017, Cao et al., 2007) A number of studies have noted a characteristic Bcl-2 family expression profile in MPM, suggesting that there may be a reliance on a single anti-apoptotic Bcl-2 protein to maintain survival. (Narasimhan et al., 1998, Segers et al., 1994, Soini et al., 1999) Addiction to specific anti-apoptotic Bcl-2 proteins has been noted in other malignancies (Simoes-Wust et al., 2000, Kondo et al., 1998) and studies suggest that different cell lines from the same cancer demonstrate addiction to different anti-apoptotic Bcl-2 proteins. (Inoue-Yamauchi et al., 2017) Predicting the addiction profile of a cancer cell creates a therapeutic opportunity for the anti-apoptotic protein of interest to be targeted, facilitating the effective induction of apoptosis. (Inoue-Yamauchi et al., 2017)

Work in the Chalmers lab using chemical BH3 profiling (Butterworth et al., 2016) has explored a key role for Bcl-xL addiction in the pathogenesis of MPM. (Jackson et al., 2020) Bcl-xL is the longer splice product of the *BCL2L1* gene which functions to inhibit Bak/Bax activation and so prevent MOMP. (Vander Heiden et al., 1997) Bcl-xL has been demonstrated to be at least as potent as Bcl-2 in preventing apoptosis in a number of human cancer cell lines following exposure to pro-apoptotic signals (Amundson et al., 2000) and numerous studies have alluded to a dominance of Bcl-xL in promoting tumour survival and treatment resistance in lung (Karczmarek-Borowska et al., 2006, Tan et al., 2011, Corcoran et al., 2013), colon (Colak et al., 2014) and ovarian (Wong et al., 2012) cancers.

1.6.7 Single agent Bcl-xL inhibition

Recognition that many tumours exist in a state in which they are 'primed for death' has come from an understanding that the intracellular balance between Bcl-2 proteins is such that cells are reliant on anti-apoptotic proteins to stay alive. Any increase in BH3-only protein expression would be anticipated to tip the cell into apoptosis due to the subsequent increased levels of free pro-apoptotic proteins. (Hennessy, 2016) Given the potential therapeutic benefit of this approach, a number of strategies have been used to manipulate Bcl-xL expression in MPM.

Early methods involved histone deacetylase inhibition (Cao et al., 2001) and antisense oligonucleotides. (Stein and Cheng, 1993) Although antisense oligonucleotide data were promising, (Smythe et al., 2002, Ozvaran et al., 2004) redundancy amongst the anti-apoptotic Bcl-2 proteins coupled with the ability of MPM cells to switch expression from one protein to another, resulted in sustained cell survival after a selective knockdown. (Ozvaran et al., 2004, Han et al., 1996) These challenges favoured an approach which could simultaneously suppress the function of numerous anti-apoptotic Bcl-2 proteins.

Development of small molecules which mimic the ability of BH3-only proteins (BH-3 mimetics) to inactivate the anti-apoptotic Bcl-2 family has been the focus of considerable effort over recent years and has resulted in the identification of a number of compounds, some of which have been taken forward in clinical trials. Early compounds such as ABT-737 and the orally bioavailable variant navitoclax (ABT-263) bind to Bcl-2, Bcl-w and Bcl-xL with subnanomolar affinity and engender apoptosis in a number of cancer cell lines. (Park et al., 2008, Wendt, 2008) Preclinical studies using navitoclax in combination with standard chemotherapies demonstrated encouraging results, (Chen et al., 2011, Ackler et al., 2010) but the clinical application of multi-protein inhibition has been limited by a number of on-target toxicities (thrombocytopenia resulting from Bcl-xL inhibition and neutropenia associated with Bcl-2 inhibition). (Zhang et al., 2007, Mason et al., 2007) This has driven the development of BH3-mimetics which selectively target individual anti-apoptotic proteins. Venetoclax (ABT-199) is a

selective Bcl-2 inhibitor which has demonstrated encouraging clinical results especially in haematological malignancies, whilst largely avoiding thrombocytopenia. (Souers et al., 2013) Selective Bcl-xL inhibitors include A-1155463 (Tao et al., 2014) and its orally bioavailable variant A-1331852. (Leverson et al., 2015) Availability of these single agent inhibitors has enabled the role of specific Bcl-2 proteins to be interrogated *in vitro* and *in vivo* to determine if their selective inhibition is sufficient for a given effect. (Leverson et al., 2015) *In vivo* studies using a range of solid tumours suggested that Bcl-xL inhibition in combination with docetaxel could produce effects as robust as that previously seen with navitoclax and chemotherapy, but without the dose limiting toxicities. (Leverson et al., 2015)

The employment of combined Bcl-2 and Bcl-xL inhibition in MPM cell lines in 2D has demonstrated significant growth inhibition associated with the induction of apoptosis, via a pathway which is mitochondrial dependent and p53 independent. (Cao et al., 2007) Furthermore, co-administration of cisplatin resulted in the synergistic induction of apoptosis *in vivo* and *in vitro*, suggesting that in MPM, BH-3 mimetics in combination with chemotherapy may have untapped therapeutic potential. (Cao et al., 2007) Studies investigating the multicellular resistance of mesothelioma spheroids suggest that the resistance to the proteasome inhibitor bortezomib, acquired when cells are grown in 3D rather than 2D, is mediated through an increased resistance to apoptosis conferred by a dependence on anti-apoptotic defences. This study also noted that despite being resistant to apoptosis, MPM spheroids overexpressed the pro-apoptotic Bcl-2 protein Bim and that exposure to ABT-737 could release this protein from sequestration by Bcl-2 and Bcl-xL, re-sensitising the spheroids to the toxic effect of bortezomib and even producing a single agent effect. (Barbone et al., 2011) Together these findings demonstrate the reliance of MPM on Bcl-xL function, confirming this protein as an attractive therapeutic target.

1.6.8 Bcl-2 protein downregulation in combination with IR

In addition to the single agent activity exhibited by Bcl-xL inhibitors, and considering the potential role of anti-apoptotic proteins in therapy resistance,

several studies have assessed the ability of these drugs to sensitize cells to other forms of therapy. The chemoresistance commonly seen in MPM, underpinned by the knowledge that most forms of chemotherapy induce apoptosis via the intrinsic pathway, which could be augmented by manipulation of Bcl-2 protein expression (Ozvaran et al., 2004) has led to a bias in the literature towards using pro-apoptotic strategies to overcome chemo-resistance in MPM, rather than radioresistance.

Resistance to IR is also a pertinent clinical issue in MPM. Whilst technological improvements in radiotherapy delivery have started to overcome some of the challenges of dose escalation, the characteristics of disease distribution and resulting treatment volumes are likely continue to preclude the employment of this modality in any capacity beyond palliation. Furthermore, despite limited *in vitro* studies, which suggest that MPM may be more radiosensitive than originally assumed, (Carmichael et al., 1989, Hakkinen et al., 1996) any potentially radical treatment is still likely to require a combined modality approach. Strategies to increase the sensitivity of mesothelioma to IR could therefore have huge potential clinical benefit in this disease.

The role of apoptosis in the radioresistance of mesothelioma cells has been explored in our own laboratory using three mesothelioma cell lines (MSTO-211H, NCI-H2052 and NCI-H226). (Jackson et al., 2020) Cells were cultured in 2D and 3D systems, where their radioresistant nature was confirmed. Viability and clonogenic survival assays were used to determine the effect of a panel of BH3-mimetics on cell survival following radiation. The BH3-mimetics A-1331852 and A-1155463 reduced cell survival as single agents and crucially, sensitised mesothelioma cells to IR. Following combination treatment, caspase 3/7 assays detected an increase in the activity of these caspases, suggesting that the reduced survival was due to the promotion of apoptosis. Inhibition of other Bcl-2 proteins with alternative small molecule inhibitors showed little efficacy, highlighting the dependency of mesothelioma cells on Bcl-xL for survival and radioresistance. Furthermore, the relative expression of anti-apoptotic Bcl-2 proteins in mesothelioma cells predicted the radiosensitising capacity of Bcl-xL

inhibition, revealing a potential biomarker of BH3 mimetic activity. This very important work has elucidated mechanisms of radioresistance in mesothelioma cells and identified clinically-relevant targets for radiosensitisation. (Jackson et al., 2020)

1.7 DNA damage responses

1.7.1 DNA damage and cell cycle arrest

The essential role played by DSB in conveying the lethal effects of IR were introduced in section 1.4.1. The ability to repair these lesions is critical for maintaining chromosomal integrity and ensuring cell survival. DSB are detected by DNA damage response (DDR) proteins, which are responsible for the tight regulation of cell cycle checkpoints in G1, S, early G2 and late G2. These checkpoints are biological pathways which block the cell from progressing through the cell cycle. This allows repair of the DNA damage before the cell attempts to replicate its DNA (G1/S checkpoint) or undergo mitosis (G2/M checkpoint), where the lethality of such damage is more likely to be manifested. The DDR protein ataxia-telangiectasia mutated (ATM) is pivotal in this process and can directly phosphorylate proteins, as well as activating several other protein kinases. Ataxia-telangiectasia and rad-3 related protein (ATR) is also critical in DDR, but it primarily focussed on protecting cells from replication stress. DDR protein driven kinase activation leads to the phosphorylation of p53, checkpoint effector kinases 1/2 (CHK1/2) and downstream proteins such as p21, cdc25, cyclin/CDK complexes and retinoblastoma proteins. Significant interaction occurs between the ATM and ATR pathways, which facilitates the mutual coordination of cell cycle arrest through the amplification of damage signals and subsequent activation of downstream DDR proteins. (Weber and Ryan, 2015, Bouwman and Jonkers, 2012, Curtin, 2012, Malumbres and Barbacid, 2009)

1.7.2 Repair of DNA-DSB

Repair of DNA DSB during cell cycle arrest is a potential mechanism through which tumours develop resistance to radiotherapy. An appreciation of this

process could therefore reveal potential targets for therapeutic manipulation. The majority of DNA DSB repair occurs by two different processes: homologous recombination repair (HRR) and non-homologous end joining (NHEJ). The principal determinant of which pathway is utilised is the cell cycle stage at the time of DNA damage. (Takata et al., 1998, Yoshida et al., 2002) HRR, which acts exclusively in the late S/G2 phase of the cell cycle, utilises the undamaged sister chromatid as a template for repair and is therefore a robustly accurate process. NHEJ, by contrast, is far more error-prone, re-joining broken ends of DNA without reference to a template. It is a simple and efficient process, but is inherently associated with the loss of genetic material, resulting from DNA end-processing. NHEJ primarily occurs in the G0 or G1 phase of the cell cycle, when cells are in a diploid state and HRR is not possible, but can be employed in all phases of the cell cycle. This is primarily due to the cellular abundance of the NHEJ activator proteins Ku70/80, which bind robustly to terminal DNA residues within seconds of a DSB occurring. (Jackson, 2002, Mahaney et al., 2009, Rothkamm et al., 2003, Beucher et al., 2009)

The method employed for DS DNA repair has been postulated to explain the fractionation sensitivity of cells at different stages of the cell cycle. (Somaiah et al., 2013, Somaiah et al., 2012) Sensitivity to fraction size in G0/G1 has been linked to the dominance of NHEJ within this phase of the cell cycle and has been suggested as an explanation for the fractionation sensitivity of late normal tissues with low proliferation indices. In contrast, the high fidelity of DS DNA repair conveyed by HRR in the S/G2 phase of the cell cycle is associated with a loss of fractionation sensitivity and increased radioresistance. (Somaiah et al., 2015) This has been demonstrated *in vitro* using cell lines displaying differential mutations in DNA repair pathways. (Somaiah et al., 2013) Cells which were able to undergo HRR displayed reduced sensitivity to fraction size and increased radioresistance. In contrast, cells which were defective in HRR but displayed functional NHEJ, retained sensitivity to fraction size. Furthermore, cells defective in NHEJ also displayed acquired radioresistance to a fractionated regime, accumulating in the late S/G2 phase and lost sensitivity to fraction size. (Somaiah et al., 2013)

Upregulation of the HRR pathway has also been suggested as an explanation for the loss of fractionation sensitivity seen clinically in breast cancer. This has been supported in a study which demonstrated HRR upregulation and enhanced S/G2 arrest in breast epidermal tissue following 5 weeks of irradiation. (Somaiah et al., 2012)

1.7.3 DNA-DSB Repair and MPM

DNA DSB repair pathways are important in the pathogenesis of MPM. Exposure to asbestos fibres has been shown to induce DS DNA breaks in mesothelial cells (Upadhyay and Kamp, 2003, Jaurand, 1997) and chromosomal deletions are observed in MPM. (Taguchi et al., 1993, Neragi-Miandoab and Sugarbaker, 2009) A study analysing the germline mutations of cancer predisposing genes revealed that 9.7% of MPM patients carry pathogenic truncating variants in DNA repair genes. These genes were primarily involved in the HRR pathway and were associated with the development of tumourigenesis at a statistically significantly lower level of asbestos exposure. These findings suggested that the pathogenesis of MPM may be linked in certain patients to a genetic predisposition which prevented cells from adequately repairing asbestos-induced DS DNA breaks. (Betti et al., 2017)

Although HRR is important in the development of MPM, a number of genes involved in the NHEJ pathway have also been implicated in this disease and its resistance to treatment. (Toumpanakis and Theocharis, 2011) Overexpression of the gene encoding the protein subunit Ku80 has been detected in MPM cell lines (Kettunen et al., 2001) and the *XRCC4* gene, the product of which is responsible for the ligation step of NHEJ, has also been found to be upregulated in clinical mesothelioma samples. (Roe et al., 2010) Such an upregulation of key DDR proteins could facilitate the repair of excessive DS DNA breaks induced by anti-cancer therapies such as IR or DNA-damaging chemotherapies and engender resistance to treatment. This makes the NHEJ an attractive pathway to target in the development of novel therapeutic strategies against MPM. (Toumpanakis and Theocharis, 2011)

1.7.4 DNA-dependent protein kinase catalytic subunit

A critical component of the NHEJ repair pathway is DNA-dependent protein kinase catalytic subunit (DNA-PKcs), a serine/threonine protein belonging to the phosphatidylinositol 3-kinase (PI3K) family. In response to a DSB, two molecules of DNA-PKcs are recruited to the lesion by the Ku70/Ku80 heterodimer. Together these molecules form a DNA repair complex, which spans the two broken ends of DNA and allows them to be tethered together. (DeFazio et al., 2002)

Phosphorylation of the threonine 2609 cluster appears to be initiated by ATM (Chen et al., 2007), while auto-phosphorylation by DNA-PKcs itself occurs at multiple sites including serine 2056, (Chen et al., 2007, Chen et al., 2005, Cui et al., 2005) threonine 3950 (Douglas et al., 2007) and threonine 2609. (Douglas et al., 2002) This auto-phosphorylation induces a critical conformational change in the protein which promotes disassociation from the Ku-DNA complex and facilitates the access of other repair proteins to the DSB. (Douglas et al., 2007) Studies using cells expressing DNA-PKcs which are unable to undergo auto-phosphorylation report extreme radiosensitivity and problems with DSB-repair defects. (Ding et al., 2003)

In addition to providing a structural support for repair, DNA-PKcs also recruits other DDR proteins to aid the ligation process and its kinase activity permits the phosphorylation of multiple substrates which are directly or indirectly involved in maintaining DNA integrity. (Collis et al., 2005) Relevant DDR proteins for DNA end processing include Artemis, an endonuclease which modifies the overhanging DNA ends, and mammalian polynucleotide kinase (PNK) which adds 5' phosphate groups to facilitate ligation. The Ligase IV/XRCC4 complex is responsible for the final stage of NHEJ, which involves ligation of the juxtaposed DNA ends. (Collis et al., 2005, Lees-Miller and Meek, 2003, Weterings and van Gent, 2004) A schematic for the processes involved in NHEJ is shown in Figure 1.6.

In addition to its role in DNA-DSB repair, DNA-PKcs has been shown to regulate cell cycle progression by regulation of cell cycle checkpoints. (Dong et al., 2017) In the absence of a proficient NHEJ pathway, irradiated cells undergo aberrant cell cycle progression, resulting in a prolonged G2/M phase arrest. (Shang et al.,

2010, Wang et al., 2002) The G2/M checkpoint prevents cells from entering mitosis before DNA damage has been repaired and is the point of the cycle at which cells are most sensitive to IR. (Morgan and Lawrence, 2015)

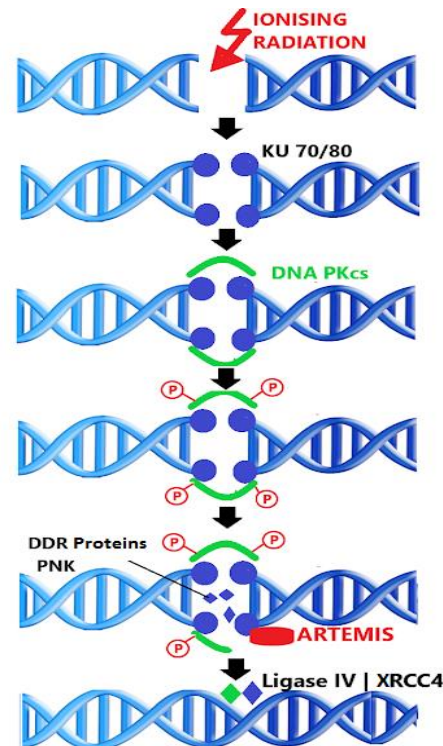


Figure 1.6 A schematic outlining the process of NHEJ

Following a DNA-DSB, two molecules of DNA-PKcs are recruited to the lesion and form a DNA repair complex. A process of sequential DNA-PKcs phosphorylation facilitates a conformational change in the protein which permits the access of other DNA repair proteins to the lesion, allowing it to be repaired and ligated.

The critical role of DNA-PKcs in NHEJ is illustrated by *in vitro* studies using mouse and human cancer cells which do not express DNA-PKcs or Ku70. These cells are compromised in their ability to repair DSB, have prolonged periods of cell cycle arrest and display enhanced radiosensitivity compared to their wild type counterparts. (Chitnis et al., 2014, Kurimasa et al., 1999, Dong et al., 2018, Dong et al., 2017, He et al., 2007). Furthermore, overexpression of DNA-PKcs has been linked with radioresistance and poor clinical outcome in several cancers. (Lee et al., 2005, Xing et al., 2008) The central role of DNA-PKcs in

repair-mediated therapeutic resistance makes it an attractive target for radiosensitisation strategies in cancer treatment.

1.7.5 Inhibition of DNA-PKcs

Preclinical experimental models of cancer exposed to broad spectrum PI3K inhibitors, such as wortmannin and LY294002, have demonstrated an association of these agents with reduced DSB repair and enhanced cellular sensitivity to IR and topoisomerase inhibitors. (Price and Youmell, 1996, Boulton et al., 2000, Rosenzweig et al., 1997) However, the unstable nature of these compounds within cells and inherent toxicity makes them unsuitable for clinical application. (Wipf and Halter, 2005)

Using the competitive PI3K inhibitor LY294002 as a template, the compound NU7026 (2-(morpholin-4-yl)-benzo-h-chromen-4-one) was developed. This is a more potent and specific inhibitor of DNA-PKcs than its predecessor and induces a greater degree of sensitivity to both IR and the DNA-damaging topoisomerase II inhibitors. (Veuger et al., 2003, Willmore et al., 2004) NU7441 (2-N-morpholino-8-dibenzothiophenyl-chromen-4-one) is a synthetic small molecule, which was developed by optimisation of NU7026. (Leahy et al., 2004) This drug is a highly potent and selective inhibitor of DNA-PK phosphorylation, with a documented IC_{50} of 14nmol/L. (Leahy et al., 2004) Pre-clinical studies have demonstrated radiosensitisation with NU7441 in several human cancer cell lines, including NSCLC, colon, breast, prostate and nasopharyngeal cancer. (Dong et al., 2018, Yang et al., 2016, Yu et al., 2015, Shaheen et al., 2011, Ciszewski et al., 2014, Zhao et al., 2006) Enhanced radiosensitivity has been associated with increased DSB and G2-arrest. (Dong et al., 2018) *In vivo* studies have demonstrated NU7441-associated potentiation of etoposide (Zhao et al., 2006) and have shown that concentrations of NU7441 required for radiosensitisation *in vitro* could be achieved and maintained in tumour tissue for up to 4 hours. (Zhao et al., 2006) The limited aqueous solubility and poor bioavailability profile of NU7441 suggests that further clinical development of this compound may be difficult. Nevertheless, the encouraging *in vitro* and *in vivo* chemo and radiosensitisation

data provide excellent justification for the further development of this drug class for therapeutic use.

A possible explanation for the potent chemo and radiosensitisation seen with DNA-PK inhibitors is the promotion of apoptosis resulting from disturbed cell cycle progression and persistent DNA damage. However, alternative non-apoptotic pathways may exist. Mitotic catastrophe has been proposed as one such mechanism (Shang et al., 2010), mediated by an ineffective G2 checkpoint which permits the premature entry of cells into mitosis with unrepaired DNA. (Vitale et al., 2011) This progression disturbs the mitotic kinetochore-microtubule structure, causing mitotic arrest due to spindle checkpoint activation, resulting in cell death. (Mikhailov et al., 2002) It has also been proposed that NU7441 may exert some of its radiosensitising properties through its impact on the HRR pathway. There have been reports of competition between the DNA damage repair pathways, with cells lacking the components of NHEJ demonstrating compensatory elevated levels of HRR. (Essers et al., 2000, Allen et al., 2002) Nevertheless, rather than stimulating HRR, DNA-PK inhibitors appear to block the pathway in a dominant negative fashion by inhibiting the dissociation of DNA-PKcs from the DNA, thereby preventing access of the HRR proteins to the lesion. (Allen et al., 2003) A similar effect has been reported during poly (ADP-ribose) polymerase-1 (PARP-1) trapping, limiting the amount of PARP-1 associated DNA repair which can occur. (Veuger et al., 2003)

It is therefore possible that a number of 'off target' effects may contribute to the radiosensitising activity of DNA-PK inhibitors.

1.8 Aims of thesis

MPM is a cancer of huge unmet need, with no effective treatment options to extend survival beyond a short number of months. The role of radiotherapy in this disease has been limited to palliation, but recent advances in radiotherapy planning and delivery has facilitated safe dose escalation within this remit, currently being investigated in the SYSTEMS-2 study.

There exists a gap in our knowledge with regard to the optimal role of radiotherapy in MPM. A lack of research into the basic radiobiology of this cancer, including its mechanisms of radioresistance, makes the selection of appropriate dose and fractionation regimes difficult and hinders our ability to simultaneously deliver tumour-selective radiosensitising drugs. There are no clinical biomarkers available to suggest which patients may benefit from radiotherapy or to monitor response to treatment. Furthermore, although radiotherapy delivery techniques have improved, it is unclear whether current technology would safely facilitate delivery of dose escalated hypofractionated radiotherapy to the entire pleura.

This thesis aims to bridge some of the gaps in our current knowledge, exploring the possibility of using radiotherapy with a more radical intent in MPM. The premise of the SYSTEMS-2 study will underpin much of this work, reflecting the importance of this randomised clinical trial of radiotherapy dose escalation as an initial step towards the employment of radical radiotherapy in this disease. A broad approach will be taken, encompassing clinical and laboratory work, in addition to radiotherapy planning and dose delivery considerations.

Specifically, this thesis aims to:

1. Facilitate the set up and delivery of SYSTEMS-2: a multicentre, phase II, randomised controlled trial of radiotherapy dose escalation for pain control in MPM.
2. Develop dose constraints which will facilitate the safe delivery of dose escalated, hypofractionated radiotherapy within the SYSTEMS-2 study.
3. Explore radiotherapy planning options which may enable further dose escalation in MPM, including MCO and isotoxic radiotherapy planning.
4. Investigate the radiobiology of two distinct MPM cell lines, using a clinically relevant 3D *in vitro* model. In particular, the response to

fractionated radiotherapy regimes will be studied and this data interrogated to determine the α/β ratio of this tumour.

5. Explore the potential for using radiosensitising drugs in MPM. The activity of NU7441 (a DNA-PKcs inhibitor) and A1331852 (a Bcl-xL inhibitor) will be studied in combination with fractionated radiotherapy using an *in vitro* 3D model of MPM. The clinical validity of these targets will be determined by IHC analysis of diagnostic biopsies taken from MPM patients.

6. Determine the expression of nine proteins, selected for their potential to influence radioresponse, in tumour biopsies taken from patients who participated in the SYSTEMS and SYSTEMS-2 studies. Expression data from the SYSTEMS cohort will be correlated with clinical trial outcomes to identify any potential biomarker of radioresponse. Baseline clinical trial data will be correlated with protein expression data from both cohorts, in an exploratory analysis.

It is hoped that this body of work will advance our understanding of the radiobiology of MPM and therefore of how radiotherapy may be best utilised to treat it.

Chapter 2: Materials and Methods

2.1 Methods used to determine dose constraints for SYSTEMS-2

2.1.1 Dose constraints

In order to generate dose constraints for the 36Gy in 6 fraction arm of SYSTEMS-2, constraints for the local thoracic SABR regimen (55Gy in 5 fractions) were used as a guide. Given the radiobiological variance between these two regimens, BED and EQD2 were calculated to allow a more useful comparison between them. The following equations were used:

$$BED = D [1 + d/(\alpha/\beta)]$$

$$EQD2 = D \frac{(d + \alpha/\beta)}{(2 + \frac{\alpha}{\beta})}$$

Where:

D= total dose

d= dose per fraction

α/β = 2, 3 or 10

Calculation of BED and EQD2 for the 36Gy in 6 fraction regime allowed an appreciation of the relative dose which would be delivered to an OAR, should it receive the full prescribed dose of 36Gy. This facilitated comparison with doses permitted within a SABR regime.

For each OAR, the maximum tolerated dose for the 55Gy in 5 fraction regimen was converted into the EQD2. In order to generate directly comparable values for SYSTEMS-2, the same maximum dose was then converted into the EQD2 for a 6 fraction regime. An α/β ratio of 3 was assumed for late normal tissue complications for all organs except the spinal cord, where an α/β ratio of 2 was employed. For acute toxicity, an α/β ratio of 10 was used. Analysis of the

relative doses delivered within the SABR regime facilitated the generation of radiobiologically safe constraints for SYSTEMS-2.

2.1.2 PTV constraints

In SYSTEMS-2 radiotherapy is delivered in accordance with International commission on radiation units 83 guidance, which recommends that dose volume specifications should be used to report a treatment plan. (Hodapp, 2012) Expected PTV coverage is therefore reported in terms of the absorbed dose (D) that covers a specified volume (v). Minimum absorbed dose will be represented by D98%, median dose by D50% and maximum dose by D2%.

The protocol for SYSTEMS-2 states that PTV constraints should not be compromised to meet OAR constraints unless the treating clinician feels that proposed plan would result in an acute toxicity. (Ashton et al., 2018) There is no maximum PTV size specified within the protocol, reflecting the geographical distribution of this malignancy and the palliative nature of this study. If there are clinical concerns about delivering the dose escalated treatment due to the size of the PTV, or potential doses to OARs, the final fraction can be omitted, delivering a total dose of 30Gy in 5 fractions. (Ashton et al., 2018)

2.1.3 Radiotherapy feasibility planning studies

Final dose constraints were submitted to the radiotherapy planning department at the Beatson West of Scotland Cancer Centre in March 2016. Five patients from the original SYSTEMS study, chosen on the basis of the close proximity of the PTV to critical radiosensitive organs were re-planned using VMAT-IMRT to assess whether the constraints were achievable. OARs for the re-planning study were contoured according to the Radiation Therapy Oncology Group (RTOG) Contouring Atlas. (Kong et al., 2011) Full details of the contouring requirements can be found in the radiotherapy planning guidelines (www.systems-2.co.uk).

In March 2019, the same radiotherapy plans were repeated by the same member of staff using the same planning technique, to assess the impact of increased experience on achievable dosimetry.

2.2 Methods used for MCO analysis of SYSTEMS-2 radiotherapy plans

2.2.1 Dose escalated radiotherapy plans (Glasgow cohort)

All SYSTEMS-2 patients have an initial radiotherapy plan generated for the dose escalated (36Gy in 6 fraction) arm of the study. Should a patient be randomised to 20Gy in 5 fractions then they are re-planned to this schedule and their original plan is de-activated. Since a record of the de-activated 36Gy plan is kept on the radiotherapy planning system, it was possible to locate a dose-escalated plan for all study patients within Glasgow. Plans from 20 such patients were optimised using the multicriteria optimisation (MCO) software which has been available at the Beatson West of Scotland Cancer Centre since September 2017. Patients whose original dose escalated plan was optimised using MCO were not included in this analysis.

2.2.2 Planning information

Radiotherapy plans for all Glasgow patients were generated with IMRT/VMAT using Eclipse planning system version 15.5. The calculation model employed the anisotropic analytical algorithm (AAA), with either 6Mv or 10Mv flattening filter free photon beams, depending on the size of the target. In order to avoid contralateral structures, partial arcs were employed, although due to PTV size and location full arcs were occasionally required. Plans were optimised through an iterative process in which dose to one organ was manipulated in respect to that received by another, until all the dose constraints and the prescribed PTV coverage were met.

2.2.3 MCO of the original 36Gy in 6 fraction plan

The dose escalated plan was copied into a new folder within Eclipse. This ensured that all test plans were maintained separately from active clinical models. Opening the plan within the External Beam Planning interface allowed the achieved dose volume histogram (DVH) for each OAR and PTV constraint to be viewed. The MCO planning software could be launched from this platform (Planning> Optimize).

2.2.4 Setting optimisation objectives

The optimisation objectives were set within the MCO platform. This detailed the required dose objectives for the PTV and OARs, in addition to a 'prioritisation setting' which could be set between 0 and 999 for each organ, reflecting the level of priority which should be attributed to that structure. PTV constraints were given the highest priority, followed by organs of particular clinical concern. It was possible to obtain increased flexibility between the generated plans by setting the dose objectives more stringently than required. As each plan was unique, the organs of primary clinical concern would depend on the size and position of the PTV. If an organ was particularly close to the PTV, then its objectives could be set more stringently and the prioritisation setting increased towards that of the PTV. Dosimetry from the original plan could be viewed in the MCO interface, allowing an appreciation of how much harder the system would need to work to achieve the set objective. Once the objectives were optimised for the structure set, trade-offs were generated and explored (>Explore trade-offs).

2.2.5 Trade-off selection

Structures were selected for trade-off, allowing the dose to one organ to be manipulated against that to another. Structures included the PTV plus one or a number of other OARs. Trade-offs were explored as 'grouped' or 'ungrouped', depending on the OAR. If the structure was required to conform to a Dmax (e.g. stomach) then selection of the 'ungrouped' option permitted visualisation of that particular dose point, but if multiple objectives needed to be met and the

dose was being evaluated across the whole OAR (e.g. contralateral lung) then a 'grouped' objective was optimal. Plans were then be generated for each objective (>Generate plans). If the initial plan had been generated and optimised within VMAT, there was greater scope for trade off explorations. This is because an optimised plan is naturally closer to the Pareto surface and the final trade off will be more efficacious when generating OAR objectives in relation to the PTV.

2.2.6 Plan generation

An optimised plan was generated from analysis of the collective PTV and OAR constraints, by calculating $3n+1$ plans for every objective set.

2.2.7 Plan Trade-off

A slider bar option was presented for each objective selected for trade-off. Moving the slider bar to the left allowed an improvement in the dose objective to the organ, whereas movement to the right incurred degradation. This is classed as Pareto surface navigation. Real time dosimetry updates illustrated the relative impact of manipulation on each OAR whereas expansion of the DVH view illustrated the effect on relative OAR doses and PTV coverage. Manipulation of the PTV was undertaken first to ensure this conformed to dose objectives. Subsequently setting the slider bar to 'stop' prevented the PTV coverage from changing and also incurred a reduction in the range available for other objectives. This is known as 'pinning the plans' to a restricted section of the Pareto surface that is of the most interest. Dose to the most clinically relevant organ was then manipulated accordingly. Once all of the available range for this structure had been utilised, the slider bar was locked down to prevent any degradation. Trade off opportunities could then be explored between other OARs until no further manipulation could be made amongst the plan collection.

2.2.8 Generating a deliverable VMAT plan

A deliverable VMAT plan could be generated using intermediate dose. This mathematically accounts for the differences between inverse optimisation and the final calculation and is particularly beneficial where there is electron density inhomogeneity within the PTV and surrounding tissue. The final plan was presented in the External Beam Planning interface and the dose was re-calculated using an AAA calculation model.

2.2.9 Plan comparison

The original and MCO plan could be compared in the Plan Evaluation interface, where DVHs illustrating the initial and new dose distribution for each OAR could be viewed. In the event that a plan failed to meet a PTV or OAR constraint, the plan collection and trade off parameters could be reviewed and re-manipulated by loading the new plan in External Beam planning and selecting 'optimize'. Once a final optimised MCO plan was selected, it was important to inspect the new dosimetry to all the OARs, even if they were not included in the trade off, to ensure that dose had not been deposited in an organ which had previously met its constraint.

2.2.10 Statistical analysis

Due to the limited number of radiotherapy plans generated, formal statistical analysis to look for a significant difference between OAR doses was not undertaken. Data are therefore presented using descriptive statistics, and clinically significant dose reductions are highlighted in the analysis. While these may be more open to interpretation than statistically significant findings, the clinical relevance of any change to the radiotherapy plan can be appreciated.

2.3 Methods used for 3D *in vitro* spheroid model

2.3.1 Cell culture

All experiments were performed using 2 commercially available mesothelioma cell lines (NCI-H2052 and MSTO-211H). All cell culture work was conducted in a class II sterile laminar flow hood, using sterile plastic ware and solutions and employing aseptic technique. Cell lines were tested regularly for mycoplasma contamination.

2.3.1.1 *Source of mesothelioma cell lines*

The cell lines NCI-H2052 (epithelioid MPM origin) and MSTO-211H (biphasic MPM origin) were a kind gift from Professor Sam Janes (University College, London).

2.3.1.2 *Growth conditions*

Cells were cultured in 75cm² cell culture flasks (Corning; reference 430641U) containing 10mls reduced serum medium (Gibco Advanced DMEM/F12 containing non-essential amino acids and 110mg/L sodium pyruvate; reference 12634-010) with 10% foetal bovine serum (Gibco; reference 10270-106), 0.5% penicillin/streptomycin (Gibco; reference 15140-122) and 0.5% L-Glutamine (Gibco; reference 25030-024). Media was stored at 4°C but warmed to 37°C in a water bath prior to use. Cells were incubated at 37°C; 5% CO₂ in air gas concentration (Galaxy 170R incubator).

2.3.1.3 *Serial passage of cells*

Cells were grown to a confluency of 85-90% from microscopic appearance, at which point the media was aspirated and 10mls of sterile phosphate buffered saline (PBS) (Oxoid; reference BR0014G) was added without disturbing the monolayer. Cells were washed by gently agitating the flask for 30 seconds. The PBS was then aspirated and 1ml pre-warmed Accutase (Gibco; reference A11105-01) was pipetted directly onto the monolayer. The flask was gently agitated to ensure that the whole surface of the flask was in direct contact with the

Accutase. The flask was transferred to the incubator and left for 5 minutes, after which time the cells were viewed under the microscope to ensure that detachment from the surface of the flask was complete. A total of 9mls media was added to the flask and the cells were pipetted a number of times to encourage generation of a single cell suspension. A fraction of this cell suspension (usually 1ml to create a 1:10 split) was transferred into a fresh 75cm² culture flask containing 10mls media and replaced in the incubator.

2.3.1.4 Counting cells

Cells were detached from the flask using the technique described in section 2.3.1.3 and suspended in a total volume of 10mls media. A haemocytometer was cleaned with 70% ethanol and the coverslip placed over the counting surface prior to loading with 10µls of cell suspension using a Gilson P10 pipette. The loaded haemocytometer was placed on the stage of an inverted brightfield AXIO microscope and the counting grid brought into focus at its lowest power. The number of cells present in the 4 corner squares of the central grid were counted and only those cells touching the lines on 2 sides of the large squares were counted 'in' to avoid counting cells twice. The total cell count was divided by 4 and multiplied by 10,000 to determine the number of cells per ml.

2.3.1.5 Cell storage and cryopreservation

In order to prepare a cell line for cryopreservation and storage, cells were grown in bulk using Corning 150cm² cell culture flasks containing 20mls media. At 90% confluency, cells were detached as detailed in section 2.3.1.3 and counted as outlined in section 2.3.1.4. The cell suspension was centrifuged using a Sigma benchtop centrifuge with a swing out rotor at 5000 RPM to pellet the cells. The supernatant was discarded and the cells re-suspended in reduced serum medium (Gibco Advanced DMEM/F12 containing non-essential amino acids and 110mg/L sodium pyruvate; reference 12634-010) with 10% DMSO at a concentration of 10⁶cells/ml and aliquoted into 1ml cryovials (Thermo Scientific; reference 377224). Aliquots were immediately transferred to a cryo 1°C freezing container (Nalgene; reference 5100-0001), filled as directed with methoxyethane and

stored at -80°C overnight. After 24 hours at -80°C , aliquots were transferred to liquid nitrogen storage tanks.

2.3.1.6 Thawing cells from liquid nitrogen

Media was prepared as per section 2.3.1.2 and pre-warmed to 37°C . Cells were retrieved from liquid nitrogen and placed immediately into dry ice for transfer to the laboratory. Aliquots were rapidly thawed in a 37°C water bath and cells were immediately transferred from the cryovial into a Corning 75cm² cell culture flask containing 10mls of pre-warmed media, using a P1000 Gilson pipette. Flasks were incubated at 37°C , 5%CO₂ overnight. The following day, the media was aspirated without disturbing the cell monolayer and replaced with 10mls fresh media. Cells were passaged a minimum of two times from frozen prior to being used in experiments.

2.3.2 Cell culture procedures for radiation only experiments

2.3.2.1 Preparation of in vitro 3D spheroid model using 96 well plates

Polystyrene 96-well spheroid microplates with clear round bottom (Corning; reference 4515) were used to culture spheroids for all radiation experiments. An individual plate was prepared for each dose of radiation planned per experiment. Cells were counted and seeded in an initial volume of 100µls media per well. Any well not being used was filled with 200µls sterile PBS in order to mitigate against 'edge effect'. Cells were seeded at day -4, following which they were incubated at 37°C to allow sufficient time for spheroids to develop. This technique is the pellet system of spheroid development. Spheroid generation was confirmed with microscopy at day -1.

2.3.2.2 Addition of media at day 0

A further 100µls of media was added to each well using a P200 Gilson pipette, bringing the total volume per well to 200µls.

2.3.2.3 Media change

This was performed at least weekly throughout the experiment. A P1000 Gilson pipette was used to aspirate the contents of the well without disturbing the spheroid. If there was a suspicion that the spheroid had been aspirated, the 96 well plate was removed from the tissue culture hood and the relevant well inspected under the microscope before the aspirate was discarded. The contents of the well were refreshed with 200µls of media as quickly as possible to prevent the spheroid drying out and plates were returned to the incubator.

2.3.3 Cell culture procedures for radiation and drug combination experiments

2.3.3.1 Preparation of 96 well plates

This was performed as outlined in section 2.3.2.1, but H2052 and 211H cells were seeded into separate 96 well plates, with 8 wells per drug concentration. For each cell line, an individual plate was prepared per radiation dose planned, to allow the effect of drug and radiotherapy dose titration to be assessed across both cell lines. Any wells not being used were filled with 200µls of PBS.

2.3.3.2 Source and preparation of radiosensitising drugs

Stocks of NU7441 and A1331852 were obtained from SelleckChem (NU7441, 5mg, reference S2638; A1331852, 5mg, reference S7801). On arrival, both drugs were reconstituted into dimethyl sulphoxide (DMSO) (Thermo Scientific; reference 20688) and aliquoted for long term storage at -80°C by Dr Mark Jackson. NU7441 was prepared at a stock concentration of 5mM while A1331852 was prepared at a stock concentration of 10mM.

2.3.3.3 Drug and DMSO preparation at day 0

At day 0, stocks of NU7441 and A1331852 were retrieved from -80°C storage, thawed at room temperature and serial dilutions prepared in media using the following equation:

$$\frac{2 \times \text{concentration required}}{\text{concentration of stock}} \times \text{total volume required}$$

Once defrosted, aliquots of NU7441 and A1331852 were stored at -20°C for the duration of the experiment. A DMSO control was prepared in media, corresponding to the maximum volume of each drug stock utilised.

2.3.3.4 Addition of media/DMSO/drug at day 0

A total of 100µls of drug (in media), DMSO (in media) or media alone was added to each well, bringing the total volume per well to 200µls. Plates were returned to the incubator for 6 hours prior to irradiation.

2.3.3.5 Drug and DMSO preparation after day 0

The drug/DMSO/media was refreshed in each well 6 hours before each dose of IR and at each media change. In order to maintain consistency between the plates, the contents of each well was refreshed even if the plate was not due to receive IR.

Aliquots of NU7441 and A1331852 were retrieved from -20°C and serial dilutions prepared using the following equation:

$$\frac{\text{concentration required}}{\text{concentration of stock}} \times \text{total volume required}$$

A relevant DMSO control was prepared corresponding to the maximum volume of each drug used.

2.3.3.6 Media change

This was performed prior to each dose of IR and at least weekly thereafter. This was performed as detailed in section 2.3.2.3, with 200µls of drug (in media), DMSO (in media) or media alone being replaced into each well.

2.3.4 Irradiation of spheroids

2.3.4.1 Delivery of ionising radiation

The spheroids were irradiated using an Xstrahl cabinet irradiator.

The 96 well plates were removed from the incubator and placed individually into the irradiation cabinet. In instances where more than one plate required the same dose of irradiation, the distance of the shelf from the source could be increased to permit concurrent treatment and the irradiation time adjusted according to the dose rate (Gy per minute) to ensure accurate dose delivery. The relative dose rates at increasing distance from the source are shown in Table 2.1. Plates were returned to the incubator immediately after irradiation. In order to maintain consistency between the plates in terms of time out of the incubator, all plates were removed for the period of irradiation

2.3.4.2 Timing of irradiation

All radiation schedules commenced on day 0. Delivery of subsequent fractions took place at 24 hour intervals, until the intended total dose had been achieved.

Table 2.1 Dose rate (in Gy/minute) delivered by the Xstrahl cabinet irradiator depending on the distance of the shelf from the source

| Shelf (mm) | Dose rate (Gy/min) |
|------------|--------------------|
| 200 | 5.56 |
| 300 | 2.47 |
| 400 | 1.39 |
| 500 | 0.9 |
| 600 | 0.63 |
| 700 | 0.48 |

This information was used to calculate the time needed to deliver the required dose of radiation.

2.3.5 Spheroid imaging

2.3.5.1 GelCount

Spheroids were imaged within the 96 well plates using the GelCount™ software (version 1.2.1.0; Oxford Optronix Ltd 2008-16). The 96 well plates were removed from the incubator in multiples of 4 and loaded into the GelCount™ cartridge. The software was programmed to photograph every well of each 96 well plate using an image resolution of 2400 dots per inch (dpi), corresponding to 10.583µm/pixel. It took approximately 1 hour to complete the count for all 4 plates, after which they were returned to the incubator and the next 4 loaded. In experiments where the total number of plates was not a multiple of 4, the final count was set to run for an hour to limit inaccuracies introduced by having plates out of the incubator for unequal amounts of time.

2.3.5.2 Timing of imaging

In each experiment, spheroids were imaged at day 0, day 1, day 2 and day 3. Following this, imaging took place at least twice per week to track growth at regular intervals following irradiation.

2.3.6 Image processing and spheroid quantification

2.3.6.1 Spyder

Data sets generated from GelCount™ were processed using the Spyder software (Scientific PYthon Development EnviRonment, version 3.6). Scripts were generated by Dr Mark Jackson which programmed the software to retain only the images from wells containing spheroids, and organise these into relevant folders. Images were saved as black images on white backgrounds (Figure 2.1)



Figure 2.1 Spheroid imaging using GelCount™ and Spyder software

Spheroids were imaged at regular intervals throughout the experiment. Each well of the 96 well plates were photographed using GelCount™ software and relevant images saved using Spyder software, to facilitate further processing.

2.3.6.2 Image J

To facilitate downstream image processing, data generated through Spyder was manipulated using the ImageJ software (National Institute of Health, USA; Java 1.8.0_144). Scripts were used to program the software to invert and crop the

original images, producing an enlarged view of the spheroid, now represented as a white image on a black background. (Figure 2.2)

2.3.6.3 Cell profiler

The area of each spheroid was quantified using the Cell Profiler programme (version 2.2.0). (Carpenter et al., 2006) This software was used to find the edge of each individual spheroid by detecting the change in pixel intensity across the image. A template pipeline was downloaded from the company website and optimised for use. The optimal settings for this analysis were:

- Discard objects outside of the diameter range: yes
- Discard objects touching the border of the image: yes
- Threshold strategy: global
- Thresholding method: RidlerCalvard
- Smoothing method for thresholding: automatic
- Threshold correction factor: 1.0

As the spheroids grew larger and became less compact, it was often necessary to change the threshold detection limits for spheroid size and pixel intensity, to ensure that the optimal outline was found at each stage of the experiment. (Figure 2.2)



Figure 2.2 Analysis of 2D images using Cell Profiler determined the area of each spheroid

Raw spheroid images were cropped and inverted using ImageJ software to facilitate further processing. An outline of the spheroid was generated using Cell profiler software, which detects pixel intensity across the image. The subsequent area was measured in pixel².

2.3.6.4 Post processing of Cell Profiler data in Excel

The data from Cell Profiler was directly exported into an Excel spreadsheet. This allowed the accuracy of the automated outline to be manual checked at each stage. Frequently, the software would detect erroneous objects in addition to the spheroid, which could then be deleted from the spreadsheet. The area for each spheroid was quoted in pixel². The micrometre: pixel ratio = 10.583: 1 (Gelcount software). Therefore, the area in pixel² was multiplied by 10.583² (112) to convert into μm^2 . The average spheroid area for each time point under each experimental condition could then be calculated and plotted to show the relative growth over time. On occasions where the spheroid had been lost from the well (e.g. by accidental aspiration during media change), data from this well was negated so that it didn't impact on the mean area calculated for each condition. Similarly, if the outlining of the spheroid was felt to be unsatisfactory despite optimisation of the settings, the spheroid was discounted and did not contribute to the data for that timepoint. On occasions where the spheroid became fragmented (e.g. following drug treatment), the largest fragment was used to represent the spheroid area. Where the spheroid was no longer measurable, but traces of cellular debris could be seen in the well (i.e. the spheroid had not been lost at media change), the area was recorded as '0' and this figure did contribute to the calculated mean area for that experimental condition.

2.3.6.5 Matlab

In addition to generating quantitative data pertaining to spheroid area, Gel Count also produced a 'mask' for each delineated object within an image. These masks could be used to estimate the spheroid volume, which may be a more clinically relevant measurement, particularly within a 3D tumour model. The Matlab software (Version 2.0; R2014a, 8.3.0.532), available from the University of Glasgow, was used to interrogate the 2D masks which were subsequently converted into a 3D volume, using the Reconstruction and visualisation from a single projection (ReVISP) software, as shown in Figure 2.3. (Piccinini et al., 2015) The resulting dataset was uploaded into an Excel spreadsheet and the values checked manually for accuracy. In instances where more than one object had been originally detected by Cell Profiler, the correct mask and corresponding value was identified by the position of the object in the image (i.e. increasing denominations left to right across the image). A similar approach was used as for the analysis of the 'area' data, in that if a spheroid had been accidentally removed or the outlining was sub-optimal, data was not counted towards the total mean volume for that time point and experimental condition. Where fragments of spheroids existed, the mask corresponding to the largest area was used to estimate volume and where the spheroid was unmeasurable the volume was recorded as '0'.

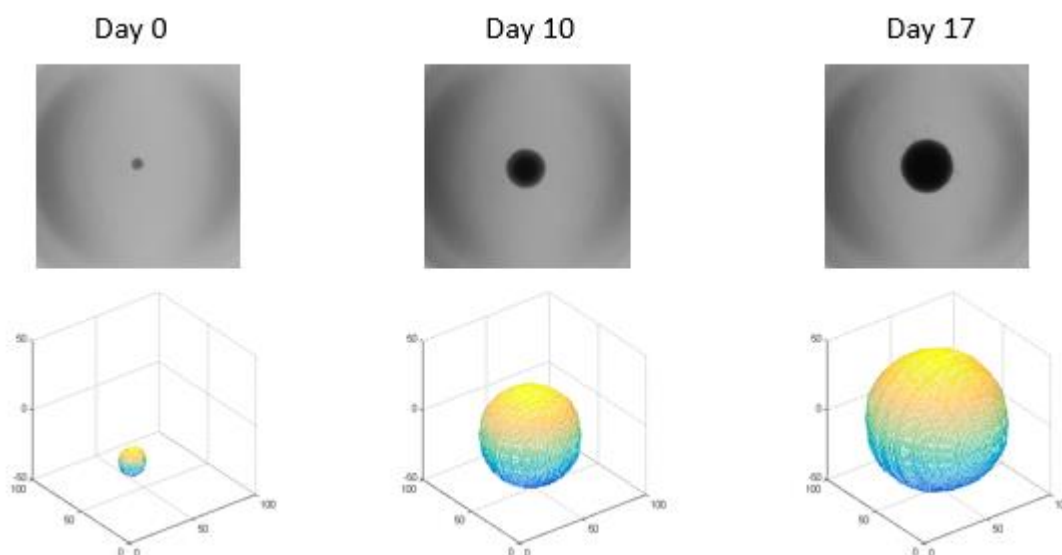


Figure 2.3 Generation of 3D volume data using 2D images

Spheroid images generated from Cell Profiler were used to determine 3D volume data using Matlab in conjunction with the ‘reconstruction and visualisation from a single projection’ (ReVISP) software. Sequential imaging permitted an estimation of the change in spheroid volume over time.

2.3.7 Statistical analysis

All statistical analyses were performed using IBM SPSS version 25 or R version 3.5.0.

2.3.7.1 Data organisation

Data for spheroid volume at day 21 was grouped in terms of radiation dose, drug dose and experiment number. Each experiment consisted of either 6 or 8 replicates per condition and the full dataset was reported and subject to analysis. Where spheroid volumes were below the lower limit of detection (but where the spheroid hadn’t been lost from the well), the volume was reset to the lowest level of detection according to the limits of the equipment used to detect and quantify the spheroids. Methods for analysing data below the level of detection have been discussed extensively in other fields. (Antweiler, 2015) It is widely accepted that complex approaches are available that outperform naïve substitution methods when a high proportion of data are below level of

detection (i.e. censored). However, in cases where the censoring proportion is low (as is the case here), the performance of substitutions methods are comparable. The smallest diameter of detection in Cell Profiler is 1 pixel unit which can be converted to μm by the multiplier 10.583. Matlab quotes final spheroid volume in μm^3 , therefore the lowest level of spheroid detection was calculated to be $1185\mu\text{m}^3$. Data were then subjected to a number of simple graphical assessments, to investigate treatment effects as well as variability within and between experiments, prior to attempting to fit a statistical model.

2.3.7.2 The linear mixed effect model

Data from each experiment were treated as independent, reflecting the distinct biological entity of a cell line cultured at a different point in time and at a different passage number. A repeated measures analysis of variance (ANOVA) model is often used to analyse data of this nature, however due to issues with missing data points (from spheroid loss) and variation in the number of replicates between experiments (i.e. an unbalanced design), this model could not be used to analyse the raw data set. Therefore, a linear mixed effect model was used. Radiotherapy dose and drug concentration were treated as fixed effects. Experiment and replicate (nested within experiment) were considered random effects, allowing the treatment inference to be generalised beyond this sample of experiments. Initially, individual replicates within each experiment were accounted for in the model; however this often created issues with model convergence, possibly due to the model being over-parameterised. An alternative method was to fit the mixed model ignoring any variability introduced by the individual replicates within experiments. This approach was justified given the minimal variability noted between the replicates (relative to, for example, between-treatment dose variability) and the well documented limitations of intra-experimental replicates in providing an independent test of the hypothesis. (Vaux et al., 2012)

In addition to the untransformed volumes, a number of data transformations were considered in order to satisfy the statistical model assumptions. Firstly, due to the scale of the raw data, transformations were performed to express

these values in log, square root and cubed root format and a 'rescaled' volume was calculated in which the raw data was divided by 10^6 . The mean and standard deviation of the entire dataset was also calculated and utilised to generate a 'standardised' volume (standardised volume = individual volume - mean volume / standard deviation).

Once a model was fitted using the raw and transformed volume data, residuals were plotted to check for normal distribution and constant variance. Radiotherapy and drug dose effects were then investigated from the best fitting model, and inferences made about main and interaction effects. Optimal fit to the linear mixed effect model was seen with either the standardised or cubed root datasets. Pairwise comparisons were generated following Sidak adjustment for multiple comparisons and used to estimate the difference between treatment doses, in addition to confidence intervals and p values.

2.3.7.3 Normalisation of data to account for the effect of IR

The linear effects model was used to analyse statistical differences between all the spheroid data. However, this approach has not been presented in the analysis of the drug/radiation spheroid volume data. In order to reveal any potentially radiosensitising effect of the selected drugs on spheroid volume, spheroid data was normalised for the effect of each IR regime. This allowed direct comparison of the therapeutic interaction between the drug and IR and data was expressed as the spheroid volume relative to the irradiated DMSO control within each fractionation regime. This normalised data was amenable to analysis using a one way ANOVA to assess differences between relative volumes. Pairwise comparisons were generated using a post hoc Tukey test.

2.3.8 Method used to estimate the α/B ratio of MPM spheroids

The α/B ratio of MPM spheroids was explored using a technique adapted from Stewart *et al* (1984), which was introduced in section 1.5.4.2. (Stewart *et al.*, 1984) To investigate the α/B ratio of MPM cell lines, fractionation schedules

were selected on the basis of previous *in vitro* 3D spheroid response data to single dose IR. Doses of 4Gy to 16Gy were delivered in 1 to 4 fractions, with individual fraction sizes of between 1Gy and 10Gy. The overall treatment time was 4 days and radiation doses of multi-fraction regimes were delivered 24 hours apart, to allow sufficient time for SLD repair. The selected endpoint of spheroid damage was assessed at multiple timepoints throughout the study, from day 10 until day 21 (in the 211H cell line) or day 28 (in the H2052 cell line). The variation in follow up time between the cell lines was a reflection of their relative ability to generate reliable data over time.

Data was plotted as volume size (mm^3) against time (days). The effect of a particular radiation regime was calculated as 'spheroid volume reduction' and was determined by subtracting the irradiated spheroid volume from that of the un-irradiated control at a chosen time point (e.g. day 21). Combining this data by fraction number allowed a response curve to be generated of total dose versus effect, for each IR regime delivered using an equal fraction number. Isoeffective dose could then be established across fractionation regimes by determining the total dose required to produce a fixed level of volume reduction. The equation of the straight line joining the data points incorporating the selected isoeffect was used to calculate the dose per fraction.

Within any multi-dose radiation schedule, each successive fraction is radiobiologically equally effective. This principal was applied by Douglas and Fowler, when investigating the effect of multiple small doses of X rays on skin reactions in mice. (Douglas and Fowler, 1976) This work identified that data conforming to the LQ model exhibits a linear relationship when plotted as the reciprocal of the total isoeffective dose (F_e) against the corresponding dose per fraction. The gradient of the line is proportional to the value of β and the y-intercept corresponds to the value of α . Manipulation of the equation of the straight line of best fit between data points therefore permitted mathematical determination of the α/β ratio.

2.4 Methods used for immunohistochemical studies

2.4.1 Tissue Acquisition

Diagnostic mesothelioma tissue samples from patients who had entered the SYSTEMS or SYSTEMS-2 study were obtained from Glasgow Biorepository. Prior to undertaking IHC analysis on these specimens, selected antibodies were optimised on mesothelioma tissue obtained from five mesothelioma patients who had not enrolled in any clinical trials. In addition to clinical samples, IHC analysis was also performed on H2052 and 211H spheroids. Cells were initially seeded at 10^2 cells per well, as described in section 2.3.2.1 and were allowed to grow for 3 weeks prior to being fixed in formalin and embedded in paraffin.

2.4.2 Sectioning and mounting of tissue

Formalin fixed paraffin embedded (FFPE) blocks containing clinical tissue were reviewed by a pathologist at the University of Glasgow to determine tissue suitability for further processing. A microtome was used to cut $4\mu\text{m}$ sections from suitable blocks and tissue was mounted onto adherent slides. Spheroid FFPE blocks were processed in the same manner.

2.4.3 Antibody optimisation

Four of the nine antibodies selected for evaluation were routinely used at the University of Glasgow IHC laboratory and were already optimised for use on human tissue. Analysis with these antibodies was performed in the University of Glasgow IHC laboratory using two autostainer platforms. Two of the five remaining antibodies (γH2Ax and DNA-PKcs) were frequently used within our laboratory on human tissue with established parameters, and three antibodies (Bcl-xL, Bcl-2 and Mcl-1) were optimised on the MPM tissue samples provided by the Biorepository. The parameters evaluated throughout the optimisation procedure are shown in Table 2.2. The final conditions chosen for antigen retrieval and optimal antibody dilutions are illustrated in Table 2.3.

Table 2.2 Parameters investigated in the process of antibody optimisation for Bcl-xL, Bcl-2 and Mcl-1 antibodies

| | pH6 | | | pH9 | | | | |
|--|-------|--------|--------|-------|-------|-------|--------|--------|
| <i>Bcl-XL anti rabbit</i> (Abcam 32370) | 1:500 | 1:1000 | 1:2000 | 1:50 | 1:300 | 1:500 | 1:1000 | 1:2000 |
| Result | - | - | - | +++ | ++ | + | - | - |
| <i>Bcl-2 anti mouse</i> (Dako M0887) | 1:50 | 1:100 | 1:200 | 1:50 | 1:100 | 1:200 | | |
| Result | - | - | - | +++ | ++ | - | | |
| <i>Bcl-2</i> (Leica NCL-L-bCl-2) | 1:200 | 1:600 | | 1:100 | 1:200 | 1:600 | 1:1200 | |
| Result | - | - | | +++ | ++ | + | - | |
| <i>Mcl-1</i> (Abcam 32087) | 1:100 | 1:500 | | 1:50 | 1:100 | 1:500 | 1:1000 | |
| Result | + | - | | +++ | +++ | ++ | - | |

Table 2.3 Final conditions selected for antigen retrieval and antibody dilution

| Antibody | Company | Code | Species | Antigen retrieval | Dilution | Positive control | Visualisation | Autostainer platform (if appropriate) |
|---------------|-----------------|-------------|---------|-------------------|----------|------------------|---------------|---------------------------------------|
| BCI-XL | Abcam | 32370 | Rabbit | pH9 | 1:300 | Tonsil | DAB | |
| BCI-2 | Leica | NCL-L-bcl-2 | Mouse | pH9 | 1:200 | Tonsil | DAB | |
| MCI-1 | Abcam | 32087 | Rabbit | pH9 | 1:500 | Tonsil | DAB | |
| γ H2Ax | Cell signalling | 9718 | Rabbit | pH6 | 1:500 | MPM tissue | DAB | |
| DNAPKcs | Abcam | GR261379-2 | Mouse | pH6 | 1:500 | MPM tissue | DAB | |

| Antibody | Company | Code | Species | Antigen retrieval | Dilution | Positive control | Visualisation | Autostainer platform (if appropriate) |
|---------------------|-----------------|--------|---------|-------------------|----------|------------------|---------------|---------------------------------------|
| p21 (WAF1/CIP1) | Dako | M7202 | Mouse | pH9 | 1:50 | MPM tissue | DAB | Dako Autostainer Link48 |
| Ki67 (MIB-1) | Dako | M7240 | Mouse | pH8 | 1:100 | MPM tissue | DAB | Dako Autostainer Link48 |
| Hif1 α | BD Biosciences | 610959 | Mouse | pH6 | 1:50 | MPM tissue | DAB | Dako Autostainer Link48 |
| Caspase 3 (Asp-175) | Cell Signalling | 9661 | Rabbit | ER2 | 1:500 | MPM tissue | DAB | Leica Bond Rx |

2.4.4 Manual immunohistochemical procedures

2.4.4.1 De-waxing slides

Paraffin wax was removed from the slides using a series of xylene and ethanol solutions, to which slides were exposed for five minutes. Completely de-waxed slides were submerged in water prior to antigen retrieval.

2.4.4.2 Antigen retrieval

Dako antigen retrieval solution (Reference S2369- pH6; Reference S2367- pH9) was diluted in water and heated in an uncovered pressure cooker for 10 minutes. Slides were transferred into the warmed solution and the covered pressure cooker was heated at full power for a further 10 minutes. Slides were left to cool for 20-30 minutes in retrieval solution.

2.4.4.3 Immunohistochemistry staining

Sections were washed twice in 10mM tris-buffered saline with tween (TBS-T) solution (pH 7.5). An endogenous peroxidase block solution (Dako Reference K4011) was applied and the slides were covered in parafilm for 10 minutes, before being washed a further two times in 10mM TBS-T solution (pH 7.5). Primary antibodies were diluted in DakoREAL diluent (Reference S2022) and 100µls of diluted antibody was added to each slide. Parafilm was applied and the slides were incubated overnight at 4°C in a humidified chamber.

Sections were washed twice in 10mM TBS-T solution (pH 7.5) prior to application of the horseradish peroxidase (HRP) labelled secondary antibody (Dako Reference K4003- anti rabbit; Dako Reference K4001- anti mouse). Slides were covered with parafilm and incubated for 40 minutes at room temperature.

Sections were washed twice in 10mM TBS-T solution (pH 7.5). A solution of 3,3'-diaminobenzidine tetrahydrochloride (DAB) was prepared using Dako Liquid DAB

and substrate chromogen solutions (Reference K3468) and one drop was applied to each slide. Parafilm was used to cover each slide and the sections were transferred to water following the development of colour. Nuclear counterstaining with Mayer's Hematoxylin was performed using the Auto-stainer in the University of Glasgow IHC laboratory and slides were mounted with coverslips.

2.4.5 Automated immunohistochemical procedures

De-waxing and antigen retrieval was performed as part of the Leica Bond Rx platform. For the Dako platform, these processes were carried out manually before the slides were placed in the autostainer.

2.4.6 Data interpretation

Prior to embarking on data analysis, time was spent with a consultant pathologist to determine typical features of malignant invasion on H+E slides. Following this training, all data analysis and interpretation was done without pathology support.

2.4.6.1 Scanning of stained slides

Following IHC staining, slides were transferred to the Glasgow Biorepository where they were scanned and loaded onto the 'Slidepath' database. Files were subsequently transferred to an external hard drive and uploaded to the 'HALO' analysis programme, supplied by the University of Glasgow.

2.4.6.2 Slide analysis

The HALO programme permitted the individual visualisation and analysis of each slide. H+E slides were studied in combination with the original pathology report to identify areas of tumour invasion and HALO was subsequently 'trained' to identify tumour cells through the manipulation of parameters of nuclear size and shape. Once optimised for an individual patient, these parameters were applied

to all relevant slides. For individual antibody, settings were then adjusted to allow the appropriate identification of weakly (1+), moderately (2+) and strongly (3+) stained tumour cells. Areas suitable for analysis were selected and a report was generated detailing the number of tumour cells detected within the fixed field, in addition to the relative strength of staining within each cell. Whilst tumour cell settings were individualised for each patient, settings for the intensity of staining were kept consistent between patient samples, to permit meaningful comparisons. The relative expression of each protein was determined through the calculation of the Histology-score ('H' Score). Using this method, the percentage of cells at each staining intensity level is calculated and an H Score is assigned using the following formula:

$$(1 \times (\% \text{ cells } 1+) + 2 \times (\% \text{ cells } 2+) + 3 \times (\% \text{ cells } 3+))$$

The final score ranges from 0-300 and gives more relative weight to higher-intensity staining in a tumour sample. The sample can then be considered positive or negative on the basis of a specific threshold.

2.4.6.3 Positive and negative controls

To determine consistency between batches of antibody staining and to ensure the specificity and sensitivity of antibody binding, positive and negative controls were included with all IHC. Tonsil tissue was primarily used as a positive control, although if this did not express the protein of interest, samples of MPM tissue which had previously demonstrated robust expression of the protein were utilised. Negative controls comprised tonsillar or MPM tissue, without addition of the primary antibody.

2.4.6.4 Statistical analysis

A number of clinical parameters were chosen to correlate with the expression levels of each protein. For biopsy specimens obtained from patients who had

taken part in SYSTEMS-2, these parameters consisted of baseline clinical trial data only, whereas those that were obtained from SYSTEMS patients could be correlated with clinical trial outcome data in addition to baseline parameters.

All statistical analysis was performed using the IBM SPSS Statistics 25 programme. Data was initially analysed through the generation of basic plots and non-parametric summary statistics, to determine whether any association could be detected between baseline clinical data and expression scores. For continuous data, (e.g. pain scores and CRP values) this comprised scatterplots with Spearman's rank correlation coefficient analysis, to determine any associated p-values. For categorical data, summary statistics were used to generate boxplots demonstrating the spread of expression data within each category. Where only two categories existed, the Mann Whitney U test was used to assess the significance of any relationship, but when data incorporated multiple categories, the Kruskal-Wallis test was employed. Data was adjusted for multiple testing using the FDR and Berferroni corrections.

Chapter 3: SYSTEMS-2

Chapter aim

This chapter will outline the design, set up and delivery of the SYSTEMS-2 study. Some of the encountered challenges will be highlighted and the strategies used to overcome them discussed.

3.1 Introduction

The concept of SYSTEMS-2 was developed following the publication of the results of the SYSTEMS study in 2015. (MacLeod et al., 2015a) This multicentre, single arm, phase II trial recruited 40 patients from 3 centres over 18 months and was the first prospective study to use validated outcome measures to assess pain responses to radiotherapy in MPM. Parallel opposed radiotherapy beams were used to deliver a standard dose of 20Gy in 5 fractions over one week to sites of pain and the study reported clinically significant pain responses 5 weeks after radiotherapy in one third of patients, with minimal toxicity.

SYSTEMS-2 is a randomised dose escalation study comparing two hypofractionated radiotherapy regimes for pain control in MPM: 20Gy in 5 fractions over 1 week versus 36Gy in 6 fractions over 2 weeks. (Ashton et al., 2018) The study is underpinned by the hypothesis that a higher dose of radiation may achieve clinically meaningful pain responses in a greater proportion of patients and could extend the duration of analgesia. Furthermore, although there is very little data available on which to determine the α/β ratio of mesothelioma, the clinical suspicion is that this cancer may exhibit a low α/β ratio and therefore may respond more favourably to hypofractionated radiotherapy. (MacLeod et al., 2015a) This hypothesis is supported by a number of other studies which have observed improved radiological or clinical responses to hypofractionated radiotherapy in MPM. (Jenkins et al., 2011, van der Zee et al., 2004) Nevertheless, the dose escalation aspect of SYSTEMS-2 may make data interpretation more complex, since the impact of dose escalation may not be distinct from that of hypofractionation.

Advanced radiotherapy techniques, principally IMRT, are being used in SYSTEMS-2 to facilitate safe dose escalation to the tumour whilst maintaining acceptable doses to normal tissues.

SYSTEMS-2 was developed through multidisciplinary collaboration between the Beatson West of Scotland Cancer Centre, Edinburgh Cancer Research Centre and the Cancer Research UK Clinical Trials Unit Glasgow. (Ashton et al., 2018) Joint funding was secured for the study in 2015 from the June Hancock Mesothelioma Research Fund and the Beatson Cancer Charity.

I was recruited into the role of Clinical Research Fellow in December 2015. My primary responsibility within this remit has been to develop and implement the SYSTEMS-2 study, initially within Glasgow, and subsequently at multiple sites across the UK. To this end I have been responsible for the production of a number of trial-specific documents, including the case report forms, laboratory manual and the radiotherapy guidelines, for which I also developed the dose constraints. I was involved in the ethics approval process and although the trial protocol was written prior to my taking the role of Clinical Research Fellow, I have contributed to all protocol amendments through the duration of the trial. I approached a number of potential sites throughout the UK with regard to joining the study and have kept in close contact with sites in set up to ensure that any problems are overcome as swiftly as possible. I liaise with regulatory bodies, such as the radiotherapy trials quality assurance team (RTTQA) and participate in the monthly trial management group (TMG) meeting. I am responsible for the clinical aspects of SYSTEMS-2 in Glasgow. This includes screening potential patients and optimising their analgesia prior to recruitment. I am responsible for planning patient radiotherapy and conducting follow up visits. Furthermore, I coordinate the central radiology review in which baseline and week 9 CT scans from all sites are assessed for radiological response to radiotherapy. Through poster and oral presentations, I have ensured that SYSTEMS-2 is well publicised, both locally, nationally and internationally. I have set up a trial specific website to ensure information is readily available to patients and clinicians and I contribute to the regular SYSTEMS-2 newsletter. I secured funding for the sample

collection associated with SYSTEMS-2 and have been involved in setting up collaborations with other research centres who wish to utilise this collection for mesothelioma research.

3.2 Methods

3.2.1 Regulatory processes

3.2.1.1 Ethical approval process

In order to obtain ethical approval for SYSTEMS-2, an integrated research application system document was submitted to the research ethics committee (REC) on 17th November 2015. The study protocol and patient information sheet (PIS) was presented at the REC review meeting on 7th December 2015 and ethical approval was granted on 19th January 2016 (REC number 15/SS/0225).

3.2.1.2 Local approval processes

Prior to SYSTEMS-2 being opened in Glasgow, the study needed to be approved by a number of local regulatory committees, including the clinical trials executive committee and radiotherapy management group. These boards reviewed the local capacity, funding and clinical demand for the study and approval from both was obtained in March 2016. Local research and development (R&D) and overall sponsor approval was granted on 12th July 2016 and SYSTEMS-2 opened to recruitment at the Beatson West of Scotland Cancer Centre on 16th August 2016.

3.2.1.3 Radiotherapy quality assurance

To ensure consistent radiotherapy plan quality across sites, quality assurance is undertaken by the RTTQA. To ensure that dose constraints can be achieved and that contouring is consistent with the protocol, centres are asked to perform a planning exercise on a 'dummy patient' (an anonymised image from a Glasgow SYSTEMS-2 patient). If sites have participated in other thoracic clinical trials

utilising IMRT, many of the QA processes can be streamlined with previous assessments.

3.2.2 Study design

SYSTEMS-2 is a multicentre, phase II randomised dose escalation study, comparing two hypofractionated schedules of radiotherapy for pain control in MPM. The study complies with Research Governance Framework for Health and Community Care, the British Good Clinical Practice regulations and the Declaration of Helsinki. SYSTEMS-2 is registered on the publically available ISRCTN database and is badged by the National Institute for Health Research. (Ashton et al., 2018) The study is sponsored by NHS Greater Glasgow and Clyde and the University of Glasgow (GN13ON388).

3.2.3 Study population

Patients with a histological or multidisciplinary team (MDT) diagnosis of MPM, in whom radiotherapy is clinically indicated for pain control, are being recruited. Potential patients are primarily identified through lung cancer or mesothelioma MDT meetings, although direct referrals from oncology or respiratory colleagues are common. The recruitment target for SYSTEMS-2 is 112 patients.

3.2.4 Inclusion criteria

- Histological and/or MDT diagnosis of MPM
- Performance status 0-2
- Predicted life expectancy of ≥ 12 weeks
- Contrast enhanced CT scan of chest and abdomen performed within 8 weeks prior to starting radiotherapy
- Worst Pain $\geq 4/10$ (0-10 numerical rating scale) after analgesia optimisation
- Ability to provide written informed consent prior to participating in the trial and any trial related procedures being performed

- Willingness to comply with scheduled visits, treatment plans and laboratory tests and other study procedures
- Patients must have a radiotherapy plan compatible with the treatment arm (30-36 Gy in 5-6 fractions) prior to randomisation

3.2.5 Exclusion criteria

- Patients who have received anti-cancer therapy within the 4 weeks of study entry that is likely to alter pain at the index site during the duration of the study
- Patients who are planned to have further anti-cancer therapy within 6 weeks of the radiotherapy treatment
- Patients who have previously received palliative radiotherapy and where there is concern that the proposed treatment volume would overlap with a previously irradiated area. This does not include patients who have received superficial photon or electron therapy to drain sites
- Psychotic disorders or cognitive impairment
- Co-existing lung tumours at the time of study entry
- Patients who are pregnant or breastfeeding
- Patients of child-bearing potential, who are unwilling to use 2 effective methods of contraception

3.2.6 Schedule of assessment

There are six planned visits within the SYSTEMS-2 study: screening, baseline, final day of radiotherapy, week 5, week 9 and week 26. A flowchart outlining the study visits is shown in Figure 3.1 and a detailed outline of the schedule of assessments is illustrated in Table 3.1.

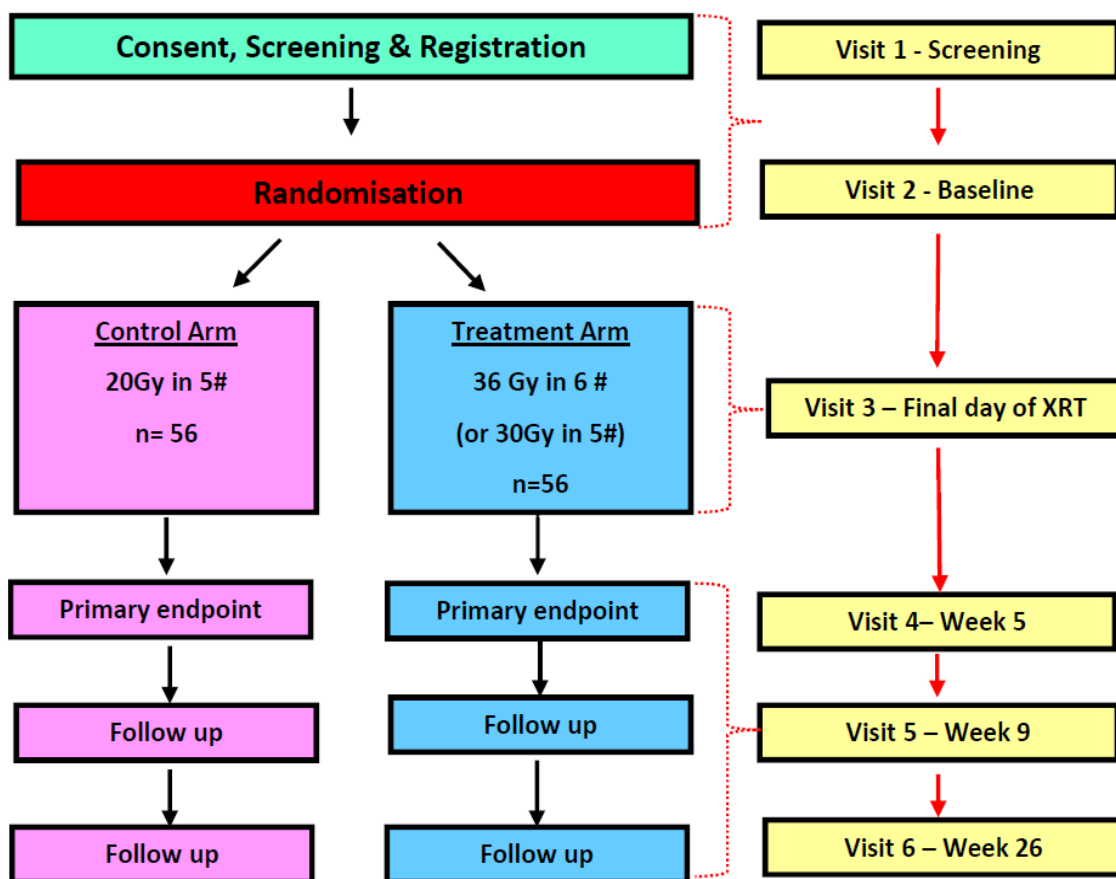


Figure 3.1 Outline of the study visits for SYSTEMS-2

Table 3.1 Schedule of assessment for SYSTEMS-2

| | Screening | Baseline | Final Day of RT | Week 5 | Week 9 | Week 26 |
|--------------------------------|----------------|------------------------------------|--|---------------|---------------|-----------------|
| | Visit 1 | Visit 2 | Visit 3 | Visit 4 | Visit 5 | Visit 6 |
| Day | -28 to -3 days | -7 to 1 days (Day 1 = RT Start) | Standard Arm: 8 +/- 3 days Treatment Arm: 15 +/- 3 days | 35 +/- 5 days | 63 +/- 7 days | 182 +/- 14 days |
| Informed consent | X | | | | | |
| Registration | X | | | | | |
| Inclusion/exclusion | X | | | | | |
| Vital signs | X | | | | | |
| Medical history | X | | | | | |
| Medication history | X | X | X | X | X | |
| Mesothelioma treatment history | X | | | | | |
| Physical examination | | X | | X | X | |
| ECOG Performance status | | X | X | X | X | |

| | Screening Visit 1 | Baseline Visit 2 | Final Day of RT Visit 3 | Week 5 Visit 4 | Week 9 Visit 5 | Week 26 Visit 6 |
|------------------------------------|----------------------|---------------------|----------------------------|-------------------|-------------------|--------------------|
| CT chest & abdomen | X | | | | X | |
| Research blood tests (optional) | | X | | X | X | |
| Routine blood tests | | X | | X | X | |
| Pregnancy Test | X | | | | | |
| Toxicity Assessment | | X | X | X | X | |
| Randomisation | | X | | | | |
| QUESTIONNAIRES: | | | | | | |
| Brief Pain Inventory | | X | X | X | X | X |
| EORTC QLQ C-30 & LC13 | | X | | X | X | |
| EQ5D | | X | | X | X | X |
| ICECAP-SCM | | X | | X | X | X |

3.2.7 Study procedures

3.2.7.1 Patient consent processes

Following the identification of a potentially eligible patient, a PIS is provided by a health care professional already known to the patient. Interested patients are given at least 24 hours to consider this document before being invited to attend for screening by the research team. Consent to obtain and use tissue and blood samples for research purposes are optional components of SYSTEMS-2 and as such, separate consent is required.

3.2.7.2 Patient registration process

Following consent, patients are registered to the study and are allocated a 3-digit sequential patient ID number.

3.2.7.3 Patient randomisation process

Patients are randomised 1:1 to dose escalated, or standard radiotherapy and are stratified according to the following factors:

1. Centre
2. Gender (male/female)
3. PS (0, 1, 2)
4. White cell count (≥ 8.3 , < 8.3)
5. Histological subtype (epithelioid, sarcomatoid, biphasic, histology unavailable)
6. Planned dose escalated treatment (30Gy or 36Gy)
7. Worst pain score (4-10)

At randomisation, each patient is issued with a unique sequential randomisation number.

3.2.7.4 Analgesia optimisation prior to randomisation

Central to the validity of SYSTEMS-2 is the step of analgesia optimisation prior to randomisation. Pain should be stabilised as much as possible to allow the effects of radiotherapy to be determined accurately. Stable pain is defined as an average pain score at the planned site of radiotherapy of between 4 and 8 for a minimum of 72 hours prior to randomisation. Whilst this is recommended, it is not absolute inclusion criteria, however, any patients whose pain score is less than 4 at the baseline visit is no longer eligible. (Ashton et al., 2018)

It is recommended that patients are reviewed by the local palliative care team at this stage. Since Glasgow was anticipated to be the primary recruiter, trial staff underwent a period of palliative care training, provided by Dr Barry Laird, Consultant in Palliative Medicine at St Columba's Hospice, Edinburgh. Any particularly challenging cases were discussed directly with Dr Laird.

To standardise prescribing practise across UK trial centres, a guideline was issued, outlining the anticipated analgesic regime for any patient being considered for SYSTEMS-2. The suggested regime adheres to the WHO pain ladder (Walker et al., 1988) and reflects the multifactorial pathophysiology of MPM associated pain, which frequently necessitates a combination of analgesics with different mechanisms of action. (MacLeod et al., 2015b) It includes regular paracetamol, preparations of sustained and immediate release morphine, an adjuvant such as pregabalin or gabapentin and a topical preparation such as a lidocaine patch.

3.2.7.5 Radiotherapy planning prior to randomisation

To avoid bias in the radiotherapy planning and target volume delineation process, all patients must have a radiotherapy plan which satisfies the planning constraints of the dose escalated arm prior to randomisation. Patients subsequently randomised to the control arm have a second plan generated to comply with the standard radiotherapy regime.

For the purposes of the trial, radiotherapy is specifically targeted at sites of pain. In order to facilitate accurate dose delivery, painful areas are demarcated by adhesive radio-opaque markers at the time of CT acquisition. CTV delineation is subsequently guided by baseline imaging information and marker position, which frequently corresponds with areas of bulky disease, sites of previous pleural intervention, rib involvement or chest wall invasion. The use of IMRT for planning is encouraged, but not mandated. If IMRT is not available, 3DCRT must be utilised. If the anatomical location of the tumour precludes delivery of 36Gy in 6 fractions, it is acceptable to omit the final fraction and treat to 30Gy in 5 fractions for the dose escalated arm.

3.2.8 Trial endpoints and objectives

3.2.8.1 Primary objective

The primary objective of the SYSTEMS-2 study is to determine whether dose escalated, hypofractionated radiotherapy increases the proportion of patients experiencing a clinically significant reduction in pain at the radiotherapy site at week five, compared to standard radiotherapy. The primary endpoint is therefore pain control at week 5. Pain is evaluated using the brief pain inventory, which was successfully implemented in the SYSTEMS study. A clinically significant response is regarded as a reduction of ≥ 2 points in the 'worse pain score' component of the brief pain inventory between the visit at baseline and week 5.

3.2.8.2 Secondary objective

The secondary objectives are to determine the relative effects of dose escalated and standard radiotherapy on acute toxicity, pain and radiological responses, overall survival and quality of life after radiotherapy.

3.2.8.3 Exploratory objectives

These include change in strong opioid use, health related QOL at week 9 and translational biomarker studies.

3.2.9 Protocol development

The initial SYSTEMS-2 protocol was written in 2015 by Dr Nick Macleod, Dr Barry Laird and Professor Anthony Chalmers. Ethical approval for the study was granted on version 2.0 and the study opened in Glasgow employing version 3.0.

3.2.9.1 Protocol amendments

A number of substantial and non-substantial amendments have been made to the original protocol since ethical approval was granted in January 2016. The majority of the substantial changes reflect clinical and logistical decisions which have been implemented to help the study run more efficiently. These are summarised below:

I. Radiotherapy planning

The original protocol stated that patients were required to have a radiotherapy plan for each treatment arm generated prior to randomisation. This was contested by the physics department at the Beatson West of Scotland Cancer Centre, who felt that this would waste time and resources. A compromise was reached whereby all patients would be planned to the dose escalated arm and subsequently re-planned to the standard arm using the same OAR and PTV delineations should they be randomised to this lower dose.

II. Baseline CT scans

The protocol states that patients should have a diagnostic CT scan of chest and abdomen with contrast within 8 weeks of the radiotherapy start date. Whilst this was usually achievable, no funding was available for these scans and it could be

difficult to ensure that they were carried out in a timely manner. Delaying the start of the radiotherapy for this reason was felt to be unethical in a cohort of patients for whom pain is a primary symptom. The decision was made to allow the radiotherapy planning scan (which specifies coverage from the apex of the chest to the iliac crest) to be carried out with intravenous contrast and using the narrowest slice width attainable. These images could then be used as baseline images for study purposes.

III. Previous chest wall radiotherapy

The initial protocol specified that patients were ineligible for SYSTEMS-2 if they had received previous palliative radiotherapy and there was concern about overlapping treatment fields at the site of pain. This created confusion at centres which continued to give prophylactic irradiation to drain sites using electrons and necessitated a protocol amendment to clarify the safety of proceeding with SYSTEMS-2 in these circumstances.

IV. Clarification of start date of RT

The initial protocol was not clear in terms of how soon after the baseline visit the radiotherapy should begin. This was clarified as being seven days and a statement was added surrounding the necessity of repeating baseline assessments should this not be achievable.

V. Assessment of renal function prior to CT scan with contrast at week 9

The protocol states that routine bloods, including renal function, should be checked at baseline, week 5 and week 9. In order to assess for any radiological response to the radiotherapy, a CT scan with contrast is required at week 9. This is often arranged at the week 5 visit, using the parameters obtained at that point to assess safety for contrast. This recommendation was updated in the light of a case where a patient attended for a CT scan two days prior to their week 9 visit and was subsequently found to have developed acute renal impairment, requiring hospitalisation. The patient had demonstrated very mild

renal impairment at week 5, but had clinically deteriorated in the intervening month, with decreased appetite and poor fluid intake. This event was reported as a serious adverse event (SAE) and was subsequently discussed at the TMG meeting and reported to the REC. The protocol was updated to suggest that if there are any concerns regarding renal function at week 5 then bloods should be repeated locally prior to the CT scan at week 9.

VI. Pain flare

Pain flares at the radiotherapy site were initially noted in a small minority of patients receiving dose escalated radiotherapy. Episodes of sharp, pleuritic pain were reported, usually occurring after the second or third fraction of radiotherapy. The symptoms are believed to be a consequence of pleural irritation and inflammation and are almost exclusively seen in the dose escalated cohort. Short courses of steroids have been used to help alleviate the pain and this advice was formalised within the protocol to ensure that practice was standardised across trial sites.

3.2.10 Site selection and opening process

The recruitment target of 112 patients is acknowledged to be ambitious, particularly for a relatively rare disease such as MPM. In order to achieve this, SYSTEMS-2 is being conducted as a multicentre study. A number of UK sites were approached by the study team, selected primarily on the basis of geographical location and MPM prevalence. The process of study set up involved the attainment of local ethical and R&D approval, in addition to liaison with the RTTQA regarding radiotherapy planning processes.

3.2.11 Central radiology review process

Radiological response is a secondary endpoint of SYSTEMS-2. The data obtained from the SYSTEMS study had been disappointing in this regard, since only 18/40 patients had been well enough to attend for their CT scan at week 12 and only one partial response was recorded. In order to increase the uptake of patients

attending for their CT scan, the date of this assessment has been brought forward to week 9. To ensure consistency within the trial, all patient images are transferred to the Beatson West of Scotland Cancer Centre via the RTTQA team for central radiology review. The week 9 and baseline CT scans are assessed by Dr Simon Sheridan (Consultant Radiologist, Queen Elizabeth University Hospital), who is blinded to the dose of radiation the patient received. Any differences between the scans are graded using the Modified RECIST criteria. (Byrne and Nowak, 2004b) The radiotherapy plans are also studied at the time of review, to ensure that the irradiated area is accurately identified.

3.2.12 Safety reporting

3.2.12.1 Adverse event reporting

Adverse events (AE), documented and graded according to the CTCAE version 4, are collected at baseline and at subsequent visits (end of radiotherapy, week 5 and week 9). The start and stop dates, severity and causality with regard to radiotherapy or disease are recorded. The exacerbation of any previous condition is classed as an AE. AEs are followed until resolution or for at least 30 days after the final fraction of radiotherapy, or until they are considered to be irreversible. Perceived lack of efficacy of the radiotherapy for pain control is not an AE.

3.2.12.2 Serious adverse event reporting

Since the safety profile of radiotherapy is well known, only events that are directly related to the administration of radiotherapy and are unexpected should be reported as a serious adverse event (SAE). A list of expected adverse events related to the administration of radiotherapy is given in the protocol (which can be found at www.systems-2.co.uk) and include nausea, fatigue and radiation dermatitis.

3.2.13 Statistical analysis

The primary endpoint of SYSTEMS-2 is to detect the difference in the proportion of patients on dose escalated radiotherapy compared to standard radiotherapy who experience a clinically significant reduction in pain at the treatment site, 5 weeks after the radiotherapy. To determine this, SYSTEMS-2 has been designed to detect an absolute increase of 20% in the proportion of responders at week 5 on dose escalated radiotherapy compared to standard radiotherapy, from 40% (the response rate reported in the SYSTEMS study (MacLeod et al., 2015a)) to 60%. This detection requires 112 patients, 56 per arm, (comparison of proportions, 90% power, 20% 1-sided level of statistical significance; equivalent to 80% power, 10% level of statistical significance). The 3-outcome design (Hong and Wang, 2007) will determine whether a phase III study is warranted.

3.2.14 Translational research

3.2.14.1 Sample collection

The SYSTEMS-2 study presents a unique opportunity to collect clinical samples from patients before and after radiotherapy which could subsequently be analysed in the context of high-quality clinical outcome data to potentially advance the treatment and monitoring of this disease. Blood samples are collected at baseline, week 5 and week 9. These are processed and stored as plasma, serum and whole blood. Samples are initially stored locally but are subsequently transferred to the Glasgow Biorepository for longer term storage. In addition to blood samples, diagnostic tumour samples are also being retrieved and stored for use in future research. The SYSTEMS-2 sample collection is summarised in Table 3.2.

Table 3.2 Summary of the SYSTEMS-2 sample collection

| | Archival Material | Baseline | Week 5 | Week 9 |
|----------------------|-------------------|----------|--------|--------|
| Plasma | | X | X | X |
| Serum | | X | X | X |
| Whole blood | | X | X | X |
| Tumour Sample (FFPE) | X | | | |

3.2.14.2 Lab manual

A SYSTEMS-2 laboratory manual was generated, detailing instructions for sample collection, processing and storage. Information was also required regarding the handling and transport of processed blood samples and of formalin fixed paraffin embedded tumour samples. This manual was completed with input from Dr Fiona Thomson at the Wolfson Wohl Cancer Research Centre and Dr Jane Hair at the Glasgow Biorepository.

3.2.14.3 Grant applications

Funding for the SYSTEMS-2 sample collection was not provided in the initial study budget. In order to secure financial backing for this and to allow provisional laboratory work on samples to commence, an application was submitted to Cancer Research UK in June 2016 for a prospective sample collection award. This application was shortlisted for consideration by the Clinical Research Committee, but was not recommended for funding.

In December 2016, a further grant application was submitted to Slater and Gordon's 'health projects and research fund'. This application was accepted in May 2017 and a proportion of the anticipated costs were secured. An additional application was submitted to the Beatson Cancer Charity in March 2017 who agreed to co-fund the outstanding costs of the sample collection and laboratory work.

3.2.15 No-cost extension

It was originally anticipated that the target sample size of 112 patients could be recruited from 5-8 study sites over a 24-month period. Due to a number of issues with site set up and patient recruitment, it became apparent in early 2018 that this target was unachievable and the possibility of a no cost extension was discussed with members of the TMG. At that time, the recruitment rate was 4.11 patients per month and a number of additional centres were due to open. An extension period of 18 months (to February 2020) was proposed, based on the anticipated recruitment numbers and opening dates collected from each site. It was predicted that if sites opened on schedule, it would be possible to reach the target sample size of 112 patients by October 2019, however a recruitment extension until February 2020 would allow some flexibility in the event of further unanticipated delays. At the end of the recruitment period, there would be a 6-month follow-up period and a further 3 months for data cleaning and analysis. This would result in study completion in November 2020.

An application for a no cost extension was submitted to the Clinical Trials Unit, the June Hancock Mesothelioma Research Fund and Beatson Cancer Charity in May 2018. This proposal was accepted by these regulatory bodies and sites have subsequently been informed of the updated recruitment timelines.

3.3 Results

3.3.1 Site set up and recruitment

Between December 2015 and July 2018, thirty nine sites across the UK were invited to take part in SYSTEMS-2. Of the sites approached, fifteen have opened the study and six are in the process of set-up at the time of writing. (Table 3.3) Time to study opening from initial confirmation of interest has varied, with 53% of sites opening within one year, 40% opening within two years and 7% taking more than two years to open the study. The delays to set up and opening have primarily been caused by capacity issues affecting clinical trial units, radiotherapy planning and delivery departments, R&D divisions and medical units. These issues affected at least four sites which are already open and have presented a significant problem for all of the sites currently in set up. Nine sites have been unable to participate in SYSTEMS-2 due to capacity problems, including five which initially expressed an interest in the study. (Table 3.3) Four of the sites did not respond to the invitation to join the study and, despite perseverance from the SYSTEMS-2 team, communication has been lost with five sites who initially expressed an interest.

Recruitment to SYSTEMS-2 has been slower than anticipated. Six sites have yet to recruit a patient, including three which have been open for more than three months and two which have been open for more than a year. (Table 3.3)

Revised projected recruitment timelines are shown in Figure 3.2.

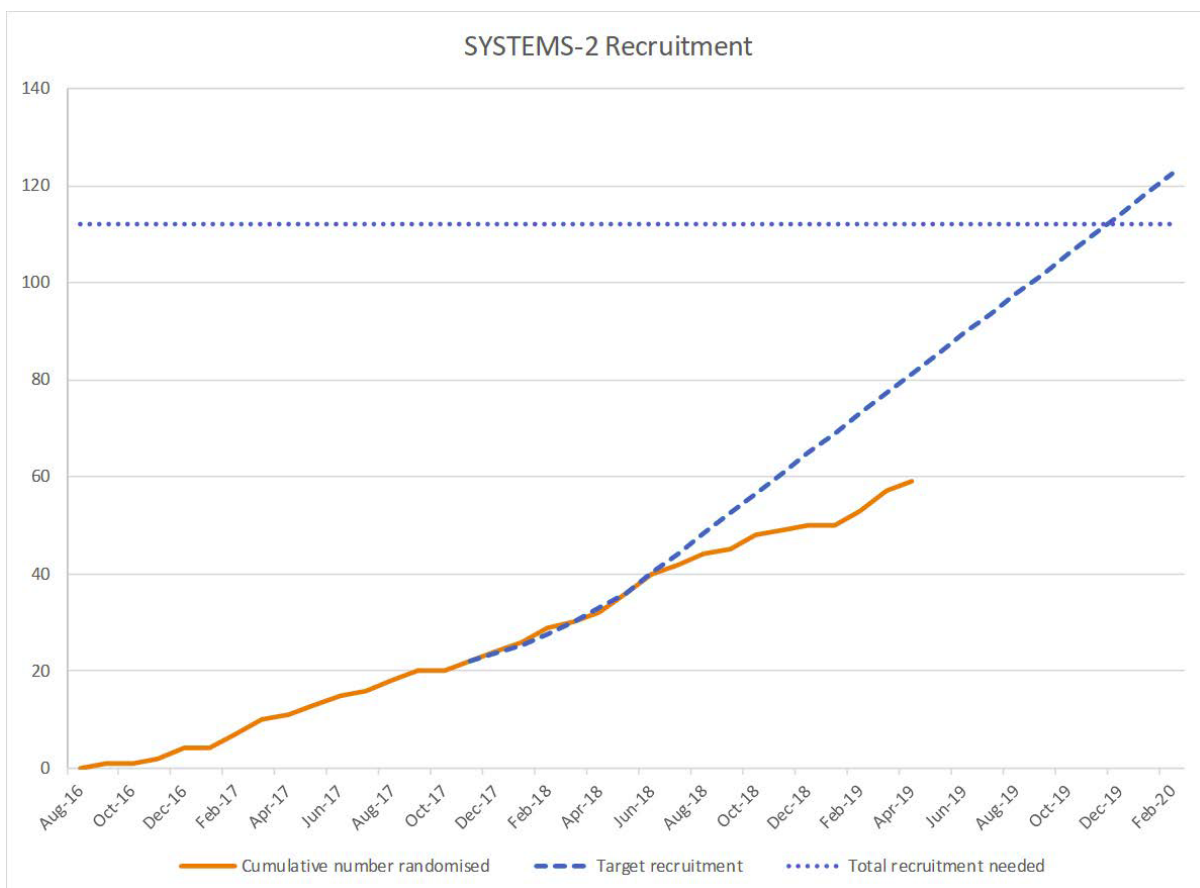


Figure 3.2 Predicted recruitment to the SYSTEMS-2 study

Anticipated recruitment to an extended time point of February 2020. Total recruitment required is represented by the light blue dotted line, target recruitment is represented by the dark blue dotted line and the current number of randomised patients is represented by the dotted red line.

Table 3.3 Outcome data for sites invited to enter SYSTEMS-2

| Nb | Site | Date of first contact | Date interest confirmed | Anticipated set-up time | Anticipated recruitment | Date opened | Recruitment to date (April 2019) | Date inability to participate confirmed | Reason for not participating |
|----|---|-----------------------|-------------------------|-------------------------|-------------------------|-------------|----------------------------------|---|------------------------------|
| 1 | Beatson West of Scotland Cancer Centre, Glasgow | N/A | N/A | N/A | 24 per year | August 2016 | 32 | | |
| 2 | University Hospital Southampton | Dec 2015 | June 2016 | Not stated | 3-4 per year | Dec 2016 | 3 | | |
| 3 | Forth Valley Royal Hospital | July 2016 | Aug 2016 | Data unavailable | Data unavailable | Jan 2017 | 0 | | |
| 4 | Weston Park Hospital Sheffield | Dec 2015 | April 2016 | 2-3 months | 3-5 per year | Feb 2017 | 6 | | |
| 5 | Royal Marsden, Sutton | Dec 2015 | Oct 2016 | 4-6 weeks | 4 per year | April 2017 | 12 | | |
| 6 | Norfolk and Norwich Hospital | April 2017 | June 2017 | 70 days | 5+ per year | Feb 2018 | 0 | | |

| Nb | Site | Date of first contact | Date interest confirmed | Anticipated set-up time | Anticipated recruitment | Date opened | Recruitment to date (April 2019) | Date inability to participate confirmed | Reason for not participating |
|----|-------------------------------------|-----------------------|-------------------------|-------------------------|-------------------------|-------------|----------------------------------|---|------------------------------|
| 7 | New Cross Hospital, Wolverhampton | Jan 2017 | March 2017 | 40 days | 2 per year | Feb 2018 | 1 | | |
| 8 | Guys and St Thomas, London | Dec 2016 | June 2017 | 3 months | 4 per year | March 2018 | 6 | | |
| 9 | Western General, Edinburgh | Aug 2016 | Oct 2016 | 3 months | 2 per year | April 2018 | 1 | | |
| 10 | Belfast City Hospital | Dec 2015 | Aug 2016 | 3-6 months | 2-4 per year | May 2018 | 2 | | |
| 11 | Southend University Hospital, Essex | Oct 2017 | Oct 2017 | Data unavailable | 8 per year | June 2018 | 2 | | |
| 12 | Royal Shrewsbury Hospital | April 2017 | Nov 2017 | 40 days | 2-3 per year | Sept 2018 | 0 | | |

| Nb | Site | Date of first contact | Date interest confirmed | Anticipated set-up time | Anticipated recruitment | Date opened | Recruitment to date (April 2019) | Date inability to participate confirmed | Reason for not participating |
|----|--|-----------------------|-------------------------|-------------------------|-------------------------|----------------|----------------------------------|---|------------------------------|
| 13 | Basildon and Thurrock University Hospitals | June 2017 | July 2017 | Data unavailable | Data unavailable | Nov 2018 | 0 | | |
| 14 | Aberdeen Royal Infirmary | April 2017 | April 2017 | Data unavailable | Data unavailable | Dec 2018 | 0 | | |
| 15 | St James University Hospital, Leeds | Dec 2015 | April 2016 | 2-3 months | 2-4 per year | Jan 2019 | 1 | | |
| 16 | Churchill Hospital, Oxford | May 2017 | Aug 2017 | 60 days | 5-10 per year | March 2019 | 0 | | |
| 17 | The Christie, Manchester | Dec 2015 | Dec 2015 | 6-8 weeks | 10-20 per year | Site in set-up | | | |

| Nb | Site | Date of first contact | Date interest confirmed | Anticipated set-up time | Anticipated recruitment | Date opened | Recruitment to date (April 2019) | Date inability to participate confirmed | Reason for not participating |
|----|--|-----------------------|-------------------------|-------------------------|-------------------------|----------------|----------------------------------|---|-------------------------------|
| 18 | Northern Centre for Cancer Care, Newcastle | July 2016 | July 2016 | Data unavailable | Data unavailable | Site in set-up | | | |
| 19 | Castlehill Hospital, Hull | Sept 2016 | March 2016 | Data unavailable | Data unavailable | Site in set-up | | | |
| 20 | Leicester Royal Infirmary | June 2016 | June 2016 | Data unavailable | Data unavailable | Site in set-up | | | |
| 21 | Kent Oncology Centre | June 2017 | June 2017 | 8-10 weeks | 2 per year | Site in set-up | | | |
| 22 | Royal Derby Hospital | May 2017 | May 2017 | Not stated | 3 per year | Site in set-up | | | |
| 23 | Nottingham University Hospital | Dec 2015 | N/A | 3 months | 5 per year | | | June 2016 | Capacity issues (RT planning) |

| Nb | Site | Date of first contact | Date interest confirmed | Anticipated set-up time | Anticipated recruitment | Date opened | Recruitment to date (April 2019) | Date inability to participate confirmed | Reason for not participating |
|----|-----------------------------------|-----------------------|-------------------------|-------------------------|-------------------------|-------------|----------------------------------|---|-----------------------------------|
| 24 | Velindre Hospital, Cardiff | Dec 2015 | April 2016 | Not stated | 6-10 per year | | | Not confirmed | Poor response |
| 25 | Royal Preston Hospital | Dec 2015 | July 2017 | 3 months | 2 per year | | | Not confirmed | Communication lost |
| 26 | Royal Stoke University Hospital | July 2018 | Sept 2018 | 40 days | 3-5 per year | | | Not confirmed | Communication lost |
| 27 | Cheltenham & Gloucester Hospitals | Sept 2016 | December 2016 | 2 weeks | 3-4 per year | | | Oct 2017 | Capacity issues (clinical trials) |
| 28 | Addenbrookes Hospital, Cambridge | Dec 2015 | N/A | | | | | Jan 2016 | Capacity issues (RT planning) |

| Nb | Site | Date of first contact | Date interest confirmed | Anticipated set-up time | Anticipated recruitment | Date opened | Recruitment to date (April 2019) | Date inability to participate confirmed | Reason for not participating |
|----|---|-----------------------|-------------------------|-------------------------|-------------------------|-------------|----------------------------------|---|---|
| 29 | Derriford Hospital, Plymouth | Dec 2015 | N/A | | | | | Sept 2016 | Capacity issues (RT planning); Lack of requirement |
| 30 | James Cook University Hospital, Middlesbrough | March 2017 | June 2017 | | | | | Jan 2018 | Capacity issues (RT planning and clinical trials) |
| 31 | Bristol Haematology & Oncology Centre | March 2017 | April 2017 | | | | | Aug 2017 | Capacity issues (RT planning & clinical trials) |
| 32 | Brighton and Sussex University Hospital | April 2017 | N/A | | | | | May 2017 | Capacity issues (clinical trials) |

| Nb | Site | Date of first contact | Date interest confirmed | Anticipated set-up time | Anticipated recruitment | Date opened | Recruitment to date (April 2019) | Date inability to participate confirmed | Reason for not participating |
|----|-------------------------------------|-----------------------|-------------------------|-------------------------|-------------------------|-------------|----------------------------------|---|---|
| 33 | The Royal Devon and Exeter Hospital | Oct 2016 | Feb 2017 | | | | | Dec 2017 | Capacity issues (RT planning) |
| 34 | Treliske Hospital, Cornwall | April 2017 | April 2017 | | | | | Aug 2017 | Capacity issues (RT planning & clinical trials) |
| 35 | North Wales Cancer Treatment Centre | July 2017 | July 2017 | | | | | Not confirmed | Communication lost |
| 36 | Royal Surrey Hospital | Jan 2017 | Jan 2017 | | | | | Not confirmed | Communication lost |
| 37 | Ninewells Hospital, Dundee | April 2017 | N/A | | | | | N/A | Communication lost |

| Nb | Site | Date of first contact | Date interest confirmed | Anticipated set-up time | Anticipated recruitment | Date opened | Recruitment to date (April 2019) | Date inability to participate confirmed | Reason for not participating |
|----|--------------------------------------|-----------------------|-------------------------|-------------------------|-------------------------|-------------|----------------------------------|---|------------------------------|
| 38 | Kings Mill Hospital, Nottinghamshire | April 2017 | N/A | | | | | N/A | Communication lost |
| 39 | Singleton Hospital, Swansea | Sept 2016 | N/A | | | | | N/A | Communication lost |
| 40 | Clatterbridge Hospital, Liverpool | Feb 2017 | N/A | | | | | N/A | Communication lost |

A total of thirty nine sites were invited to enter SYSTEMS-2 between December 2015 and July 2018. Current recruitment figures are shown for open sites and sites in set up are indicated. Sites which have declined to enter the study are listed, with the stated reason.

3.3.2 Radiotherapy delivery technique

Of the sixteen sites which are currently recruiting to SYSTEMS-2, nine are using IMRT/VMAT for radiotherapy planning, two are utilising 3DCRT and four are employing a combination of both. Data was unavailable for one site. Of the fifty nine patients currently randomised, 10 have been stratified to a 30Gy/5 fraction dose escalated regime. One patient has so far been ineligible for the study due to the inability to generate a safe dose escalated plan (Table 3.4).

Table 3.4 Planning methods employed by current SYSTEMS-2 sites.

| Site | Planning Technique | Nb of patients treated with 30Gy/5# | Nb of patients ineligible for SYSTEMS-2 due to inability to generate safe dose escalated plan |
|---|--------------------|-------------------------------------|---|
| Beatson West of Scotland Cancer Centre, Glasgow | VMAT | 1 | 0 |
| University Hospital Southampton | 3DCRT | 0 | 0 |
| Forth Valley Royal Hospital | VMAT | 0 | 0 |
| Weston Park Hospital Sheffield | VMAT | 1 | 0 |
| Royal Marsden, Sutton | IMRT | 5 | 0 |
| Norfolk and Norwich Hospital | 3DCRT/ IMRT | 0 | 0 |

| Site | Planning Technique | Nb of patients treated with 30Gy/5# | Nb of patients ineligible for SYSTEMS-2 due to inability to generate safe dose escalated plan |
|--|--------------------|-------------------------------------|---|
| New Cross Hospital, Wolverhampton | 3DCRT/IMRT | 0 | 1 |
| Guys and St Thomas, London | VMAT | 1 | 0 |
| Western General, Edinburgh | 3DCRT | 0 | 0 |
| Belfast City Hospital | VMAT | 1 | 0 |
| Southend University Hospital, Essex | VMAT | 1 | 0 |
| Royal Shrewsbury Hospital | 3DCRT/IMRT/VMAT | 0 | 0 |
| Basildon and Thurrock University Hospitals | Data unavailable | 0 | 0 |
| Aberdeen Royal Infirmary | VMAT | 0 | 0 |

| Site | Planning Technique | Nb of patients treated with 30Gy/5# | Nb of patients ineligible for SYSTEMS-2 due to inability to generate safe dose escalated plan |
|-------------------------------------|-------------------------|-------------------------------------|---|
| St James University Hospital, Leeds | VMAT | 0 | 0 |
| Churchill Hospital, Oxford | 3DCRT/ IMRT/ VMAT | 0 | 0 |

3.3.3 Glasgow Screening Cohort

Within Glasgow, a total of sixty patients were screened for SYSTEMS-2 between August 2016 and April 2019. Of these, twenty nine patients passed screening and proceeded directly to study registration, twenty two failed screening, two died during the period of analgesia optimisation and seven passed screening, but were not registered for the trial. Data for the patients who failed screening, or who passed but did not enter the study, is shown in Table 3.5.

Of the seven patients who passed screening but were not registered to SYSTEMS-2, four chose not to participate, two were entered into an alternative clinical trial and one suffered a deterioration in their PS prior to registration. (Table 3.5) Of the twenty two patients who failed screening, eight were PS \geq 3, two had undergone previous standard dose radiotherapy at the site of pain and twelve had an inadequate pain score, either at first assessment or after the optimisation of their analgesia. (Table 3.5) The reasons for not entering patients into SYSTEMS-2 following initial screening are summarised in Figure 3.3.

The typical analgesic regimes required to reduce MPM associated pain to a score of $\leq 3/10$ are presented in Table 3.5. Morphine was prescribed in 83% of these patients and three or more different types of painkiller were required in 67% of the cohort, reflecting the poly-pharmaceutical approach required in this disease. Close follow up of this group suggested that pain control deteriorated in a substantial proportion (66.7%) of patients, within weeks or months of the initial control. Of the eight Glasgow patients who experienced a worsening pain score, only three were of adequate PS to be considered for SYSTEMS-2, reflecting the association between pain, disease progression and clinical deterioration. In total, thirty two patients have been registered for SYSTEMS-2 in Glasgow to date, including three patients who initially failed screening.

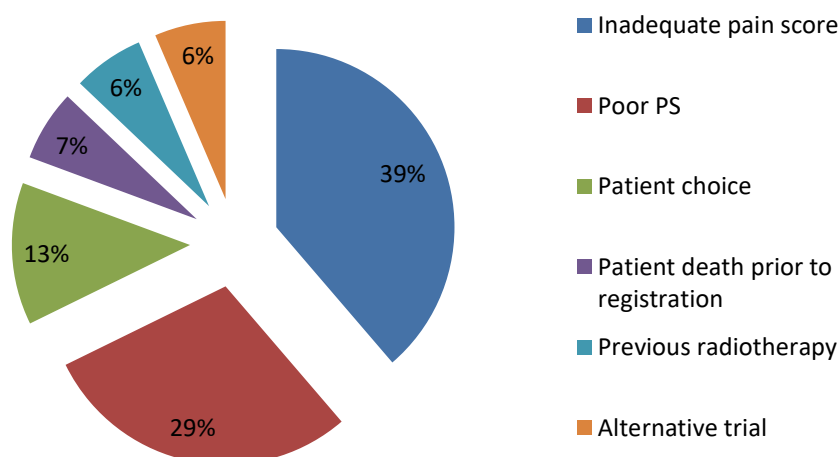


Figure 3.3 Summary of screening outcomes in patients who were not registered for SYSTEMS-2

Data is taken from thirty one patients screened in Glasgow between August 2016 and April 2019. Patients with an inadequate pain score may be re-screened for SYSTEMS-2 should their pain control deteriorate.

Table 3.5 Screening outcomes for patients who did not enter SYSTEMS-2 immediately

| | Referral date | Referral source | Screening outcome | Reason for failing screening | Analgesia regime if pain score $\leq 4/10$ | Pain outcome | Reason for not participating | Other information |
|---|---------------|-----------------|------------------------|--|--|----------------------------------|------------------------------|-------------------|
| 1 | 21/07/2016 | Respiratory | Failed | Poor PS | N/A | N/A | N/A | SFRT |
| 2 | 22/09/2016 | MDT | Failed | Previous RT at site of pain | N/A | N/A | N/A | |
| 3 | 14/10/2016 | MDT | Passed; not registered | N/A | N/A | N/A | Patient declined study | |
| 4 | 01/11/2016 | Oncology | Failed | Poor PS | N/A | N/A | N/A | |
| 5 | 12/12/2016 | Respiratory | Failed | Poor PS | N/A | N/A | N/A | SFRT |
| 6 | 12/12/2016 | Oncology | Failed | Pain score $< 4/10$ after analgesia optimisation | Paracetamol, Shortec | Recurred after 2 months- poor PS | N/A | |

| | Referral date | Referral source | Screening outcome | Reason for failing screening | Analgesia regime if pain score \leq 4/10 | Pain outcome | Reason for not participating | Other information |
|----|---------------|-----------------|-------------------------|---|--|--|------------------------------|--------------------|
| 7 | 12/12/2016 | Oncology | Failed | Pain score <4/10 after analgesia optimisation | Paracetamol, MST, Oramorph, Pregabalin, Lidocaine patch, Dexamethasone | Recurred after 4 months- entered SYSTEMS-2 | N/A | |
| 8 | 22/12/2016 | Respiratory | Died prior to screening | N/A | N/A | N/A | N/A | |
| 9 | 16/01/2017 | Respiratory | Failed | Pain score <4/10 after analgesia optimisation | Paracetamol, MST | No further pain | N/A | |
| 10 | 26/01/2017 | Oncology | Failed | Poor PS | N/A | N/A | N/A | |
| 11 | 07/03/2017 | Oncology | Failed | Pain score <4/10 on initial visit | Paracetamol | No further pain | N/A | Systemic treatment |
| 12 | 17/03/2017 | Respiratory | Failed | Previous RT | N/A | N/A | N/A | Cordotomy |

| | Referral date | Referral source | Screening outcome | Reason for failing screening | Analgesia regime if pain score $\leq 4/10$ | Pain outcome | Reason for not participating | Other information |
|----|---------------|-----------------|------------------------|--|--|------------------------------------|-------------------------------------|-------------------|
| 13 | 21/03/2017 | Oncology | Failed | Pain score $< 4/10$ on initial visit | Paracetamol | No further pain | N/A | |
| 14 | 27/03/2017 | Respiratory | Failed | Poor PS | N/A | N/A | N/A | |
| 15 | 10/05/2017 | Oncology | Failed | Poor PS | N/A | N/A | N/A | SFRT |
| 16 | 17/05/2017 | Oncology | Passed; not registered | N/A | N/A | N/A | Decline in PS prior to registration | SFRT |
| 17 | 26/05/2017 | Oncology | Failed | Pain score $< 4/10$ after analgesia optimisation | Paracetamol, Longtec, Shortec, Lidocaine patch | Recurred after 1 month- poor PS | N/A | |
| 18 | 05/06/2017 | Oncology | Failed | Pain score $< 4/10$ after analgesia optimisation | Paracetamol, Longtec, Shortec, Gabapentin, Lidocaine patch | Recurred after 2 months- SYSTEMS-2 | N/A | |

| | Referral date | Referral source | Screening outcome | Reason for failing screening | Analgesia regime if pain score ≤4/10 | Pain outcome | Reason for not participating | Other information |
|----|---------------|-----------------|-------------------------|---|--|------------------------------------|------------------------------|-------------------|
| 19 | 24/08/2017 | Oncology | Passed; not registered | N/A | N/A | N/A | Patient declined study | |
| 20 | 07/11/2017 | Oncology | Failed | Pain score <4/10 after analgesia optimisation | Paracetamol, MST, Sevredol, Amitriptylline | Recurred after 7 months- poor PS | N/A | |
| 21 | 17/11/2017 | Respiratory | Died prior to screening | N/A | N/A | N/A | N/A | |
| 22 | 27/11/2017 | Oncology | Failed | Pain score <4/10 after analgesia optimisation | Paracetamol, Longtec, Shortec, Pregabalin | Recurred after 4 months- poor PS | N/A | |
| 23 | 03/01/2018 | Oncology | Failed | Pain score <4/10 after analgesia optimisation | Paracetamol, MST, Lidocaine patch | Recurred after 2 months- SYSTEMS-2 | N/A | |

| | Referral date | Referral source | Screening outcome | Reason for failing screening | Analgesia regime if pain score $\leq 4/10$ | Pain outcome | Reason for not participating | Other information |
|----|---------------|-----------------|------------------------|--|---|----------------------------------|------------------------------|-----------------------------|
| 24 | 02/02/2018 | Respiratory | Passed; not registered | N/A | N/A | N/A | Patient declined study | Systemic treatment |
| 25 | 11/05/2018 | MDT | Failed | Poor PS | N/A | N/A | N/A | |
| 26 | 17/05/2018 | MDT | Failed | Pain score $< 4/10$ after analgesia optimisation | Paracetamol, MST, Oramorph, Pregabalin, Lidocaine patch | Recurred after 2 months- poor PS | N/A | SFRT |
| 27 | 08/06/2018 | Respiratory | Failed | Poor PS | N/A | N/A | N/A | |
| 28 | 28/08/2018 | Oncology | Failed | Pain score $< 4/10$ after analgesia optimisation | Paracetamol, Oramorph, Pregabalin | No further pain | N/A | Systemic treatment |
| 29 | 07/01/2019 | Oncology | Passed; not registered | N/A | N/A | N/A | Alternative clinical trial | Given RT off study for pain |

| | Referral date | Referral source | Screening outcome | Reason for failing screening | Analgesia regime if pain score $\leq 4/10$ | Pain outcome | Reason for not participating | Other information |
|----|---------------|-----------------|------------------------|------------------------------|--|--------------|------------------------------|-------------------------------|
| 30 | 13/02/2019 | Oncology | Passed; not registered | N/A | N/A | N/A | Alternative clinical trial | Given RT off study for pain |
| 31 | 12/04/2019 | MDT | Passed; not registered | N/A | N/A | N/A | Patient declined study | Patient declined RT off study |

Data is taken from thirty one Glasgow patients who were screened for SYSTEMS-2, but did not enter the study immediately. Patients were referred between July 2016 and April 2019. The source and date of the referral is indicated, in addition to the screening outcome. Reason for screen failure is given and the analgesic regime of any patient whose pain score was $<4/10$ is shown. Patients who had controlled pain were closely monitored and patients who subsequently became eligible for SYSTEMS-2 are indicated. Eligible patients who did not enter the study are shown, in addition to the reason for not participating. Additional information is provided where relevant. SFRT (single fraction radiotherapy).

3.3.4 Collaborations

The SYSTEMS-2 sample collection has attracted high quality collaborations. Professor Andrew Mellor's translational immunology group in Newcastle are studying levels of Kynurenine and Tryptophan in blood samples to estimate the activity of the intercellular enzyme indoleamine 2,3-dioxygenase (IDO). IDO is believed to have a role in the immune checkpoint pathways and may have the potential to mediate anti-tumour immune activity. Previous studies have suggested that elevated IDO activity is correlated with poor clinical outcomes in several types of cancers. (Godin-Ethier et al., 2011) Furthermore, a recent study assessing fluctuating levels of this enzyme before and after radiotherapy in non-small cell lung cancer suggested that radiotherapy appeared to influence systemic IDO activity and that it exerted a significant impact on metastatic risk and overall survival. (Wang et al., 2018) Following approval from the TMG and the successful provision of a Material Transfer Agreement from both local R&D departments, plasma and serum samples from the Glasgow patient cohort have been sent to Newcastle to allow investigation of the pre- and post- radiotherapy levels of IDO activity in this MPM population. Following the final reporting of SYSTEMS-2, this data could be used to determine whether IDO levels are predictive of clinical response in this disease.

3.4 Discussion

SYSTEMS-2 has been successfully opened at a total of sixteen sites throughout the UK, but set up has been difficult, with a number of sites experiencing similar issues and delays. Furthermore, recruitment to the study has been slow, reflecting the inherent challenges of recruiting to a palliative study in a relatively rare disease.

The primary challenges to site set up and patient recruitment, in addition to the steps taken to overcome them, are outlined below.

3.4.1 Challenges of site set up

3.4.1.1 Staff shortages and capacity issues

Between December 2015 and July 2018, a total of 39 sites were invited to join the SYSTEMS-2 study. Despite very enthusiastic responses, only 38% of these sites have joined to date. (Table 3.3) The main reasons stated for inability to participate have been staff shortages (across medical, radiotherapy planning and clinical trial departments) and a lack of capacity to take on clinical trials within radiotherapy departments. Unfortunately, these issues affected many sites who had expressed an initial interest to participate, including some of the larger centres from areas with a high incidence of MPM, such as Leicester Royal Infirmary, Newcastle, Velindre Hospital (Cardiff), Addenbrookes (Cambridge) and Bristol.

The Christie Hospital, who were expected to participate from study start in 2016, were unable to commit to taking on SYSTEMS-2 due to capacity issues until January 2018. At the time of writing, the process of set-up is still ongoing at this site, working towards opening in summer 2019. The Christie is anticipated to be a significant addition to SYSTEMS-2, given their projected recruitment target of 10-20 patients per year. Furthermore, Leicester Royal Infirmary, who see up to 130 potentially eligible patients per year, have as yet been unable to participate due to lack of thoracic clinical oncology staff and radiotherapy capacity issues. A potential resolution to the problems at Leicester was to set up a formal referral service to Sheffield, which had already opened SYSTEMS-2. Although this initially seemed to be a good solution, no patients have been treated on the study using this pathway. Despite approaching various funding committees, hotel costs could not be secured for these patients who therefore would need to travel for treatment each day. The return distance of 148 miles may serve as a barrier to robust recruitment in this cohort of patients.

The issues surrounding local staff shortages are a government matter and as such cannot readily be influenced for the purposes of this study. Nevertheless, the capacity issues within radiotherapy departments which have represented a

common barrier to the implementation of SYSTEMS-2, along with many other important radiotherapy studies throughout the UK, have been raised with the National Cancer Research Institute Clinical and Translational Radiotherapy Research Group to be addressed at a national level.

3.4.1.2 Perceived lack of requirement

Surprisingly, in addition to staff shortages, an anticipated lack of need for this study was given as a reason for SYSTEMS-2 not to be implemented at Derriford Hospital, Plymouth. The PI confirmed that very few fractions of radiotherapy are given at this centre for pain control and stated that the lung cancer clinic is run alongside the palliative care clinic. As such, it was felt that patients receive excellent palliation and very seldom required irradiation. This statement suggests that good palliative care may be the key to pain control in this disease, further strengthening the approach of analgesia optimisation prior to randomisation.

3.4.1.3 Introduction of the health research authority system

In addition to sites being affected by local issues, set-up at some of the English sites was further hindered by the introduction of the new Health Research Authority system, which was established as an executive non-departmental public body sponsored by the Department of Health on 1 January 2015. The aim of this system is to combine local R&D processes with REC approval. An application was made for SYSTEMS-2 to be added to the Health Research Authority trial portfolio, but the backlog caused by the transition to a new system resulted in a substantial delay.

3.4.1.4 Radiotherapy planning QA

It is acknowledged that the radiotherapy planning for SYSTEMS-2 can be challenging and that it may be difficult to generate an acceptable plan in terms of OAR dosimetry without compromising PTV coverage. A number of sites have

struggled with the radiotherapy planning exercise during the RTTQA assessment process and this has occasionally impacted on trial opening times.

Specific issues raised by sites included whether the OAR constraints needed to be reduced if fewer fractions were delivered and whether it was acceptable to modify the PTV around the organ which was breaching the constraint. Furthermore, some sites were unclear as to whether the PTV could be altered, depending on which treatment regimen the patient received. In terms of contouring, there were also questions raised surrounding margins that needed to be added to treatment volumes. The protocol states that the CTV should be outlined as the area believed to be causing pain and that a margin of 1-2cm should be added to this to create the PTV. In most radiotherapy planning the gross tumour volume (GTV) is outlined for treatment and a margin added to create the CTV, onto which a further margin is added to form the PTV. Since within SYSTEMS-2 we are not aiming to treat the entire GTV this volume was not mentioned in the planning guidelines, which caused confusion.

Throughout this process, queries were answered swiftly and engagement of the radiotherapy planning team at the Beatson West of Scotland Cancer Centre facilitated the sharing of planning solutions, helping to overcome many of these issues. The creation of a Rapidplan model, discussed in Chapter 4, will help to speed up the planning process and ensure that plans are able to meet the required dose constraints at VMAT centres.

3.4.2 Challenges of patient recruitment

Recruitment to SYSTEMS-2 has been slow, even when sites have opened as planned. The collection of screening logs from sites indicates that a number of patients are considered for the study who do not subsequently take part, for a number of reasons.

3.4.2.1 Inadequate performance status

The onset of difficult pain tends to indicate disease progression and is often accompanied by a deterioration in general health and PS. It is not uncommon therefore for patients to fail screening due to an inadequate PS or because they are deemed unlikely to survive for 12 weeks. Analysis of Glasgow screening data indicates that 29% of screen failures are due to poor PS. (Figure 3.3)

When SYSTEMS-2 was first opened in Glasgow, many of the initial consultations, particularly to optimise analgesia, were conducted as home visits. Although this was more convenient for the patient and seemed to be good for recruitment, it was more difficult to accurately determine PS in a patient's home environment. Bringing the same patients to clinic for formal screening or randomisation often served to highlight this discrepancy and a number of these patients did not proceed on the study.

3.4.2.2 Inadequate pain score

Resolution of the worst pain score to <4/10 following analgesia optimisation has been observed throughout all sites and is the most common cause of screen failure (39%) in Glasgow patients to date (Figure 3.3). In addition, some registered patients have failed to be randomised due to inadequate pain scores at their baseline visit. Close monitoring of this group of patients in Glasgow has indicated that pain often returns at a later date, at which point patients may be eligible for SYSTEMS-2. Nevertheless, an associated decline in PS often precludes study entry at this stage.

3.4.2.3 Patient decision not to participate

In the screened Glasgow cohort, 10.3% of eligible patients decided not to participate in SYSTEMS-2. The catchment area of the Beatson West of Scotland Cancer Centre is vast and although patients can be admitted for the duration of their radiotherapy, follow up visits may necessitate travelling significant

distances. This may be an overwhelming prospect in this patient population and is a primary reason quoted for not wishing to participate in the study.

3.4.2.4 Competing trials

In recent months, recruitment to SYSTEMS-2 has been marginally impacted by other studies. In particular, the ATOMIC-Meso study, which opened in Glasgow in August 2018, is the only existing UK trial to offer a specific systemic treatment for sarcomatoid MPM. This subtype of MPM is associated with rapid progression and a very poor prognosis and patients are understandably often very keen to receive treatment within this study. Should these patients also have pain they could receive radiotherapy within the SYSTEMS-2 trial, however the study protocol dictates that systemic treatment is precluded for six weeks after the radiotherapy has been given. At least two patients in Glasgow have recently opted to have standard radiotherapy 'off study' for their pain in order to proceed to systemic treatment more quickly. This issue was discussed at the TMG in January 2019, however the six week 'washout period' after radiation is critical in ensuring that pain responses at week 5 cannot be attributed to any other intervention and is therefore central to study validity.

3.4.3 Measures taken to enhance trial recruitment

3.4.3.1 Trial promotion

Local recruitment to SYSTEMS-2 has been encouraged through the promotion of the study to respiratory, palliative care and oncology colleagues. Oral presentations, delivered at MDTs, lunchtime meetings and designated teaching sessions, have outlined the study aims, recruitment criteria and referral process, to teams at a number of hospitals and hospices throughout the west of Scotland. Furthermore, posters have been distributed to sites for display in clinical areas, to facilitate the advertisement of the trial amongst patient groups who may recognise themselves as being eligible. Given the rapid patient decline observed in the SYSTEMS study, it was also hoped that an enhanced awareness of the study amongst appropriate teams would facilitate the referral of patients at an earlier stage in their disease trajectory.

Promotion has also taken place on a national and international level, with study-specific oral and poster presentations being delivered at a number of conferences, including the British Thoracic Oncology Group conference (2016/17), the European Society of Radiation Oncology conference 2018 and the International Mesothelioma Interest Group meeting (2016/18).

In addition to promoting the study to healthcare professionals, time has also been invested in ensuring that the mesothelioma population and their families are aware of SYSTEMS-2. Annual participation in the June Hancock Mesothelioma Research Fund 'meet the researchers' event allows patients to ask questions about the study and understand more about the role of radiotherapy in the palliation of this disease.

3.4.3.2 Social media presence

The SYSTEMS-2 study website (www.systems-2.co.uk) was set up in 2016. It is a valuable resource which has aided recruitment by ensuring that up to date, accurate trial information is easily accessible to both patients and health care professionals. The website contains useful information on MPM, links to study documentation and the study newsletters. Updates are also provided online about current recruitment status. Regular updates on trial recruitment and site status are also communicated through a SYSTEMS-2 Twitter account.

3.4.3.3 Newsletter

A designated SYSTEMS-2 newsletter is published on a quarterly basis and distributed to all sites that are open or in set up. In addition to providing general updates on trial-specific matters and tips for maximising recruitment, the newsletter includes site-specific recruitment and screening numbers.

3.4.3.4 Extended site number

It was originally planned that SYSTEMS-2 would open at five to eight sites across the UK. Given the delays experienced in site set up and the slow recruitment seen, the number of sites potential sites has been extended to twenty.

3.4.3.5 Protocol amendments

A number of the protocol amendments (section 3.2.9.1) were specifically implemented to facilitate the ease of recruitment to SYSTEMS-2.

3.4.3.6 Study screening logs

These are collected on a monthly basis to provide information on the screening activity at each site.

3.4.3.7 TMG oversight

Recruitment from each site is continuously monitored and discussed within the TMG. Sites identified as being poor recruiters are contacted by the study team to discuss any local barriers to recruitment, and possible resolutions.

3.4.3.8 Webex-conferencing

A webex conference to discuss trial recruitment is planned for summer 2019. All open sites have been invited to participate, in addition to sites in set up. It is hoped that this supportive and positive discussion will help to overcome any problems which are being experienced or any specific barriers to recruitment.

3.4.4 Issues of analgesia optimisation

Whilst the analgesia optimisation step is crucial to the validity of SYSTEMS-2, this process can be associated with a number of challenges in this patient cohort.

3.4.4.1 Polypharmacy

The multifactorial pathophysiology of the pain experienced in MPM often requires the use of a number of different analgesics with alternative mechanisms of action, as illustrated in Table 3.5. Therefore, most SYSTEMS-2 patients are usually on a combination of at least four different regular medications for pain, in addition to medication to take on an 'as required' basis. This elderly population frequently have other comorbidities, for which other long term medications are required and the issue of polypharmacy can result in problems with compliance, side effects and confusion about which medicines to take. This problem is particularly common in patients who live alone, without any support. In order to overcome some of these issues, Glasgow patients are encouraged to keep a clear list of their medications and when they should be taken. Once their analgesia has been fully optimised, a request is made for a 'dosset box' to be provided by their local pharmacy in order to lessen the chance of a patient-related medication error. Patients are also encouraged to keep 'pain diary', in which pain scores and the use of breakthrough analgesia is recorded. In addition to creating an accurate picture of their analgesic requirements, this is also helpful when assessing pain responses. Laxatives are routinely co-prescribed with opioids and oxycodone is often preferentially prescribed over morphine to prevent toxicity, particularly if patients are frail.

3.4.4.2 Multiple healthcare providers

This patient group are often under the care of multiple healthcare professionals, in addition to the research study team. These usually include respiratory, palliative care, oncology and general practitioners. Although one team in particular may take responsibility for optimising analgesia, changes can be made by any of these specialists which can be confusing for patients and makes accurate recording of analgesic requirements difficult for the study team. Furthermore, if analgesia is changed following radiotherapy, this can make the interpretation of pain scores at week 5 challenging and could invalidate results. Within Glasgow, this issue has been addressed by careful communication with all the teams involved in the patient's care. Any changes made to analgesia in clinic

are communicated promptly to the GP and palliative care team by telephone and in writing, to allow accurate update of their online records.

3.4.4.3 Frequent hospital admissions

The long latency period of MPM and its association with industrialised, polluted environments, means that this disease primarily affects an older patient demographic, who frequently have additional comorbidities. These factors, in combination with the aggressive nature of MPM, result in relatively frequent hospital admissions in this vulnerable patient population. During these admissions, analgesia prescriptions are reviewed as part of good medical practise and are sometimes altered on discharge. It is not always clear in these circumstances why changes have been made, which can make accurate recording for trial purposes problematic.

3.4.5 Challenges of pain assessments

MPM is an insidious disease which affects the entire hemithorax and can often result in patients having large areas of pain or multiple sites of discomfort. In this situation, it can be difficult to ascertain the exact location of the 'worst' area of pain, since this is the area which will be scored on the brief pain inventory and targeted for treatment. Usually however, it is possible to treat even relatively large areas of the chest wall within a single PTV and encompass more than one site of pain. On occasion, patients have returned to clinic at week 5 with a new site of discomfort which may now represent their 'worst' area of pain. In this situation, it is paramount that the questions on the brief pain inventory are answered in relation to area which was originally treated and for this reason, patients are talked through this questionnaire carefully, rather than being left to complete it independently.

3.5 Summary

SYSTEMS-2 is the first randomised study of radiotherapy dose escalation to be attempted in MPM, a disease in which research has been chronically underfunded

and for which very few treatment options exist. This important trial recruited its first patient in Glasgow in August 2016 and has subsequently opened at a total of sixteen sites around the UK, recruiting a total of sixty six patients to April 2019. A number of challenges have been encountered, in both site set up and patient recruitment, but the study team have worked hard to address these problems, adopting novel and innovative strategies to overcome them where possible.

Chapter 4: Development of dose constraints for SYSTEMS-2

Chapter aim

This chapter will describe the process through which the OAR dose constraints for the SYSTEMS-2 study were generated and tested.

4.1 Introduction

4.1.1 Selection of hypofractionated radiotherapy regime for SYSTEMS-2

Within SYSTEMS-2, the analgesic properties of two hypofractionated radiotherapy regimes are being compared (20Gy in 5 fractions over 1 week and 36Gy in 6 fractions over two weeks). The dose of 20Gy in 5 fractions is a standard palliative radiotherapy dose used in a number of tumour sites and was the regime used in the original SYSTEMS study. (MacLeod et al., 2015a) This modest dose is tolerable to most radiosensitive organs and was demonstrated in SYSTEMS to be associated with very little toxicity. Delivery is usually achieved with a simple set up of parallel opposed pairs, without the requirement for dosimetry analysis to specific OARs. This allows rapid plan generation and swift administration for symptomatic relief.

The premise behind the selection of a 36Gy in 6 fraction regime for the dose escalated arm of SYSTEMS-2 lies in the assumption that MPM may have a low α/β ratio and therefore may respond more favourably to a larger dose per fraction. The regime of 36Gy in 6 fractions allows a significantly larger dose to be delivered per fraction and facilitates the completion of treatment in a timely fashion, without incurring an unacceptable number of hospital visits.

Dose escalation is associated with an increased potential for normal tissue toxicity. While the poor prognosis of MPM means that most of the patients would not live long enough to develop the problematic late tissue toxicity frequently associated with hypofractionated regimes, the delivery of 6Gy per fraction could still overwhelm cellular repair mechanisms and cause acute toxicities if normal

tissue tolerances are not respected. This may result in unacceptable side effects which could negate the palliative benefit of radiotherapy. The SYSTEMS-2 protocol therefore mandates the use of more sophisticated radiotherapy delivery techniques, such as 3DCRT or IMRT, to facilitate safe dose escalation. While IMRT provides an effective way of shaping dose to the tumour site and allows sparing of OARs, the inverse planning process used with this technique means that unless radiosensitive structures are outlined and allocated an appropriate constraint, the planning system may allow dose to be deposited in these regions, giving rise to hotspots greater than the highest 'prescribed' dose of 36Gy. Consequentially, appropriate dose constraints for a number of OARs needed to be developed and validated for this hypofractionated regime, prior to opening the study.

4.1.2 Established dose constraints for lung radiotherapy

A century of experience with conventionally fractionated radiotherapy has afforded the oncological community a robust appreciation of normal tissue tolerances for 2Gy per fraction regimes. These are outlined in the 2010 QUANTEC (Quantitative Analysis of Normal Tissue Effects in the Clinic) guidelines on an organ by organ basis. (Bentzen et al., 2010) Conversely, there is far less data available to guide dose constraints for safe delivery of hypofractionated treatments.

Moderately hypofractionated radiotherapy regimes (delivering 2.1 - 5Gy per fraction) have been utilised in the treatment of locally advanced non-small cell lung cancer (NSCLC) for a number of years (Thirion et al., 2004) and a regime of 55Gy/20 fractions was approved in the UK by NICE in 2011, despite a lack of established constraints to guide doses to OARs. (Swanick et al., 2015) A comprehensive systematic review published in 2016 by Fleming *et al.* provides a summary of dose-volume constraints for moderately hypofractionated regimes within the lung. (Fleming et al.) Toxicity data from numerous ongoing clinical trials of hypofractionated radiotherapy in NSCLC will provide robust additional information to allow these doses to be further modified in the future.

Ablative radiotherapy regimes (>8Gy per fraction) generally cause cell death on the linear (exponential) portion of the cell survival curve, where tissues have very limited capacity for self-repair. These regimes therefore have a huge capacity to cause acute and late effects and doses delivered to OARs must be carefully considered. (Timmerman, 2008) Stereotactic radiosurgery and intraoperative data in humans and animals have generated toxicity profiles associated with large single doses of radiotherapy, although the applicability of such constraints to regimes which are delivered non-invasively and to undisturbed tissue is debatable. (Timmerman, 2008) More recently, the success of SABR has generated early normal tissue toxicity data which can be used as a starting point to guide practice. Some of the earliest dose constraints for SABR were published by Timmerman in 2008 (Timmerman, 2008), but relative inexperience with the technique at the time and limited long-term follow-up meant that few of these recommendations were validated. Increasing experience with SABR, including within several clinical trials where robust toxicity data can be generated, has permitted the refinement and modification of these constraints. Many studies have reported toxicity data following SABR at various sites which have been summarised in a variety of documents, (Timmerman, 2008, Benedict et al., 2010, Lo et al., 2013) the most comprehensive of which is the AAPM-101 report, published in 2010. (Benedict et al., 2010) In 2017, these recommendations were revised in light of more recent data and published as a UK consensus on normal tissue constraints for SABR. (Hanna et al., 2018) These constraints will undoubtedly be adjusted again in the future as further prospective toxicity data is collected and our understanding of local normal tissue responses to such extreme hypofractionation is developed.

4.1.3 Developing dose constraints for SYSTEMS-2

The dose constraints for SYSTEMS-2 have been generated using local thoracic SABR dose constraints as a guide. The local constraints originated primarily from the Timmerman paper (Timmerman, 2008), but have been adjusted over time, according to local experience. It should be noted however that there are large discrepancies between this palliative study and a SABR approach, particularly in terms of treatment intent, fraction size, total delivered dose and PTV size.

These differences mean that SABR dose constraints could not be directly applied to SYSTEMS-2 and needed modification, to establish radiobiological equivalence.

4.2 Results

4.2.1 Typical PTV sizes for SYSTEMS-2 are an order of magnitude greater than those for SABR

To demonstrate the difference between SABR and SYSTEMS-2 in terms of planning target volume, dosimetric data from the last five patients treated with thoracic SABR at the Beatson West of Scotland Cancer Centre were reviewed. PTV sizes from these plans were compared with the PTV sizes for the five SYSTEMS patients who were re-planned in this study. This data is presented in Table 4.1 and demonstrates that the typical PTV for SYSTEMS-2 is an order of magnitude greater than that seen in SABR.

Table 4.1 Comparative values for planning target volumes in SABR and SYSTEMS-2

| Lung SABR | | SYSTEMS-2 |
|-------------|------------------------------|------------------------------|
| | 56.62 cm ³ | 841.9 cm ³ |
| | 17.27 cm ³ | 636.1 cm ³ |
| | 28.9 cm ³ | 582 cm ³ |
| | 12.12 cm ³ | 1126.3 cm ³ |
| | 65.5 cm ³ | 693.6 cm ³ |
| Mean | 36.082 cm³ | 775.98 cm³ |
| SD | 23.81 cm³ | 218.55 cm³ |

4.2.2 Radiobiological analysis of local SABR dose constraints has guided the development of constraints for a 6 fraction regime within SYSTEMS-2

To conceptualise the radiobiological differences between a SABR regime of 55Gy in 5 fractions and the SYSTEMS-2 regime of 36Gy in 6 fractions, these regimes were expressed in terms of their BED and EQD2. Calculations were performed using an α/β ratio of 10Gy for acute tissue reactions and of 3Gy for late normal tissue toxicity. These values are illustrated in Table 4.2.

Table 4.2 BED and EQD2 for a 55Gy/5 fraction thoracic SABR regime and 36Gy/6 fraction SYSTEMS-2 regime

| Regime | α/β (Gy) | BED | EQD2 |
|------------------|------------------------|-----------------------|---------|
| 55Gy/5 fractions | 3 | 256Gy ₃ | 154Gy |
| | 10 | 115.5Gy ₁₀ | 96.25Gy |
| 36Gy/6 fractions | 3 | 108Gy ₃ | 64.8Gy |
| | 10 | 57.6Gy ₁₀ | 48Gy |

Local thoracic SABR OAR dose constraints are shown in Table 4.3. To determine the comparative radiobiological impact of applying these constraints directly within SYSTEMS-2, parameters of BED and EQD2 were calculated for delivery of the maximum permitted dose to a structure, in either 5 fractions or 6 fractions. For the spinal cord, calculations were performed using an α/β ratio of 2Gy, while for all other organs, late complications were modelled using an α/β ratio of 3Gy and for acute toxicities, an α/β ratio of 10Gy was assumed. These parameters are illustrated in Table 4.3.

Table 4.3 Comparison of maximum SABR OAR dose constraints delivered in 5 or 6 fractions, expressed as EQD2 and BED

| Organ | SABR Constraint | α/β (Gy) | Maximum SABR dose | Radiobiological values for SABR constraint in 5 fractions | Radiobiological values for SABR constraint in 6 fractions |
|-----------------------------|-----------------|---------------------|-------------------|---|---|
| Spinal cord | Dmax 1cc | 2 | 28Gy | EQD2 = 53.2Gy BED = 106.4Gy ₂ | EQD2 = 46.69Gy BED = 93.38Gy ₂ |
| Oesophagus | Dmax 1cc | 3 | 28.5Gy | EQD2 = 49.59Gy BED = 82.65Gy ₃ | EQD2 = 44.18Gy BED = 73.62Gy ₃ |
| | | 10 | 28.5Gy | EQD2 = 37.29Gy BED = 44.75Gy ₁₀ | EQD2 = 35.03Gy BED = 42.04Gy ₁₀ |
| Ipsilateral brachial plexus | Dmax 1cc | 3 | 29Gy | EQD2 = 51.04Gy BED = 85.07Gy ₃ | EQD2 = 45.41Gy BED = 75.7Gy ₃ |
| | | 10 | 29Gy | EQD2 = 38.18Gy BED = 45.82Gy ₁₀ | EQD2 = 35.84Gy BED = 43.01Gy ₁₀ |
| Heart | Dmax 1cc | 3 | 29Gy | EQD2 = 51.04Gy BED = 85.07Gy ₃ | EQD2 = 45.41Gy BED = 75.7Gy ₃ |
| | | 10 | 29Gy | EQD2 = 38.18Gy BED = 45.82Gy ₁₀ | EQD2 = 35.84Gy BED = 43.01Gy ₁₀ |
| Trachea and bronchus | Dmax 1cc | 3 | 35Gy | EQD2 = 70Gy BED = 116.67Gy ₃ | EQD2 = 61.81Gy BED = 103.02Gy ₃ |
| | | 10 | 35Gy | EQD2 = 49.58Gy BED = 59.5Gy ₁₀ | EQD2 = 46.17Gy BED = 55.4Gy ₁₀ |

| Organ | SABR Constraint | α/β (Gy) | Maximum SABR dose | Radiobiological values for SABR constraint in 5 fractions | Radiobiological values for SABR constraint in 6 fractions |
|---------------|------------------|---------------------|-------------------|---|---|
| Great vessels | Dmax 0.5cc | 3 | 53Gy | EQD2 = 144.16Gy BED = 240.27Gy ₃ | EQD2 = 125.4Gy BED = 209Gy ₃ |
| | | 10 | 53Gy | EQD2 = 90.98Gy BED = 109.2Gy ₁₀ | EQD2 = 83.17Gy BED = 99.8Gy ₁₀ |
| Liver | Mean liver dose | 3 | 15.2Gy | EQD2 = 18.36Gy BED = 30.6Gy ₃ | EQD2 = 16.81Gy BED = 28.02Gy ₃ |
| | | 10 | 15.2Gy | EQD2 = 16.52Gy BED = 19.82Gy ₁₀ | EQD2 = 15.87Gy BED = 19.05Gy ₁₀ |
| Kidneys | Mean kidney dose | 3 | 10Gy | EQD2 = 10Gy BED = 16.67Gy ₃ | EQD2 = 9.34Gy BED = 15.57Gy ₃ |
| | | 10 | 10Gy | EQD2 = 10Gy BED = 12.0Gy ₁₀ | EQD2 = 9.73Gy BED = 11.67Gy ₁₀ |
| Stomach | Dmax 0.5cc | 3 | 35Gy | EQD2 = 70Gy BED = 116.67Gy ₃ | EQD2 = 61.81Gy BED = 103.02Gy ₃ |
| | | 10 | 35Gy | EQD2 = 49.58Gy BED = 59.5Gy ₁₀ | EQD2 = 46.17Gy BED = 55.4Gy ₁₀ |
| Small bowel | Dmax 0.5cc | 3 | 35Gy | EQD2 = 70Gy BED = 116.67Gy ₃ | EQD2 = 61.81Gy BED = 103.02Gy ₃ |
| | | 10 | 35Gy | EQD2 = 49.58Gy BED = 59.5Gy ₁₀ | EQD2 = 46.17Gy BED = 55.4Gy ₁₀ |

(Dmax: maximum dose; cc: cubic centimetres)

Initial dose constraints were generated based on the relative concern of inducing acute radiation toxicity within structures and are shown in Table 4.4. For organs where acute toxicity was a particular concern, (oesophagus, stomach, small bowel, liver) the SYSTEMS-2 constraint was kept in line with the EQD2 of the SABR 5 fraction dose limit. Analysis of data for the stomach and small bowel suggested that delivery of the full dose proposed in SYSTEMS-2 (36Gy in 6 fractions, EQD2 = 48Gy; α/β ratio = 10) would not exceed the SABR constraint in these tissues (35Gy in 5 fractions, EQD2 = 49.58Gy; α/β ratio = 10) and therefore the initial constraint on these organs was 36Gy. The SABR constraint to the oesophagus was slightly tighter (28.5Gy in 5 fractions). This was reflected in the SYSTEMS-2 dose constraint of 30Gy, which was radiobiologically similar to that delivered in a SABR regime, assuming an α/β ratio of 10Gy (EQD2 of 30Gy/6 = 37.5Gy; EQD2 of 28.5Gy/5 = 37.3Gy).

A more cautious approach was taken with the dose to the spinal cord, given the serial nature of this organ. Direct application of the SABR constraint of 28Gy affords the radiobiological advantage of dose delivery across a greater number of fractions and reflects the guarded approach that needs to be taken with such tissue.

For organs in which radiation effects were felt to be less likely to result in acute clinical symptoms (e.g. trachea, brachial plexus), the maximum recommended dose was 36Gy. Although for some organs this exceeded the EQD2 of the SABR regime, clinically this was felt to be within safe limits, since the purpose of this exercise was to prevent excessive doses being deposited in these tissues during the inverse planning process. In the case of the contralateral lung constraint, the V5 was increased from <1% to <5%, reflecting the palliative nature of this study.

**Table 4.4 Initial dose constraints for SYSTEMS-2 presented as EQD2 and BED
(SABR constraints presented for radiobiological comparison)**

| Organ | Constraint | α/B (Gy) | SYSTEMS- 2 dose constraints and radiobiological values | SABR dose constraints and radiobiological values |
|-----------------------------------|-------------------|---------------------------------------|---|---|
| Spinal cord | Dmax 1cc | 2 | 28Gy EQD2 = 46.67Gy BED = 93.38Gy ₂ | 28Gy EQD2 = 53.2Gy BED = 106.4Gy ₂ |
| Oesophagus | Dmax 1cc | 3 | 30Gy EQD2 = 48Gy BED = 80Gy ₃ | 28.5Gy EQD2 = 49.6Gy BED = 82.65Gy ₃ |
| | | 10 | 30Gy EQD2 = 37.5Gy BED = 45Gy ₁₀ | 28.5Gy EQD2 = 37.29Gy BED = 44.75Gy ₁₀ |
| Ipsilateral brachial plexus | Dmax 1cc | 3 | 36Gy EQD2 = 64.8Gy BED = 108Gy ₃ | 29Gy EQD2 = 51.04Gy BED = 85.07Gy ₃ |
| Heart | Dmax 1cc | 3 | 36Gy EQD2 = 64.8Gy BED = 108Gy ₃ | 29Gy EQD2 = 51.04Gy BED = 85.07Gy ₃ |
| Trachea and bronchus | Dmax 1cc | 3 | 36Gy EQD2 = 64.8Gy BED = 108Gy ₃ | 35Gy EQD2 = 70Gy BED = 116.67Gy ₃ |
| Great vessels | Dmax 0.5cc | 3 | 36Gy EQD2 = 64.8Gy BED = 108Gy ₃ | 53Gy EQD2 = 144.16Gy BED = 240.27Gy ₃ |

| Organ | Constraint | α/B (Gy) | SYSTEMS- 2 dose constraints and radiobiological values | SABR dose constraints and radiobiological values |
|--------------------|------------------|--------------------|---|---|
| Contralateral lung | V5 | | <5% | <1% |
| Liver | Mean liver dose | 3 | 16Gy EQD2 = 18.14Gy BED = 30.24Gy ₃ | 15.2Gy EQD2 = 18.36Gy BED = 30.6Gy ₃ |
| | | 10 | 16Gy EQD2 = 16.89Gy BED = 20.27Gy ₁₀ | 15.2Gy EQD2 = 16.52Gy BED = 19.82 Gy ₁₀ |
| Kidneys | Mean kidney dose | 3 | 10Gy EQD2 = 9.34Gy BED = 15.57Gy ₃ | 10Gy EQD2 = 10Gy BED = 16.67Gy ₃ |
| Stomach | Dmax 0.5cc | 3 | 36Gy EQD2 = 64.8Gy BED = 108Gy ₃ | 35Gy EQD2 = 70Gy BED = 116.67Gy ₃ |
| | | 10 | 36Gy EQD2 = 48Gy BED = 57.6Gy ₁₀ | 35Gy EQD2 = 49.58Gy BED = 59.5Gy ₁₀ |
| Small bowel | Dmax 0.5cc | 3 | 36Gy EQD2 = 64.8Gy BED = 108Gy ₃ | 35Gy EQD2 = 70Gy BED = 116.67Gy ₃ |
| | | 10 | 36Gy EQD2 = 48Gy BED = 57.6Gy ₁₀ | 35Gy EQD2 = 49.58Gy BED = 59.5Gy ₁₀ |

Further adjustments were made to the constraints in Table 4.4 following review by leading thoracic radiotherapy clinicians at the Beatson West of Scotland Cancer Centre and at the Leeds Cancer Centre (also due to participate in SYSTEMS-2). It was suggested that a contralateral lung V5 of <5% would be unachievable with rotational radiotherapy techniques and the volumetric parameters for contralateral lung dose were therefore adjusted to V20 <10% (and ideally <5%), V10 <50% and V5 <70%. Mean lung dose would be collected from centres for analysis purposes, but no specific constraint was allocated. Dmax constraint for all organs was reduced to 0.5cc to align with current practise. A more cautious approach to the spinal cord was suggested to reflect uncertainties in the precise α/β ratio for this organ. The maximum dose was reduced to 27Gy, allowing for an EQD2 of <50Gy where $\alpha/\beta= 1$ and of <44Gy where $\alpha/\beta= 2$. Finally, the stomach and small bowel constraints were reduced to 30Gy to correspond with the maximal oesophagus dose.

The final dose constraints put forward for planning feasibility studies are shown in Table 4.5.

Table 4.5 Dose constraints submitted to Beatson West of Scotland Cancer Centre radiotherapy department for planning feasibility studies

| Organ | Constraint | SYSTEMS- 2 dose |
|-----------------------------|------------|-----------------|
| Spinal cord | Dmax 0.5cc | 27Gy |
| Oesophagus | Dmax 0.5cc | 30Gy |
| Ipsilateral brachial plexus | Dmax 0.5cc | 36Gy |
| Heart | Dmax 0.5cc | 36Gy |
| Trachea and bronchus | Dmax 0.5cc | 36Gy |

| Organ | Constraint | SYSTEMS- 2 dose |
|--------------------|-------------------|------------------------|
| Contralateral lung | V5 | 70% |
| | V10 | 50% |
| | V20 | 10% |
| Liver | Mean liver dose | 16Gy |
| Great vessels | Dmax 0.5cc | 36Gy |
| Kidneys | Mean kidney dose | 10Gy |
| Stomach | Dmax 0.5cc | 30Gy |
| Small bowel | Dmax 0.5cc | 30Gy |

The anticipated PTV coverage for SYSTEMS-2 plans is shown in Table 4.6.

Table 4.6 Expected PTV coverage

| | Constraint | Prescribed dose |
|-------------|-------------------|------------------------|
| PTV minimum | D98% | 95% |
| PTV median | D50% | 100% |
| PTV maximum | D2% | 107% |

4.2.3 VMAT planning studies highlight the challenge of achieving adequate PTV coverage without breaching OAR dose constraints

To test the deliverability of the proposed SYSTEMS-2 dose constraints, a planning feasibility study was conducted at the Beatson West of Scotland Cancer Centre prior to study opening. Five patients who had taken part in the original SYSTEMS study were selected on the basis of the close proximity of critical OARs to the PTV. Organs were contoured according to the radiotherapy planning guidelines and VMAT planning was conducted using Eclipse planning system version 15.5. The doses achieved in this exercise are shown in Table 4.7.

Adequate PTV coverage was achieved in 2/5 patients (Patient 3 and Patient 5), however, this was associated with OAR breaches in both. In Patient 3, the contralateral lung V5 was 73.6% (constraint: V5< 70%) and in Patient 5, the oesophageal dose exceeded the constraint of 30Gy to 0.5cc by 4.7Gy. In Patients 2 and 4, all OAR constraints were met, but the D98% of >95% was not achieved (94.6% and 94% in Patients 2 and 4 respectively). In Patient 1, PTV coverage was suboptimal (D98%= 92.8%) and dose to 0.5cc of oesophagus (32.2Gy) breached the objective.

Table 4.7 Dosimetry data from VMAT planning studies undertaken on 5 patients from the original SYSTEMS trial

| Organ | Constraint | Maximum Dose | Pt 1 | Pt 2 | Pt 3 | Pt 4 | Pt 5 |
|-----------------------------|---------------|--------------|-------------|------|------|------|-------------|
| Spinal cord | Dmax 0.5cc | 27Gy | 26.3 | 6.6 | 21.9 | 14.2 | 26.9 |
| Oesophagus | Dmax 0.5cc | 30Gy | 32.2 | 14 | 15.8 | 19.5 | 34.7 |
| Ipsilateral brachial plexus | Dmax 0.5cc | 36Gy | 33.7 | 0.2 | 3.8 | 2.4 | 0.4 |
| Heart | Dmax 0.5cc | 36 Gy | 16.4 | 24.8 | 25.4 | 34.9 | 29.5 |

| Organ | Constraint | Maximum | Pt 1 | Pt 2 | Pt 3 | Pt 4 | Pt 5 |
|-----------------------------------|------------------|---------|-------------|-------------|-------------|-----------|---------|
| | | Dose | | | | | |
| Trachea | Dmax 0.5cc | 36Gy | 25.8 | 0.8 | 17.4 | 14 | 10.3 |
| Bronchus | Dmax 0.5cc | 36Gy | 20.5 | 15.6 | 18.8 | 31.1 | 33.4 |
| Great vessels | Dmax 0.5cc | 36Gy | 22.3 | 12.7 | 19.9 | 35.4 | 22.8 |
| Contralateral lung | <70% | V5Gy | 57 | 13.4 | 73.6 | 67.1 | 21.5 |
| | <50% | V10Gy | 7 | 0 | 2.8 | 7.4 | 0.1 |
| | <10% | V20Gy | <0.1 | <0.1 | <0.1 | <0.1 | <0.1 |
| Liver | Mean Liver Dose | 16Gy | 0.2 | 2.5 | 0.4 | 1.4 | 5.3 |
| Kidneys (individual and combined) | Mean Kidney Dose | 10Gy | 0.2 | 0.5 | 0.3/0.2 | 0.3/0.2 | 0.9/1.3 |
| Stomach | Dmax 0.5cc | 30Gy | 0.4 | 14 | 2 | 15.7 | 10.1 |
| Small bowel | Dmax 0.5cc | 30Gy | 0.3 | 6.4 | 0.9 | 0.7 | 1.5 |
| PTV | D98% | >95 | 92.8 | 94.6 | 98 | 94 | 95.8 |
| | D50% | 100 | 101.5 | 100.9 | 102 | 100 | 100.8 |
| | D2% | <107 | 106.7 | 104.8 | 106.1 | 105 | 106.7 |

(Instances where the dose constraint could not be met are highlighted in red)

4.2.4 Planner experience impacts on the quality of a SYSTEMS-2 radiotherapy plan

To determine the impact of planner experience on the quality of radiotherapy plans which could be generated, further VMAT planning was undertaken for the same five patients in March 2019, when SYSTEMS-2 had been open in Glasgow for over 2.5 years. This work was conducted by the same planner who undertook the original VMAT planning work and who has been responsible for planning most of the Glasgow SYSTEMS-2 cohort to date. The plans met all of the prescribed PTV constraints without breaching any OAR constraints. The dosimetry achieved is shown in Table 4.8.

Table 4.8 Dosimetry data from VMAT planning studies undertaken in March 2019

| Organ | Constraint | Maximum Dose | Pt 1 | Pt 2 | Pt 3 | Pt 4 | Pt 5 |
|-----------------------------|---------------|--------------|------|------|------|------|------|
| Spinal cord | Dmax 0.5cc | 27Gy | 26.8 | 6.8 | 18 | 14.6 | 26.1 |
| Oesophagus | Dmax 0.5cc | 30Gy | 26.7 | 14.3 | 18.2 | 20.2 | 27.7 |
| Ipsilateral brachial plexus | Dmax 0.5cc | 36Gy | 35.5 | 0.3 | 3.3 | 2.6 | 0.4 |
| Heart | Dmax 0.5cc | 36Gy | 15 | 19.5 | 27.2 | 34.8 | 19.4 |
| Trachea | Dmax 0.5cc | 36Gy | 25.1 | 0.8 | 18.3 | 14.6 | 8.9 |
| Bronchus | Dmax 0.5cc | 36Gy | 22.0 | 18.1 | 25.8 | 32.8 | 33.1 |
| Great vessels | Dmax 0.5cc | 36Gy | 26 | 12.3 | 22.1 | 35.3 | 25.1 |

| Organ | Constraint | Maximum Dose | Pt 1 | Pt 2 | Pt 3 | Pt 4 | Pt 5 |
|--------------------|------------------|--------------|-------|-------|-------|-------|-------|
| Liver | Mean Liver Dose | 16Gy | 0.2 | 2.5 | 0.3 | 8.4 | 4.8 |
| Stomach | Dmax 0.5cc | 30Gy | 0.3 | 14.2 | 1.7 | 2.2 | 9.6 |
| Small bowel | Dmax 0.5cc | 30Gy | 0.2 | 6.4 | 0.7 | 0.2 | 1.1 |
| Contralateral lung | <70% | V5Gy | 66.3 | 2.5 | 60 | 67.2 | 46.9 |
| | <50% | V10Gy | 13.4 | 3.3 | 7.5 | 7.7 | 6.6 |
| | <10% | V20Gy | <0.1 | 5.5 | <0.1 | <0.1 | <0.1 |
| Kidneys | Mean Kidney Dose | 10Gy | 0.1 | 0.5 | 0.3 | 0.2 | 0.7 |
| PTV | D98% | >95 | 95.3 | 95.1 | 95.6 | 98 | 96 |
| | D50% | 100 | 100.7 | 101.4 | 101 | 101.3 | 101.1 |
| | D2% | <107 | 104 | 105.3 | 106.1 | 106 | 106.2 |

(Improvements in OAR dose or PTV coverage (compared to Table 4.7) are shown in green. Increases in the OAR dose from the original plan are shown in blue. All OAR dose constraints were met.)

Improved PTV coverage was associated with an increase in D98% in 4/5 patients and a reduction in D2% for 2/5 patients. (Table 4.8) The DVH shown in Figure 4.1 illustrates the improvement in PTV coverage achieved for Patient 1, where D98% was increased from 92.8% to 95.3% and D2% was reduced from 106.7% to 104%.

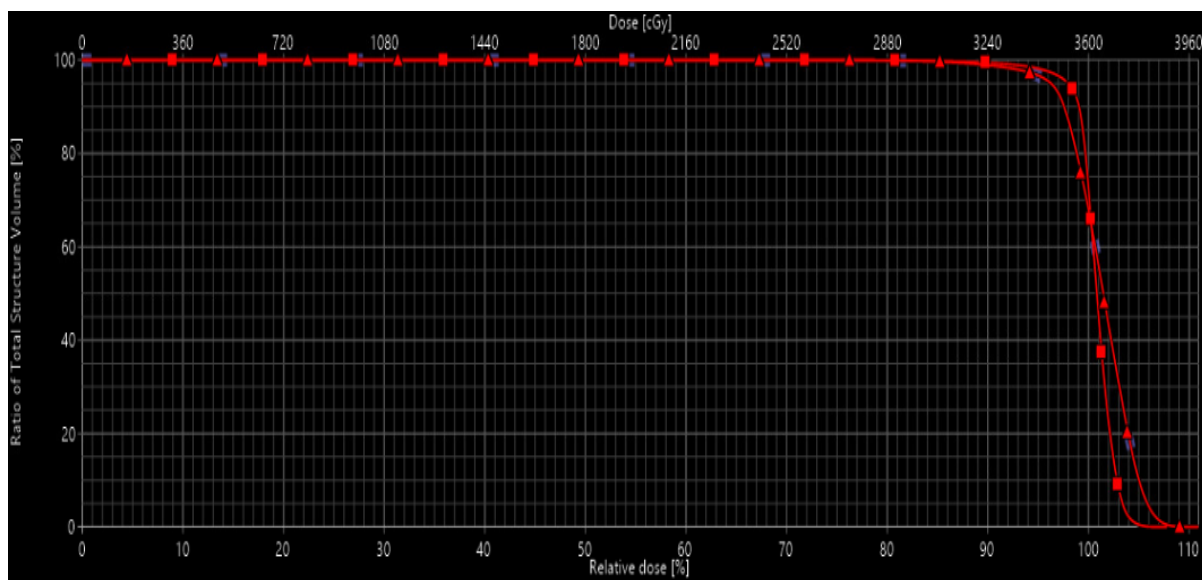


Figure 4.1 DVH illustrating the improvement in PTV coverage achieved for Patient 1

Original plan (triangles); March 2019 plan (squares)

Reductions were seen in dose deposition within a number of structures in the VMAT re-plans. For example, in Patient 5, dose to 0.5cc of oesophagus was reduced from 34.7Gy in the original VMAT plan to 27.7Gy in the March 2019 plan (Figure 4.2), while dose to 0.5cc of heart was reduced from 29.5Gy to 19.4Gy in the same patient. These improvements were marginally offset by an increase in contralateral lung dose (V5 increased from 21.5% to 46.9% and V10 from 0.1% to 6.6% in the original and March 2019 plans respectively). Nevertheless, these doses were still well within the trial specific constraints and the improvement in the oesophageal dose to <30Gy to 0.5cc meant that this plan satisfied all objectives. In Patient 3, the contralateral lung V5 was reduced from 73.6% to 60%, (Figure 4.3) which allowed this plan to meet the objective of V5 <70%. The V10 was increased from 2.8% to 7.5%, but this was still well below the trial objective of V10 <50%.

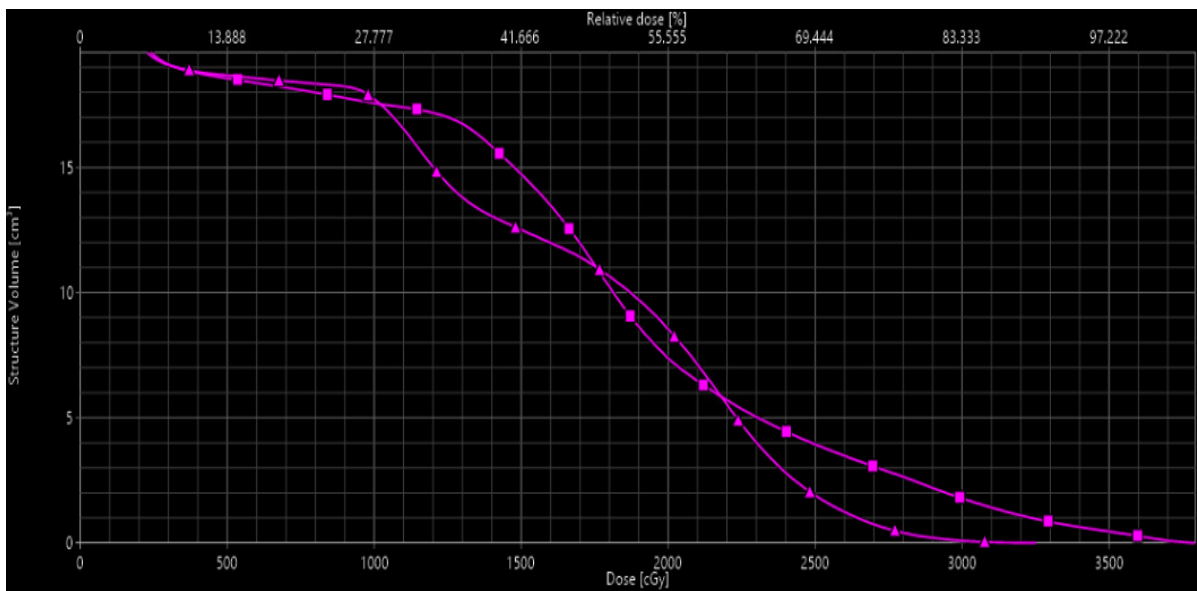


Figure 4.2 DVH showing improvements in oesophageal dose for Patient 5

Original plan (squares); March 2019 plan (triangles)

36Gy/6 plan (Original)

36Gy/6 plan (March 2019)

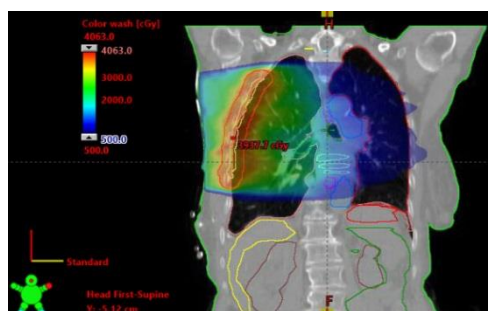


Figure 4.3 Plan showing distribution of dose to 5Gy

Contralateral lung V5 is reduced from 73.6% in original plan to 60% in March 2019.

4.3 Discussion

4.3.1 Clinical considerations of the SYSTEMS-2 dose constraints

There are little data to support precise dose constraints to OARs for hypofractionated radiotherapy regimes, particularly in the palliative setting. Nevertheless, clinically relevant data has been generated from increasing experience with SABR. Whilst SYSTEMS-2 is not directly comparable to SABR, the radiobiological analysis of doses tolerated within a locally delivered 5 fraction SABR regime has permitted a conversion to acceptable doses for a 6 fraction regime. Particular attention has been paid to organs in which acute toxicity could cause symptoms and caution has been applied to the dose delivered to the radio-intolerant spinal cord.

The majority of the dose constraints listed in the local SABR guidelines are quoted as the maximum volume of an organ which can receive a threshold dose or higher (Dmax to 'x'cc). Direct conversion of this dose using the EQD2 principle allowed the generation of applicable dose constraints for SYSTEMS-2, using the same volumetric parameters. Dmax 0.5cc represents a volume which is both clinically realistic and comparable when calculated across different planning systems and is therefore appropriate to apply to a multicentre clinical trial. In the case of parallel organs, such as the lungs, percentage volumetric constraints are often more appropriate to guide the maximum percentage of an OAR that can receive a threshold dose or higher. Published toxicity data on IMRT in mesothelioma (Allen et al., 2006, Miles et al., 2008, Rice et al., 2007a), in addition to local clinical experience with SABR and moderately hypofractionated thoracic radiotherapy regimes, has permitted development of clinically appropriate contralateral lung constraints for SYSTEMS-2. Given the anticipated PTV sizes associated with SYSTEMS-2 and the potential for a greater volume of any OARs to be irradiated, percentage dose volume metrics may be a more appropriate guide for some parallel organs. The challenge of adopting clinically appropriate percentage volumetric dose constraints in novel hypofractionation regimes has been acknowledged in the QUANTEC guidelines, (Bentzen et al., 2010) but SYSTEMS-2 will provide a robust mechanism through which such data

can be generated, by allowing correlation of toxicity outcomes with achieved volumetric parameters.

It could be argued that the SYSTEMS-2 doses are overly cautious, particularly for the spinal cord and oesophagus, especially if interpreted in the context of the recently published UK consensus document. (Hanna et al., 2018) Constraints quoted for these organs within a 5 fraction regime are more generous than in our local guidance (30Gy for spinal cord and 34Gy for oesophagus compared to 28Gy and 28.5Gy respectively within the local protocol). Radiobiologically, this would equate to EQD2 of 60Gy for spinal cord (α/β ratio= 2) and 47.6Gy for oesophagus (α/β ratio= 10). Nevertheless, as illustrated in Table 4.1, PTV size in SYSTEMS-2 will be far greater than that accepted for a SABR regime and therefore it is appropriate to remain cautious.

Of the four organs permitted to receive the full dose of 36Gy in 6 fractions (EQD2 64.8Gy where $\alpha/\beta= 3$; 48Gy where $\alpha/\beta= 10$), the trachea/proximal bronchus and great vessels are within the EQD2 dose of the SABR regime (70Gy and 144Gy respectively where $\alpha/\beta=3$; 49.6Gy and 91Gy where $\alpha/\beta=10$). In contrast, the ipsilateral brachial plexus and heart exceed the EQD2 dose of a SABR regime (51.04Gy in both organs where $\alpha/\beta=3$; 38.18Gy where $\alpha/\beta=10$).

In standard lung radiotherapy, planned and delivered locally by VMAT, the brachial plexus is not classified as an OAR. Radiobiologically, this standard lung regime of 55Gy in 20 fractions is similar to that delivered in SYSTEMS-2 (EQD2 = 63.25Gy and 64.8Gy respectively where $\alpha/\beta=3$) and therefore it was felt this organ could tolerate full dose to a constraint of 0.5cc.

Radiation induced heart disease (RIHD) can have devastating consequences following the administration of radical doses of radiotherapy, particularly in lung and breast cancers. (Madan et al., 2015) The dose constraints of a SABR regime in particular, would be modelled around the prevention of this complication,

given the curative intent of treatment. Analysis of the recently published UK SABR consensus guidelines suggests that an 8 fraction regime should have a maximum heart dose of <50Gy (optimal) and <60Gy (mandatory). Radiobiologically, this equates to an EQD2 of 92.5Gy and 126Gy respectively, using an α/β ratio of 3. For comparison, the SYSTEMS-2 dose constraint has an EQD2 of 64.8Gy ($\alpha/\beta= 3$). The latency period associated with RIHD is in the region of 10-15 years (Madan et al., 2015) and therefore patients participating in SYSTEMS-2 are unlikely to live long enough to develop these long term complications.

More recently published data, however, has suggested that radiation to the heart may be associated with more acute toxicity than previously appreciated. A paper published by Atkins *et al* in 2019 suggests that in lung cancer patients, treated with radical thoracic radiotherapy, mean heart dose was associated with a statistically significant increased risk of major adverse cardiac events. (Atkins et al., 2019) Within the median follow up period of 20.4 months, 10.3% of patients had developed an acute cardiac event, including myocardial infarct, heart failure, requirement for re-vascularisation and cardiac-specific death. In patients with pre-existing cardiac risk factors, the risk of adverse cardiac events was increased and critically, no threshold dose was identified below which there was no risk. Advances in systemic therapy has led to improved outcomes in locally advanced NSCLC, with median survival times of more than 2 years. (Bradley et al., 2015, Senan et al., 2016) The identification of clinically significant post-radiotherapy cardiac events in a more condensed time-frame than tends to be seen following the treatment of other cancers, such as breast or lymphoma, (van Nimwegen et al., 2015, Darby et al., 2013) has prompted the requirement for early recognition and treatment of cardiac-related events and stricter planning criteria to lower heart doses in thoracic radiotherapy for NSCLC. Whilst the SYSTEMS-2 cardiac dose constraint of 36Gy in 6 fractions to 0.5cc was felt to be clinically acceptable in this palliative study of mesothelioma patients, future radiotherapy studies in this cohort would likely need to adopt similar strategies in cardiac risk assessment and dose modification.

No dose constraint has been applied to the ipsilateral (treated) lung for several reasons. Firstly, the pleural thickening associated with MPM reduces the capacity for lung expansion on the affected side. This, in combination with other features of this disease including pleural fluid collections and areas of collapse mean that the baseline functional reserve in the ipsilateral lung is often poor. Secondly, areas of chest wall pain can be extensive and the size of the PTV often reflects this. It was felt that implementation of a dose constraint on the affected side would therefore be futile. Since the ipsilateral lung is not required to be outlined for planning purposes, dosimetric data (e.g. mean lung dose, V20) is not being collected. In contrast, dose constraints to the contralateral lung have been carefully selected and whilst there is no constraint denoted for contralateral mean lung dose, this is being collected from sites to permit retrospective analysis. Although dose escalated, hypofractionated radiotherapy has never been attempted in MPM, IMRT has been used to deliver radical doses of conventionally fractionated radiotherapy to the pleural surface following surgical resection for a number of years, particularly in the United States. Publication of toxicity data from 3 large institutions utilising this technique reported unacceptably high rates of fatal pneumonitis. (Miles et al., 2008, Rice et al., 2007a, Allen et al., 2006) As a result, contralateral lung dose is now carefully considered, in particular V20, which has a statistically significant predictive association with pneumonitis. (Rice et al., 2007a)

Whilst the contralateral lung constraints are slightly more lenient than suggested for V5 and V20 in a SABR regime, this reflects the palliative nature of SYSTEMS-2. Nevertheless, the ability to generate a largely unilateral plan despite a rotational delivery technique, means that the V20 is often negligible and this is clearly illustrated in Table 4.7.

Since SYSTEMS-2 opened to recruitment, dose constraints for two hypofractionated radiotherapy regimes in MPM have been published. (Gomez et al., 2019, Parisi et al., 2017) These regimes, both of which deliver radiotherapy to the entire hemithorax, are more closely aligned to SYSTEMS-2 in terms of dose per fraction, than a SABR protocol. Constraints used by Marc de Perrot's team to

deliver accelerated hemithoracic radiotherapy (25Gy in 5 fractions with an optional 5Gy integrated boost to GTV and tract sites) to 62 patients in the 'SMART' study (Cho et al., 2014, de Perrot et al., 2016) were recently published by Gomez *et al.* (Gomez et al., 2019) These constraints are generally more conservative than those employed in SYSTEMS-2, particularly in terms of the dose to the contralateral lung ($V_7 < 20\%$) and spinal cord ($D_{max} < 22\text{Gy}$). Furthermore, doses to heart and liver are individualised depending on disease location and constraints are determined for maximum structure dose, rather than maximum dose to 0.5cc of structure. This cautious approach reflects the radical nature of this study, in which patients are required to undergo extensive surgery within a week of completing radiotherapy, and potentially chemotherapy, depending on post-operative nodal staging. Furthermore, the life expectancy of this patient cohort is likely to be longer than that anticipated in SYSTEMS-2 and therefore late normal tissue toxicity has to be considered.

In 2017, Parisi *et al* published constraints employed to deliver 25Gy in 5 fractions, with an inhomogeneous boost to the GTV of 37.5Gy to 36 patients after PD or biopsy for MPM. (Parisi et al., 2017) These dose constraints, which are quoted in terms of EQD2, are more closely aligned to those employed in SYSTEMS-2. The doses to the contralateral lung ($V_5 < 5\%$) and spinal cord (EQD2 25Gy, α/β ratio= 3) are more conservative, but greater doses are permitted to the oesophagus, kidney and liver than are acceptable for SYSTEMS-2.

The discrepancies between these published constraints reflect not only differences in treatment volumes and intent, but also the lack of established data on which to base them. The rigorous setting of a clinical trial, where toxicity data is collected at regular intervals, is the optimal setting in which to test the safety of the SYSTEMS-2 dose constraints, and to generate comparative data to the regimes employed by de Perrot and Parisi.

4.3.2 A planning study of five cases suggests that the SYSTEMS-2 PTV constraints are challenging to meet without breaching OAR constraints

The protocol for SYSTEMS-2 states that OAR dose constraints should be used as a guide for radiotherapy planning, but that the dose to the PTV should not be compromised to meet them. This approach could be criticised in a study of palliative intent and results in a more complex radiotherapy planning process. Nevertheless, ensuring that the PTV received the intended fixed total dose across all dose escalated plans was felt to be an important factor in aiding accurate data interpretation and maintaining study validity in this randomised controlled trial. The use of alternative dose escalation approaches, such as isotoxic radiotherapy planning, would result in different dose escalated regimes being delivered to the PTV and may not generate sufficiently robust data to answer the relatively simple research question posed in SYSTEMS-2.

Within this planning study, the SYSTEMS-2 dose constraints were tested on five patients who took part in the initial SYSTEMS study. Capacity within the radiotherapy planning unit at the Beatson West of Scotland Cancer Centre, combined with time constraints, meant that re-planning more patients was not feasible. Cases were specifically selected as being challenging from a radiotherapy planning perspective, in terms of PTV size and location. Therefore, while the limited number of cases in this planning study could be criticised, they permitted robust initial testing of the dose constraints.

Not all of the proposed dose constraints could be met for every patient who was planned with VMAT and there was difficulty meeting a D98% of 95% in 3/5 patients. In Patients 1 and 5, the oesophageal dose breached the constraint of 30Gy to 0.5cc. Both of these patients had bulky tumours which abutted the oesophagus for several centimetres. In the case of Patient 5, the oesophagus was within the PTV for 2 centimetres. In Patient 3 the V5 was slightly in excess of the V5 constraint of 70%. Nevertheless, the favourable dosimetry achieved for V10 and V20 means that this plan may have been clinically acceptable.

The difficulty in achieving the required PTV coverage in this planning study was concerning, nevertheless, in a clinical situation these plans would have been formally reviewed by clinical staff in conjunction with the radiotherapy planner and compromises could have been made to OAR constraints in an attempt to ensure adequate PTV coverage. The final decision to accept the plan lies with the treating clinician and if there are concerns about doses to OARs then the final dose can be omitted, treating to 30Gy in 5 fractions in the dose escalated arm. It was accepted that for some plans it may be difficult to achieve all the OAR constraints and a clinical decision would need to be made at that point as to whether to treat to a total dose of 36Gy or 30Gy. The results from this initial planning study were therefore felt to be representative of the likely real-life scenario and the proposed constraints were accepted and taken forward to be used in SYSTEMS-2.

4.3.3 The quality of the radiotherapy plan is influenced by the familiarity of the planner with SYSTEMS-2 planning

Since SYSTEMS-2 opened in Glasgow in August 2016, thirty two patients have been treated locally and at the time of writing, there have been no patients for whom concerns about PTV size or dose delivery to OARs have prevented randomisation or necessitated a dose reduction to 30Gy/5 fractions. This perhaps reflects the dosimetry advantages gained from familiarity with a planning technique. The observation that clinically superior plans can be produced if a planner is familiar with the planning technique has been noted in other studies utilising IMRT in MPM and has been linked with a reduction in toxicity. (Patel et al., 2012) Data from the planning studies conducted in March 2019 supports the suggestion. All five VMAT plans, generated from patients who had participated in the original SYSTEMS study, had originally failed to meet trial constraints. This was due to inadequate PTV coverage, excessive OAR doses, or both. When the same five patients were re-planned using the same treatment planning system, to the same dose and fractionation, by the same planner with the benefit of over two years experience with SYSTEMS-2 radiotherapy planning, all plans met the specified PTV prescription and OAR constraints.

The challenge presented by the complexity of the SYSTEMS-2 radiotherapy plans was felt to be a potential barrier to site engagement with the study and subsequently to patient recruitment. In order to help other centres overcome any difficulties with the radiotherapy planning, the physics department at the Beatson West of Scotland Cancer Centre have been able to share their planning solutions and are currently developing a RapidPlan model which can be shared with any site running SYSTEMS-2 with VMAT or IMRT. It is anticipated that this will facilitate the rapid generation of high quality, robust plans, enabling patients to be treated quickly within the study.

4.4 Summary

Novel dose constraints for the delivery of hypofractionated, dose escalated radiotherapy within a UK-wide clinical trial have been generated. The robust nature of a randomised clinical trial will provide the perfect setting in which the safety of these selected doses can be adequately tested.

Chapter 5: Assessing the impact of MCO on SYSTEMS-2 dose escalated VMAT plans

Chapter aim

This chapter aims to determine whether MCO can be used to improve the quality of dose escalated clinical VMAT plans generated for the Glasgow cohort of SYSTEMS-2.

5.1 Introduction

Within the SYSTEMS-2 study, radiotherapy is targeted specifically at sites of pain. In some patients, painful areas coincide with specific areas of bulky disease, rib infiltration or chest wall involvement, which can be encompassed within a relatively modest treatment volume. In many cases however, the pathophysiology of pain is multifactorial, arising from a combination of nerve involvement, disseminated pleural disease and the infiltration of local structures. This gives rise to a more diffuse pattern of pain, frequently involving large regions of the chest wall and necessitates a more extensive treatment volume. Furthermore, nerve root involvement can often give rise to neuropathic pain and adequate treatment of this necessitates close proximity of the CTV to critical radiosensitive structures.

The selection of the OAR dose constraints for SYSTEMS-2 has been discussed in Chapter 4. They are particularly cautious, due to concerns about the induction of acute toxicities with this novel dose/fractionation regime, which could negate any palliative benefit of the treatment. The use of IMRT/VMAT also introduces the issue of dose bathing and therefore all organs are allocated a constraint to prevent excessive dose being deposited within them during the inverse planning process. These multiple constraints, in addition to a large PTV in close proximity to OARs, makes the radiotherapy planning difficult and time consuming and the inability to generate a clinically acceptable dose escalated plan has been recorded as a reason for patient ineligibility.

MCO has been demonstrated in a number of studies to lower radiation doses to OARs without compromising PTV coverage and has improved on both IMRT and VMAT plans within a number of tumour types, including prostate, pancreatic, glioblastoma and non-small cell lung cancer. (Teichert et al., 2019, Wala et al., 2013, Kamran et al., 2016, Muller et al., 2017) Time taken to produce a clinically acceptable plan is also reported to be reduced with this planning solution. (Teichert et al., 2019, Muller et al., 2017, Craft et al., 2012b) MCO software was introduced at the Beatson West of Scotland Cancer Centre in September 2017, but is not routinely used for planning SYSTEMS-2 patients. All of the SYSTEMS-2 Glasgow cohort have been planned with VMAT and would be candidates for re-optimisation with MCO. Furthermore, regardless of the dose which was actually delivered, all trial patients have a clinically acceptable dose escalated plan generated prior to randomisation. A planning study was therefore undertaken using dose escalated clinical plans to determine whether MCO could achieve any further reductions in OAR dose without compromising PTV coverage.

5.2 Results

5.2.1. MCO generated clinically superior radiotherapy plans for the majority of SYSTEMS-2 patients

To determine the value of MCO in reducing doses to OARs, the dose escalated VMAT radiotherapy plans of 20 patients from the Glasgow cohort of the SYSTEMS-2 study were identified and analysed with MCO. Plans which improved OAR sparing without breaching any trial specific dose constraints or compromising PTV coverage were deemed to be acceptable. Plans which were identified as 'failing' (i.e. those breaching any OAR constraint or failing to comply with the prescribed PTV coverage) were re-analysed through MCO a number of times to investigate whether dose distribution could be improved. Following this process, thirteen MCO plans were generated that improved OAR sparing compared to the clinical plans, whilst maintaining the PTV coverage. Seven plans were deemed to be unacceptable.

The dose reductions achieved by MCO in those plans which passed this planning study are shown in Tables 5.1 and 5.2 and Figures 5.1 and 5.2. Due to the limited number of acceptable plans, formal statistical analyses were not performed and descriptive statistics are used to describe this data. Clinically significant reductions in mean dose to OARs were observed in a number of cases. For example, a dose reduction of 599cGy was achieved in the mean dose to liver (patient 11) and of 670cGy in mean dose to stomach (patient 5). Furthermore, notable dose reductions to contralateral lung were achieved, including a 34% reduction in V5 (patient 7) and a 23% reduction in V10 (patient 3). The maximum point dose and maximum dose to 0.5cc of the OAR were also dramatically reduced in a number of cases and to a number of structures. This improvement is particularly relevant for serial organs, such as the spinal cord which can lose their complete functionality if even a small volume receives a dose above the tolerance limit. In the case of patient 11, for example, a maximal point dose reduction of 613cGy and 0.5cc dose reduction of 569cGy to the spinal cord was achieved. Clinically relevant reductions in cord dose were also seen in patients 1, 2, 6 and 13.

5.2.2 No predictive pattern was identified between PTV location and MCO dose sparing

To determine whether MCO is more effective at sparing structures contralateral or ipsilateral to the PTV, data were analysed according to the hemithorax which required radiotherapy. Similar levels of sparing were observed in a number of bilateral structures regardless of the side of the PTV. For example, in patients requiring radiotherapy to the left hemithorax, mean bronchial dose was reduced by an average of 191cGy±281cGy (left) and 198cGy±222cGy (right) (Table 5.1 and Figure 5.1A) and in patients with right sided disease, this reduction was 149cGy±186cGy and 145cGy±145cGy (left and right main bronchi respectively). (Table 5.2 and Figure 5.2A)

Analysis of the sparing achieved for unilateral structures revealed variable results. The average reduction in mean stomach dose was similar regardless of the side of the PTV: 298cGy± 272cGy in patients with left sided MPM, (Table 5.1

and Figure 5.1A) and $279\text{cGy} \pm 178\text{cGy}$ for those with right sided disease. (Table 5.2 and Figure 5.2A) For some structures, more effective ipsilateral dose sparing was observed. For example, in patients with right sided MPM, mean liver dose was reduced by an average of $267\text{cGy} \pm 239\text{cGy}$, (Table 5.2 and Figure 5.2A) compared to $136\text{cGy} \pm 107\text{cGy}$ in left sided disease. (Table 5.1 and Figure 5.1A) For other structures, contralateral dose sparing was predominant: mean heart dose was reduced by an average of $171\text{cGy} \pm 94\text{cGy}$ in left sided disease, (Table 5.1 and Figure 5.1A) compared to $300\text{cGy} \pm 189\text{cGy}$ on the right. (Table 5.2 and Figure 5.2A)

Table 5.1 Changes to OAR doses achieved with MCO in left sided MPM

| Organ/constraint | Patient | | | | | | Mean | Standard Deviation |
|--------------------|---------|------|------|-------|------|------|----------------|--------------------|
| | 1 | 2 | 3 | 4 | 5 | 6 | | |
| PTV | | | | | | | | |
| D98 (%) | 0.6 | 1 | 0.2 | 2.3 | 0.1 | -0.1 | 0.68 | 0.88 |
| D50 (%) | -1.6 | 0.6 | 1.7 | 0.9 | 0.8 | 0.2 | 0.43 | 1.11 |
| D2 (%) | -0.9 | 0.4 | 0 | 0.7 | 2 | -2 | 0.03 | 1.38 |
| Spinal cord | | | | | | | | |
| Min (cGy) | 0 | -0.8 | 0 | -1.1 | 0 | 0 | -0.32 | 0.50 |
| Max (cGy) | -300 | -418 | 108 | -237 | -295 | -452 | -265.67 | 200.21 |
| Mean (cGy) | -46 | -71 | -90 | -39 | -47 | -82 | -62.50 | 21.32 |
| 0.5cc (cGy) | -239 | -417 | -131 | -232 | -299 | -433 | -291.83 | 116.52 |
| Stomach | | | | | | | | |
| Min (cGy) | -236 | -40 | -30 | -234 | -738 | -1 | -213.17 | 277.47 |
| Max (cGy) | -59 | -684 | -26 | -930 | 127 | 0 | -262.00 | 433.86 |
| Mean (cGy) | -168 | -370 | -43 | -534 | -670 | -1 | -297.67 | 271.81 |
| 0.5cc (cGy) | 41 | -712 | -30 | -978 | -53 | -1 | -288.83 | 440.06 |
| Liver | | | | | | | | |
| Min (cGy) | -12 | -13 | -2 | -12.3 | -57 | -1 | -16.22 | 20.69 |
| Max (cGy) | -216 | -134 | -80 | -536 | -421 | -13 | -233.33 | 204.48 |
| Mean (cGy) | -172 | -286 | -22 | -134 | -197 | -6 | -136.17 | 107.16 |
| 0.5cc (cGy) | -290 | -379 | -74 | -531 | -499 | -13 | -297.67 | 215.74 |

| Organ/constraint | Patient | | | | | | Mean | Standard Deviation |
|-------------------|---------|------|------|-------|------|-------|----------------|--------------------|
| | 1 | 2 | 3 | 4 | 5 | 6 | | |
| Oesophagus | | | | | | | | |
| Min (cGy) | -3 | -4 | -6 | -5.4 | -2 | -6 | -4.40 | 1.67 |
| Max (cGy) | -156 | -816 | -332 | -677 | -568 | -1028 | -596.17 | 318.01 |
| Mean (cGy) | -120 | -347 | -188 | -253 | -172 | -345 | -237.50 | 94.16 |
| 0.5cc (cGy) | -134 | -872 | -328 | -628 | -678 | -1002 | -607.00 | 326.59 |
| L Kidney | | | | | | | | |
| Min (cGy) | -1 | -2 | -2 | -1.9 | -18 | 0 | -4.15 | 6.83 |
| Max (cGy) | -28 | -10 | -31 | -9 | -123 | 0 | -33.50 | 45.43 |
| Mean (cGy) | -2 | -4 | -5 | -4 | 128 | -1 | 18.67 | 53.58 |
| 0.5cc (cGy) | -25 | -11 | -27 | -3 | -160 | 0 | -37.67 | 60.94 |
| R Kidney | | | | | | | | |
| Min (cGy) | -2 | -8 | -1 | -4.9 | -11 | 0 | -4.48 | 4.32 |
| Max (cGy) | -93 | -46 | -14 | -10.9 | -189 | -9 | -60.32 | 70.79 |
| Mean (cGy) | -10 | -18 | -5 | -12 | -61 | -4 | -18.33 | 21.51 |
| 0.5cc (cGy) | -42 | -119 | -12 | -18 | -159 | -9 | -59.83 | 63.68 |
| Heart | | | | | | | | |
| Min (cGy) | -299 | -203 | -133 | -18 | -25 | -5 | -113.83 | 119.60 |
| Max (cGy) | -46 | -66 | -317 | -243 | 69 | -48 | -108.50 | 143.14 |
| Mean (cGy) | -263 | -220 | -242 | -180 | -106 | -16 | -171.17 | 94.06 |
| 0.5cc (cGy) | -89 | -47 | -336 | -344 | 23 | -49 | -140.33 | 158.83 |

| Organ/constraint | Patient | | | | | | Mean | Standard Deviation |
|------------------------|---------|------|------|-------|------|-------|----------------|--------------------|
| | 1 | 2 | 3 | 4 | 5 | 6 | | |
| Gt vessels | | | | | | | | |
| Min (cGy) | -2 | -5 | 0 | -0.9 | -4 | -5 | -2.82 | 2.15 |
| Max (cGy) | -49 | -100 | -151 | -152 | -775 | -746 | -328.83 | 336.65 |
| Mean (cGy) | -78 | -96 | -184 | -64 | -133 | -303 | -143.00 | 89.51 |
| 0.5cc (cGy) | -58 | -222 | -232 | -160 | -756 | -809 | -372.83 | 323.75 |
| L Main Bronchus | | | | | | | | |
| Min (cGy) | -22 | -22 | -588 | -9 | -11 | -109 | -126.83 | 229.03 |
| Max (cGy) | 259 | 219 | -311 | -163 | -16 | -1103 | -185.83 | 499.60 |
| Mean (cGy) | -14 | -35 | -379 | -18.4 | -14 | -685 | -190.90 | 281.48 |
| 0.5cc (cGy) | 77 | -1 | -457 | -62 | -17 | -1033 | -248.83 | 427.67 |
| R Main Bronchus | | | | | | | | |
| Min (cGy) | -24 | -27 | -510 | | -12 | -63 | -127.20 | 214.84 |
| Max (cGy) | -526 | -66 | -534 | -129 | -20 | -674 | -324.83 | 284.40 |
| Mean (cGy) | -128 | -39 | -513 | -50 | -15 | -444 | -198.17 | 221.50 |
| 0.5cc (cGy) | -409 | -70 | -537 | -114 | -18 | -644 | -298.67 | 265.86 |
| Small Bowel | | | | | | | | |
| Min (cGy) | 0 | -5 | -4 | -0.5 | -17 | | -5.30 | 6.89 |
| Max (cGy) | -240 | -50 | -40 | -378 | 172 | | -107.20 | 210.18 |
| Mean (cGy) | -11 | -9 | -7 | -14 | -387 | | -85.60 | 168.51 |
| 0.5cc (cGy) | -263 | -48 | -39 | -392 | -91 | | -166.60 | 155.05 |

| Organ/constraint | Patient | | | | | | Mean | Standard Deviation |
|-----------------------|---------|-------|--------|-------|------|-------|----------------|--------------------|
| | 1 | 2 | 3 | 4 | 5 | 6 | | |
| Large Bowel | | | | | | | | |
| Min (cGy) | 0 | 0 | -1 | -0.4 | | | -0.35 | 0.47 |
| Max (cGy) | 20 | -15 | -54 | -138 | | | -46.75 | 67.93 |
| Mean (cGy) | -30 | -11 | -8 | -21 | | | -17.50 | 10.02 |
| 0.5cc (cGy) | -8 | -14 | -47 | -151 | | | -55.00 | 66.26 |
| Ipsilateral BP | | | | | | | | |
| Min (cGy) | -1 | -2 | -3 | -1.8 | 0 | -28 | -5.97 | 10.84 |
| Max (cGy) | -4 | -2 | -42 | 12.3 | -2 | -59 | -16.12 | 27.79 |
| Mean (cGy) | -2 | -2 | -14 | -1.1 | -2 | -46 | -11.18 | 17.75 |
| 0.5cc (cGy) | -4 | -3 | -34 | 5 | -2 | -10 | -8.00 | 13.61 |
| Trachea | | | | | | | | |
| Min (cGy) | -3 | -3 | -5 | -4.3 | -3 | -38 | | |
| Max (cGy) | -17 | -20 | -348 | -5 | -8 | -848 | -207.67 | 341.24 |
| Mean (cGy) | -8 | -8 | -95 | -6.3 | -4 | -583 | -117.38 | 230.84 |
| 0.5cc (cGy) | -19 | -20 | -421 | -8 | -9 | -843 | -220.00 | 345.95 |
| CL lung | | | | | | | | |
| V5 (%) | -21.2 | -19.9 | -12.4 | -13.2 | -6.4 | -20.1 | -15.53 | 5.84 |
| V10 (%) | -5.9 | -2.5 | -22.94 | 0 | -0.7 | -1.5 | -6.71 | 9.29 |
| V20 (%) | -0.2 | 0 | -0.3 | 0 | 0 | 0 | -0.08 | 0.13 |

Table 5.2 Changes to OAR doses achieved with MCO in right sided MPM

| Organ/constraint | Patient | | | | | | | Mean | Standard Deviation |
|--------------------|---------|------|------|------|------|------|------|----------------|--------------------|
| | 7 | 8 | 9 | 10 | 11 | 12 | 13 | | |
| PTV | | | | | | | | | |
| D98 (%) | 0.9 | -0.6 | -0.2 | 0 | -1.5 | 0.8 | -1.6 | -0.31 | 1.00 |
| D50 (%) | 0.4 | 1.2 | 1.5 | 2.1 | -2 | 0.8 | -1 | 0.43 | 1.45 |
| D2 (%) | 0.3 | 1.8 | 1 | 1.3 | -0.6 | 1.3 | -1.3 | 0.54 | 1.13 |
| Spinal cord | | | | | | | | | |
| Min (cGy) | -3 | -1.4 | -0.4 | -0.1 | -2 | -1 | -1 | -1.27 | 0.98 |
| Max (cGy) | -164 | -394 | -395 | -89 | -613 | 217 | -370 | -258.29 | 270.45 |
| Mean (cGy) | -112 | -96 | -47 | -38 | -214 | -86 | -117 | -101.43 | 58.14 |
| 0.5cc (cGy) | -162 | -436 | -382 | 54 | -569 | -5 | -459 | -279.86 | 242.01 |
| Stomach | | | | | | | | | |
| Min (cGy) | -146 | -32 | -25 | -128 | -151 | -43 | -6 | -75.86 | 62.92 |
| Max (cGy) | -731 | -417 | -352 | -573 | -847 | -958 | -55 | -561.86 | 313.29 |
| Mean (cGy) | -372 | -201 | -93 | -365 | -495 | -413 | -18 | -279.57 | 177.70 |
| 0.5cc (cGy) | -662 | -399 | -317 | -557 | -846 | -909 | -47 | -533.86 | 304.79 |
| Liver | | | | | | | | | |
| Min (cGy) | -2 | -4 | -3 | -3 | -10 | -1 | 0 | -3.29 | 3.25 |
| Max (cGy) | -134 | -392 | -176 | 30 | -64 | 123 | -12 | -89.29 | 166.86 |
| Mean (cGy) | -192 | -530 | -170 | -372 | -599 | 0 | -6 | -267.00 | 239.74 |
| 0.5cc (cGy) | -128 | -661 | -196 | -3 | -75 | -126 | -13 | -171.71 | 226.20 |

| Organ/constraint | 7 | 8 | 9 | 10 | 11 | 12 | 13 | Mean | Standard Deviation |
|-------------------------|----------|----------|----------|-----------|-----------|-----------|-----------|----------------|---------------------------|
| Oesophagus | | | | | | | | | |
| Min (cGy) | -9 | -4 | -9 | -3 | -2.8 | -2 | -18 | -6.83 | 5.72 |
| Max (cGy) | -755 | -570 | -724 | -573 | -1084 | 225 | -428 | -558.43 | 402.78 |
| Mean (cGy) | -378 | -223 | -352 | -153 | -286 | -152 | -215 | -251.29 | 90.41 |
| 0.5cc (cGy) | -680 | -581 | -699 | -539 | -1041 | 30 | -506 | -573.71 | 320.33 |
| L Kidney | | | | | | | | | |
| Min (cGy) | -20 | -7 | -5 | -2 | -31 | -13 | -2 | -11.43 | 10.78 |
| Max (cGy) | -397 | -51 | -27 | 3 | -389 | -237 | -20 | -159.71 | 178.08 |
| Mean (cGy) | -91 | -18 | -12 | -5 | -205 | -53 | -5 | -55.57 | 73.05 |
| 0.5cc (cGy) | -373 | -47 | -21 | -51 | -351 | -198 | -18 | -151.29 | 156.47 |
| R Kidney | | | | | | | | | |
| Min (cGy) | -6 | -3 | -4 | -2 | -6 | -2 | 0 | -3.29 | 2.21 |
| Max (cGy) | 16 | -52 | -27 | -24 | -1053 | -21 | -9 | -167.14 | 391.16 |
| Mean (cGy) | -37 | -16 | -9 | -9 | -117 | -24 | -2 | -30.57 | 39.82 |
| 0.5cc (cGy) | 19 | -50 | -18 | -23 | -1140 | -29 | 0 | -177.29 | 425.08 |
| Heart | | | | | | | | | |
| Min (cGy) | -361 | -41 | -189 | -32 | -25 | -56 | -16 | -102.86 | 128.26 |
| Max (cGy) | 39 | -1211 | -197 | -377 | -408 | 91 | -272 | -333.57 | 431.82 |
| Mean (cGy) | -565 | -295 | -550 | -265 | -113 | -116 | -195 | -299.86 | 188.78 |
| 0.5cc (cGy) | -2 | -935 | -342 | -424 | -461 | 68 | -254 | -335.71 | 332.59 |

| Organ/constraint | 7 | 8 | 9 | 10 | 11 | 12 | 13 | Mean | Standard Deviation |
|-------------------------|----------|----------|----------|-----------|-----------|-----------|-----------|----------------|---------------------------|
| Gt vessels | | | | | | | | | |
| Min (cGy) | -4 | -4 | -2 | -2 | -5 | -1 | 0 | -2.57 | 1.81 |
| Max (cGy) | -250 | -590 | 68 | -233 | -984 | 294 | -180 | -267.86 | 419.20 |
| Mean (cGy) | -296 | -107 | -141 | -77 | -180 | -96 | -303 | -171.43 | 93.62 |
| 0.5cc (cGy) | -440 | -619 | -118 | -309 | -908 | 481 | -175 | -298.29 | 437.76 |
| L Main Bronchus | | | | | | | | | |
| Min (cGy) | | -37 | -60 | -10 | -27 | -40 | -330 | -84.00 | 121.62 |
| Max (cGy) | | -120 | -350 | -19 | -49 | -49 | -548 | -189.17 | 213.38 |
| Mean (cGy) | | -47 | -296 | -16 | -32 | -43 | -462 | -149.33 | 185.79 |
| 0.5cc (cGy) | | -86 | -379 | -24 | -42 | -46 | -574 | -191.83 | 229.86 |
| R Main Bronchus | | | | | | | | | |
| Min (cGy) | | -26 | -58 | -10 | -21 | -55 | -324 | -82.33 | 119.92 |
| Max (cGy) | | -678 | -683 | -26 | -36 | -52 | -283 | -293.00 | 314.91 |
| Mean (cGy) | | -136 | -339 | -17 | -22 | -49 | -307 | -145.00 | 144.70 |
| 0.5cc (cGy) | | -545 | -683 | -24 | -29 | -48 | -274 | -267.17 | 287.76 |
| Small Bowel | | | | | | | | | |
| Min (cGy) | -10 | -1 | -3 | 0 | -4 | 0 | -1 | -2.71 | 3.55 |
| Max (cGy) | -258 | -48 | -244 | -600 | -267 | -351 | -11 | -254.14 | 196.17 |
| Mean (cGy) | -51 | -11 | -12 | -44 | -57 | -23 | -4 | -28.86 | 21.47 |
| 0.5cc (cGy) | -242 | -48 | -253 | -566 | -224 | -339 | -10 | -240.29 | 185.41 |

| Organ/constraint | 7 | 8 | 9 | 10 | 11 | 12 | 13 | Mean | Standard Deviation |
|-----------------------|-------|-------|------|-------|------|-------|------|----------------|--------------------|
| Large Bowel | | | | | | | | | |
| Min (cGy) | -1 | 0 | -3 | -1 | | -1 | 0 | -1.00 | 1.10 |
| Max (cGy) | -56 | -103 | -2 | -472 | | -3 | -10 | -107.67 | 182.81 |
| Mean (cGy) | -10 | -33 | -2 | -68 | | -2 | -3 | -19.67 | 26.49 |
| 0.5cc (cGy) | -45 | -98 | -4 | -423 | | -3 | -10 | -97.17 | 163.73 |
| Ipsilateral BP | | | | | | | | | |
| Min (cGy) | -7 | -4 | -7 | 1 | -2 | -4 | -6 | -4.14 | 2.91 |
| Max (cGy) | -12 | -7 | -6 | -7 | -1 | -5 | -16 | -7.71 | 4.89 |
| Mean (cGy) | -7 | -5 | -5 | -4 | -2 | -3 | -15 | -5.86 | 4.34 |
| 0.5cc (cGy) | -11 | -7 | -8 | -6 | -2 | -4 | -16 | -7.71 | 4.64 |
| Trachea | | | | | | | | | |
| Min (cGy) | -9 | -4 | -8 | -4 | -3 | -1 | -11 | -5.71 | 3.64 |
| Max (cGy) | -200 | -27 | -39 | -11 | -14 | -55 | -484 | -118.57 | 173.89 |
| Mean (cGy) | -50 | -7 | -27 | -4 | -6 | -13 | -206 | -44.71 | 72.96 |
| 0.5cc (cGy) | -184 | -21 | 1 | -11 | -14 | -53 | -398 | -97.14 | 147.07 |
| CL lung | | | | | | | | | |
| V5 (%) | -34 | -0.59 | -9.4 | -7.1 | -4.3 | -4.4 | -15 | -10.68 | 11.25 |
| V10 (%) | -1.35 | 0 | 0 | -13.2 | 0 | -13.2 | -29 | -8.11 | 11.04 |
| V20 (%) | 0 | 0 | 0 | 0 | 0 | 0 | -0.4 | -0.06 | 0.15 |

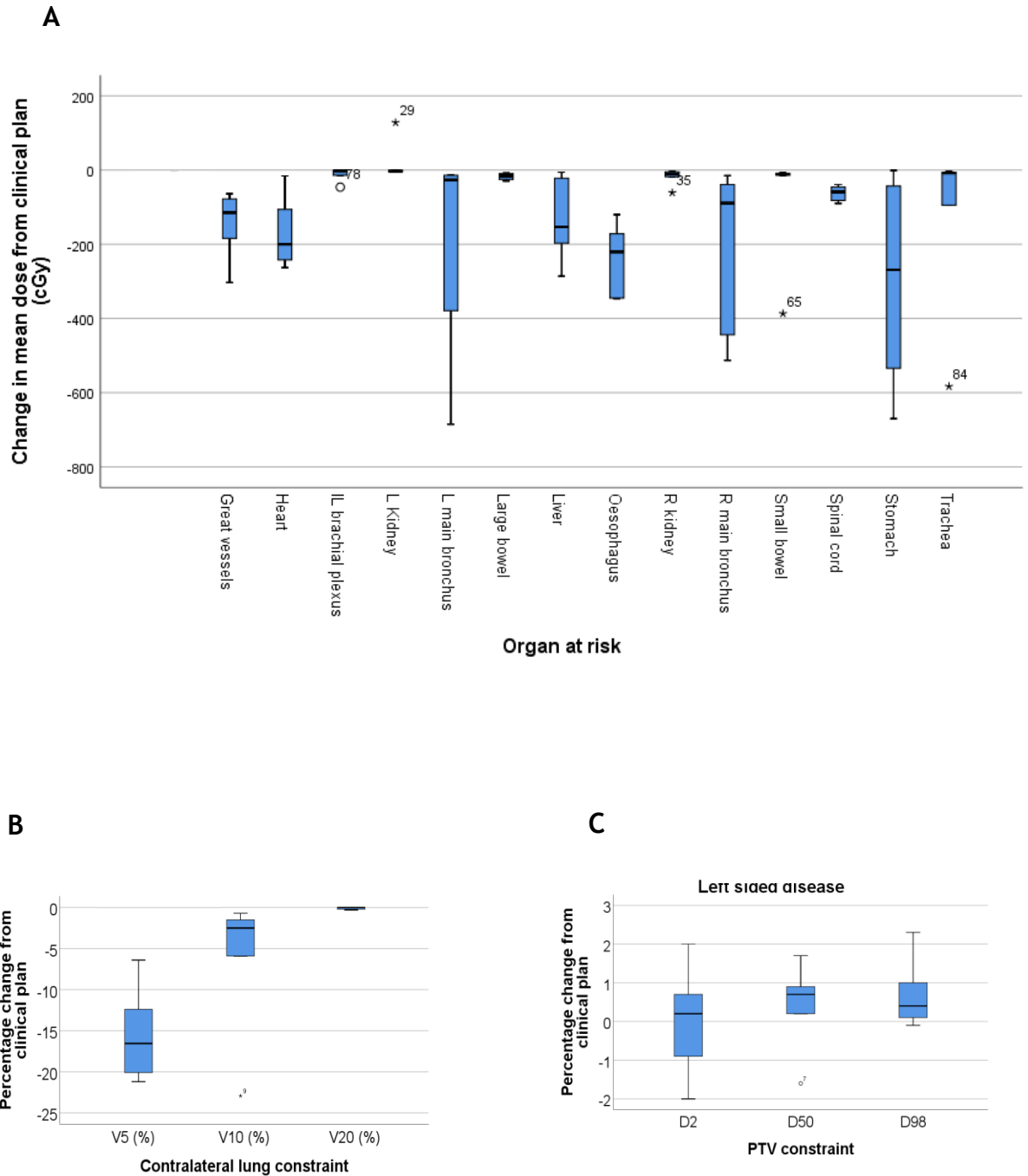


Figure 5.1 Changes in dosimetry achieved with MCO compared to clinical VMAT plans in patients with left sided MPM

The dose escalated VMAT plans of six SYSTEMS-2 patients with left sided MPM were replanned using MCO. Data are expressed as MCO-associated changes in the radiation dose received by OARs (A), changes in contralateral lung dosimetry (B) and changes in PTV coverage (C). Data are presented as box and whisker plots, plotted according to the Tukey method.

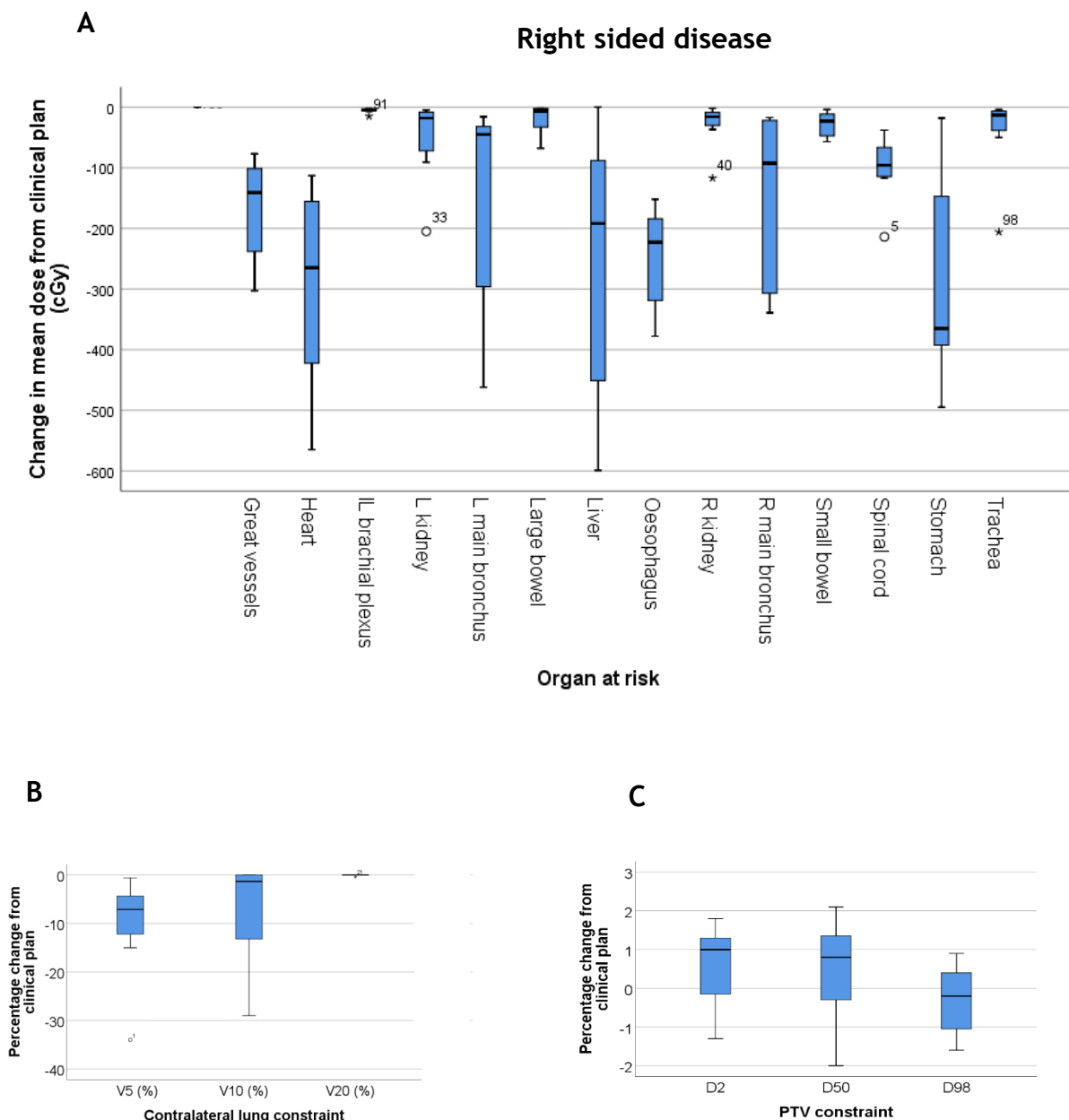


Figure 5.2 Changes in dosimetry achieved with MCO compared to clinical VMAT plans in patients with right sided MPM

The dose escalated VMAT plans of seven SYSTEMS-2 patients with right sided MPM were replanned using MCO. Data are expressed as MCO-associated changes in the radiation dose received by OARs (A), changes in contralateral lung dosimetry (B) and changes in PTV coverage (C). Data are presented as box and whisker plots, plotted according to the Tukey method.

5.2.3 MCO achieved clinically significant reductions in multiple OAR doses without compromising PTV coverage

Analysis of individual MCO plans revealed that dramatic dose reductions could be achieved in critical OARs without incurring unacceptable dose escalation to other structures. For all plans which passed the planning study, MCO reduced the mean organ dose for every structure, with the exception of Patient 5, in whom the dose to the left kidney was increased by 128cGy, from 892cGy to 1020cGy (V10: 44%). This rise was associated with a consequential reduction in mean stomach dose of 670cGy (from 2054cGy to 1384cGy) and a reduction in the mean small bowel dose of 387cGy (from 658cGy to 271cGy). Spinal cord was better spared (Dmax 0.5cc: 745cGy, compared to 1044cGy in the clinical plan), as was oesophagus (Dmax 0.5cc reduction of 678cGy, from 2014cGy to 1336cGy) and liver (Dmax 0.5cc reduced by 499cGy, from 2174cGy to 1675cGy). (Figures 5.3 and 5.5) Furthermore, the contralateral lung was better spared, with a reduction in V5 of 6.4% (from 11% to 4.6%). These improvements in dose delivery to OARs were achieved in the context of acceptable PTV coverage, illustrated in Figure 5.4) with the MCO plan achieving D98 of 95.1%, D50 of 101% and D2 of 105% (compared to 95%, 100.2% and 103% respectively in the clinical plan).

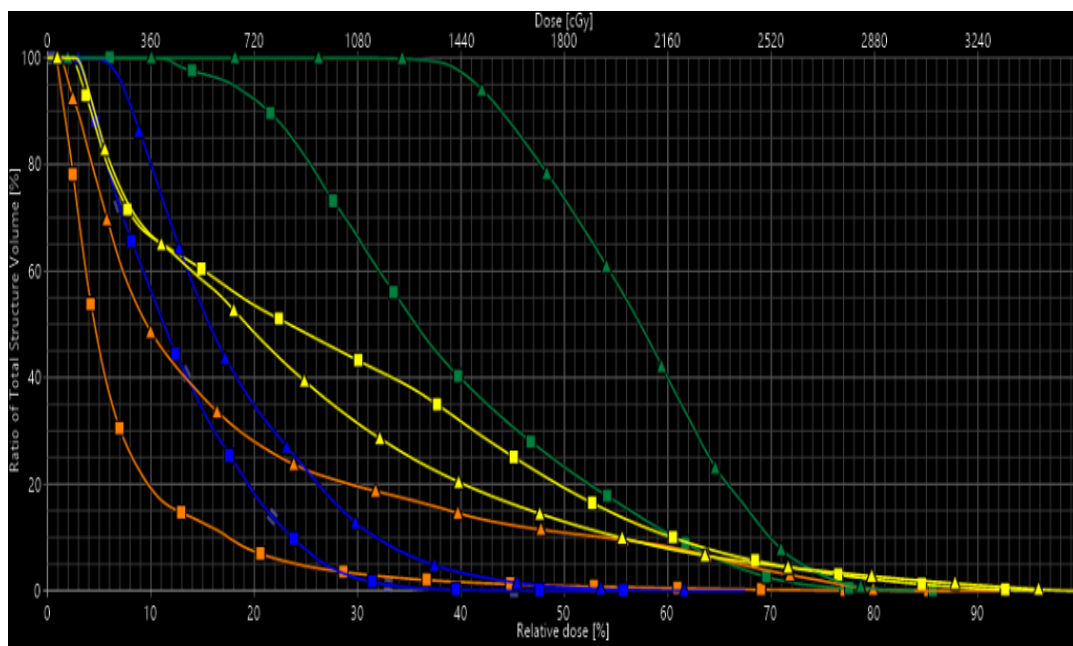


Figure 5.3 Dose volume histogram comparing OARs doses from the clinical VMAT plan (triangle markers) with the MCO generated plan (square markers) for patient 5

Represented OARs are liver (blue), kidney (yellow), stomach (green) and small bowel (orange). Data are presented as dose delivered to total structure volume (%)

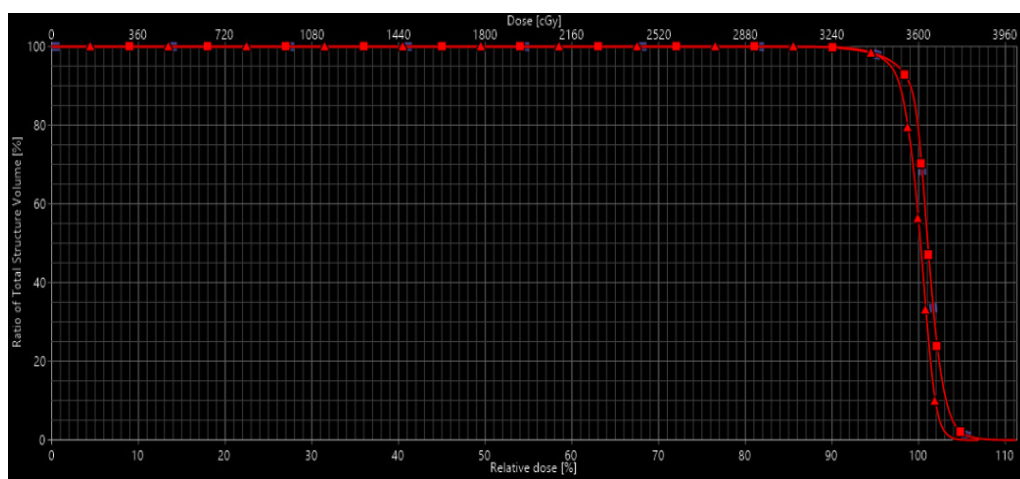


Figure 5.4 Dose volume histogram showing PTV coverage in the clinical VMAT plan (triangle markers) and MCO plan (square markers) for patient 5

Data are presented as dose delivered to total structure volume (%)

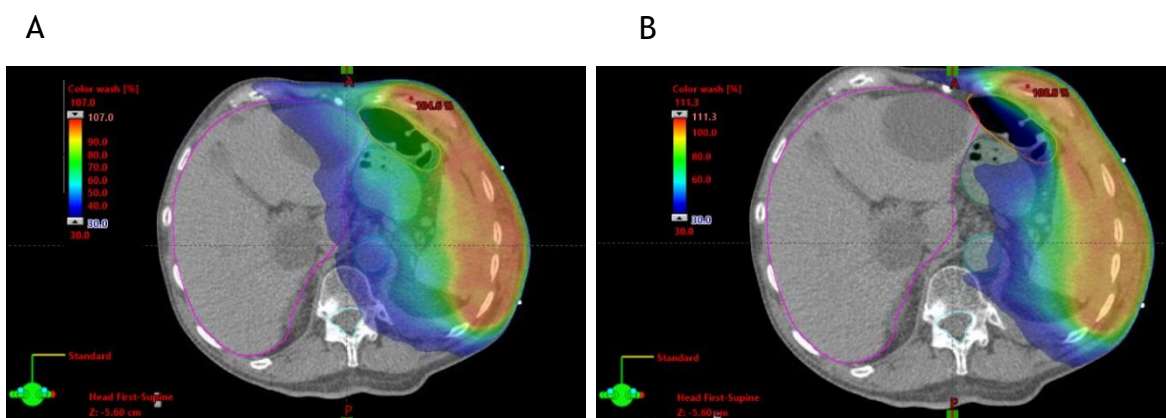


Figure 5.5 Comparison of the 30% isodose distribution between the clinical VMAT plan (A) and the MCO plan (B) for patient 5

The MCO plan for patient 7 achieved a reduction in the contralateral lung V5 of 34% (from 36% to 2%), illustrated in Figure 5.8. This improvement was associated with reductions in mean heart dose (565cGy), mean oesophageal dose (378cGy) and mean stomach dose (372cGy). (Figure 5.6) The PTV coverage remained satisfactory (D98 of 96.4%, D50 of 101% and D2 of 104.6%) and is shown in Figure 5.7.

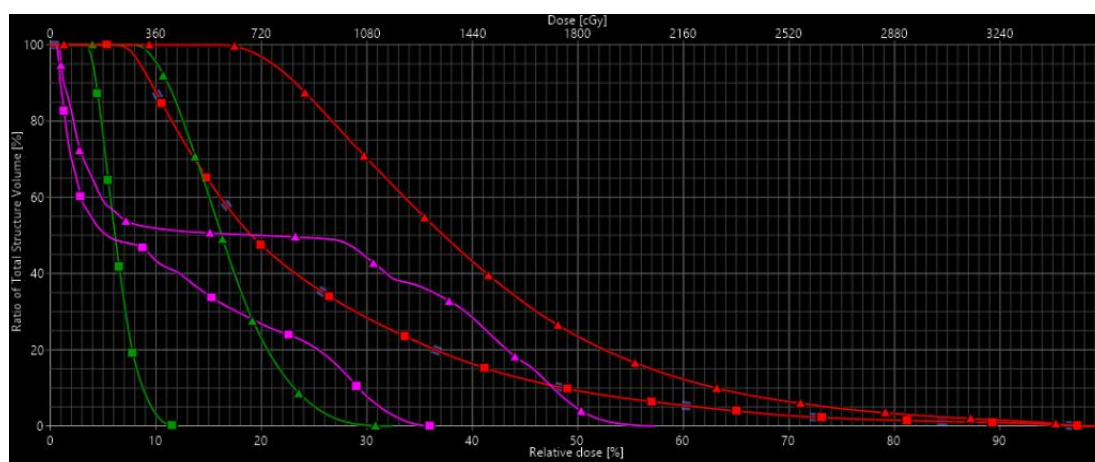


Figure 5.6 Dose volume histograms comparing OARs doses from the clinical VMAT plan (triangle markers) with the MCO generated plan (square markers) for patient 7

Represented OARs are heart (red), stomach (green) and oesophagus (purple). Data are presented as dose delivered to total structure volume (%).

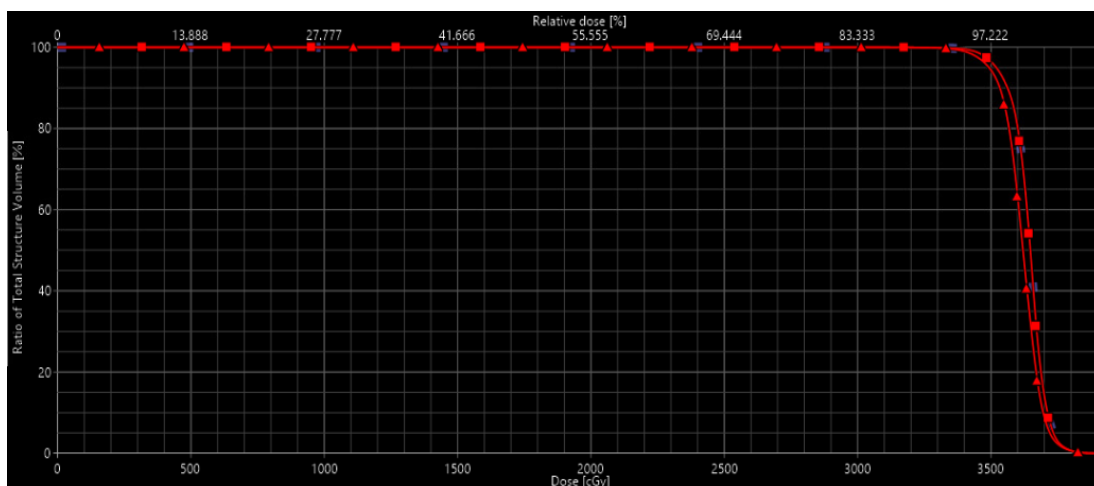


Figure 5.7 Dose volume histogram showing PTV coverage in the clinical VMAT plan (triangle markers) and MCO plan (square markers) for patient 7

Data are presented as dose delivered to total structure volume (%)

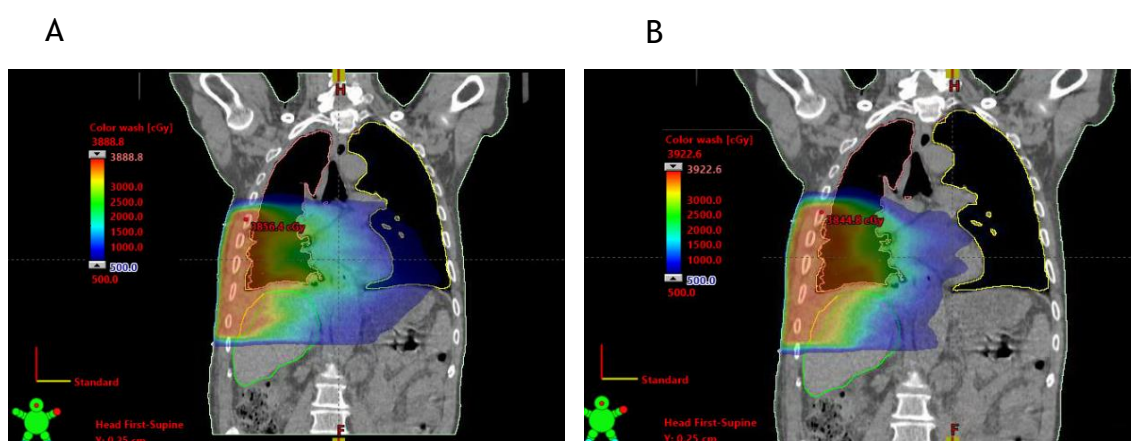


Figure 5.8 Comparison of the 500cGy isodose distribution between the clinical VMAT plan (A) and the MCO plan (B) for patient 7

Analysis of the MCO plan for patient 11 reveals dramatic reductions in dose delivered to critical OARs without any compensatory rise in dose delivered to other organs. Mean doses to stomach, oesophagus and liver were reduced by 495cGy (from 660cGy to 165cGy), 286cGy (from 598cGy to 312cGy) and 599cGy (from 1539cGy to 940cGy) respectively. Dmax to 0.5cc spinal cord was reduced by 569cGy (from 1221cGy to 652cGy) and to great vessels by 908cGy (from 1894cGy to 986cGy). These changes are illustrated in Figures 5.9 and 5.11. The MCO plan reduced contralateral lung V5 by 4.3% (from 5% to 0.3%). Both V10 and

V20 were <0.1% in the clinical and MCO plan. The PTV coverage in the MCO plan was within the trial stipulated limits, achieving a D98 of 95.2%, D50 of 101% and D2 of 105.4%. This compares to 96.7%, 103% and 106% respectively in the original clinical VMAT plan. (Figure 5.10)

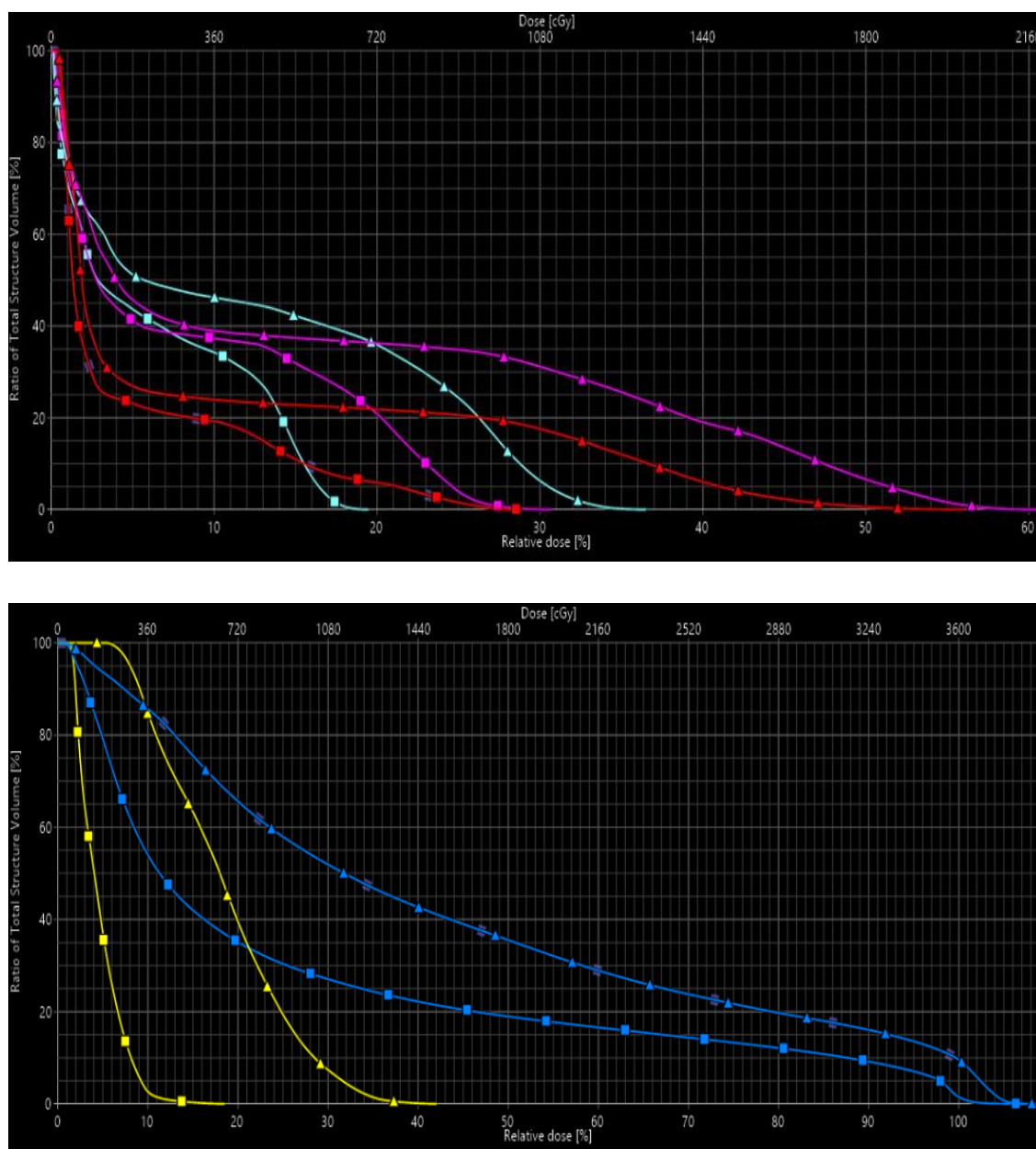


Figure 5.9 Dose volume histograms comparing OARs doses from the clinical VMAT plan (triangle markers) with the MCO generated plan (square markers) for patient 11

Represented OARs are great vessels (red), spinal cord (turquoise), oesophagus (purple), liver (blue) and stomach (yellow). Data are presented as dose delivered to total structure volume (%).

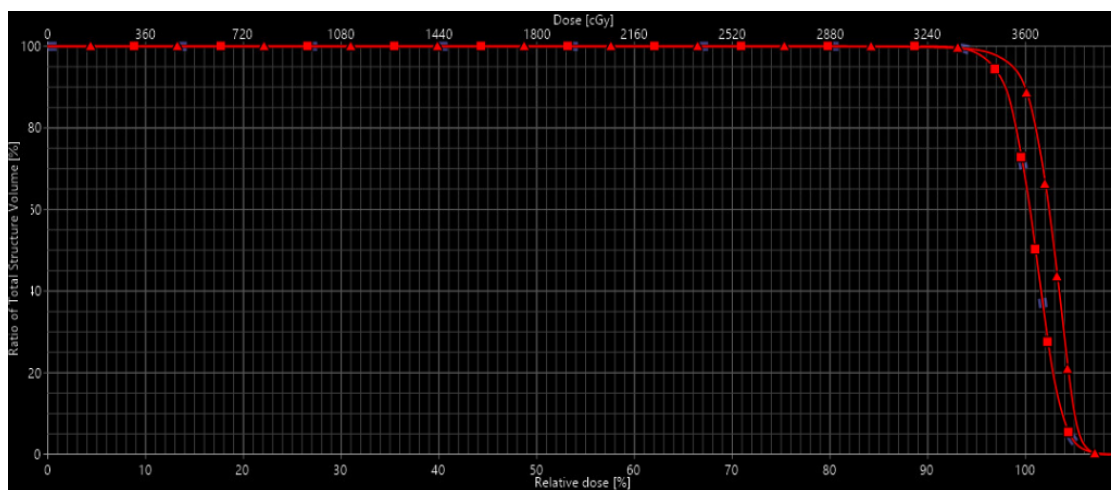


Figure 5.10 Dose volume histogram showing PTV coverage in the clinical VMAT plan (triangle markers) and MCO plan (square markers) for patient 11. Data are presented as dose delivered to total structure volume (%).

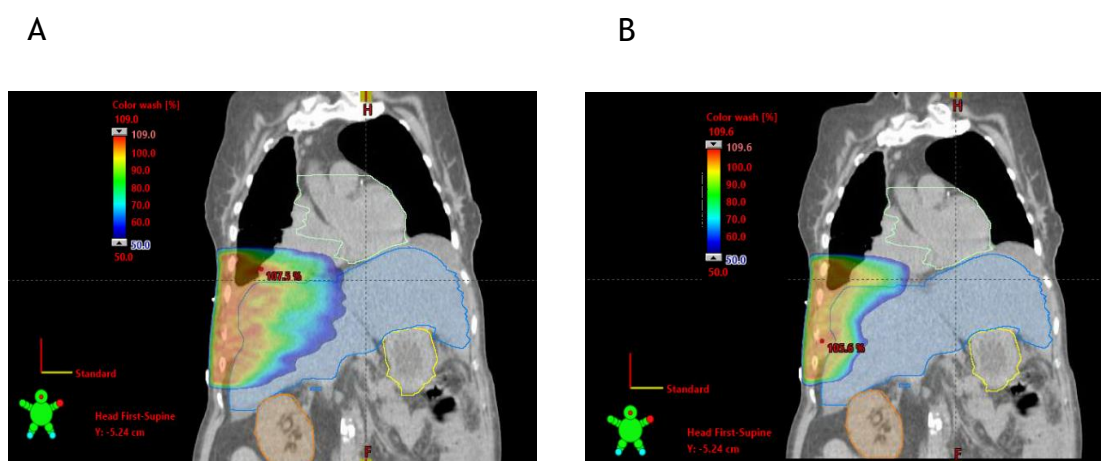


Figure 5.11 Comparison of the 50% isodose distribution between the clinical VMAT plan (A) and the MCO plan (B) for patient 11

5.2.4 Plans which failed this planning study were predominantly left sided, but were not associated with significantly larger PTV sizes

A comparison of the plans which passed this planning study and those which did not, are presented in Table 5.3. Plans were analysed with regard to their PTV size and location, the number of OARs directly within the PTV and the number of treatment volumes encompassed within a single plan.

Of the seven plans which failed (patient numbers 14-20), six had disease within the left hemithorax and two had more than one PTV, representing multiple sites of pain, which were combined to form one treatment volume. In contrast, all of the plans which passed the planning study had only one PTV.

The inclusion of OARs within the PTV was seen in a number of plans, often for several centimetres. For example, in patient number 11, which passed the MCO planning study, the heart was in the PTV for 3.5cm, the oesophagus for 2.8cm and the liver for 4cm.

Comparison between the two groups suggests that there was no significant difference in the size of the treatment volumes. The average PTV size in the plans which passed this planning study was $1163.2\text{cm}^3 \pm 318.5 \text{cm}^3$, whereas in the plans which failed the average size was $1156 \text{cm}^3 \pm 556 \text{cm}^3$, ($p = 0.97$).

Table 5.3 Comparison of plan parameters

| Patient number | PTV number | PTV location | OARs in PTV | PTV size (cm ³) | Outcome of MCO plan |
|----------------|------------|------------------|---|-----------------------------|---------------------|
| 1 | 1 | Left upper lobe | None | 648 | Passed |
| 2 | 1 | Left lower lobe | Great vessels (6cm) | 1268 | Passed |
| 3 | 1 | Left lower lobe | Heart (2.2cm) | 1700 | Passed |
| 4 | 1 | Left lower lobe | Heart (3cm) | 978 | Passed |
| 5 | 1 | Left lower lobe | Great vessels (3cm), Spinal canal (2cm) | 1322 | Passed |
| 6 | 1 | Left lower lobe | None | 1132 | Passed |
| 7 | 1 | Right lower lobe | None | 871 | Passed |
| 8 | 1 | Right lower lobe | Liver (6cm) | 1094 | Passed |
| 9 | 1 | Right lower lobe | Liver (10.2cm) | 869 | Passed |

| Patient number | PTV number | PTV location | OARs in PTV | PTV size (cm ³) | Outcome of MCO plan |
|----------------|------------|---|--|-----------------------------|---------------------|
| 10 | 1 | Right lower lobe | Heart (3cm), Liver (6cm) | 1623 | Passed |
| 11 | 1 | Right lower lobe | Heart (3.5cm), Oesophagus (2.8cm), Liver (4cm) | 1186 | Passed |
| 12 | 1 | Right middle lobe | Great vessels (1cm) | 1530 | Passed |
| 13 | 1 | Right lower lobe | Liver (1cm) | 900 | Passed |
| 14 | 1 | Left upper lobe | Brachial plexus (2.2cm), Great vessels (8.5cm) | 415 | Failed |
| 15 | 1 | Left lower lobe | Heart (5.8cm), Great vessels (7.4cm) | 1043 | Failed |
| 16 | 2 | Left upper lobe and left lower chest wall | Small bowel (1cm) | 1136 | Failed |
| 17 | 2 | Left upper and left lower lobe | Stomach (3.5cm) | 2051 | Failed |
| 18 | 1 | Right middle lobe | Spinal cord (1.75cm) | 1452 | Failed |
| 19 | 1 | Left upper lobe | Great vessels (7.2cm), Heart (0.8cm) | 579 | Failed |
| 20 | 1 | Left lower lobe | Great vessels (6cm) | 1419 | Failed |

An analysis of the doses achieved to the OARs and PTV within the plans which failed is presented in Table 5.4. This data highlights that MCO was associated with clinically significant dose reductions to OARs in plans which subsequently failed this planning study. For example, in patient 14, significant dose reductions were seen to the spinal cord (4.6Gy to 0.5cc) and trachea (3.3Gy to 0.5cc), but this was offset by an increase in dose to the great vessels which was in excess of the dose constraint of 36Gy to 0.5cc. Furthermore, the PTV coverage was inadequate in this plan, not meeting the prescription of D98% >95%. Similarly, in patient 16, the small bowel constraint of 30Gy to 0.5cc could not be met, but

doses to 0.5cc of the oesophagus and stomach were reduced by 1.84Gy and 4.6Gy respectively. The PTV coverage was also improved from a D98% of 95.9% in the original plan to 96.2% in the MCO plan. These gains were offset by an increase in the dose to the spinal cord, from 15.18Gy to 0.5cc in the original plan, to 19.7Gy in the MCO plan. This dose is within the constraint of 27Gy to 0.5cc, as set out in the SYSTEMS-2 protocol.

In some patients, MCO offered very few improvements to OAR dose or PTV coverage from the original VMAT plan and was associated with excessive doses to a number of organs. For example, in patient 20, the MCO plan increased dose to the great vessels, stomach and small bowel, breaching trial dose constraints. Dose to the heart was also increased from the original plan, from 33.5Gy to 35.3Gy to 0.5cc, although this remained within the trial specified constraint of 36Gy to 0.5cc. These compromises were not compensated for by improved PTV coverage: D98% = 95.4% in the original plan compared to 95.5% in the MCO plan and the D2 was greater with the MCO, indicating a hot spot.

Table 5.4 PTV and OAR parameters achieved in plans which failed the planning study

| Patient number | OARs | Dose to 0.5cc (Gy) | | PTV coverage | |
|----------------|-----------------|--------------------|----------|------------------------------|-----------------------------|
| | | Original plan | MCO plan | Original plan | MCO plan |
| 14 | Spinal cord | 25.5 | 20.9 | D98% = 95.6% D2% = 105.5% | D98% = 94.9% D2% = 106% |
| | Oesophagus | 28.5 | 28 | | |
| | Trachea | 33.8 | 30.5 | | |
| | Brachial plexus | 36 | 35.4 | | |
| | Great vessels | 35.8 | 36.7 | | |
| 15 | Spinal cord | 25.6 | 23.7 | D98% = 96.4% D2% = 106.9% | D98% = 95.2% D2% = 106% |
| | Stomach | 27.2 | 25.7 | | |
| | Oesophagus | 27.3 | 25.4 | | |
| | Great vessels | 35.9 | 36.5 | | |
| 16 | Cord | 15.18 | 19.77 | D98% = 95.9% D2% = 105% | D98% = 96.2% D2 = 106.1% |
| | Small bowel | 29.89 | 31.77 | | |
| | Oesophagus | 26.34 | 24.5 | | |
| | Stomach | 22.4 | 17.81 | | |

| Patient number | OARs | Dose to 0.5cc (Gy) | | PTV coverage | |
|----------------|--|--|--|------------------------------|------------------------------|
| | | Original plan | MCO plan | Original plan | MCO plan |
| 17 | Brachial plexus Oesophagus Spinal cord Stomach Trachea | 35.31 28.3 26.66 29.10 25.23 | 32.32 29 24.73 32.54 24.3 | D98% = 95.3% D2 = 106.9% | D98% = 94.9% D2% = 106.9% |
| 18 | Spinal cord Oesophagus Trachea | 25.34 27.64 24.1 | 28.84 28.65 22.8 | D98% = 95.4% D2 = 104.3% | D98% = 97.4% D2% = 105.8% |
| 19 | Great vessels Heart Oesophagus Spinal cord | 35.65 35.74 16.41 7.6 | 36.31 37.2 14.45 6.3 | D98% = 95.1% D2% = 104.2% | D98% = 95.2% D2% = 104.1% |
| 20 | Great vessels Stomach Spinal cord Heart Small bowel | 35 28.4 26.8 33.5 29.54 | 37.3 30.29 24.3 35.3 30.54 | D98% = 95.4% D2% = 105.2% | D98% = 95.5% D2% = 106.2% |

(Improvements in OAR dose are shown in green. Increases in the OAR dose from the original plan are shown in blue where the constraint is still met and in red where it is breached.)

5.3 Discussion

The data presented in this chapter shows that MCO can be used to produce clinically superior radiotherapy plans for the majority of patients with MPM, without compromising PTV coverage or exceeding OAR constraints. Radiotherapy planning can be difficult in this patient cohort, due to the large target volumes which are often in close proximity to radiosensitive structures. This data is amongst the first to assess the role of MCO in the radiotherapy planning in this patient population and may impact on future planning, in both the palliative and radical settings.

5.3.1 MCO can significantly reduce dose to organs which are associated with problematic acute toxicities

MCO was able to improve on the clinical VMAT dose escalated plans of 13/20 SYSTEMS-2 patients. Clinically significant dose reductions were observed in a number of organs, with some of the greatest gains observed in structures particularly vulnerable to acute radiation toxicity, such as liver and stomach. Furthermore, the increased conformity achieved with MCO enabled dose to be sculpted away from an OAR, even when the PTV was bordering this structure, as illustrated by the liver dosimetry in Figure 5.11. The reductions in dose were sometimes associated with a consequential dose increase to an alternative structure, but the trial constraints were not exceeded. The dosimetric changes were achieved with minimal effect on PTV coverage, with plans continuing to adhere to the trial PTV prescription.

The VMAT planning for SYSTEMS-2 employs partial arcs to reduce dose to contralateral structures, particularly the contralateral lung. However, in many cases, the size and location of the PTV precludes this and full arcs are required to deliver the treatment. In spite of this, relatively unilateral plans were generated, usually achieving a contralateral lung V20 of <0.1%. Re-planning with MCO demonstrated the ability to further improve the contralateral lung dose, achieving reductions in both V5 and V10 of $15.5\% \pm 5.8\%$ and $6.7\% \pm 9.3\%$ respectively in left sided disease and of $10.7\% \pm 11.3\%$ and $8.1\% \pm 11\%$ respectively when the disease was on the right. These improvements are clinically significant, since V5 has been linked with the development of pneumonitis. (Rice et al., 2007a)

The variety of sparing observed in this planning study for structures contralateral and ipsilateral to the PTV is likely due to a combination of factors, including the size and location of the PTV, the use of full versus partial arcs and the quality of the initial treatment plan.

5.3.2 Plans generated by MCO may be clinically acceptable despite breaching dose constraints

All patients included in this planning study had an acceptable clinical dose escalated clinical plan and had taken part in SYSTEMS-2. It was observed that 7/20 of these plans could not be improved upon with MCO, without breaching trial specific dose constraints. Details of these plans, including PTV size and location are shown in Tables 5.3 and 5.4.

Only one of the plans which failed incorporated right sided disease, possibly suggesting that the benefit of MCO may be influenced by disease laterality. The principle right sided OAR is the liver, whereas there are numerous left sided OARs (heart, stomach, bowel loops). Arguably, this makes the planning of left sided MPM more difficult and it could be that the MCO trade off between OARs in this setting is more challenging. However, it is difficult to draw any firm conclusions from such a limited dataset, in which the initial distribution of disease was unequal (12 left sided cases and 8 right sided).

Two of the plans which were rejected had more than one PTV: patients 16 and 17 both had two areas of pain and both areas were treated. The total PTV in each case was a combination of the two individual treatment volumes. In contrast, all of the accepted plans contained single PTVs, suggesting that this may be a contributing factor to plan failure.

The direct inclusion of OARs within the PTV did not necessarily seem to predispose to plan failure, suggesting that this can be tolerated within the planning constraints.

Failure of MCO to improve on the clinical plan may be because the original plan was sufficiently close to the Pareto surface, with MCO offering little scope for further optimisation. This is demonstrated clearly in patients 18, 19 and 20. In other plans, however, clinically significant reductions were achieved in a

number of OARs, but this was at the expense of a dose breach in an alternative organ. Due to the strict terms of this re-planning study, these plans were not deemed to be satisfactory, but many of them may have been clinically acceptable. Dose breaches were often minimal and were usually offset by significant dose reductions in OARs where early normal tissue effects are problematic (e.g. liver, stomach, oesophagus). The protocol of SYSTEMS-2 states that the dose constraints are not mandated and should be used as a guide to planning only; the final decision of whether or not to accept a plan lies with the treating clinician. (Ashton et al., 2018) A pragmatic view should be taken in this palliative setting to ensure that quality of life is preserved and therefore many of the MCO plans which were rejected in this study may have been clinically acceptable.

5.3.3 The future role of MCO in SYSTEMS-2 radiotherapy planning

The dose reductions achieved with MCO within this planning study are impressive and would likely reduce treatment related toxicity, which is already being carefully monitored, within this palliative clinical trial cohort. The deliverability of these plans is implied by the ‘aperture shape controller’ function within the MCO software, which does not allow an undeliverable plan to be calculated. Nevertheless, further ‘in house’ quality assurance processes are underway to ensure that the presented plans are clinically achievable. Assuming that these processes confirm deliverability, it is likely that MCO will be used to further enhance the radiotherapy planning process for the remainder of the Glasgow SYSTEMS-2 cohort. This, in conjunction with the findings presented in Chapter 4 which demonstrated a link between plan quality and planner experience, suggests that the highest quality plans should be achieved for patients recruited to this study.

Furthermore, this cohort of MCO optimised plans could serve as a useful resource in the building of an effective RapidPlan model for SYSTEMS-2. A study by Miguel *et al*, investigating the role of MCO in head and neck radiotherapy, reported that the optimal plan was created by performing MCO on a plan generated through a RapidPlan model which had been built using a training cohort of plans previously

optimised with MCO. (Miguel-Chumacero et al., 2018) Creating such a resource for SYSTEMS-2, which could be shared amongst sites, would facilitate the creation of high quality radiotherapy plans for trial patients and may encourage other sites to join the study. Furthermore, it could promote consistency between plans generated at different hospitals, in addition to reducing planning time.

5.3.4 The potential for further dose escalation with MCO

The data presented in this chapter was generated using plans created for a dose of 36Gy in 6 fractions and suggests that further dose escalation may be safely achievable in MPM using MCO. This introduces the possibility of using radiotherapy for MPM in a more radical setting than is currently practised in the UK. It is already accepted that in other types of cancer (e.g. NSCLC), local control cannot be reliably achieved using conventional radiotherapy dosing schedules and techniques. (Nguyen et al., 2010) This, in combination with the demonstration of a clear radiotherapy dose-response relationship in NSCLC (Martel et al., 1999) has led to strategies aiming to escalate the dose of radiation delivered to the tumour. Nevertheless, results of the RTOG 0617 study suggest that conventionally fractionated dose escalated regimes, which increase overall treatment time, are not the optimal strategy in NSCLC. (Bradley et al., 2015) Novel radiotherapy approaches are now being used, which permit the radiation dose to the tumour to be escalated, depending on the normal tissue constraints. (van Baardwijk et al., 2008, van Baardwijk et al., 2010) 'Isotoxic radiotherapy', delivered using IMRT and a hyperfractionated accelerated regime, is currently being assessed in a UK feasibility study in patients with stage III NSCLC. (Haslett et al., 2016) Future MCO planning studies within the SYSTEMS-2 cohort will aim to investigate delivery of a dose escalated radiotherapy regime to the whole pleura, incorporating isotoxically prescribed boosts to areas of bulky disease and/or pain, depending on the results of the SYSTEMS-2 study.

5.3.5 Physician led radiotherapy planning using MCO

In addition to generating clinically superior radiotherapy plans, MCO allows the treatment planning to be distributed amongst clinical staff. A study by Kierkels *et al* demonstrated that novice treatment planners were able to produce head and neck radiotherapy plans which were almost indistinguishable from those generated conventionally and took less time to create (on average 43 minutes with MCO versus 205 minutes with conventional planning). (Kierkels et al., 2015) A further study by Muller *et al* which investigated the role of physician led MCO radiotherapy planning in brain and prostate tumours concluded that this is a feasible approach which could improve departmental efficiencies. (Muller et al., 2017) Within the current study, all MCO plans were generated by a physician with no prior experience of radiotherapy planning. Physician-led MCO radiotherapy planning may potentially bring many benefits, the most important of which is the background clinical knowledge of the case and the ability to manipulate the dose to various structures, according to the clinical situation.

5.4 Summary

This data demonstrates that physician led MCO planning can achieve clinically significant improvements in the dose escalated radiotherapy plans of SYSTEMS-2 patients, sparing OARs without compromising PTV coverage. This technique is likely to influence future radiotherapy planning in this disease, in both the palliative and radical settings. Furthermore, these MCO plans will contribute to a 'training cohort' in the generation of a Rapidplan model which can be shared amongst sites to facilitate high quality radiotherapy planning in the SYSTEMS-2 study.

Chapter 6: Characterising the radiosensitivity of mesothelioma using an *in vitro* 3D model

Chapter aim

The aim of this chapter is to explore the radiosensitivity and radiobiology of MPM using a clinically relevant in vitro spheroid model. Spheroids generated from two distinct MPM cell lines will be exposed to varying doses of radiotherapy, delivered using different fractionation regimes. The same model will be used to identify an isoeffective dose of IR, which could be used to estimate the α/β ratio of MPM. This information would be extremely useful in the planning and development of future clinical trials of radiotherapy in this disease, by guiding optimal fraction size.

6.1 Introduction

6.1.1 Clinical assessment of radiosensitivity in MPM

MPM is generally regarded as an inherently radioresistant tumour, for which the role of radiotherapy is limited exclusively to palliation of pain, employing modest doses of radiation which can be tolerated by nearby OARs. (Ashton et al., 2017) This reputation may be underpinned more by the difficulties of delivering a tumouricidal dose to the pleural cavity using traditional RT techniques, than by direct evidence of radioresistance. Furthermore, since follow up cross sectional imaging is not routinely performed after palliative treatments, the radiological impact of even modest doses of IR are rarely determined, making the true radiosensitivity of MPM difficult to ascertain in a clinical setting.

A limited number of studies have attempted to define the radiological response of MPM to IR in a clinical setting. (Jenkins et al., 2011, Linden et al., 1996) Linden *et al* observed just one radiological response out of 31 patients treated with an IR dose of 40Gy in 20 fractions, (Linden et al., 1996) however, a

retrospective study by Jenkins *et al* report more encouraging data with a regime employing 3Gy per fraction. (Jenkins et al., 2011) In this series of 54 patients, a dose of 36Gy in 12 fractions was delivered over 2.5 weeks to sites of pain and bulky disease. CT imaging was conducted in fit patients after 2 months and compared to baseline imaging using the Modified RECIST criteria. (Byrne and Nowak, 2004b) An overall radiological response rate of 43% was reported, with a median reduction from baseline measurements of 32% within the radiotherapy field and a median increase of 22% from baseline measurements outside of the field. Furthermore, patients who had responded to RT had a significantly longer overall survival than non-responders (7.2 months versus 2.8 months; $p= 0.001$), suggesting that hypofractionated radiotherapy may be more effective in MPM and could be linked to improved overall survival. (Jenkins et al., 2011) A similar sensitivity to fraction size has been observed by van der Zee *et al*, who reported a 54% clinical response rate to 40Gy in 10 fractions in a cohort of MPM patients treated for intervention site recurrence. (van der Zee et al., 2004) Whilst these data suggest an encouraging role for hypofractionation in MPM, they should be interpreted cautiously given their single arm design and the use of different total doses.

In the SYSTEMS study, in which 20Gy was delivered in 4Gy per fraction, (MacLeod et al., 2015a) radiological data was collected at week 12 from 18 patients out of 40 and scored according to the Modified RECIST criteria. (Byrne and Nowak, 2004b) Only one partial response was identified, suggesting that MPM was radioresistant at this dose, despite hypofractionation and that clinical response did not correlate with a notable reduction in tumour bulk. (MacLeod et al., 2015a) The impact of dose escalated hypofractionated radiotherapy in comparison to this standard dose is currently being assessed in the SYSTEMS-2 study, in which radiological data is collected at week 9. (Ashton et al., 2018)

6.1.2 *In vivo* studies of MPM radiosensitivity

In vivo studies of radiosensitivity require the tumour under investigation to grow reliably in a xenograft model, such that any regression following IR treatment can be accurately determined. Experiences within our own laboratory with

regard to this have been unsuccessful. Three MPM cell lines (H2052, 211H and H226) were used to establish subcutaneous xenografts in nude mice, however, only 211H cells were able to form tumours, which spontaneously regressed (data not shown). Further attempts with subcutaneous deposition of this cell line in SCID mice demonstrated tumour growth, but these were prone to ulceration and necrosis and were therefore unreliable. For this reason, preclinical models utilising cell lines have been employed for the investigation of this malignancy.

6.1.3 *In vitro* studies of MPM radiosensitivity

6.1.3.1 2D models of MPM

Despite the radioresistant reputation of MPM in the clinic, there is evidence to suggest that MPM cell lines grown *in vitro* may be relatively radiosensitive. (Carmichael et al., 1989, Hakkinen et al., 1996)

The first study to investigate the *in vitro* radiation response of MPM was conducted by Carmichael *et al.* (Carmichael et al., 1989) A clonogenic assay was used to investigate the effect of single radiation doses of between 1 and 12Gy on seventeen human lung cancer cell lines, including two MPM cell lines. Cells were incubated for 2-4 weeks following IR and differences in radiosensitivity were distinguished by comparisons of the MID, SF2Gy and values of α and β . While the observed responses of small cell and non-small cell lung cancer (SCLC and NSCLC) were largely similar to what would be expected in clinical practice, mesothelioma was noted to be unexpectedly sensitive to radiation *in vitro*. The SF2Gy was reported to be 0.34 - 0.35 and almost no shoulder was observed in cell survival curves, suggestive of limited capacity for SLD repair. (Carmichael et al., 1989) The α/β ratios reported for these cell lines were 5Gy and 26Gy, suggesting that they may have different sensitivities to fractionation.

Further work by Hakkinen *et al* in 1996 studied the radiosensitivity, cell growth kinetics, radiation-induced cell cycle delay and genomic integrity of six different mesothelioma cell lines. (Hakkinen et al., 1996) Cells were exposed to single

radiation doses ranging from 1 to 8Gy, following which they were allowed to grow for 7 to 8 days to allow enough time for any damage to manifest. An MTT assay was conducted and the LQ model was used to determine the SF2Gy and the α/β ratio for each cell line. A large difference in radiosensitivity was noted between the cell lines, with SF2Gy varying from 0.36 (± 0.06) to 0.81 (± 0.08). Aneuploid cell lines (M28K and M38K) were relatively radioresistant. M28K cells had a SF2Gy of 0.74 (± 0.09), and reported α and β values of 0.083Gy^{-1} ($\pm 0.015\text{Gy}^{-1}$) and 0.019Gy^{-2} ($\pm 0.004\text{Gy}^{-2}$) respectively. Similarly, the SF2Gy in M38K cells was 0.81 (± 0.08), with α of 0.089Gy^{-1} ($\pm 0.015\text{Gy}^{-1}$) and β of 0.012Gy^{-2} ($\pm 0.003\text{Gy}^{-2}$). Predicted α/β ratios of 4Gy and 7Gy were reported for M28K and M38K cell lines respectively, suggesting that they may be sensitive to changes in dose per fraction. Diploid cell lines were found to be more radiosensitive, with a poorly defined shoulder in their survival curve. M14 cells were the most radiosensitive, with a reported SF2Gy of 0.36 (± 0.06) and values of α and β of 0.48Gy^{-1} ($\pm 0.04\text{Gy}^{-1}$) and 0.005Gy^{-2} ($\pm 0.005\text{Gy}^{-2}$) respectively. The predicted α/β ratio of this cell line was 92Gy, suggesting that these cells would not respond to changes in dose per fraction. (Hakkinen et al., 1996) This study provides interesting insight into the radiosensitivity of MPM; however, such contradictory data limits the potential for general clinical applicability.

6.1.3.2 3D models of MPM

Despite the popularity of 3D tumour models and their established role in radiobiological studies, (Santini et al., 1999) there is a paucity of radiation research utilising 3D spheroid models of MPM, even though this tumour exhibits characteristics which particularly favour its investigation in such a system.

In vivo, MPM forms a 3D mass from a 2D pleural monolayer. The resistance to therapeutic strategies seen clinically with this disease may in part be due to this adopted morphology. (Barbone et al., 2008, Daubriac et al., 2009) A recent study identified a total of 209 genes which were differentially expressed between mesothelioma cells cultured in a monolayer or as a spheroid culture, (Barbone et al., 2016) suggesting that changes in gene expression may also contribute to the resistant phenotype. Furthermore, cytological preparations of

pleural fluid often reveal the presence of cellular aggregates, similar to spheroids, containing a collagen-based extracellular matrix core. (Delahaye et al., 1990) These cores are strongly suggestive of malignancy and in a study by Delahaye *et al*, were detected in the pleural effusions of 64% of patients with MPM versus 4% of patients with adenocarcinoma. (Delahaye et al., 1990) The source of the aggregates is unclear, but they are suspected to be derived from shearing of the primary tumour or from breakage of papillary structures. (Kim et al., 2005) Data suggest that these non-adherent tumour aggregates are able to resist loss of anchorage-induced apoptosis (anoikis) through de-regulation of cell signalling pathways (PI3/Akt, ERK and SAPK/JNK), and through the sequestration of the BH3-only pro-apoptotic protein Bim by anti-apoptotic proteins. (Daubriac et al., 2009) These aggregates have also been demonstrated to increase in size over time, displaying an ability to grow without anchorage to a substrate. (Daubriac et al., 2009) The ability to survive and grow in a non-adherent environment facilitates the development of new MPM foci and may explain the multifocal nature of this disease within the pleural cavity. (Daubriac et al., 2009) These properties have been replicated *in vitro* by MPM tumour fragment spheroids grown in non-adherent conditions, which were observed to proliferate at a similar rate to the original tumour for up to four weeks. (Kim et al., 2005) The ability of mesothelioma to form structures similar to spheroids *in vivo* lends weight to the rationale for using a spheroid model to study this highly aggressive and resistant tumour.

6.1.4 Validation of a 3D *in vitro* model of MPM

Given the suitability of MPM to be studied in a 3D spheroid model, early work from our laboratory, conducted by Dr Mark Jackson, assessed the relative performance of various cell survival assays to determine the radiosensitivity of three MPM cell lines (data not shown). These included clonogenic and cell viability assays as well as a 3D spheroid model. Each independent experimental technique confirmed the observation that MPM is resistant to small doses of IR (2Gy) but that larger doses of 10Gy, delivered as a single fraction, were associated with markedly decreased cell survival. This work also validated the 3D *in vitro* spheroid model as a robust system in which to study the effects of fractionated IR in mesothelioma.

6.2 Results

6.2.1 MPM cells exhibit radiosensitivity to IR in a dose dependent manner

Prior to embarking on detailed studies of MPM radiosensitivity, pilot studies were conducted to establish the optimal conditions of the *in vitro* 3D spheroid model, specifically in terms of seeding density and radiation dose. Previous work from our lab suggested that delivery of a single 2Gy fraction of IR to MPM spheroids, seeded at a density 10^4 cells per well, did not have any significant impact on spheroid size at 3 weeks (data not shown). To determine the optimal radiation dose which caused maximum spheroid growth delay, MPM cells were seeded at densities of 10^2 , 10^3 and 10^4 cells per well and left to form spheroids before being exposed to single IR doses of between 4Gy and 12Gy. Sham irradiated spheroids were included as a control. Spheroid size was monitored over 21 days and image reconstruction using ReVISP software was used to generate a 3D volume from a 2D image.

At a seeding density of 10^2 cells per well, sham irradiated spheroids progressively increased in volume over 3 weeks. For example, in the H2052 model, the mean spheroid volume was 0.005mm^3 ($\pm 0.0007\text{mm}^3$) on day 0 and 0.5mm^3 ($\pm 0.02\text{mm}^3$) by day 21. (Figure 6.1) Similarly, sham irradiated 211H spheroids increased their mean volume from 0.004mm^3 ($\pm 0.001\text{mm}^3$) on day 0 to 1.1mm^3 ($\pm 0.2\text{mm}^3$) on day 21. (Figure 6.2) In contrast, irradiated spheroids increased their volume more slowly and in a manner which was dependent on radiation dose. After 21 days, spheroids exposed to 7Gy were markedly smaller than those treated with 4Gy (Figures 6.1 to 6.4). This trend was observed in both cell lines. To illustrate, at day 5, the mean volume of H2052 spheroids exposed to 4Gy and 7Gy were similar ($0.01\text{mm}^3 \pm 0.002\text{mm}^3$ and $0.009\text{mm}^3 \pm 0.002\text{mm}^3$ respectively), but by day 21, those treated with 4Gy had grown to a volume of 0.24mm^3 ($\pm 0.05\text{mm}^3$) whereas the 7Gy group had a mean volume of 0.07mm^3 ($\pm 0.02\text{mm}^3$) at the same time point (Figure 6.1). In the 211H model, the day 5 volumes of 4Gy and 7Gy treated spheroids were 0.04mm^3 ($\pm 0.01\text{mm}^3$) and 0.02mm^3 ($\pm 0.006\text{mm}^3$) respectively, but by day 21 the volume of spheroids

exposed to 4Gy had increased to 0.9mm^3 ($\pm 0.4\text{mm}^3$) whereas those exposed to 7Gy had increased only marginally to 0.12mm^3 ($\pm 0.08\text{mm}^3$) (Figure 6.3).

Whilst relative volumes of both H2052 and 211H spheroids were similarly affected by exposure to 5Gy, 6Gy and 7Gy, a differential effect on spheroid volume was noted between the two cell lines following exposure to 4Gy. In the 211H model, the growth curve of spheroids treated with 4Gy was similar to that of the sham irradiated controls. For example the mean spheroid volume at day 21 in the sham irradiated group was 1.09mm^3 ($\pm 0.22\text{mm}^3$), compared to 0.87mm^3 ($\pm 0.38\text{mm}^3$) in the group which had been exposed to 4Gy. (Figure 6.3) In contrast, the growth trajectories of sham irradiated H2052 spheroids and those exposed to 4Gy IR were distinct. (Figure 6.1) At day 21, the mean spheroid volume in the sham irradiated group was 0.48mm^3 ($\pm 0.02\text{mm}^3$), whereas in the group which had received 4Gy the mean volume was 0.24mm^3 ($\pm 0.05\text{mm}^3$).

In both cell lines, exposure to 6Gy and 7Gy effectively delayed spheroid growth. (Figures 6.1 and 6.3) For example, in the H2052 cell line, the mean day 21 spheroid volume was 0.06mm^3 ($\pm 0.02\text{mm}^3$) after exposure to 6Gy, compared to 0.07mm^3 ($\pm 0.02\text{mm}^3$) in the group receiving 7Gy. This observation suggests that 6Gy may be sufficient to maximally delay MPM growth at this seeding density. At IR doses above 8Gy, no change in spheroid volume was observed in either cell line from day 0 (data not shown). Variability between replicates was observed to be much greater in the 211H cell line than in the H2052 model. This is illustrated by the greater standard deviation observed between Figure 6.1 and Figure 6.3. Furthermore, this variability became more pronounced towards the end of the experiment, as the spheroids increased in volume. For example, at day 0, sham irradiated 211H spheroids displayed a mean volume of 0.004mm^3 , associated with a standard deviation of $\pm 0.001\text{mm}^3$. By day 21, the mean volume had increased to 1.09mm^3 and the standard deviation was $\pm 0.22\text{mm}^3$. In contrast, the mean and standard deviation of H2052 spheroid volumes at day 0 and 21 were $0.005\text{mm}^3 \pm 0.0007\text{mm}^3$ and $0.48\text{mm}^3 \pm 0.02\text{mm}^3$ respectively. Expressing this error data using the coefficient of variance (CV) parameter (standard

deviation/mean), the CV for the 211H cell line at day 21 is 20.2%, compared to 4.2% in the H2052 cell line.

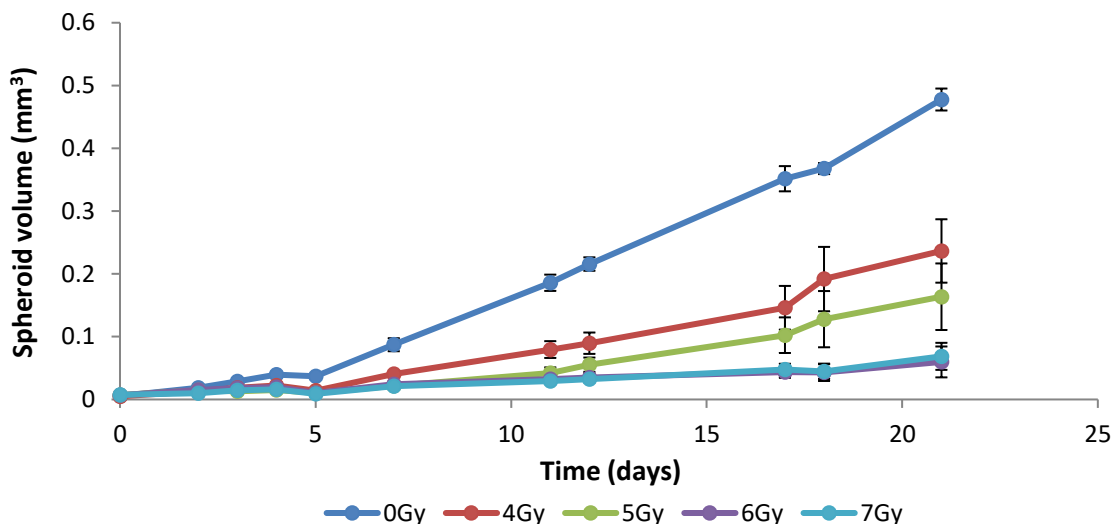


Figure 6.1 H2052 spheroid volumes following exposure to single IR fractions

H2052 spheroids, seeded at a density of 10^2 cells per well, were exposed to single doses of IR between 4Gy and 7Gy and growth was monitored over 21 days. A sham irradiated control was included. Data are expressed as spheroid volume (mm^3) against time (days). Data was generated from a single experiment, employing 6 replicate spheroids per condition and error bars represent the standard deviation of replicates within the experimental group.

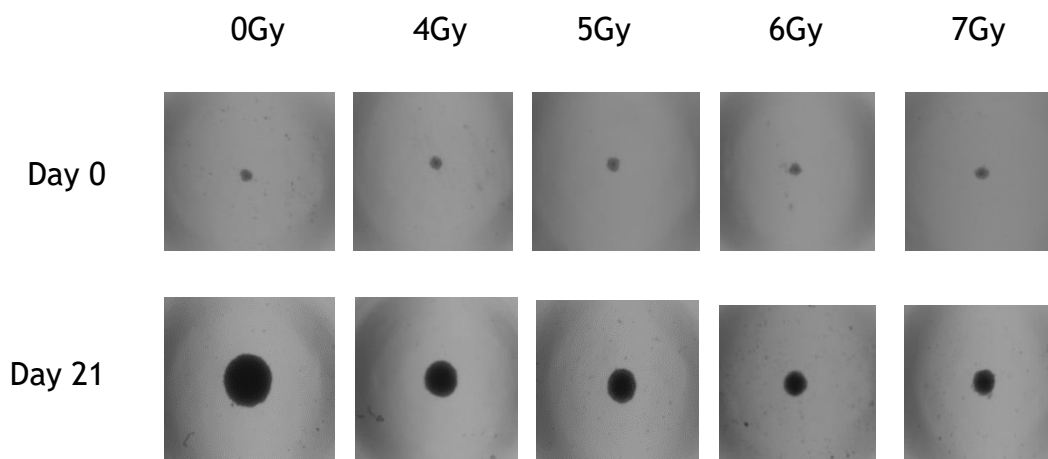


Figure 6.2 Representative H2052 spheroids at day 0 and day 21 following irradiation with increasing doses of IR

H2052 spheroids, seeded at a density of 10^2 cells per well, were irradiated with single fractions of IR between 4 and 7Gy. A sham irradiated group were included as a control. Spheroid growth was monitored for 21 days by regular brightfield imaging.

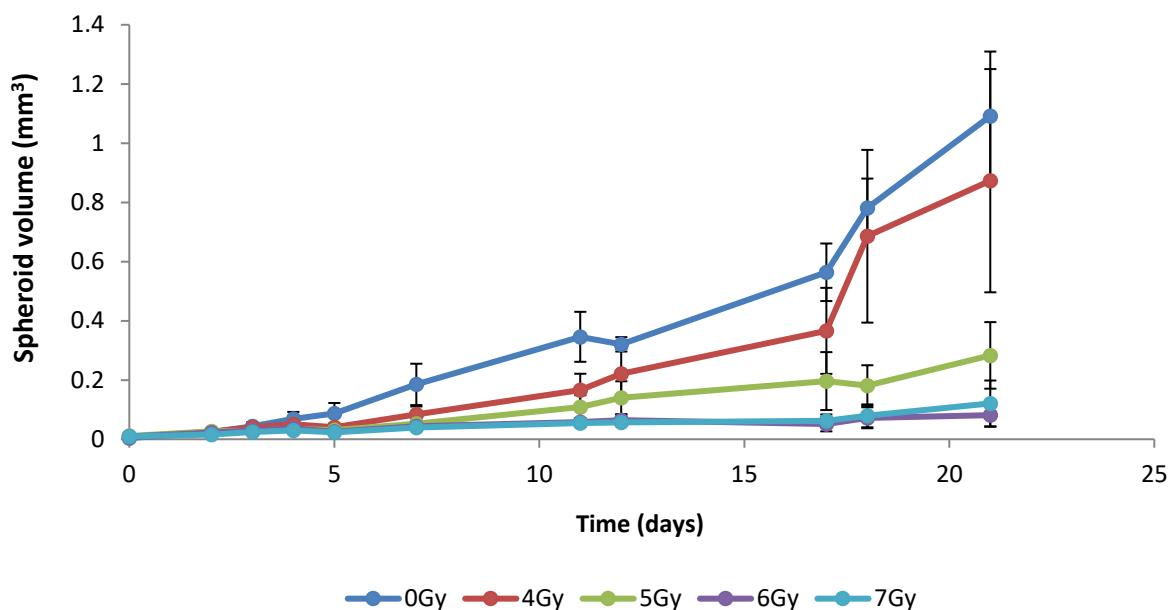


Figure 6.3 211H spheroid volumes following exposure to single fractions of IR

211H spheroids, seeded at a density of 10^2 cells per well, were exposed to single doses of IR between 4Gy and 7Gy and subsequent growth was monitored over 21 days. A sham irradiated control was included. Data are expressed as spheroid volume (mm^3) against time (days). Data was generated from a single experiment, employing 6 replicate spheroids per condition and error bars represent the standard deviation of replicates within the experimental group.

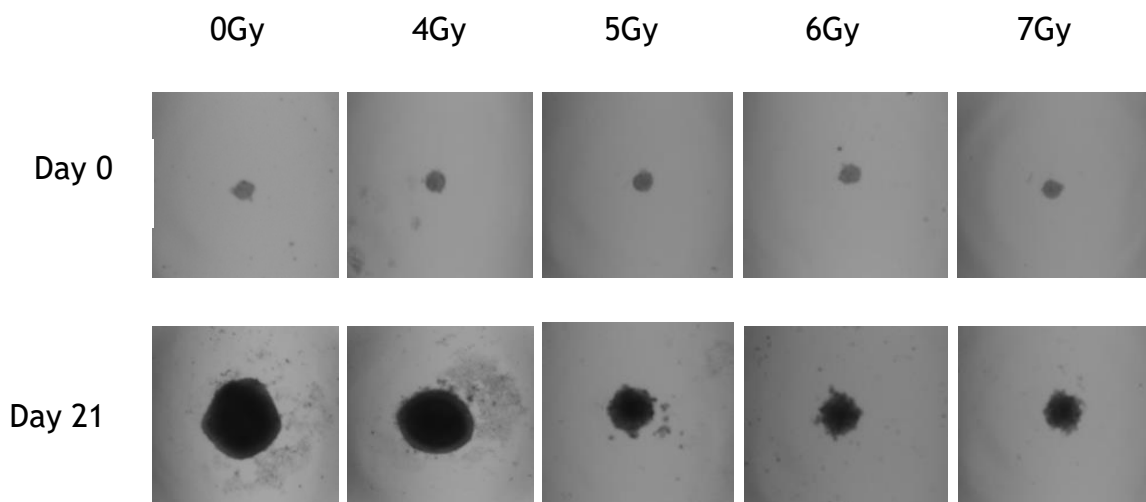


Figure 6.4 Representative 211H spheroids sizes at day 0 and day 21 following irradiation with increasing doses of IR

211H spheroids, seeded at a density of 10^2 cells per well, were irradiated with single fractions of IR between 4 and 7Gy. A sham irradiated group were included as a control. Spheroid growth was monitored for 21 days by regular brightfield imaging.

To determine the effect of initial cell number on radiosensitivity, spheroids were established at higher seeding densities and treated with IR as before. At a seeding density of 10^3 cells per well, H2052 spheroid growth was maximally delayed by an IR dose of 6Gy ($0.18\text{mm}^3 \pm 0.03\text{mm}^3$ at day 21 compared to $0.05\text{mm}^3 \pm 0.003\text{mm}^3$ at day 0). (Figure 6.5) In contrast, maximal growth delay was not seen until a dose of 11Gy was delivered to 211H spheroids seeded at a density of 10^3 cells per well (day 21 volume of $0.17\text{mm}^3 \pm 0.06\text{mm}^3$ compared to $0.08\text{mm}^3 \pm 0.002\text{mm}^3$ at day 0). (Figure 6.6)

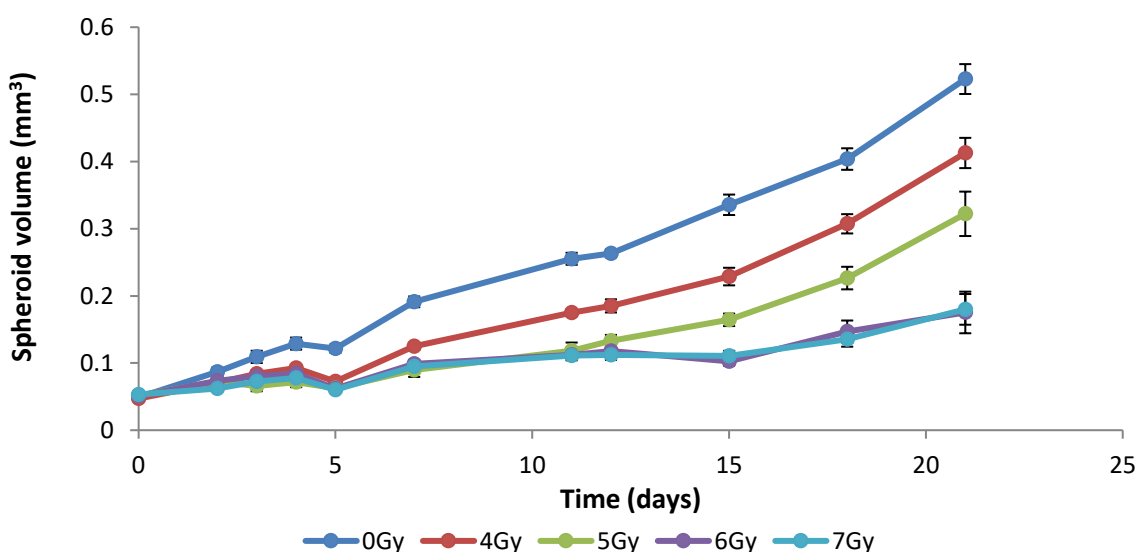


Figure 6.5 H2052 spheroid volumes following exposure to single fractions of IR

H2052 spheroids, seeded at a density of 10^3 cells per well, were exposed to single doses of IR between 4Gy and 7Gy and subsequent growth was monitored over 21 days. A sham irradiated control was included. Data are expressed as spheroid volume (mm^3) against time (days). Data was generated from a single experiment, employing 6 replicate spheroids per condition and error bars represent the standard deviation of replicates within the experimental group.

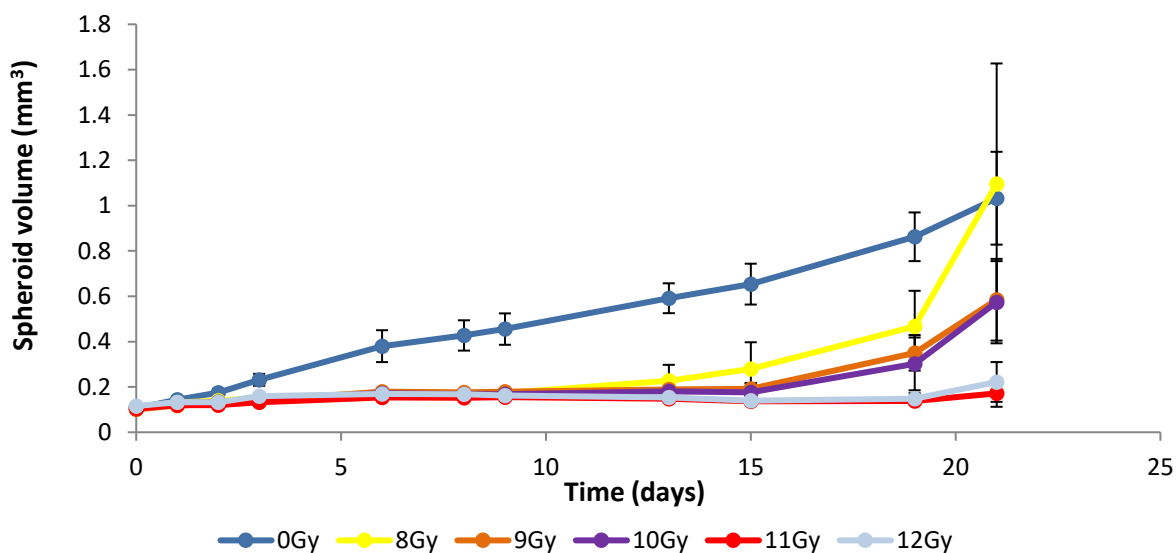


Figure 6.6 211H spheroid volumes following exposure to single fractions of IR

211H spheroids, seeded at a density of 10^3 cells per well, were exposed to single doses of IR between 8Gy and 12Gy and subsequent growth was monitored over 21 days. A sham irradiated control was included. Data are expressed as spheroid volume (mm^3) against time (days). Data was generated from a single experiment, employing 6 replicate spheroids per condition and error bars represent the standard deviation of replicates within the experimental group.

When the seeding density was further escalated to 10^4 cells per well, an IR dose of 6Gy was still able to adequately delay spheroid growth in the H2052 model ($0.3\text{mm}^3 \pm 0.02\text{mm}^3$) at day 21 compared to $0.23\text{mm}^3 (\pm 0.009\text{mm}^3)$ at day 0 (Figure 6.7). In the 211H model, the maximum growth delay was achieved with an IR dose of 11Gy until day 19 ($0.21\text{mm}^3 \pm 0.04\text{mm}^3$ compared to $0.27\text{mm}^3 \pm 0.02\text{mm}^3$ at day 0), however by day 21 the average spheroid volume observed with this dose had risen to $0.39\text{mm}^3 (\pm 0.13\text{mm}^3)$. (Figure 6.8)

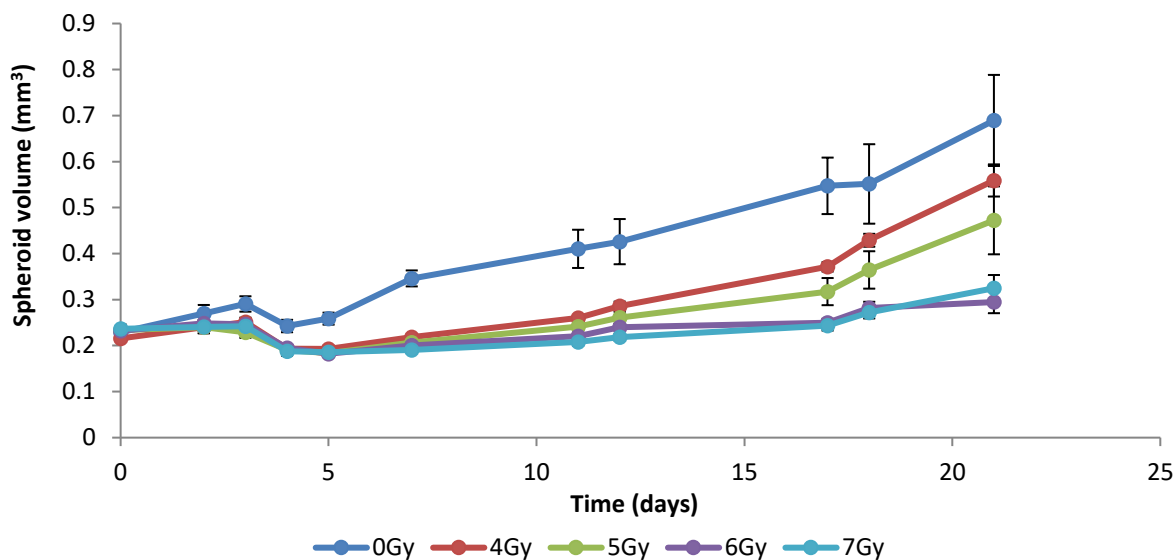


Figure 6.7 H2052 spheroid volumes following exposure to single fractions of IR

H2052 spheroids, seeded at a density of 10^4 cells per well, were exposed to single doses of IR between 4Gy and 7Gy and subsequent growth was monitored over 21 days. A sham irradiated control was included. Data are expressed as spheroid volume (mm^3) against time (days). Data was generated from a single experiment, employing 6 replicate spheroids per condition and error bars represent the standard deviation of replicates within the experimental group.

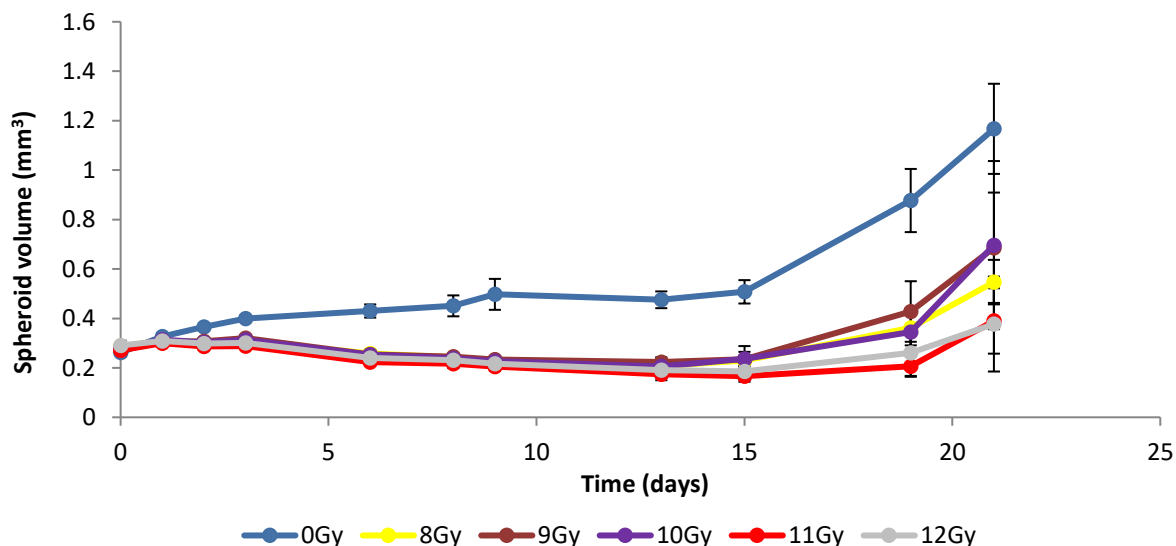


Figure 6.8 211H spheroid volumes following exposure to single fractions of IR

211H spheroids, seeded at a density of 10^4 cells per well, were exposed to single doses of IR between 8Gy and 12Gy and subsequent growth was monitored over 21 days. A sham irradiated control was included. Data are expressed as spheroid volume (mm^3) against time (days). Data was generated from a single experiment, employing 6 replicate spheroids per condition and error bars represent the standard deviation of replicates within the experimental group.

Together, these data demonstrate that IR can delay the growth of MPM spheroids and that larger doses of IR are associated with more efficacious control. Greater doses of IR were required to adequately delay the growth of 211H spheroids, particularly at higher seeding densities.

An optimal seeding density of 10^2 cells per well was selected for ongoing studies using this model, in combination with IR doses of 6Gy to 8Gy. These parameters were chosen to reduce the variability between 211H replicates at later experimental time points and to ensure that MPM spheroid growth could be adequately delayed by the selected doses of IR.

6.2.2 Hypofractionated radiotherapy regimens delay MPM spheroid growth with improved efficacy

Pilot studies have demonstrated that a single fraction of 6Gy IR optimally delays the growth of MPM spheroids, seeded at a density of 10^2 cells per well, over a period of 21 days. In the clinic, however, radiotherapy is typically delivered over a number of treatments (usually employing a dose of 2Gy per fraction), since this preferentially spares the late responding normal tissue owing to its typically low α/B ratio. As the α/B ratio of MPM remains largely unknown, studies were performed using the 3D *in vitro* spheroid model to determine whether MPM might be similarly spared by conventional fractionation. H2052 and 211H cells were seeded at a density of 10^2 cells per well and left to form spheroids before being irradiated with fractionated radiation schedules with total doses of either 6Gy or 8Gy. (Table 6.1) Where required, multiple radiation doses were delivered with a 24-hour inter fraction interval. Sham irradiated spheroids were included as a control. Spheroid growth was monitored for 21 days and data are reported as mean spheroid volume at day 21, averaged from 3 to 7 individual experiments, each incorporating 6 to 8 replicates per condition.

Table 6.1 Fractionated radiotherapy regimes

| Total dose | Conventionally fractionated regimes | Moderately hypofractionated regimes | Maximally hypofractionated regimes |
|------------|-------------------------------------|-------------------------------------|------------------------------------|
| 6Gy | 3x2Gy | 2x3Gy | 1x6Gy |
| 8Gy | 4x2Gy | 2x4Gy | 1x8Gy |

Spheroids were exposed to a total IR dose of 6Gy or 8Gy, delivered in regimes employing different doses per fraction. Fractionated treatments were delivered 24 hours apart and spheroid growth was monitored for 21 days.

Delivery of a total IR dose of 6Gy to MPM spheroids was associated with a significant reduction in volume compared to the sham irradiated controls, regardless of how it was delivered. For example, the mean volume of sham irradiated H2052 spheroids was $0.5\text{mm}^3 (\pm 0.04\text{mm}^3)$ at day 21, compared to $0.26\text{mm}^3 (\pm 0.05\text{mm}^3)$ in the group exposed to 3x2Gy ($p < 0.0001$), $0.23\text{mm}^3 (\pm 0.04\text{mm}^3)$ in those treated with 2x3Gy ($p < 0.0001$) and just $0.07\text{mm}^3 (\pm 0.02\text{mm}^3)$ in the 1x6Gy group ($p < 0.0001$). (Figure 6.9A) A similar trend was observed in the 211H spheroids. In this model, the sham irradiated spheroids displayed a mean volume of $0.93\text{mm}^3 (\pm 0.19\text{mm}^3)$, compared to $0.45\text{mm}^3 (\pm 0.08\text{mm}^3)$ in those treated with 3x2Gy ($p < 0.05$), $0.43\text{mm}^3 (\pm 0.11\text{mm}^3)$ in the group receiving 2x3Gy ($p < 0.05$) and $0.15\text{mm}^3 (\pm 0.11\text{mm}^3)$ in the spheroids exposed to 1x6Gy ($p < 0.0001$). (Figure 6.9B)

Although all IR regimes delivered a total dose of 6Gy and were associated with a reduction in spheroid volume, the delivery of the dose in a single 6Gy fraction produced significantly smaller spheroids at day 21 than regimes employing 2Gy or 3Gy per fraction. For example, in the 211H model, delivery of 1x6Gy was associated with a mean spheroid volume of $0.15\text{mm}^3 (\pm 0.11\text{mm}^3)$ at day 21, compared to $0.45\text{mm}^3 (\pm 0.08\text{mm}^3)$ in the group exposed to 3x2Gy ($p < 0.0001$) and $0.43\text{mm}^3 (\pm 0.11\text{mm}^3)$ in those treated with 2x3Gy ($p < 0.0001$). (Figure 6.9B) The same pattern was seen in the H2052 model. (Figure 6.9A)

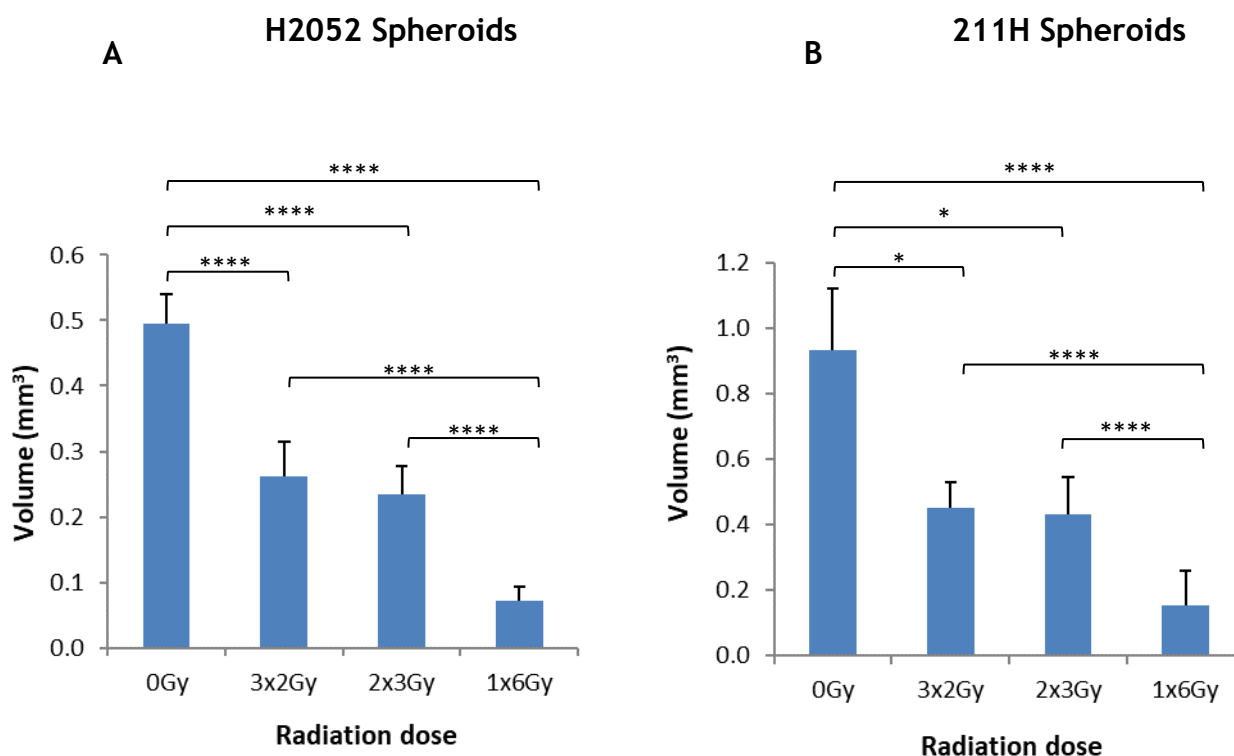


Figure 6.9 The effect of 6Gy on H2052 (A) and 211H (B) spheroid volumes at day 21

Spheroids were exposed to a total IR dose of 6Gy, delivered in different doses per fraction and growth was monitored over 21 days. Data is expressed as the mean spheroid volume at day 21, averaged from 3 to 7 individual experiments, each incorporating 6 to 8 replicates per condition (0Gy n=7; 3x2Gy n=3; 2x3Gy n=3; 1x6Gy n=3). Error bars reflect the standard deviation of the means. Statistical significance was determined with a linear mixed effect model, using the cubed root of the transformed data value. (*p<0.05; ****p<0.0001)

Exposure of MPM spheroids to a total IR dose of 8Gy reduced spheroid volume in a manner similar to that observed with 6Gy. In both cell lines, exposure to 8Gy significantly reduced day 21 spheroid volume compared to the sham irradiated control, regardless of the delivery regime, and the greatest reduction in volume was seen with a single 8Gy fraction. (Figure 6.10 A and B) In contrast to the data generated for 6Gy regimes, significant differences in day 21 spheroid volumes were observed between groups treated with conventionally fractionated and moderately hypofractionated IR regimes. For example, in the H2052 model, exposure to 4x2Gy IR was associated with a mean spheroid volume of 0.22mm³

($\pm 0.05\text{mm}^3$) at day 21, compared to $0.15\text{mm}^3(\pm 0.04\text{mm}^3)$ in spheroids exposed to $2\times 4\text{Gy}$ ($p<0.0001$). (Figure 6.10A) Similarly, 211H spheroids exposed to $4\times 2\text{Gy}$ IR had a mean day 21 volume of $0.5\text{mm}^3(\pm 0.2\text{mm}^3)$, compared to $0.32\text{mm}^3(\pm 0.21\text{mm}^3)$ in the $2\times 4\text{Gy}$ group ($p<0.001$). (Figure 6.10B)

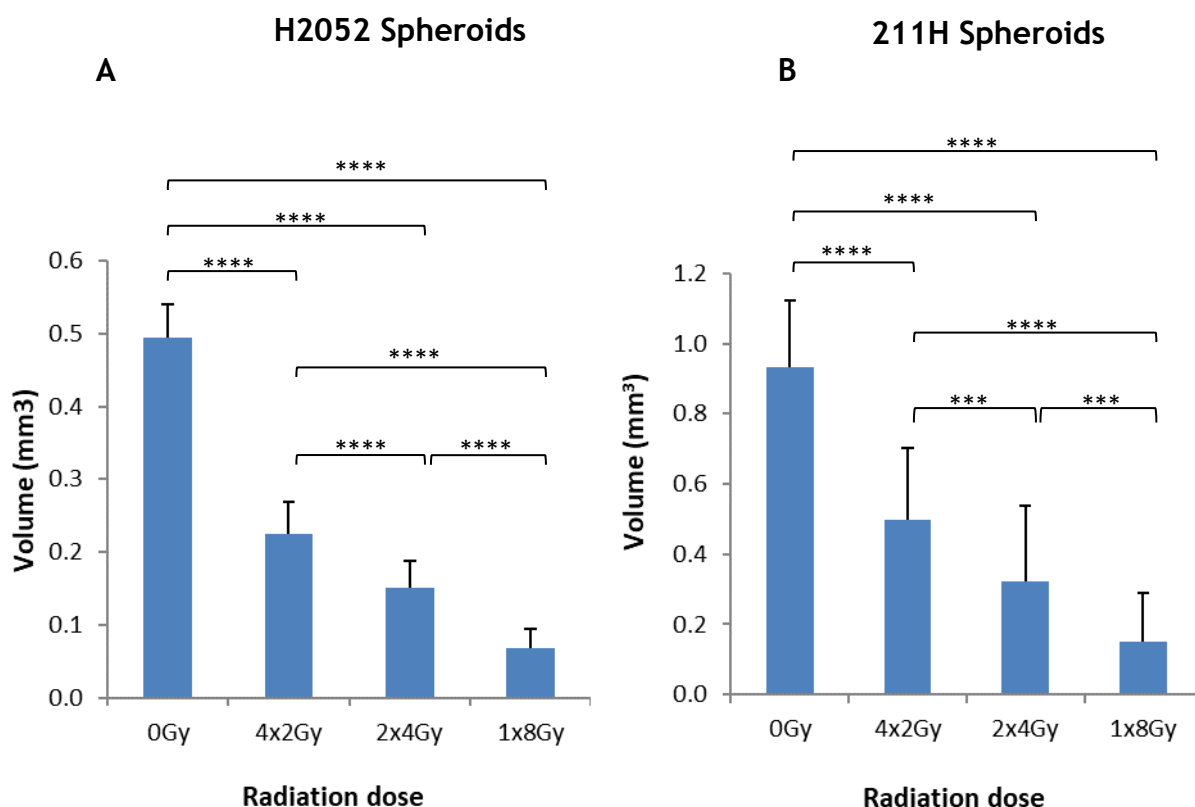


Figure 6.10 The effect of 8Gy on H2052 (A) and 211H (B) spheroid volumes day at 21

Spheroids were exposed to a total IR dose of 8Gy, delivered in different doses per fraction and growth was monitored over 21 days. Data is expressed as the mean spheroid volume at day 21, averaged from 7 individual experiments, each incorporating 6-8 replicates per condition. Error bars reflect the standard deviation of the means. Statistical significance was determined with a linear mixed effect model, using the cubed root of the transformed data value. (**p=0.001; ****p<0.0001)

In summary, these data suggest that MPM is sensitive to changes in radiation dose per fraction and that the most efficacious delay of spheroid growth is achieved with hypofractionated radiation regimes. These observations have clinical relevance, since the decision to select hypofractionated radiation regimes for the SYSTEMS-2 study was underpinned by the assumption that MPM has a low α/β ratio and may respond more favourably to IR delivered in larger doses per fraction.

6.2.3 Estimation of isoeffective radiation doses suggest MPM spheroids exhibit a low α/β ratio

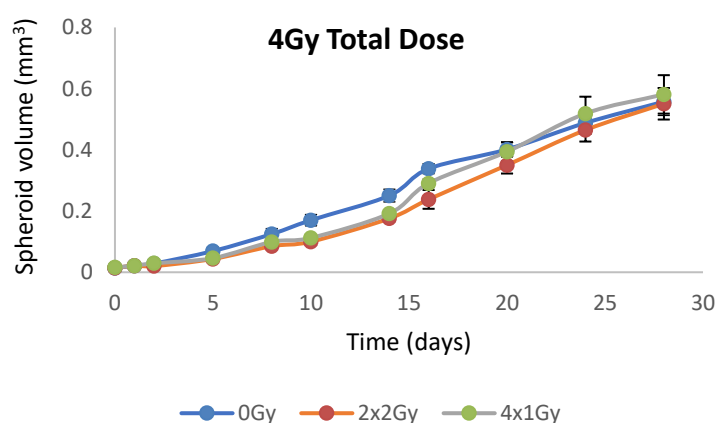
To further explore the assumptions made about the α/β ratio of MPM within the SYSTEMS-2 clinical trial, additional *in vitro* studies were conducted using the 3D spheroid model of MPM. Cells were seeded at a density of 10^2 cells per well and left to form spheroids before being irradiated with a selection of IR regimes that employed a variety of total doses, given over a number of different fractionation schedules. (Table 6.2) A sham irradiated group was included as a control and spheroid volume was monitored for 21 days in the 211H model and for 28 days in the H2052 model. Treatment effect was defined as volume reduction from the sham irradiated control and was used to generate a dose effect curve within radiation regimes utilising equal numbers of fractions. An isoeffective dose was then identified across radiation regimes and used to estimate the α/β ratio.

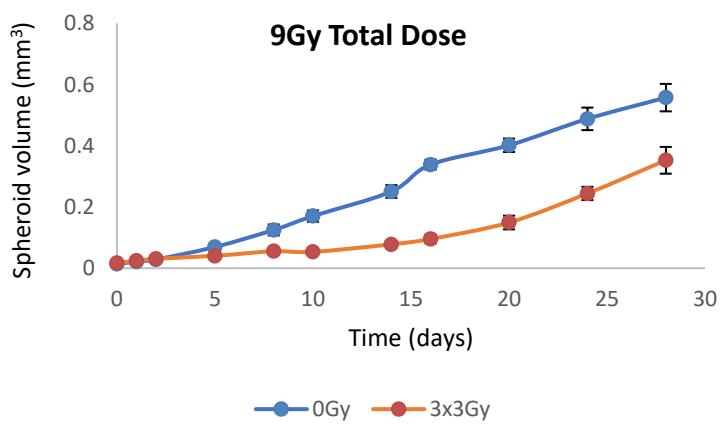
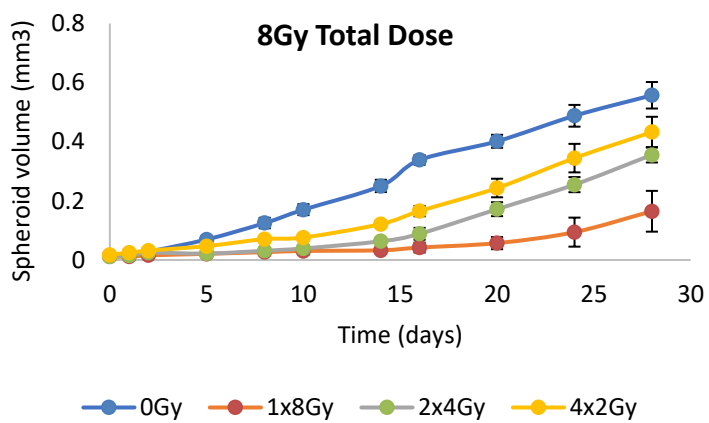
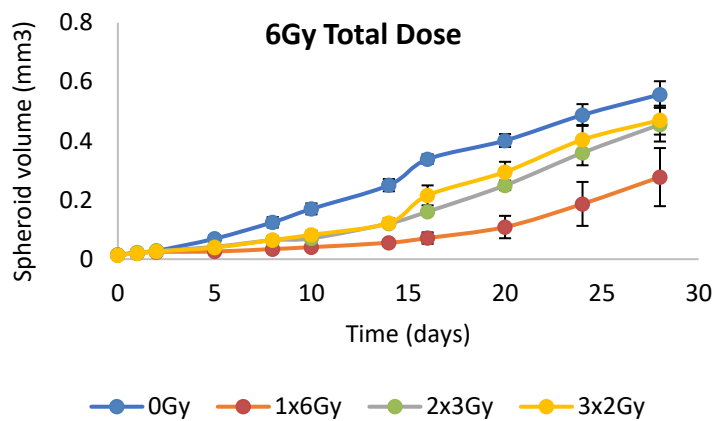
For clarity, the process used to estimate treatment effect, the generation of dose effect curves and calculations of isoeffective dose are illustrated for H2052 spheroids at day 14. (Table 6.3 and Figures 6.13-6.14) The remainder of the data for the H2052 and 211H cell lines are presented in Appendix 1.

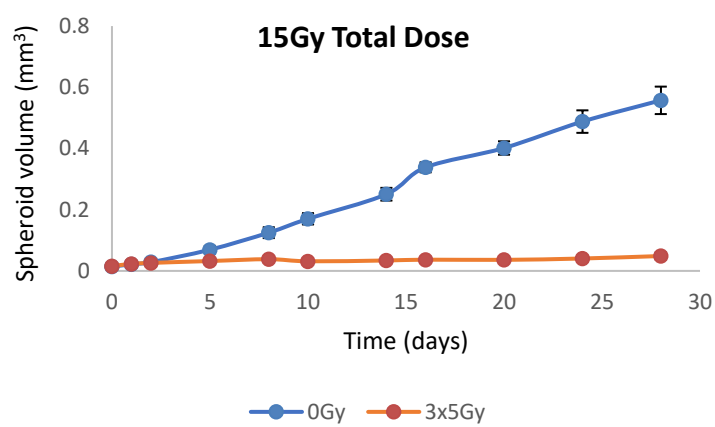
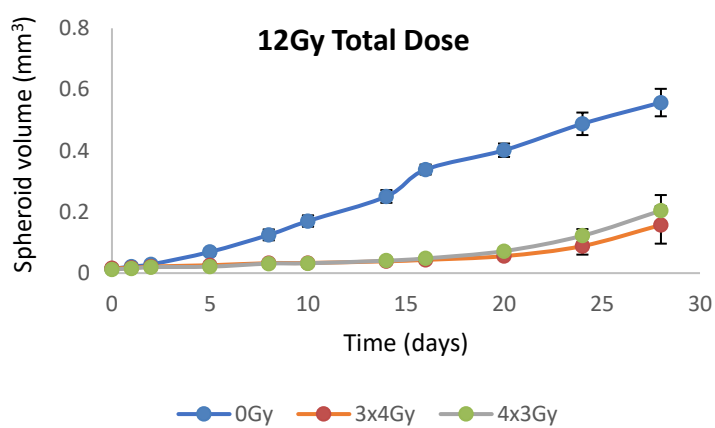
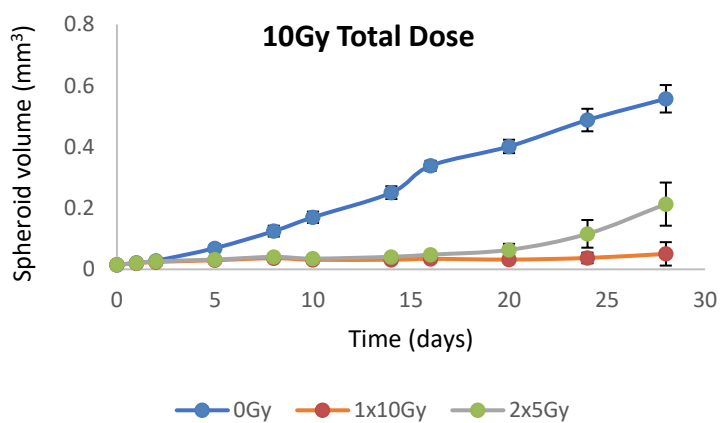
Table 6.2 Radiation schedules delivered to MPM spheroids to investigate tumour α/β ratio

| Regime fraction number | Total dose | Dose per fraction |
|-------------------------------|-------------------|--------------------------|
| 1 | 6Gy | 6Gy |
| | 8Gy | 8Gy |
| | 10Gy | 10Gy |
| 2 | 4Gy | 2Gy |
| | 6Gy | 3Gy |
| | 8Gy | 4Gy |
| | 10Gy | 5Gy |
| 3 | 6Gy | 2Gy |
| | 9Gy | 3Gy |
| | 12Gy | 4Gy |
| | 15Gy | 5Gy |
| 4 | 4Gy | 1Gy |
| | 8Gy | 2Gy |
| | 12Gy | 3Gy |
| | 16Gy | 4Gy |

Exposure of MPM spheroids to IR reduced spheroid volume in a dose dependent manner, as had been observed in earlier work. This is illustrated in both the single fraction and fractionated regimes, with greater total doses delaying spheroid growth more effectively. For example, in the H2052 model, delivery of 10Gy as a single fraction resulted in a mean day 28 spheroid volume of 0.05mm^3 ($\pm 0.04\text{mm}^3$) whereas a 6Gy single fraction produced a mean day 28 spheroid volume of 0.28mm^3 ($\pm 0.1\text{mm}^3$). (Figure 6.11) In the 211H model, delivery of a total dose of 9Gy as a 3x3Gy regime produced a mean day 21 spheroid volume of 0.27mm^3 ($\pm 0.16\text{mm}^3$), as compared to delivery of 6Gy in a 3x2Gy regime which produced a mean day 21 spheroid volume of 0.55mm^3 ($\pm 0.08\text{mm}^3$) (Figure 6.12). Furthermore, the influence of fractionation on spheroid growth was again observed in this data set, with more hypofractionated regimes delaying growth with greater efficacy. For example, in the H2052 model, delivery of 10Gy as a single fraction was associated with a mean day 28 spheroid volume of 0.05mm^3 ($\pm 0.04\text{mm}^3$), whereas delivery of the same dose as 2x5Gy allowed the spheroid volume to increase to 0.21mm^3 ($\pm 0.07\text{mm}^3$) by day 28. (Figure 6.11) Similarly, delivery of 8Gy as 2x4Gy was associated with a reduced mean day 21 volume ($0.47\text{mm}^3 \pm 0.3\text{mm}^3$) compared to delivery of the same dose as 4x2Gy ($0.64\text{mm}^3 \pm 0.18\text{mm}^3$) in the 211H model. (Figure 6.12)







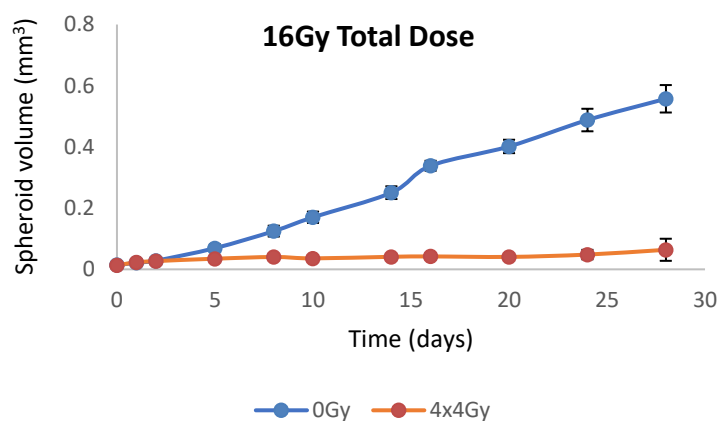
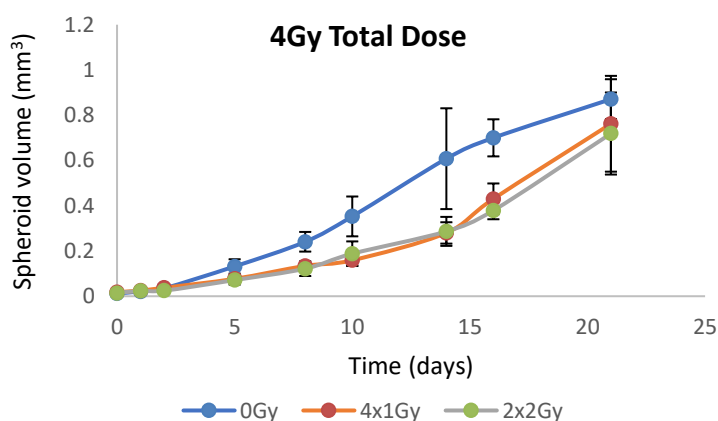
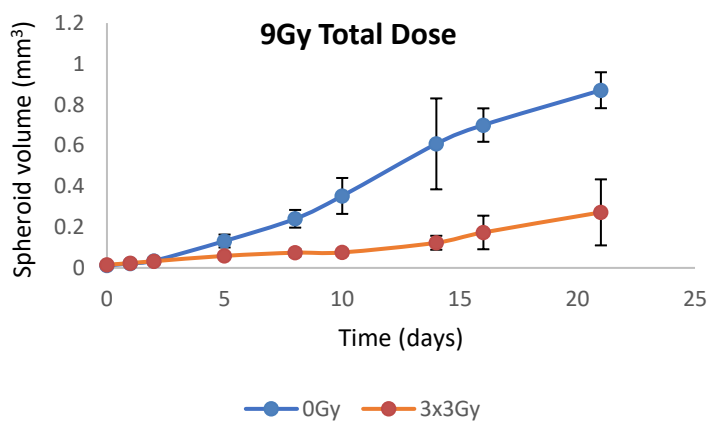
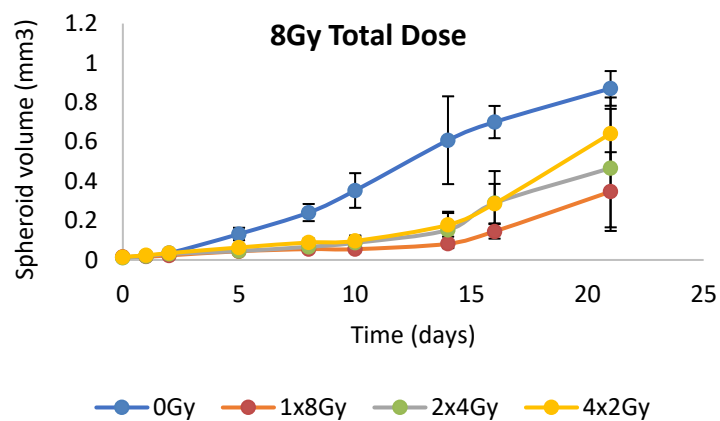
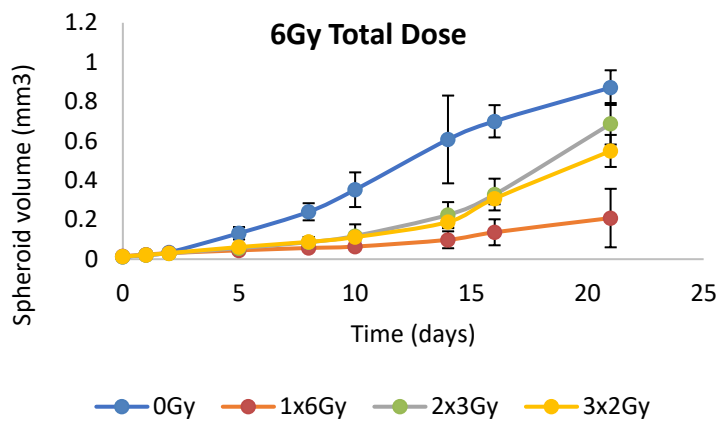
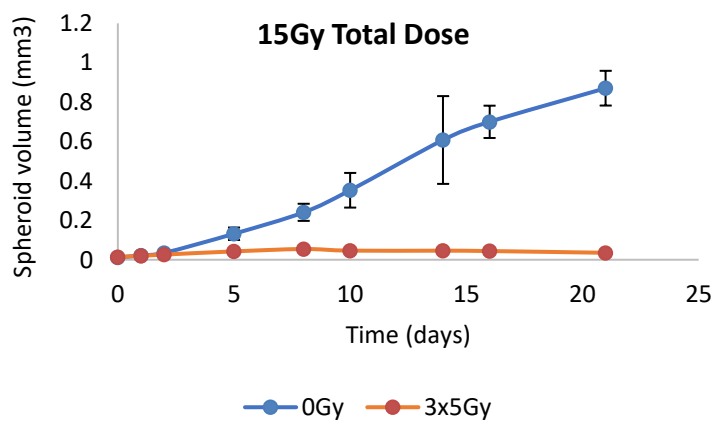
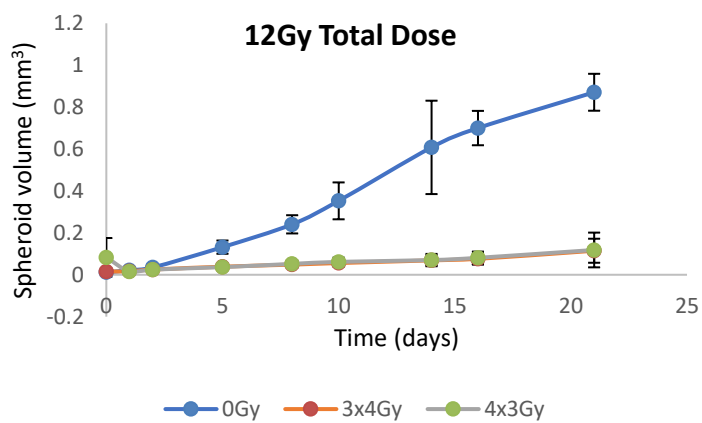
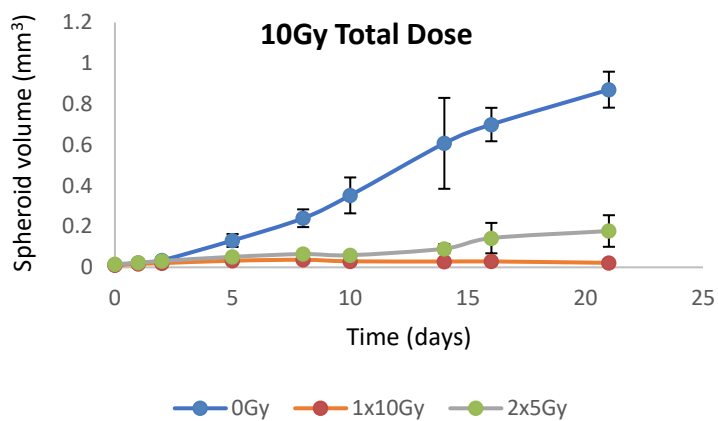


Figure 6.11 H2052 spheroid growth delay curves following exposure to IR

H2052 cells were seeded at 10^2 cells per well and allowed to form spheroids before being exposed to different doses of IR. IR was delivered either as single fractions, two fractions, three fractions, or as a four fraction regime. For clarity, data are plotted according to total dose delivered rather than by fractionation regime. Spheroid growth was monitored for 28 days and 3D volume data was generated from 2D images. Data is expressed as spheroid volume (mm^3) against time (days) and was generated from a single experiment, incorporating 6 replicates per condition. Error bars represent the standard deviation between the replicates.







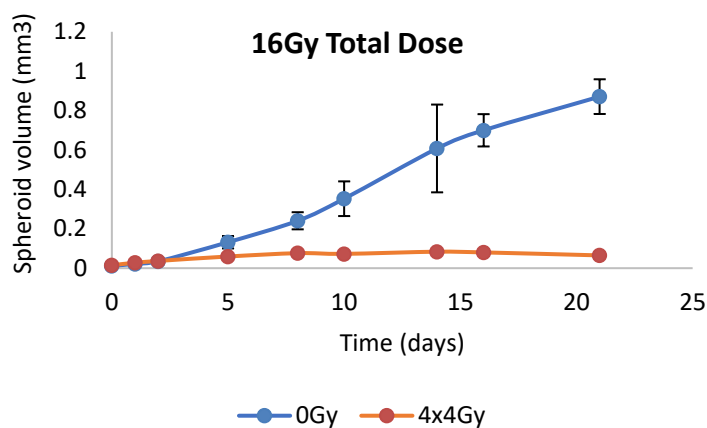


Figure 6.12 211H spheroid growth delay curves following exposure to IR

211H cells were seeded at 10^2 cells per well and allowed to form spheroids before being exposed to IR of differing doses. IR was delivered either as single fractions, two fractions, three fractions, or as a four fraction regime. For clarity, data are plotted according to total dose delivered rather than by fractionation regime. Growth was monitored for 21 days and 3D volume data was generated from 2D images. Data is expressed as spheroid volume (mm^3) against time (days) and was generated from a single experiment, incorporating 6 replicates per condition. Error bars represent the standard deviation between the replicates.

Useful estimations of treatment effect were observed from both MPM models from day 10 onwards. Prior to this, levels of spheroid damage were so similar between fractionation regimes that dose response curves could not accurately distinguish between IR doses. Furthermore, at these early time points, the size of effect was so limited that it was often not possible to identify a common level between the regimes.

The day 14 volumes of irradiated H2052 spheroids and sham irradiated controls are illustrated in Table 6.3. The reduction in spheroid volume compared to that of the sham irradiated control was calculated and dose effect curves generated to illustrate the impact of different doses of IR, delivered in an equal number of fractions (Figure 6.13). A common effect level was selected, for example, 0.2mm^3 , and the required total dose of IR necessary to reduce growth by this amount was determined for each fraction number.

Table 6.3 H2052 spheroid volume reduction caused by each IR regime at day

14

| | Regime | Total dose | Volume (mm ³) | Volume reduction from control (mm ³) |
|-------------------------|--------|------------|---------------------------|--|
| Sham-irradiated control | 0Gy | 0Gy | 0.2506 | 0 |
| Single fraction | 1x6Gy | 6Gy | 0.0556 | 0.1950 |
| | 1x8Gy | 8Gy | 0.0327 | 0.2179 |
| | 1x10Gy | 10Gy | 0.0314 | 0.2191 |
| Two fractions | 2x2Gy | 4Gy | 0.1760 | 0.0746 |
| | 2x3Gy | 6Gy | 0.1209 | 0.1297 |
| | 2x4Gy | 8Gy | 0.0632 | 0.1873 |
| | 2x5Gy | 10Gy | 0.0410 | 0.2095 |
| Three fractions | 3x2Gy | 6Gy | 0.1227 | 0.1279 |
| | 3x3Gy | 9Gy | 0.0780 | 0.1726 |
| | 3x4Gy | 12Gy | 0.0386 | 0.2120 |
| | 3x5Gy | 15Gy | 0.0340 | 0.2165 |
| Four fractions | 4x1Gy | 4Gy | 0.1921 | 0.0585 |
| | 4x2Gy | 8Gy | 0.1215 | 0.1291 |
| | 4x3Gy | 12Gy | 0.0407 | 0.2098 |
| | 4x4Gy | 16Gy | 0.0410 | 0.2095 |

The mean volume of irradiated H2052 spheroids is subtracted from the mean volume of the sham irradiated controls to provide an estimate of the relative effect (damage) of each IR schedule on spheroid volume at day 14.

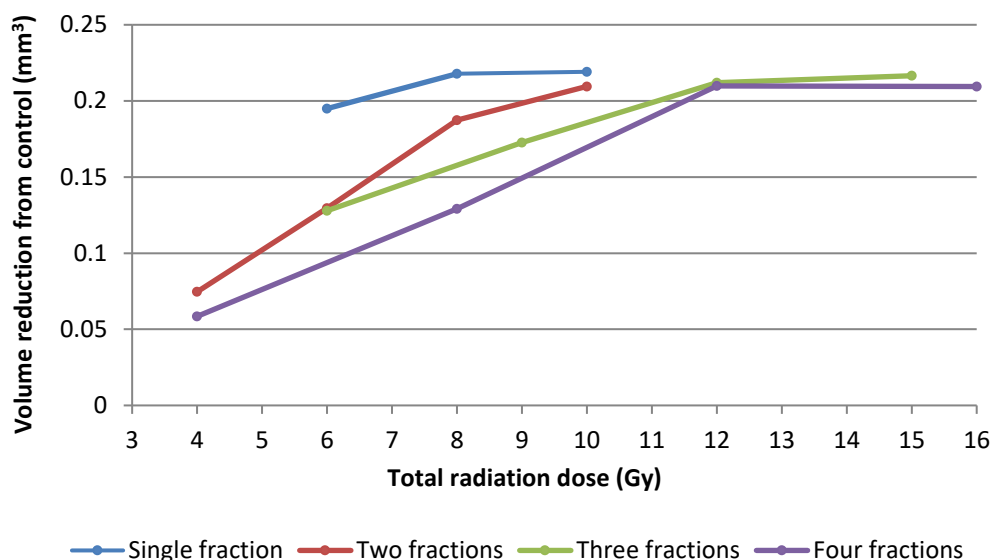


Figure 6.13 Dose effect curves illustrating the impact of different fractionation schedules on H2052 spheroid damage at day 14

Spheroid volume reductions from the sham irradiated control were used to generate a dose response curve for IR schedules delivered as a single fraction, two fractions, three fractions or four fractions. A common level of effect amongst all response curves was selected and the total dose of IR required to generate this effect determined.

Table 6.4 Dosimetry information on the IR regimes required to reduce H2052 spheroid volume by 0.2mm³ from the sham irradiated control at day 14

| Number of fractions (n) | Effect (mm ³) | Total dose (D) | Dose per fraction (D/n) | Reciprocal total dose (1/D) |
|-------------------------|---------------------------|----------------|-------------------------|-----------------------------|
| 1 | 0.2 | 6.441 | 6.441 | 0.155 |
| 2 | 0.2 | 9.141 | 4.571 | 0.109 |
| 3 | 0.2 | 11.089 | 3.696 | 0.090 |
| 4 | 0.2 | 11.513 | 2.878 | 0.087 |

The relative total IR dose is established from the dose response curves. The dose per fraction and reciprocal of the total dose is calculated for each regime.

The reciprocal of the total dose required for a given isoeffect and the corresponding dose per fraction were calculated. (Table 6.4) Plotting these values gives a straight line, with gradient proportional to the value of β and y-intercept corresponding to the value of α . At day 14, the estimated α/β ratio in H2052 cells was 1.1. (Figure 6.14 and Table 6.5)

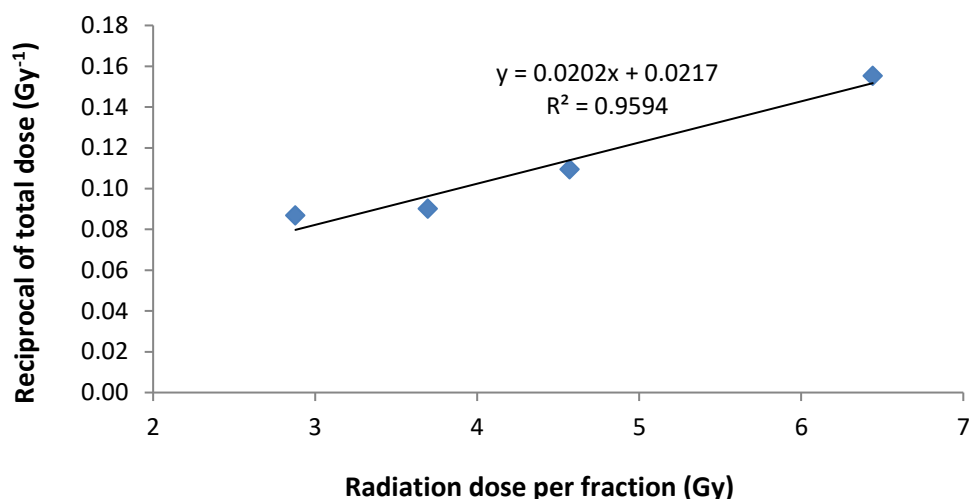


Figure 6.14 Estimate of the α/β ratio of H2052 spheroids

Plotting the reciprocal of the total IR dose required to reduce spheroid volume by 0.2mm^3 at day 14 from the sham irradiated control, against the corresponding dose per fraction gives a line, whose slope is proportional to β and whose intercept on the vertical axis corresponds to the value of α . The equation for the regression line was used to calculate the α/β ratio and the fit of the data points is indicated by R^2 .

This procedure was used to identify isoeffective dose levels of IR on each day that the spheroids were imaged. These data were subsequently used to estimate the α/β ratio of the cell lines, using the equation derived from the line of best fit between the data points. Multiple results were generated over the course of the study, which allowed the reproducibility and reliability of the method to be assessed.

An element of variability was observed in the α/β ratio estimates generated from the H2052 model, but data suggest that this cell line exhibits a mean α/β ratio of 1.67 (95% CI 1.0 -2.3). (Table 6.5)

Table 6.5 Estimated α/β ratios from H2052 spheroids

| Day | Isoeffect level (mm ³) | Estimated α/β ratio (Gy) |
|--------------------------------------|------------------------------------|-------------------------------------|
| 10 | 0.13 | 0.8 |
| 14 | 0.2 | 1.1 |
| 16 | 0.28 | 2.3 |
| 21 | 0.3 | 1.2 |
| 24 | 0.35 | 2.9 |
| 28 | 0.3 | 1.7 |
| Mean | | 1.67 |
| $\bar{x} \pm 1.96 (\delta/\sqrt{n})$ | | 1.0 - 2.3 |

Isoeffective data from four dose response curves were utilised to generate the estimate of α/β ratio on each day of imaging. The average α/β ratio is quoted with 95% confidence intervals.

Analysis of the data from the 211H model highlighted a greater degree of variability amongst α/β ratio estimates. Whilst the estimate from day 10 reflected that seen in the H2052 model, data generated from subsequent time points saw the estimate rise progressively. To illustrate, the α/β ratio estimate at day 14 was 2.5Gy (using an isoeffect level of 0.51mm³) whereas by day 21 it had risen to 3.8Gy (using an isoeffect level of 0.65mm³). This cell line displayed a mean α/β ratio of 2.63 (95% CI 1.3- 3.9). (Table 6.6)

Table 6.6 Estimated α/β ratios from 211H spheroids.

| Day | Isoeffect level (mm ³) | Estimated α/β ratio (Gy) |
|--------------------------------------|------------------------------------|-------------------------------------|
| 10 | 0.29 | 0.8 |
| 14 | 0.51 | 2.5 |
| 16 | 0.55 | 3.4 |
| 21 | 0.65 | 3.8 |
| Mean | | 2.63 |
| $\bar{x} \pm 1.96 (\delta/\sqrt{n})$ | | 1.3 - 3.9 |

Isoeffective data from four dose response curves were utilised to generate the estimate of α/β ratio on each day of imaging. The average α/β ratio is quoted with 95% confidence intervals.

Although it may not be possible to establish a definitive α/β ratio for MPM using these data, results suggest that the α/β ratio may be lower than that exhibited by many other cancers. Considered with the other data presented in this chapter, specifically the sensitivity of MPM cell lines to changes in IR dose per fraction and the superior effect of dose hypofractionation in the delay of spheroid growth, these data add further support to the hypothesis that MPM exhibits a low α/β ratio and so would be optimally treated with hypofractionated radiation regimes.

6.3 Discussion

The radiobiology and radiosensitivity of MPM have not been well characterised and the limited number of *in vitro* studies exploring this to date have focussed on the impact of single fractions of IR, using 2D experimental models to generate measures of cell survival. (Carmichael et al., 1989, Hakkinen et al., 1996) Earlier studies in our own laboratory used 2D clonogenic survival assays to investigate the radiobiology of 211H and H2052 cell lines. (Jackson et al., 2020) Data from this work generated cell survival curves which fitted the LQ model and although parameters for α and β were calculated, the α/β ratio has not

been formally reported, due to a large degree of variability seen between the 3 biological replicates in the experiment, resulting in wide confidence intervals around the mean.

This study is the first to use a more clinically relevant 3D *in vitro* model to assess specifically the impact of dose fractionation on MPM spheroids and to use this data to provide an informed estimate of α/β ratio. The challenges of generating robust measures of radiosensitivity from 3D models have been discussed in section 1.5.4. Nevertheless, a 3D spheroid approach has several strengths within the setting of MPM, in particular the ability to replicate more closely the properties of an *in vivo* tumour and to mimic the cellular aggregates found in pleural effusions that correlate with disease aggression. (Delahaye et al., 1990) Furthermore, this model allows for an estimation of volume, which is the parameter used for assessment of tumour in the clinical setting. The ReVISP software, (Piccinini et al., 2015) used to assess volume, is specifically designed to take into account spheroid protuberances and irregularities, facilitating the generation a more realistic 3D representation than other systems, which assume a sphere or ellipsoid morphology. (Gaylord and Clowes, 1906, Woglom, 1925, Tomayko and Reynolds, 1989) This is a particularly important consideration for the 211H spheroids, which exhibited an irregular growth pattern.

6.3.1 Cell line considerations

All experiments were conducted using two cell lines (H2052 and 211H), originally derived from patients with epithelioid and biphasic MPM respectively. Intrinsic differences between the behaviour of these cells lines cultured as spheroids were observed.

The growth characteristics displayed by these two cell lines were markedly different. When grown in 3D, H2052 cells formed compact structures, forming regularly shaped spheroids with sharply circumscribed borders. While the rate of growth changed following treatment with IR, the regular growth pattern of the spheroids was preserved, rendering them easy to delineate. In contrast, 211H

cells displayed an irregular growth pattern, forming loosely packed spheroids with a hazy border. Frequently, cellular projections could be seen from one side of the spheroid and as the volume increased, the spheroid lost its structural integrity. Cells became detached from the main body of the spheroid and the structure became increasingly difficult to delineate accurately. For this reason, 211H spheroid replicates displayed greater variability in their shape and volume than their H2052 counterparts, particularly at later experimental time points. Acknowledging these limitations, data from both cell lines are represented and discussed.

6.3.2 The radiation dose-dependent response of MPM to IR

In keeping with the studies of Carmichael and Hakkinen, in which the radiosensitivity of two MPM cell lines were established using a clonogenic assay, data presented here suggest that MPM cell lines are radiosensitive, and that the degree of radiosensitivity can vary between them. (Carmichael et al., 1989, Hakkinen et al., 1996) Data show that the growth of MPM spheroids, seeded at a density of 10^2 cells per well, was impaired by doses of IR greater than 4Gy, delivered as single doses. Whilst doses of IR above 6Gy were found to optimally delay spheroid growth at this seeding density, some spheroid recovery was observed following exposure to 4Gy and 5Gy. This dose dependent nature of the spheroid response to IR is likely a reflection of the extent of DNA damage inflicted by the IR and the capacity of the cell to repair it. For example, exposure to a single fraction of 6Gy IR would cause extensive DNA damage, which is likely to overwhelm molecular pathways of repair and cause significant cellular senescence or death. This is reflected in poor growth and reduced day 21 spheroid volumes in both MPM models exposed to this dose. Conversely, exposure to a single IR dose of 4Gy IR would be predicted to induce fewer DNA DS breaks. The ability of spheroids to recover from the insult and continue to grow, suggests that cellular repair pathways remain functional and so this dose of IR is insufficient to significantly impact on the growth of MPM spheroids.

The variable response of the two cell lines to equal doses of IR suggests that 211H spheroids may be more radioresistant than their H2052 counterparts, in

keeping with the aggressive and treatment resistant nature of non-epithelioid MPM. The exact control exerted on spheroid growth by a specific dose of IR cannot be accurately ascertained in a single study and the lack of experimental repeats performed here is a clear limitation. However, this was preliminary work, conducted with the aim of generating pilot data with which to demonstrate 'proof of principle' and inform the optimal cell seeding density and radiation doses for subsequent studies of dose fractionation.

6.3.3 The response of MPM to hypofractionated IR

In vitro 3D spheroid models have previously been demonstrated as a robust system in which to investigate the effect of dose hypofractionation on cancer cell radioresponse. (Kaaijk et al., 1997) Data generated within this study suggests that MPM spheroids are sensitive to changes in IR dose per fraction and that their growth is most effectively delayed by hypofractionated regimes. This observation suggests that there is a capacity for SLD repair in these cells.

Following exposure to a single dose of 6Gy, spheroid volumes were significantly lower than with a regime delivering the same total dose in a number of smaller fractions (i.e. 3x2Gy or 2x3Gy). Fractionated IR causes proportionately less DNA damage with each exposure and a treatment gap of 24 hours allows the cell time to repair any SLD. This allows recovery before the next dose of IR is given and facilitates tumour sparing in the same way that dose fractionation spares late tissue toxicity. Delivery of the same total dose in a hypofractionated manner appears to dramatically impact on the level of spheroid growth delay achieved.

This finding was further supported by the observation that spheroid volumes were significantly different between the conventionally and moderately fractionated regimes when a total dose of 8Gy IR was employed. This was not seen in the 6Gy model, potentially due to the relatively small difference between 2Gy per fraction and 3Gy per fraction schedules, but exposure to a more hypofractionated regime utilising 4Gy per fraction resulted in significantly smaller spheroids at day 21 than in the 4x2Gy group. In keeping with previous

findings, the most efficacious growth delay was observed with the maximum dose per fraction of 1x8Gy.

Despite this novel data in an MPM model, the discovery that tumour control can be more efficacious with hypofractionated radiotherapy is not new. In the case of prostate and breast cancer, recently generated radiobiological data have altered clinical practise, (Yarnold et al., 2011, Miralbell et al., 2012) but published values for α/β in a number of tumour sites suggest that many cancers will exhibit sparing with fractionated radiotherapy. (van Leeuwen et al., 2018) Crucially, it is the degree of sparing compared to normal tissue which will guide fractionation protocols between tumour types. A clear limitation of this study is the lack of control group from which the relative sparing displayed by MPM could be estimated. Future studies should include cell lines with known α/β ratios to provide an optimal comparator.

6.3.4 Estimating the α/β ratio of MPM

6.3.4.1 Technique selection

The technique used to generate estimates of MPM α/β ratio was adapted from a paper by Stewart *et al* (1984). (Stewart et al., 1984) Reduction in spheroid volume was used as a measure of effect, facilitating the generation of dose effect curves. Isoeffective doses between the differing radiation schedules were determined and α/β ratio was estimated by plotting the dose per fraction against the reciprocal of the total dose required for the isoeffect.

Analysis of the dose effect curves demonstrates a profound influence of fractionation in this model, signified by the observation that the total radiation dose required to reduce spheroid volume by a given level increased progressively with increasing fraction number. As reported by Stewart *et al*, capacity for SLD repair can be assessed from the dose effect curves, by comparing the total dose required in different fractionation regimes to produce the same effect level. In keeping with previous findings, this analysis confirmed our observation that MPM

spheroids are susceptible to changes in dose per fraction and that the most effective spheroid growth delay is achieved with hypofractionated treatments.

By analysing data in this manner, the estimated mean α/β ratio of the H2052 MPM cell line was 1.67Gy (95% CI 1.0Gy- 2.3Gy) and 2.63Gy (95% CI 1.3Gy- 3.9Gy) in the 211H cell line. Both cell lines therefore demonstrate relatively low α/β ratios compared to other types of cancer (van Leeuwen et al., 2018) and support the values obtained for the JMN cell line by Carmichael (Carmichael et al., 1989) and the aneuploid MPM cell lines investigated by Hakkinen *et al.* (Hakkinen et al., 1996)

Although values of α and β have been generated for MPM, this data cannot be used as a direct measure of cell line radiosensitivity. This is because the output measure in these experiments was 'spheroid volume' rather than classical radiobiological parameter of 'cell survival'. Nevertheless, while the raw values may not be directly reflective of radiosensitivity, the ratio between them is a valid predictor of the response to dose per fraction.

6.3.4.2 Limitations of the selected technique

Whilst this method has generated MPM α/β ratios which were similar to those reported by other groups, there were a number of problems encountered with the technique which may have influenced our results.

Firstly, it was observed that the isoeffective data points did not always conform to a linear relationship and occasionally there were data points which appeared to deviate from the trend. For H2052 this was most frequently data representing the single fraction of IR, whereas in the 211H dataset this was less consistently problematic. The presence of data points not conforming to the fit increased uncertainty in this method and the cause and impact of this issue needs to be carefully considered. Whilst the dose and fractionation regimes for this work were selected on the basis of previous spheroid irradiation data, the effects

observed following exposure to single fractions of IR were much greater than those seen in the other fractionation regimes. Consequently, equivalent effects were often at the extreme of the single fraction data. It was observed by Stewart *et al* that whilst the choice of isoeffect does not affect the outcome of the analysis, data taken from extremes of curves may be less reliable. (Stewart *et al.*, 1984) However, this problem was not exclusively seen when data was taken from an extreme of a data set. Therefore, it may be that single fraction data should be avoided for this type of experiment and that multi-fraction data alone should be used to calculate precise measures of radiosensitivity. In future experiments, this issue could be further explored by selecting single fractions of lower doses, whose effect levels would more reliably align with those seen in the other fractionation regimes. Alternatively, single fraction data could be omitted altogether and replaced with an increased number of multi-fraction radiation regimes. Despite this acknowledged limitation, values generated for the parameter R^2 were above 0.9 for all of the H2052 data, with the exception of data from day 10 which had an R^2 value of 0.89. This suggests that the data points are adequately close to the regression line for this data to be considered valid. For the 211H data, values for R^2 ranged from 0.72 to 0.89, suggesting that conformity to the regression line was more limited.

A further issue noted with this technique was the increasing α/β ratio over time observed in the 211H cell line. Clinical studies have shown that over the course of a radiotherapy regime, the α/β ratio of tissue can increase, potentially through upregulation of the HRR pathway. (Somaiah *et al.*, 2012) Specific analysis of the DNA repair pathways employed by the spheroids was outwith the scope of this project, but alterations in DDR may provide an explanation for this observation, in addition to radiobiological factors, such as hypoxia or proliferation. An alternative explanation may lie in the irregular growth pattern of the 211H spheroids, leading to increased experimental variability. The accuracy of the chosen technique relies on consistent spheroid responses which can be accurately determined and robustly compared across fractionation regimes. The growth pattern of the 211H cell line may render it a suboptimal choice for such an experimental approach and future work may incorporate alternative cell lines, with more regular growth patterns.

Due to time constraints, this study was only performed once. Clearly it is difficult to draw definitive conclusions regarding tumour α/β ratio from data generated in a single dose response experiment, performed using only 2 cell lines. Nevertheless, the α/β data generated from this 3D model compliments that generated earlier in our lab in which 2D clonogenic modelling was performed on the same 2 cell lines. (Jackson et al., 2020) The α/β values obtained from this work have not been published due to uncertainties in their accuracy, reflected in the wide confidence intervals around the mean. They were however, estimated to be lower than those classically estimated for cancer. The combination of these dataset does lend weight to the suggestion that MPM may be more fraction size dependent than previously thought, although clearly further confirmatory studies need to be conducted. Given the range of radiosensitivities and variations in α/β ratios observed in other studies using MPM cell lines, it would be useful to repeat this work on a panel of cell lines, using both clonogenic assays and tumour growth delay approaches to gain further insight.

Finally, whilst the approach used in this study has been based on that published by Stewart *et al*, (Stewart et al., 1984) there are important differences between these studies which need to be considered when assessing data reliability. In the Stewart paper, a comprehensive fractionation schedule was employed, employing 1-64 fractions, delivering between 0.9Gy and 16Gy per fraction. Responses were measured over 48 weeks, using 3 robust functional endpoints which could be reliably measured and used in combination to determine radiobiological parameters. In contrast, the α/β ratio estimate in this study is generated from the assessment of a single endpoint over a maximum of 28 days after irradiation with 1-4 fractions employing 1Gy to 10Gy per fraction. The difficulty in obtaining accurate data at early timepoints has already been discussed, and the restrictions imposed by experimental size limited the number of data points which could be generated within each fractionation regime. Although the premise of the experiments are similar, data generated from this study will be inherently less robust than that generated by Stewart *et al*.

6.3.4.3 Strengths of the selected technique

Despite these limitations, the chosen technique was reliable and informative. Both previous studies of MPM radiosensitivity were performed on cells in 2D. (Carmichael et al., 1989, Hakkinen et al., 1996) The current model utilises a 3D *in vitro* system, which represents an intermediate level of complexity between cells in monolayers and *in vivo* tumours. Despite the inherent challenges of determining robust radiobiological parameters from 3D systems, the increased therapeutic resistance displayed by cells in 3D (Kobayashi et al., 1993, Desoize and Jardillier, 2000, Barbone et al., 2008) may permit a more accurate estimation of true tumour radiosensitivity than can be achieved in 2D models and therefore such data may reflect the clinical scenario more closely. The data generated in this work complements that generated in 2D in our laboratory using the same cell lines, in which the α/β ratio was estimated to be low.

The decision to expose spheroids to IR every 24 hours in the multi-fractionated regimes was informed by clinical practise and based on an assumption, supported by the literature surrounding the kinetics of cellular DNA repair, (Mariotti et al., 2013, Kochan et al., 2017) that this would allow sufficient time for SLD repair between exposures. Although it cannot be completely assured that SLD repair is fully completed in this timeframe, the greater spheroid recovery seen in fractionated regimes suggests that this methodology is sound.

In order to limit the impact of radiobiological factors, such as repopulation, on spheroid volume over time, treatment time was limited to four days and spheroid growth data was collected for a maximum of four weeks. Nevertheless, it cannot be guaranteed that the observed results are completely due to spheroid radiosensitivity, since factors such as re-oxygenation or proliferation, which could not be actively controlled, may have influenced outcomes. However, as such factors influence clinical outcome following radiotherapy, consideration in the model system may be advantageous from a translational perspective.

6.3.4.4 Alternative methods to determine spheroid response to IR

In contrast to 2D models of cell survival, established methods of determining radiobiological parameters from 3D models are scarce. The technique used by Stewart *et al* was adopted because of the similarities between the functional parameters assessed in their work and the measures of spheroid growth reduction generated in this model. An alternative method of assessing spheroid response to multi fraction irradiation has been proposed by Stuschke *et al*. (Stuschke *et al.*, 1992, Stuschke *et al.*, 1990, Stuschke *et al.*, 1995) This method utilises a 'spheroid control assay' to determine the radiation dose necessary to control the growth of 50% of the spheroids from which parameters of radiosensitivity can be calculated. In this assay, spheroids are transferred to 24 well plates 48 hours after irradiation and subsequently grown as monolayers over a 3 month period to determine the level of control exerted by the various radiation regimes. The timeframes necessary to generate such data and the deviation from methods of spheroid analysis which had already been established in our laboratory meant that this approach was not taken. Furthermore, allowing the spheroids to continue to grow as 3D structures rather than as monolayers, facilitates a more accurate representation of the tumour response to IR compared to the approach used by Stuschke *et al*, and suggests that our data may be more robust.

6.3.5 Clinical translation of data

It was not feasible to directly employ clinically relevant doses of IR within this *in vitro* study, since preliminary data suggested that doses sufficient for achieving control of spheroid growth were less than 15Gy, much lower than the total doses of 20Gy or 36Gy delivered in the SYSTEMS-2 study (data not shown). Doses of IR which delivered similar fraction sizes to those being investigated in SYSTEMS-2 were therefore selected (i.e. 4Gy or 6Gy per fraction). It could be argued that a requirement of between 6Gy to 8Gy to control the growth of spheroids initially seeded at 100 cells per well may not reflect a level of radiosensitivity which could be clinically applicable to the bulk of tumours often seen in this disease. Nevertheless, this pre-clinical model demonstrates proof of concept that MPM is

susceptible to radiation, sensitive to changes in dose per fraction and responds more effectively to hypofractionated radiotherapy regimes.

6.4 Summary

These data are the first to use a clinically relevant 3D *in vitro* model to investigate the radiobiological properties of MPM and challenges some of the most firmly held conceptions of this disease. Results suggest that following exposure to sufficient doses, growth of MPM *in vitro* can be effectively delayed by radiation. Furthermore, whilst a definitive α/β ratio has proved difficult to determine, data show that MPM is sensitive to changes in radiation dose per fraction and is most effectively controlled by hypofractionated regimes. These observations complement clonogenic data generated previously within our lab and taken together with data from fractionation studies, suggest that this tumour may have an α/β ratio lower than many other cancers and may exhibit sparing with fractionated regimes. This finding is clinically pertinent, given the choice of radiation dose and fractionation currently being investigated in the SYSTEMS-2 study. Outcome data from this clinical trial is awaited, but a more accurate understanding of the radiobiology of this disease will aid the selection of appropriate dose and fractionation regimes for future radiotherapy trials in MPM.

Chapter 7: Assessing the impact of novel radiosensitising drugs with fractionated radiotherapy on MPM spheroids

Chapter aim

This purpose of this chapter is to explore the activity of two commercially available compounds shown to radiosensitise MPM in 2D, using an in vitro 3D spheroid model. The compounds, which have different molecular targets, will be delivered with fractionated radiotherapy regimes, to determine whether they can radiosensitise MPM in 3D and whether their efficacy is affected by fractionation schedule.

7.1 Introduction

7.1.1 The rationale for using radiosensitisers

Radiotherapy is an effective method of killing tumour cells, but can also damage healthy tissue, leading to normal tissue toxicity. The delivery of a sufficiently tumouricidal dose is therefore often precluded by the close proximity of normal radiosensitive structures to tumour targets. Dose fractionation is used to facilitate safe dose escalation by preferentially sparing normal tissues from late side effects. As explained in section 1.4.4, late tissue effects usually exhibit a low α/β ratio and are sensitive to changes in radiation dose per fraction, whereas tumour clonogen killing and acute tissue reactions are characterised by high α/β ratios and are relatively insensitive to changes in dose per fraction. This discrepancy means that dose fractionation is selectively beneficial in sparing late tissue toxicity. To make tumours more sensitive to the effects of IR, drugs which selectively augment the effect of IR in tumour cells are delivered in combination with radiotherapy.

The superior clinical outcomes achieved when radiotherapy is delivered with such radiosensitising agents has been demonstrated in a variety of tumour types (Herskovic et al., 1992, Sultana et al., 2007, Rose et al., 1999, Rowell and O'Rourke N, 2004, Tobias et al., 2010) and has led to a combined approach becoming the standard of care in a number of malignancies. (Herskovic et al.,

1992, Sultana et al., 2007, Pignon et al., 2009, Curran et al., 2011)

Traditionally, chemotherapeutic agents that cause DNA damage, such as platinum compounds or topoisomerase inhibitors, were used to enhance the cancer cell kill resulting from exposure to IR. More recently, however, as our understanding of the molecular pathways governing cancer cell survival has grown, an interest has developed in the production of novel radiosensitising agents which target the pathways of resistance to IR. Commonly targeted pathways include those responsible for DNA-damage repair, intercellular signalling and transduction pathways and apoptosis. Many small molecules that affect these processes are being taken forward in clinical trials. (Zaidi et al., 2009)

The advantage of combining IR with a selective radiosensitising agent is that improved tumour kill can be achieved without necessitating an increase in radiation dose and therefore without incurring any escalation in normal tissue toxicity. In MPM, where tumour encases the irregularly shaped pleural cavity and lies in close proximity to a number of normal radiosensitive structures, safe delivery of radical doses of IR is particularly challenging. The discovery of an efficacious radiosensitising agent would therefore likely be of marked clinical benefit in this disease.

7.1.2 Rationale for investigating the radiosensitising properties of DNA damage repair proteins

The fundamental role of DNA damage in the pathogenesis of MPM (Betti et al., 2017) and the implication that genetic aberrations within the NHEJ pathway may contribute to treatment resistance in this disease (Kettunen et al., 2001, Roe et al., 2010) has led to an interest in DNA damage repair proteins as potential therapeutic targets in MPM. (Toumpanakis and Theocharis, 2011) The critical role of DNA-PKcs in the NHEJ DNA repair pathway and its association with repair-mediated radioresistance has been described in section 1.7.4. This serine/threonine kinase is a member of the phosphatidylinositol 3-kinase (PI3K) family, for which a number of inhibitors have been developed. Broad spectrum PI3K inhibitors, such as wortmannin and LY294002, (Nakamura et al., 1997,

Arcaro and Wymann, 1993) and those which are progressively more specific for DNA-PKcs, such as NU7026 (Willmore et al., 2004) and NU7441 (Leahy et al., 2004) (discussed in section 1.7.5) have been described.

Manipulation of DNA-PKcs function with the selective inhibitor NU7441 has been investigated as a strategy to enhance tumour responses to radiotherapy (Yu et al., 2015, Shaheen et al., 2011, Ciszewski et al., 2014, Zhao et al., 2006) and chemotherapy (Yanai et al., 2017) in a number of malignancies, and whilst NU7441 has been demonstrated to promote extensive radiosensitisation in non-small cell lung cancer cell lines, (Saha et al., 2014) there is a paucity of research surrounding the use of this inhibitor in MPM. Nevertheless, unpublished data from our own lab suggests that NU7441 may demonstrate therapeutic activity in this disease. Studies investigating the activity of NU7441 in a 2D *in vitro* model, using two different MPM cell lines, showed that this drug exhibited single agent activity, with an EC50 1.69 μ M in 211H cells and 2.35 μ M in H2052 cells. Furthermore, when delivered with IR, 1 μ M NU7441 radiosensitized MPM cells with a sensitizer enhancement ratio (SER) of 1.85 and 2.43 in 211H and H2052 cells respectively.

Given the potent radiosensitising activity seen with this drug in previous studies, NU7441 was selected for use within our 3D spheroid model, where it was anticipated to act as a positive control. Inhibition of DNA-PK is unlikely to result in tumour specific radiosensitisation because the adjacent normal tissues also use the NHEJ pathway to repair DNA damage. Therefore, even if a therapeutic interaction with IR is demonstrated in MPM spheroids, NU7441 would not be our first choice of drug in the clinic because of the likelihood of exacerbating normal tissue effects.

7.1.3 Rationale for investigating the radiosensitising properties of BH-3 mimetics

The critical role of the intrinsic apoptotic pathway in mediating cellular death following IR and the reliance of MPM on anti-apoptotic BCL-2 proteins to evade apoptosis, suggests that manipulation of this pathway with BH3 mimetics may provide a valuable therapeutic opportunity for radiosensitisation in this disease. Whilst IR can induce apoptosis in both tumour cells and normal tissue, concurrent exposure to a BH3 mimetic, that would increase cellular levels of free pro-apoptotic proteins, may preferentially promote apoptosis in MPM cells, which are naturally more susceptible to this process. Any therapeutic activity demonstrated with this approach may therefore be tumour specific

The validity of utilising BH3 mimetics as a therapeutic approach in cells which are 'primed for death' has been demonstrated in other malignancies. Exposure of Bcl-xL dependent human acute T lymphoblastic leukaemia cell lines to the Bcl-xL inhibitor A1331852 as a single agent resulted in reduced cell survival and a reported EC50 of 6nM. (Leverson et al., 2015) Furthermore, the potential for BH3 mimetics to overcome MPM resistance to apoptosis has been demonstrated *in vitro* in 2D studies and *in vivo*, where dual blockade of Bcl-2 and Bcl-xL with 2-methoxy antimycin A3 engendered apoptosis, both as a single agent and in combination with chemotherapy. (Cao et al., 2007) The role of BH3 mimetics as radiosensitisers has been assessed in other studies, where an ability to overcome acquired radioresistance of breast cancer cells and increase the radiosensitivity of cervical cancer HeLa cells, via an apoptotic-driven pathway, has been demonstrated. (Wu et al., 2014, Li et al., 2012, Wang et al., 2012) Nevertheless, the only available data surrounding the use of BH3 mimetics as a potential radiosensitiser in MPM has been generated in our own lab. (Jackson et al., 2020) Results suggest that inhibition of apoptosis may underpin the radioresistance observed in this disease and that this tumour characteristic may be mediated in 2D culture by a dependence on Bcl-xL. When Bcl-xL activity was inhibited in 211H and H2052 cell lines using A1331852, cell survival was reduced. In addition to displaying single agent activity (EC50 270nM in 211H cells and 133nM in H2052 cells), A1331852 also sensitised these cells to IR, via an apoptosis driven pathway, with a SER of 1.55 in 211H cells (1 μ M A1331852) and 1.80 in H2052

cells (0.3 μ M A1331852). (Jackson et al., 2020) Having identified clinically-relevant targets for radiosensitisation, this encouraging work can be taken forward to establish the impact of dose fractionation on BH3 mimetic activity in MPM cell lines cultured in 3D.

7.1.4 Selection of radiosensitisers for investigation in MPM

Two novel radiosensitising agents have therefore been selected for investigation with fractionated IR in a 3D model of MPM. These agents are NU7441, a selective inhibitor of DNA-PKcs, and A1331852, a selective Bcl-xL inhibitor.

7.1.5 Selection of an appropriate platform to investigate radiosensitisation of MPM

The specific attributes of the *in vitro* 3D spheroid system that make it a robust platform on which to study MPM have been discussed in sections 1.5.3 and 6.1.3.2. Nevertheless, the increased resistance to apoptosis observed when MPM is cultured in 3D (Barbone et al., 2008) and the ability of MPM to form structures similar to spheroids *in vivo* (Delahaye et al., 1990, Kim et al., 2005) makes this a particularly strong model on which to perform these investigations.

The *in vitro* 3D spheroid model will therefore be used for this work. The single agent activities of the drug and IR alone will be explored before any therapeutic interactions between them are investigated.

7.1.6 Confirming target proteins in experimental and clinical samples

To confirm that these target proteins are present in MPM spheroids, DNA-PKcs and Bcl-xL expression will be quantified by IHC staining of FFPE H2052 and 211H spheroids. Given the redundancy of function known to exist between the anti-apoptotic Bcl-2 proteins, (Ozvaran et al., 2004, Han et al., 1996) and the differential relative expression of anti-apoptotic Bcl-2 proteins in mesothelioma cells observed in our own lab, levels of Mcl-1 and Bcl-2 will also be explored.

To determine the potential translational impact of this *in vitro* work to the clinic, IHC will be used to determine the expression profile of DNA-PKcs and anti-apoptotic Bcl-2 proteins in the clinical samples of mesothelioma patients who took part in the SYSTEMS and SYSTEMS-2 studies.

7.2 Results

7.2.1 Fractionation determines efficacy of IR in delaying MPM spheroid growth

To determine the sensitivity of MPM cells to IR, spheroids were treated and allowed to grow for 21 days. The effect of fractionation on MPM growth was assessed by exposing the spheroids to different radiation regimes. To control for the total dose received, all irradiated spheroids were treated with a dose of 8Gy, but this was delivered in schedules with different doses per fraction. Spheroid size was monitored by regular imaging and 3D volume was determined by reconstruction of 2D representations. For simplicity, data are presented as the mean spheroid volume at the end of the experiment.

Exposure of MPM spheroids to a total dose of 8Gy IR reduced growth by day 21, regardless of the fractionation regime. In the H2052 model, for example, the sham irradiated spheroids grew to a volume of $0.52 \pm 0.03\text{mm}^3$ by day 21, compared to those receiving a single 8Gy fraction of IR, which grew to only $0.1 \pm 0.03\text{mm}^3$ ($p < 0.0001$) (Figure 7.1A). Similarly, in the 211H spheroids, exposure to a single dose of 8Gy resulted in a day 21 volume of $0.25 \pm 0.11\text{mm}^3$, as compared to $1.03 \pm 0.26\text{mm}^3$ in the sham irradiated controls ($p < 0.0001$) (Figure 7.1B). In keeping with data shown in section 6.2.2, delivery of a total dose of 8Gy reduced the growth of both H2052 and 211H spheroids in a manner that was dependent on fractionation schedule, with hypofractionated regimes demonstrating the greatest efficacy. (Figure 7.1)

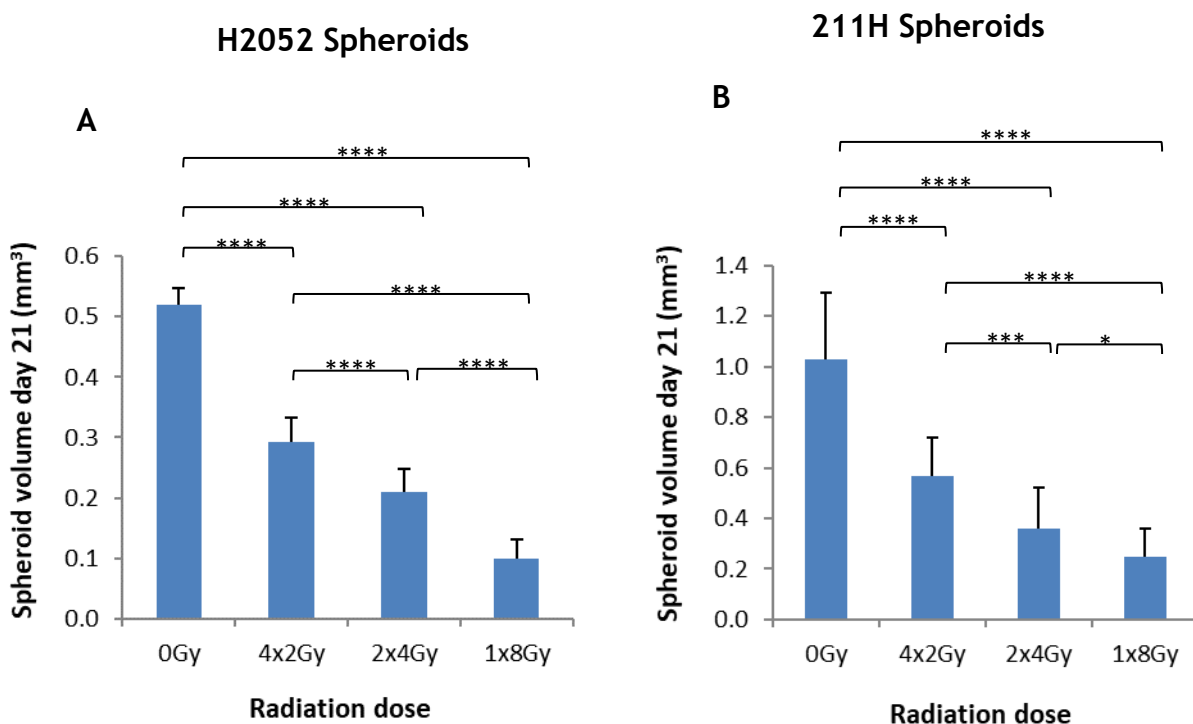


Figure 7.1 The effect of radiation alone on MPM spheroid volume at day 21

Spheroids were exposed to a total IR dose of 8Gy, delivered in different doses per fraction and growth was monitored over 21 days. Data is expressed as the mean spheroid volume in mm³ at day 21, averaged from 4 individual experiments, each incorporating 6-8 replicates per condition. Error bars reflect the standard deviation of the means. Statistical significance was determined with a linear mixed effect model, using the cubed root of the transformed data value. (*p<0.05; ***p<0.001; ****p<0.0001)

7.2.2 NU7441 did not exert any single agent activity in MPM cell lines

To determine the single agent activity of NU7441, MPM spheroids were treated with increasing concentrations of the drug or a DMSO control and were allowed to grow for 21 days. Spheroid size was monitored and data are presented as the mean spheroid volumes at day 21. Exposure of MPM spheroids to NU7441 at concentrations of 0.03μM to 0.3μM had no impact on the spheroid volume observed at day 21 in either cell line model. For example, the mean volume of H2052 spheroids treated with 0.3μM NU7441 was 0.49 ± 0.07mm³ at day 21, compared to 0.52 ± 0.03 mm³ in those which had been treated with the DMSO control (Figure 7.2A). Similarly, in the 211H model, exposure to the DMSO control allowed spheroids to grow to a volume of 1.03 ± 0.3mm³ by day 21,

compared to $1.09 \pm 0.2 \text{ mm}^3$ in spheroids treated with $0.3 \mu\text{M}$ NU7441 (Figure 7.2B).

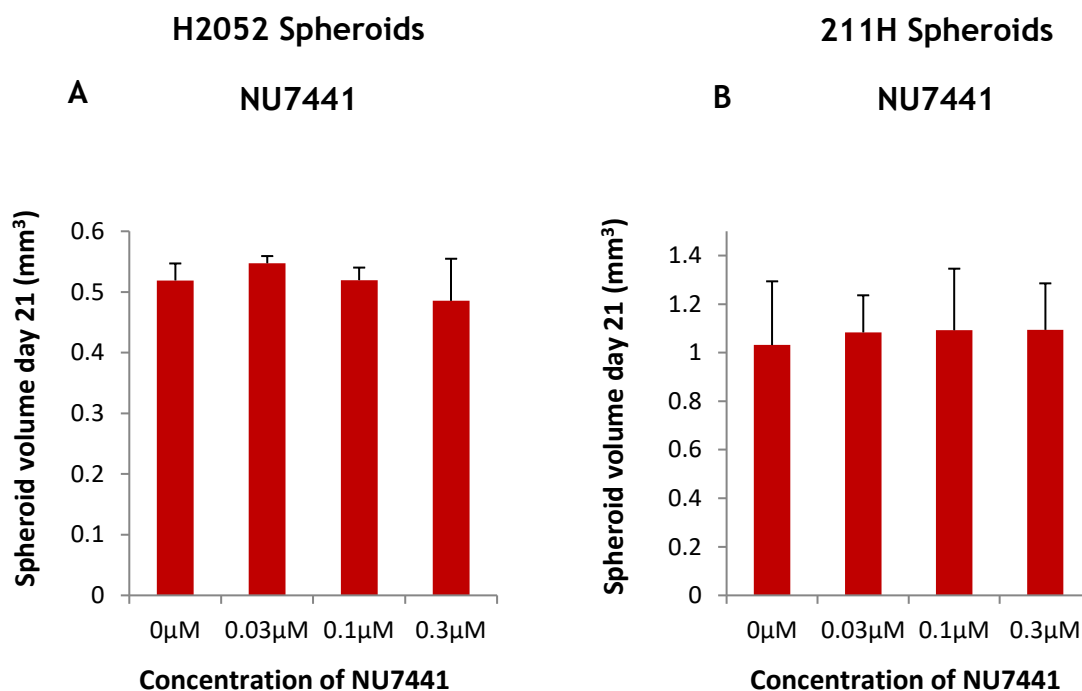


Figure 7.2 The effect of NU7441 alone on MPM spheroid volume at day 21

Spheroids were exposed to increasing concentrations of NU7441 and growth was monitored over 21 days. Data is expressed as the mean spheroid volume in mm^3 at day 21, averaged from 3-4 individual experiments ($0 \mu\text{M}$ $n=4$; $0.03 \mu\text{M}$ $n=3$; $0.1 \mu\text{M}$ $n=3$; $0.3 \mu\text{M}$ $n=4$). Each experiment incorporated 6-8 replicates per condition. Error bars reflect the standard deviation of the means. Statistical significance was determined with a linear mixed effect model, using the cubed root of the transformed data value.

7.2.3 Combination of NU7441 with IR exhibits a therapeutic interaction

To determine whether NU7441 was capable of sensitizing MPM spheroids to IR, spheroids were treated concomitantly with varying concentrations of the drug and a single IR dose of 8Gy. Spheroid size was monitored over 21 days and 3D volume was determined by reconstruction of 2D images. To reveal any potential radiosensitising activity, data are plotted as spheroid volume relative to the irradiated DMSO control, following correction for the effect of a single IR dose of 8Gy. This analysis acts to reveal any therapeutic interaction, for example if co-administration of IR with the drug reduces the spheroid volume more effectively than with IR alone.

Combination of NU7441 with a single 8Gy fraction of IR significantly reduced MPM spheroid volumes at day 21, compared to the irradiated DMSO control. For example, exposure to 8Gy IR and 0.03 μ M NU7441 reduced the relative H2052 spheroid volume to 72% \pm 6% of the control ($p < 0.001$) and the same radiation dose combined with 0.3 μ M NU7441 reduced it to 27% \pm 16% ($p < 0.0001$). (Figure 7.3A) In addition to being significantly different from the irradiated DMSO control, these volumes were also significantly different from each other ($p < 0.01$) (Figure 7.3A). A similar trend was observed in the 211H model with this drug, where for example, the relative spheroid volume reduction seen with 0.1 μ M NU7441 and 8Gy IR (47% \pm 12% of the control) was significantly different than that induced by exposure to 0.3 μ M NU7441 and 8Gy IR (20% \pm 6% of the control) ($p < 0.05$). (Figure 7.3B) These data indicate that the combination of NU7441 and IR is associated with a therapeutic interaction in MPM spheroids, the magnitude of which is dependent on the concentration of NU7441. This radiosensitising effect was also evident in the volume data, shown in Appendix 2.

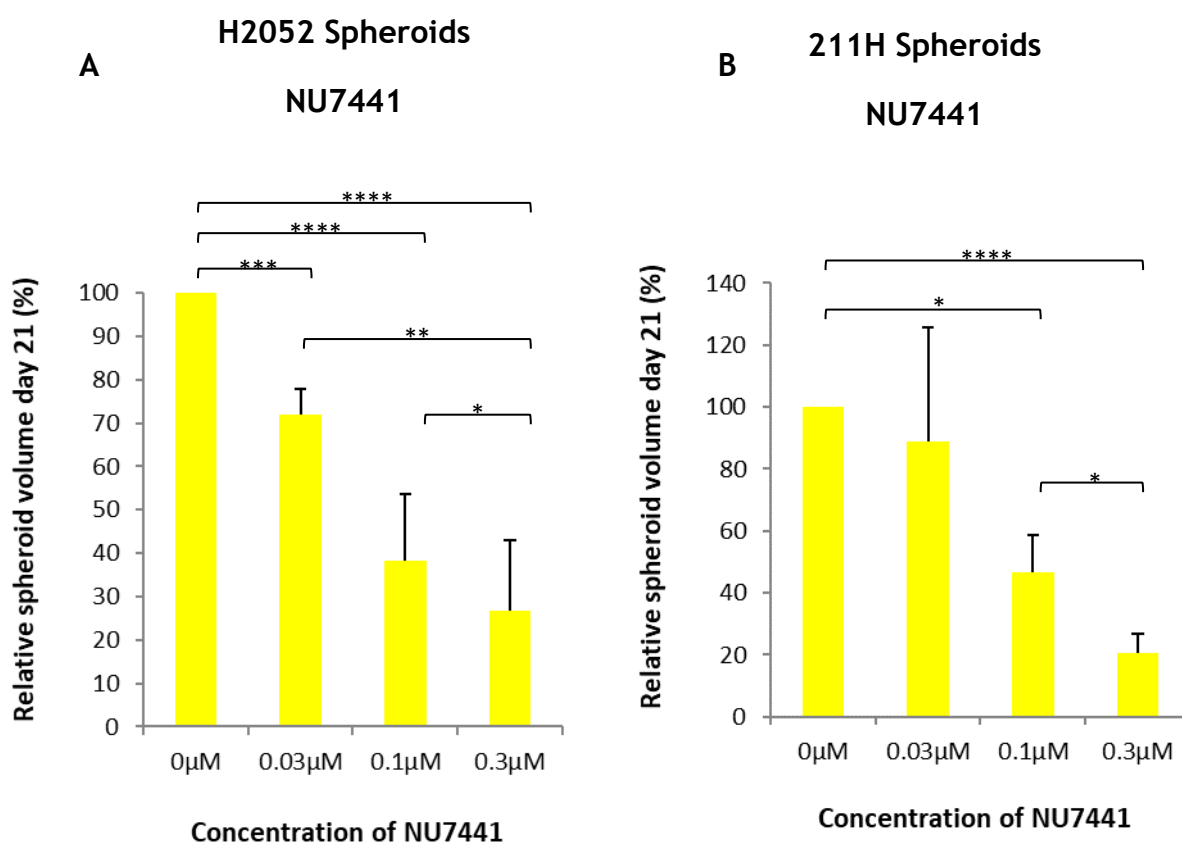


Figure 7.3 The effect of combination therapy with NU7441 and IR on relative MPM spheroid volume at day 21

Spheroids were exposed to increasing concentrations of NU7441 delivered with a single 8Gy fraction of IR and growth was monitored over 21 days. Data is expressed as the mean day 21 spheroid volume relative to the DMSO control, following correction for the effect of a single IR dose of 8Gy. Data were generated from 3-4 independent experiments (0μM n=4; 0.03μM n=3; 0.1μM n=3; 0.3μM n=4), with each experiment incorporating 6-8 replicates per condition. Error bars represent the standard deviations of the normalised means. Statistical analysis was performed using one way ANOVA and pairwise comparisons were generated with a post hoc Tukey test. (*p<0.05, **p<0.01, ***p<0.001; ****p<0.0001)

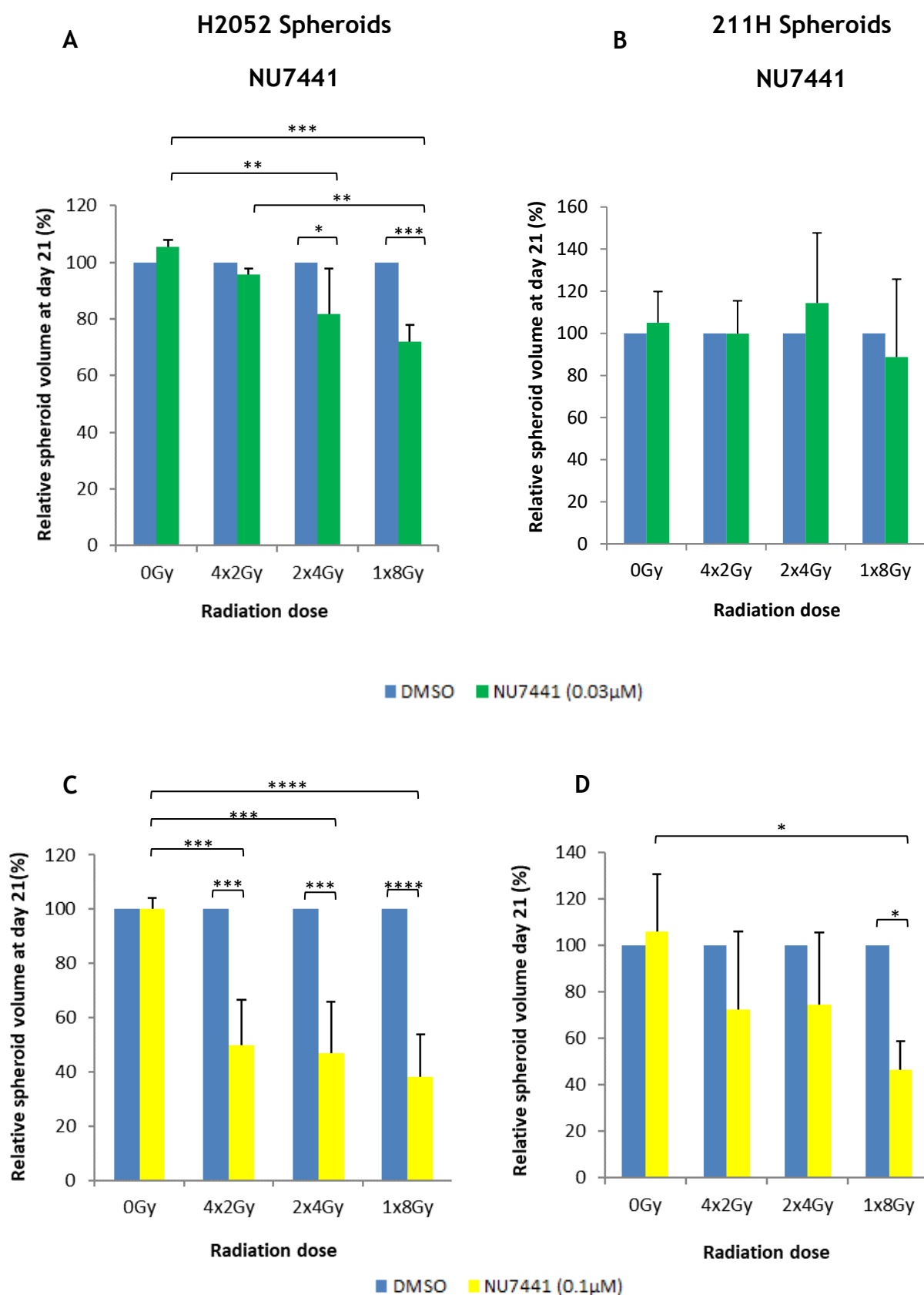
7.2.4 An enhanced radiosensitising effect of NU7441 was detected with hypofractionated IR at low drug concentrations

NU7441 has been observed to cause a radiosensitising effect in MPM spheroids when delivered with a single 8Gy fraction of IR, but clinically radiotherapy is delivered in a large number of small fractions, typically of 2Gy each. To assess the impact of fractionation on the radiosensitising effect of NU7441, MPM spheroids were treated with increasing concentrations of this drug in

combination with radiotherapy regimes delivering a total dose of 8Gy, over a different number of fractions. Data showing the day 21 spheroid volumes obtained under each condition can be found in Appendix 2, but for the purposes of highlighting therapeutic interaction, data are plotted as volume relative to DMSO control, following correction for the effect of each of the fractionation schedules alone (Figure 7.4 A-F).

In the H2052 model, exposure to a combination of 0.03 μ M NU7441 and IR was only associated with a significant reduction in the relative day 21 spheroid volume when hypofractionated radiation regimes were employed (Figure 7.4A). For example, when 0.03 μ M NU7441 was delivered with 2Gy per fraction (4x2Gy), the relative spheroid volume was not significantly different to the irradiated DMSO control (96% \pm 2%), whereas delivery of the same concentration of NU7441 with 2x4Gy and 1x8Gy IR reduced the relative spheroid volumes to 82% \pm 16% ($p < 0.05$) and 72% \pm 6% ($p < 0.001$) of each irradiated control respectively. The difference observed in relative volume reduction between the 4x2Gy spheroids and 1x8Gy spheroids was associated with a p value of < 0.01 , suggesting that the therapeutic interaction of NU7441 at this concentration is significantly greater when larger doses per fraction are employed. No therapeutic interaction was observed with 0.03 μ M NU7441 in the 211H model, regardless of fractionation regime (Figure 7.4B). When the NU7441 concentration was increased to 0.1 μ M, combination with IR in the H2052 model significantly reduced the day 21 spheroid volumes relative to the irradiated DMSO control across all fractionation regimes and the magnitude of the reductions were similar, regardless of the dose per fraction. (Figure 7.4C) In the 211H model, combination of 0.1 μ M NU7441 with 1x8Gy IR significantly reduced the day 21 spheroid volume relative to the irradiated control (47% \pm 12%; $p < 0.05$), but no significant reductions were observed in the 2x4Gy or 4x2Gy regimes (Figure 7.4D). Combination of IR with 0.3 μ M NU7441 reduced the relative spheroid volume at day 21 in both cell lines, with no significant differences noted in the magnitude of therapeutic interaction between fractionation regimes (Figure 7.4E and F) Together, these data suggest that NU7441 exerts a potent radiosensitising effect on MPM cells in a concentration dependent manner. Where the concentration of the drug was reduced sufficiently to allow a differential response to be detected, the

therapeutic interaction of NU7441 was marginally more efficacious with hypofractionated radiotherapy regimes.



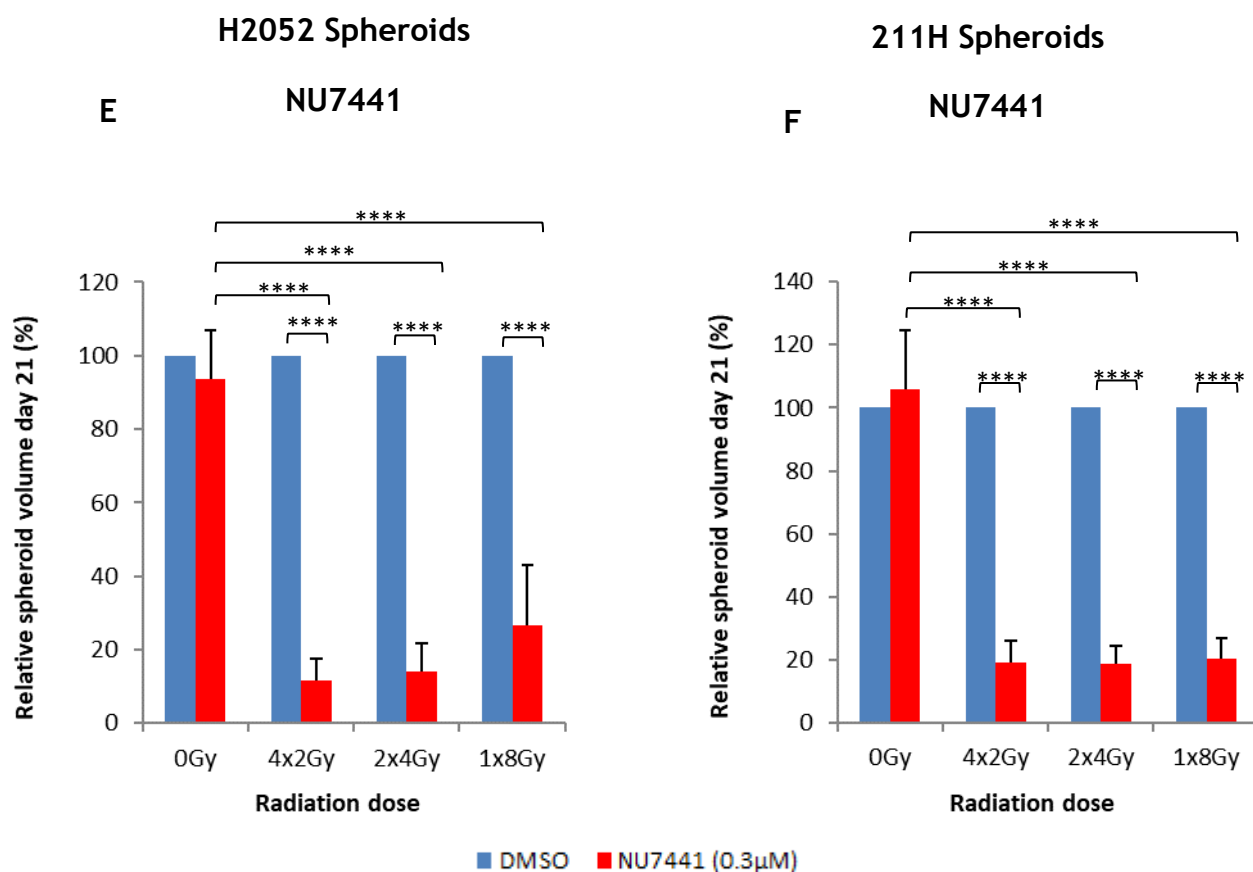


Figure 7.4 The effect of NU7441 on relative MPM spheroid volume at day 21, normalised for the effect of fractionation regime

Spheroids were exposed to increasing concentrations of NU7441 in combination with fractionated radiotherapy and their growth was monitored for 21 days. Data is expressed as the mean day 21 spheroid volume relative to DMSO control, following correction for the effect of each fractionation regime. Data were generated from 3-4 independent experiments (0µM n=4; 0.03µM n=3; 0.1µM n=3; 0.3µM n=4), with each experiment incorporating 6-8 replicates per condition. Error bars represent the standard deviations of the normalised means. Statistical analysis was performed using one way ANOVA and pairwise comparisons were generated with a post hoc Tukey test. (*p<0.05; **p<0.01; ***p<0.001; ****p<0.0001)

7.2.5 A1331852 exhibits single agent activity in H2052 cells

To determine the single agent activity of A1331852, MPM spheroids were treated with increasing concentrations of the drug or a DMSO control and were allowed to grow for 21 days. Spheroid size was monitored and data are presented as the mean spheroid volumes at day 21.

Exposing H2052 spheroids to concentrations of A1331852 above 0.1µM reduced their growth in a concentration-dependent manner (Figure 7.5A). Spheroids exposed to the DMSO control grew to a volume of $0.52 \pm 0.03\text{mm}^3$ by day 21, whereas those exposed to A1331852 at a concentration of 0.3µM and 3µM grew to only $0.45 \pm 0.03\text{mm}^3$ ($p<0.0001$) and $0.31 \pm 0.01 \text{mm}^3$ ($p<0.0001$) respectively. In addition to being significantly different from the DMSO control, these volumes were also significantly different from each other ($p<0.0001$), a trend which was repeated across the different concentrations. This pattern of growth reduction indicates that A1331852 exerts concentration-dependent single agent activity against H2052 spheroids *in vitro*. In contrast, no A1331852-mediated single agent therapeutic activity was observed in the 211H cell line (Figure 7.5B).

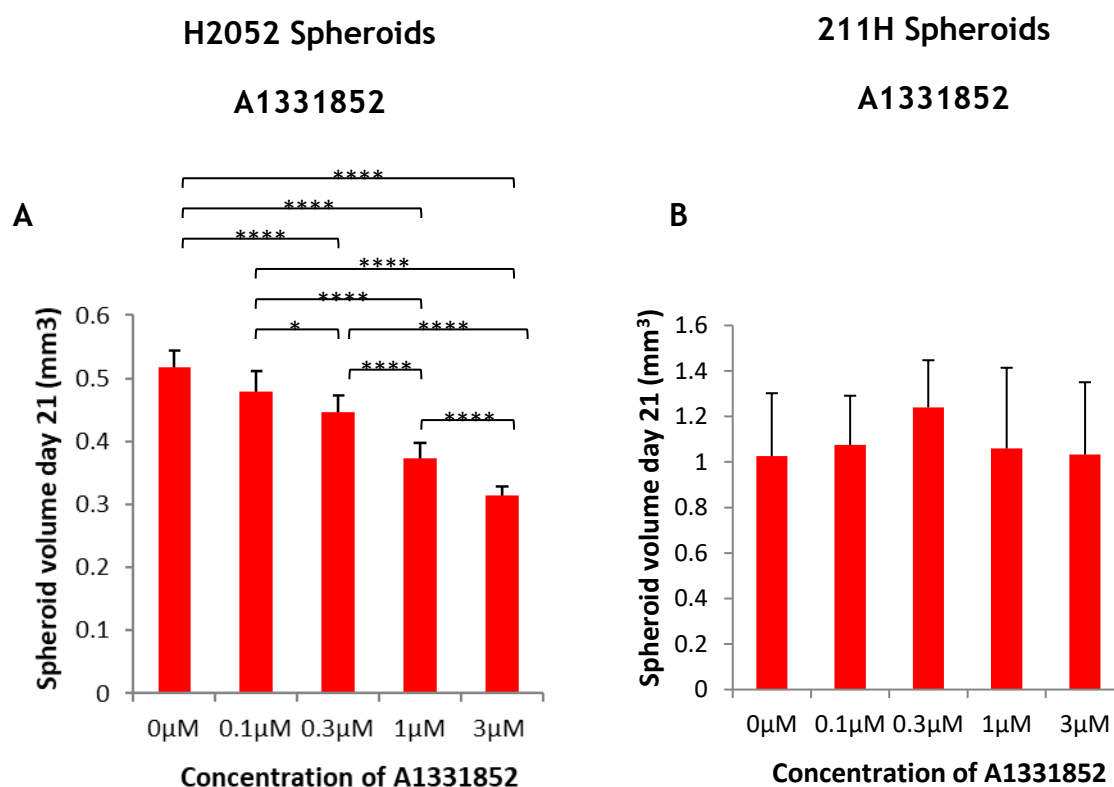


Figure 7.5 The effect of A1331852 alone on MPM spheroid volume at day 21

Spheroids were exposed to increasing concentrations of A1331852 and growth was monitored over 21 days. Data is expressed as the mean spheroid volume in mm³ at day 21, averaged from 2-4 individual experiments (0µM n=4; 0.1µM n=3; 0.3µM n=4; 1µM n=4; 3µM n=2). Each experiment incorporated 6-8 replicates per condition. Error bars reflect the standard deviation of the means. Statistical significance was determined with a linear mixed effect model, using either the standardised volume value or the cubed root of the transformed data value. (* $p<0.05$; **** $p<0.0001$)

7.2.6 The combination of A1331852 with IR exhibits a therapeutic interaction

To determine whether A1331852 was capable of sensitizing MPM spheroids to IR, spheroids were treated concomitantly with varying concentrations of the drug and a single IR dose of 8Gy. Spheroid size was monitored over 21 days and 3D volume was determined by reconstruction of 2D images. Data are plotted as spheroid volume relative to irradiated control following correction for the effect of a single IR dose of 8Gy.

The combination of A1331852 and IR (delivered as a single 8Gy fraction), significantly reduced the day 21 MPM spheroid volumes, relative to the DMSO controls treated with the same IR regime (Figure 7.6). For example, exposure of H2052 spheroids to 3 μ M A1331852 with an 8Gy single fraction reduced the relative day 21 volume to 0.8% \pm 0.02% of the irradiated DMSO control ($p < 0.0001$) (Figure 7.6A). Similarly, in the 211H model, exposure to 8Gy IR with 3 μ M A1331852 reduced the relative day 21 spheroid volume to 7% \pm 9% of the irradiated DMSO control ($p < 0.001$) (Figure 7.6B). Together, these data suggest that the combination A1331852 with IR is associated with significant radiosensitisation in MPM spheroids.

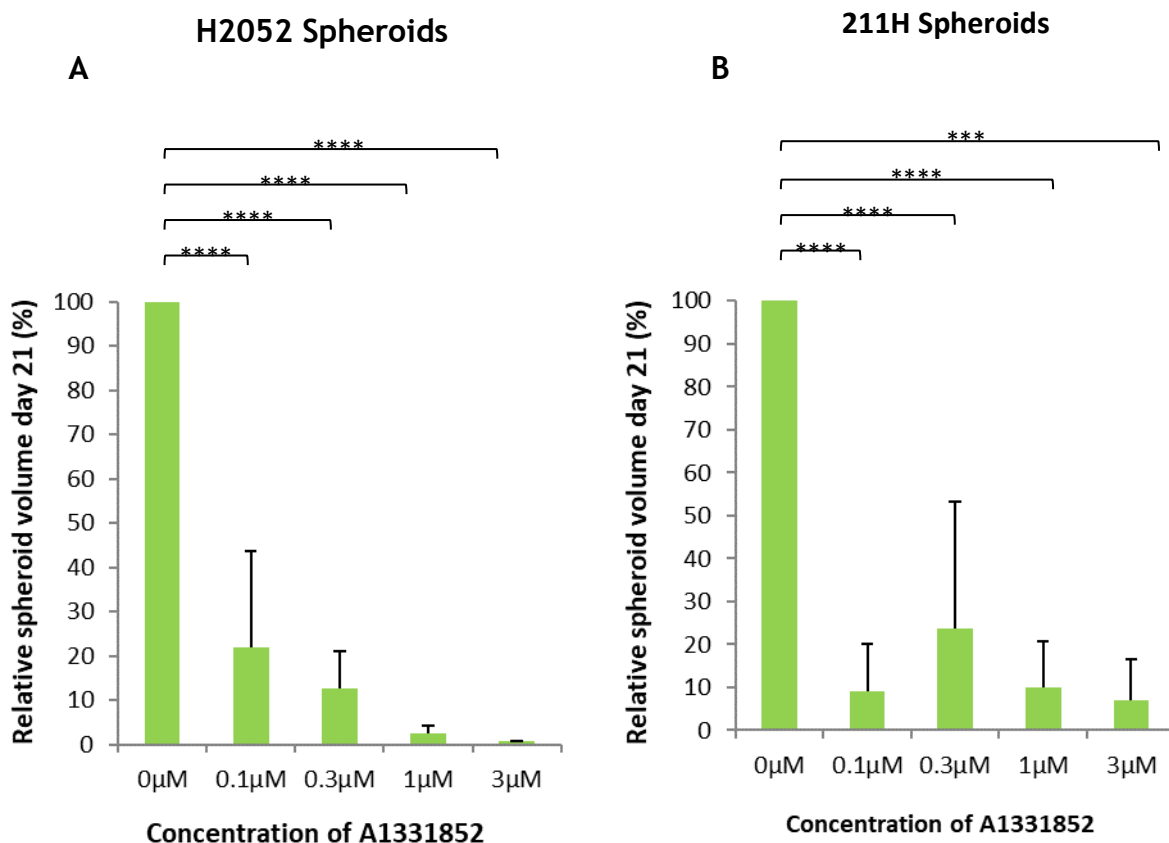


Figure 7.6 The effect of combination therapy with A1331852 and IR on relative MPM spheroid volume at day 21

Spheroids were exposed to increasing concentrations of A1331852 delivered with a single 8Gy fraction of IR and growth was monitored over 21 days. Data is expressed as the mean day 21 spheroid volume relative to DMSO control, following correction for the effect of a single IR dose of 8Gy. Data were generated from 2-4 independent experiments (0μM n=4; 0.1μM n=3; 0.3μM n=4; 1μM n=4; 3μM n=2), with each experiment incorporating 6-8 replicates per condition. Error bars represent the standard deviations of the normalised means. Statistical analysis was performed using one way ANOVA and pairwise comparisons were generated with a post hoc Tukey test. (**p<0.001; ****p<0.0001)

7.2.7 The radiosensitising effects of A1331852 is enhanced with hypofractionated IR

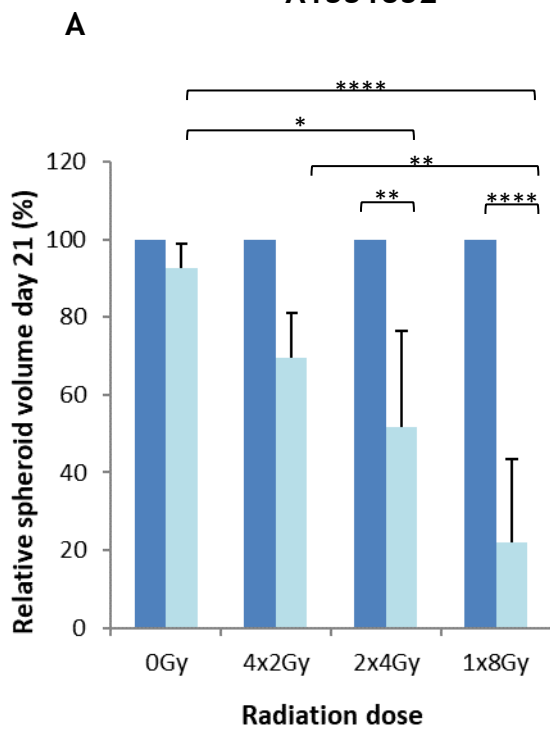
To assess the impact of fractionation on the radiosensitising effect of A1331852, MPM spheroids were treated with increasing concentrations of this drug in combination with radiotherapy regimes delivering a total dose of 8Gy, over a

different number of fractions. Data are plotted as volume relative to DMSO control, following correction for the effect of each of the fractionation schedules alone (Figure 7.7). Data showing the day 21 spheroid volumes obtained under each condition can be found in Appendix 2.

Exposure of MPM spheroids to IR with A1331852 at a concentration of 0.1 μ M reduced the day 21 spheroid volume relative to the DMSO control, regardless of the fractionation regime (Figure 7.7A and B). Nevertheless, the reduction in relative spheroid volume was greater when A1331852 was combined with hypofractionated regimes than when it was administered with IR delivered in smaller doses per fraction. For example, in the H2052 model, administration of 0.1 μ M A1331852 with 2x4Gy reduced the day 21 spheroid volume to 52% \pm 25% of the irradiated DMSO control ($p < 0.01$), whereas the same drug concentration given in combination with 1x8Gy reduced the volume to 22% \pm 22% of its irradiated control ($p < 0.0001$) (Figure 7.7A). Similarly, in the 211H spheroids, 0.1 μ M A1331852 combined with 4x2Gy reduced the day 21 spheroid volume to 56% \pm 26% of the irradiated DMSO control ($p < 0.05$), while the same concentration administered with 1x8Gy reduced it to 9% \pm 10% ($p < 0.0001$) (Figure 7.7B). In addition to being statistically different from their irradiated DMSO controls, these relative spheroid volumes are statistically different from each other ($p < 0.01$). This data suggest that the magnitude of the therapeutic interaction between A1331852 and IR increases with progressively hypofractionated radiotherapy regimes. Similar effects were seen in both MPM cell lines when IR was delivered with increasing concentrations of A1331852. The magnitude of the therapeutic effect increased in a concentration-dependent manner, such that at the highest concentrations of A1331852 explored, there was no discernible difference in the relative spheroid volumes between the fractionation regimes. For example, combination of 3 μ M A1331852 with 4x2Gy IR reduced H2052 relative spheroid volume to 2.3% \pm 3% of the irradiated DMSO control and combination of the same concentration with 1x8Gy IR reduced the spheroid volume to 0.8% \pm 0.02% of the control (Figure 7.7G and H).

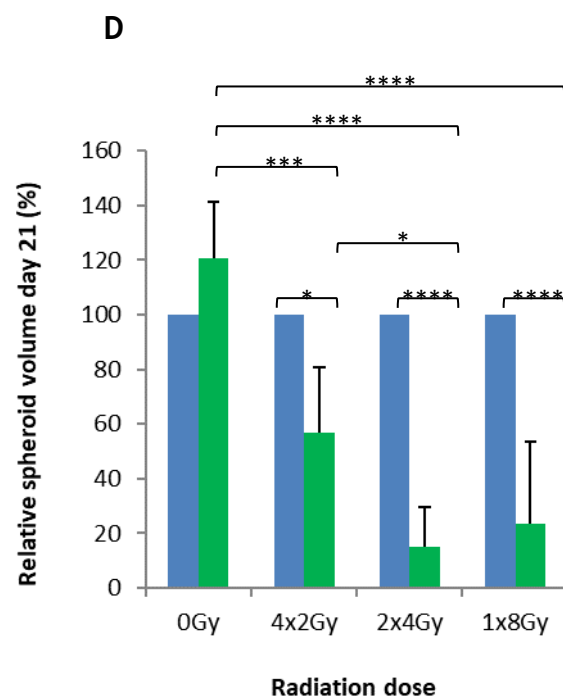
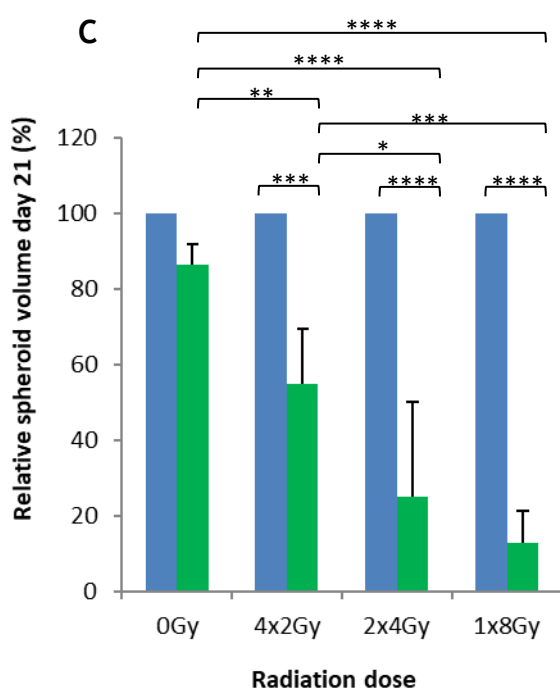
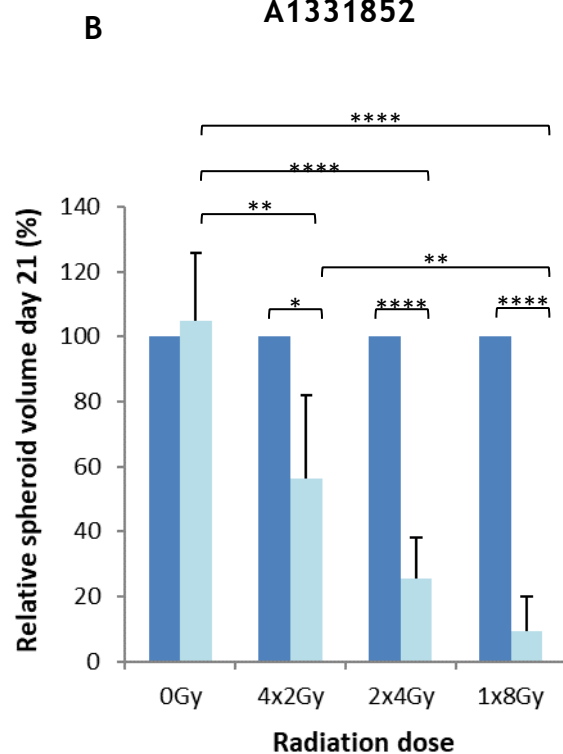
H2052 Spheroids

A1331852



211H Spheroids

A1331852



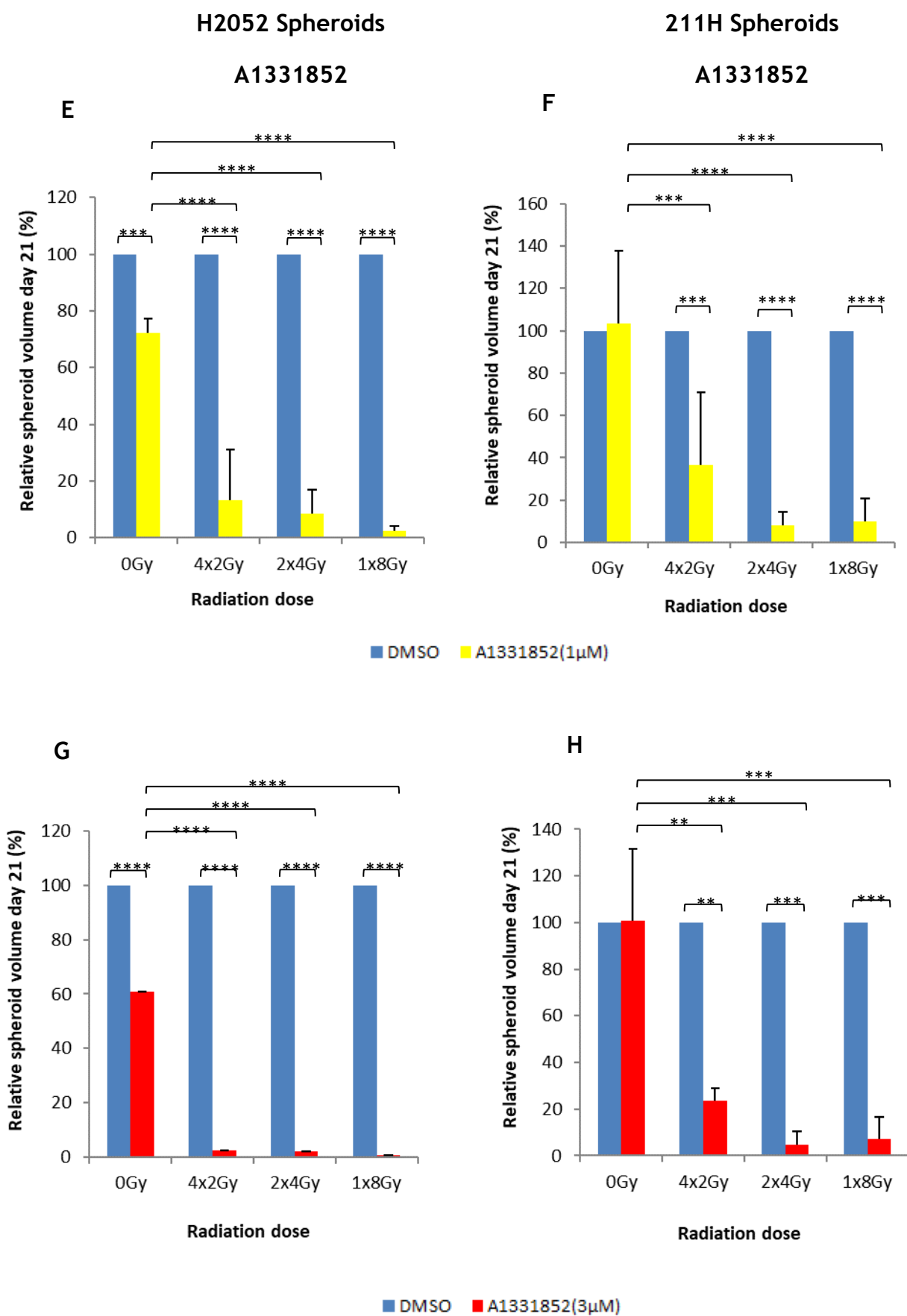


Figure 7.7 The effect of A1331852 on relative MPM spheroid volume at day 21, normalised for the effect of fractionation regime

(Figure 7.7) Spheroids were exposed to increasing concentrations of A1331852 in combination with fractionated radiotherapy and their growth was monitored for 21 days. Data is expressed as the mean day 21 spheroid volume relative to DMSO control, following correction for the effect of each fractionation regime. Data were generated from 2-4 independent experiments (0 μ M n=4; 0.1 μ M n=3; 0.3 μ M n=4; 1 μ M n=4; 3 μ M n=2), with each experiment incorporating 6-8 replicates per condition. Error bars represent the standard deviations of the normalised means. Statistical analysis was performed using one way ANOVA and pairwise comparisons were generated with a post hoc Tukey test. (*p<0.05; **p<0.01; ***p<0.001; ****p<0.0001)

In summary, these data suggest that both NU7441 and A1331852 are potent radiosensitisers of MPM spheroids. At concentrations which allowed the differential effect of the drugs within each fractionation regime to be determined, both NU7441 and A1331852 demonstrated increased efficacy with hypofractionated radiotherapy. This effect is more clearly demonstrated when radiotherapy was combined with A1331852 than with NU7441.

7.2.8 MPM spheroids strongly express Bcl-xL and DNA-PKcs, but Bcl-2 and Mcl-1 are differentially expressed between H2052 and 211H cell lines

To confirm that DNA-PKcs and Bcl-xL are expressed in MPM spheroids and to therefore elucidate the likely mechanism of the observed radiosensitising effect of NU7441 and A1131852, unirradiated MPM spheroids were stained for these target proteins using IHC. For completeness, levels of Bcl-2 and Mcl-1 were also explored, given the level of redundancy known to exist between the anti-apoptotic Bcl-2 proteins. Cells were seeded at 10² cells per well, left to form spheroids and cultured for three weeks to ensure that they were a suitable size for further processing. At day 21, spheroids were fixed in formalin, sectioned and subjected to IHC, with appropriate positive and negative controls.

Expression of DNA-PKcs and anti-apoptotic Bcl-2 proteins was analysed using the 'Halo' software, in which thresholds were set to detect positively stained cells. The structure of H2052 spheroids was well maintained throughout this process, whereas the integrity of 211H spheroids was degraded through fixing, sectioning and IHC staining. Consequentially, the spatial expression of these proteins is less clear in the 211H group than in the H2052 spheroids. (Figure 7.8 and Figure 7.10)

A total of 95% of cells in the H2052 spheroids were scored positive for DNA-PKcs staining, compared to 83% of cells in 211H spheroids. (Figure 7.8 and Figure 7.9)

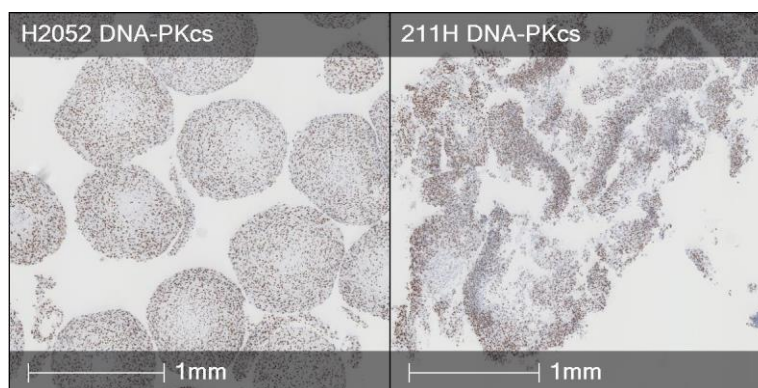


Figure 7.8 Relative expression of DNA-PKcs in H2052 and 211H spheroids

Cells were seeded at 10^2 cells per well and cultured for 3 weeks before being fixed, sectioned and stained for DNA-PKcs using IHC. Cell nuclei were counterstained with haematoxylin. Images were obtained by scanning slides into Halo software where analysis was also performed.

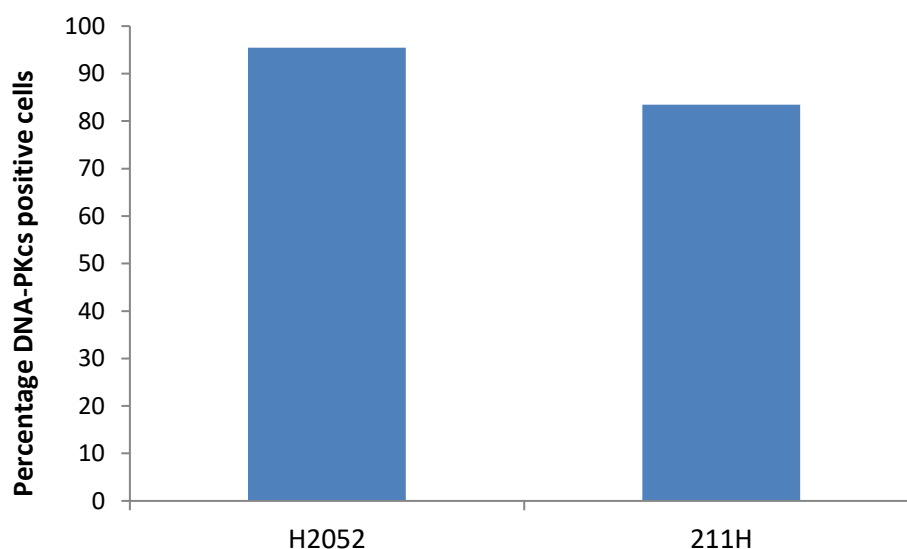


Figure 7.9 Percentage of cellular expression of DNA-PKcs in H2052 and 211H cells

The number of DNA-PKcs positively stained cells within each spheroid was determined using the Halo software. Data are expressed as the percentage of positive cells.

In H2052 spheroids, expression of Bcl-xL was dominant, with 98% of cells within the spheroids scoring positive for this stain. Much lower expression of Mcl-1 was observed (12.5% of cells scoring positive) and minimal Bcl-2 expression was seen, with only 0.003% of cells within the spheroids scoring positive for this protein. (Figure 7.10 and Figure 7.11) In contrast, within the 211H spheroids, relatively high expression of both Bcl-xL and Mcl-1 was observed (99% and 88% of cells scoring positive for these proteins respectively). Bcl-2 expression in 211H spheroids was much lower, with 15.6% of cells scoring positive for this protein. (Figure 7.10 and Figure 7.11)

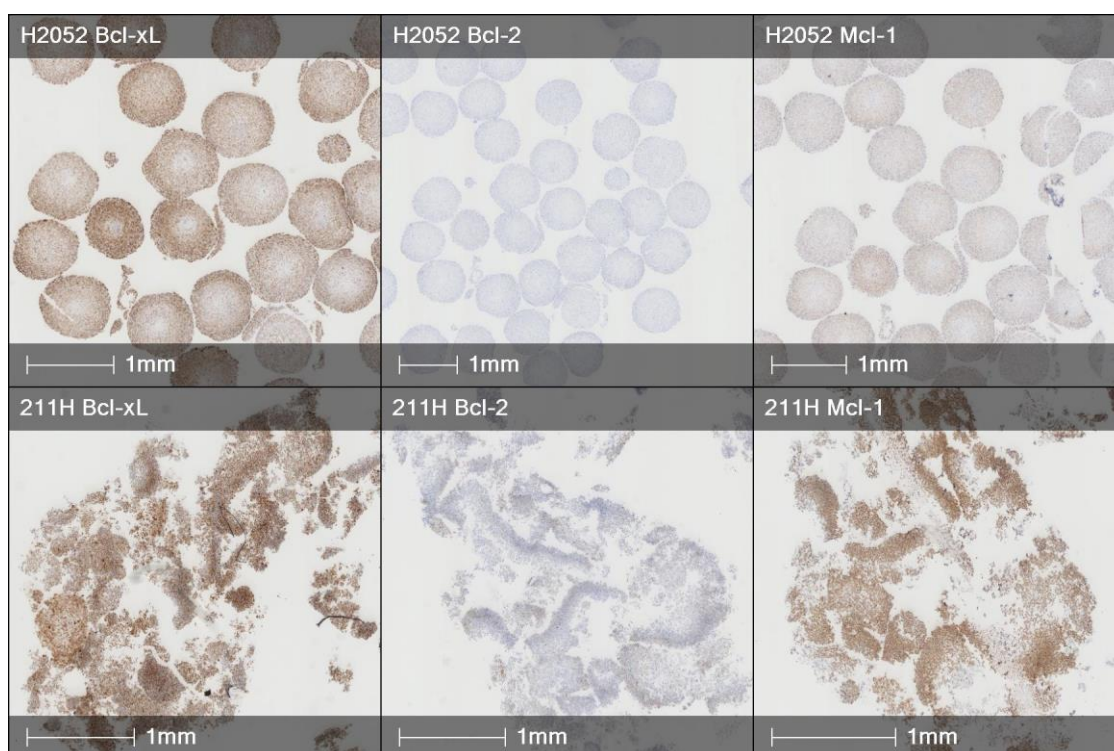


Figure 7.10 Relative expression of Bcl-xL, Bcl-2 and Mcl-1 in H2052 and 211H spheroids

Cells were seeded at 10^2 cells per well and cultured for 3 weeks before being fixed, sectioned and stained for anti-apoptotic Bcl-2 proteins using IHC. Cell nuclei were counterstained with haematoxylin. Images were obtained by scanning slides into Halo software, where analysis was also performed.

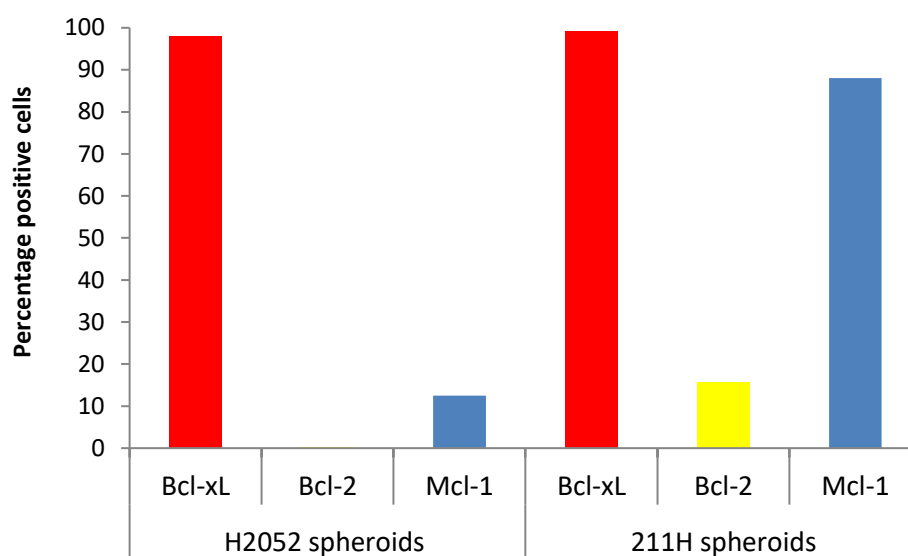


Figure 7.11 MPM expression of anti-apoptotic Bcl-2 proteins

The number of cells which stained positive for Bcl-xL, Bcl-2 and Mcl-1 within each spheroid was determined using the Halo software. Data are expressed as the percentage of positive cells for each protein.

7.2.9 DNA-PKcs is robustly expressed in MPM tissue

Having established that DNA-PKcs and Bcl-xL are expressed in MPM cells *in vitro*, MPM tumour samples were analysed, to determine whether the selected drugs were likely to be useful radiosensitisers in the clinic. Diagnostic FFPE samples of 18 patients who subsequently participated in the SYSTEMS and SYSTEMS-2 studies were sectioned and stained. Corresponding H+E samples were used to identify areas of malignant infiltration and tumour cell protein expression was scored as absent, weak, moderate or strong. These data were used to determine an H score for each tissue sample analysed. Antibody performance and technique consistency was assessed by including a positive and negative control (no primary antibody) with each analysis. Appropriate clinical biopsy samples, identified during the process of antibody optimisation, were used for this purpose. Typical expression levels in positive and negative controls and the expected staining pattern are shown in Figure 7.12. Representative images and corresponding expression data are also presented from 5 patients, incorporating examples from patients with epithelioid and sarcomatoid subtypes of MPM. (Figure 7.13)

Analysis of the positive control identified nuclear staining for DNA-PKcs. (Figure 7.12) This is consistent with the expression of this protein in regions of DNA damage repair and, together with the lack of background staining in the negative control, supports the specificity of the antibody employed. The same pattern of staining was seen in all of the clinical samples analysed, with strong levels of expression being observed throughout the presented cohort. (Figure 7.13) This correlated with high tumour DNA-PKcs H scores, shown in Table 7.1, which ranged from 225 to 278. Analysis of the tumour DNA-PKcs H scores for all 18 patients suggested that these findings were representative of the full cohort, where a mean tumour H score of 244 ± 28 was calculated. (Data shown and further discussed in Chapter 8)

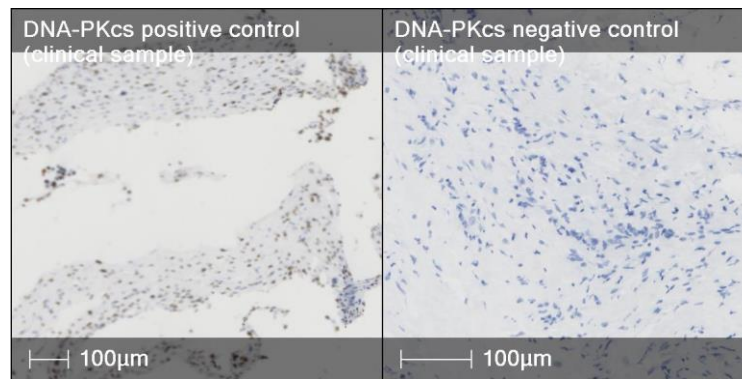


Figure 7.12 Expression of DNA-PKcs in MPM tissue selected as positive and negative controls

FFPE diagnostic tissue samples obtained from patients subsequently diagnosed with MPM were sectioned and stained for DNA-PKcs expression using IHC. Cell nuclei were counterstained with haematoxylin. A nuclear pattern of staining was demonstrated, consistent with the known distribution of this protein. Minimal background staining was observed in the negative control. Images were obtained by scanning slides into Halo software.

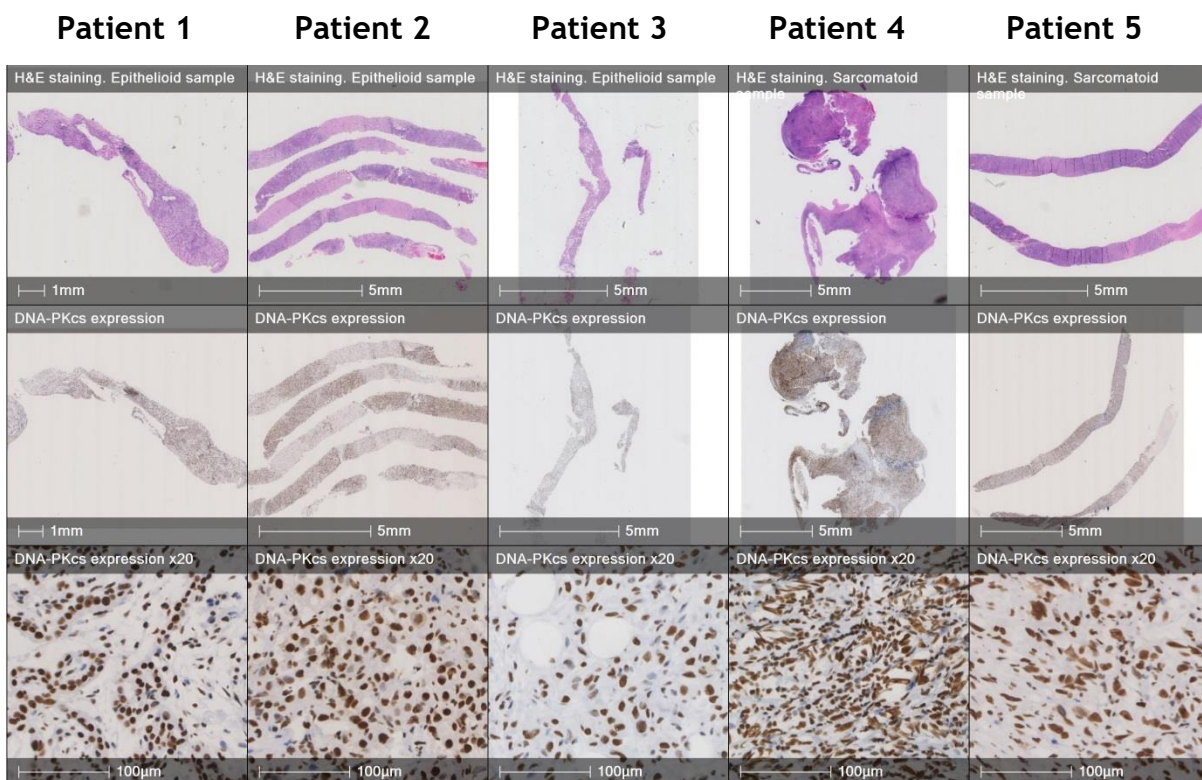


Figure 7.13 Expression of DNA-PKcs in MPM tissue

FFPE diagnostic tissue samples from patients who subsequently entered the SYSTEMS or SYSTEMS-2 study were sectioned before being stained for DNA-PKcs expression using IHC. Cell nuclei were counterstained with haematoxylin. Images were obtained by scanning slides into Halo software, where analysis was also performed. Representative images are displayed from five patients with either epithelioid or sarcomatoid disease.

Table 7.1 Levels of DNA-PKcs expression in MPM cells

| Clinical sample | Histology | % Positive Cells | % 1+ Cells | % 2+ Cells | % 3+ Cells | H-Score |
|-----------------|-------------|------------------|------------|------------|------------|---------|
| 1 | Epithelioid | 96.5 | 6.19 | 23.54 | 66.76 | 253.56 |
| 2 | Epithelioid | 99.7 | 1.99 | 16.46 | 81.26 | 278.67 |
| 3 | Epithelioid | 92.7 | 7.91 | 36.59 | 48.18 | 225.63 |
| 4 | Sarcomatoid | 98.3 | 3.22 | 27.54 | 67.51 | 260.85 |
| 5 | Sarcomatoid | 99.2 | 3.79 | 30.69 | 64.72 | 259.35 |

Tumour cells were identified in the biopsy specimens shown in Figure 7.11 and the relative expression of DNA-PKcs was determined. The intensity of staining was graded as absent, weak, moderate or strong. H scores were calculated using the equation (1x (% cells 1+) + 2x (% cells 2+) + 3x (% cells 3+)).

7.2.10 Anti-apoptotic Bcl-2 proteins are expressed with differential intensities in MPM tissue

To determine whether the Bcl-xL is present in clinical samples from patients with MPM, and therefore whether A1331852 may represent a clinically useful radiosensitiser in this disease, Bcl-xL, Bcl-2 and Mcl-1 expression in clinical tissue samples was assessed by IHC staining. Diagnostic FFPE samples of 18 patients who subsequently participated in the SYSTEMS and SYSTEMS-2 studies were sectioned and stained. Corresponding H+E samples were used to identify areas of malignant infiltration and tumour cell protein expression was scored as absent, weak, moderate or strong, facilitating the calculation of an H score for each tissue sample. A positive (tonsil tissue) and negative (tonsil tissue or clinical sample) control was also included. Typical expression levels in positive and negative controls and the expected staining pattern are shown in Figure 7.14. Representative images and corresponding expression data are presented from 5 patients, incorporating examples from patients with epithelioid, biphasic and sarcomatoid subtypes of MPM. (Figure 7.15 and Table 2)

Strong expression of all three anti-apoptotic Bcl-2 proteins was consistently seen in the positive controls, although the geographical distribution varied. Bcl-xL and Mcl-1 expression was highest in the follicles whereas expression of Bcl-2 dominated in the lymph cells. (Figure 7.14) Analysis at high magnification (x20) confirmed cytoplasmic staining in all three proteins, consistent with mitochondrial localization. A circular staining pattern resulted, which tended to exclude the nuclei and remained consistent with the pattern observed in clinical samples. Minimal background staining was detected in the negative control. (Figure 7.14)

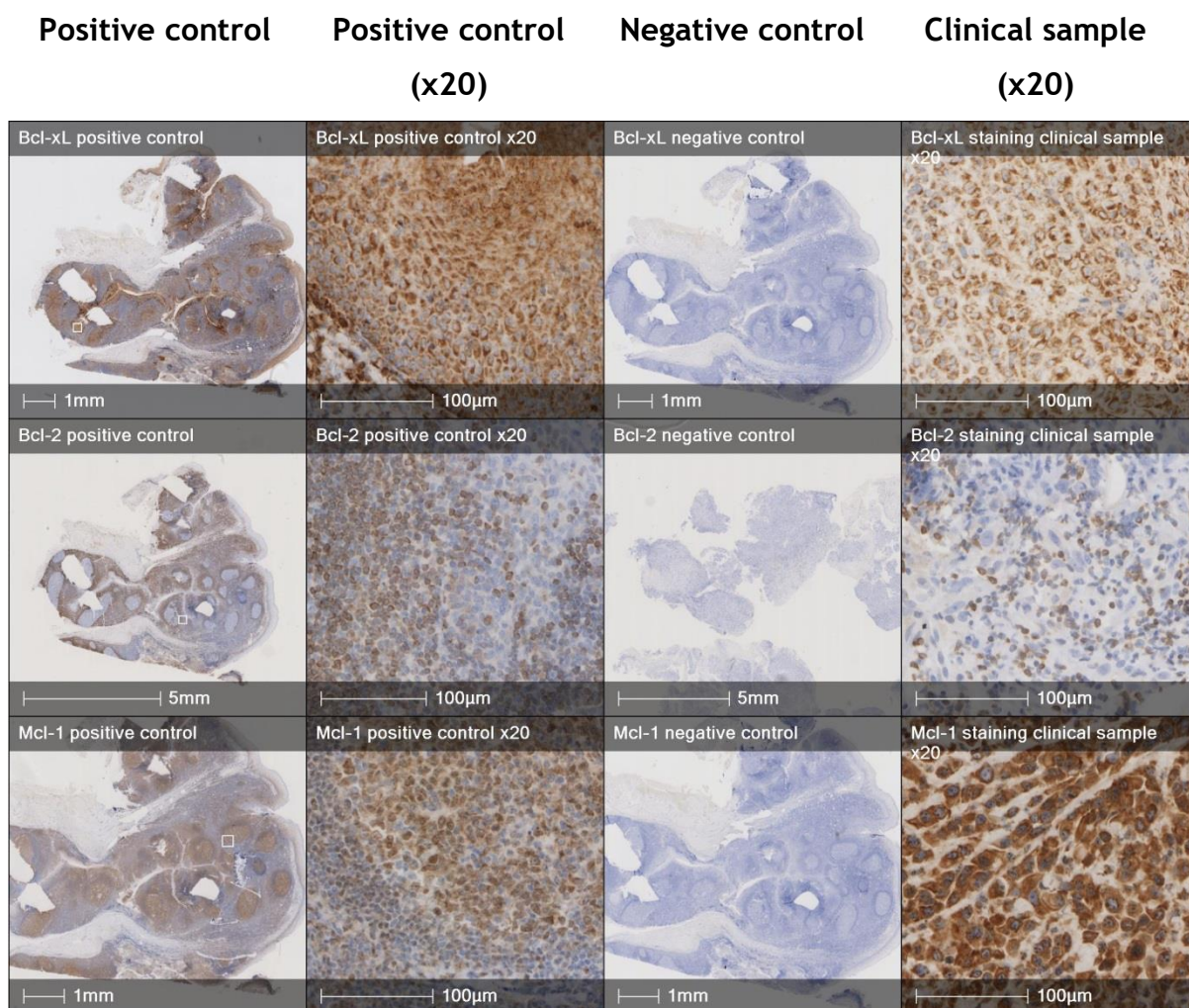


Figure 7.14 Expression of Bcl-xL, Bcl-2 and Mcl-1 in positive and negative controls and in clinical samples

FFPE tissue samples were sectioned and stained for Bcl-xL, Bcl-2 and Mcl-1 expression using IHC. Cell nuclei were counterstained with haematoxylin. Images were obtained by scanning slides into Halo software. Cytoplasmic staining was demonstrated, consistent with the known distribution of these proteins. At a magnification of x20, the same staining pattern was observed in clinical samples from MPM patients. Minimal background staining was observed in the negative controls.

Analysis of the clinical samples show that Bcl-xL, Bcl-2 and Mcl-1 were expressed in all of the biopsy specimens, but that the levels of expression differed. (Figure 7.15) Both Bcl-xL and Mcl-1 were strongly expressed in the tissue specimens, and this correlated with high levels of tumour expression. Accordingly, H scores of between 138 and 211 were recorded for Bcl-xL, and of between 123 and 264 for

Mcl-1, in this representative cohort. (Table 7.2) Expression of Bcl-2 was visibly lower in all the biopsy samples (Figure 7.15) and H scores for tumour expression of this protein was also notably reduced (between 9 and 91). (Table 7.2)

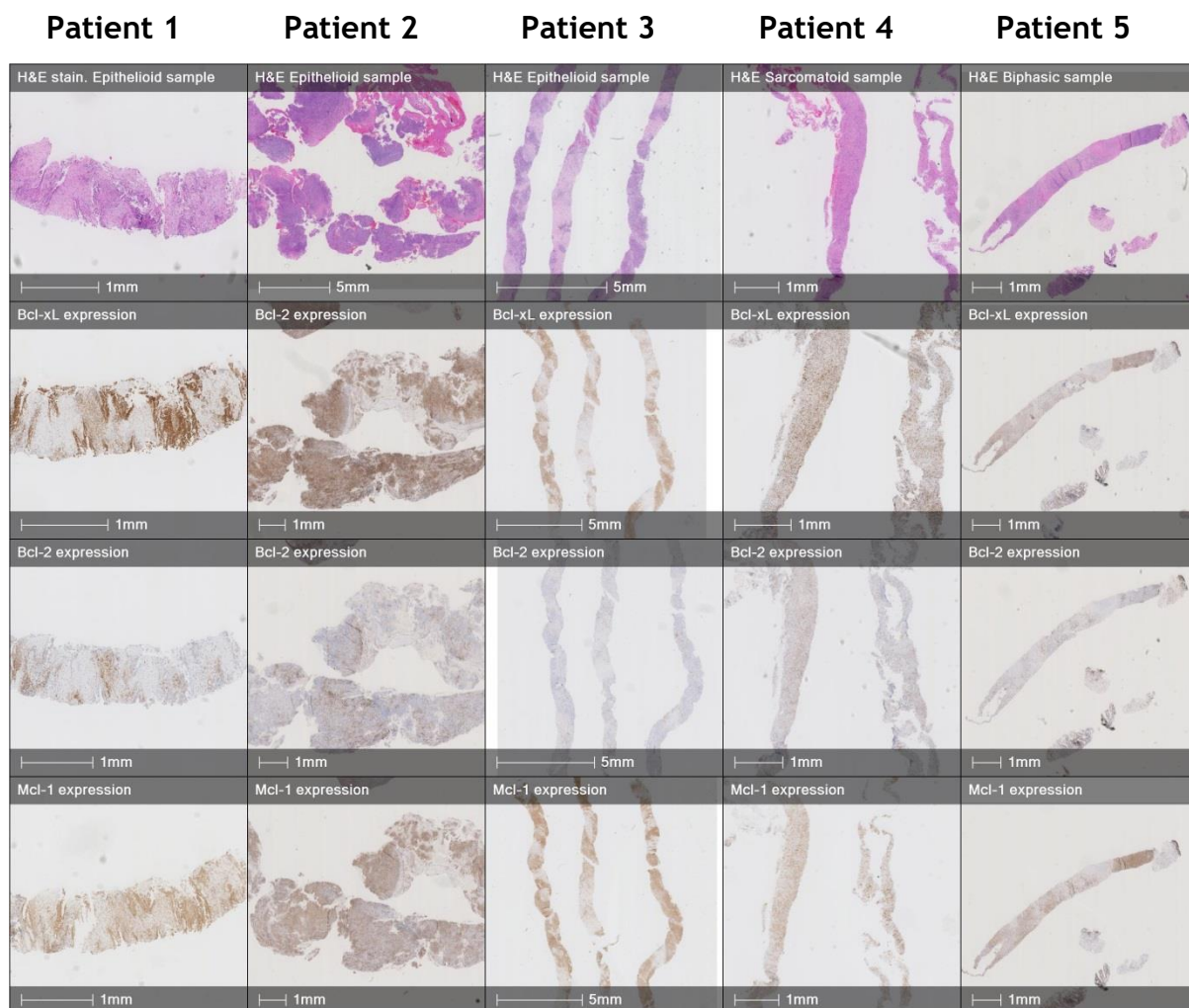


Figure 7.15 Expression of Bcl-xL, Bcl-2 and Mcl-1 in MPM tissue

FFPE diagnostic tissue samples from patients who subsequently entered the SYSTEMS or SYSTEMS-2 study were sectioned and stained for Bcl-xL, Bcl-2 and Mcl-1 expression using IHC. Cell nuclei were counterstained with haematoxylin. Images were obtained by scanning slides into Halo software, where analysis was also performed. Representative images are displayed from five patients with epithelioid, sarcomatoid or biphasic disease.

Table 7.2 Expression of Bcl-xL, Bcl-2 and Mcl-1 in MPM cells

| Protein | Patient | Histology | % +ve Cells | % 1+ Cells | % 2+ Cells | % 3+ Cells | H-Score |
|---------|---------|-------------|-------------|------------|------------|------------|---------|
| Bcl-xL | 1 | Epithelioid | 74.64 | 9.01 | 13.71 | 51.92 | 192.20 |
| | 2 | Epithelioid | 78.31 | 5.70 | 12.38 | 60.23 | 211.16 |
| | 3 | Epithelioid | 72.06 | 14.53 | 26.37 | 31.16 | 160.74 |
| | 4 | Sarcomatoid | 90.81 | 56.31 | 21.14 | 13.36 | 138.67 |
| | 5 | Biphasic | 81.83 | 44.49 | 9.02 | 28.32 | 147.49 |
| Bcl-2 | 1 | Epithelioid | 32.33 | 19.06 | 8.20 | 5.07 | 50.66 |
| | 2 | Epithelioid | 34.31 | 13.71 | 7.90 | 12.70 | 67.61 |
| | 3 | Epithelioid | 9.01 | 8.43 | 0.46 | 0.11 | 9.69 |
| | 4 | Sarcomatoid | 70.40 | 56.24 | 6.80 | 7.36 | 91.91 |
| | 5 | Biphasic | 17.49 | 9.35 | 5.72 | 2.42 | 28.04 |
| Mcl-1 | 1 | Epithelioid | 83.36 | 19.16 | 36.44 | 27.76 | 175.31 |
| | 2 | Epithelioid | 57.46 | 13.49 | 21.75 | 22.22 | 123.64 |
| | 3 | Epithelioid | 98.26 | 4.26 | 21.39 | 72.60 | 264.85 |
| | 4 | Sarcomatoid | 71.41 | 25.80 | 30.63 | 14.98 | 132.00 |
| | 5 | Biphasic | 80.09 | 19.46 | 30.17 | 30.47 | 171.19 |

Tumour cells were identified in the biopsy specimens shown in Figure 7.15 and the expression of each protein of interest was determined. The intensity of staining was graded as absent, weak, moderate or strong. H scores were calculated using the equation (1x (% cells 1+) + 2x (% cells 2+) + 3x (% cells 3+)).

Combined analysis of data from all 18 patients samples revealed that the variation in protein expression identified in this representative cohort was consistent with that of the complete data set. Within the complete cohort, the mean tumour H score for Bcl-xL expression was 122 (± 54), compared to 61 (± 54) for Bcl-2 expression. Mean tumour H score for Mcl-1 expression was 164 (± 68), which was significantly greater than that for Bcl-2 ($p = 0.02$) but not statistically different from Bcl-xL expression. (Figure 7.16)

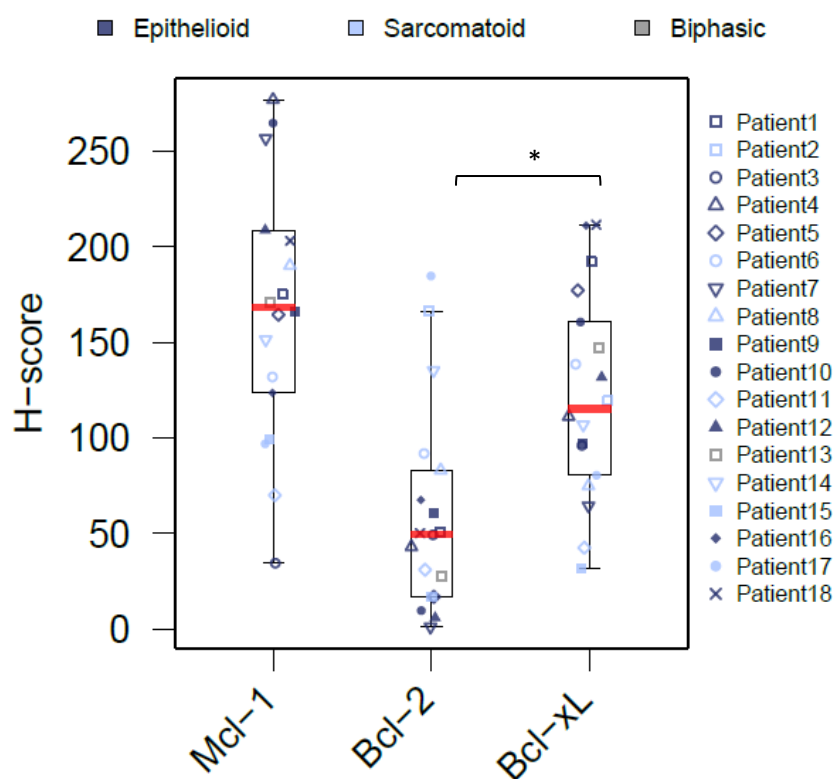


Figure 7.16 Expression of Bcl-xL, Bcl-2 and Mcl-1 in MPM tissue

FFPE samples from 18 patients who subsequently entered the SYSTEMS or SYSTEMS-2 clinical trial were sectioned and stained for expression of Bcl-xL, Bcl-2 and Mcl-1. Tumour cells were identified and their expression of each protein was graded as absent, weak, moderate or strong. H scores were calculated using the equation $(1 \times (\% \text{ cells } 1+) + 2 \times (\% \text{ cells } 2+) + 3 \times (\% \text{ cells } 3+))$. Data are represented as box and whisker plots box. The median is indicated by the red horizontal line in the box and the whiskers were plotted according to the Tukey method. Statistical analysis was conducted using the Kruskal-Wallis test with false discovery rate (FDR) correction of the p values (* $p < 0.05$)

Taken together, this data suggests that both DNA-PKcs and Bcl-xL are expressed in MPM tissue and are therefore valid targets of radiosensitisation in this disease.

7.3 Discussion

7.3.1 The growth of MPM spheroids is delayed by ionising radiation and A1331852, but unaffected by NU7441

The delivery of a total dose of 8Gy IR alone caused a significant reduction in MPM spheroid volume by day 21, compared to the sham irradiated controls, regardless of how it was delivered. In keeping with the findings of chapter 6, the fraction size significantly impacted on the growth of the spheroid by day 21, with progressively larger doses per fraction causing a greater reduction in spheroid volume than smaller fraction sizes.

Significant A1331852-mediated single agent therapeutic activity was noted in the H2052 cell line at concentrations of 0.3 μ M and above. Quantification of this activity through the calculation of an EC50 value has not been possible, primarily because the experiment was not designed for this purpose, so the maximum therapeutic effect was not determined. Nevertheless, impressive levels of single agent activity have been observed in other studies when Bcl-xL dependent cell lines are exposed to this drug, with a reported EC50 of 6nM in human acute T lymphoblastic leukaemia cells. (Leverson et al., 2015) Furthermore, previous data generated in our lab using traditional 2D cell viability assays suggests that A1331852 exerts single agent activity in H2052 MPM cells with an EC50 of 0.133 μ M. (Jackson et al., 2020) Whilst this data cannot be directly compared with that from our 3D model, the absence of significant single agent activity at A1331852 concentrations lower than 0.3 μ M suggests that H2052 MPM cells cultured in 3D are more resistant to the cytotoxic effects of this agent than previously seen in 2D models. This observation is in keeping with the multicellular resistance demonstrated by 3D spheroids in other studies. (Barbone et al., 2008, Desoize and Jardillier, 2000)

No single agent activity was observed for any of the concentrations of A1331852 investigated in the 211H model. Previous data shows that when exposed to 211H cells in 2D, A1331852 exhibited single agent activity with an EC50 of 0.27 μ M, suggesting that 211H cells are more resistant to this drug than H2052 cells.

(Jackson et al., 2020) The current data supports this finding, and further corroborates the theory that MPM cells in 3D demonstrate multicellular resistance. (Barbone et al., 2008)

A potential explanation for the difference in sensitivity to A1331852 observed between H2052 and 211H cells may be provided by 2D *in vitro* data generated in our laboratory by Dr Mark Jackson. In this work, relative expression of anti-apoptotic Bcl-2 proteins within three different MPM cell lines was determined by Western blot. This data suggested that H2052 cells preferentially express Bcl-xL, whereas 211H cells do not demonstrate 'addiction' to any particular Bcl-2 protein, expressing approximately equal levels of all the anti-apoptotic proteins assessed. (Jackson et al., 2020) This data is further substantiated by IHC data presented in Figure 7.10, where relative expression of the anti-apoptotic Bcl-2 proteins was determined in 211H and H2052 spheroids. Bcl-xL was robustly expressed in both H2052 and 211H spheroids, but expression levels of Mcl-1 and Bcl-2 were much lower in the H2052 cells. The dependency of H2052 cells on Bcl-xL for survival makes these cells particularly sensitive to A1331852. In 211H cells, the delicate balance of pro- and anti-apoptotic proteins would be less susceptible to disruption with Bcl-xL inhibition, since the other anti-apoptotic proteins could compensate for any changes in Bcl-xL activity and maintain cell survival in the presence of A1331852. Thus, an approach capable of simultaneously targeting multiple Bcl-2 proteins, using broader spectrum or combination BH3-mimetics, might be advantageous in MPM subtypes expressing multiple Bcl-2 proteins.

Exposure of MPM spheroids to NU7441 alone did not reveal any single agent activity. This is in contrast to 2D data generated previously in our lab, where single agent activity was observed with NU7441 and EC50 values of 1.69 μ M and 2.35 μ M were reported in 211H and H2052 cell lines respectively. In addition to the increased drug resistance demonstrated by cells grown in 3D, an explanation for this observation may be a low baseline burden of DNA damage within the spheroids and consequentially reduced NHEJ activity. Under these conditions, exposure to NU7441 would not be expected to exert an influence on spheroid

growth; the effect of the drug only becomes apparent when the level of DNA damage is increased by exposure to IR. This theory is supported by other studies, demonstrating a lack of single agent activity of NU7441 in human cancer cell lines, but subsequently revealing extensive radiosensitisation when the drug was delivered with IR. (Zhao et al., 2006, Shaheen et al., 2011) Supplementary IHC data, quantifying spheroid-associated DS-DNA breaks before and after exposure to 10Gy IR, also supports this suggestion. This data is presented in Appendix 3 and shows that γ H2Ax expression, which is a marker of DS-DNA damage, increases dramatically following exposure to IR in both cell lines.

7.3.2 Both NU7441 and A1331852 exert a radiosensitising effect on MPM cells when delivered with a single fraction of IR

Data shows that when spheroids are exposed to a combination of IR and either NU7441 or A1331852, a greater reduction in spheroid volume is observed than when they are exposed to either the drug or IR alone. This observation implies a therapeutic interaction and suggests that these drugs can exert a radiosensitisation effect on MPM cells in 3D. Robust expression of both DNA-PKcs and Bcl-xL in MPM spheroids observed with IHC, lends support to the proposed mechanism of radiosensitisation being due to the selective inhibition of these target proteins.

7.3.2.1 NU7441

The combination of a single 8Gy dose of IR with increasing concentrations of NU7441 resulted in progressively smaller relative spheroid volumes at day 21. This suggests that radiosensitisation with NU7441 occurs in a concentration-dependent manner, a hypothesis which is supported by data from a number of other studies. (Ciszewski et al., 2014, Shaheen et al., 2011, Saha et al., 2014) Mechanistically, this dose dependency makes sense when the function of NU7441 is considered. IR causes DNA damage and if the cell is unable to repair this damage then it dies, or is left unable to replicate. NU7441 exerts its radiosensitising effect by preventing DNA damage repair via the NHEJ pathway. As discussed in section 1.7.2, the NHEJ pathway is one of the two crucial

pathways of DS-DNA repair. Inhibition of this process leads to persistent DNA damage, prolonged cell cycle delay and the promotion of cell death, by apoptosis or mitotic catastrophe. Therefore, the greater the drug concentration present during IR, the greater the impact on the NHEJ pathway; consequentially, fewer cells will survive the insult of IR and the radiosensitisation effect of the drug will be larger. In addition to its impact on the NHEJ pathway, NU7441 has been reported to inhibit the HRR pathway of DNA damage repair (Allen et al., 2003) and to cause PARP-1 inhibition. (Veuger et al., 2003) One of the weaknesses of this study is that we have not definitively clarified the mechanistic pathway of the radiosensitising activity observed.

NU7441 has been demonstrated to be a potent radiosensitiser in a number of other pre-clinical studies using a variety of different cell lines cultured in 2D. (Ciszewski et al., 2014, Yang et al., 2016, Dong et al., 2017, Shaheen et al., 2011, Zhao et al., 2006) Ciszewski *et al* reported a 4 to 12 fold increase in breast cancer cell line radiosensitivity when 1 μ M NU7441 was combined with doses of IR of between 2Gy and 8Gy. (Ciszewski et al., 2014) The same concentration of NU7441 sensitised human nasopharyngeal cancer cells to IR (2Gy- 8Gy) (Dong et al., 2017) and in a different study, hormone sensitive and insensitive prostate cancer cells, were radiosensitised by 1 μ M NU7441. (Shaheen et al., 2011) Potent radiosensitising activity, associated with persistent DNA-DS breaks and G2/M arrest was demonstrated by clonogenic assay, following the exposure of human colon cancer cells to 1 μ M NU7441. (Zhao et al., 2006)

Direct correlation of our data with that generated in these 2D studies is difficult because of the differences in concentrations of NU7441 used, the variation in methods used to report effects and the inherent challenges of comparing outcome measures generated from a 3D spheroid model assessing volume and a 2D cell viability assay measuring cell survival directly. It is usual in drug-radiation studies to generate cell survival curves and normalise for the effect of the drug, since this makes separation between survival curves clear. However, in our 3D model, accurate survival curves could not be generated because the surviving fraction of cells corresponding to the observed change in spheroid

volume is unknown. Furthermore, since our study was primarily assessing the effect of hypofractionation on drug activity, data has been corrected to account for the effect of radiation alone, to allow any therapeutic interaction arising from the change in fraction size to be revealed. This necessary discrepancy in data analysis renders any direct comparisons of our data and that generated in these 2D studies very challenging. Nevertheless, in agreement with 2D radiosensitisation, a clear therapeutic interaction was observed in the MPM spheroid model.

Whilst NU7441 induced radiosensitisation of both MPM cell lines, the efficacy of the drug seemed to be greater in the H2052 model, in which spheroid volume was reduced compared to the irradiated DMSO control at all concentrations of NU7441 explored. By contrast, in the 211H model, significant reductions from the irradiated DMSO control were only noted at concentrations of 0.1 μ M and 0.3 μ M NU7441, suggesting that this cell line may be less susceptible to the radiosensitising effects of this agent. Previous radiosensitisation studies performed in our lab support these findings. In these 2D studies, exposure of 211H cells to 1 μ M NU7441 in combination with IR radiosensitised the cells with a SER of 1.85, whereas a greater degree of radiosensitisation was observed using the same drug concentration and IR in H2052 cells (SER 2.43). Although direct correlation with this 2D data is not possible, the principal remains that 211H seems to be more resistant to radiosensitisation than H2052 cells.

As discussed in chapter 6, the 211H cell line was derived from a patient with biphasic MPM. This histological subtype is known to be inherently more aggressive and resistant to treatment than the epithelioid MPM, from which the H2052 cell line was generated. There are no published studies detailing the genetic profile of these two cell lines, however, they are both represented within the catalogue of somatic mutations in cancer database (<https://cancer.sanger.ac.uk/cosmic>). Analysis of this resource did not reveal any known genetic mutations within the NHEJ pathway in either cell line. In contrast, a single missense heterozygous mutation was identified within the *Rad54B* gene in the H2052 cell line. This gene has a functional role in the HRR

pathway of DDR, coding for the Rad54B protein which binds to double-stranded DNA and exerts ATPase activity in the presence of DNA. Mutations within this gene are known to be important in malignancies of the lung, breast and colon. (McAndrew et al., 2016) Within the 211H cell line, three genetic mutations were identified within genes encoding proteins of the HRR pathway: *Eme1*, *Rad51B* and *Top3b*. Only the mutation in *Top3b* has been validated and is reported as a missense heterozygous mutation. This gene codes for DNA topoisomerase 3-beta-1, an enzyme which controls the transient breaking and re-joining of single strand DNA during transcription, impacting on the supercoiling and topology of DNA. It has an important role in maintaining genome stability. (Gene) Although it could be surmised that the differences in radiosensitivity observed between the H2052 and 211H cell lines may in part due to their ability to repair DNA damage following IR, the functional impact of these mutations is not reported, making it difficult to draw any firm conclusions. Further analysis of the catalogue of somatic mutations in cancer database did not identify these mutations being present in human pleural mesothelioma tissue, regardless of subtype.

7.3.2.2 A1331852

The radiosensitising properties of BH3 mimetics have been investigated in a number of *in vitro* studies, where their effects have been studied on breast cancer cells and cervical cancer HeLa cells. (Wu et al., 2014, Li et al., 2012, Wang et al., 2012) Li *et al* used a 2D clonogenic assay to examine the activity of ABT 737 (a BH3 mimetic which targets both Bcl-2 and Bcl-xL) in breast cancer cell lines with acquired radioresistance. Cells were exposed to 1µM of the drug for 24 hours before being exposed to IR doses of 4Gy, 8Gy and 12Gy. Results suggested that radiosensitivity could be restored in these cell lines by exposure to ABT 737. A reduction in survival fraction from approximately 0.8 to 0.08 was observed when 8Gy IR was employed in combination with the drug and the associated radiosensitivity appeared to be mediated through an increase in apoptosis. (Li et al., 2012) Breast cancer cells were also used to investigate ABT 737 associated radiosensitisation in a study by Wu *et al*. (Wu et al., 2014) Clonogenic assays were used to determine the effect of 2.5µM ABT 737 given in combination with 4Gy IR. Data revealed a significant radiosensitising effect, with a reduction in the number of surviving clones to 11.2% in the combination group

compared to 39.7% in the group treated with ABT 737 alone and 65.2% in the group exposed to 4Gy IR alone. Simultaneous analysis of apoptosis markers suggested that this increase in cell death was apoptosis-dependent. (Wu et al., 2014) Wang *et al* used ABT 737 at a concentration of 10 μ M to treat cervical cancer HeLa cell lines prior to exposure to IR doses of 2Gy, 4Gy, 6Gy and 8Gy. (Wang et al., 2012) Results of a clonogenic assay suggested that combination treatment was associated with significant radiosensitisation, via an apoptosis-dependent pathway.

Despite these encouraging findings, the potential to make direct comparisons with, or mechanistic inferences from, such data are limited, since all of these studies used 2-D assays to assess the impact of ABT-737, a far less selective BH3 mimetic than the specific Bcl-xL inhibitor employed in our 3-D model. Previous data generated in our own lab studying A1331852 in MPM clonogenic assays provides a representation of the size of the radiosensitisation effect seen with this drug in 2D. Data suggested that H2052 cells were radiosensitised by 0.3 μ M A1331852 (SER 1.80) and that 211H cells underwent radiosensitisation following exposure to 1 μ M A1331852 (SER 1.55), via an apoptosis driven pathway. (Jackson et al., 2020)

Of particular relevance to the selection of a 3D platform on which to investigate the activity of a Bcl-xL inhibitor in MPM, is data from Barbone *et al*, which shows that MPM cells express a different repertoire of Bcl-2 proteins when they are grown in 3D. (Barbone et al., 2011) Furthermore, gene expression profiling studies have reported that in 3D culture, MPM cells downregulate genes associated with apoptosis. (Kim et al., 2012) Therefore, despite encouraging 2D data, it was important to confirm that Bcl-xL inhibition is effective in 3D, since this is more closely representative of the clinical scenario.

Consistent with the 2D radiosensitisation data, a clear therapeutic interaction was seen in our spheroid model between A1331852 and IR. No difference in the relative efficacy of A1331852 was identified between H2052 and 211H spheroids

at the concentrations investigated in this 3D model, suggesting that this drug may be efficacious in both histological subtypes of MPM represented. Furthermore, the ability of the drug to produce a radiosensitising effect where no single agent activity was observed, supports a combination approach.

Whilst our data shows that A1331852 induces a potent radiosensitising effect compared to the irradiated DMSO control, no statistical differences were noted between the relative spheroid volumes at day 21 with increasing concentrations of the drug, in either cell line. This observation suggests that even the minimum concentration investigated was above the threshold at which a concentration-dependent effect could be observed. Future experimentation would aim to determine the concentration-dependency of the effect by assaying at lower concentrations.

7.3.3 Optimal radiosensitisation with hypofractionated IR is more consistently demonstrated with A1331852 than with NU7441

The combination of NU7441 with differently fractionated IR regimes confirmed the previously noted concentration dependent radiosensitising effect of this drug and improved efficacy in the H2052 cell line. The impact of dose fractionation observed with NU7441 was much less dramatic than with A1331852 and although increased efficacy was observed with hypofractionation, this was only revealed at a concentration of 0.1 μ M in the 211H model and at 0.03 μ M in the H2052 model.

In the case of A1331852, the dependency of radiosensitisation on dose per fraction was clearly demonstrated, showing the influence of fractionation on this class of agent for the first time. The separation of relative spheroid volumes according to fractionation schedule is very clear in the H2052 model at all concentrations of A1331852 under 1 μ M. In the 211H model, while concentrations of 0.3 μ M or less caused a clear difference in relative spheroid volumes when delivered with 4x2Gy, the separation of spheroid volumes between 2x4Gy and 1x8Gy was less distinct. This perhaps reflects the irregular growth pattern of this

cell line, (previously discussed in chapter 6.3.1), leading to an increase in variability between experimental replicates, and rendering subtle differences in spheroid size difficult to detect.

The disparity observed between the interaction of these drugs with hypofractionated IR may be in part explained by the mechanistic properties of the drugs and the influence of competing pathways.

An elegant explanation for the observed interaction of NU7441 with fractionated IR may be provided by the work of Somaiah *et al.*, in which the influence of specific DNA repair pathways have been investigated in relation to cellular response to fractionated radiotherapy. (Somaiah *et al.*, 2015, Somaiah *et al.*, 2013) *In vitro* studies using cell lines deficient in different DDR pathways have identified that loss of fraction size sensitivity is associated with the dominance of the HRR pathway, while cells proficient in NHEJ remain sensitive to dose fractionation. (Somaiah *et al.*, 2013) Data presented in this study implies that sensitivity to dose fractionation in MPM spheroids may be primarily mediated by NHEJ. Loss of this pathway through exposure to NU7441 may promote a reliance on the HRR pathway for DDR, resulting in the observed loss of fraction size sensitivity. This observation suggests that the HRR pathway remains functional in these cell lines, despite the mutations in the *Rad54B* and *Top3b* genes discussed previously.

The differential impact exerted by A1331852 across fractionation regimes may be explained by considering the impact of dose fractionation on pro-apoptotic pathways. Although all spheroids in this study received a total dose of 8Gy, the differential way in which the dose was delivered would have greatly influenced the cellular response. Exposure to a single dose of 8Gy is likely to cause significant DNA damage, providing a robust pro-death stimulus sufficient for activation of apoptosis. Conversely, dividing this dose into four fractions of 2Gy, delivered with a gap of 24 hours between each fraction would result in far more containable levels of cellular stress and more time to repair injuries between

fractions. Consequentially, cells exposed to smaller doses per fraction are far less likely to trigger pro-apoptotic pathways as a response to IR. Cells exposed to hypofractionated RT already have an excess of pro-apoptotic signals and the addition of a Bcl-xL inhibitor further disrupts the delicate balance exerted by the Bcl-2 family of proteins. These cells are therefore far more likely to die by apoptosis than cells exposed to more conventionally fractionated radiotherapy regimes.

An additional factor in the differential response to fractionated IR observed between NU7441 and A1331852 may be a more direct link between Bcl-2 inhibition and cell death compared to DNA-PKcs inhibition. It may be that cells continue to survive following genetic damage and that the anticipated volume of cell death does not correlate with the observed experimental output. In contrast, disturbing the delicate balance of Bcl-2 proteins with a BH3 mimetic may be more likely to result in commitment to cell death through the induction of MOMP.

7.3.4 DNA-PKcs and Bcl-xL are clinically relevant targets of radiosensitisation

IHC data provides confirmation that both DNA-PKcs and Bcl-xL are strongly expressed in the tissue samples of patients with epithelioid, biphasic and sarcomatoid MPM and suggests that these protein targets are clinically appropriate and could potentially serve as effective radiosensitisers in all histological subtypes of this disease.

The finding that Bcl-2 and Mcl-1 are also expressed in clinical samples may be clinically relevant. The binding groove of Mcl-1 is substantially different from that of Bcl-xL or Bcl-2 (Czabotar et al., 2007) and most Bcl-xL or Bcl-2 inhibitors don't bind to Mcl-1 with any considerable affinity. (Hennessy, 2016) This lack of target heterogeneity is demonstrated in studies investigating the effect of ABT-737 as a single agent, which report that Mcl-1 confers resistance to this drug (Woo et al., 2009) and can be a major factor of resistance in lung cancer

spheroids. (Yang et al., 2009) Similar studies in MPM found that although Mcl-1 didn't block the spheroid response to ABT 737, reduction of these protein levels (e.g. by siRNA) enhanced the effect of the drug, suggesting that Mcl-1 may blunt the response. (Barbone et al., 2011)

The expression of multiple Bcl-2 proteins in clinical samples introduces the possibility that MPM tissue may not display the same level of dependency on specific anti-apoptotic Bcl-2 proteins as immortalised cell lines and that increased resistance to A1331852 may be encountered. A broader spectrum BH3 mimetic may be required to induce clinically relevant levels of radiosensitisation in patients and this possibility requires further investigation.

7.3.5 Clinical application of data

This work is amongst the first to assess the impact of radiosensitising drugs on the therapeutic ratio of IR in MPM cell lines and is the first work conducted to date to assess the impact of radiotherapy dose fractionation on the efficacy of these drugs in a clinically relevant 3D spheroid model. Data suggest that the therapeutic efficacy of IR can be dramatically enhanced in MPM by the addition of both the DNA-PKcs inhibitor, NU7441 and by the specific Bcl-xL inhibitor A1331852. Furthermore, it appears that A1331852 in particular exerts its optimal radiosensitising effect when it is delivered with a hypofractionated radiation dose, an observation which may be of therapeutic potential, especially given the emerging evidence of a low α/β ratio in this disease.

In order for any therapeutic interaction demonstrated *in vitro* to be translated into a viable clinical opportunity, the drug should be able to selectively sensitise tumour over normal tissue to radiation. While both drugs investigated in this study displayed clear radiosensitising activity in MPM, their clinical potential may differ in this regard. The radiosensitising activity of NU7441 is unlikely to be discriminatory, whereas A1331852 could potentially exert selective MPM activity in combination with IR because of the reliance of MPM cells on anti-apoptotic proteins for survival. Any therapeutic interaction demonstrated with this drug

may therefore represent a tumour specific effect which could be translated into a therapeutic option.

Although BH-3 mimetics may selectively induce radiosensitivity in MPM cells, the normal tissue effects of this drug need to be considered if systemic administration is to be attempted. Bcl-xL is expressed at the RNA and protein level in a number of normal tissues, including brain, lung, GI tract, endocrine tissue and reproductive organs.

(<https://www.proteinatlas.org/ENSG00000171552-BCL2L1/tissue>) Clinical studies using multitarget BH3 mimetics have previously reported 'on target' normal tissue toxicities to be dose limiting, leading to a reduced interest in these drugs. Nevertheless, the reported toxicities are primarily haematological, with Bcl-xL inhibition causing thrombocytopenia and neutropenia associated with Bcl-2 inhibition. (Zhang et al., 2007, Mason et al., 2007) Subsequently, *in vivo* studies using a range of solid tumours have suggested that single agent Bcl-xL inhibition in combination with docetaxel chemotherapy could produce robust clinical effects, without inducing dose limiting toxicities. (Leverson et al., 2015) The radiosensitising activity observed with Bcl-xL inhibitors in this study introduces the possibility of using them in combination with IR, rather than as single agents. In this situation, efficacy may be maintained with shorter treatment duration and lower drug concentrations, thereby reducing haematological effects. Furthermore, the combined use of Bcl-xL inhibition and chemotherapy probably exacerbates systemic toxicity, whereas the effects of Bcl-xL inhibition and IR should be localised to the treatment field, thereby minimising the effect on the bone marrow.

7.4 Summary

This study has demonstrated concentration-dependent single agent activity of A1131852 in H2052 MPM cells in 3D. Furthermore, it has confirmed that both NU7441 and A1331852 are potent radiosensitisers in two independent MPM cell lines, which robustly express the relevant target proteins, in a clinically relevant 3D model. Radiosensitisation was found to be greater with hypofractionated radiation and the validity of the selected proteins as clinically relevant targets

has been confirmed through the IHC analysis of diagnostic tissue samples obtained from MPM patients. Although both radiosensitisers worked with optimal efficacy with hypofractionated radiotherapy, this trend was far more evident with the BH3 mimetic than with the DNA-PKcs inhibitor. These findings are clinically pertinent, since data presented in chapter 6 suggests that MPM may have a low α/β ratio and therefore would be likely to respond more favourably to a hypofractionated radiotherapy regime. The addition of a radiosensitiser which is potentially tumour selective, efficacious across histological subtypes and optimally effective when combined with hypofractionated radiotherapy therefore has great potential in this disease.

Chapter 8: Assessment of potential biomarkers of radiotherapy response in MPM

Aim

The aim of this chapter is to determine the expression of selected proteins, chosen for their potential to influence radiotherapy response, in diagnostic tissue samples collected from patients participating in the SYSTEMS and SYSTEMS-2 studies. Pilot data on the correlation of protein expression with radiation responses will be generated using tissue collected from SYSTEMS patients and clinical trial outcome data. Biopsy tissue collected from SYSTEMS-2 patients will be used at this stage to determine whether protein expression can be linked to baseline clinical parameters.

8.1 Introduction

8.1.1 Predictive biomarkers of radiotherapy response

Radiotherapy is employed in the treatment of more than half of newly diagnosed malignancies. (Delaney et al., 2005) It is a key component in the curative management of many common cancers (Glimelius et al., 2013, Horwich et al., 2013, Senkus et al., 2013) and is the cornerstone of symptom palliation. (Lutz et al., 2014) Whilst advances in radiotherapy delivery have allowed treatments to be personalised to patient anatomy, predictive biomarkers, which would allow radiotherapy to be tailored to tumour and normal tissue biology, are lacking. (Forker et al., 2015) Such biomarkers could inform decisions on radical treatment options, dosing strategies and optimal end of life care.

The crucial role of predictive biomarkers in systemic therapies has been demonstrated in breast and lung cancer, where the ability to detect and target genetic mutations in HER2, EGFR and ALK have revolutionised cancer-related outcomes in select groups of patients. (Slamon et al., 2001, Verma et al., 2012, Mitsudomi et al., 2010, Shaw et al., 2011) Several studies have identified a number of encouraging candidates reported to predict a radiotherapy benefit at a number of different tumour sites. (Drukker et al., 2014, Soderlund et al.,

2007, Eschrich et al., 2009, Eschrich et al., 2012, Choudhury et al., 2010, Noordermeer et al., 2012, Torres-Roca et al., 2005) These include genetic signatures, such as the radiosensitivity index, (Torres-Roca et al., 2005, Eschrich et al., 2012, Eschrich et al., 2009) as well as a number of DNA-damage repair markers (Soderlund et al., 2007, Choudhury et al., 2010, Noordermeer et al., 2012). Nevertheless, none of these candidate biomarkers have been robustly assessed in a clinical trial randomising between radiotherapy and no radiotherapy, to allow a predictive value to be determined. (Forker et al., 2015)

The SYSTEMS-2 clinical trial provides a unique opportunity to conduct MPM-specific radiotherapy biomarker research. Within this study, original diagnostic tumour biopsies are obtained from a well characterised population in whom radiotherapy response will be documented at several time points using a validated pain scale and imaging. Correlation of clinical trial radiotherapy outcomes with immuno-histochemical data on selected protein expression could potentially help to identify a biomarker of radiotherapy response. Furthermore, the identification of proteins associated with radio-resistance could inform future targets for radiosensitisation in this disease.

Since the SYSTEMS-2 trial is still recruiting, radiotherapy outcome data is currently unavailable. Nevertheless, protein expression in biopsy samples taken from the Glasgow patient cohort can be determined at this stage and correlated with baseline clinical trial data in an exploratory analysis. Furthermore, pilot data into the association of selected protein expression with radiotherapy response can be generated using biopsy samples obtained from patients who participated in SYSTEMS, from which full outcome data is available.

8.1.2 Selection of proteins for investigation

A total of nine proteins have been selected for investigation. These have been chosen for their potential to impact on radiotherapy response and include proteins associated with DNA repair, proliferation, hypoxia and the control of apoptosis.

8.1.2.1 Anti-apoptotic Bcl-2 proteins: Mcl-1, Bcl-2 and Bcl-xL

A large body of evidence indicates that defects in apoptotic pathways are common in mesothelioma and may provide an important mechanism of radio-resistance. (Fennell and Rudd, 2004, Narasimhan et al., 1998, Segers et al., 1994, Soini et al., 1999) Furthermore, *in vitro* studies by our own group have confirmed the radio-resistant nature of a panel of human mesothelioma cells to low doses of radiation and showed that these cells are extremely refractory to induction of apoptosis. Small molecule inhibitors of Bcl-xL reduced cell survival as single-agents and, crucially, sensitized mesothelioma cells to IR. This reduction in survival was associated with increased levels of caspase-3/7 activity and apoptosis. (Manuscript submitted) As discussed in section 1.6.6, these proteins represent promising and novel targets for radiosensitisation, and preclinical data presented earlier in this thesis have confirmed that their selective inhibition radiosensitises MPM spheroids in a clinically relevant 3D *in vitro* model. Expression of these proteins in archival tissue specimens taken for diagnostic purposes might therefore have predictive value in determining which patients will benefit from radiotherapy.

8.1.2.2 Activated caspase 3

The central role of executioner caspase 3 in the final common pathway of apoptosis has been discussed in section 1.6.4. Using an antibody which is specific to the activated form of caspase 3, baseline levels of activity will be determined in MPM patient samples and used to assess whether this information could be used to predict radioresponse.

8.1.2.3 P21

The cyclin dependent kinase inhibitor, p21, is a principal mediator of cell cycle arrest. (Abbas and Dutta, 2009) It is able to inhibit all cyclin/CDK complexes, (Xiong et al., 1993) but primarily exerts its effect through the inhibition of CDK2, (Wade Harper et al., 1993, Abbas and Dutta, 2009) which operates in the G1/S phase of the cell cycle. In addition to mediating p53-dependent growth arrest in G1 phase, (Deng et al., 1995) p21 has been implicated in the promotion

of cell cycle arrest in response to a number of p53 independent stimuli, demonstrating an ability to act as an effective sensor and effector of many anti-proliferative signals. (Abbas and Dutta, 2009) As well as mediating cell cycle arrest, p21 has a dominant role in promoting cellular senescence and differentiation, in addition to modulating DNA damage repair. (Abbas and Dutta, 2009)

P21 is also thought to have a role in the control of apoptosis, although the mechanism is not fully understood, with reports of both pro- and anti-apoptotic functions of the protein. (Roninson, 2002, Gartel, 2005) Furthermore, despite its robust cytoprotective properties, evidence suggests that under certain circumstances, p21 can drive cell proliferation and take on an oncogenic role, potentially mediated through the inhibition of apoptosis. (Roninson, 2002)

8.1.2.4 DNA-PKcs

Ionising radiation mediates its cytotoxic effect through the generation of DS-DNA breaks and repair of these lesions represents a potential mechanism through which tumours develop resistance to radiotherapy. As discussed in section 1.7.2, the NHEJ pathway is a crucial pathway of DS-DNA damage repair, in which the protein DNA-PKcs is fundamental. (DeFazio et al., 2002, Chen et al., 2005, Chen et al., 2007, Cui et al., 2005, Douglas et al., 2007, Douglas et al., 2002, Ding et al., 2003) Mutations within the NHEJ pathway have been implicated in the resistance of MPM to treatment (Toumpanakis and Theocharis, 2011, Kettunen et al., 2001, Roe et al., 2010) and data presented earlier in this thesis demonstrated that specific disruption of NHEJ by inhibition of DNA-PKcs can radiosensitise MPM spheroids *in vitro*. Levels of DNA-PKcs expression within clinical samples may therefore not only be useful in determining response to IR, but also to potentially identify patients with tumours that may be amenable to radiosensitisation.

8.1.2.5 *Ki67*

Tumour proliferation rate can impact on radiation response through the processes of repopulation and re-assortment. Tumour initiating cells that survive IR and are capable of rapid proliferation can repopulate the tumour, reducing the efficiency of radiotherapy and mediate treatment resistance. Conversely, the rapid progression of proliferating cells through the cell cycle increases the chance of a cell which was in a radioresistance phase of the cycle redistributing to the radiosensitive late G2/M phase in a multi-fractionated regime. The Ki67 protein is a marker of cellular proliferation, present during all active phases of the cell cycle but absent in quiescent (G0) cells. (Bruno and Darzynkiewicz, 1992) Data suggests that tissue proliferation indices are inversely correlated with sensitivity to fraction size. (Thames et al., 1990, Hopewell et al., 2003) Correlation of the baseline tumour proliferation rate with responses to the hypofractionated radiotherapy delivered in SYSTEMS-2 would therefore be of radiobiological interest.

8.1.2.6 *HIF1 α*

The impact of tumour hypoxia on radiation response is dictated by the oxygen fixation hypothesis, (Gray et al., 1953) previously discussed in section 1.5.3. In addition to being resistant to radiotherapy, hypoxic tumours further prevent effective treatment, by favouring the enrichment of tumour cells with stem-like properties (Ghattass et al., 2013) and by promoting disease progression through the activity of the α and β subunits of hypoxia-inducible factor-1 (HIF-1) and HIF-2. (Nabavi et al., 2016) Under hypoxic conditions, HIF1 α becomes stable and accumulates, associating with the constitutively expressed HIF1 β to affect the transcription of target genes. (Kallio et al., 1997) Detection of HIF1 α expression can therefore be associated with tissue hypoxia and will be used in this study as a surrogate marker of hypoxia in baseline biopsy specimens. The role of hypoxia in MPM pathogenesis, progression and resistance to treatment has not been well studied, (Nabavi et al., 2016) although evidence suggests that hypoxic cells can be found within MPM tissue (Ravenna et al., 2014) and studies using fluoromisonidazole PET-CT identified hypoxic areas in bulky tumour masses in MPM patients. (Francis et al., 2015)

8.1.2.7 γ H2Ax

Double stranded DNA breaks can be detected by the focal localisation of the phosphorylated histone γ H2Ax, with each focus representing an individual DSB. (Kuo and Yang, 2008) Phosphorylation of this protein by ATM and ATR occurs immediately after the formation of a DS-DNA break and is the first step in the recruitment of DDR proteins to the break. Foci of γ H2Ax form rapidly after IR, with a maximal response 30 minutes after exposure, subsequently declining over a period of hours as the cells repair the damage. (Redon et al., 2009)

Determining the expression of this protein in tissue samples taken from treatment naïve MPM patients will provide an indication of the baseline level of DNA damage within the tumour and may also provide some insight into the relative capability for repair.

By analysing FFPE tissue taken from patients participating in SYSTEMS and SYSTEMS-2, the expression of these 9 proteins of interest will be determined. In addition to providing pilot data on prospective biomarkers of radiotherapy response, this information could represent a valuable resource in the future research of this disease, given the paucity of MPM IHC samples currently available within public datasets (e.g. ProteinAtlas and The Cancer Genome Atlas Project).

8.2 Results

8.2.1 IHC validity in MPM samples is enhanced by the generation of reliable positive controls

To determine the expression of selected proteins within diagnostic MPM tissue, FFPE tissue blocks were obtained from patients who entered the SYSTEMS or SYSTEMS-2 study. The blocks were sectioned and subjected to IHC staining for the proteins of interest. One slide from each block was stained with H&E, to determine tissue architecture and distinguish areas of malignant infiltration. Areas of tumour invasion were identified and protein expression within tumour cells was determined by scoring for staining intensity. This allowed an H score to

be generated, which served as a comparator for relative protein expression between samples.

In total, 21 blocks were obtained for this purpose from the Glasgow Biorepository over the course of two years. Of these samples, 8 originated from patients who took part in SYSTEMS and 13 were from SYSTEMS-2 patients. Following review of the H&E and the initial pathology report, 3 samples were discounted from the final analysis, because no tumour cells could be identified. This left 7 samples from SYSTEMS patients and 11 from SYSTEMS-2 for further analysis and correlation studies. These samples comprised 10 samples of epithelioid subtype, 7 samples of sarcomatoid subtype and 1 sample expressing a biphasic pattern of disease.

A total of 9 proteins were selected for analysis. These included 6 which were expressed in the nucleus (DNA-PKcs, γ H2Ax, P21, Activated caspase 3, Ki67 and HIF1 α) and 3 which localised to the mitochondria, represented by cytoplasmic staining (Bcl-xL, Bcl-2 and Mcl-1).

To determine consistency between batches of antibody staining and to ensure the specificity and sensitivity of antibody binding, positive and negative controls were included with all IHC. These comprised human tonsil tissue, or MPM tissue previously demonstrated to express sufficient levels of protein to act as a reliable control. Negative controls, comprised human tonsil or MPM tissue, with no primary antibody. Patterns of staining were consistent between different batches of IHC. (Figure 8.1) Robust positive control samples were identified for each protein, with the exception of 'activated caspase 3', in which only the germinal centre of tonsillar tissue could be reliably demonstrated to express this protein on a weak basis. (Figure 8.1) Representative images of protein expression in epithelioid and non-epithelioid MPM tissue, with corresponding H&E are shown in Figure 8.1, in addition to the typical levels of staining achieved in positive controls. Representative negative controls for IHC performed manually and on the autostainer are shown in Figure 8.2.

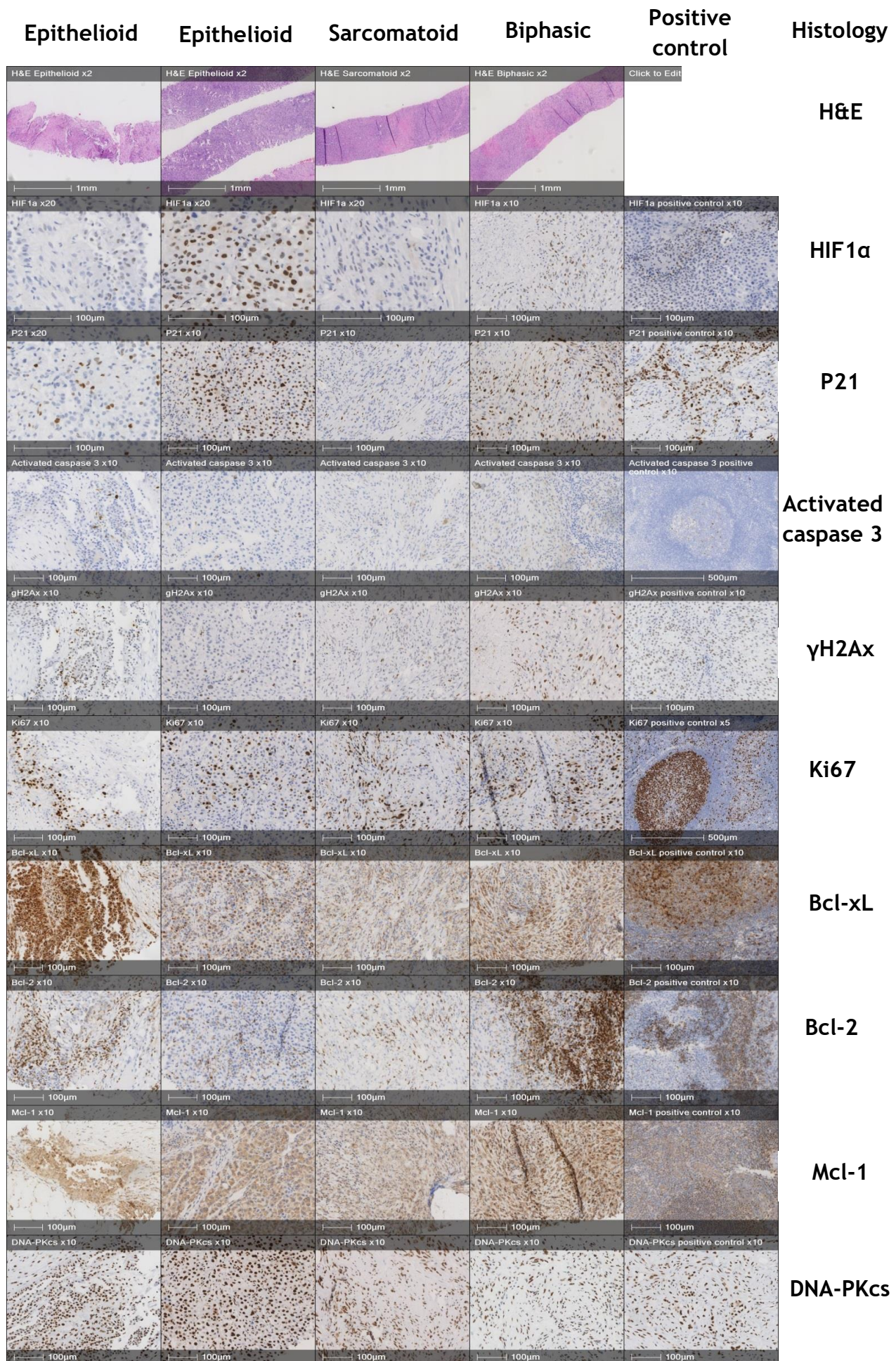


Figure 8.1 Representative expression profiles of selected proteins in MPM biopsy tissue and positive controls

(Figure 8.1) Tissue from FFPE samples obtained from MPM patients were stained for their expression of 9 selected proteins. Proteins demonstrated either a nuclear or a cytoplasmic staining pattern. Data validity was confirmed using positive controls of human tonsil tissue, or MPM tissue previously demonstrated to have high protein expression. Representative images are shown from two patients with epithelioid disease, one patient with sarcomatoid disease and one with biphasic histology. Nuclei were counterstained with haematoxylin and images were obtained by scanning slides into Halo software, where analysis was also carried out.

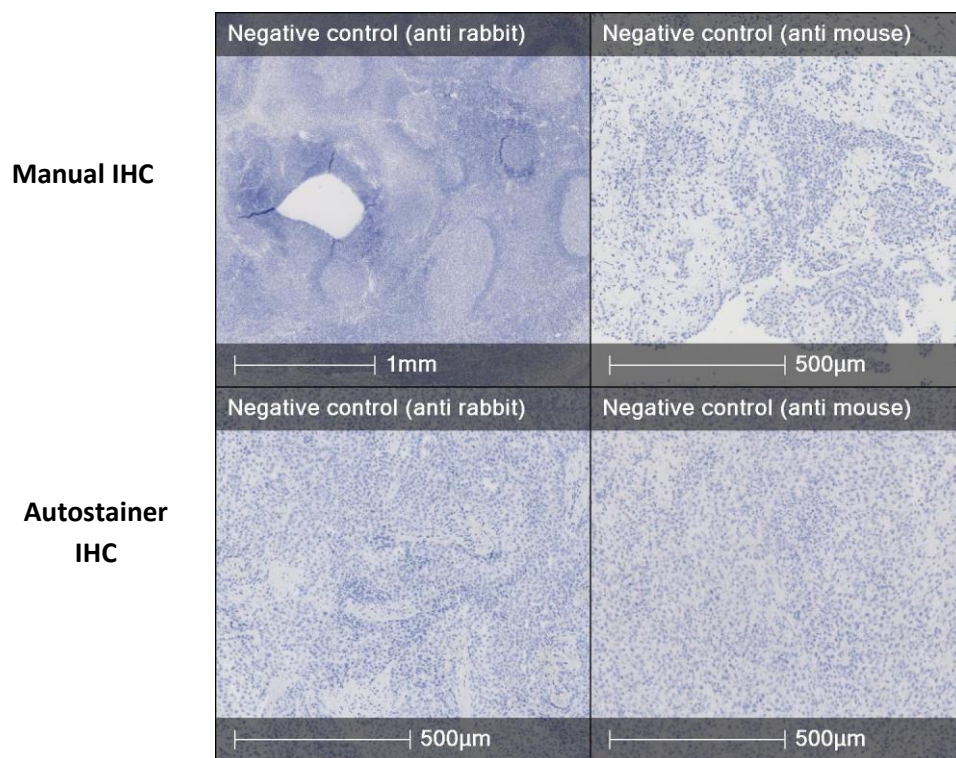


Figure 8.2 Negative controls determining binding specificity of rabbit and mouse primary antibodies

To determine that staining is dependent on the primary antibodies employed for IHC, tonsillar or MPM tissue was subjected to the IHC staining process, but without the addition of the primary antibody. Negative controls were run during both the manual and automated IHC.

8.2.2 MPM tissue exhibits heterogeneity in protein expression

Expression of all 9 proteins of interest was detected within the MPM tissue samples, but the level of expression differed between proteins and between patients. (Figure 8.1 and Figure 8.3) For example, strong expression of DNA-PKcs was noted throughout all 18 samples, with a mean H score of 242 ± 28 , whereas expression of activated caspase 3 and HIF1 α were uniformly low, with mean H scores of 7 ± 6 and 14 ± 16 respectively. (Figure 8.3) Expression data for other proteins suggest a high level of variation in the expression of a single protein between different tissue samples. For example, the mean H score of Bcl-2 expression was 61, with a standard deviation of 54, suggesting substantial variability within the dataset. Similar levels of variance around the mean were seen with Bcl-xL, Ki67, Mcl-1, γ H2Ax and p21 expression. (Figure 8.3)

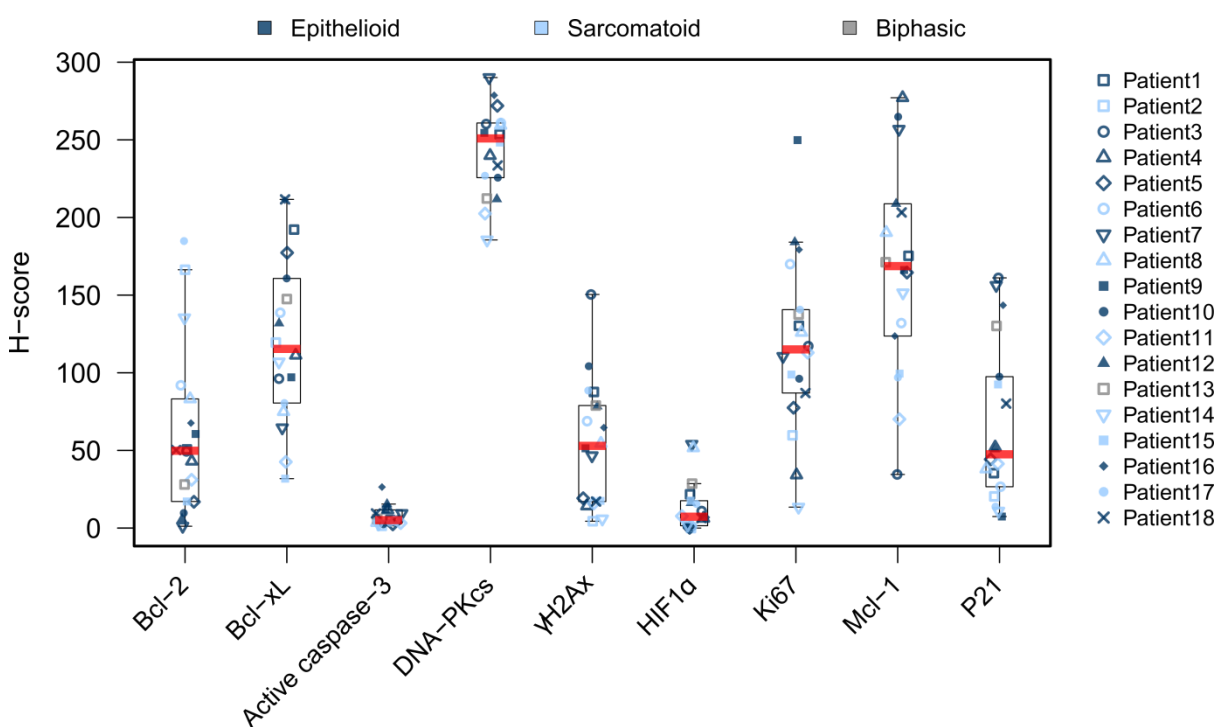


Figure 8.3 Expression of selected proteins in MPM tissue samples

Data were generated from IHC analysis of 18 diagnostic tissue samples comprising 10 epithelioid, 7 sarcomatoid and 1 biphasic subtype. Tumour cells were identified and their expression of each protein was graded as absent, weak, moderate or strong. H scores were calculated using the equation $(1 \times (\% \text{ cells } 1+) + 2 \times (\% \text{ cells } 2+) + 3 \times (\% \text{ cells } 3+))$. Data are presented as box and whisker plots, plotted according to the Tukey method and the median is denoted by the horizontal red line.

8.2.3 Protein expression is not significantly different between histological subtypes of MPM

To determine whether protein expression varied between epithelioid and non-epithelioid MPM, data was dichotomised by histological subtype and analysed using the Mann Whitney U test, with false discovery rate (FDR) p value correction. This analysis revealed no significant differences in H-scores between tissue subtypes.

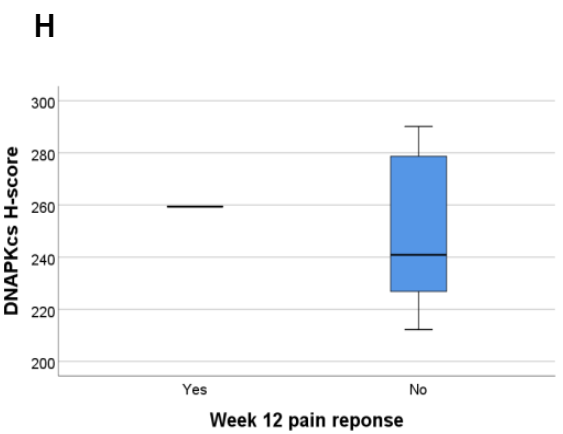
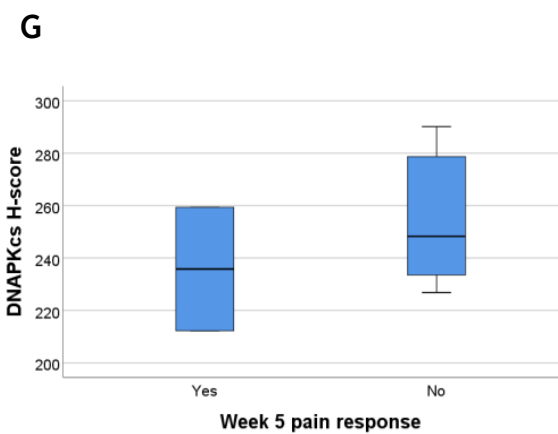
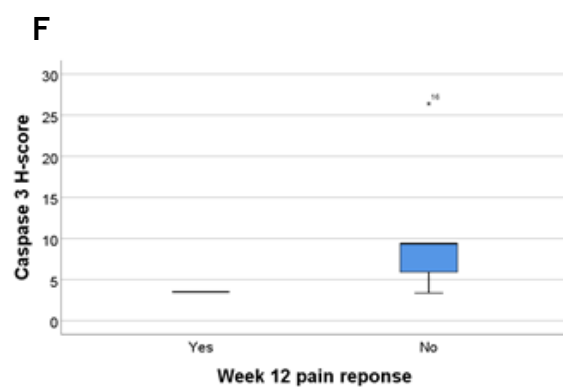
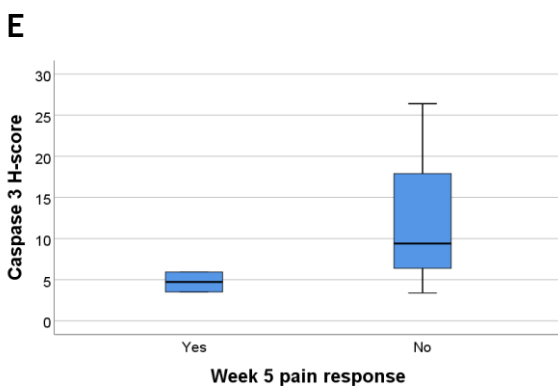
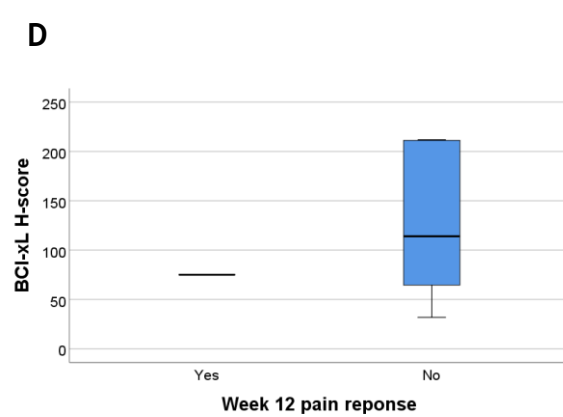
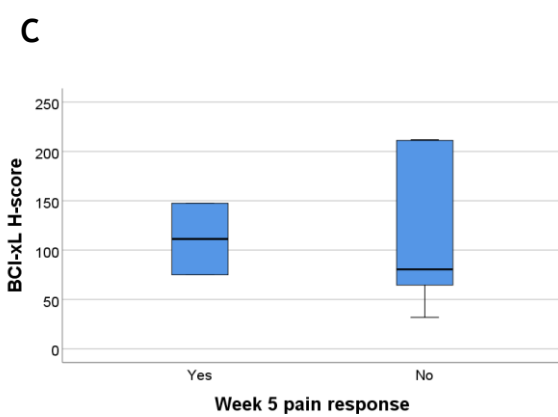
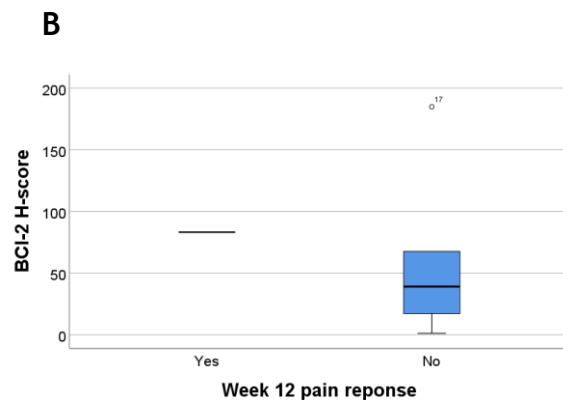
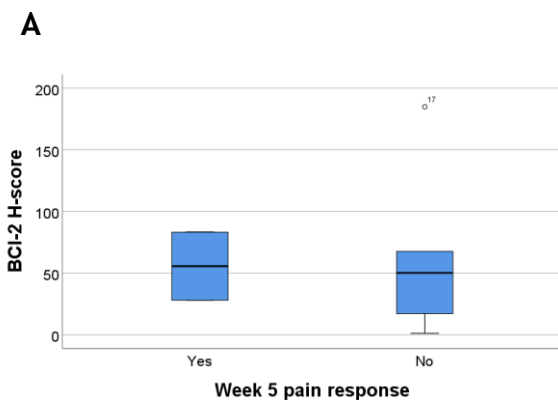
8.2.4 No correlation was found between baseline clinical parameters and protein expression in MPM tissue

To determine whether protein expression could be predictive of clinical parameters, tumour H scores generated from SYSTEMS and SYSTEMS-2 patients were correlated with clinical trial information. In cases where the biopsy specimens were obtained from patients who had taken part in SYSTEMS-2, these parameters consisted of baseline clinical trial data only, whereas those that were obtained from SYSTEMS patients could also be correlated with clinical trial outcome data, such as pain response to radiotherapy.

No statistically significant interactions were found when H scores from SYSTEMS patients were correlated with pain response to radiotherapy, either at week 5 or at week 12. A pain response was defined as a $\geq 30\%$ reduction in pain from the baseline, assessed using the brief pain inventory. This data is shown in Figure 8.4 A-R.

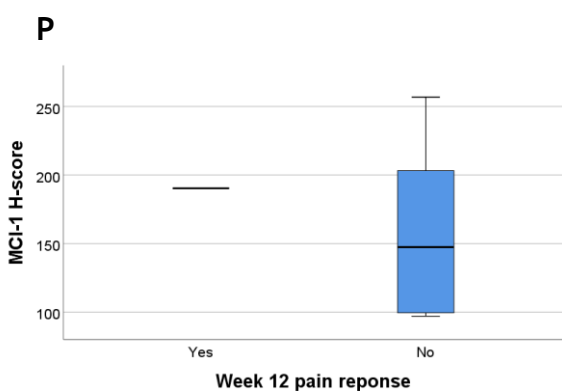
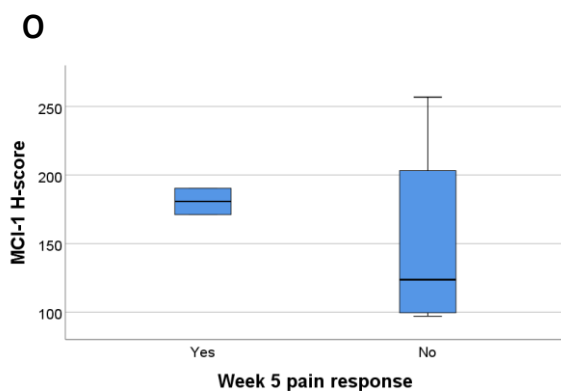
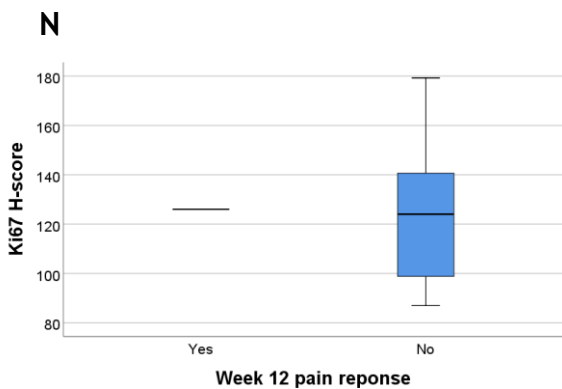
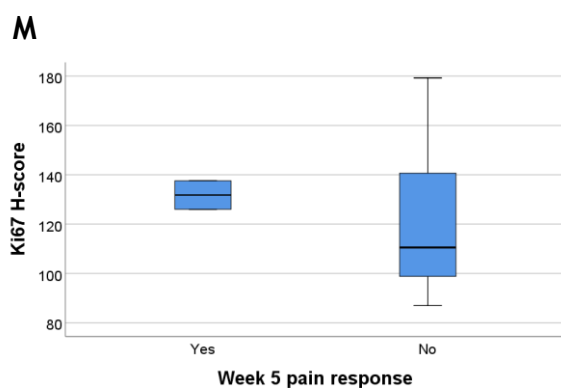
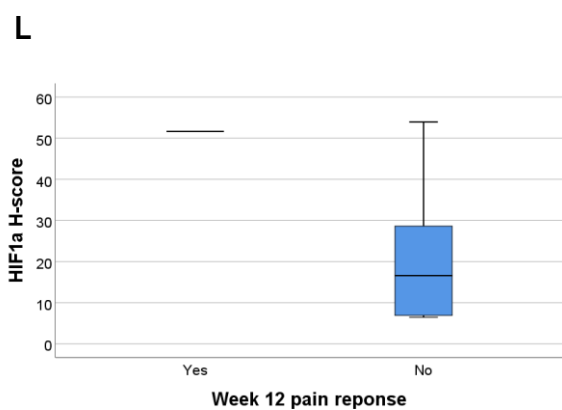
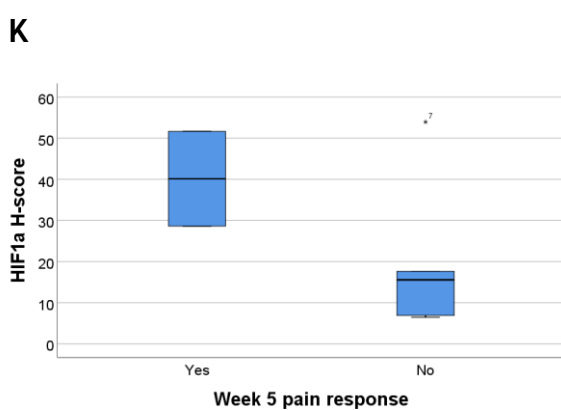
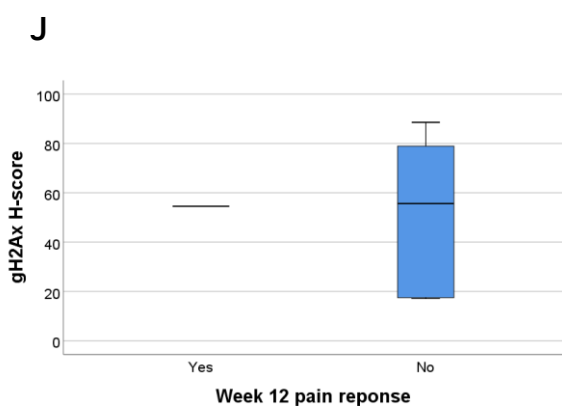
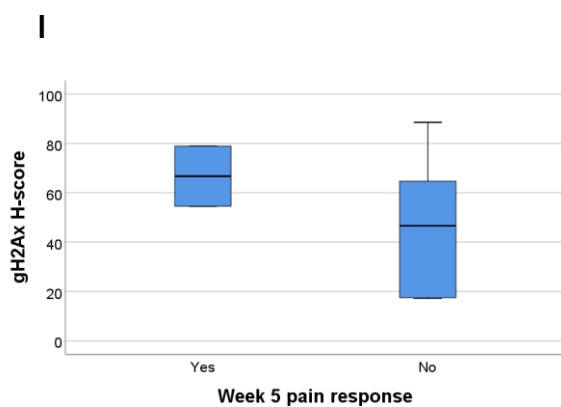
Week 5

Week 12



Week 5

Week 12



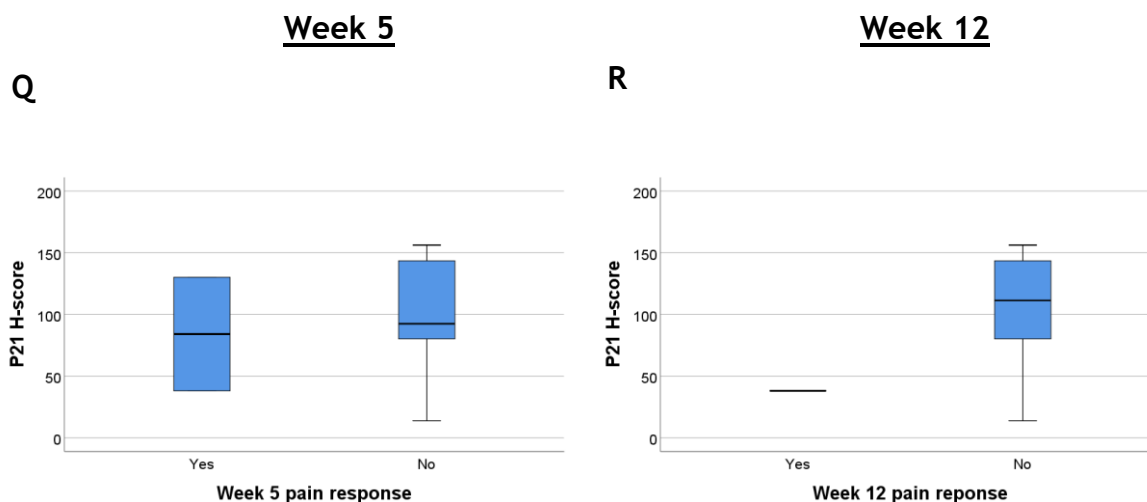


Figure 8.4 A-R Correlation of protein H-scores in tissue samples taken from SYSTEMS patients with pain outcomes at week 5 and 12 after radiotherapy

Data were generated from IHC analysis of 7 diagnostic tissue samples comprising 3 epithelioid, 3 sarcomatoid and 1 biphasic subtype. Tumour cells were identified and their expression of each protein was graded as absent (0), weak (1+), moderate (2+) or strong (3+). H scores were calculated using the equation $1x (\% \text{ cells } 1+) + 2x (\% \text{ cells } 2+) + 3x (\% \text{ cells } 3+)$. Data are presented as box and whisker plots, plotted according to the Tukey method and the median is denoted by the horizontal line. Statistical analyses were performed using the Mann Whitney U Test.

On initial analysis, statistically significant correlations were revealed between a number of baseline parameters and protein expression. These associations included Bcl-xL and DNA-PKcs expression with the requirement for pleurodesis, expression of activated caspase 3 with histological subtype, Ki67 expression with stage of disease at the time of requiring radiotherapy and a raised baseline CRP correlating with expression of Ki67 and γ H2Ax.

Following correction for multiple testing using both FDR and Bonferroni corrections however, all of these significant findings were lost at the $p > 0.05$ level. The initial p values associated with each investigated interaction, in addition to those obtained following Bonferroni and FDR correction are shown in Table 8.1. Further graphical illustrations of this dataset can be found in Appendix 4.

| | HIF1 | P21 | Act casp 3 | γ H2A x | Ki67 | Bcl- xL | Bcl-2 | Mcl- 1 | DNA PKcs |
|----------------------------------|-------|-------|------------------|-------------------|-------|------------|-------|-----------|-------------|
| Stage of disease | | | | | | | | | |
| P value | 0.233 | 0.878 | 0.878 | 0.477 | 0.025 | 1 | 0.96 | 0.785 | 0.956 |
| FDR | 1 | 1 | 1 | 1 | 0.486 | 1 | 1 | 1 | 1 |
| Bonferroni | 1 | 1 | 1 | 1 | 1 | 1 | 1 | 1 | 1 |
| Pain response (week 5)* | | | | | | | | | |
| P value | 0.381 | 0.857 | 0.533 | 0.571 | 0.857 | 1 | 0.86 | 0.857 | 0.571 |
| FDR | 1 | 1 | 1 | 1 | 1 | 1 | 1 | 1 | 1 |
| Bonferroni | 1 | 1 | 1 | 1 | 1 | 1 | 1 | 1 | 1 |
| Pain response (week 12)* | | | | | | | | | |
| P value | 0.571 | 0.571 | 0.667 | 1 | 1 | 0.857 | 0.57 | 0.857 | 0.857 |
| FDR | 1 | 1 | 1 | 1 | 1 | 1 | 1 | 1 | 1 |
| Bonferroni | 1 | 1 | 1 | 1 | 1 | 1 | 1 | 1 | 1 |
| CRP* | | | | | | | | | |
| P value | 0.872 | 0.957 | 0.505 | 0.005 | 0.005 | 0.957 | 0.21 | 0.266 | 0.704 |
| FDR | 1 | 1 | 1 | 0.225 | 0.225 | 1 | 1 | 1 | 1 |
| Bonferroni | 1 | 1 | 1 | 0.45 | 0.45 | 1 | 1 | 1 | 1 |

8.3 Discussion

8.3.1 Proteins of interest were expressed in MPM tissue

Data confirmed that all 9 proteins were expressed in the diagnostic biopsies of MPM patients, at differing levels of intensity. Expression of some proteins (e.g. DNA-PKcs and HIF1 α) was relatively uniform in all biopsy specimens, whereas others displayed a large degree of variability between patients, indicated by the substantial standard deviations observed within some of the datasets. MPM is

known to be a highly heterogeneous tumour (Oehl et al., 2018) and random sampling during the biopsy process may in part explain the variation in protein levels observed.

The validity of expression data was confirmed through the use of positive and negative controls. Where possible, MPM tissue was used for this purpose. This enhances confidence in our data, since control and target tissue were processed in the same way, reducing the potential for technical variation to influence results. Staining was found to correlate well with the anticipated subcellular distribution of each protein.

Reliable positive controls were obtained for all proteins, with the exception of activated caspase 3. Despite use of this antibody with a variety of different tissues, staining could only be repeatedly seen in the germinal centres of human tonsil tissue, and this was of weak intensity. MPM cells *in vitro* are inherently resistant to apoptosis (Fennell and Rudd, 2004, Narasimhan et al., 1998) and the manipulation of apoptotic pathways to enhance radiosensitivity in MPM has been explored earlier in this thesis. The low expression of activated caspase 3 observed in these tumour samples may be due to a baseline resistance to apoptosis in these treatment naïve patients. Nevertheless, without a positive control which robustly expresses this protein to act as a comparator, accurate interpretation of this data is difficult. Future IHC analysis on SYSTEMS and SYSTEMS-2 tissue samples should aim to use a different positive control tissue, for example, tissue treated with apoptosis-inducing drugs, or select an alternative antibody for detection of activated caspase 3 than the one used in this study.

The variability seen in protein expression between biopsy specimens makes it difficult to make generalised comment on the relevance of these proteins in MPM. Nevertheless, DNA-PKcs was found to be robustly expressed in all tissue samples analysed, suggesting that the NHEJ pathway of DNA damage repair may be an important process in this tumour. Furthermore, this observation lends

weight to data presented in chapter 7, which highlighted the radiosensitising properties of the DNA-PKcs inhibitor NU7441 in MPM and the apparent importance of the NHEJ pathway in fractionation sensitivity in this tumour. Expression of HIF1 α was found to be uniformly low across tissue samples. This is an interesting finding and suggests that hypoxia may not be a significant pathogenic driver in this tumour. Representative images shown in Figure 8.1 demonstrate that areas of HIF1 α expression were detected in some samples, but these were small pockets of HIF1 α positive cells, indicating only limited areas of hypoxia. Data presented by Francis *et al.* suggest that areas of significant hypoxia in MPM are found in bulky tumour deposits. (Francis *et al.*, 2015) An alternative explanation for our findings may therefore be that whilst bulky areas of disease are likely to have been targeted for biopsy, sufficient depth may not have been reached to allow central hypoxic areas of tumour to be sampled.

8.3.2 Protein expression in MPM tissue could not be correlated with baseline clinical parameters in this limited dataset

Although initial statistical analysis using the Mann Whitney U and Spearman Rank Correlation tests identified a number of statistically significant associations between baseline clinical characteristics and protein expression, the statistical significance all correlations was lost at the $p > 0.05$ level, following correction for multiple comparisons. This is a clear limitation of the sample size utilised in this study and larger sample sizes will be required to thoroughly investigate correlations in future analyses.

The lack of detected interaction between baseline clinical trial data and protein expression may not necessarily be surprising, given that the proteins were selected for their potential to impact on radiation response. Disappointingly, correlation of protein expression from SYSTEMS patients with clinical trial outcome data failed to identify any potential biomarker of radiotherapy response. Nevertheless, only 7 samples out of a potential 30 were obtained for this analysis, severely limiting the power of this dataset to reveal any significant association. Analysis of protein expression in SYSTEMS-2 biopsy specimens is ongoing and in addition to the current dataset, will provide a far more robust

cohort for correlation with pain and radiological response data when SYSTEMS-2 completes recruitment and reports its outcomes.

8.3.3 Study limitations

There are a number of weaknesses in this study, the most important of which was the limited number of patient samples obtained on which to carry out IHC and subsequent correlation analyses. Originally, it had been anticipated that tissue would be obtained from the majority of the Glasgow cohort of SYSTEMS-2 patients and all of Glasgow's SYSTEMS patients with histological diagnoses of MPM. Together, this totalled more than 60 FFPE blocks. Despite timely request for this tissue, capacity issues within Glasgow Biorepository meant that approval of the request was delayed by 13 months and a lack of on-site storage meant that subsequent retrieval of the blocks was slow. Furthermore, staffing issues resulted in a substantial delay in the review and sectioning of blocks by a consultant pathologist. To overcome this issue, the tissue blocks were released directly from the Biorepository in batches, to be reviewed and sectioned by histopathology staff at the University of Glasgow. Following this process, blocks were returned and a further batch collected. Despite these measures, only 21 FFPE samples were obtained, 3 of which did not contain tumour cells and could not be included in subsequent analysis. This issue has limited the ability to draw robust conclusions from our dataset.

In addition to the number of samples obtained, there were also problems with the quality of the samples received. These diagnostic biopsies were often obtained through medical thoracoscopy rather than through a video assisted thoracoscopic procedure. Consequentially, they were small and susceptible to non-specific staining at the edge of the sample. If not recognised, this 'edge effect' could falsely increase the H score, thereby invalidating our results. This problem was overcome through selection of the region of interest at digital analysis, to prevent cells at the edge contributing to the expression score. However, this further reduced the volume of tissue in which to locate tumour cells.

A further issue was that some of the tissue samples were degraded through the IHC process. This meant that they appeared histologically different from their respective H&E sample, rendering the process of tumour identification more difficult. In addition, some tissue samples became detached from the slide, making them blurred at microscopy and rendering analysis impossible.

Areas of malignant invasion were identified through the inspection of H&E slides with the corresponding pathology report. This was often challenging because of the recognised diagnostic difficulties in MPM (Inai, 2008, Henderson et al., 2013) and also because malignant cells were often diffusely infiltrated within normal pleura, making them hard to identify. Subsequent IHC slide analysis was performed individually, with parameters of cell size and shape manipulated on the 'Halo' software to facilitate the identification of tumour cells within the specimen. Confirmation of the selected cells in a field of view as malignant was performed before the entire sample was analysed. Despite these measures, non-malignant cells may still have been inadvertently included in the analysis.

Finally, although a period of training was undertaken with a consultant pathologist prior to embarking on data analysis, the lack of formal pathology input with regard to the identification of areas of malignant invasion and the generation of subsequent H scores, is an acknowledged limitation of this work.

8.4 Summary

In summary, the data reported here demonstrate that the selected proteins of interest are expressed in MPM tissue at differing levels of intensity, with most displaying variable expression between biopsy samples. Exploratory analyses correlating clinical trial data with protein expression did not reveal any statistically significant interactions and disappointingly, no potential biomarkers of radiotherapy response were identified from analysis of the limited number of SYSTEMS samples. A more robust correlation analysis will be performed when SYSTEMS-2 has completed recruitment and reported its radiotherapy outcomes.

Chapter 9: Final discussion

9.1 The changing landscape of MPM research

Over the last few years, there has been a focused effort within the UK to fund research into cancers of unmet need. This policy has facilitated basic scientific research into malignancies such as MPM, which had been chronically underfunded. As a result, a gradual understanding of the biology of this malignancy is being established and methods to overcome its resistance to a variety of therapeutic strategies are being investigated. Efforts to standardise patient care across the UK have intensified, with British Thoracic Society guidance recommending that every patient should be discussed at a central MDT, where the most appropriate treatment options can be considered. (Woolhouse et al., 2018)

The research drive in MPM has led to increasing clinical trial availability, particularly for systemic therapies, where early data, especially around immunotherapy has been encouraging. (Alley et al., 2017) Although to date, clinical trials have only demonstrated a role for radiotherapy in the palliation of MPM, (MacLeod et al., 2015a) a number of phase II studies have been conducted to assess radiotherapy in the multimodality setting, following chemotherapy and surgery. (Federico et al., 2013, Krug et al., 2009, Weder et al., 2007, Van Schil et al., 2010, Hasegawa et al., 2016) Despite the encouraging survival data reported, the lack of randomisation and inherent biases associated with surgical studies (typified by the exclusion of patients who were not fit enough for surgery), makes it difficult to draw firm conclusions from these data.

SYSTEMS-2 is the first randomised study of radiotherapy dose escalation to be attempted in MPM. (Ashton et al., 2018) The challenges of conducting randomised clinical trials in relatively rare diseases have been discussed in the literature. (Lilford et al., 1995, Tan et al., 2003) The added difficulties of conducting such trials in a palliative context is also acknowledged, (McWhinney et al., 1994, Grande and Todd, 2000) and have been outlined within this thesis. Nevertheless, the importance of overcoming these issues to permit the

recruitment of adequate numbers of patients from which high quality data can be generated is evidenced by the fact that only two randomised clinical trials of radical treatment in MPM have been published to date (Stahel et al., 2015, Treasure et al., 2011) and both have generally been regarded as inconclusive, largely due to insufficient power. (Rimner et al., 2016a, Rusch et al., 2013)

The future of MPM research is likely to be guided in part by a recently published landmark article detailing the molecular characterisation of 216 cases of MPM. This analysis, which was based on exome sequencing, identified only a small number of coding mutations (on average 24 ± 11 per tumour), suggesting that the mutational burden of MPM is much lower than in most other cancers. (Bueno et al., 2016) Furthermore, this molecular analysis revealed that the dominant protein alterations in MPM are loss-of-function mutations in tumour suppressor genes. Very few oncogene driver mutations were identified, suggesting that patients with MPM are unlikely to respond to currently available small molecule inhibitors. (Bueno et al., 2016) The low mutational burden of MPM, in combination with the lack of obviously druggable targets suggests that a multi-modal approach is likely to be required for the successful treatment of this disease, further substantiating the importance of radiotherapy research in MPM. (Blyth and Murphy, 2018)

There is escalating evidence to suggest that hypofractionated RT may provide a specific anti-tumour activation of the immune system. (Bernstein et al., 2016) Demonstration of a cytotoxic T cell response to hypofractionated radiotherapy in MPM mouse models, (De La Maza et al., 2017, Wu et al., 2015) provides a compelling strategy for a combination approach with immunotherapy in the future treatment of this disease.

9.2 Dose constraints

The SYSTEMS-2 study necessitated generation of novel dose constraints for a hypofractionated thoracic radiotherapy regime. Local SABR thoracic protocols were used as a template on which these constraints were modelled and they

have also been interpreted in light of the more recently published UK consensus on normal tissue constraints for SABR. (Hanna et al., 2018) Nevertheless, substantial differences exist between the radiotherapy delivered in SABR and SYSTEMS-2, particularly in terms of PTV size, dose per fraction and treatment intent.

The recent publications by Gomez *et al* and Parisi *et al* of normal tissue dose constraints for hypofractionated radiotherapy regimes in MPM, offer appropriate comparisons. These constraints were noted to be more conservative than those suggested for SYSTEMS-2, reflecting the more radical approach taken in these studies. Nevertheless, the rigorous setting of a clinical trial, where toxicity data is collected at regular intervals, is the optimal setting in which to test the safety of the SYSTEMS-2 dose constraints, and to generate robust comparative data to the regimes employed by de Perrot and Parisi. Future hypofractionated radiotherapy protocols are likely to be guided by toxicity data generated from SYSTEMS-2 and this data may also facilitate the development of macroscopic models of normal tissue volume effects, particularly for acute tissue complications following large doses per fraction. Hypofractionated radiotherapy regimes with radical intent however, would need to give greater consideration to the issue of late normal tissue complications, which were largely negated by the life expectancy of the SYSTEMS-2 cohort.

9.3. Dose delivery

Safe dose escalation in SYSTEMS-2 has been achieved through the use of 3D conformal radiotherapy or IMRT/VMAT, which facilitates sparing of normal tissue without compromising dose to the tumour. Large PTV volumes and close proximity of radiosensitive structures makes the radiotherapy planning for SYSTEMS-2 challenging. This is evidenced by the fact that none of the ‘test’ patients at the Beatson West of Scotland Cancer Centre met every dose constraint and at some recruiting centres, patients have not been randomised on the study due to the inability to generate a suitable dose escalated plan.

Radical radiotherapy planning for MPM is likely to be even more challenging, since doses to OARs will need to be maintained at an acceptable level, in the context of further dose escalation to a larger PTV. Recent procurement of MCO planning software by the Beatson West of Scotland Cancer Centre has permitted the re-planning study presented in this thesis, which suggests that clinically significant dose reductions can be achieved in a number of OARs without compromising the PTV coverage. These data suggest that further dose escalation to the PTV may be possible without breaching dose constraints. Ongoing planning studies at the Beatson West of Scotland Cancer Centre will determine whether the entire pleura could be treated to the dose escalated regime of 36Gy in 6 fractions without compromising OAR constraints and isotoxic radiotherapy planning studies will investigate the maximal dose achievable in the pleura. Outcomes from this work will be crucial in guiding further dose escalation in MPM.

The potential for radical radiotherapy in MPM is enhanced by ongoing advances in radiotherapy planning and delivery, which are likely to afford further protection to OARs by increasing dose conformity. These developments include 4D CT planning, which facilitates an appreciation of intra-fraction motion of the target volume, and the advent of methods which reduce the impact of respiratory tumour motion on radiotherapy planning: 'respiratory gated radiotherapy techniques'. (Giraud and Houle, 2013) In 2004 Ling *et al* described how these methods could be employed to facilitate dose escalation without increasing toxicity, (Ling et al., 2004) and subsequently they have been widely employed to improve geometric precision and dosimetry at a number of tumour sites affected by respiratory motion such as lung, breast and liver. (Underberg et al., 2005, Saito et al., 2014, Berg et al., 2018, Wagman et al., 2003)

Other developments which are likely to impact on radiotherapy delivery in the future include the integration of radiobiological modelling into treatment planning systems (Mesbahi et al., 2019, D'Andrea et al., 2018) and functional imaging techniques. Modern functional imaging provides a surrogate for the visualisation of a variety of tumour characteristics, including metabolism,

hypoxia, perfusion and proliferation. (Thorwarth, 2015) Integration of this information with radiotherapy planning offers a powerful tool through which plans can be further personalised and dose can be tailored to overcome biology-driven radiation resistance. (Nestle et al., 2009, van der Heide et al., 2012)

The advance of MRI-guided radiotherapy offers further opportunities for dose escalation to the pleura. MRI is already used in the treatment planning of a number of different cancers, where the improved resolution of soft tissue allows more precise delineation of treatment volumes and OARs than can be achieved by CT. This imaging is currently used in the staging of MPM where surgery is being considered, since improved soft tissue visualisation facilitates the accurate assessment of diaphragmatic, chest wall and mediastinal involvement. (Stewart et al., 2003)

Combining MRI with a linac in a single unit has been challenging, since the magnetic field impacts on dose distribution and the movement of the linac influences the magnetic field. (Chin et al., 2020) Nevertheless, overcoming these issues has permitted the development of a system from which online adaptive RT planning can be performed with greater accuracy than can currently be achieved with onboard CT scanners. (Lütgendorf-Caucig et al., 2011) MRI guided radiotherapy offers the ability to make accurate daily online corrections to account for positional and volume changes of OAR and target volumes, and the ability to continuously image while the beam is on permits live verification of tumour coverage and OAR dosimetry. This technology has great potential in tumour sites where inter and intrafraction motion causes doubt over treatment accuracy (e.g. thorax). (Chin et al., 2020) Furthermore, a number of dosimetric studies of adaptive radiotherapy planning have confirmed promising results, demonstrating less normal tissue irradiation in a number of tumour sites, including in lung cancer. (Møller et al., 2016, Nijkamp et al., 2008, Castelli et al., 2015) MRI-guided radiotherapy in MPM could facilitate the improved coverage of a radical PTV, permitting further dose escalation, while reducing toxicities in critical neighbouring normal tissue. Furthermore, combination of MRI with functional modalities (eg. MRI/PET, diffusion-weighted MRI) may

complement MR guided radiotherapy to allow synergies between the systems, facilitating the implementation of focal boosts to areas of hypoxia or increased cell proliferation. (Rosenkrantz et al., 2016)

Finally, the growing availability of proton therapy throughout the UK is expected to offer further opportunities for dose escalation in MPM. While protons have been investigated extensively in locally advanced non-small cell lung cancer (NSCLC), (Remick et al., 2017, Higgins et al., 2017, Chang et al., 2017, Chao et al., 2017) their clinical application in MPM has been limited to date, to a small number of institutional series. (Pan et al., 2015, Badiyan et al., 2018, Lee et al., 2017) A planning study by Krayenbuehl *et al*, comparing the dosimetry achieved with IMRT and protons in eight MPM patients post EPP, suggested that although protons could reduce dose to most OARs, they are more susceptible to changing air cavities and therefore adaptive radiotherapy planning may be required. (Krayenbuehl et al., 2010)

9.4 Radiobiological considerations of MPM

A fundamental consideration of any radiotherapy regime is the underlying radiosensitivity of the tumour and adjacent normal tissues, in addition to their relative sensitivity to changes in dose per fraction. There is a paucity of information surrounding the radiobiology of mesothelioma and the challenge of delivering tumouricidal doses using traditional radiotherapy techniques has afforded this tumour a reputation for radioresistance. Within this thesis, the radioresponse of mesothelioma cell lines has been examined using a clinically relevant 3D model. Data suggest that the growth of mesothelioma spheroids can be delayed with radiation, intimating that if a suitable radiation dose could be selectively achieved within the pleural cavity, radiotherapy may offer a valid therapeutic option for patients with MPM. Furthermore, the discovery that spheroid growth is sensitive to changes in dose per fraction and optimally delayed with hypofractionated radiotherapy, supports the hypothesis that MPM has a low α/β ratio, an assumption which underpinned the selection of dose and fractionation for the SYSTEMS-2 study. Although a definitive α/β ratio for MPM spheroids could not be established, data suggest that the two cell lines explored

have different α/β ratios, and that these values are low, consistent with their observed response to hypofractionation of dose.

This novel data supporting a low tumour α/β ratio is clinically relevant and may be used to guide optimal dose and fractionation schedules for future clinical trials of radiotherapy in MPM. Of particular relevance is the fact that tumours with a low α/β ratio treated with hypofractionated regimes require a lower total dose of radiation to achieve tumour control than with conventionally fractionated treatment. This was demonstrated in the case of prostate cancer within the CHIP study (Dearnaley et al., 2016) and is particularly important in MPM, where multiple dose limiting organs are in close proximity to the PTV. The development of hypofractionated radiotherapy regimes for the treatment of both breast and prostate cancer has been guided by a clinical suspicion that these tumours exhibit a low α/β ratio. Clinical data to support this proposal has been generated over time, but *in vitro* studies utilising tumour cell lines to determine the α/β ratio provided an important early step in establishing best practise in the treatment of these malignancies. (Algan et al., 1996, Chapman, 2014, Leith et al., 1993, DeWeese et al., 1998, Babazadeh Toloti et al., 2018)

9.5 The potential for radiosensitisation in MPM

Even if the low α/β ratio of MPM suggests that a lower total dose could be employed without compromising tumour kill, the frailty of this patient population and the volume of the pleural cavity that would receive radiation in any radical approach, means that treatment related toxicity would remain a significant concern. For this reason, the potential role of two radiosensitising drugs has been explored in combination with fractionated radiotherapy, to determine efficacy in 3D models of MPM. The DNA-PK inhibitor, NU7441, which targets the NHEJ pathway of DDR, was selected as a positive control. Since both tumour and normal tissue utilise the NHEJ pathway, radiosensitisation mediated by this approach would not be tumour specific and concerns about associated exacerbation of normal tissue toxicity would be likely to limit clinical translation. In contrast, the selective Bcl-xL inhibitor, A1331852, which acts as a BH3 mimetic, is likely to be more active in tumour tissue, given the reliance of

MPM cells on anti-apoptotic Bcl-2 proteins. Therefore, radiosensitisation mediated by this approach would be likely to be tumour selective and have greater clinical potential. Both agents were found to be potent radiosensitisers in MPM, suggesting that apoptotic and DDR pathways are important in the MPM-mediated resistance to radiotherapy. The tumour selectivity offered through an apoptosis-mediated approach and the observation that A1331852 displayed optimal therapeutic activity in combination with hypofractionated radiotherapy, highlights this drug as a promising candidate in future radiosensitising strategies in MPM.

Tumour sensitivity to radiation may, in the future, be enhanced by selective drug delivery. An elegant approach to this, currently being investigated at the University of Greenwich, exploits the arginine dependency of MPM. In this work, funded by the University Alliance DTA Scheme (<https://unialliance.ac.uk/dta/>), an anticancer agent is tagged to an arginine molecule which is preferentially taken up by MPM tissue. Current strategies centre on the delivery of chemotherapeutic agents to the tumour, but if a radiosensitising agent could be tagged to arginine in the same way, then concurrent radiation would be selectively more toxic to the tumour than to the normal surrounding tissues.

Alternative approaches of selective drug delivery to the tumour include the employment of gold nanoparticles targeted to MPM cells, the efficacy of which has recently been demonstrated in an *in vitro* system, using Pemetrexed-loaded nanoparticles targeted to CD146. (Cova et al., 2019) Furthermore, the anatomical distribution of MPM is such that in many cases, selective drug delivery may be simply achieved through direct treatment administration into the pleural space.

9.6 Biomarkers of MPM radiosensitivity

A radical treatment approach may not be suitable for all patients with MPM, not only because of patient-related factors, such as frailty and comorbidities, but also because of tumour specific considerations. It was noted in the SYSTEMS

study that one third of patients had a clinically significant pain response at week five. In contrast, approximately one third had a pain response which was not significant and one third had no improvement in their pain. (MacLeod et al., 2015a) There is no clear explanation why some patients responded to radiation and others did not, although this is likely to reflect a combination of physical factors, including tumour bulk, position and infiltration of surrounding structures, in addition to psychological factors and underlying tumour biology. Although a predictive link has been reported between the EORTC prognostic index and radiation response, (Jenkins et al., 2011) this association has not been validated and there remains no predictive indicator for radiotherapy response in MPM. The identification of a biomarker that would distinguish a subset of patients with radio-responsive disease would bring with it enormous clinical implications, especially in the radical setting, where the trade-off between tumour control and normal tissue toxicity is paramount. Unfortunately, the data presented in this thesis is too preliminary to identify a potential biomarker of radiation response from the SYSTEMS study, although pilot data was obtained using the limited dataset available. The SYSTEMS-2 study continues to recruit and it is anticipated that this much larger trial will generate biomarker information that might establish an initial correlation between protein expression and radiotherapy outcomes in this well studied patient population. The work conducted to date, in which IHC conditions have been optimised for the selected proteins of interest will facilitate rapid analysis of FFPE samples from SYSTEMS-2. In addition to guiding patient selection for radiotherapy, biomarker research may identify proteins which confer radio-resistance, providing targets for future therapy in this disease. The impact of this for patients could be enormous and could change the landscape of this disease from one of palliation to prolonged disease control or cure within a short number of years. For this reason, biomarker research is an area of intense research in MPM. Of particular relevance is research into predictive biomarkers of tumour fractionation sensitivity, where markers of proliferation and checkpoint proteins may be implicated. (Somaiah et al., 2015) If, as suggested by other groups investigating the α/β ratio of MPM, (Hakkinen et al., 1996, Carmichael et al., 1989) the range of fractionation sensitivities within this tumour type is broad, then a biomarker to identify those patients who may selectively benefit from hypofractionation of dose would be clinically invaluable.

9.7 Summary

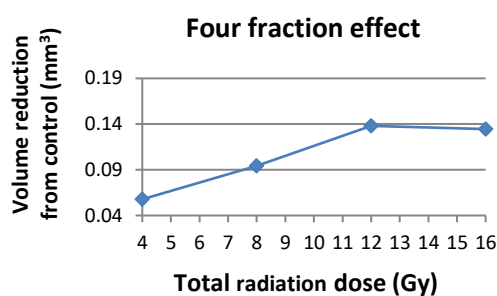
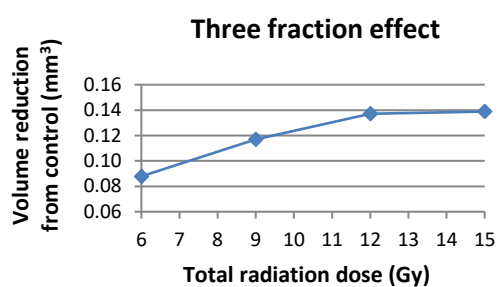
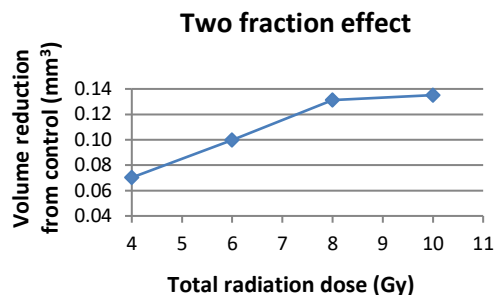
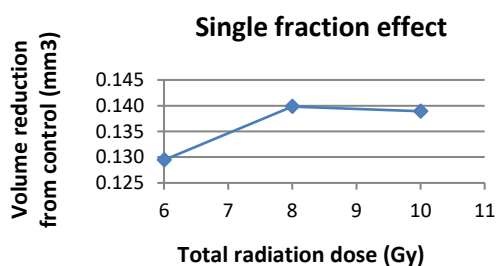
The research presented in this thesis has been conducted at a time when the role of radiotherapy in MPM is in transition. Traditionally regarded as having only a palliative role in the management of this disease, radiotherapy is starting to be used with the aim of disease control, in combination with other treatment modalities, with encouraging data reported from a number of non-randomised, phase I/II studies conducted outside of the UK. (Cho et al., 2014, Minatel et al., 2014, Rice et al., 2007b, Krug et al., 2009, Van Schil et al., 2010)

SYSTEMS-2 will provide the first randomised controlled data of patient outcomes following dose escalated, hypofractionated radiotherapy in MPM. Despite the palliative intent of this study, it represents an important step towards a more radical approach to the management of this disease, at a time when the boundaries of modern radiotherapy planning are being pushed to investigate the limits of radical treatment in a number of cancers.

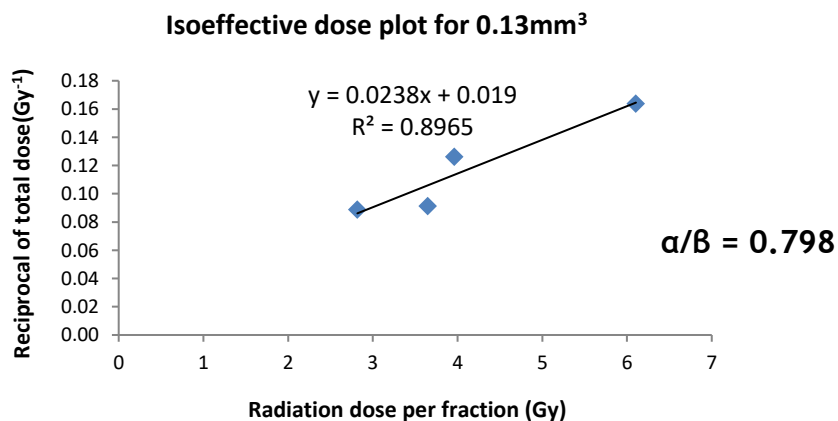
Within this thesis, important radiobiological parameters of MPM have been investigated. Data suggests that MPM is more radiosensitive than traditionally assumed and considerable evidence has been generated to support the hypothesis that MPM exhibits a low α/β ratio. These radiobiological observations could have important implications for the design of future clinical trials of radiotherapy in MPM and are presented in this thesis in combination with data pertaining to a number of strategies which may safely facilitate further dose escalation in MPM, beyond that being investigated in SYSTEMS-2. It is hoped that this body of work will be used to inform future radiotherapy practise in MPM and will advance the possibility of using radiotherapy with radical intent in the treatment of patients with this cancer of unmet need.

Appendix 1: Isoeffective data

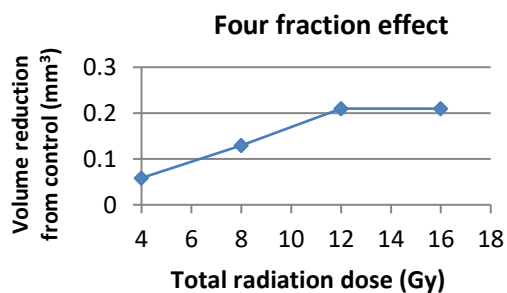
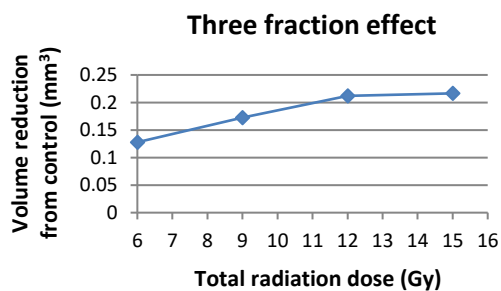
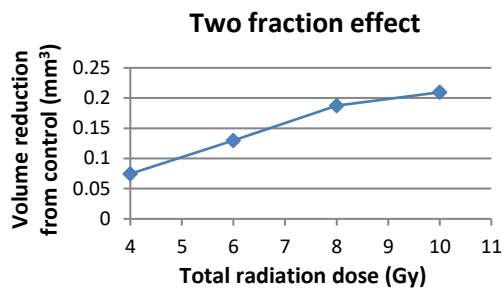
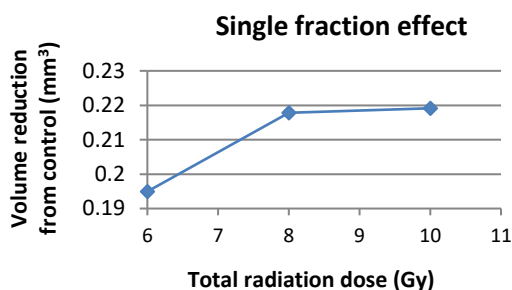
H2052 Data: Day 10



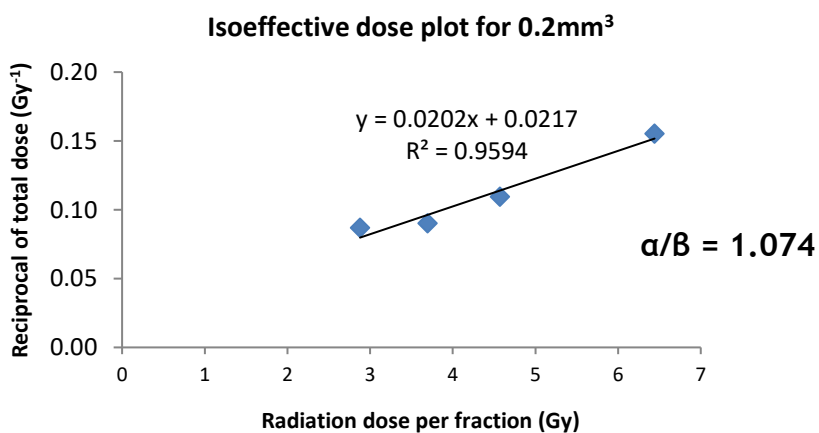
| Fraction number | Effect size (mm ³) | Total dose (Gy) | Dose per fraction (Gy) | Reciprocal total dose |
|-----------------|--------------------------------|-----------------|------------------------|-----------------------|
| 1 | 0.13 | 6.105 | 6.105 | 0.164 |
| 2 | 0.13 | 7.923 | 3.961 | 0.126 |
| 3 | 0.13 | 10.950 | 3.650 | 0.091 |
| 4 | 0.13 | 11.269 | 2.817 | 0.089 |



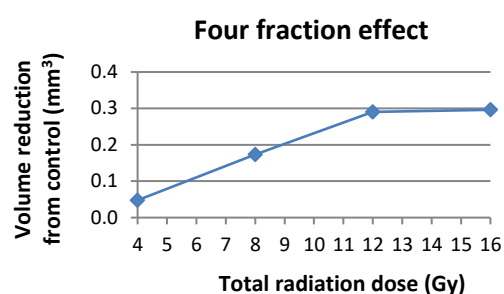
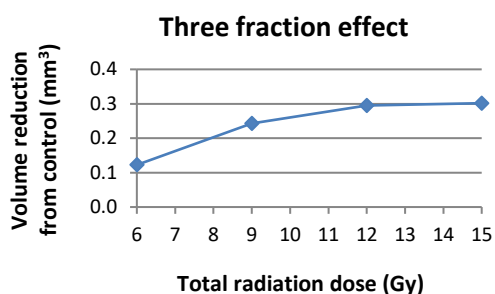
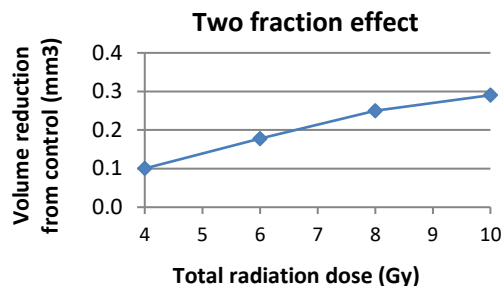
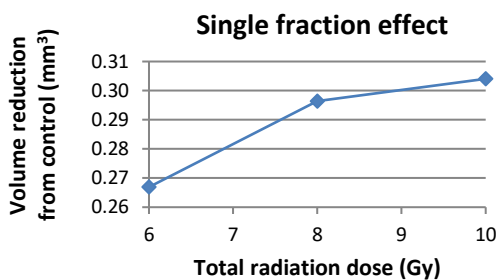
H2052 Data: Day 14



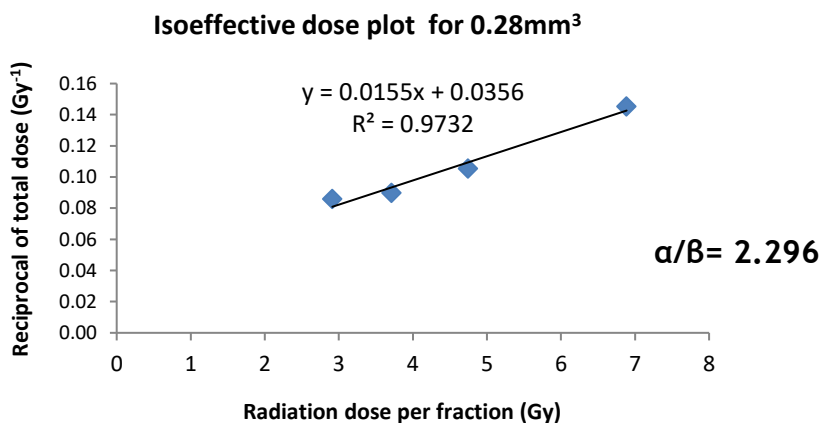
| Fraction number | Effect size (mm ³) | Total dose (Gy) | Dose per fraction (Gy) | Reciprocal total dose |
|-----------------|--------------------------------|-----------------|------------------------|-----------------------|
| 1 | 0.2 | 6.441 | 6.441 | 0.155 |
| 2 | 0.2 | 9.141 | 4.571 | 0.109 |
| 3 | 0.2 | 11.089 | 3.696 | 0.090 |
| 4 | 0.2 | 11.513 | 2.878 | 0.087 |



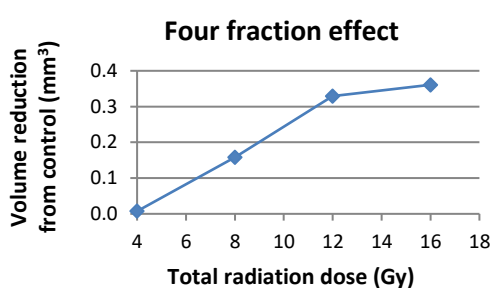
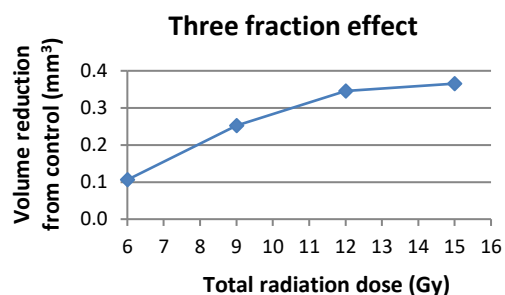
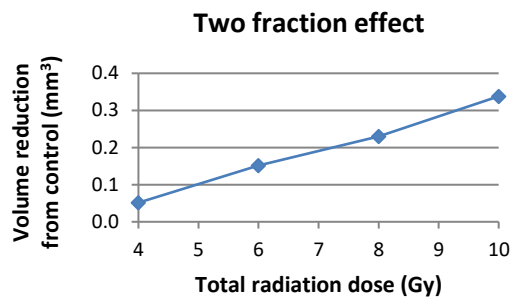
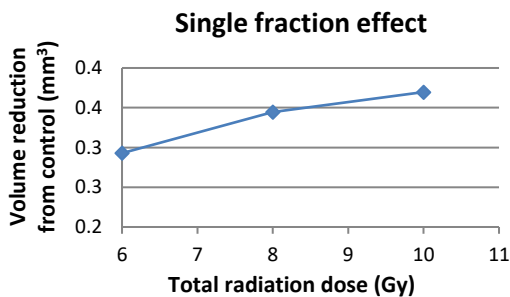
H2052 Data: Day 16



| Fraction number | Effect size (mm ³) | Total dose (Gy) | Dose per fraction (Gy) | Reciprocal total dose |
|-----------------|--------------------------------|-----------------|------------------------|-----------------------|
| 1 | 0.28 | 6.886 | 6.886 | 0.145 |
| 2 | 0.28 | 9.489 | 4.744 | 0.105 |
| 3 | 0.28 | 11.133 | 3.711 | 0.090 |
| 4 | 0.28 | 11.648 | 2.912 | 0.086 |

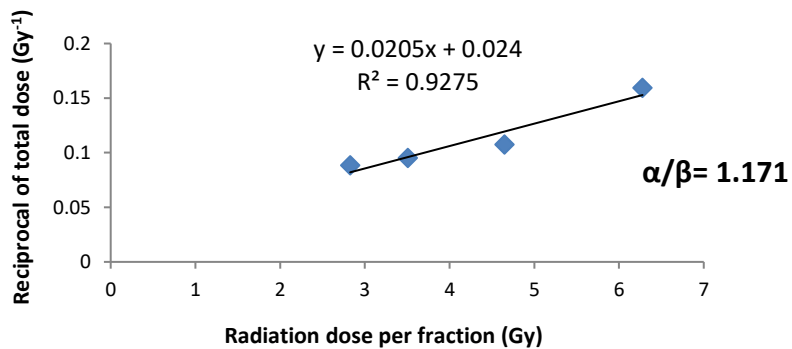


H2052 Data: Day 21

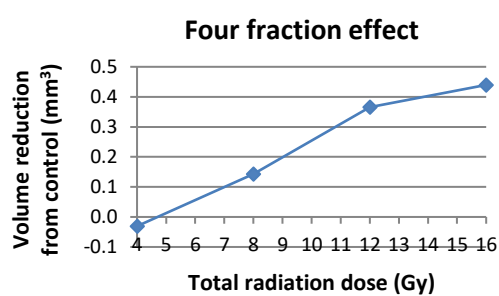
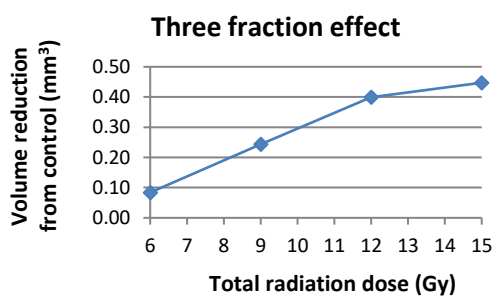
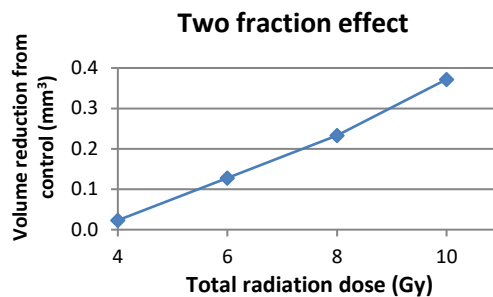
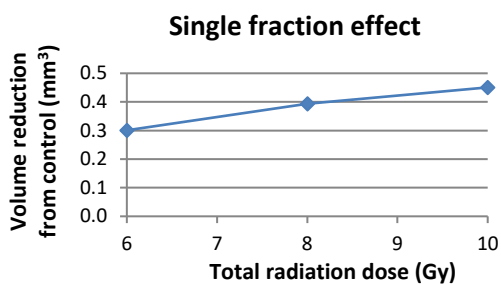


| Fraction number | Effect size (mm ³) | Total dose (Gy) | Dose per fraction (Gy) | Reciprocal total dose |
|-----------------|--------------------------------|-----------------|------------------------|-----------------------|
| 1 | 0.3 | 6.278 | 6.278 | 0.159 |
| 2 | 0.3 | 9.299 | 4.649 | 0.108 |
| 3 | 0.3 | 10.523 | 3.508 | 0.095 |
| 4 | 0.3 | 11.309 | 2.827 | 0.088 |

Isoeffective dose plot for 0.3mm³

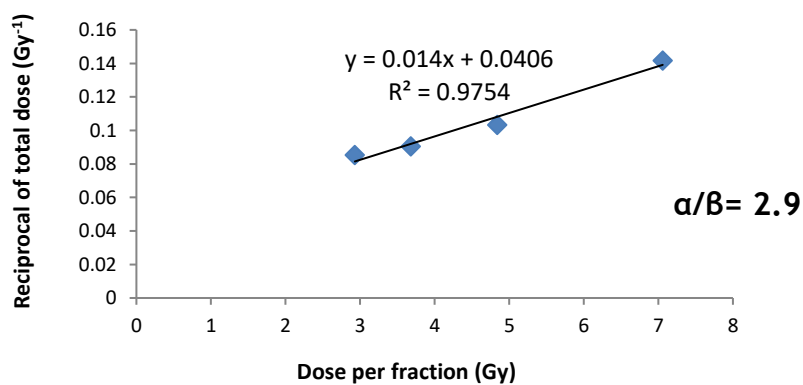


H2052 Data: Day 24

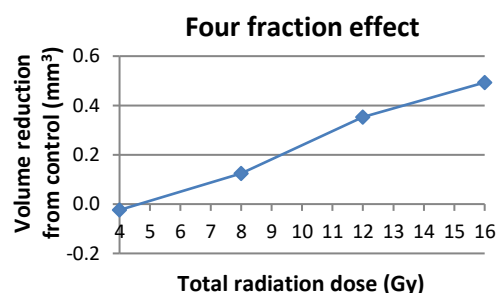
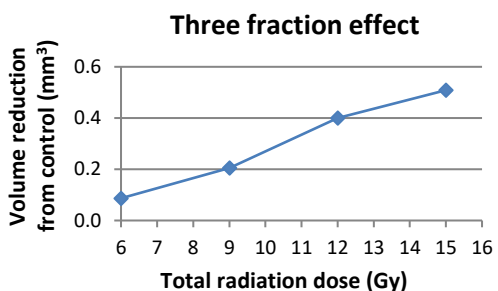
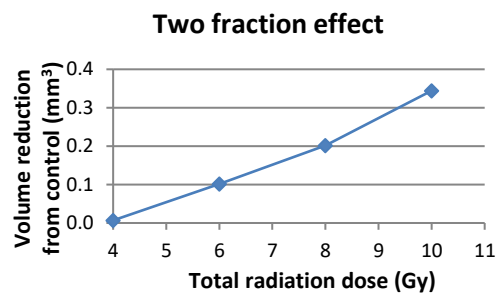
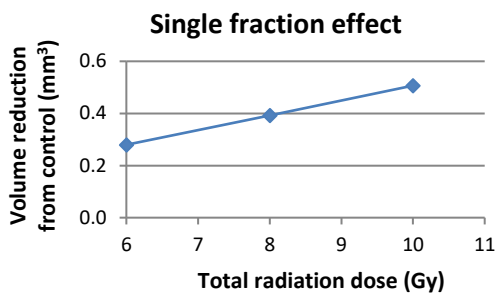


| Fraction number | Effect size (mm ³) | Total dose (Gy) | Dose per fraction (Gy) | Reciprocal total dose |
|-----------------|--------------------------------|-----------------|------------------------|-----------------------|
| 1 | 0.35 | 7.058 | 7.058 | 0.142 |
| 2 | 0.35 | 9.685 | 4.842 | 0.103 |
| 3 | 0.35 | 11.047 | 3.682 | 0.091 |
| 4 | 0.35 | 11.719 | 2.930 | 0.085 |

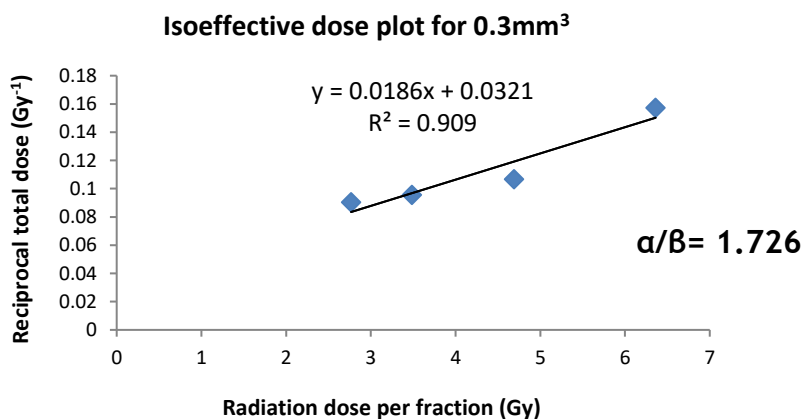
Isoeffective dose plot for 0.35mm³



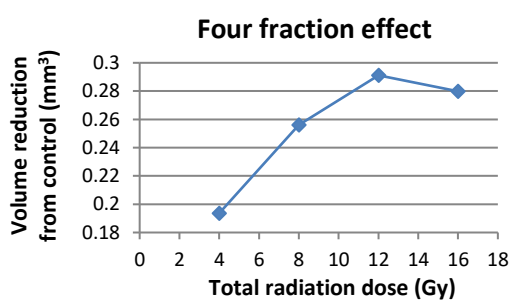
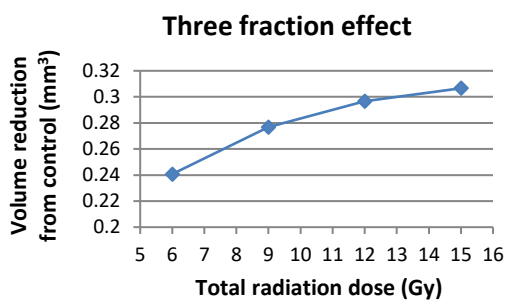
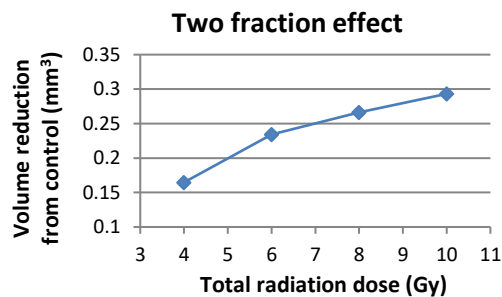
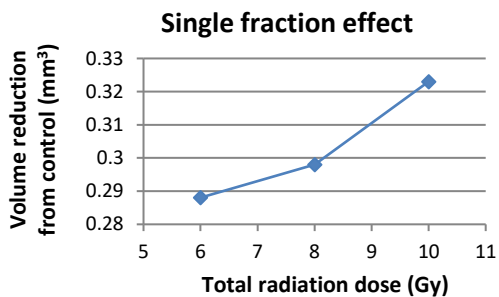
H2052 Data: Day 28



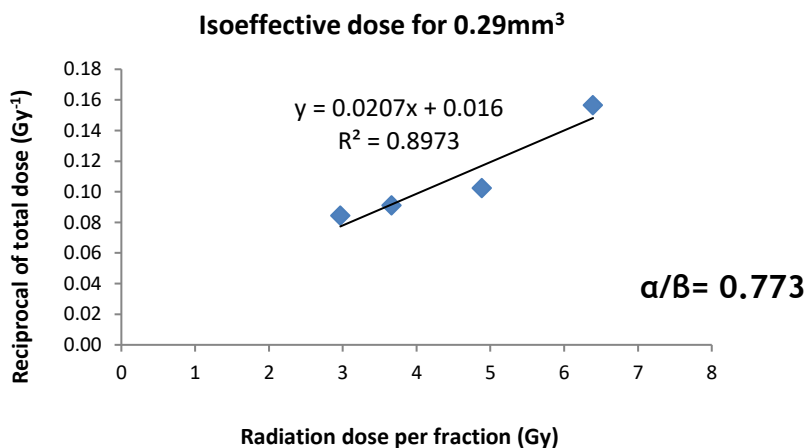
| Fraction number | Effect size (mm ³) | Total dose (Gy) | Dose per fraction (Gy) | Reciprocal total dose |
|-----------------|--------------------------------|-----------------|------------------------|-----------------------|
| 1 | 0.3 | 6.360709 | 6.360709 | 0.157215 |
| 2 | 0.3 | 9.379644 | 4.689822 | 0.106614 |
| 3 | 0.3 | 10.46214 | 3.49 | 0.095583 |
| 4 | 0.3 | 11.06791 | 2.766978 | 0.090351 |



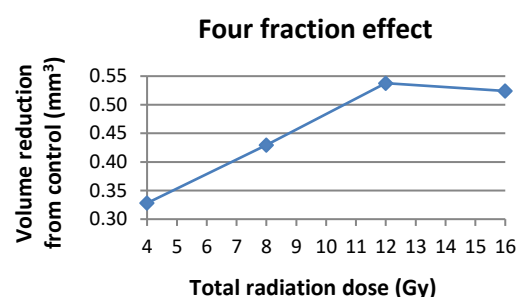
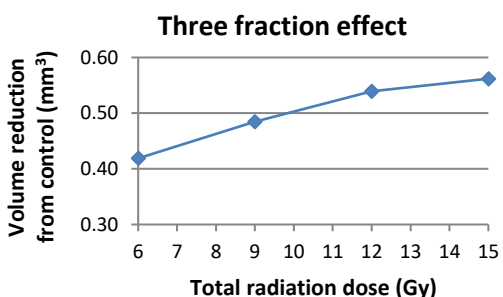
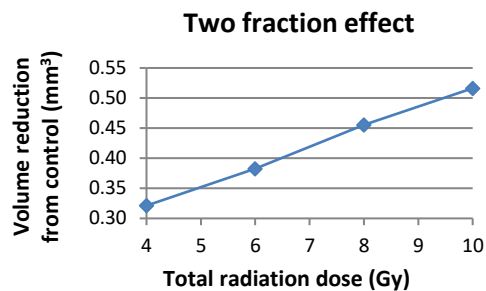
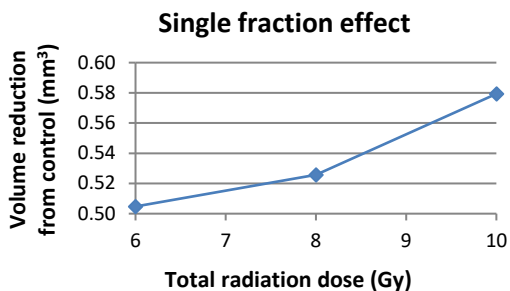
211H Data: Day 10



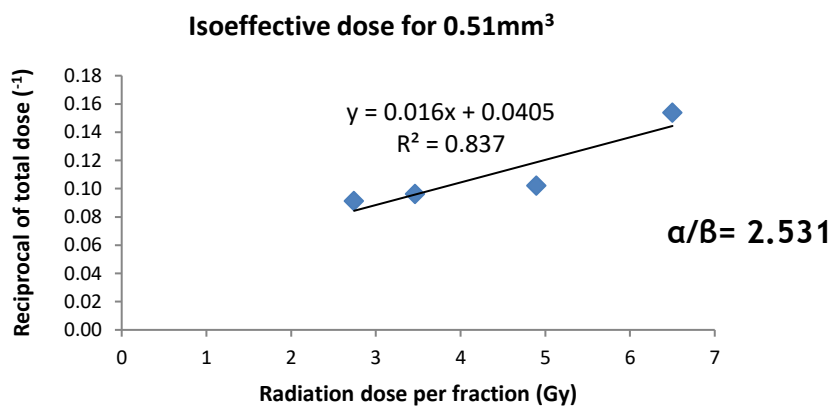
| Fraction number | Effect size (mm ³) | Total dose (Gy) | Dose per fraction (Gy) | Reciprocal total dose |
|-----------------|--------------------------------|-----------------|------------------------|-----------------------|
| 1 | 0.29 | 6.392 | 6.392 | 0.156 |
| 2 | 0.29 | 9.770 | 4.885 | 0.102 |
| 3 | 0.29 | 10.981 | 3.660 | 0.091 |
| 4 | 0.29 | 11.870 | 2.967 | 0.084 |



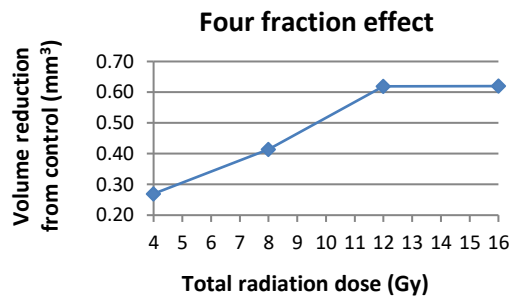
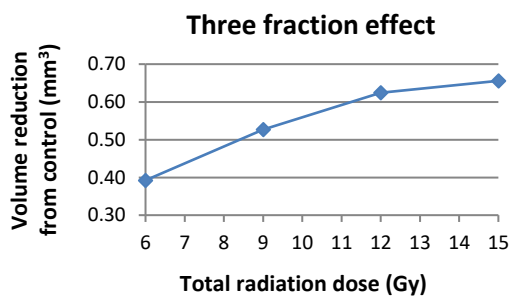
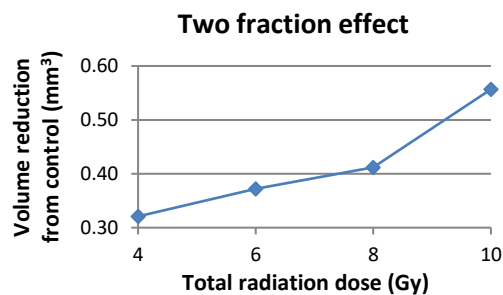
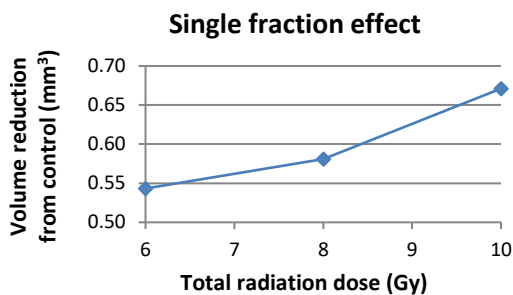
211H Data: Day 14



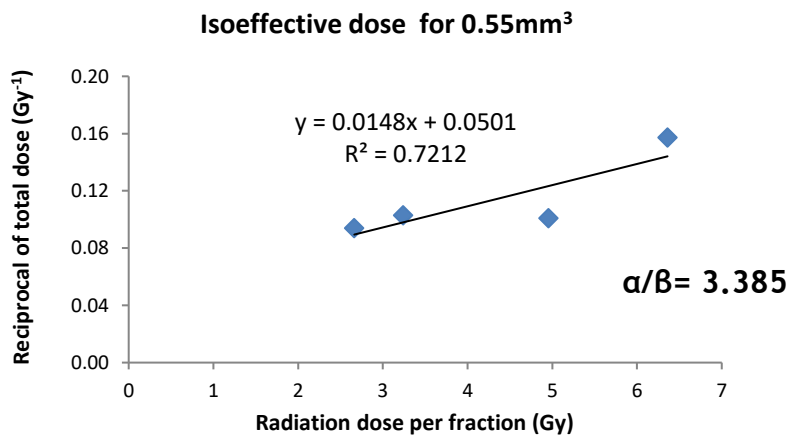
| Fraction number | Effect size (mm ³) | Total dose (Gy) | Dose per fraction (Gy) | Reciprocal total dose |
|-----------------|--------------------------------|-----------------|------------------------|-----------------------|
| 1 | 0.51 | 6.501 | 6.501 | 0.154 |
| 2 | 0.51 | 9.793 | 4.896 | 0.102 |
| 3 | 0.51 | 10.394 | 3.465 | 0.096 |
| 4 | 0.51 | 10.973 | 2.743 | 0.091 |



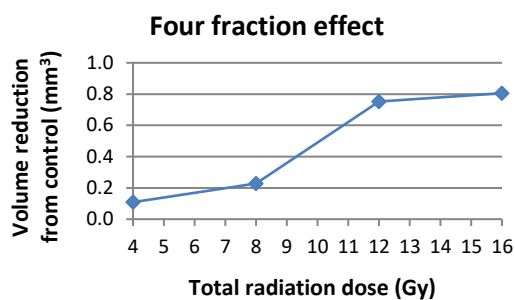
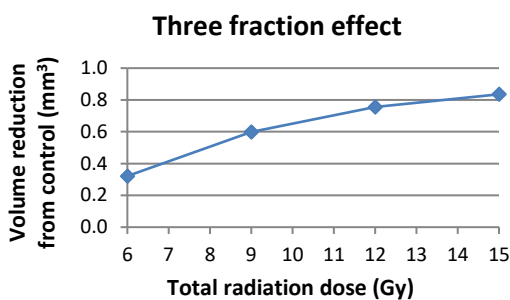
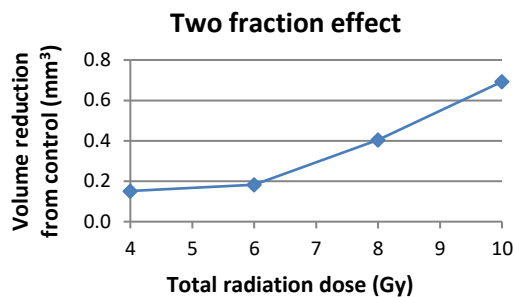
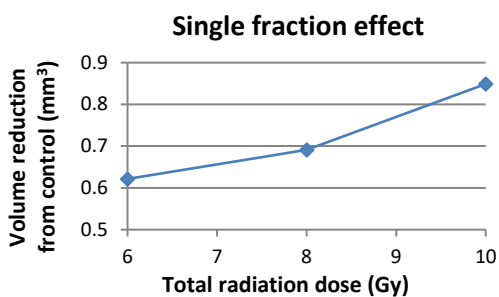
211H Data: Day 16



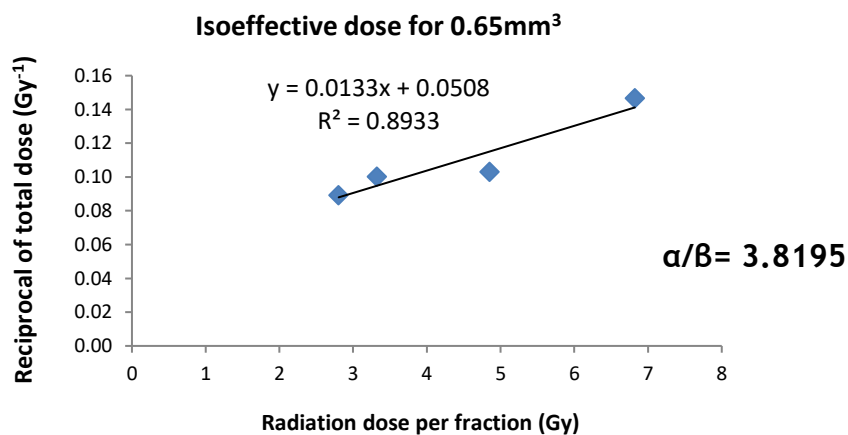
| Fraction number | Effect size (mm ³) | Total dose (Gy) | Dose per fraction (Gy) | Reciprocal total dose |
|-----------------|--------------------------------|-----------------|------------------------|-----------------------|
| 1 | 0.55 | 6.360 | 6.360 | 0.157 |
| 2 | 0.55 | 9.908 | 4.954 | 0.101 |
| 3 | 0.55 | 9.726 | 3.242 | 0.103 |
| 4 | 0.55 | 10.651 | 2.663 | 0.094 |



211H Data: Day 21

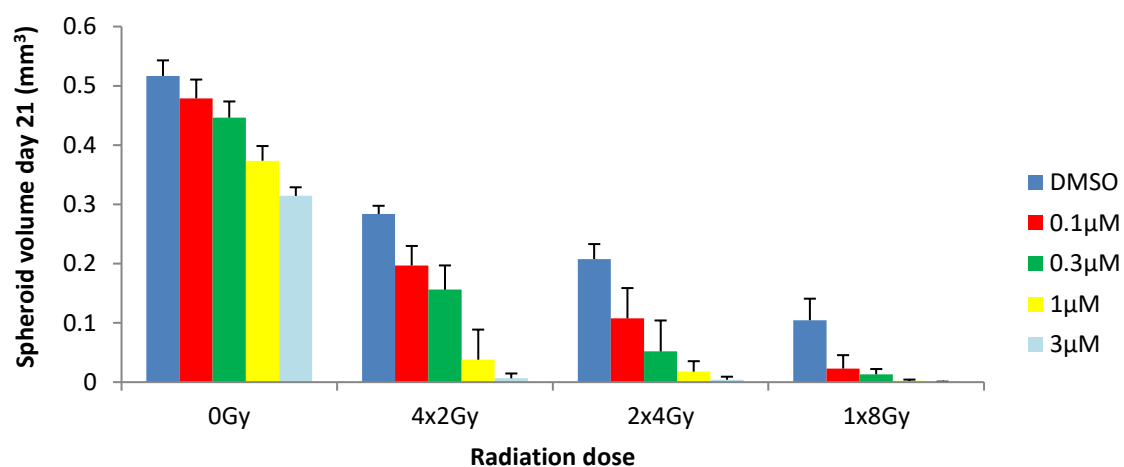


| Fraction number | Effect size (mm ³) | Total dose (Gy) | Dose per fraction (Gy) | Reciprocal total dose |
|-----------------|--------------------------------|-----------------|------------------------|-----------------------|
| 1 | 0.65 | 6.821 | 6.821 | 0.147 |
| 2 | 0.65 | 9.703 | 4.852 | 0.103 |
| 3 | 0.65 | 9.976 | 3.325 | 0.100 |
| 4 | 0.65 | 11.215 | 2.804 | 0.089 |

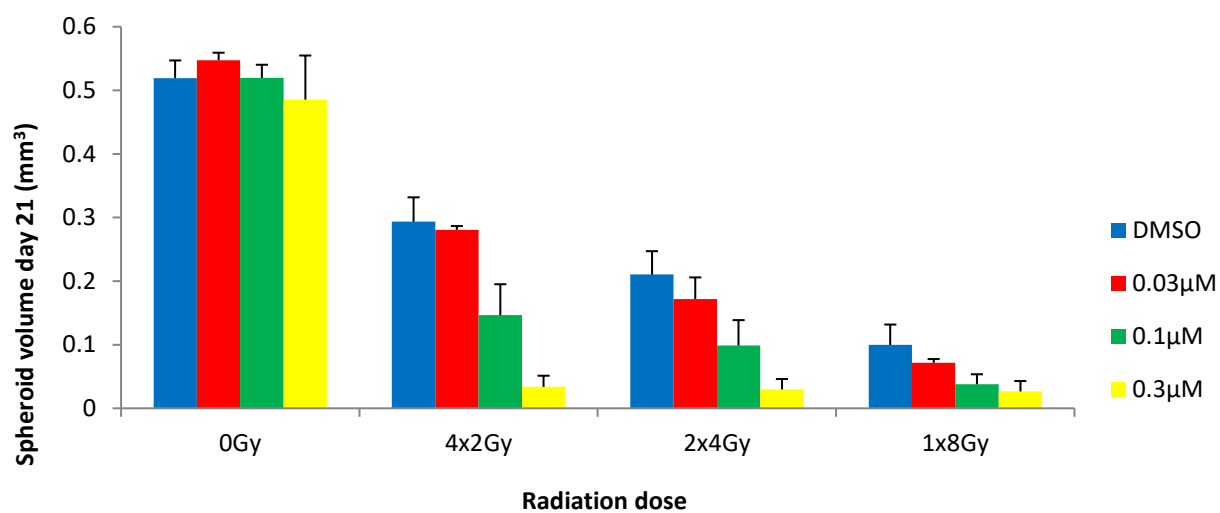


Appendix 2: Volume data for radiosensitising drug experiments

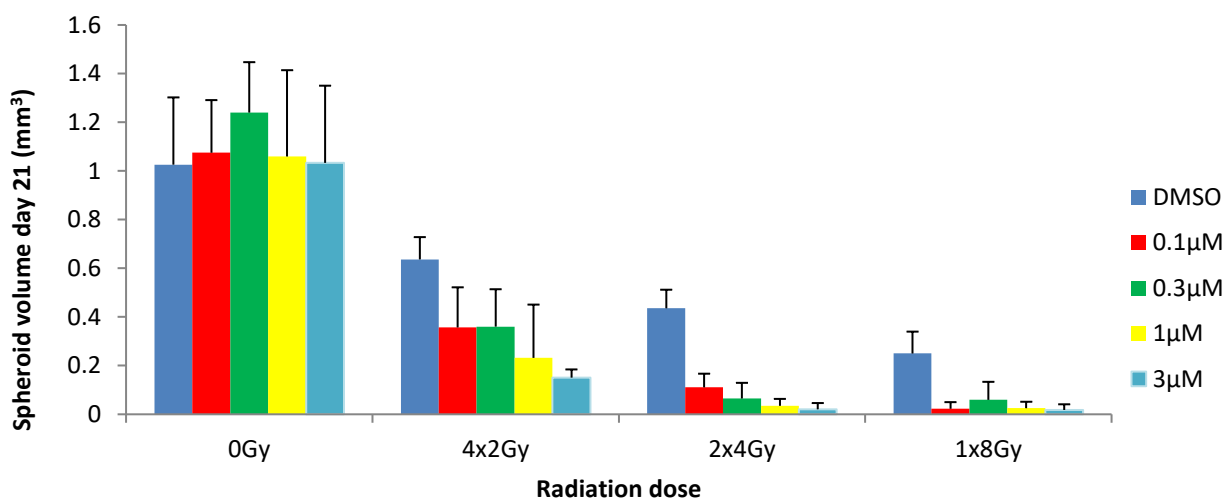
Effect of A1331852 & fractionated radiotherapy on H2052 spheroid volume at day 21



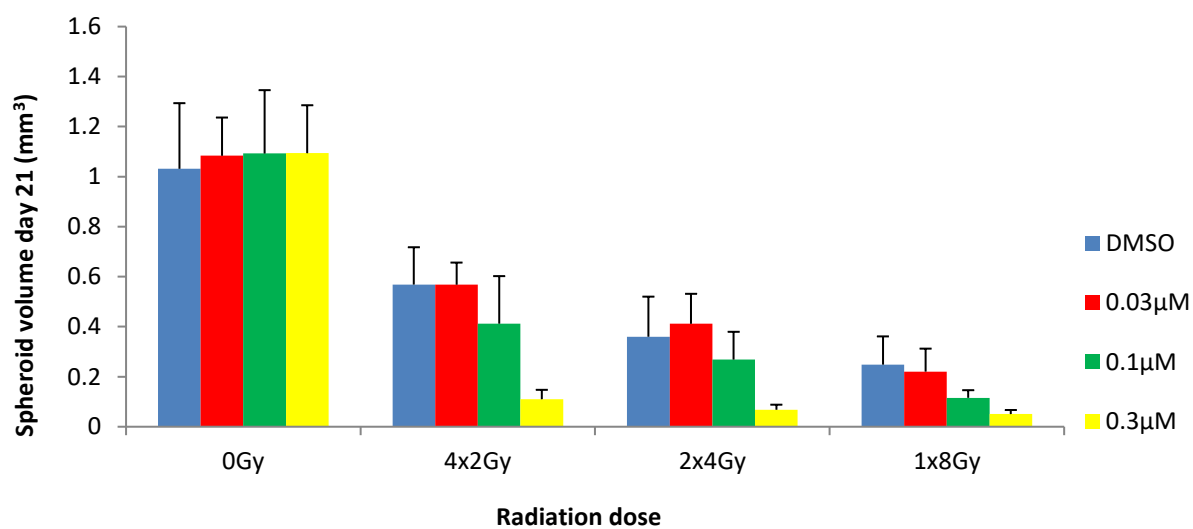
Effect of NU7441 & fractionated radiotherapy on H2052 spheroid volume at day 21



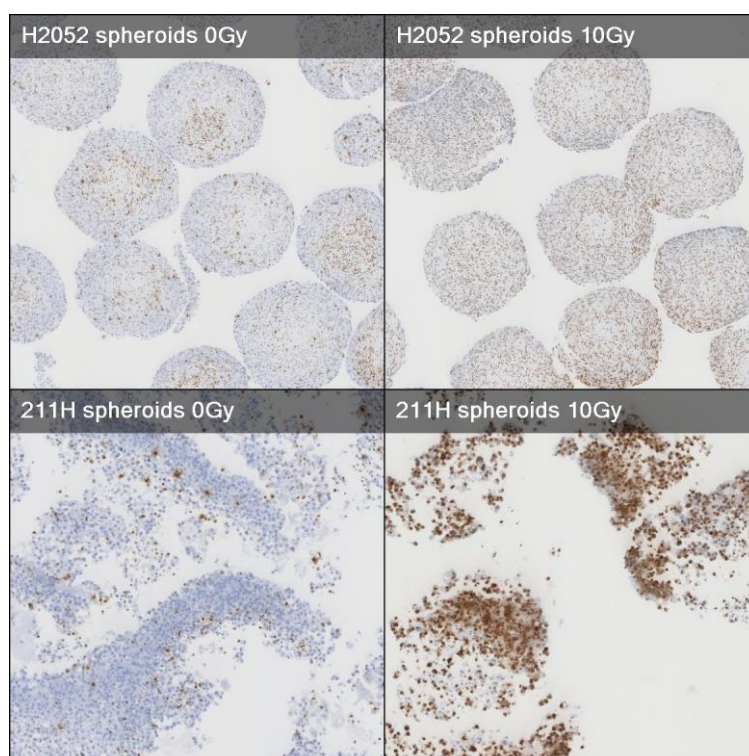
Effect of A1331852 & fractionated radiotherapy on 211H spheroid volume at day 21



Effect of NU7441 & fractionated radiotherapy on 211H spheroid volume at day 21



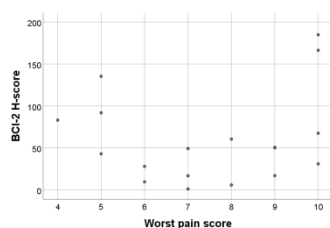
Appendix 3: γ H2Ax expression



| Condition | Percentage γ H2Ax positive cells |
|------------|---|
| 211H 0Gy | 40.5621 |
| 211H 10Gy | 95.7347 |
| H2052 0Gy | 49.7587 |
| H2052 10Gy | 80.6842 |

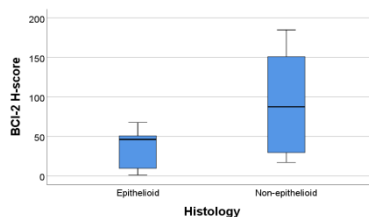
Appendix 4: IHC Correlation data Bcl-2 correlation data

Worst pain score at baseline



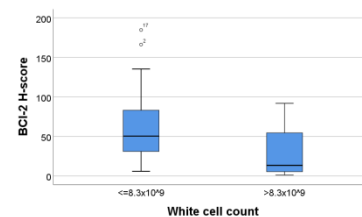
Spearman's rank correlation $p = 0.617$

Histology



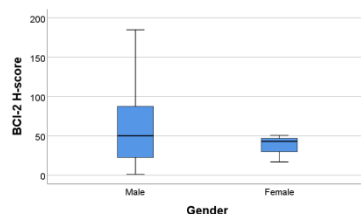
Mann Whitney test $p = 0.55$

White cell count



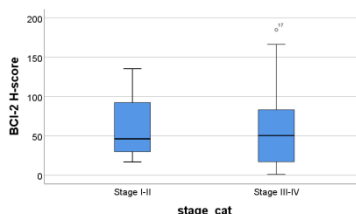
Mann Whitney test $p = 0.158$

Gender



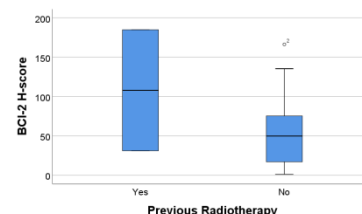
Mann Whitney test $p = 0.574$

Stage of disease



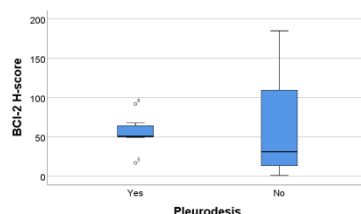
Mann Whitney test $p = 0.959$

Previous radiotherapy



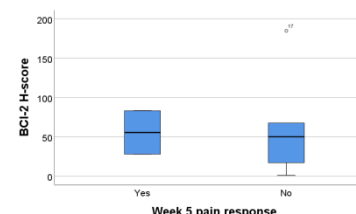
Mann Whitney test $p = 0.471$

Pleurodesis



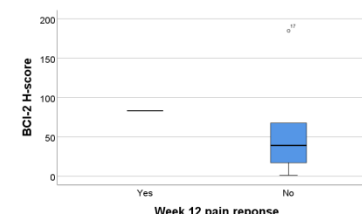
Mann Whitney test $p = 0.536$

Week 5 pain response



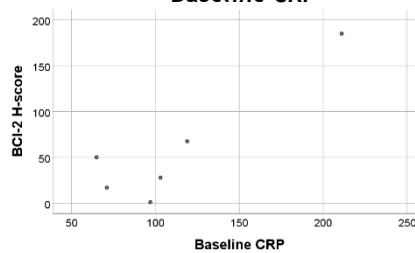
Mann Whitney test $p = 0.857$

Week 12 pain response



Mann Whitney test $p = 0.571$

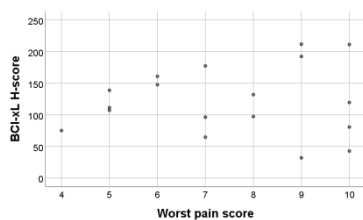
Baseline CRP



Spearman's rank correlation $p = 0.208$

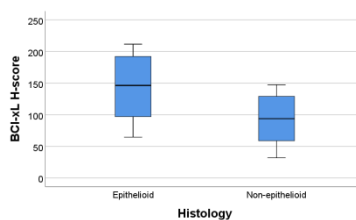
Bcl-xL correlation data

Worst pain score at baseline



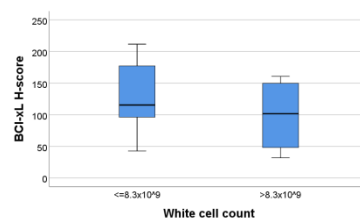
Spearman's rank correlation $p = 0.921$

Histology



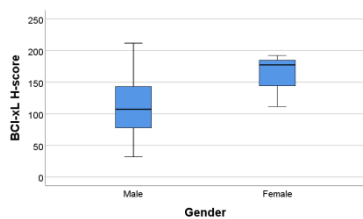
Mann Whitney test $p = 0.068$

White cell count



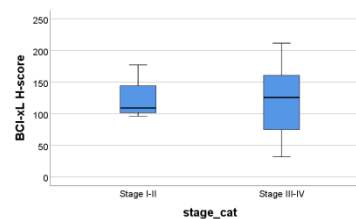
Mann Whitney test $p = 0.442$

Gender



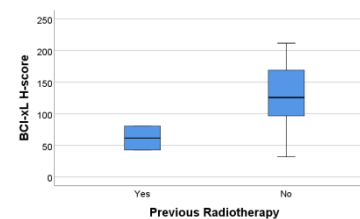
Mann Whitney test $p = 0.203$

Stage of disease



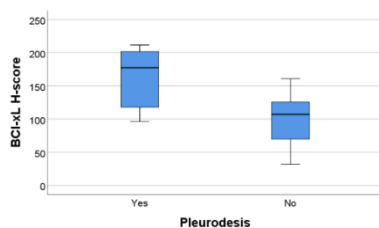
Mann Whitney test $p = 1.0$

Previous radiotherapy



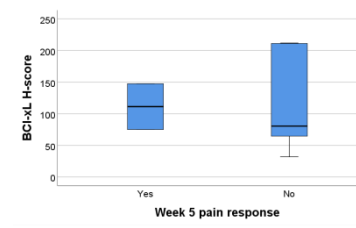
Mann Whitney test $p = 0.118$

Week 5 pain response



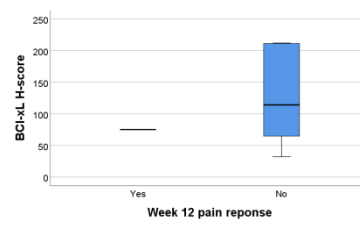
Mann Whitney test $p = 0.027$

Week 12 pain response



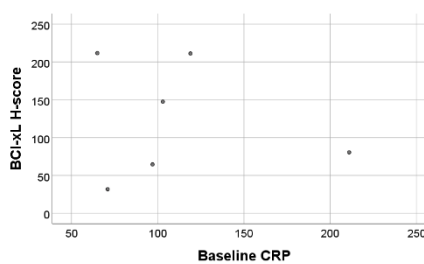
Mann Whitney test $p = 1$

Pleurodesis



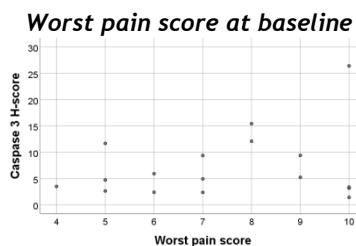
Mann Whitney test $p = 0.857$

Baseline CRP

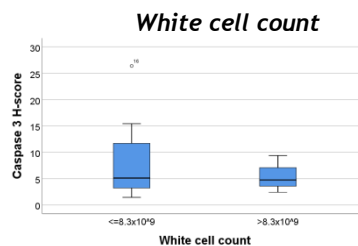


Spearman's rank correlation $p = 0.957$

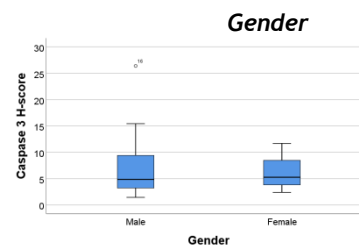
Activated caspase 3 correlation data



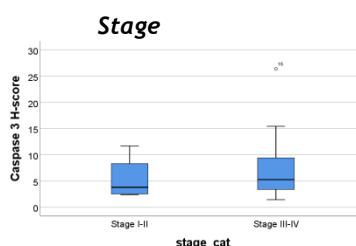
Spearman's rank correlation $p= 0.078$



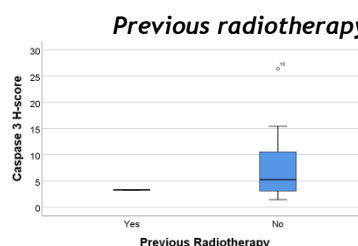
Mann Whitney test $p= 0.676$



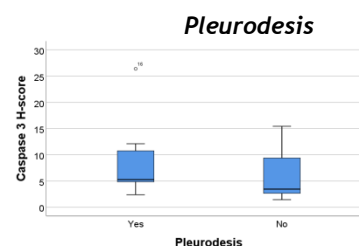
Mann Whitney test $p= 0.953$



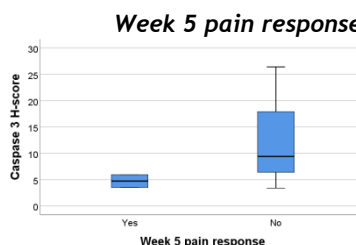
Mann Whitney test $p= 0.878$



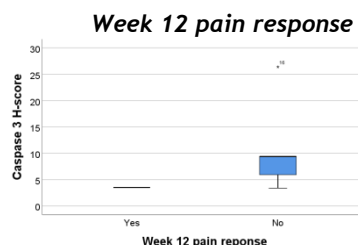
Mann Whitney test $p= 0.368$



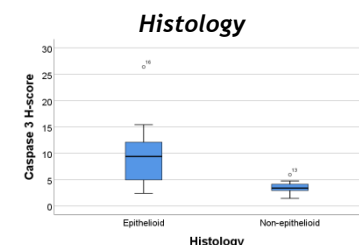
Mann Whitney test $p= 0.315$



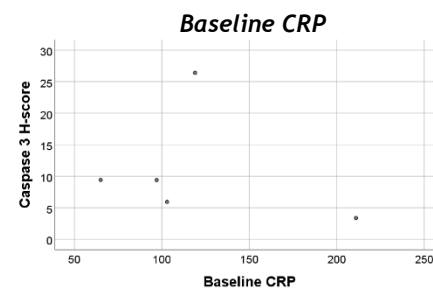
Mann Whitney test $p= 0.533$



Mann Whitney test $p= 0.667$



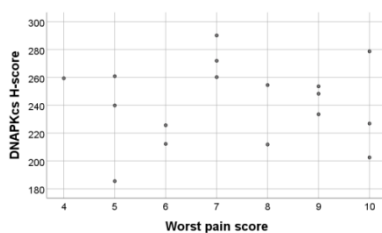
Spearman's rank correlation $p= 0.50$



Mann Whitney test $p= 0.043$

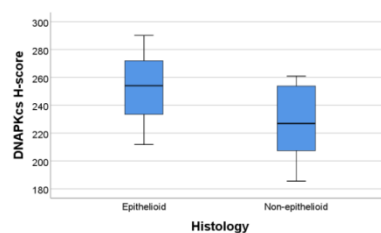
DNA-PKcs correlation data

Worst pain score at baseline



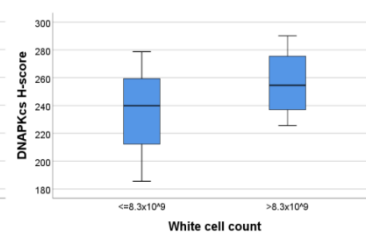
Spearman's rank correlation $p= 0.869$

Histology



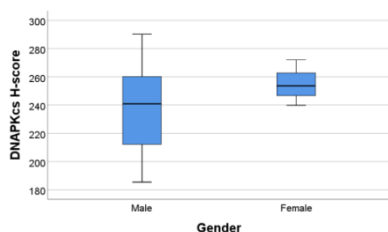
Mann Whitney test $p= 0.161$

White cell count



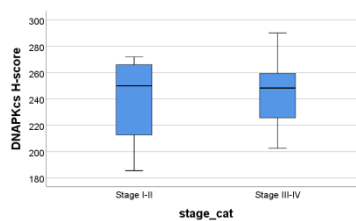
Mann Whitney test $p= 0.35$

Gender



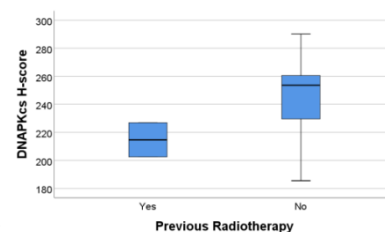
Mann Whitney test $p= 0.51$

Stage of disease



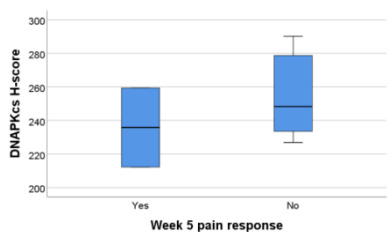
Mann Whitney test $p= 0.956$

Previous radiotherapy



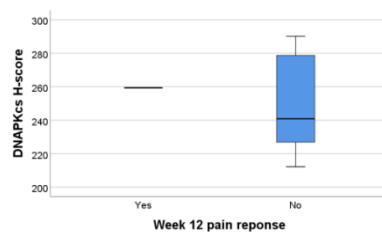
Mann Whitney test $p= 0.176$

Week 5 pain response



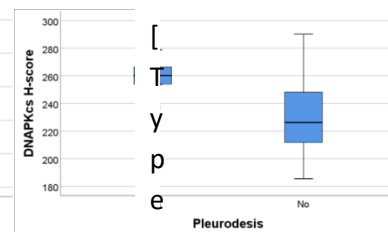
Mann Whitney test $p= 0.571$

Week 12 pain response



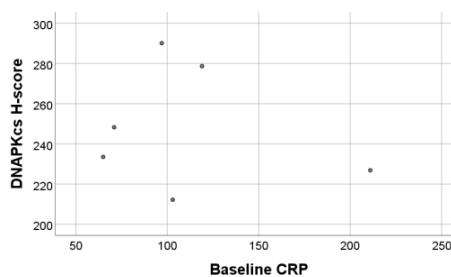
Mann Whitney test $p= 0.857$

Pleurodesis



Mann Whitney test $p= 0.023$

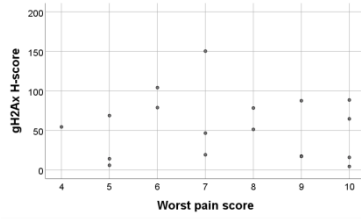
Baseline CRP



Spearman's rank correlation $p= 0.704$

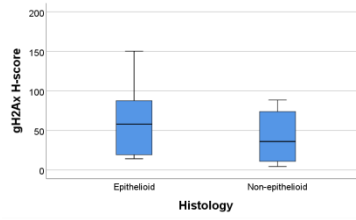
γH2Ax correlation data

Worst pain score at baseline



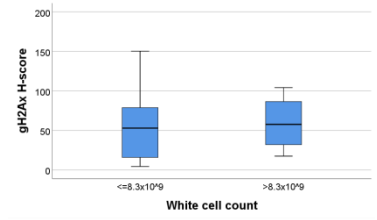
Spearman's rank correlation $p= 0.792$

Histology



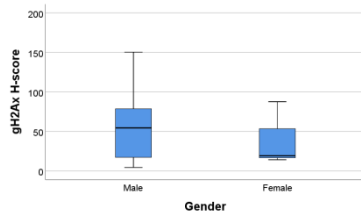
Mann Whitney test $p= 0.360$

White cell count



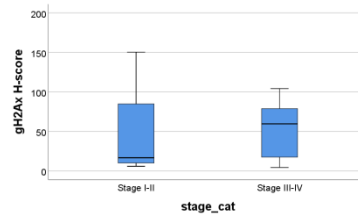
Mann Whitney test $p= 0.645$

Gender



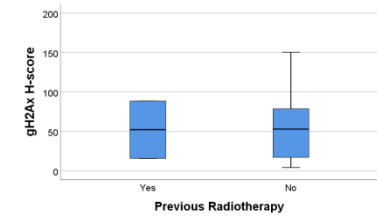
Mann Whitney test $p= 0.738$

Stage of disease



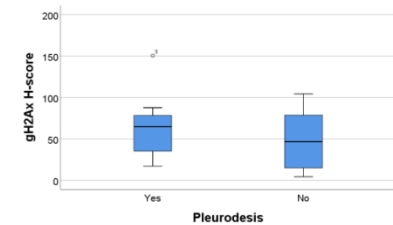
Mann Whitney test $p= 0.477$

Previous radiotherapy



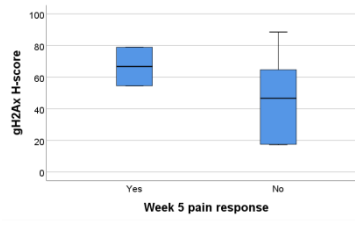
Mann Whitney test $p= 0.941$

Pleurodesis



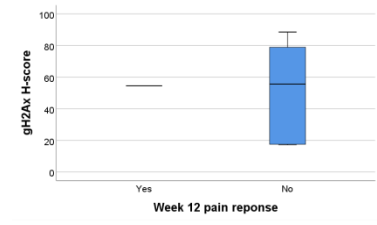
Mann Whitney test $p= 0.375$

Week 5 pain response



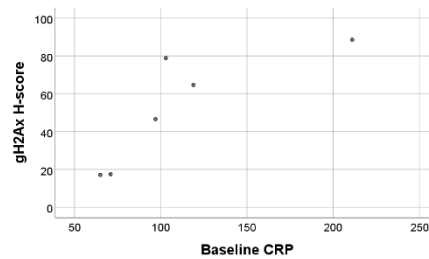
Mann Whitney test $p= 0.571$

Week 12 pain response



Mann Whitney test $p= 1.0$

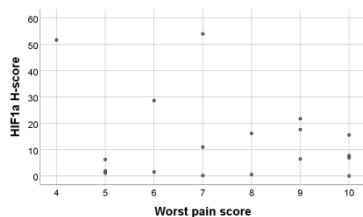
Baseline CRP



Spearman's rank correlation $p= 0.005$

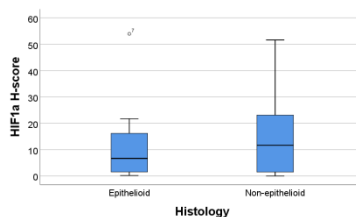
HIF1α correlation data

Worst pain score at baseline



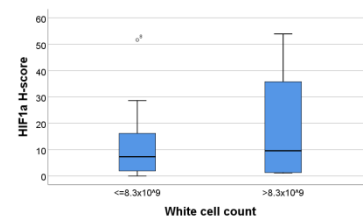
Spearman's rank correlation $p = 0.895$

Histology



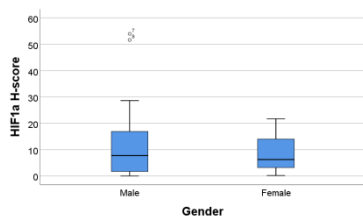
Mann Whitney test $p = 0.762$

White cell count



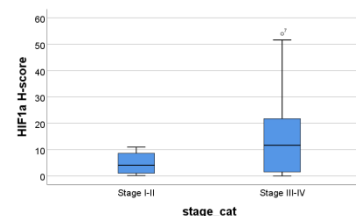
Mann Whitney test $p = 0.798$

Gender



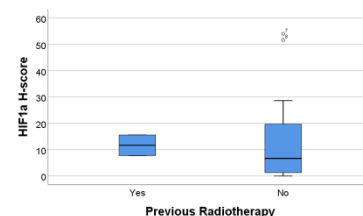
Mann Whitney test $p = 0.654$

Stage of disease



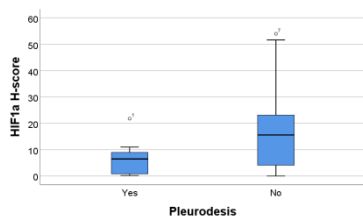
Mann Whitney test $p = 0.233$

Previous radiotherapy



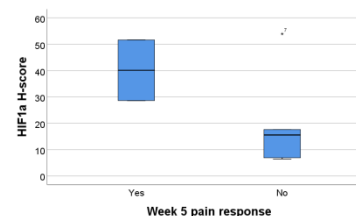
Mann Whitney test $p = 0.732$

Pleurodesis



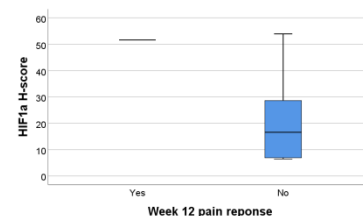
Mann Whitney test $p = 0.211$

Week 5 pain response



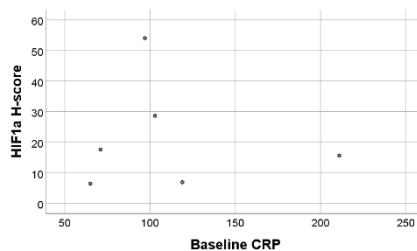
Mann Whitney test $p = 0.381$

Week 12 pain response



Mann Whitney test $p = 0.571$

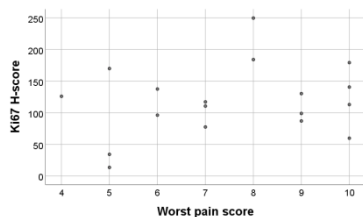
Baseline CRP



Spearman's rank correlation $p = 0.872$

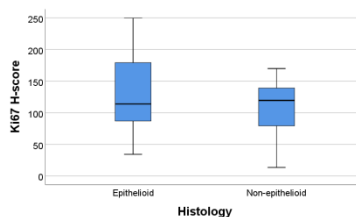
Ki67 correlation data

Worst pain score at baseline



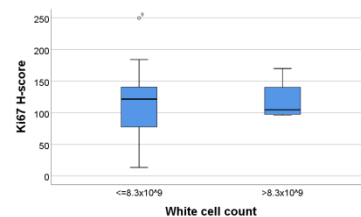
Spearman's rank correlation $p = 0.437$

Histology



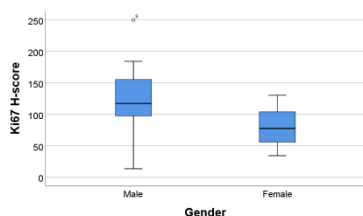
Mann Whitney test $p = 0.829$

White cell count



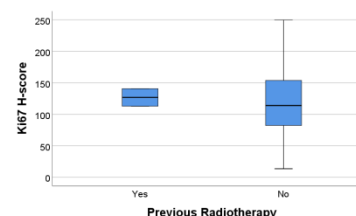
Mann Whitney test $p = 0.878$

Gender



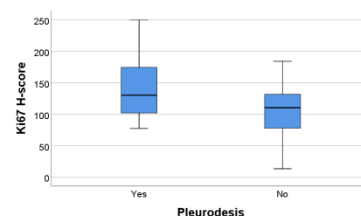
Mann Whitney test $p = 0.250$

Previous radiotherapy



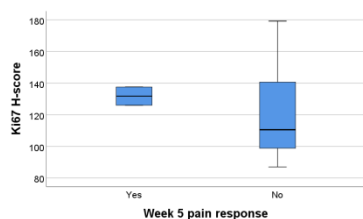
Mann Whitney test $p = 0.641$

Pleurodesis



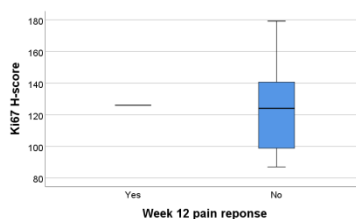
Mann Whitney test $p = 0.246$

Week 5 pain response



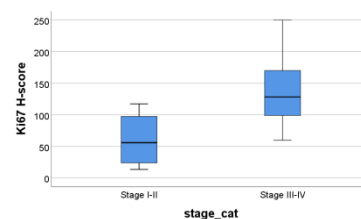
Mann Whitney test $p = 0.857$

Week 12 pain response



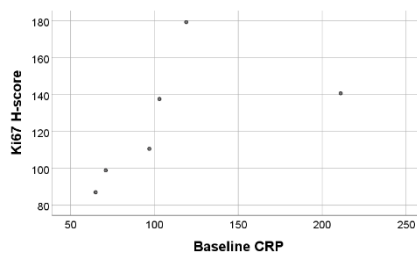
Mann Whitney test $p = 1.0$

Stage of disease



Mann Whitney test $p = 0.025$

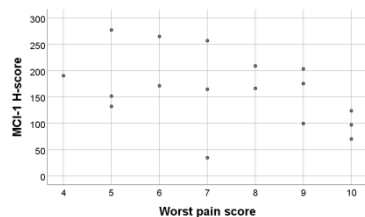
Baseline CRP



Spearman's rank correlation $p = 0.005$

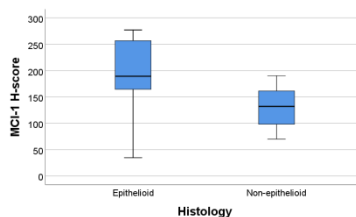
Mcl-1 correlation data

Worst pain score at baseline



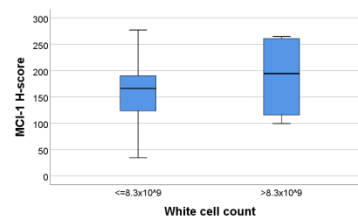
Spearman's rank correlation $p = 0.083$

Histology



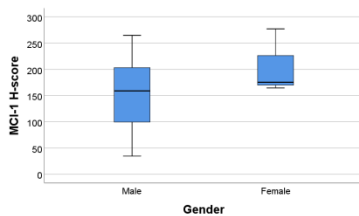
Mann Whitney test $p = 0.07$

White cell count



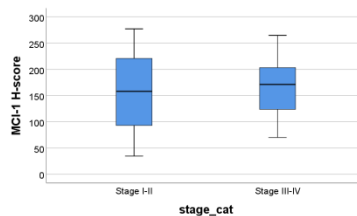
Mann Whitney test $p = 0.624$

Gender



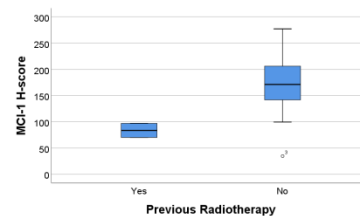
Mann Whitney test $p = 0.3$

Stage of disease



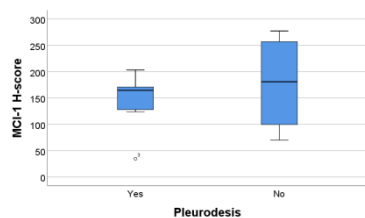
Mann Whitney test $p = 0.785$

Previous radiotherapy



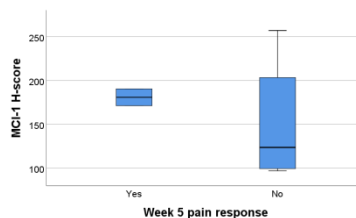
Mann Whitney test $p = 0.06$

Pleurodesis



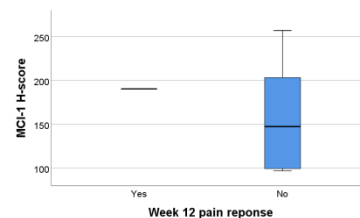
Mann Whitney test $p = 0.364$

Week 5 pain response



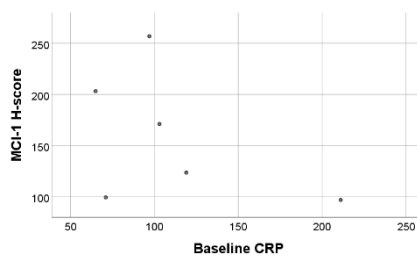
Mann Whitney test $p = 0.857$

Week 12 pain response



Mann Whitney test $p = 0.857$

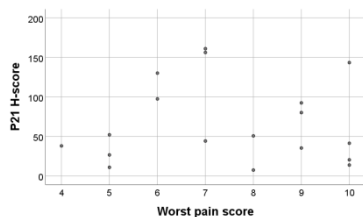
Baseline CRP



Spearman's rank correlation $p = 0.266$

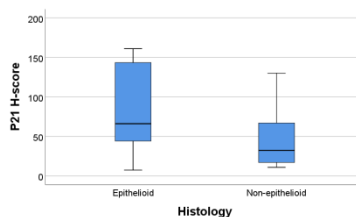
P21 correlation data

Worst pain score



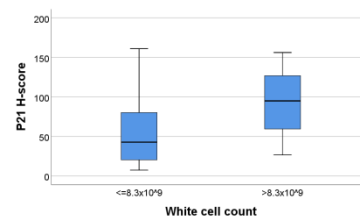
Spearman's rank correlation $p= 0.856$

Histology



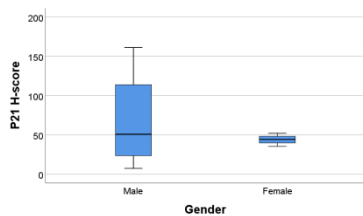
Mann Whitney test $p= 0.101$

White cell count



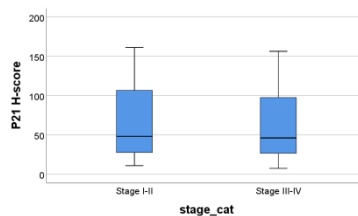
Mann Whitney test $p= 0.277$

Gender



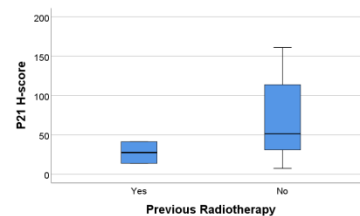
Mann Whitney test $p= 0.824$

Stage of disease



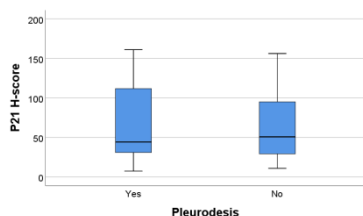
Mann Whitney test $p= 0.878$

Previous radiotherapy



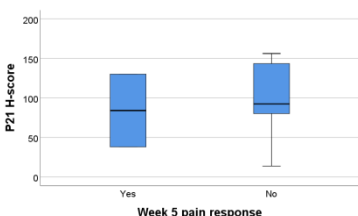
Mann Whitney test $p= 0.327$

Pleurodesis



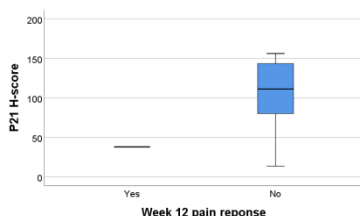
Mann Whitney test $p= 1.0$

Week 5 pain response



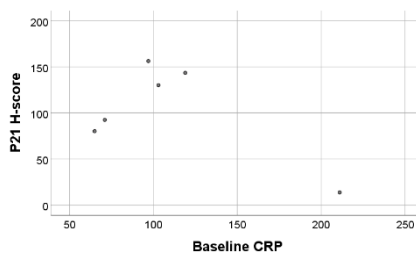
Mann Whitney test $p= 0.857$

Week 12 pain response



Mann Whitney test $p= 0.571$

Baseline CRP



Spearman's rank correlation $p= 0.957$

References

2016. National Lung Cancer Audit, Pleural Mesothelioma Report 2016. *London, UK: Royal College of Physicians.*
- ABBAS, T. & DUTTA, A. 2009. p21 in cancer: intricate networks and multiple activities. *Nature reviews. Cancer*, 9, 400-414.
- ABBOTT, D. W., HOLT, J. T. & FREEMAN, M. L. 1998. Double-Strand Break Repair Deficiency and Radiation Sensitivity in BRCA2 Mutant Cancer Cells. *JNCI: Journal of the National Cancer Institute*, 90, 978-985.
- ACKLER, S., MITTEN, M. J., FOSTER, K., OLEKSIJEW, A., REFICI, M., TAHIR, S. K., XIAO, Y., TSE, C., FROST, D. J., FESIK, S. W., ROSENBERG, S. H., ELMORE, S. W. & SHOEMAKER, A. R. 2010. The Bcl-2 inhibitor ABT-263 enhances the response of multiple chemotherapeutic regimens in hematologic tumors in vivo. *Cancer Chemother Pharmacol*, 66, 869-80.
- AGUILAR-MADRID, G., ROBLES-PEREZ, E., JUAREZ-PEREZ, C. A., ALVARADO-CABRERO, I., RICO-MENDEZ, F. G. & JAVIER, K. G. 2010. Case-control study of pleural mesothelioma in workers with social security in Mexico. *Am J Ind Med*, 53, 241-51.
- AHAMAD, A., STEVENS, C. W., SMYTHE, W. R., LIAO, Z., VAPORCIYAN, A. A., RICE, D., WALSH, G., GUERRERO, T., CHANG, J., BELL, B., KOMAKI, R. & FORSTER, K. M. 2003. Promising early local control of malignant pleural mesothelioma following postoperative intensity modulated radiotherapy (IMRT) to the chest. *Cancer J*, 9, 476-84.
- AISNER, J., BOUTIN, C., BUTCHART, E. G., CHAHINIAN, P., FABER, L. P., HEELAN, R., MATTSO, K., PASS, H. I., PATZ, E. F., ROBINSON, B., RUSCH, V. W., TAMMILEHTO, L., VOGELZANG, N. J., AISNER, S., ANTMAN, K. H., BELANI, C. P., BIGNON, J., BRODIN, O., FEINS, R., GINSBERG, R., HAMMAR, S., HERNDON, J., HILLARDEL, G., ILSON, D., KELLER, S., KELSEN, D., KRASNA, M., MAASILTA, P., MONNET, I., ROGGLI, V. L., RUFFIE, P., SALMINEN, U., SALTZ, L., STRAUSS, G., VIALLAT, J. R. & VONBULTZINGSLOWEN, F. 1995. A PROPOSED NEW INTERNATIONAL TNM STAGING SYSTEM FOR MALIGNANT PLEURAL MESOTHELIOMA. *Chest*, 108, 1122-1128.
- ALGAN, O., STOBBE, C. C., HELT, A. M., HANKS, G. E. & CHAPMAN, J. D. 1996. Radiation inactivation of human prostate cancer cells: the role of apoptosis. *Radiat Res*, 146, 267-75.
- ALLEN, A. M., CZERMINSKA, M., JANNE, P. A., SUGARBAKER, D. J., BUENO, R., HARRIS, J. R., COURT, L. & BALDINI, E. H. 2006. Fatal pneumonitis associated with intensity-modulated radiation therapy for mesothelioma. *Int J Radiat Oncol Biol Phys*, 65, 640-5.
- ALLEN, A. M., SCHOFIELD, D., HACKER, F., COURT, L. E. & CZERMINSKA, M. 2007. Restricted field IMRT dramatically enhances IMRT planning for mesothelioma. *Int J Radiat Oncol Biol Phys*, 69, 1587-92.
- ALLEN, C., HALBROOK, J. & NICKOLOFF, J. A. 2003. Interactive competition between homologous recombination and non-homologous end joining. *Mol Cancer Res*, 1, 913-20.
- ALLEN, C., KURIMASA, A., BRENNEMAN, M. A., CHEN, D. J. & NICKOLOFF, J. A. 2002. DNA-dependent protein kinase suppresses double-strand break-induced and spontaneous homologous recombination. *Proc Natl Acad Sci U S A*, 99, 3758-63.
- ALLEY, E. W., LOPEZ, J., SANTORO, A., MOROSKY, A., SARAF, S., PIPERDI, B. & VAN BRUMMELEN, E. 2017. Clinical safety and activity of pembrolizumab in patients with malignant pleural mesothelioma (KEYNOTE-028): preliminary results from a non-randomised, open-label, phase 1b trial. *The Lancet Oncology*, 18, 623-630.
- AMUNDSON, S. A., MYERS, T. G., SCUDIERO, D., KITADA, S., REED, J. C. & FORNACE, A. J., JR. 2000. An informatics approach identifying markers of chemosensitivity in human cancer cell lines. *Cancer Res*, 60, 6101-10.
- ANTWEILER, R. C. 2015. Evaluation of Statistical Treatments of Left-Censored Environmental Data Using Coincident Uncensored Data Sets. II. Group Comparisons. *Environmental Science & Technology*, 49, 13439-13446.
- APPENZOLLER, L. M., MICHALSKI, J. M., THORSTAD, W. L., MUTIC, S. & MOORE, K. L. 2012. Predicting dose-volume histograms for organs-at-risk in IMRT planning. *Med Phys*, 39, 7446-61.

- ARCARO, A. & WYMAN, M. P. 1993. Wortmannin is a potent phosphatidylinositol 3-kinase inhibitor: the role of phosphatidylinositol 3,4,5-trisphosphate in neutrophil responses. *Biochem J*, 296 (Pt 2), 297-301.
- ASHTON, M., O'ROURKE, N., CURRIE, S., RIMNER, A. & CHALMERS, A. 2017. The role of radical radiotherapy in the management of malignant pleural mesothelioma: A systematic review. *Radiother Oncol*, 125, 1-12.
- ASHTON, M., O'ROURKE, N., MACLEOD, N., LAIRD, B., STOBO, J., KELLY, C., ALEXANDER, L., FRANKS, K., MOORE, K., CURRIE, S., VALENTINE, R. & CHALMERS, A. J. 2018. SYSTEMS-2: A randomised phase II study of radiotherapy dose escalation for pain control in malignant pleural mesothelioma. *Clin Transl Radiat Oncol*, 8, 45-49.
- ATKINS, K. M., RAWAL, B., CHAUNZWA, T. L., LAMBA, N., BITTERMAN, D. S., WILLIAMS, C. L., KOZONO, D. E., BALDINI, E. H., CHEN, A. B., NGUYEN, P. L., D'AMICO, A. V., NOHRIA, A., HOFFMANN, U., AERTS, H. J. W. L. & MAK, R. H. 2019. Cardiac Radiation Dose, Cardiac Disease, and Mortality in Patients With Lung Cancer. 73, 2976-2987.
- BAAS, P., FENNEL, D., KERR, K. M., VAN SCHIL, P. E., HAAS, R. L., PETERS, S. & COMMITTEE, E. G. 2015. Malignant pleural mesothelioma: ESMO Clinical Practice Guidelines for diagnosis, treatment and follow-up. *Ann Oncol*, 26 Suppl 5, v31-9.
- BABAZADEH TOLOTI, S., RAFAT MOTAVALLI, L., MIRI HAKIMABAD, H., MOHAMMADI-YEGANEH, S. & RAJAB-BOLOKAT, E. 2018. Assessment of in vitro radiosensitivity parameters of breast cancer cells following exposure to radiotherapy hospital-based facilities. *Iranian Journal of Medical Physics*, 15, 132-139.
- BADIYAN, S. N., MOLITORIS, J. K., ZHU, M., GLASS, E., DIWANJI, T. & SIMONE, C. B., 2ND 2018. Proton beam therapy for malignant pleural mesothelioma. *Transl Lung Cancer Res*, 7, 189-198.
- BALDINI, E. H., RECHT, A., STRAUSS, G. M., DECAMP, M. M., JR., SWANSON, S. J., LIPTAY, M. J., MENTZER, S. J. & SUGARBAKER, D. J. 1997. Patterns of failure after trimodality therapy for malignant pleural mesothelioma. *Ann Thorac Surg*, 63, 334-8.
- BALL, D. L. & CRUICKSHANK, D. G. 1990. The treatment of malignant mesothelioma of the pleura: review of a 5-year experience, with special reference to radiotherapy. *Am J Clin Oncol*, 13, 4-9.
- BARBONE, D., RYAN, J. A., KOLHATKAR, N., CHACKO, A. D., JABLONS, D. M., SUGARBAKER, D. J., BUENO, R., LETAI, A. G., COUSSENS, L. M., FENNEL, D. A. & BROADDUS, V. C. 2011. The Bcl-2 repertoire of mesothelioma spheroids underlies acquired apoptotic multicellular resistance. *Cell Death Dis*, 2, e174.
- BARBONE, D., VAN DAM, L., FOLLO, C., JITHESH, P. V., ZHANG, S. D., RICHARDS, W. G., BUENO, R., FENNEL, D. A. & BROADDUS, V. C. 2016. Analysis of Gene Expression in 3D Spheroids Highlights a Survival Role for ASS1 in Mesothelioma. *PLoS One*, 11, e0150044.
- BARBONE, D., YANG, T. M., MORGAN, J. R., GAUDINO, G. & BROADDUS, V. C. 2008. Mammalian target of rapamycin contributes to the acquired apoptotic resistance of human mesothelioma multicellular spheroids. *J Biol Chem*, 283, 13021-30.
- BARIS, I., SIMONATO, L., ARTVINLI, M., POOLEY, F., SARACCI, R., SKIDMORE, J. & WAGNER, C. 1987. Epidemiological and environmental evidence of the health effects of exposure to erionite fibres: a four-year study in the Cappadocian region of Turkey. *Int J Cancer*, 39, 10-7.
- BASER, M. E., DE RIENZO, A., ALTOMARE, D., BALSARA, B. R., HEDRICK, N. M., GUTMANN, D. H., PITTS, L. H., JACKLER, R. K. & TESTA, J. R. 2002. Neurofibromatosis 2 and malignant mesothelioma. *Neurology*, 59, 290-1.
- BAYMAN, N., APPEL, W., ASHCROFT, L., BALDWIN, D. R., BATES, A., DARLISON, L., EDWARDS, J. G., EZHIL, V., GILLIGAN, D., HATTON, M., JEGANNATHAN, A., MANSY, T., PEAKE, M. D., PEMBERTON, L., RINTOUL, R. C., SNEE, M., RYDER, W. D., TAYLOR, P. & FAIVRE-FINN, C. 2019. Prophylactic Irradiation of Tracts in Patients With Malignant Pleural Mesothelioma: An Open-Label, Multicenter, Phase III Randomized Trial. *J Clin Oncol*, 37, 1200-1208.
- BECKETT, P., EDWARDS, J., FENNEL, D., HUBBARD, R., WOOLHOUSE, I. & PEAKE, M. D. 2015. Demographics, management and survival of patients with malignant pleural

- mesothelioma in the National Lung Cancer Audit in England and Wales. *Lung Cancer*, 88, 344-348.
- BEDDOWES, E., SPICER, J., CHAN, P. Y., KHADEIR, R., CORBACHO, J. G., REPANA, D., STEELE, J. P., SCHMID, P., SZYSZKO, T., COOK, G., DIAZ, M., FENG, X., JOHNSTON, A., THOMSON, J., SHEAFF, M., WU, B. W., BOMALASKI, J., PACEY, S. & SZLOSAREK, P. W. 2017. Phase 1 Dose-Escalation Study of Pegylated Arginine Deiminase, Cisplatin, and Pemetrexed in Patients With Argininosuccinate Synthetase 1-Deficient Thoracic Cancers. *J Clin Oncol*, 35, 1778-1785.
- BEGG, A. C. & MOOREN, E. 1989. Rapid fluorescence-based assay for radiosensitivity and chemosensitivity testing in mammalian cells in vitro. *Cancer Res*, 49, 565-9.
- BENEDICT, S. H., YENICE, K. M., FOLLOWILL, D., GALVIN, J. M., HINSON, W., KAVANAGH, B., KEALL, P., LOVELOCK, M., MEEKS, S., PAPIEZ, L., PURDIE, T., SADAGOPAN, R., SCHELL, M. C., SALTER, B., SCHLESINGER, D. J., SHIU, A. S., SOLBERG, T., SONG, D. Y., STIEBER, V., TIMMERMAN, R., TOME, W. A., VERELLEN, D., WANG, L. & YIN, F. F. 2010. Stereotactic body radiation therapy: the report of AAPM Task Group 101. *Med Phys*, 37, 4078-101.
- BENTZEN, S. M., CONSTINE, L. S., DEASY, J. O., EISBRUCH, A., JACKSON, A., MARKS, L. B., TEN HAKEN, R. K. & YORKE, E. D. 2010. Quantitative Analyses of Normal Tissue Effects in the Clinic (QUANTEC): an introduction to the scientific issues. *International journal of radiation oncology, biology, physics*, 76, S3-S9.
- BERG, M., LORENZEN, E. L., JENSEN, I., THOMSEN, M. S., LUTZ, C. M., REFSGAARD, L., NISSEN, H. D. & OFFERSEN, B. V. 2018. The potential benefits from respiratory gating for breast cancer patients regarding target coverage and dose to organs at risk when applying strict dose limits to the heart: results from the DBCG HYPO trial. *Acta Oncol*, 57, 113-119.
- BERNSTEIN, M. B., KRISHNAN, S., HODGE, J. W. & CHANG, J. Y. 2016. Immunotherapy and stereotactic ablative radiotherapy (ISABR): a curative approach? *Nat Rev Clin Oncol*, 13, 516-24.
- BETTI, M., CASALONE, E., FERRANTE, D., ASPESI, A., MORLEO, G., BIASI, A., SCULCO, M., MANCUSO, G., GUARRERA, S., RIGHI, L., GROSSO, F., LIBENER, R., PAVESI, M., MARIANI, N., CASADIO, C., BOLDORINI, R., MIRABELLI, D., PASINI, B., MAGNANI, C., MATULLO, G. & DIANZANI, I. 2017. Germline mutations in DNA repair genes predispose asbestos-exposed patients to malignant pleural mesothelioma. *Cancer Lett*, 405, 38-45.
- BEUCHER, A., BIRRAUX, J., TCHOUANDONG, L., BARTON, O., SHIBATA, A., CONRAD, S., GOODARZI, A. A., KREMLER, A., JEGGO, P. A. & LOBRICH, M. 2009. ATM and Artemis promote homologous recombination of radiation-induced DNA double-strand breaks in G2. *EMBO J*, 28, 3413-27.
- BIBBY, A. C. & MASKELL, N. A. 2018. Current treatments and trials in malignant pleural mesothelioma. 12, 2161-2169.
- BISSETT, D., MACBETH, F. R. & CRAM, I. 1991. The role of palliative radiotherapy in malignant mesothelioma. *Clin Oncol (R Coll Radiol)*, 3, 315-7.
- BLYTH, K. G. & MURPHY, D. J. 2018. Progress and challenges in Mesothelioma: From bench to bedside. *Respir Med*, 134, 31-41.
- BORASCHI, P., NERI, S., BRACCINI, G., GIGONI, R., LEONCINI, B. & PERRI, G. 1999. Magnetic resonance appearance of asbestos-related benign and malignant pleural diseases. *Scand J Work Environ Health*, 25, 18-23.
- BOTT, M., BREVET, M., TAYLOR, B. S., SHIMIZU, S., ITO, T., WANG, L., CREANEY, J., LAKE, R. A., ZAKOWSKI, M. F., REVA, B., SANDER, C., DELSITE, R., POWELL, S., ZHOU, Q., SHEN, R., OLSHEN, A., RUSCH, V. & LADANYI, M. 2011. The nuclear deubiquitinase BAP1 is commonly inactivated by somatic mutations and 3p21.1 losses in malignant pleural mesothelioma. *Nat Genet*, 43, 668-72.
- BOTTOMLEY, A., COENS, C., EFFICACE, F., GAAFAR, R., MANEGOLD, C., BURGERS, S., VINCENT, M., LEGRAND, C. & VAN MEERBEECK, J. P. 2007. Symptoms and Patient-Reported Well-Being: Do They Predict Survival in Malignant Pleural Mesothelioma? A Prognostic Factor Analysis of EORTC-NCIC 08983: Randomized Phase III Study of Cisplatin With or. *Journal of Clinical Oncology*, 25, 5770-5776.

- BOULTON, S., KYLE, S. & DURKACZ, B. W. 2000. Mechanisms of enhancement of cytotoxicity in etoposide and ionising radiation-treated cells by the protein kinase inhibitor wortmannin. *Eur J Cancer*, 36, 535-41.
- BOUTIN, C., REY, F. & VIALLAT, J. R. 1995. Prevention of malignant seeding after invasive diagnostic procedures in patients with pleural mesothelioma. A randomized trial of local radiotherapy. *Chest*, 108, 754-8.
- BOUWMAN, P. & JONKERS, J. 2012. The effects of deregulated DNA damage signalling on cancer chemotherapy response and resistance. *Nat Rev Cancer*, 12, 587-98.
- BRADLEY, J. D., PAULUS, R., KOMAKI, R., MASTERS, G., BLUMENSCHNEIN, G., SCHILD, S., BOGART, J., HU, C., FORSTER, K., MAGLIOCCO, A., KAVADI, V., GARCES, Y. I., NARAYAN, S., IYENGAR, P., ROBINSON, C., WYNN, R. B., KOPROWSKI, C., MENG, J., BEITLER, J., GAUR, R., CURRAN, W. & CHOY, H. 2015. Standard-dose versus high-dose conformal radiotherapy with concurrent and consolidation carboplatin plus paclitaxel with or without cetuximab for patients with stage IIIA or IIIB non-small-cell lung cancer (RTOG 0617): a randomised, two-by-two factorial phase 3 study. *The Lancet Oncology*, 16, 187-199.
- BRENNER, D. J., MARTINEZ, A. A., EDMUNDSON, G. K., MITCHELL, C., THAMES, H. D. & ARMOUR, E. P. 2002. Direct evidence that prostate tumors show high sensitivity to fractionation (low alpha/beta ratio), similar to late-responding normal tissue. *Int J Radiat Oncol Biol Phys*, 52, 6-13.
- BROADDUS, V. C., DANSEN, T. B., ABAYASIRIWARDANA, K. S., WILSON, S. M., FINCH, A. J., SWIGART, L. B., HUNT, A. E. & EVAN, G. I. 2005. Bid mediates apoptotic synergy between tumor necrosis factor-related apoptosis-inducing ligand (TRAIL) and DNA damage. *J Biol Chem*, 280, 12486-93.
- BROCK, W. A., BAKER, F. L., WIKE, J. L., SIVON, S. L. & PETERS, L. J. 1990. Cellular radiosensitivity of primary head and neck squamous cell carcinomas and local tumor control. *Int J Radiat Oncol Biol Phys*, 18, 1283-6.
- BRUNO, S. & DARZYNKIEWICZ, Z. 1992. Cell cycle dependent expression and stability of the nuclear protein detected by Ki-67 antibody in HL-60 cells. *Cell Prolif*, 25, 31-40.
- BUDUHAN, G., MENON, S., AYE, R., LOUIE, B., MEHTA, V. & VALLIÈRES, E. 2009. Trimodality Therapy for Malignant Pleural Mesothelioma. *The Annals of Thoracic Surgery*, 88, 870-876.
- BUENO, R., STAWISKI, E. W., GOLDSTEIN, L. D., DURINCK, S., DE RIENZO, A., MODRUSAN, Z., GNAD, F., NGUYEN, T. T., JAISWAL, B. S., CHIRIEAC, L. R., SCIRANGHELLA, D., DAO, N., GUSTAFSON, C. E., MUNIR, K. J., HACKNEY, J. A., CHAUDHURI, A., GUPTA, R., GUILLORY, J., TOY, K., HA, C., CHEN, Y. J., STINSON, J., CHAUDHURI, S., ZHANG, N., WU, T. D., SUGARBAKER, D. J., DE SAUVAGE, F. J., RICHARDS, W. G. & SESHAGIRI, S. 2016. Comprehensive genomic analysis of malignant pleural mesothelioma identifies recurrent mutations, gene fusions and splicing alterations. *Nat Genet*, 48, 407-16.
- BUIKHUISEN, W. A., HIDDINGA, B. I., BAAS, P. & VAN MEERBEECK, J. P. 2015. Second line therapy in malignant pleural mesothelioma: A systematic review. *Lung Cancer*, 89, 223-231.
- BUTTERWORTH, K. T. 2019. Evolution of the Supermodel: Progress in Modelling Radiotherapy Response in Mice. *Clinical Oncology*, 31, 272-282.
- BUTTERWORTH, M., PETTITT, A., VARADARAJAN, S. & COHEN, G. M. 2016. BH3 profiling and a toolkit of BH3-mimetic drugs predict anti-apoptotic dependence of cancer cells. *Br J Cancer*, 114, 638-41.
- BYDDER, S., PHILLIPS, M., JOSEPH, D. J., CAMERON, F., SPRY, N. A., DEMELKER, Y. & MUSK, A. W. 2004. A randomised trial of single-dose radiotherapy to prevent procedure tract metastasis by malignant mesothelioma. *Br J Cancer*, 91, 9-10.
- BYRNE, M. J. & NOWAK, A. K. 2004a. Modified RECIST criteria for assessment of response in malignant pleural mesothelioma. *Annals of Oncology*, 15, 257-260.
- BYRNE, M. J. & NOWAK, A. K. 2004b. Modified RECIST criteria for assessment of response in malignant pleural mesothelioma. *Ann Oncol*, 15, 257-60.
- CAO, X., RODARTE, C., ZHANG, L., MORGAN, C. D., LITTLEJOHN, J. & SMYTHE, W. R. 2007. Bcl2/bcl-xL inhibitor engenders apoptosis and increases chemosensitivity in mesothelioma. *Cancer Biol Ther*, 6, 246-52.

- CAO, X. X., MOHUIDDIN, I., ECE, F., MCCONKEY, D. J. & SMYTHE, W. R. 2001. Histone deacetylase inhibitor downregulation of bcl-xl gene expression leads to apoptotic cell death in mesothelioma. *Am J Respir Cell Mol Biol*, 25, 562-8.
- CARBONE, M., PASS, H. I., RIZZO, P., MARINETTI, M., DI MUZIO, M., MEW, D. J., LEVINE, A. S. & PROCOPIO, A. 1994. Simian virus 40-like DNA sequences in human pleural mesothelioma. *Oncogene*, 9, 1781-90.
- CARMICHAEL, J., DEGRAFF, W. G., GAMSON, J., RUSSO, D., GAZDAR, A. F., LEVITT, M. L., MINNA, J. D. & MITCHELL, J. B. 1989. Radiation sensitivity of human lung cancer cell lines. *Eur J Cancer Clin Oncol*, 25, 527-34.
- CARPENTER, A. E., JONES, T. R., LAMPRECHT, M. R., CLARKE, C., KANG, I. H., FRIMAN, O., GUERTIN, D. A., CHANG, J. H., LINDQUIST, R. A., MOFFAT, J., GOLLAND, P. & SABATINI, D. M. 2006. CellProfiler: image analysis software for identifying and quantifying cell phenotypes. *Genome Biology*, 7, R100.
- CASTELLI, J., SIMON, A., LOUVEL, G., HENRY, O., CHAJON, E., NASSEF, M., HAIGRON, P., CAZOULAT, G., OSPINA, J. D., JEGOUX, F., BENEZERY, K. & DE CREVOISIER, R. 2015. Impact of head and neck cancer adaptive radiotherapy to spare the parotid glands and decrease the risk of xerostomia. *Radiat Oncol*, 10, 6.
- CAVAZZA, A., TRAVIS, L. B., TRAVIS, W. D., WOLFE, J. T., 3RD, FOO, M. L., GILLESPIE, D. J., WEIDNER, N. & COLBY, T. V. 1996. Post-irradiation malignant mesothelioma. *Cancer*, 77, 1379-85.
- CHANG, J. Y., VERMA, V., LI, M., ZHANG, W., KOMAKI, R., LU, C., ALLEN, P. K., LIAO, Z., WELSH, J., LIN, S. H., GOMEZ, D., JETER, M., O'REILLY, M., ZHU, R. X., ZHANG, X., LI, H., MOHAN, R., HEYMACH, J. V., VAPORCIYAN, A. A., HAHN, S. & COX, J. D. 2017. Proton Beam Radiotherapy and Concurrent Chemotherapy for Unresectable Stage III Non-Small Cell Lung Cancer: Final Results of a Phase 2 Study. *JAMA Oncol*, 3, e172032.
- CHANYAVANICH, V., DAS, S. K., LEE, W. R. & LO, J. Y. 2011. Knowledge-based IMRT treatment planning for prostate cancer. *Med Phys*, 38, 2515-22.
- CHAO, H. H., BERMAN, A. T., SIMONE, C. B., 2ND, CIUNCI, C., GABRIEL, P., LIN, H., BOTH, S., LANGER, C., LELIONIS, K., RENGAN, R., HAHN, S. M., PRABHU, K., FAGUNDES, M., HARTSELL, W., MICK, R. & PLASTARAS, J. P. 2017. Multi-Institutional Prospective Study of Reirradiation with Proton Beam Radiotherapy for Locoregionally Recurrent Non-Small Cell Lung Cancer. *J Thorac Oncol*, 12, 281-292.
- CHAPMAN, J. D. 2003. Single-hit mechanism of tumour cell killing by radiation. *Int J Radiat Biol*, 79, 71-81.
- CHAPMAN, J. D. 2014. Can the two mechanisms of tumor cell killing by radiation be exploited for therapeutic gain? *Journal of Radiation Research*, 55, 2-9.
- CHAPMAN, J. D., STOBBE, C. C., GALES, T., DAS, I. J., ZELLMER, D. L., BIADE, S. & MATSUMOTO, Y. 1999. Condensed chromatin and cell inactivation by single-hit kinetics. *Radiat Res*, 151, 433-41.
- CHEN, B. P., CHAN, D. W., KOBAYASHI, J., BURMA, S., ASAITHAMBY, A., MOROTOMI-YANO, K., BOTVINICK, E., QIN, J. & CHEN, D. J. 2005. Cell cycle dependence of DNA-dependent protein kinase phosphorylation in response to DNA double strand breaks. *J Biol Chem*, 280, 14709-15.
- CHEN, B. P., UEMATSU, N., KOBAYASHI, J., LERENTHAL, Y., KREMLER, A., YAJIMA, H., LOBRICH, M., SHILOH, Y. & CHEN, D. J. 2007. Ataxia telangiectasia mutated (ATM) is essential for DNA-PKcs phosphorylations at the Thr-2609 cluster upon DNA double strand break. *J Biol Chem*, 282, 6582-7.
- CHEN, J., JIN, S., ABRAHAM, V., HUANG, X., LIU, B., MITTEN, M. J., NIMMER, P., LIN, X., SMITH, M., SHEN, Y., SHOEMAKER, A. R., TAHIR, S. K., ZHANG, H., ACKLER, S. L., ROSENBERG, S. H., MAECKER, H., SAMPATH, D., LEVERSON, J. D., TSE, C. & ELMORE, S. W. 2011. The Bcl-2/Bcl-X(L)/Bcl-w inhibitor, navitoclax, enhances the activity of chemotherapeutic agents in vitro and in vivo. *Mol Cancer Ther*, 10, 2340-9.
- CHEUNG, M. & TESTA, J. R. 2017. BAP1, a tumor suppressor gene driving malignant mesothelioma. *Translational lung cancer research*, 6, 270-278.

- CHIN, S., ECCLES, C. L., MCWILLIAM, A., CHUTER, R., WALKER, E., WHITEHURST, P., BERRESFORD, J., VAN HERK, M., HOSKIN, P. J. & CHOUDHURY, A. 2020. Magnetic resonance-guided radiation therapy: A review. *J Med Imaging Radiat Oncol*, 64, 163-177.
- CHINNAIYAN, A. M. 1999. The apoptosome: heart and soul of the cell death machine. *Neoplasia*, 1, 5-15.
- CHIPUK, J. E., MOLDOVEANU, T., LLAMBI, F., PARSONS, M. J. & GREEN, D. R. 2010. The BCL-2 family reunion. *Mol Cell*, 37, 299-310.
- CHITNIS, M. M., LODHIA, K. A., ALEKSIC, T., GAO, S., PROTHEROE, A. S. & MACAULAY, V. M. 2014. IGF-1R inhibition enhances radiosensitivity and delays double-strand break repair by both non-homologous end-joining and homologous recombination. *Oncogene*, 33, 5262-73.
- CHO, B. C., FELD, R., LEIGHL, N., OPITZ, I., ANRAKU, M., TSAO, M. S., HWANG, D. M., HOPE, A. & DE PERROT, M. 2014. A feasibility study evaluating Surgery for Mesothelioma After Radiation Therapy: the "SMART" approach for resectable malignant pleural mesothelioma. *J Thorac Oncol*, 9, 397-402.
- CHO, J., DINNIWELL, R. & DE PERROR, M. 2010. Comparing adjuvant hemithoracic radiation using 3D conformal (3DCRT) vs. intensity modulated radiotherapy (IMRT) techniques in malignant pleural mesothelioma (MPM) patients treated with extrapleural pneumonectomy (EPP). *ESTRO*, S547.
- CHOUDHURY, A., NELSON, L. D., TEO, M. T., CHILKA, S., BHATTARAI, S., JOHNSTON, C. F., ELLIOTT, F., LOWERY, J., TAYLOR, C. F., CHURCHMAN, M., BENTLEY, J., KNOWLES, M. A., HARNDEN, P., BRISTOW, R. G., BISHOP, D. T. & KILTIE, A. E. 2010. MRE11 expression is predictive of cause-specific survival following radical radiotherapy for muscle-invasive bladder cancer. *Cancer Res*, 70, 7017-26.
- CHRENEK, M. A., WONG, P. & WEAVER, V. M. 2001. Tumour-stromal interactions. Integrins and cell adhesions as modulators of mammary cell survival and transformation. *Breast Cancer Res*, 3, 224-9.
- CISZEWSKI, W. M., TAVECCHIO, M., DASTYCH, J. & CURTIN, N. J. 2014. DNA-PK inhibition by NU7441 sensitizes breast cancer cells to ionizing radiation and doxorubicin. *Breast Cancer Res Treat*, 143, 47-55.
- CLEELAND, C. S. & RYAN, K. M. 1994. Pain assessment: global use of the Brief Pain Inventory. *Ann Acad Med Singapore*, 23, 129-38.
- CLIVE, A. O., TAYLOR, H., DOBSON, L., WILSON, P., DE WINTON, E., PANAKIS, N., PEPPERELL, J., HOWELL, T., STEWART, S. A., PENZ, E., JORDAN, N., MORLEY, A. J., ZAHAN-EVANS, N., SMITH, S., BATCHELOR, T. J. P., MARCHBANK, A., BISHOP, L., IONESCU, A. A., BAYNE, M., COOPER, S., KERRY, A., JENKINS, P., TOY, E., VIGNESWARAN, V., GILDERSLEVE, J., AHMED, M., MCDONALD, F., BUTTON, M., LEWANSKI, C., COMINS, C., DAKSHINAMOORTHY, M., LEE, Y. C. G., RAHMAN, N. M. & MASKELL, N. A. 2016. Prophylactic radiotherapy for the prevention of procedure-tract metastases after surgical and large-bore pleural procedures in malignant pleural mesothelioma (SMART): a multicentre, open-label, phase 3, randomised controlled trial. *Lancet Oncol*, 17, 1094-1104.
- COLAK, S., ZIMBERLIN, C. D., FESSLER, E., HOGDAL, L., PRASETYANTI, P. R., GRANDELA, C. M., LETAI, A. & MEDEMA, J. P. 2014. Decreased mitochondrial priming determines chemoresistance of colon cancer stem cells. *Cell Death And Differentiation*, 21, 1170.
- COLLIS, S. J., DEWEESE, T. L., JEGGO, P. A. & PARKER, A. R. 2005. The life and death of DNA-PK. *Oncogene*, 24, 949-61.
- COOLEN, J., DE KEYZER, F., NAFTEUX, P., DE WEVER, W., DOOMS, C., VANSTEENKISTE, J., ROEBBEN, I., VERBEKEN, E., DE LEYN, P., VAN RAEMDONCK, D., NACKAERTS, K., DYMARKOWSKI, S. & VERSCHAKELLEN, J. 2012. Malignant pleural disease: diagnosis by using diffusion-weighted and dynamic contrast-enhanced MR imaging--initial experience. *Radiology*, 263, 884-92.
- CORCORAN, R. B., CHENG, K. A., HATA, A. N., FABER, A. C., EBI, H., COFFEE, E. M., GRENINGER, P., BROWN, R. D., GODFREY, J. T., COHOON, T. J., SONG, Y., LIFSHITS, E., HUNG, K. E., SHIODA, T., DIAS-SANTAGATA, D., SINGH, A., SETTLEMAN, J., BENES, C. H., MINO-KENUDSON, M., WONG, K. K. & ENGELMAN, J. A. 2013. Synthetic lethal interaction of combined BCL-XL

- and MEK inhibition promotes tumor regressions in KRAS mutant cancer models. *Cancer Cell*, 23, 121-8.
- CORY, S. & ADAMS, J. M. 2002. The Bcl2 family: regulators of the cellular life-or-death switch. *Nat Rev Cancer*, 2, 647-56.
- COVA, E., PANDOLFI, L., COLOMBO, M., FRANGIPANE, V., INGHILLERI, S., MOROSINI, M., MRAKIC-SPOSTA, S., MORETTI, S., MONTI, M., PIGNOCHINO, Y., BENVENUTI, S., PROSPERI, D., STELLA, G., MORBINI, P. & MELONI, F. 2019. Pemetrexed-loaded nanoparticles targeted to malignant pleural mesothelioma cells: an in vitro study. *International journal of nanomedicine*, 14, 773-785.
- CRAFT, D., MCQUAID, D., WALA, J., CHEN, W., SALARI, E. & BORTFELD, T. 2012a. Multicriteria VMAT optimization. *Med Phys*, 39, 686-96.
- CRAFT, D. L., HALABI, T. F., SHIH, H. A. & BORTFELD, T. R. 2006. Approximating convex Pareto surfaces in multiobjective radiotherapy planning. *Medical Physics*, 33, 3399-3407.
- CRAFT, D. L., HONG, T. S., SHIH, H. A. & BORTFELD, T. R. 2012b. Improved planning time and plan quality through multicriteria optimization for intensity-modulated radiotherapy. *Int J Radiat Oncol Biol Phys*, 82, e83-90.
- CREANEY, J., FRANCIS, R. J., DICK, I. M., MUSK, A. W., ROBINSON, B. W. S., BYRNE, M. J. & NOWAK, A. K. 2011. Serum Soluble Mesothelin Concentrations in Malignant Pleural Mesothelioma: Relationship to Tumor Volume, Clinical Stage and Changes in Tumor Burden. *Clinical Cancer Research*, 17, 1181.
- CREANEY, J., YEOMAN, D., DEMELKER, Y., SEGAL, A., MUSK, A. W., SKATES, S. J. & ROBINSON, B. W. S. 2008. Comparison of osteopontin, megakaryocyte potentiating factor, and mesothelin proteins as markers in the serum of patients with malignant mesothelioma. *Journal of Thoracic Oncology*, 3, 851-857.
- CUI, X., YU, Y., GUPTA, S., CHO, Y.-M., LEES-MILLER, S. P. & MEEK, K. 2005. Autophosphorylation of DNA-dependent protein kinase regulates DNA end processing and may also alter double-strand break repair pathway choice. *Molecular and cellular biology*, 25, 10842-10852.
- CURRAN, W. J., JR, PAULUS, R., LANGER, C. J., KOMAKI, R., LEE, J. S., HAUSER, S., MOVASAS, B., WASSERMAN, T., ROSENTHAL, S. A., GORE, E., MACHTAY, M., SAUSE, W. & COX, J. D. 2011. Sequential vs Concurrent Chemoradiation for Stage III Non-Small Cell Lung Cancer: Randomized Phase III Trial RTOG 9410. *JNCl: Journal of the National Cancer Institute*, 103, 1452-1460.
- CURTIN, N. J. 2012. DNA repair dysregulation from cancer driver to therapeutic target. *Nat Rev Cancer*, 12, 801-17.
- CZABOTAR, P. E., LEE, E. F., VAN DELFT, M. F., DAY, C. L., SMITH, B. J., HUANG, D. C., FAIRLIE, W. D., HINDS, M. G. & COLMAN, P. M. 2007. Structural insights into the degradation of Mcl-1 induced by BH3 domains. *Proc Natl Acad Sci U S A*, 104, 6217-22.
- CZABOTAR, P. E., LESSENE, G., STRASSER, A. & ADAMS, J. M. 2014. Control of apoptosis by the BCL-2 protein family: implications for physiology and therapy. *Nat Rev Mol Cell Biol*, 15, 49-63.
- D'ANDREA, M., STROLIN, S., UNGANIA, S., CACCIATORE, A., BRUZZANITI, V., MARCONI, R., BENASSI, M. & STRIGARI, L. 2018. Radiobiological Optimization in Lung Stereotactic Body Radiation Therapy: Are We Ready to Apply Radiobiological Models? *Frontiers in Oncology*, 7.
- DALE, R. G. 1985. The application of the linear-quadratic dose-effect equation to fractionated and protracted radiotherapy. *Br J Radiol*, 58, 515-28.
- DALE, R. G. 1989. Time-dependent tumour repopulation factors in linear-quadratic equations--implications for treatment strategies. *Radiother Oncol*, 15, 371-81.
- DARBY, S. C., EWERTZ, M., MCGALE, P., BENNET, A. M., BLOM-GOLDMAN, U., BRØNNUM, D., CORREA, C., CUTTER, D., GAGLIARDI, G., GIGANTE, B., JENSEN, M.-B., NISBET, A., PETO, R., RAHIMI, K., TAYLOR, C. & HALL, P. 2013. Risk of Ischemic Heart Disease in Women after Radiotherapy for Breast Cancer. 368, 987-998.
- DAUBRIAC, J., FLEURY-FEITH, J., KHEUANG, L., GALIPON, J., SAINT-ALBIN, A., RENIER, A., GIOVANNINI, M., GALATEAU-SALLE, F. & JAURAND, M. C. 2009. Malignant pleural

- mesothelioma cells resist anoikis as quiescent pluricellular aggregates. *Cell Death Differ*, 16, 1146-55.
- DE GRAAF-STRUKOWSKA, L., VAN DER ZEE, J., VAN PUTTEN, W. & SENAN, S. 1999. Factors influencing the outcome of radiotherapy in malignant mesothelioma of the pleura—a single-institution experience with 189 patients. *International Journal of Radiation Oncology*Biophysics*, 43, 511-516.
- DE LA MAZA, L., WU, M., WU, L., YUN, H., ZHAO, Y., CATRAL, M., MCCART, A., CHO, B. J. & DE PERROT, M. 2017. In Situ Vaccination after Accelerated Hypofractionated Radiation and Surgery in a Mesothelioma Mouse Model. *Clin Cancer Res*, 23, 5502-5513.
- DE PERROT, M., FELD, R., LEIGHL, N. B., HOPE, A., WADDELL, T. K., KESHAVJEE, S. & CHO, B. C. 2016. Accelerated hemithoracic radiation followed by extrapleural pneumonectomy for malignant pleural mesothelioma. *J Thorac Cardiovasc Surg*, 151, 468-73.
- DE RIENZO, A. & TESTA, J. R. 2000. Recent advances in the molecular analysis of human malignant mesothelioma. *Clin Ter*, 151, 433-8.
- DEACON, J. M., WILSON, P. A. & PECKHAM, M. J. 1985. The radiobiology of human neuroblastoma. *Radiother Oncol*, 3, 201-9.
- DEARNALEY, D., SYNDIKUS, I., MOSSOP, H., KHOO, V., BIRTLE, A., BLOOMFIELD, D., GRAHAM, J., KIRKBRIDE, P., LOGUE, J., MALIK, Z., MONEY-KYRLE, J., O'SULLIVAN, J. M., PANADES, M., PARKER, C., PATTERSON, H., SCRASE, C., STAFFURTH, J., STOCKDALE, A., TREMLETT, J., BIDMEAD, M., MAYLES, H., NAISMITH, O., SOUTH, C., GAO, A., CRUICKSHANK, C., HASSAN, S., PUGH, J., GRIFFIN, C. & HALL, E. 2016. Conventional versus hypofractionated high-dose intensity-modulated radiotherapy for prostate cancer: 5-year outcomes of the randomised, non-inferiority, phase 3 CHHiP trial. *Lancet Oncol*, 17, 1047-1060.
- DEFAZIO, L. G., STANSEL, R. M., GRIFFITH, J. D. & CHU, G. 2002. Synapsis of DNA ends by DNA-dependent protein kinase. *The EMBO journal*, 21, 3192-3200.
- DEGUEN, B., GOUTEBROZE, L., GIOVANNINI, M., BOISSON, C., VAN DER NEUT, R., JAURAND, M. C. & THOMAS, G. 1998. Heterogeneity of mesothelioma cell lines as defined by altered genomic structure and expression of the NF2 gene. *Int J Cancer*, 77, 554-60.
- DELAHAYE, M., DE JONG, A. A., VERSNEL, M. A., HOOGSTEDEN, H. C., TEELING, P. & VAN DER KWAST, T. H. 1990. Cytopathology of malignant mesothelioma. Reappraisal of the diagnostic value of collagen cores. *Cytopathology*, 1, 137-45.
- DELANEY, G., JACOB, S., FEATHERSTONE, C. & BARTON, M. 2005. The role of radiotherapy in cancer treatment: estimating optimal utilization from a review of evidence-based clinical guidelines. *Cancer*, 104, 1129-37.
- DENG, C., ZHANG, P., HARPER, J. W., ELLEDGE, S. J. & LEDER, P. 1995. Mice lacking p21CIP1/WAF1 undergo normal development, but are defective in G1 checkpoint control. *Cell*, 82, 675-84.
- DESOIZE, B. & JARDILLIER, J.-C. 2000. Multicellular resistance: a paradigm for clinical resistance? *Critical Reviews in Oncology/Hematology*, 36, 193-207.
- DEWEESE, T. L., SHIPMAN, J. M., DILLEHAY, L. E. & NELSON, W. G. 1998. Sensitivity of human prostatic carcinoma cell lines to low dose rate radiation exposure. *J Urol*, 159, 591-8.
- DING, Q., REDDY, Y. V., WANG, W., WOODS, T., DOUGLAS, P., RAMSDEN, D. A., LEES-MILLER, S. P. & MEEK, K. 2003. Autophosphorylation of the catalytic subunit of the DNA-dependent protein kinase is required for efficient end processing during DNA double-strand break repair. *Mol Cell Biol*, 23, 5836-48.
- DONG, J., REN, Y., ZHANG, T., WANG, Z., LING, C. C., LI, G. C., HE, F., WANG, C. & WEN, B. 2018. Inactivation of DNA-PK by knockdown DNA-PKcs or NU7441 impairs non-homologous end-joining of radiation-induced double strand break repair. *Oncol Rep*, 39, 912-920.
- DONG, J., ZHANG, T., REN, Y., WANG, Z., LING, C. C., HE, F., LI, G. C., WANG, C. & WEN, B. 2017. Inhibiting DNA-PKcs in a non-homologous end-joining pathway in response to DNA double-strand breaks. *Oncotarget*, 8, 22662-22673.
- DOUGLAS, B. G. & FOWLER, J. F. 1976. The effect of multiple small doses of x rays on skin reactions in the mouse and a basic interpretation. *Radiat Res*, 66, 401-26.
- DOUGLAS, P., CUI, X., BLOCK, W. D., YU, Y., GUPTA, S., DING, Q., YE, R., MORRICE, N., LEES-MILLER, S. P. & MEEK, K. 2007. The DNA-Dependent Protein Kinase Catalytic Subunit Is

- Phosphorylated In Vivo on Threonine 3950, a Highly Conserved Amino Acid in the Protein Kinase Domain. *Molecular and Cellular Biology*, 27, 1581-1591.
- DOUGLAS, P., SAPKOTA, G. P., MORRICE, N., YU, Y., GOODARZI, A. A., MERKLE, D., MEEK, K., ALESSI, D. R. & LEES-MILLER, S. P. 2002. Identification of in vitro and in vivo phosphorylation sites in the catalytic subunit of the DNA-dependent protein kinase. *Biochem J*, 368, 243-51.
- DRUKKER, C. A., ELIAS, S. G., NIJENHUIS, M. V., WESSELING, J., BARTELINK, H., ELKHUIZEN, P., FOWBLE, B., WHITWORTH, P. W., PATEL, R. R., DE SNOO, F. A., VAN 'T VEER, L. J., BEITSCH, P. D. & RUTGERS, E. J. 2014. Gene expression profiling to predict the risk of locoregional recurrence in breast cancer: a pooled analysis. *Breast Cancer Res Treat*, 148, 599-613.
- DUBESSY, C., MERLIN, J. M., MARCHAL, C. & GUILLEMIN, F. 2000. Spheroids in radiobiology and photodynamic therapy. *Crit Rev Oncol Hematol*, 36, 179-92.
- DUMANE, V., RIMNER, A., YORKE, E. & ROSENWEIG, K. 2016. Volumetric-modulated arc therapy for malignant pleural mesothelioma after pleurectomy/decortication. *Applied Radiation Oncology*, 5, 28-37.
- ELMORE, S. 2007. Apoptosis: a review of programmed cell death. *Toxicol Pathol*, 35, 495-516.
- ERNST, A., HOFMANN, S., AHMADI, R., BECKER, N., KORSHUNOV, A., ENGEL, F., HARTMANN, C., FELSBURG, J., SABEL, M., PETERZIEL, H., DURCHDEWALD, M., HESS, J., BARBUS, S., CAMPOS, B., STARZINSKI-POWITZ, A., UNTERBERG, A., REIFENBERGER, G., LICHTER, P., HEROLD-MENDE, C. & RADLWIMMER, B. 2009. Genomic and expression profiling of glioblastoma stem cell-like spheroid cultures identifies novel tumor-relevant genes associated with survival. *Clin Cancer Res*, 15, 6541-50.
- ESCHRICH, S. A., FULP, W. J., PAWITAN, Y., FOEKENS, J. A., SMID, M., MARTENS, J. W., ECHEVARRIA, M., KAMATH, V., LEE, J. H., HARRIS, E. E., BERGH, J. & TORRES-ROCA, J. F. 2012. Validation of a radiosensitivity molecular signature in breast cancer. *Clin Cancer Res*, 18, 5134-43.
- ESCHRICH, S. A., PRAMANA, J., ZHANG, H., ZHAO, H., BOULWARE, D., LEE, J. H., BLOOM, G., ROCHA-LIMA, C., KELLEY, S., CALVIN, D. P., YEATMAN, T. J., BEGG, A. C. & TORRES-ROCA, J. F. 2009. A gene expression model of intrinsic tumor radiosensitivity: prediction of response and prognosis after chemoradiation. *Int J Radiat Oncol Biol Phys*, 75, 489-96.
- ESSERS, J., VAN STEEG, H., DE WIT, J., SWAGEMAKERS, S. M., VERMEIJ, M., HOEIJMAKERS, J. H. & KANAAR, R. 2000. Homologous and non-homologous recombination differentially affect DNA damage repair in mice. *EMBO J*, 19, 1703-10.
- FADOK, V. A., DE CATHELINAEU, A., DALEKE, D. L., HENSON, P. M. & BRATTON, D. L. 2001. Loss of phospholipid asymmetry and surface exposure of phosphatidylserine is required for phagocytosis of apoptotic cells by macrophages and fibroblasts. *J Biol Chem*, 276, 1071-7.
- FARRAR, J. T., PORTENOY, R. K., BERLIN, J. A., KINMAN, J. L. & STROM, B. L. 2000. Defining the clinically important difference in pain outcome measures. *Pain*, 88, 287-94.
- FEDERICO, R., ADOLFO, F., GIUSEPPE, M., LORENZO, S., MARTINO, D. T., ANNA, C., ADRIANO, P., GINO, C., FRANCESCA, R., MATTEO, C., GBENGA, K., PAOLO, M. & FRANCESCO, F. 2013. Phase II trial of neoadjuvant pemetrexed plus cisplatin followed by surgery and radiation in the treatment of pleural mesothelioma. *BMC Cancer*, 13, 22.
- FENNELL, D. A. & RUDD, R. M. 2004. Defective core-apoptosis signalling in diffuse malignant pleural mesothelioma: opportunities for effective drug development. *Lancet Oncol*, 5, 354-62.
- FERTIL, B., DERTINGER, H., COURDI, A. & MALAISE, E. P. 1984. Mean inactivation dose: a useful concept for intercomparison of human cell survival curves. *Radiat Res*, 99, 73-84.
- FLEMING, C., CAGNEY, D. N., O'KEEFFE, S., BRENNAN, S. M., ARMSTRONG, J. G. & MCCLEAN, B. Normal tissue considerations and dose volume constraints in the moderately hypofractionated treatment of non-small cell lung cancer. *Radiotherapy and Oncology*, 119, 423-431.
- FLORES, R. M., PASS, H. I., SESHAN, V. E., DYCOCO, J., ZAKOWSKI, M., CARBONE, M., BAINS, M. S. & RUSCH, V. W. 2008. Extrapleural pneumonectomy versus pleurectomy/decortication in the surgical management of malignant pleural mesothelioma: Results in 663 patients. *Journal of Thoracic and Cardiovascular Surgery*, 135, 620-6.

- FOGLIATA, A., REGGIORI, G., STRAVATO, A., LOBEFALO, F., FRANZESE, C., FRANCESCHINI, D., TOMATIS, S., MANCOSU, P., SCORSETTI, M. & COZZI, L. 2017. RapidPlan head and neck model: the objectives and possible clinical benefit. *Radiation Oncology*, 12, 73.
- FORKER, L. J., CHOUDHURY, A. & KILTIE, A. E. 2015. Biomarkers of Tumour Radiosensitivity and Predicting Benefit from Radiotherapy. *Clinical Oncology*, 27, 561-569.
- FORSSELL, G. 1910. Quelques observations de radiumthérapie de tumeurs cancéreuses. *Arch d'Electr Med Exper et Cliniques*, 18, 801-802.
- FOWLER, J., CHAPPELL, R. & RITTER, M. 2001. Is alpha/beta for prostate tumors really low? *Int J Radiat Oncol Biol Phys*, 50, 1021-31.
- FOWLER, J. F. 1983. Dose response curves for organ function or cell survival. *Br J Radiol*, 56, 497-500.
- FOWLER, J. F. 1992. Brief summary of radiobiological principles in fractionated radiotherapy. *Seminars in Radiation Oncology*, 2, 16-21.
- FRACASSO, G. & COLOMBATTI, M. 2000. Effect of therapeutic macromolecules in spheroids. *Crit Rev Oncol Hematol*, 36, 159-78.
- FRANCIS, R. J., SEGARD, T., MORANDEAU, L., LEE, Y. C., MILLWARD, M. J., SEGAL, A. & NOWAK, A. K. 2015. Characterization of hypoxia in malignant pleural mesothelioma with FMISO PET-CT. *Lung Cancer*, 90, 55-60.
- FRITZ, P., WEBER, K. J., FRANK, C. & FLENTJE, M. 1996. Differential effects of dose rate and superfractionation on survival and cell cycle of V79 cells from spheroid and monolayer culture. *Radiother Oncol*, 39, 73-9.
- GARTEL, A. L. 2005. The conflicting roles of the cdk inhibitor p21(CIP1/WAF1) in apoptosis. *Leuk Res*, 29, 1237-8.
- GAYLORD, H. R. & CLOWES, G. H. A. 1906. On spontaneous cure of cancer. *Surg. Gynecol. Obstet.*, 2, 633-658.
- GEMBA, K., FUJIMOTO, N., AOE, K., KATO, K., TAKESHIMA, Y., INAI, K. & KISHIMOTO, T. 2013. Treatment and survival analyses of malignant mesothelioma in Japan. *Acta Oncologica*, 52, 803-808.
- GENE, E. TOP3B DNA topoisomerase III beta *Entrez Gene*.
- GHATTASS, K., ASSAH, R., EL-SABBAN, M. & GALI-MUHTASIB, H. 2013. Targeting hypoxia for sensitization of tumors to radio- and chemotherapy. *Curr Cancer Drug Targets*, 13, 670-85.
- GILL, R. R., UMEOKA, S., MAMATA, H., TILLEMANN, T. R., STANWELL, P., WOODHAMS, R., PADERA, R. F., SUGARBAKER, D. J. & HATABU, H. 2010. Diffusion-weighted MRI of malignant pleural mesothelioma: preliminary assessment of apparent diffusion coefficient in histologic subtypes. *AJR Am J Roentgenol*, 195, W125-30.
- GIRAUD, P. & HOULE, A. 2013. Respiratory Gating for Radiotherapy: Main Technical Aspects and Clinical Benefits. *ISRN Pulmonology*, 2013, 13.
- GIRAUD, P., SYLVESTRE, A., ZEFKILI, S., LISBONA, A., BONNETTE, P., LE PIMPEC BARTHES, F., PARIS, E., PERIGAUD, C., SAVIGNONI, A. & MAHE, M. A. 2011. Helical tomotherapy for resected malignant pleural mesothelioma: dosimetric evaluation and toxicity. *Radiother Oncol*, 101, 303-6.
- GLIMELIUS, B., TIRET, E., CERVANTES, A., ARNOLD, D. & GROUP, O. B. O. T. E. G. W. 2013. Rectal cancer: ESMO Clinical Practice Guidelines for diagnosis, treatment and follow-up†. *Annals of Oncology*, 24, vi81-vi88.
- GODIN-ETHIER, J., HANAFLI, L. A., PICCIRILLO, C. A. & LAPOINTE, R. 2011. Indoleamine 2,3-dioxygenase expression in human cancers: clinical and immunologic perspectives. *Clin Cancer Res*, 17, 6985-91.
- GOMEZ-ROMAN, N., STEVENSON, K., GILMOUR, L., HAMILTON, G. & CHALMERS, A. J. 2017. A novel 3D human glioblastoma cell culture system for modeling drug and radiation responses. *Neuro Oncol*, 19, 229-241.
- GOMEZ, D. R., RIMNER, A., SIMONE, C. B., 2ND, CHO, B. C. J., DE PERROT, M., ADJEI, A. A., BUENO, R., GILL, R. R., HARPOLE, D. H., JR., HESDORFFER, M., HIRSCH, F. R., JACKSON, A. A., PASS, H. I., RICE, D. C., RUSCH, V. W., TSAO, A. S., YORKE, E. & ROSENZWEIG, K. 2019. The Use of Radiation Therapy for the Treatment of Malignant Pleural Mesothelioma: Expert Opinion

- from the National Cancer Institute Thoracic Malignancy Steering Committee, International Association for the Study of Lung Cancer, and Mesothelioma Applied Research Foundation. *J Thorac Oncol*, 14, 1172-1183.
- GOODHEAD, D. T. 1994. Initial events in the cellular effects of ionizing radiations: clustered damage in DNA. *Int J Radiat Biol*, 65, 7-17.
- GRANDE, G. E. & TODD, C. J. 2000. Why are trials in palliative care so difficult? *Palliat Med*, 14, 69-74.
- GRAY, L. H., CONGER, A. D., EBERT, M., HORNSEY, S. & SCOTT, O. C. 1953. The concentration of oxygen dissolved in tissues at the time of irradiation as a factor in radiotherapy. *Br J Radiol*, 26, 638-48.
- GROSSO, F., STEELE, N., NOVELLO, S., NOWAK, A. K., POPAT, S., GREILLIER, L., JOHN, T., LEIGHL, N. B., RECK, M., TAYLOR, P., PLANCHARD, D., SØRENSEN, J. B., SOCINSKI, M. A., WANGENHEIM, U. V., LOEMBÉ, A. B., BARRUECO, J., MORSLI, N. & SCAGLIOTTI, G. 2017. Nintedanib Plus Pemetrexed/Cisplatin in Patients With Malignant Pleural Mesothelioma: Phase II Results From the Randomized, Placebo-Controlled LUME-Meso Trial. *Journal of Clinical Oncology*, 35, 3591-3600.
- GUO, G., CHMIELECKI, J., GOPARAJU, C., HEGUY, A., DOLGALEV, I., CARBONE, M., SEEPO, S., MEYERSON, M. & PASS, H. I. 2015. Whole-exome sequencing reveals frequent genetic alterations in BAP1, NF2, CDKN2A, and CUL1 in malignant pleural mesothelioma. *Cancer Res*, 75, 264-9.
- GUPTA, V., KRUG, L. M., LASER, B., HUDKA, K., FLORES, R., RUSCH, V. W. & ROSENZWEIG, K. E. 2009. Patterns of local and nodal failure in malignant pleural mesothelioma after extrapleural pneumonectomy and photon-electron radiotherapy. *J Thorac Oncol*, 4, 746-50.
- HAKKINEN, A. M., LAASONEN, A., LINNAINMAA, K., MATTSON, K. & PYRHONEN, S. 1996. Radiosensitivity of mesothelioma cell lines. *Acta Oncol*, 35, 451-6.
- HALL, E. J. 1973. *Radiobiology for the radiologist*, Hagerstown, Md. : Medical Dept., Harper & Row, [1973] ©1973.
- HAN, Z., CHATTERJEE, D., EARLY, J., PANTAZIS, P., HENDRICKSON, E. A. & WYCHE, J. H. 1996. Isolation and characterization of an apoptosis-resistant variant of human leukemia HL-60 cells that has switched expression from Bcl-2 to Bcl-xL. *Cancer Res*, 56, 1621-8.
- HANAHAAN, D. & WEINBERG, R. A. 2000. The hallmarks of cancer. *Cell*, 100, 57-70.
- HANNA, G. G., MCDONALD, F., MURRAY, L., HARROW, S., LANDAU, D., AHMED, M. & FRANKS, K. N. 2018. UK Consensus on Normal Tissue Dose Constraints for Stereotactic Radiotherapy: Reply to Ghafoor et al. *Clin Oncol (R Coll Radiol)*, 30, 456.
- HASANI, A., ALVAREZ, J. M., WYATT, J. M., BYDDER, S., MILLWARD, M., BYRNE, M., MUSK, A. W. & NOWAK, A. K. 2009. Outcome for patients with malignant pleural mesothelioma referred for Trimodality therapy in Western Australia. *J Thorac Oncol*, 4, 1010-6.
- HASEGAWA, S., OKADA, M., TANAKA, F., YAMANAKA, T., SOEJIMA, T., KAMIKONYA, N., TSUJIMURA, T., FUKUOKA, K., YOKOI, K. & NAKANO, T. 2016. Trimodality strategy for treating malignant pleural mesothelioma: results of a feasibility study of induction pemetrexed plus cisplatin followed by extrapleural pneumonectomy and postoperative hemithoracic radiation (Japan Mesothelioma Interest Group 0601 Trial). *Int J Clin Oncol*, 21, 523-30.
- HASLETT, K., FRANKS, K., HANNA, G. G., HARDEN, S., HATTON, M., HARROW, S., MCDONALD, F., ASHCROFT, L., FALK, S., GROOM, N., HARRIS, C., MCCLOSKEY, P., WHITEHURST, P., BAYMAN, N. & FAIVRE-FINN, C. 2016. Protocol for the isotoxic intensity modulated radiotherapy (IMRT) in stage III non-small cell lung cancer (NSCLC): a feasibility study. *BMJ Open*, 6, e010457.
- HASSAN, R., SHARON, E., THOMAS, A., ZHANG, J., LING, A., MIETTINEN, M., KREITMAN, R. J., STEINBERG, S. M., HOLLEVOET, K. & PASTAN, I. 2014. Phase 1 study of the antimesothelin immunotoxin SS1P in combination with pemetrexed and cisplatin for front-line therapy of pleural mesothelioma and correlation of tumor response with serum mesothelin, megakaryocyte potentiating factor, and cancer antigen 125. *Cancer*, 120, 3311-9.

- HE, F., LI, L., KIM, D., WEN, B., DENG, X., GUTIN, P. H., LING, C. C. & LI, G. C. 2007. Adenovirus-mediated expression of a dominant negative Ku70 fragment radiosensitizes human tumor cells under aerobic and hypoxic conditions. *Cancer Res*, 67, 634-42.
- HEELAN, R. T., RUSCH, V. W., BEGG, C. B., PANICEK, D. M., CARAVELLI, J. F. & EISEN, C. 1999. Staging of malignant pleural mesothelioma: Comparison of CT and MR imaging. *American Journal of Roentgenology*, 172, 1039-1047.
- HEHLGANS, S., EKE, I., DEUSE, Y. & CORDES, N. 2008. Integrin-linked kinase: Dispensable for radiation survival of three-dimensionally cultured fibroblasts. *Radiotherapy and Oncology*, 86, 329-335.
- HELOU, J., CLEMENT-COLMOU, K., SYLVESTRE, A., CAMPION, L., AMESSIS, M., ZEFKILI, S., RAPHAEL, J., BONNETTE, P., LE PIMPEC BARTHES, F., PERIGAUD, C., MAHE, M. A. & GIRAUD, P. 2013. [Helical tomotherapy in the treatment of malignant pleural mesothelioma: The impact of low doses on pulmonary and oesophageal toxicity]. *Cancer Radiother*, 17, 755-62.
- HENDERSON, D. W., REID, G., KAO, S. C., VAN ZANDWIJK, N. & KLEBE, S. 2013. Challenges and controversies in the diagnosis of malignant mesothelioma: Part 2. Malignant mesothelioma subtypes, pleural synovial sarcoma, molecular and prognostic aspects of mesothelioma, BAP1, aquaporin-1 and microRNA. *Journal of Clinical Pathology*, 66, 854.
- HENNESSY, E. J. 2016. Selective inhibitors of Bcl-2 and Bcl-xL: Balancing antitumor activity with on-target toxicity. *Bioorg Med Chem Lett*, 26, 2105-14.
- HERNDON, J. E., GREEN, M. R., CHAHINIAN, A. P., CORSON, J. M., SUZUKI, Y. & VOGELZANG, N. J. 1998. Factors predictive of survival among 337 patients with mesothelioma treated between 1984 and 1994 by the Cancer and Leukemia Group B. *Chest*, 113, 723-31.
- HERSKOVIC, A., MARTZ, K., AL-SARRAF, M., LEICHMAN, L., BRINDLE, J., VAITKEVICIUS, V., COOPER, J., BYHARDT, R., DAVIS, L. & EMAMI, B. 1992. Combined chemotherapy and radiotherapy compared with radiotherapy alone in patients with cancer of the esophagus. *N Engl J Med*, 326, 1593-8.
- HIDA, T., MATSUMOTO, S., HAMASAKI, M., KAWAHARA, K., TSUJIMURA, T., HIROSHIMA, K., KAMEI, T., TAGUCHI, K., IWASAKI, A., ODA, Y., HONDA, H. & NABESHIMA, K. 2015. Deletion status of p16 in effusion smear preparation correlates with that of underlying malignant pleural mesothelioma tissue. *Cancer Science*, 106, 1635-1641.
- HIGGINS, K. A., O'CONNELL, K., LIU, Y., GILLESPIE, T. W., MCDONALD, M. W., PILLAI, R. N., PATEL, K. R., PATEL, P. R., ROBINSON, C. G., SIMONE, C. B., 2ND, OWONIKOKO, T. K., BELANI, C. P., KHURI, F. R., CURRAN, W. J., RAMALINGAM, S. S. & BEHERA, M. 2017. National Cancer Database Analysis of Proton Versus Photon Radiation Therapy in Non-Small Cell Lung Cancer. *Int J Radiat Oncol Biol Phys*, 97, 128-137.
- HILL-KAYSER, C. E., AVERY, S., MESINA, C. F., JAMES, P., FRIEDBERG, J. S., CENGEL, K., LIN, L. L., HAHN, S. M. & RENGAN, R. 2009. Hemithoracic radiotherapy after extrapleural pneumonectomy for malignant pleural mesothelioma: a dosimetric comparison of two well-described techniques. *J Thorac Oncol*, 4, 1431-7.
- HILL, M. M., ADRAIN, C., DURIEZ, P. J., CREAGH, E. M. & MARTIN, S. J. 2004. Analysis of the composition, assembly kinetics and activity of native Apaf-1 apoptosomes. *EMBO J*, 23, 2134-45.
- HODAPP, N. 2012. [The ICRU Report 83: prescribing, recording and reporting photon-beam intensity-modulated radiation therapy (IMRT)]. *Strahlenther Onkol*, 188, 97-9.
- HODGSON, J. T. & DARNTON, A. 2000. The quantitative risks of mesothelioma and lung cancer in relation to asbestos exposure. *Annals of Occupational Hygiene*, 44, 565-601.
- HONG, S. & WANG, Y. 2007. A three-outcome design for randomized comparative phase II clinical trials. *Stat Med*, 26, 3525-34.
- HOPEWELL, J. W., NYMAN, J. & TURESSON, I. 2003. Time factor for acute tissue reactions following fractionated irradiation: a balance between repopulation and enhanced radiosensitivity. *Int J Radiat Biol*, 79, 513-24.
- HORNSEY, S. 1970. Differences in survival of jejunal crypt cells after radiation delivered at different dose-rates. *Br J Radiol*, 43, 802-6.

- HORWICH, A., PARKER, C., DE REIJK, T., KATAJA, V. & GROUP, O. B. O. T. E. G. W. 2013. Prostate cancer: ESMO Clinical Practice Guidelines for diagnosis, treatment and follow-up†. *Annals of Oncology*, 24, vi106-vi114.
- HOWEL, D., ARBLASTER, L., SWINBURNE, L., SCHWEIGER, M., RENVOIZE, E. & HATTON, P. 1997. Routes of asbestos exposure and the development of mesothelioma in an English region. *Occup Environ Med*, 54, 403-9.
- HUSSEIN, M., SOUTH, C. P., BARRY, M. A., ADAMS, E. J., JORDAN, T. J., STEWART, A. J. & NISBET, A. 2016. Clinical validation and benchmarking of knowledge-based IMRT and VMAT treatment planning in pelvic anatomy. *Radiotherapy and Oncology*, 120, 473-479.
- INAI, K. 2008. Pathology of mesothelioma. *Environmental health and preventive medicine*, 13, 60-64.
- INOUE-YAMAUCHI, A., JENG, P. S., KIM, K., CHEN, H. C., HAN, S., GANESAN, Y. T., ISHIZAWA, K., JEBIWOTT, S., DONG, Y., PIETANZA, M. C., HELLMANN, M. D., KRIS, M. G., HSIEH, J. J. & CHENG, E. H. 2017. Targeting the differential addiction to anti-apoptotic BCL-2 family for cancer therapy. *Nat Commun*, 8, 16078.
- JACKSON, M. R., ASHTON, M., KOESSINGER, A. L., DICK, C., VERHEIJ, M. & CHALMERS, A. J. 2020. Mesothelioma Cells Depend on the Antiapoptotic Protein Bcl-xL for Survival and Are Sensitized to Ionizing Radiation by BH3-Mimetics. *Int J Radiat Oncol Biol Phys*, 106, 867-877.
- JACKSON, S. P. 2002. Sensing and repairing DNA double-strand breaks. *Carcinogenesis*, 23, 687-696.
- JASSEM, J., RAMLAU, R., SANTORO, A., SCHUETTE, W., CHEMAISSANI, A., HONG, S., BLATTER, J., ADACHI, S., HANAUSKE, A. & MANEGOLD, C. 2008. Phase III Trial of Pemetrexed Plus Best Supportive Care Compared With Best Supportive Care in Previously Treated Patients With Advanced Malignant Pleural Mesothelioma. *Journal of Clinical Oncology*, 26, 1698-1704.
- JAU RAND, M. C. 1997. Mechanisms of fiber-induced genotoxicity. *Environ Health Perspect*, 105 Suppl 5, 1073-84.
- JAU RAND, M. C. & FLEURY-FEITH, J. 2005. Pathogenesis of malignant pleural mesothelioma. *Respirology*, 10, 2-8.
- JAU RAND, M. C., KAPLAN, H., THIO LLET, J., PINCHON, M. C., BERNAUDIN, J. F. & BIGNON, J. 1979. Phagocytosis of chrysotile fibers by pleural mesothelial cells in culture. *The American journal of pathology*, 94, 529-538.
- JENKINS, P., MILLINER, R. & SALMON, C. 2011. Re-evaluating the role of palliative radiotherapy in malignant pleural mesothelioma. *European Journal of Cancer*, 47, 2143-2149.
- JOHNSTONE, R. W., RUEFLI, A. A. & LOWE, S. W. 2002. Apoptosis: a link between cancer genetics and chemotherapy. *Cell*, 108, 153-64.
- JOINER, M. & VAN DER KOGEL, A. 2009. Basic Clinical Radiobiology. CRC Press.
- KAAIJK, P., TROOST, D., SMINIA, P., HULSHOF, M. C., VAN DER KRACHT, A. H., LEENSTRA, S. & BOSCH, D. A. 1997. Hypofractionated radiation induces a decrease in cell proliferation but no histological damage to organotypic multicellular spheroids of human glioblastomas. *Eur J Cancer*, 33, 645-51.
- KALLIO, P. J., PONGRATZ, I., GRADIN, K., MCGUIRE, J. & POELLINGER, L. 1997. Activation of hypoxia-inducible factor 1alpha: posttranscriptional regulation and conformational change by recruitment of the Arnt transcription factor. *Proceedings of the National Academy of Sciences of the United States of America*, 94, 5667-5672.
- KAMRAN, S. C., MUELLER, B. S., PAETZOLD, P., DUNLAP, J., NIEMIERKO, A., BORTFELD, T., WILLERS, H. & CRAFT, D. 2016. Multi-criteria optimization achieves superior normal tissue sparing in a planning study of intensity-modulated radiation therapy for RTOG 1308-eligible non-small cell lung cancer patients. *Radiother Oncol*, 118, 515-20.
- KARCZMAREK-BOROWSKA, B., FILIP, A., WOJCIEROWSKI, J., SMOLEN, A., KOROBOWICZ, E., KORSZEN-PILECKA, I. & ZDUNEK, M. 2006. Estimation of prognostic value of Bcl-xL gene expression in non-small cell lung cancer. *Lung Cancer*, 51, 61-9.
- KATADA, H., HIGASHIGUCHI, R., MARUYAMA, H., EMI, Y., YOKOSE, Y., TAKAHASHI, S., MIKAMI, R. & KONISHI, Y. 1983. Effects of chrysotile asbestos on lung and pleural carcinogenesis of N-bis(2-hydroxypropyl)nitrosamine in rats. *Cancer Lett*, 17, 313-20.

- KAUR, G. & DUFOUR, J. M. 2012. Cell lines: Valuable tools or useless artifacts. *Spermatogenesis*, 2, 1-5.
- KAWASHIMA, M., OZAWA, S., HAGA, A., SAKUMI, A., KUROKAWA, C., SUGIMOTO, S., KARASAWA, K., NAKAGAWA, K. & SASAI, K. 2013. Comparison of total MU and segment areas in VMAT and step-and-shoot IMRT plans. *Radiol Phys Technol*, 6, 14-20.
- KELLAND, L. R. & BINGLE, L. 1988. Radiosensitivity and characterisation of a newly established cell line from an epithelioid sarcoma. *Br J Cancer*, 58, 322-5.
- KELLERER, A. M. & HUG, O. 1972. Theory of dose-effect relations. *Encyclopedia of Medical Radiology*, 2, 1-42.
- KETTUNEN, E., NISSEN, A. M., OLLIKAINEN, T., TAAVITSAINEN, M., TAPPER, J., MATTSON, K., LINNAINMAA, K., KNUUTILA, S. & EL-RIFAI, W. 2001. Gene expression profiling of malignant mesothelioma cell lines: cDNA array study. *Int J Cancer*, 91, 492-6.
- KIERKELS, R. G. J., VISSER, R., BIJL, H. P., LANGENDIJK, J. A., VAN 'T VELD, A. A., STEENBAKKERS, R. J. H. M. & KOREVAAR, E. W. 2015. Multicriteria optimization enables less experienced planners to efficiently produce high quality treatment plans in head and neck cancer radiotherapy. *Radiation Oncology*, 10, 87.
- KIM, H., PHUNG, Y. & HO, M. 2012. Changes in global gene expression associated with 3D structure of tumors: an ex vivo matrix-free mesothelioma spheroid model. *PLoS One*, 7, e39556.
- KIM, K. U., WILSON, S. M., ABAYASIRIWARDANA, K. S., COLLINS, R., FJELLBIRKELAND, L., XU, Z., JABLONS, D. M., NISHIMURA, S. L. & BROADDUS, V. C. 2005. A novel in vitro model of human mesothelioma for studying tumor biology and apoptotic resistance. *Am J Respir Cell Mol Biol*, 33, 541-8.
- KIRSCHNER, M. B., PULFORD, E., HODA, M. A., ROZSAS, A., GRIGGS, K., CHENG, Y. Y., EDELMAN, J. J. B., KAO, S. C., HYLAND, R., DONG, Y. W., LASZLO, V., KLIKOVITS, T., VALLELY, M. P., GRUSCH, M., HEGEDUS, B., DOME, B., KLEPETKO, W., VAN ZANDWIJK, N., KLEBE, S. & REID, G. 2015. Fibulin-3 levels in malignant pleural mesothelioma are associated with prognosis but not diagnosis. *British Journal of Cancer*, 113, 963-969.
- KITAMURA, F., ARAKI, S., SUZUKI, Y., YOKOYAMA, K., TANIGAWA, T. & IWASAKI, R. 2002. Assessment of the mutations of p53 suppressor gene and Ha- and Ki-ras oncogenes in malignant mesothelioma in relation to asbestos exposure: a study of 12 American patients. *Ind Health*, 40, 175-81.
- KOBAYASHI, H., MAN, S., GRAHAM, C. H., KAPITAIN, S. J., TEICHER, B. A. & KERBEL, R. S. 1993. Acquired multicellular-mediated resistance to alkylating agents in cancer. *Proc Natl Acad Sci U S A*, 90, 3294-8.
- KOCHAN, J. A., DESCLOS, E. C. B., BOSCH, R., MEISTER, L., VRIEND, L. E. M., VAN ATTIKUM, H. & KRAWCZYK, P. M. 2017. Meta-analysis of DNA double-strand break response kinetics. *Nucleic acids research*, 45, 12625-12637.
- KONDO, S., SHINOMURA, Y., KANAYAMA, S., HIGASHIMOTO, Y., KIYOHARA, T., ZUSHI, S., KITAMURA, S., UEYAMA, H. & MATSUZAWA, Y. 1998. Modulation of apoptosis by endogenous Bcl-xL expression in MKN-45 human gastric cancer cells. *Oncogene*, 17, 2585-91.
- KONG, F.-M., RITTER, T., QUINT, D. J., SENAN, S., GASPAR, L. E., KOMAKI, R. U., HURKMANS, C. W., TIMMERMAN, R., BEZJAK, A., BRADLEY, J. D., MOVSAS, B., MARSH, L., OKUNIEFF, P., CHOY, H. & CURRAN, W. J. 2011. Consideration of Dose Limits for Organs at Risk of Thoracic Radiotherapy: Atlas for Lung, Proximal Bronchial Tree, Esophagus, Spinal Cord, Ribs, and Brachial Plexus. *International Journal of Radiation Oncology*Biophysics*, 81, 1442-1457.
- KRAYENBUEHL, J., DIMMERLING, P., CIERNIK, I. F. & RIESTERER, O. 2014. Clinical outcome of postoperative highly conformal versus 3D conformal radiotherapy in patients with malignant pleural mesothelioma. *Radiat Oncol*, 9, 32.
- KRAYENBUEHL, J., HARTMANN, M., LOMAX, A. J., KLOECK, S., HUG, E. B. & CIERNIK, I. F. 2010. Proton Therapy for Malignant Pleural Mesothelioma After Extrapleural Pleuropneumectomy. *International Journal of Radiation Oncology*Biophysics*, 78, 628-634.

- KRAYENBUEHL, J., OERTEL, S., DAVIS, J. B. & CIERNIK, I. F. 2007. Combined photon and electron three-dimensional conformal versus intensity-modulated radiotherapy with integrated boost for adjuvant treatment of malignant pleural mesothelioma after pleuropneumectomy. *Int J Radiat Oncol Biol Phys*, 69, 1593-9.
- KRUG, L. M., KINDLER, H. L., CALVERT, H., MANEGOLD, C., TSAO, A. S., FENNELL, D., ÖHMAN, R., PLUMMER, R., EBERHARDT, W. E. E., FUKUOKA, K., GAAFAR, R. M., LAFITTE, J.-J., HILLERDAL, G., CHU, Q., BUIKHUISEN, W. A., LUBINIECKI, G. M., SUN, X., SMITH, M. & BAAS, P. 2015. Vorinostat in patients with advanced malignant pleural mesothelioma who have progressed on previous chemotherapy (VANTAGE-014): a phase 3, double-blind, randomised, placebo-controlled trial. *The Lancet Oncology*, 16, 447-456.
- KRUG, L. M., PASS, H. I., RUSCH, V. W., KINDLER, H. L., SUGARBAKER, D. J., ROSENZWEIG, K. E., FLORES, R., FRIEDBERG, J. S., PISTERS, K., MONBERG, M., OBASAJU, C. K. & VOGELZANG, N. J. 2009. Multicenter phase II trial of neoadjuvant pemetrexed plus cisplatin followed by extrapleural pneumonectomy and radiation for malignant pleural mesothelioma. *J Clin Oncol*, 27, 3007-13.
- KUO, L. J. & YANG, L. X. 2008. Gamma-H2AX - a novel biomarker for DNA double-strand breaks. *In Vivo*, 22, 305-9.
- KURIMASA, A., OUYANG, H., DONG, L. J., WANG, S., LI, X., CORDON-CARDO, C., CHEN, D. J. & LI, G. C. 1999. Catalytic subunit of DNA-dependent protein kinase: impact on lymphocyte development and tumorigenesis. *Proc Natl Acad Sci U S A*, 96, 1403-8.
- LAW, M. R., GREGOR, A., HODSON, M. E., BLOOM, H. J. & TURNER-WARWICK, M. 1984. Malignant mesothelioma of the pleura: a study of 52 treated and 64 untreated patients. *Thorax*, 39, 255-9.
- LEAHY, J. J., GOLDING, B. T., GRIFFIN, R. J., HARDCASTLE, I. R., RICHARDSON, C., RIGOREAU, L. & SMITH, G. C. 2004. Identification of a highly potent and selective DNA-dependent protein kinase (DNA-PK) inhibitor (NU7441) by screening of chromenone libraries. *Bioorg Med Chem Lett*, 14, 6083-7.
- LEE, H., ZENG, J., BOWEN, S. R. & RENGAN, R. 2017. Proton Therapy for Malignant Pleural Mesothelioma: A Three Case Series Describing the Clinical and Dosimetric Advantages of Proton-Based Therapy. *Cureus*, 9, e1705-e1705.
- LEE, S. W., CHO, K. J., PARK, J. H., KIM, S. Y., NAM, S. Y., LEE, B. J., KIM, S. B., CHOI, S. H., KIM, J. H., AHN, S. D., SHIN, S. S., CHOI, E. K. & YU, E. 2005. Expressions of Ku70 and DNA-PKcs as prognostic indicators of local control in nasopharyngeal carcinoma. *Int J Radiat Oncol Biol Phys*, 62, 1451-7.
- LEES-MILLER, S. P. & MEEK, K. 2003. Repair of DNA double strand breaks by non-homologous end joining. *Biochimie*, 85, 1161-73.
- LEITH, J. T., QUARANTO, L., PADFIELD, G., MICHELSON, S. & HERCBERGS, A. 1993. Radiobiological studies of PC-3 and DU-145 human prostate cancer cells: x-ray sensitivity in vitro and hypoxic fractions of xenografted tumors in vivo. *Int J Radiat Oncol Biol Phys*, 25, 283-7.
- LEKSELL, L. 1951. The stereotaxic method and radiosurgery of the brain. *Acta Chir Scand*, 102, 316-9.
- LETAI, A. G. 2008. Diagnosing and exploiting cancer's addiction to blocks in apoptosis. *Nat Rev Cancer*, 8, 121-32.
- LEUNG, A. N., MULLER, N. L. & MILLER, R. R. 1990. CT IN DIFFERENTIAL-DIAGNOSIS OF DIFFUSE PLEURAL DISEASE. *American Journal of Roentgenology*, 154, 487-492.
- LEVERSON, J. D., PHILLIPS, D. C., MITTEN, M. J., BOGHAERT, E. R., DIAZ, D., TAHIR, S. K., BELMONT, L. D., NIMMER, P., XIAO, Y., MA, X. M., LOWES, K. N., KOVAR, P., CHEN, J., JIN, S., SMITH, M., XUE, J., ZHANG, H., OLEKSIJEV, A., MAGOC, T. J., VAIDYA, K. S., ALBERT, D. H., TARRANT, J. M., LA, N., WANG, L., TAO, Z. F., WENDT, M. D., SAMPATH, D., ROSENBERG, S. H., TSE, C., HUANG, D. C., FAIRBROTHER, W. J., ELMORE, S. W. & SOUERS, A. J. 2015. Exploiting selective BCL-2 family inhibitors to dissect cell survival dependencies and define improved strategies for cancer therapy. *Sci Transl Med*, 7, 279ra40.
- LI, J.-Y., LI, Y.-Y., JIN, W., YANG, Q., SHAO, Z.-M. & TIAN, X.-S. 2012. ABT-737 reverses the acquired radioresistance of breast cancer cells by targeting Bcl-2 and Bcl-xL. *Journal of Experimental & Clinical Cancer Research*, 31, 102.

- LILFORD, R. J., THORNTON, J. G. & BRAUNHOLTZ, D. 1995. Clinical trials and rare diseases: a way out of a conundrum. *BMJ*, 311, 1621-5.
- LIM, E. 2016. 195 A feasibility study comparing (extended) pleurectomy decortication versus no pleurectomy decortication in the multimodality management of patients with malignant pleural mesothelioma: the MARS 2 study. *Lung Cancer*, 91, S71.
- LINDEN, C. J., MERCKE, C., ALBRECHTSSON, U., JOHANSSON, L. & EWERS, S. B. 1996. Effect of hemithorax irradiation alone or combined with doxorubicin and cyclophosphamide in 47 pleural mesotheliomas: a nonrandomized phase II study. *European Respiratory Journal*, 9, 2565.
- LING, C. C., YORKE, E., AMOLS, H., MECHALAKOS, J., ERDI, Y., LEIBEL, S., ROSENZWEIG, K. & JACKSON, A. 2004. High-tech will improve radiotherapy of NSCLC: A hypothesis waiting to be validated. *International Journal of Radiation Oncology*Biophysics*Physics*, 60, 3-7.
- LIU, W., BODLE, E., CHEN, J. Y., GAO, M., ROSEN, G. D. & BROADDUS, V. C. 2001. Tumor necrosis factor-related apoptosis-inducing ligand and chemotherapy cooperate to induce apoptosis in mesothelioma cell lines. *Am J Respir Cell Mol Biol*, 25, 111-8.
- LIU, W., ERNST, J. D. & BROADDUS, V. C. 2000. Phagocytosis of crocidolite asbestos induces oxidative stress, DNA damage, and apoptosis in mesothelial cells. *Am J Respir Cell Mol Biol*, 23, 371-8.
- LO, S. S., SAHGAL, A., CHANG, E. L., MAYR, N. A., TEH, B. S., HUANG, Z., SCHEFTER, T. E., YAO, M., MACHTAY, M., SLOTMAN, B. J. & TIMMERMAN, R. D. 2013. Serious complications associated with stereotactic ablative radiotherapy and strategies to mitigate the risk. *Clin Oncol (R Coll Radiol)*, 25, 378-87.
- LOPEZ-RIOS, F., ILLEI, P. B., RUSCH, V. & LADANYI, M. 2004. Evidence against a role for SV40 infection in human mesotheliomas and high risk of false-positive PCR results owing to presence of SV40 sequences in common laboratory plasmids. *Lancet*, 364, 1157-66.
- LOW, E. M., KHOURY, G. G., MATTHEWS, A. W. & NEVILLE, E. 1995. Prevention of tumour seeding following thoracoscopy in mesothelioma by prophylactic radiotherapy. *Clin Oncol (R Coll Radiol)*, 7, 317-8.
- LÜTGENDORF-CAUCIG, C., FOTINA, I., STOCK, M., PÖTTER, R., GOLDNER, G. & GEORG, D. 2011. Feasibility of CBCT-based target and normal structure delineation in prostate cancer radiotherapy: multi-observer and image multi-modality study. *Radiother Oncol*, 98, 154-61.
- LUTZ, S. T., JONES, J. & CHOW, E. 2014. Role of radiation therapy in palliative care of the patient with cancer. *J Clin Oncol*, 32, 2913-9.
- MAASILTA, P. 1991. Deterioration in lung function following hemithorax irradiation for pleural mesothelioma. *Int J Radiat Oncol Biol Phys*, 20, 433-8.
- MACLEOD, N., CHALMERS, A., O'ROURKE, N., MOORE, K., SHERIDAN, J., MCMAHON, L., BRAY, C., STOBO, J., PRICE, A., FALLON, M. & LAIRD, B. J. 2015a. Is Radiotherapy Useful for Treating Pain in Mesothelioma?: A Phase II Trial. *J Thorac Oncol*, 10, 944-50.
- MACLEOD, N., KLEPSTAD, P., FALLON, M. & LAIRD, B. 2015b. Pain Management in Mesothelioma. 5.
- MACLEOD, N., PRICE, A., O'ROURKE, N., FALLON, M. & LAIRD, B. 2014. Radiotherapy for the treatment of pain in malignant pleural mesothelioma: a systematic review. *Lung Cancer*, 83, 133-8.
- MADAN, R., BENSON, R., SHARMA, D. N., JULKA, P. K. & RATH, G. K. 2015. Radiation induced heart disease: Pathogenesis, management and review literature. *Journal of the Egyptian National Cancer Institute*, 27, 187-193.
- MAHANEY, B. L., MEEK, K. & LEES-MILLER, S. P. 2009. Repair of ionizing radiation-induced DNA double strand breaks by non-homologous end-joining. *The Biochemical journal*, 417, 639-650.
- MALUMBRES, M. & BARBACID, M. 2009. Cell cycle, CDKs and cancer: a changing paradigm. *Nat Rev Cancer*, 9, 153-66.
- MARIOTTI, L. G., PIROVANO, G., SAVAGE, K. I., GHITA, M., OTTOLENGHI, A., PRISE, K. M. & SCHETTINO, G. 2013. Use of the γ -H2AX assay to investigate DNA repair dynamics following multiple radiation exposures. *PLoS one*, 8, e79541-e79541.

- MARTEL, M. K., TEN HAKEN, R. K., HAZUKA, M. B., KESSLER, M. L., STRAWDERMAN, M., TURRISI, A. T., LAWRENCE, T. S., FRAASS, B. A. & LICHTER, A. S. 1999. Estimation of tumor control probability model parameters from 3-D dose distributions of non-small cell lung cancer patients. *Lung Cancer*, 24, 31-7.
- MASKELL, N. A., GLEESON, F. V. & DAVIES, R. J. 2003. Standard pleural biopsy versus CT-guided cutting-needle biopsy for diagnosis of malignant disease in pleural effusions: a randomised controlled trial. *Lancet*, 361, 1326-1330.
- MASON, K. D., CARPINELLI, M. R., FLETCHER, J. I., COLLINGE, J. E., HILTON, A. A., ELLIS, S., KELLY, P. N., EKERT, P. G., METCALF, D., ROBERTS, A. W., HUANG, D. C. & KILE, B. T. 2007. Programmed anuclear cell death delimits platelet life span. *Cell*, 128, 1173-86.
- MATTSON, K., HOLSTI, L. R., TAMMILEHTO, L., MAASILTA, P., PYRHONEN, S., MANTYLA, M., KAJANTI, M., SALMINEN, U. S., RAUTONEN, J. & KIVISAARI, L. 1992. Multimodality treatment programs for malignant pleural mesothelioma using high-dose hemithorax irradiation. *Int J Radiat Oncol Biol Phys*, 24, 643-50.
- MCANDREW, E. N., LEPAGE, C. C. & MCMANUS, K. J. 2016. The synthetic lethal killing of RAD54B-deficient colorectal cancer cells by PARP1 inhibition is enhanced with SOD1 inhibition. *Oncotarget*, 7, 87417-87430.
- MCELVENNY, D. M., DARNTON, A. J., PRICE, M. J. & HODGSON, J. T. 2005. Mesothelioma mortality in Great Britain from 1968 to 2001. *Occupational Medicine*, 55, 79-87.
- MCPMAHON, S. J. 2018. The linear quadratic model: usage, interpretation and challenges. *Phys Med Biol*, 64, 01tr01.
- MCWHINNEY, I. R., BASS, M. J. & DONNER, A. 1994. Evaluation of a palliative care service: problems and pitfalls. *Bmj*, 309, 1340-2.
- MENIAWY, T. M., CREANEY, J., LAKE, R. A. & NOWAK, A. K. 2013. Existing models, but not neutrophil-to-lymphocyte ratio, are prognostic in malignant mesothelioma. *Br J Cancer*, 109, 1813-20.
- MESBAHI, A., RASOULI, N., MOHAMMADZADEH, M., NASIRI MOTLAGH, B. & OZAN TEKIN, H. 2019. Comparison of Radiobiological Models for Radiation Therapy Plans of Prostate Cancer: Three-dimensional Conformal versus Intensity Modulated Radiation Therapy. *Journal of biomedical physics & engineering*, 9, 267-278.
- MIGUEL-CHUMACERO, E., CURRIE, G., JOHNSTON, A. & CURRIE, S. 2018. Effectiveness of Multi-Criteria Optimization-based Trade-Off exploration in combination with RapidPlan for head & neck radiotherapy planning. *Radiat Oncol*, 13, 229.
- MIKHAILOV, A., COLE, R. W. & RIEDER, C. L. 2002. DNA damage during mitosis in human cells delays the metaphase/anaphase transition via the spindle-assembly checkpoint. *Curr Biol*, 12, 1797-806.
- MILANO, M. T. & ZHANG, H. 2010. Malignant Pleural Mesothelioma: A Population-Based Study of Survival. *Journal of Thoracic Oncology*, 5, 1841-1848.
- MILES, E. F., LARRIER, N. A., KELSEY, C. R., HUBBS, J. L., MA, J., YOO, S. & MARKS, L. B. 2008. Intensity-modulated radiotherapy for resected mesothelioma: the Duke experience. *Int J Radiat Oncol Biol Phys*, 71, 1143-50.
- MINATEL, E., TROVO, M., POLESEL, J., BARESE, T., BEARZ, A., FRANCHIN, G., GOBITTI, C., RUMEILEH, I. A., DRIGO, A., FONTANA, P., PAGAN, V. & TROVO, M. G. 2014. Radical pleurectomy/decortication followed by high dose of radiation therapy for malignant pleural mesothelioma. Final results with long-term follow-up. *Lung Cancer*, 83, 78-82.
- MINATEL, E., TROVO, M., POLESEL, J., RUMEILEH, I. A., BARESE, T., BEARZ, A., DEL CONTE, A., FRANCHIN, G., GOBITTI, C., DRIGO, A., DASSIE, A., PAGAN, V. & TROVO, M. G. 2012. Tomotherapy after pleurectomy/decortication or biopsy for malignant pleural mesothelioma allows the delivery of high dose of radiation in patients with intact lung. *J Thorac Oncol*, 7, 1862-1866.
- MINCHINTON, A. I. & TANNOCK, I. F. 2006. Drug penetration in solid tumours. *Nat Rev Cancer*, 6, 583-92.
- MIRALBELL, R., ROBERTS, S. A., ZUBIZARRETA, E. & HENDRY, J. H. 2012. Dose-fractionation sensitivity of prostate cancer deduced from radiotherapy outcomes of 5,969 patients in

- seven international institutional datasets: alpha/beta = 1.4 (0.9-2.2) Gy. *Int J Radiat Oncol Biol Phys*, 82, e17-24.
- MITSUDOMI, T., MORITA, S., YATABE, Y., NEGORO, S., OKAMOTO, I., TSURUTANI, J., SETO, T., SATOUCHI, M., TADA, H., HIRASHIMA, T., ASAMI, K., KATAKAMI, N., TAKADA, M., YOSHIOKA, H., SHIBATA, K., KUDOH, S., SHIMIZU, E., SAITO, H., TOYOOKA, S., NAKAGAWA, K. & FUKUOKA, M. 2010. Gefitinib versus cisplatin plus docetaxel in patients with non-small-cell lung cancer harbouring mutations of the epidermal growth factor receptor (WJTOG3405): an open label, randomised phase 3 trial. *The Lancet Oncology*, 11, 121-128.
- MOHIUDDIN, I., CAO, X., OZVARAN, M. K., ZUMSTEIN, L., CHADA, S. & SMYTHE, W. R. 2002. Phosphatase and tensin analog gene overexpression engenders cellular death in human malignant mesothelioma cells via inhibition of AKT phosphorylation. *Ann Surg Oncol*, 9, 310-6.
- MOLLBERG, N. M., VIGNESWARAN, Y., KINDLER, H. L., WARNES, C., SALGIA, R., HUSAIN, A. N. & VIGNESWARAN, W. T. 2012. Quality of Life After Radical Pleurectomy Decortication for Malignant Pleural Mesothelioma. *Annals of Thoracic Surgery*, 94, 1086-1093.
- MØLLER, D. S., HOLT, M. I., ALBER, M., TVILUM, M., KHALIL, A. A., KNAP, M. M. & HOFFMANN, L. 2016. Adaptive radiotherapy for advanced lung cancer ensures target coverage and decreases lung dose. *Radiother Oncol*, 121, 32-38.
- MUELLER-KLIESER, W. 1987. Multicellular spheroids. A review on cellular aggregates in cancer research. *J Cancer Res Clin Oncol*, 113, 101-22.
- MUELLER-KLIESER, W. 1997. Three-dimensional cell cultures: from molecular mechanisms to clinical applications. *Am J Physiol*, 273, C1109-23.
- MULLER, B. S., SHIH, H. A., EFSTATHIOU, J. A., BORTFELD, T. & CRAFT, D. 2017. Multicriteria plan optimization in the hands of physicians: a pilot study in prostate cancer and brain tumors. *Radiat Oncol*, 12, 168.
- MURTHY, S. S. & TESTA, J. R. 1999. Asbestos, chromosomal deletions, and tumor suppressor gene alterations in human malignant mesothelioma. *J Cell Physiol*, 180, 150-7.
- MYCHALEZAK, B., NORI, D., ARMSTRONG, J., MARTINI, N. & HARRISON, L. 1989. Results of treatment of malignant pleural mesothelioma with surgery, brachytherapy and external beam irradiation. *Endocurie Hypertherm Oncol*, 5, 245.
- NABAVI, N., BENNEWITH, K. L., CHURG, A., WANG, Y., COLLINS, C. C. & MUTTI, L. 2016. Switching off malignant mesothelioma: exploiting the hypoxic microenvironment. *Genes & cancer*, 7, 340-354.
- NAHUM, A. E. 2015. The radiobiology of hypofractionation. *Clin Oncol (R Coll Radiol)*, 27, 260-9.
- NAKAMURA, M., NAKASHIMA, S., KATAGIRI, Y. & NOZAWA, Y. 1997. Effect of wortmannin and 2-(4-morpholinyl)-8-phenyl-4H-1-benzopyran-4-one (LY294002) on N-formyl-methionyl-leucyl-phenylalanine-induced phospholipase D activation in differentiated HL60 cells: possible involvement of phosphatidylinositol 3-kinase in phospholipase D activation. *Biochem Pharmacol*, 53, 1929-36.
- NAKANO, K. & VOUSDEN, K. H. 2001. PUMA, a novel proapoptotic gene, is induced by p53. *Mol Cell*, 7, 683-94.
- NARASIMHAN, S. R., YANG, L., GERWIN, B. I. & BROADDUS, V. C. 1998. Resistance of pleural mesothelioma cell lines to apoptosis: relation to expression of Bcl-2 and Bax. *Am J Physiol*, 275, L165-71.
- NELSON-REES, W. A., DANIELS, D. W. & FLANDERMEYER, R. R. 1981. Cross-contamination of cells in culture. *Science*, 212, 446-52.
- NERAGI-MIANDOAB, S. & SUGARBAKER, D. J. 2009. Chromosomal deletion in patients with malignant pleural mesothelioma. *Interact Cardiovasc Thorac Surg*, 9, 42-4.
- NESTLE, U., WEBER, W., HENTSCHEL, M. & GROSU, A. L. 2009. Biological imaging in radiation therapy: role of positron emission tomography. *Phys Med Biol*, 54, R1-25.
- NGUYEN, N. P., BISHOP, M., BOROK, T. J., WELSH, J., HAMILTON, R., COHEN, D., NGUYEN, L. M. & VINCENT, V. H. 2010. Pattern of failure following chemoradiation for locally advanced non-small cell lung cancer: potential role for stereotactic body radiotherapy. *Anticancer Res*, 30, 953-61.

- NI, Z., LIU, Y., KESHAVA, N., ZHOU, G., WHONG, W. & ONG, T. 2000. Analysis of K-ras and p53 mutations in mesotheliomas from humans and rats exposed to asbestos. *Mutat Res*, 468, 87-92.
- NIJKAMP, J., POS, F. J., NUVER, T. T., DE JONG, R., REMEIJER, P., SONKE, J. J. & LEBESQUE, J. V. 2008. Adaptive radiotherapy for prostate cancer using kilovoltage cone-beam computed tomography: first clinical results. *Int J Radiat Oncol Biol Phys*, 70, 75-82.
- NOORDERMEER, S. M., WENNEMERS, M., BERGEVOET, S. M., VAN DER HEIJDEN, A., TONNISSEN, E., SWEEP, F. C., JANSEN, J. H., SPAN, P. N. & VAN DER REIJDEN, B. A. 2012. Expression of the BRCA1 complex member BRE predicts disease free survival in breast cancer. *Breast Cancer Res Treat*, 135, 125-33.
- O'BRIEN, M. E. R., WATKINS, D., RYAN, C., PRIEST, K., CORBISHLEY, C., NORTON, A., ASHLEY, S., ROWELL, N. & SAYER, R. 2006. A randomised trial in malignant mesothelioma (M) of early (E) versus delayed (D) chemotherapy in symptomatically stable patients: the MED trial. *Annals of Oncology*, 17, 270-275.
- O'ROURKE, N., GARCIA, J. C., PAUL, J., LAWLESS, C., MCMENEMIN, R. & HILL, J. 2007. A randomised controlled trial of intervention site radiotherapy in malignant pleural mesothelioma. *Radiother Oncol*, 84, 18-22.
- ODA, E., OHKI, R., MURASAWA, H., NEMOTO, J., SHIBUE, T., YAMASHITA, T., TOKINO, T., TANIGUCHI, T. & TANAKA, N. 2000. Noxa, a BH3-only member of the Bcl-2 family and candidate mediator of p53-induced apoptosis. *Science*, 288, 1053-8.
- OEHL, K., VRUGT, B., OPITZ, I. & MEERANG, M. 2018. Heterogeneity in Malignant Pleural Mesothelioma. *International journal of molecular sciences*, 19, 1603.
- OZVARAN, M. K., CAO, X. X., MILLER, S. D., MONIA, B. A., HONG, W. K. & SMYTHE, W. R. 2004. Antisense oligonucleotides directed at the bcl-xl gene product augment chemotherapy response in mesothelioma. *Mol Cancer Ther*, 3, 545-50.
- PAN, H. Y., JIANG, S., SUTTON, J., LIAO, Z., CHANCE, W. W., FRANK, S. J., ZHU, X. R., LI, H., FONTANILLA, H. P., ZHANG, X. & GOMEZ, D. R. 2015. Early experience with intensity modulated proton therapy for lung-intact mesothelioma: A case series. *Pract Radiat Oncol*, 5, e345-53.
- PAPP, T., SCHIPPER, H., PEMSEL, H., BASTROP, R., MULLER, K. M., WIETHEGE, T., WEISS, D. G., DOPP, E., SCHIFFMANN, D. & RAHMAN, Q. 2001. Mutational analysis of N-ras, p53, p16INK4a, p14ARF and CDK4 genes in primary human malignant mesotheliomas. *Int J Oncol*, 18, 425-33.
- PARISI, E., ROMEO, A., SARNELLI, A., GHIGI, G., BELLIA, S. R., NERI, E., MICHELETTI, S., DIPALMA, B., ARPA, D., FURINI, G., BURGIO, M. A., GENESTRETI, G., GURIOLI, C., SANNA, S., BOVOLATO, P., REA, F., STORME, G., SCARPI, E., ARIENTI, C., TESEI, A. & POLICO, R. 2017. High dose irradiation after pleurectomy/decortication or biopsy for pleural mesothelioma treatment. *Cancer Radiother*, 21, 766-773.
- PARK, C.-M., BRUNCKO, M., ADICKES, J., BAUCH, J., DING, H., KUNZER, A., MARSH, K. C., NIMMER, P., SHOEMAKER, A. R., SONG, X., TAHIR, S. K., TSE, C., WANG, X., WENDT, M. D., YANG, X., ZHANG, H., FESIK, S. W., ROSENBERG, S. H. & ELMORE, S. W. 2008. Discovery of an Orally Bioavailable Small Molecule Inhibitor of Prosurvival B-Cell Lymphoma 2 Proteins. *Journal of Medicinal Chemistry*, 51, 6902-6915.
- PASS, H. I. 2012. Fibulin-3 as a Blood and Effusion Biomarker for Pleural Mesothelioma (vol 367, pg 1417, 2012). *New England Journal of Medicine*, 367, 1768-1768.
- PATEL, P. R., YOO, S., BROADWATER, G., MARKS, L. B., MILES, E. F., D'AMICO, T. A., HARPOLE, D. & KELSEY, C. R. 2012. Effect of increasing experience on dosimetric and clinical outcomes in the management of malignant pleural mesothelioma with intensity-modulated radiation therapy. *Int J Radiat Oncol Biol Phys*, 83, 362-8.
- PETERSON, J. T., JR., GREENBERG, S. D. & BUFFLER, P. A. 1984. Non-asbestos-related malignant mesothelioma. A review. *Cancer*, 54, 951-60.
- PICCININI, F., TESEI, A., ARIENTI, C. & BEVILACQUA, A. 2015. Cancer multicellular spheroids: volume assessment from a single 2D projection. *Comput Methods Programs Biomed*, 118, 95-106.

- PIETENPOL, J. A. & STEWART, Z. A. 2002. Cell cycle checkpoint signaling: cell cycle arrest versus apoptosis. *Toxicology*, 181-182, 475-81.
- PIGNON, J. P., LE MAITRE, A., MAILLARD, E. & BOURHIS, J. 2009. Meta-analysis of chemotherapy in head and neck cancer (MACH-NC): an update on 93 randomised trials and 17,346 patients. *Radiother Oncol*, 92, 4-14.
- PISTOLESI, M. & RUSTHOVEN, J. 2004. Malignant pleural mesothelioma - Update, current management, and newer therapeutic strategies. *Chest*, 126, 1318-1329.
- PRICE, B. D. & YOUMELL, M. B. 1996. The phosphatidylinositol 3-kinase inhibitor wortmannin sensitizes murine fibroblasts and human tumor cells to radiation and blocks induction of p53 following DNA damage. *Cancer Res*, 56, 246-50.
- RAMOS-NINO, M. E., VIANALE, G., SABO-ATTWOOD, T., MUTTI, L., PORTA, C., HEINTZ, N. & MOSSMAN, B. T. 2005. Human mesothelioma cells exhibit tumor cell-specific differences in phosphatidylinositol 3-kinase/AKT activity that predict the efficacy of Onconase. *Mol Cancer Ther*, 4, 835-42.
- RANA, S. B. 2013. Volumetric intensity modulated arc therapy in lung cancer: Current literature review. *Clinical Cancer Investigation Journal*, 2, 9-13.
- RAVENNA, L., CARDILLO, I., CURZIO, G., BALDI, A., MATTIONI, M., VINCENZI, B., RUSSO, M., SODDU, S. & VERDINA, A. 2014. Mesothelioma and Hypoxia: Modulation of the Inflammation-Related Phenotype and Identification of Prognostic Markers. *Cancer Science & Therapy*, 6, 378-387.
- REDON, C. E., DICKEY, J. S., BONNER, W. M. & SEDELNIKOVA, O. A. 2009. γ -H2AX as a biomarker of DNA damage induced by ionizing radiation in human peripheral blood lymphocytes and artificial skin. *Advances in space research : the official journal of the Committee on Space Research (COSPAR)*, 43, 1171-1178.
- REGAUD, C., NOGIER, T. 1911. Stérilization rontgenienne totale et définitive, sans radiodermite, des testicules du Belier adulte; conditions de sa réalisation. *Compt. Rend. Sec. de Biol.*, 70, 202-203.
- REMICK, J. S., SCHONEWOLF, C., GABRIEL, P., DOUCETTE, A., LEVIN, W. P., KUCHARCZUK, J. C., SINGHAL, S., PECHET, T. T. V., RENGAN, R., SIMONE, C. B., 2ND & BERMAN, A. T. 2017. First Clinical Report of Proton Beam Therapy for Postoperative Radiotherapy for Non-Small-Cell Lung Cancer. *Clin Lung Cancer*, 18, 364-371.
- RICE, D. C., SMYTHE, W. R., LIAO, Z., GUERRERO, T., CHANG, J. Y., MCALEER, M. F., JETER, M. D., CORREA, A., VAPORCIYAN, A. A., LIU, H. H., KOMAKI, R., FORSTER, K. M. & STEVENS, C. W. 2007a. Dose-dependent pulmonary toxicity after postoperative intensity-modulated radiotherapy for malignant pleural mesothelioma. *Int J Radiat Oncol Biol Phys*, 69, 350-7.
- RICE, D. C., STEVENS, C. W., CORREA, A. M., VAPORCIYAN, A. A., TSAO, A., FORSTER, K. M., WALSH, G. L., SWISHER, S. G., HOFSTETTER, W. L., MEHRAN, R. J., ROTH, J. A., LIAO, Z. & SMYTHE, W. R. 2007b. Outcomes after extrapleural pneumonectomy and intensity-modulated radiation therapy for malignant pleural mesothelioma. *Ann Thorac Surg*, 84, 1685-92; discussion 1692-3.
- RIMNER, A., SIMONE, C. B., 2ND, ZAUDERER, M. G., CENGEL, K. A. & RUSCH, V. W. 2016a. Hemithoracic radiotherapy for mesothelioma: lack of benefit or lack of statistical power? *The Lancet Oncology*, 17, e43-e44.
- RIMNER, A., ZAUDERER, M. G., GOMEZ, D. R., ADUSUMILLI, P. S., PARHAR, P. K., WU, A. J., WOO, K. M., SHEN, R., GINSBERG, M. S., YORKE, E. D., RICE, D. C., TSAO, A. S., ROSENZWEIG, K. E., RUSCH, V. W. & KRUG, L. M. 2016b. Phase II Study of Hemithoracic Intensity-Modulated Pleural Radiation Therapy (IMPRINT) As Part of Lung-Sparing Multimodality Therapy in Patients With Malignant Pleural Mesothelioma. *J Clin Oncol*, 34, 2761-8.
- ROE, O. D., ANDERSSON, E., SANDECK, H., CHRISTENSEN, T., LARSSON, E. & LUNDGREN, S. 2010. Malignant pleural mesothelioma: genome-wide expression patterns reflecting general resistance mechanisms and a proposal of novel targets. *Lung Cancer*, 67, 57-68.
- ROFSTAD, E. K., WAHL, A. & BRUSTAD, T. 1986. Radiation response of multicellular spheroids initiated from five human melanoma xenograft lines. Relationship to the radioresponsiveness in vivo. *Br J Radiol*, 59, 1023-9.

- ROFSTAD, E. K., WAHL, A. & BRUSTAD, T. 1987. Radiation sensitivity in vitro of cells isolated from human tumor surgical specimens. *Cancer Res*, 47, 106-10.
- RONINSON, I. B. 2002. Oncogenic functions of tumour suppressor p21(Waf1/Cip1/Sdi1): association with cell senescence and tumour-promoting activities of stromal fibroblasts. *Cancer Lett*, 179, 1-14.
- ROSE, P. G., BUNDY, B. N., WATKINS, E. B., THIGPEN, J. T., DEPPE, G., MAIMAN, M. A., CLARKE-PEARSON, D. L. & INSALACO, S. 1999. Concurrent cisplatin-based radiotherapy and chemotherapy for locally advanced cervical cancer. *N Engl J Med*, 340, 1144-53.
- ROSENKRANTZ, A. B., FRIEDMAN, K., CHANDARANA, H., MELSAETHER, A., MOY, L., DING, Y. S., JHAVERI, K., BELTRAN, L. & JAIN, R. 2016. Current Status of Hybrid PET/MRI in Oncologic Imaging. *AJR Am J Roentgenol*, 206, 162-72.
- ROSENZWEIG, K. E., YOUPELL, M. B., PALAYOOR, S. T. & PRICE, B. D. 1997. Radiosensitization of human tumor cells by the phosphatidylinositol3-kinase inhibitors wortmannin and LY294002 correlates with inhibition of DNA-dependent protein kinase and prolonged G2-M delay. *Clinical Cancer Research*, 3, 1149-1156.
- ROSENZWEIG, K. E., ZAUDERER, M. G., LASER, B., KRUG, L. M., YORKE, E., SIMA, C. S., RIMNER, A., FLORES, R. & RUSCH, V. 2012. Pleural intensity-modulated radiotherapy for malignant pleural mesothelioma. *Int J Radiat Oncol Biol Phys*, 83, 1278-83.
- ROTHKAMM, K., KRUGER, I., THOMPSON, L. H. & LOBRICH, M. 2003. Pathways of DNA double-strand break repair during the mammalian cell cycle. *Mol Cell Biol*, 23, 5706-15.
- ROWELL, N. P. & O'ROURKE N, P. 2004. Concurrent chemoradiotherapy in non-small cell lung cancer. *Cochrane Database Syst Rev*, CD002140.
- RUDD, R. M. 2010. Malignant mesothelioma. *British Medical Bulletin*, 93, 105-123.
- RUSCH, V., BALDINI, E. H., BUENO, R., DE PERROT, M., FLORES, R., HASEGAWA, S., KLEPETKO, W., KRUG, L., LANG-LAZDUNSKI, L., PASS, H., WEDER, W. & SUGARBAKER, D. J. 2013. The role of surgical cytoreduction in the treatment of malignant pleural mesothelioma: Meeting summary of the International Mesothelioma Interest Group Congress, September 11-14, 2012, Boston, Mass. *The Journal of Thoracic and Cardiovascular Surgery*, 145, 909-910.
- RUSCH, V. W., CHANSKY, K., KINDLER, H. L., NOWAK, A. K., PASS, H. I., RICE, D. C., SHEMANSKI, L., GALATEAU-SALLÉ, F., MCCAUGHAN, B. C., NAKANO, T., RUFFINI, E., VAN MEERBEECK, J. P., YOSHIMURA, M., GOLDSTRAW, P., RAMI-PORTA, R., ASAMURA, H., BALL, D., BEER, D., BEYRUTI, R., BOLEJACK, V., CHANSKY, K., CROWLEY, J., DETTERBECK, F. C., EBERHARDT, W. E. E., EDWARDS, J., GALATEAU-SALLÉ, F., GIROUX, D., GLEESON, F., GROOME, P., HUANG, J., KENNEDY, C., KIM, J., KIM, Y. T., KINGSBURY, L., KONDO, H., KRASNIK, M., KUBOTA, K., LERUT, T., LYONS, G., MARINO, M., MAROM, E. M., VAN MEERBEECK, J. P., MITCHELL, A., NAKANO, T., NICHOLSON, A. G., NOWAK, A., PEAKE, M., RICE, T. W., ROSENZWEIG, K., RUFFINI, E., RUSCH, V. W., SAIJO, N., VAN SCHIL, P., SCULIER, J.-P., SHEMANSKI, L., STRATTON, K., SUZUKI, K., TACHIMORI, Y., THOMAS, C. F., TRAVIS, W. D., TSAO, M. S., TURRISI, A., VANSTEENKISTE, J., WATANABE, H., WU, Y.-L., BAAS, P., ERASMUS, J., HASEGAWA, S., INAI, K., KERNSTINE, K., KINDLER, H., KRUG, L., NACKAERTS, K., PASS, H., RICE, D., FALKSON, C., FILOSSO, P. L., GIACCONE, G., KONDO, K., LUCCHI, M., OKUMURA, M., BLACKSTONE, E., ASAMURA, H., BATIREL, H., BILLE, A., PASTORINO, U., CALL, S., CANGIR, A., CEDRES, S., FRIEDBERG, J., GALATEAU-SALLÉ, F., HASAGAWA, S., KERNSTINE, K., KINDLER, H., MCCAUGHAN, B., NAKANO, T., NOWAK, A., OZTURK, C. A., PASS, H., DE PERROT, M., et al. 2016. The IASLC Mesothelioma Staging Project: Proposals for the M Descriptors and for Revision of the TNM Stage Groupings in the Forthcoming (Eighth) Edition of the TNM Classification for Mesothelioma. *Journal of Thoracic Oncology*, 11, 2112-2119.
- RUSCH, V. W., ROSENZWEIG, K., VENKATRAMAN, E., LEON, L., RABEN, A., HARRISON, L., BAINS, M. S., DOWNEY, R. J. & GINSBERG, R. J. 2001. A phase II trial of surgical resection and adjuvant high-dose hemithoracic radiation for malignant pleural mesothelioma. *J Thorac Cardiovasc Surg*, 122, 788-95.
- SAELEN, X., FESTJENS, N., VANDE WALLE, L., VAN GURP, M., VAN LOO, G. & VANDENABEELE, P. 2004. Toxic proteins released from mitochondria in cell death. *Oncogene*, 23, 2861-74.

- SAHA, D., LAN, Y., HSU, F., TUMATI, V., ZHANG, Z., LIN, Y. & CHEN, B. 2014. 208 Combined treatment of a DNA-PKcs inhibitor (NU7441) and ionizing radiation causes a differential mode of cell death in a panel of NSCLC cell lines and exhibits robust radiosensitisation. *European Journal of Cancer*, 50, 68.
- SAITO, T., MATSUYAMA, T., TOYA, R., FUKUGAWA, Y., TOYOFUKU, T., SEMBA, A. & OYA, N. 2014. Respiratory gating during stereotactic body radiotherapy for lung cancer reduces tumor position variability. *PLoS one*, 9, e112824-e112824.
- SAKAHIRA, H., ENARI, M. & NAGATA, S. 1998. Cleavage of CAD inhibitor in CAD activation and DNA degradation during apoptosis. *Nature*, 391, 96-9.
- SAKAI, Y., YAMAGAMI, S. & NAKAZAWA, K. 2010. Comparative analysis of gene expression in rat liver tissue and monolayer- and spheroid-cultured hepatocytes. *Cells Tissues Organs*, 191, 281-8.
- SANCAR, A., LINDSEY-BOLTZ, L. A., UNSAL-KACMAZ, K. & LINN, S. 2004. Molecular mechanisms of mammalian DNA repair and the DNA damage checkpoints. *Annu Rev Biochem*, 73, 39-85.
- SANTINI, M. T., RAINALDI, G. & INDOVINA, P. L. 1999. Multicellular tumour spheroids in radiation biology. *Int J Radiat Biol*, 75, 787-99.
- SAUNDERS, J., ASHTON, M., HALL, C., LAIRD, B. & MACLEOD, N. 2019. Pain management in patients with malignant mesothelioma: challenges and solutions. *Lung Cancer (Auckl)*, 10, 37-46.
- SCHERPEREEL, A., ASTOUL, P., BAAS, P., BERGHMANS, T., CLAYSON, H., DE VUYST, P., DIENEMANN, H., GALATEAU-SALLE, F., HENNEQUIN, C., HILLERDAL, G., LE PÉCHOUX, C., MUTTI, L., PAIRON, J. C., STAHEL, R., VAN HOUTTE, P., VAN MEERBEECK, J., WALLER, D. & WEDER, W. 2010. Guidelines of the European Respiratory Society and the European Society of Thoracic Surgeons for the management of malignant pleural mesothelioma. *European Respiratory Journal*, 35, 479.
- SCHULER, M. & GREEN, D. R. 2001. Mechanisms of p53-dependent apoptosis. *Biochem Soc Trans*, 29, 684-8.
- SCHWACHOFER, J. H., CROOIJMANS, R. P., VAN GASTEREN, J. J., HOOGENHOUT, J., JERUSALEM, C. R., KAL, H. B. & THEEUWES, A. G. 1989. Radiosensitivity of different human tumor cells lines grown as multicellular spheroids determined from growth curves and survival data. *Int J Radiat Oncol Biol Phys*, 17, 1015-20.
- SCORSETTI, M., BIGNARDI, M., CLIVIO, A., COZZI, L., FOGLIATA, A., LATTUADA, P., MANCOSU, P., NAVARRIA, P., NICOLINI, G., URSO, G., VANETTI, E., VIGORITO, S. & SANTORO, A. 2010. Volumetric modulation arc radiotherapy compared with static gantry intensity-modulated radiotherapy for malignant pleural mesothelioma tumor: a feasibility study. *Int J Radiat Oncol Biol Phys*, 77, 942-9.
- SEGERS, K., RAMAEL, M., SINGH, S. K., WEYLER, J., VAN MEERBEECK, J., VERMEIRE, P. & VAN MARCK, E. 1994. Immunoreactivity for bcl-2 protein in malignant mesothelioma and non-neoplastic mesothelium. *Virchows Arch*, 424, 631-4.
- SEKIDO, Y. 2013. Molecular pathogenesis of malignant mesothelioma. *Carcinogenesis*, 34, 1413-9.
- SEANAN, S., BRADE, A., WANG, L. H., VANSTEENKISTE, J., DAKHIL, S., BIESMA, B., MARTINEZ AGUILLO, M., AERTS, J., GOVINDAN, R., RUBIO-VIQUEIRA, B., LEWANSKI, C., GANDARA, D., CHOY, H., MOK, T., HOSSAIN, A., ISCOE, N., TREAT, J., KOUSTENIS, A., SAN ANTONIO, B., CHOUAKI, N. & VOKES, E. 2016. PROCLAIM: Randomized Phase III Trial of Pemetrexed-Cisplatin or Etoposide-Cisplatin Plus Thoracic Radiation Therapy Followed by Consolidation Chemotherapy in Locally Advanced Nonsquamous Non-Small-Cell Lung Cancer. *J Clin Oncol*, 34, 953-62.
- SENKUS, E., KYRIAKIDES, S., PENAULT-LLORCA, F., POORTMANS, P., THOMPSON, A., ZACKRISSON, S., CARDOSO, F. & GROUP, O. B. O. T. E. G. W. 2013. Primary breast cancer: ESMO Clinical Practice Guidelines for diagnosis, treatment and follow-up†. *Annals of Oncology*, 24, vi7-vi23.
- SHAHEEN, F. S., ZNOJEK, P., FISHER, A., WEBSTER, M., PLUMMER, R., GAUGHAN, L., SMITH, G. C., LEUNG, H. Y., CURTIN, N. J. & ROBSON, C. N. 2011. Targeting the DNA double strand break repair machinery in prostate cancer. *PLoS One*, 6, e20311.

- SHAM, E. & DURAND, R. E. 1998. Cell kinetics and repopulation mechanisms during multifraction irradiation of spheroids. *Radiother Oncol*, 46, 201-7.
- SHANG, Z. F., HUANG, B., XU, Q. Z., ZHANG, S. M., FAN, R., LIU, X. D., WANG, Y. & ZHOU, P. K. 2010. Inactivation of DNA-dependent protein kinase leads to spindle disruption and mitotic catastrophe with attenuated checkpoint protein 2 Phosphorylation in response to DNA damage. *Cancer Res*, 70, 3657-66.
- SHAW, A. T., YEAP, B. Y., SOLOMON, B. J., RIELY, G. J., GAINOR, J., ENGELMAN, J. A., SHAPIRO, G. I., COSTA, D. B., OU, S.-H. I., BUTANEY, M., SALGIA, R., MAKI, R. G., VARELLA-GARCIA, M., DOEBELE, R. C., BANG, Y.-J., KULIG, K., SELARU, P., TANG, Y., WILNER, K. D., KWAK, E. L., CLARK, J. W., IAFRATE, A. J. & CAMIDGE, D. R. 2011. Effect of crizotinib on overall survival in patients with advanced non-small-cell lung cancer harbouring ALK gene rearrangement: a retrospective analysis. *The Lancet Oncology*, 12, 1004-1012.
- SHUKER, L., HARRISON, P. & POOLE, S. 1997. Fibrous materials in the environment. *Leicester: MRC Institute for environment and health*.
- SIMÕES-WUST, A. P., OLIE, R. A., GAUTSCHI, O., LEECH, S. H., HANER, R., HALL, J., FABBRO, D., STAHEL, R. A. & ZANGEMEISTER-WITTKKE, U. 2000. Bcl-xl antisense treatment induces apoptosis in breast carcinoma cells. *Int J Cancer*, 87, 582-90.
- SLAMON, D. J., LEYLAND-JONES, B., SHAK, S., FUCHS, H., PATON, V., BAJAMONDE, A., FLEMING, T., EIERMANN, W., WOLTER, J., PEGRAM, M., BASELGA, J. & NORTON, L. 2001. Use of Chemotherapy plus a Monoclonal Antibody against HER2 for Metastatic Breast Cancer That Overexpresses HER2. *New England Journal of Medicine*, 344, 783-792.
- SLEE, E. A., ADRAIN, C. & MARTIN, S. J. 2001. Executioner caspase-3, -6, and -7 perform distinct, non-redundant roles during the demolition phase of apoptosis. *J Biol Chem*, 276, 7320-6.
- SMYTHE, W. R., MOHUIDDIN, I., OZVERAN, M. & CAO, X. X. 2002. Antisense therapy for malignant mesothelioma with oligonucleotides targeting the bcl-xl gene product. *J Thorac Cardiovasc Surg*, 123, 1191-8.
- SODERLUND, K., STAL, O., SKOOG, L., RUTQVIST, L. E., NORDENSKJOLD, B. & ASKMALM, M. S. 2007. Intact Mre11/Rad50/Nbs1 complex predicts good response to radiotherapy in early breast cancer. *Int J Radiat Oncol Biol Phys*, 68, 50-8.
- SOINI, Y., KINNULA, V., KAARTEENAHO-WIIK, R., KURTTILA, E., LINNAINMAA, K. & PAAKKO, P. 1999. Apoptosis and expression of apoptosis regulating proteins bcl-2, mcl-1, bcl-X, and bax in malignant mesothelioma. *Clin Cancer Res*, 5, 3508-15.
- SOMAIHA, N., ROTHKAMM, K. & YARNOLD, J. 2015. Where Do We Look for Markers of Radiotherapy Fraction Size Sensitivity? *Clin Oncol (R Coll Radiol)*, 27, 570-8.
- SOMAIHA, N., YARNOLD, J., DALEY, F., PEARSON, A., GOTHARD, L., ROTHKAMM, K. & HELLEDAY, T. 2012. The relationship between homologous recombination repair and the sensitivity of human epidermis to the size of daily doses over a 5-week course of breast radiotherapy. *Clin Cancer Res*, 18, 5479-88.
- SOMAIHA, N., YARNOLD, J., LAGERQVIST, A., ROTHKAMM, K. & HELLEDAY, T. 2013. Homologous recombination mediates cellular resistance and fraction size sensitivity to radiation therapy. *Radiother Oncol*, 108, 155-61.
- SOUERS, A. J., LEVERSON, J. D., BOGHAERT, E. R., ACKLER, S. L., CATRON, N. D., CHEN, J., DAYTON, B. D., DING, H., ENSCHEDE, S. H., FAIRBROTHER, W. J., HUANG, D. C., HYMOWITZ, S. G., JIN, S., KHAW, S. L., KOVAR, P. J., LAM, L. T., LEE, J., MAECKER, H. L., MARSH, K. C., MASON, K. D., MITTEN, M. J., NIMMER, P. M., OLEKSIJEW, A., PARK, C. H., PARK, C. M., PHILLIPS, D. C., ROBERTS, A. W., SAMPATH, D., SEYMOUR, J. F., SMITH, M. L., SULLIVAN, G. M., TAHIR, S. K., TSE, C., WENDT, M. D., XIAO, Y., XUE, J. C., ZHANG, H., HUMERICKHOUSE, R. A., ROSENBERG, S. H. & ELMORE, S. W. 2013. ABT-199, a potent and selective BCL-2 inhibitor, achieves antitumor activity while sparing platelets. *Nat Med*, 19, 202-8.
- SOYSAL, O., KARAOGLANOGLU, N., DEMIRACAN, S., TOPCU, S., TASTEPE, I., KAYA, S., UNLU, M. & CETIN, G. 1997. Pleurectomy/decortication for palliation in malignant pleural mesothelioma: results of surgery. *Eur J Cardiothorac Surg*, 11, 210-3.
- STAHEL, R. A., RIESTERER, O., XYRAFAS, A., OPITZ, I., BEYELER, M., OCHSENBEIN, A., FRUH, M., CATHOMAS, R., NACKAERTS, K., PETERS, S., MAMOT, C., ZIPPELIUS, A., MORDASINI, C., CASPAR, C. B., ECKHARDT, K., SCHMID, R. A., AEBERSOLD, D. M., GAUTSCHI, O., NAGEL,

- W., TOPFER, M., KRAYENBUEHL, J., RIBI, K., CIERNIK, I. F. & WEDER, W. 2015. Neoadjuvant chemotherapy and extrapleural pneumonectomy of malignant pleural mesothelioma with or without hemithoracic radiotherapy (SAKK 17/04): a randomised, international, multicentre phase 2 trial. *Lancet Oncol*, 16, 1651-8.
- STEEL, G. G. & PEACOCK, J. H. 1989. Why are some human tumours more radiosensitive than others? *Radiother Oncol*, 15, 63-72.
- STEIN, C. A. & CHENG, Y. C. 1993. Antisense oligonucleotides as therapeutic agents--is the bullet really magical? *Science*, 261, 1004-12.
- STERZING, F., SROKA-PEREZ, G., SCHUBERT, K., MUNTER, M. W., THIEKE, C., HUBER, P., DEBUS, J. & HERFARTH, K. K. 2008. Evaluating target coverage and normal tissue sparing in the adjuvant radiotherapy of malignant pleural mesothelioma: helical tomotherapy compared with step-and-shoot IMRT. *Radiother Oncol*, 86, 251-7.
- STEWART, D., WALLER, D., EDWARDS, J., JEYAPALAN, K. & ENTWISLE, J. 2003. Is there a role for pre-operative contrast-enhanced magnetic resonance imaging for radical surgery in malignant pleural mesothelioma? *European Journal of Cardio-Thoracic Surgery*, 24, 1019-1024.
- STEWART, D. J., MARTIN-UCAR, A., PILLING, J. E., EDWARDS, J. G., O'BYRNE, K. J. & WALLER, D. A. 2004. The effect of extent of local resection on patterns of disease progression in malignant pleural mesothelioma. *The Annals of Thoracic Surgery*, 78, 245-252.
- STEWART, F. A., SORANSON, J. A., ALPEN, E. L., WILLIAMS, M. V. & DENEKAMP, J. 1984. Radiation-induced renal damage: the effects of hyperfractionation. *Radiat Res*, 98, 407-20.
- STUSCHKE, M., BUDACH, V., BAMBERG, M. & BUDACH, W. 1990. Methods for analysis of censored tumor growth delay data. *Radiat Res*, 122, 172-80.
- STUSCHKE, M., BUDACH, V., KLAES, W. & SACK, H. 1992. Radiosensitivity, repair capacity, and stem cell fraction in human soft tissue tumors: an in vitro study using multicellular spheroids and the colony assay. *Int J Radiat Oncol Biol Phys*, 23, 69-80.
- STUSCHKE, M., BUDACH, V., STUBEN, G., STREFFER, C. & SACK, H. 1995. Heterogeneity in the fractionation sensitivities of human tumor cell lines: studies in a three-dimensional model system. *Int J Radiat Oncol Biol Phys*, 32, 395-408.
- SUGARBAKER, D. J., GARCIA, J. P., RICHARDS, W. G., HARPOLE, D. H., HEALYBALDINI, E., DECAMP, M. M., MENTZER, S. J., LIPTAY, M. J., STRAUSS, G. M. & SWANSON, S. J. 1996. Extrapleural pneumonectomy in the multimodality therapy of malignant pleural mesothelioma - Results in 120 consecutive patients. *Annals of Surgery*, 224, 288-294.
- SUGARBAKER, D. J., JAKLITSCH, M. T., BUENO, R., RICHARDS, W., LUKANICH, J., MENTZER, S. J., COLSON, Y., LINDEN, P., CHANG, M., CAPALBO, L., OLDREAD, E., NERAGI-MIANDOAB, S., SWANSON, S. J. & ZELLOS, L. S. 2004. Prevention, early detection, and management of complications after 328 consecutive extrapleural pneumonectomies. *J Thorac Cardiovasc Surg*, 128, 138-46.
- SULTANA, A., TUDUR SMITH, C., CUNNINGHAM, D., STARLING, N., TAIT, D., NEOPTOLEMOS, J. P. & GHANEH, P. 2007. Systematic review, including meta-analyses, on the management of locally advanced pancreatic cancer using radiation/combined modality therapy. *Br J Cancer*, 96, 1183-90.
- SWANICK, C. W., LIN, S. H., SUTTON, J., NAIK, N. S., ALLEN, P. K., LEVY, L. B., LIAO, Z., WELSH, J. W., KOMAKI, R., CHANG, J. Y. & GOMEZ, D. R. 2015. Use of simultaneous radiation boost achieves high control rates in patients with non-small-cell lung cancer who are not candidates for surgery or conventional chemoradiation. *Clin Lung Cancer*, 16, 156-63.
- SYLVESTRE, A., GIRAUD, P., ZEFKILI, S., LISBONA, A., SAVIGNONI, A., BONNETTE, P., LE PIMPEC BARTHE, F., MICHAUD, J., PERIGAUD, C. & MAHÉ, M. 2010. Helical Tomotherapy for Resected Malignant Pleural Mesothelioma: The French Clinical Experience. *International Journal of Radiation Oncology • Biology • Physics*, 78, S538.
- TAGUCHI, T., JHANWAR, S. C., SIEGFRIED, J. M., KELLER, S. M. & TESTA, J. R. 1993. Recurrent deletions of specific chromosomal sites in 1p, 3p, 6q, and 9p in human malignant mesothelioma. *Cancer Res*, 53, 4349-55.

- TAIOLI, E., WOLF, A. S., CAMACHO-RIVERA, M. & FLORES, R. M. 2014. Women With Malignant Pleural Mesothelioma Have a Threefold Better Survival Rate Than Men. *The Annals of Thoracic Surgery*, 98, 1020-1024.
- TAKATA, M., SASAKI, M. S., SONODA, E., MORRISON, C., HASHIMOTO, M., UTSUMI, H., YAMAGUCHI-IWAI, Y., SHINOHARA, A. & TAKEDA, S. 1998. Homologous recombination and non-homologous end-joining pathways of DNA double-strand break repair have overlapping roles in the maintenance of chromosomal integrity in vertebrate cells. *EMBO J*, 17, 5497-508.
- TAN, N., MALEK, M., ZHA, J., YUE, P., KASSEES, R., BERRY, L., FAIRBROTHER, W. J., SAMPATH, D. & BELMONT, L. D. 2011. Navitoclax enhances the efficacy of taxanes in non-small cell lung cancer models. *Clin Cancer Res*, 17, 1394-404.
- TAN, S.-B., DEAR, K. B. G., BRUZZI, P. & MACHIN, D. 2003. Strategy for randomised clinical trials in rare cancers. *BMJ*, 327, 47-49.
- TAO, Z.-F., HASVOLD, L., WANG, L., WANG, X., PETROS, A. M., PARK, C. H., BOGHAERT, E. R., CATRON, N. D., CHEN, J., COLMAN, P. M., CZABOTAR, P. E., DESHAYES, K., FAIRBROTHER, W. J., FLYGARE, J. A., HYMOWITZ, S. G., JIN, S., JUDGE, R. A., KOEHLER, M. F. T., KOVAR, P. J., LESSENE, G., MITTEN, M. J., NDUBAKU, C. O., NIMMER, P., PURKEY, H. E., OLEKSIJEW, A., PHILLIPS, D. C., SLEEBES, B. E., SMITH, B. J., SMITH, M. L., TAHIR, S. K., WATSON, K. G., XIAO, Y., XUE, J., ZHANG, H., ZOBEL, K., ROSENBERG, S. H., TSE, C., LEVERSON, J. D., ELMORE, S. W. & SOUERS, A. J. 2014. Discovery of a Potent and Selective BCL-XL Inhibitor with in Vivo Activity. *ACS Medicinal Chemistry Letters*, 5, 1088-1093.
- TEICHERT, K., CURRIE, G., KÜFER, K.-H., MIGUEL-CHUMACERO, E., SÜSS, P., WALCZAK, M. & CURRIE, S. 2019. Targeted multi-criteria optimisation in IMRT planning supplemented by knowledge based model creation. *Operations Research for Health Care*, 100185.
- TESTA, J. R., CHEUNG, M., PEI, J., BELOW, J. E., TAN, Y., SEMENTINO, E., COX, N. J., DOGAN, A. U., PASS, H. I., TRUSA, S., HESDORFFER, M., NASU, M., POWERS, A., RIVERA, Z., COMERTPAY, S., TANJI, M., GAUDINO, G., YANG, H. & CARBONE, M. 2011. Germline BAP1 mutations predispose to malignant mesothelioma. *Nat Genet*, 43, 1022-5.
- THACKER, J. & ZDZIENICKA, M. Z. 2003. The mammalian XRCC genes: their roles in DNA repair and genetic stability. *DNA Repair (Amst)*, 2, 655-72.
- THAMES, H. D., BENTZEN, S. M., TURESSON, I., OVERGAARD, M. & VAN DEN BOGAERT, W. 1990. Time-dose factors in radiotherapy: a review of the human data. *Radiother Oncol*, 19, 219-35.
- THERASSE, P., ARBUCK, S. G., EISENHAEUER, E. A., WANDERS, J., KAPLAN, R. S., RUBINSTEIN, L., VERWEIJ, J., VAN GLABBEKE, M., VAN OOSTEROM, A. T., CHRISTIAN, M. C. & GWYTHYER, S. G. 2000. New guidelines to evaluate the response to treatment in solid Tumors. *Journal of the National Cancer Institute*, 92, 205-216.
- THIEKE, C., KUFER, K. H., MONZ, M., SCHERRER, A., ALONSO, F., OELFKE, U., HUBER, P. E., DEBUS, J. & BORTFELD, T. 2007. A new concept for interactive radiotherapy planning with multicriteria optimization: first clinical evaluation. *Radiother Oncol*, 85, 292-8.
- THIRION, P., HOLMBERG, O., COLLINS, C. D., O'SHEA, C., MORIARTY, M., POMEROY, M., O'SULLIVAN, C., BUCKNEY, S. & ARMSTRONG, J. 2004. Escalated dose for non-small-cell lung cancer with accelerated hypofractionated three-dimensional conformal radiation therapy. *Radiother Oncol*, 71, 163-6.
- THOMA, C. R., ZIMMERMANN, M., AGARKOVA, I., KELM, J. M. & KREK, W. 2014. 3D cell culture systems modeling tumor growth determinants in cancer target discovery. *Adv Drug Deliv Rev*, 69-70, 29-41.
- THOMAS, A., GIESLER, T. & WHITE, E. 2000. p53 mediates bcl-2 phosphorylation and apoptosis via activation of the Cdc42/JNK1 pathway. *Oncogene*, 19, 5259-69.
- THORWARTH, D. 2015. Functional imaging for radiotherapy treatment planning: current status and future directions-a review. *The British journal of radiology*, 88, 20150056-20150056.
- TIMMERMAN, R. D. 2008. An overview of hypofractionation and introduction to this issue of seminars in radiation oncology. *Semin Radiat Oncol*, 18, 215-22.
- TOBIAS, J. S., MONSON, K., GUPTA, N., MACDOUGALL, H., GLAHOLM, J., HUTCHISON, I., KADALAYIL, L., HACKSHAW, A., HEAD, U. K. & NECK CANCER TRIALISTS, G. 2010.

- Chemoradiotherapy for locally advanced head and neck cancer: 10-year follow-up of the UK Head and Neck (UKHAN1) trial. *Lancet Oncol*, 11, 66-74.
- TOBLER, M., WATSON, G. & LEAVITT, D. D. 2002. Intensity-modulated photon arc therapy for treatment of pleural mesothelioma. *Med Dosim*, 27, 255-9.
- TOL, J. P., DELANEY, A. R., DAHELE, M., SLOTMAN, B. J. & VERBAKEL, W. F. A. R. 2015. Evaluation of a Knowledge-Based Planning Solution for Head and Neck Cancer. *International Journal of Radiation Oncology*Biological*Physics*, 91, 612-620.
- TOMAYKO, M. M. & REYNOLDS, C. P. 1989. Determination of subcutaneous tumor size in athymic (nude) mice. *Cancer Chemother Pharmacol*, 24, 148-54.
- TORRES-ROCA, J. F., ESCHRICH, S., ZHAO, H., BLOOM, G., SUNG, J., MCCARTHY, S., CANTOR, A. B., SCUTO, A., LI, C., ZHANG, S., JOVE, R. & YEATMAN, T. 2005. Prediction of radiation sensitivity using a gene expression classifier. *Cancer Res*, 65, 7169-76.
- TOUMPANAKIS, D. & THEOCHARIS, S. E. 2011. DNA repair systems in malignant mesothelioma. *Cancer Lett*, 312, 143-9.
- TREASURE, T., LANG-LAZDUNSKI, L., WALLER, D., BLISS, J. M., TAN, C., ENTWISLE, J., SNEE, M., O'BRIEN, M., THOMAS, G., SENAN, S., O'BYRNE, K., KILBURN, L. S., SPICER, J., LANDAU, D., EDWARDS, J., COOMBES, G., DARLISON, L., PETO, J. & FOR THE, M. T. 2011. Extra-pleural pneumonectomy versus no extra-pleural pneumonectomy for patients with malignant pleural mesothelioma: clinical outcomes of the Mesothelioma and Radical Surgery (MARS) randomised feasibility study. *The Lancet Oncology*, 12, 763-772.
- TREASURE, T. & SEDRAKYAN, A. 2004. Pleural mesothelioma: little evidence, still time to do trials. *Lancet*, 364, 1183-5.
- TREGLIA, G., SADEGHI, R., ANNUNZIATA, S., LOCOCO, F., CAFAROTTI, S., BERTAGNA, F., PRIOR, J. O., CERIANI, L. & GIOVANELLA, L. 2014. Diagnostic accuracy of 18F-FDG-PET and PET/CT in the differential diagnosis between malignant and benign pleural lesions: a systematic review and meta-analysis. *Acad Radiol*, 21, 11-20.
- UNDERBERG, R., VAN SORNSSEN DE KOSTE, J., SLOTMAN, B. & SENAN, S. 2005. Advantages of Respiration-Gated Radiotherapy for Stage III Lung Cancer. *International Journal of Radiation Oncology • Biology • Physics*, 63, S415.
- UPADHYAY, D. & KAMP, D. W. 2003. Asbestos-induced pulmonary toxicity: role of DNA damage and apoptosis. *Exp Biol Med (Maywood)*, 228, 650-9.
- VAETH, J. M. & PURCELL, T. R. 1964. RADIATION RESPONSE OF DIFFUSE PLEURAL MESOTHELIOMA: A CASE REPORT. *Radiol Clin*, 33, 319-27.
- VAN BAARDWIJK, A., BOSMANS, G., BOERSMA, L., WANDERS, S., DEKKER, A., DINGEMANS, A. M., BOOTSMA, G., GERAEDTS, W., PITZ, C., SIMONS, J., LAMBIN, P. & DE RUYSSCHER, D. 2008. Individualized radical radiotherapy of non-small-cell lung cancer based on normal tissue dose constraints: a feasibility study. *Int J Radiat Oncol Biol Phys*, 71, 1394-401.
- VAN BAARDWIJK, A., WANDERS, S., BOERSMA, L., BORGER, J., OLLERS, M., DINGEMANS, A. M., BOOTSMA, G., GERAEDTS, W., PITZ, C., LUNDE, R., LAMBIN, P. & DE RUYSSCHER, D. 2010. Mature results of an individualized radiation dose prescription study based on normal tissue constraints in stages I to III non-small-cell lung cancer. *J Clin Oncol*, 28, 1380-6.
- VAN DER HEIDE, U. A., HOUWELING, A. C., GROENENDAAL, G., BEETS-TAN, R. G. & LAMBIN, P. 2012. Functional MRI for radiotherapy dose painting. *Magn Reson Imaging*, 30, 1216-23.
- VAN DER ZEE, J., VAN DE POL, M. & PRAAG, J. O. 2004. Survey on the prophylactic as well as symptomatic treatment of intervention sites of malignant pleural mesothelioma in the Netherlands and Belgium. *Radiother Oncol*, 70, 99.
- VAN LEEUWEN, C. M., OEI, A. L., CREZEE, J., BEL, A., FRANKEN, N. A. P., STALPERS, L. J. A. & KOK, H. P. 2018. The alfa and beta of tumours: a review of parameters of the linear-quadratic model, derived from clinical radiotherapy studies. *Radiation oncology (London, England)*, 13, 96-96.
- VAN LOO, G., SAELENS, X., VAN GURP, M., MACFARLANE, M., MARTIN, S. J. & VANDENABEELE, P. 2002. The role of mitochondrial factors in apoptosis: a Russian roulette with more than one bullet. *Cell Death Differ*, 9, 1031-42.
- VAN MEERBEECK, J. P., GAAFAR, R., MANEGOLD, C., VAN KLAVEREN, R. J., VAN MARCK, E. A., VINCENT, M., LEGRAND, C., BOTTOMLEY, A., DEBRUYNE, C. & GIACCONE, G. 2005.

- Randomized phase III study of cisplatin with or without raltitrexed in patients with malignant pleural mesothelioma: An intergroup study of the European Organisation for Research and Treatment of Cancer Lung Cancer Group and the National Cancer Institute of Canada. *Journal of Clinical Oncology*, 23, 6881-6889.
- VAN NIMWEGEN, F. A., SCHAAPVELD, M., JANUS, C. P. M., KROL, A. D. G., PETERSEN, E. J., RAEMAEKERS, J. M. M., KOK, W. E. M., ALEMAN, B. M. P. & VAN LEEUWEN, F. E. 2015. Cardiovascular Disease After Hodgkin Lymphoma Treatment: 40-Year Disease Risk. *JAMA Internal Medicine*, 175, 1007-1017.
- VAN SCHIL, P. E., BAAS, P., GAAFAR, R., MAAT, A. P., VAN DE POL, M., HASAN, B., KLOMP, H. M., ABDELRAHMAN, A. M., WELCH, J. & VAN MEERBEECK, J. P. 2010. Trimodality therapy for malignant pleural mesothelioma: results from an EORTC phase II multicentre trial. *Eur Respir J*, 36, 1362-9.
- VANDER HEIDEN, M. G., CHANDEL, N. S., WILLIAMSON, E. K., SCHUMACKER, P. T. & THOMPSON, C. B. 1997. Bcl-xL regulates the membrane potential and volume homeostasis of mitochondria. *Cell*, 91, 627-37.
- VAUX, D. L., FIDLER, F. & CUMMING, G. 2012. Replicates and repeats--what is the difference and is it significant? A brief discussion of statistics and experimental design. *EMBO Rep*, 13, 291-6.
- VERMA, S., MILES, D., GIANNI, L., KROP, I. E., WELSLAU, M., BASELGA, J., PEGRAM, M., OH, D.-Y., DIÉRAS, V., GUARDINO, E., FANG, L., LU, M. W., OLSEN, S. & BLACKWELL, K. 2012. Trastuzumab Emtansine for HER2-Positive Advanced Breast Cancer. *New England Journal of Medicine*, 367, 1783-1791.
- VEUGER, S. J., CURTIN, N. J., RICHARDSON, C. J., SMITH, G. C. & DURKACZ, B. W. 2003. Radiosensitization and DNA repair inhibition by the combined use of novel inhibitors of DNA-dependent protein kinase and poly(ADP-ribose) polymerase-1. *Cancer Res*, 63, 6008-15.
- VILLANOVA, F., PROCOPIO, A. & RIPPO, M. R. 2008. Malignant mesothelioma resistance to apoptosis: recent discoveries and their implication for effective therapeutic strategies. *Curr Med Chem*, 15, 631-41.
- VINCI, M., GOWAN, S., BOXALL, F., PATTERSON, L., ZIMMERMANN, M., COURT, W., LOMAS, C., MENDIOLA, M., HARDISSON, D. & ECCLES, S. A. 2012. Advances in establishment and analysis of three-dimensional tumor spheroid-based functional assays for target validation and drug evaluation. *BMC Biol*, 10, 29.
- VITALE, I., GALLUZZI, L., CASTEDO, M. & KROEMER, G. 2011. Mitotic catastrophe: a mechanism for avoiding genomic instability. *Nat Rev Mol Cell Biol*, 12, 385-92.
- VIVO, C., LECOMTE, C., LEVY, F., LEROY, K., KIROVA, Y., RENIER, A., KHEUANG, L., PIEDBOIS, P., CHOPIN, D. & JAURAND, M. C. 2003. Cell cycle checkpoint status in human malignant mesothelioma cell lines: response to gamma radiation. *British journal of cancer*, 88, 388-395.
- VOGELZANG, N. J., RUSTHOVEN, J. J., SYMANOWSKI, J., DENHAM, C., KAUKEL, E., RUFFIE, P., GATZEMEIER, U., BOYER, M., EMRI, S., MANEGOLD, C., NIYIKIZA, C. & PAOLETTI, P. 2003. Phase III study of pemetrexed in combination with cisplatin versus cisplatin alone in patients with malignant pleural mesothelioma. *J Clin Oncol*, 21, 2636-44.
- WADE HARPER, J., ADAMI, G. R., WEI, N., KEYOMARSI, K. & ELLEDGE, S. J. 1993. The p21 Cdk-interacting protein Cip1 is a potent inhibitor of G1 cyclin-dependent kinases. *Cell*, 75, 805-816.
- WAGMAN, R., YORKE, E., FORD, E., GIRAUD, P., MAGERAS, G., MINSKY, B. & ROSENZWEIG, K. 2003. Respiratory gating for liver tumors: use in dose escalation. *Int J Radiat Oncol Biol Phys*, 55, 659-68.
- WAGNER, J. C., SLEGGES, C. A. & MARCHAND, P. 1960. Diffuse pleural mesothelioma and asbestos exposure in the North Western Cape Province. *Br J Ind Med*, 17, 260-71.
- WALA, J., CRAFT, D., PALY, J., ZIETMAN, A. & EFSTATHIOU, J. 2013. Maximizing dosimetric benefits of IMRT in the treatment of localized prostate cancer through multicriteria optimization planning. *Med Dosim*, 38, 298-303.

- WALKER, V. A., HOSKIN, P. J., HANKS, G. W. & WHITE, I. D. 1988. Evaluation of WHO analgesic guidelines for cancer pain in a hospital-based palliative care unit. *J Pain Symptom Manage*, 3, 145-9.
- WALLER, D. A., MORRITT, G. N. & FORTY, J. 1995. VIDEO-ASSISTED THORACOSCOPIC PLEURECTOMY IN THE MANAGEMENT OF MALIGNANT PLEURAL EFFUSION. *Chest*, 107, 1454-1456.
- WANG, H., YANG, Y. B., SHEN, H. M., GU, J., LI, T. & LI, X. M. 2012. ABT-737 induces Bim expression via JNK signaling pathway and its effect on the radiation sensitivity of HeLa cells. *PLoS One*, 7, e52483.
- WANG, N. S., JAURAND, M. C., MAGNE, L., KHEUANG, L., PINCHON, M. C. & BIGNON, J. 1987. The interactions between asbestos fibers and metaphase chromosomes of rat pleural mesothelial cells in culture. A scanning and transmission electron microscopic study. *The American journal of pathology*, 126, 343-349.
- WANG, W., HUANG, L., JIN, J. Y., JOLLY, S., ZANG, Y., WU, H., YAN, L., PI, W., LI, L., MELLOR, A. L. & KONG, F. S. 2018. IDO Immune Status after Chemoradiation May Predict Survival in Lung Cancer Patients. *Cancer Res*, 78, 809-816.
- WARTENBERG, M., LING, F. C., MUSCHEN, M., KLEIN, F., ACKER, H., GASSMANN, M., PETRAT, K., PUTZ, V., HESCHELER, J. & SAUER, H. 2003. Regulation of the multidrug resistance transporter P-glycoprotein in multicellular tumor spheroids by hypoxia-inducible factor (HIF-1) and reactive oxygen species. *FASEB J*, 17, 503-5.
- WEBER, A. M. & RYAN, A. J. 2015. ATM and ATR as therapeutic targets in cancer. *Pharmacol Ther*, 149, 124-38.
- WEDER, W., STAHEL, R. A., BERNHARD, J., BODIS, S., VOGT, P., BALLABENI, P., LARDINOIS, D., BETTICHER, D., SCHMID, R., STUPP, R., RIS, H. B., JERMANN, M., MINGRONE, W., ROTH, A. D. & SPILIOPOULOS, A. 2007. Multicenter trial of neo-adjuvant chemotherapy followed by extrapleural pneumonectomy in malignant pleural mesothelioma. *Ann Oncol*, 18, 1196-202.
- WELSH, J. S., PATEL, R. R., RITTER, M. A., HARARI, P. M., MACKIE, T. R. & MEHTA, M. P. 2002. Helical tomotherapy: an innovative technology and approach to radiation therapy. *Technol Cancer Res Treat*, 1, 311-6.
- WENDT, M. D. 2008. Discovery of ABT-263, a Bcl-family protein inhibitor: observations on targeting a large protein-protein interaction *Expert Opinion on Drug Discovery*, 3, 1123-1143.
- WETERINGS, E. & VAN GENT, D. C. 2004. The mechanism of non-homologous end-joining: a synopsis of synapsis. *DNA Repair (Amst)*, 3, 1425-35.
- WHELDON, T. E., LIVINGSTONE, A., WILSON, L., O'DONOGHUE, J. & GREGOR, A. 1985. The radiosensitivity of human neuroblastoma cells estimated from regrowth curves of multicellular tumour spheroids. *Br J Radiol*, 58, 661-4.
- WIGGINS, J. 2007. BTS statement on malignant mesothelioma in the UK, 2007. *Thorax*, 62, ii1.
- WILCOX, B. E., SUBRAMANIAM, R. M., PELLER, P. J., AUGHENBAUGH, G. L., NICHOLS III, F. C., AUBRY, M. C. & JETT, J. R. 2009. Utility of integrated computed tomography-positron emission tomography for selection of operable malignant pleural mesothelioma. *Clin Lung Cancer*, 10, 244-8.
- WILLERS, H., TAGHIAN, A. G., LUO, C. M., TRESZEZAMSKY, A., SGROI, D. C. & POWELL, S. N. 2009. Utility of DNA repair protein foci for the detection of putative BRCA1 pathway defects in breast cancer biopsies. *Mol Cancer Res*, 7, 1304-9.
- WILLIAMS, F. H. 1901. Treatment of certain forms of cancer by the X-rays. *Journal of the American Medical Association*, 37, 688-691.
- WILLMORE, E., DE CAUX, S., SUNTER, N. J., TILBY, M. J., JACKSON, G. H., AUSTIN, C. A. & DURKACZ, B. W. 2004. A novel DNA-dependent protein kinase inhibitor, NU7026, potentiates the cytotoxicity of topoisomerase II poisons used in the treatment of leukemia. *Blood*, 103, 4659-65.
- WIPF, P. & HALTER, R. J. 2005. Chemistry and biology of wortmannin. *Org Biomol Chem*, 3, 2053-61.
- WITHERS, H. R. 1975. Four R's of radiotherapy. *Advances in Radiation Biology*, 241-247.

- WOGLOM, W. H. 1925. Regression of the Jensen Rat Sarcoma. *The Journal of Cancer Research*, 9, 171-189.
- WONG, M., TAN, N., ZHA, J., PEALE, F. V., YUE, P., FAIRBROTHER, W. J. & BELMONT, L. D. 2012. Navitoclax (ABT-263) Reduces Bcl-xL-Mediated Chemoresistance in Ovarian Cancer Models. *Molecular Cancer Therapeutics*, 11, 1026.
- WOO, H. N., SEO, Y. W., MOON, A. R., JEONG, S. Y., JEONG, S. Y., CHOI, E. K. & KIM, T. H. 2009. Effects of the BH3-only protein human Noxa on mitochondrial dynamics. *FEBS Lett*, 583, 2349-54.
- WOOLHOUSE, I., BISHOP, L., DARLISON, L., DE FONSEKA, D., EDEY, A., EDWARDS, J., FAIVRE-FINN, C., FENNELL, D. A., HOLMES, S., KERR, K. M., NAKAS, A., PEEL, T., RAHMAN, N. M., SLADE, M., STEELE, J., TSIM, S. & MASKELL, N. A. 2018. British Thoracic Society Guideline for the investigation and management of malignant pleural mesothelioma. *Thorax*, 73, i1-i30.
- WOOLHOUSE, I. & MASKELL, N. A. 2018. Introducing the new BTS guideline: the investigation and management of pleural malignant mesothelioma. *Thorax*, 73, 210-212.
- WU, D., HIROSHIMA, K., MATSUMOTO, S., NABESHIMA, K., YUSA, T., OZAKI, D., FUJINO, M., YAMAKAWA, H., NAKATANI, Y., TADA, Y., SHIMADA, H. & TAGAWA, M. 2013. Diagnostic Usefulness of p16/CDKN2A FISH in Distinguishing Between Sarcomatoid Mesothelioma and Fibrous Pleuritis. *American Journal of Clinical Pathology*, 139, 39-46.
- WU, H., SCHIFF, D. S., LIN, Y., NEBOORI, H. J., GOYAL, S., FENG, Z. & HAFFTY, B. G. 2014. Ionizing radiation sensitizes breast cancer cells to Bcl-2 inhibitor, ABT-737, through regulating Mcl-1. *Radiat Res*, 182, 618-25.
- WU, L., WU, M. O., DE LA MAZA, L., YUN, Z., YU, J., ZHAO, Y., CHO, J. & DE PERROT, M. 2015. Targeting the inhibitory receptor CTLA-4 on T cells increased abscopal effects in murine mesothelioma model. *Oncotarget*, 6, 12468-80.
- XIA, P., HWANG, A. B. & VERHEY, L. J. 2002. A leaf sequencing algorithm to enlarge treatment field length in IMRT. *Med Phys*, 29, 991-8.
- XING, J., WU, X., VAPORCIYAN, A. A., SPITZ, M. R. & GU, J. 2008. Prognostic significance of ataxia-telangiectasia mutated, DNA-dependent protein kinase catalytic subunit, and Ku heterodimeric regulatory complex 86-kD subunit expression in patients with nonsmall cell lung cancer. *Cancer*, 112, 2756-64.
- XIONG, Y., HANNON, G. J., ZHANG, H., CASSO, D., KOBAYASHI, R. & BEACH, D. 1993. p21 is a universal inhibitor of cyclin kinases. *Nature*, 366, 701-704.
- YAES, R. J., PATEL, P. & MARUYAMA, Y. 1991. On using the linear-quadratic model in daily clinical practice. *Int J Radiat Oncol Biol Phys*, 20, 1353-62.
- YAJNIK, S., ROSENZWEIG, K. E., MYCHALCZAK, B., KRUG, L., FLORES, R., HONG, L. & RUSCH, V. W. 2003. Hemithoracic radiation after extrapleural pneumonectomy for malignant pleural mesothelioma. *Int J Radiat Oncol Biol Phys*, 56, 1319-26.
- YAMADA, K. M. & CUKIERMAN, E. 2007. Modeling tissue morphogenesis and cancer in 3D. *Cell*, 130, 601-10.
- YAN, T. D., TIN, M., BOYER, M., MCLEAN, J., P, G. B. & MCCAUGHAN, B. C. 2009. Treatment failure after extrapleural pneumonectomy for malignant pleural mesothelioma. *J Thorac Dis*, 1, 23-8.
- YANAI, M., MAKINO, H., PING, B., TAKEDA, K., TANAKA, N., SAKAMOTO, T., YAMAGUCHI, K., KODANI, M., YAMASAKI, A., IGISHI, T. & SHIMIZU, E. 2017. DNA-PK Inhibition by NU7441 Enhances Chemosensitivity to Topoisomerase Inhibitor in Non-Small Cell Lung Carcinoma Cells by Blocking DNA Damage Repair. *Yonago Acta Med*, 60, 9-15.
- YANG, C., WANG, Q., LIU, X., CHENG, X., JIANG, X., ZHANG, Y., FENG, Z. & ZHOU, P. 2016. NU7441 Enhances the Radiosensitivity of Liver Cancer Cells. *Cell Physiol Biochem*, 38, 1897-905.
- YANG, T. M., BARBONE, D., FENNELL, D. A. & BROADDUS, V. C. 2009. Bcl-2 family proteins contribute to apoptotic resistance in lung cancer multicellular spheroids. *Am J Respir Cell Mol Biol*, 41, 14-23.
- YARNOLD, J., BENTZEN, S. M., COLES, C. & HAVILAND, J. 2011. Hypofractionated whole-breast radiotherapy for women with early breast cancer: myths and realities. *Int J Radiat Oncol Biol Phys*, 79, 1-9.

- YATES, D. H., CORRIN, B., STIDOLPH, P. N. & BROWNE, K. 1997. Malignant mesothelioma in south east England: clinicopathological experience of 272 cases. *Thorax*, 52, 507-12.
- YEGLES, M., SAINT-ETIENNE, L., RENIER, A., JANSON, X. & JAURAND, M.-C. 1993. Induction of Metaphase and Anaphase/Telophase Abnormalities by Asbestos Fibers in Rat Pleural Mesothelial Cells In Vitro. *American Journal of Respiratory Cell and Molecular Biology*, 9, 186-191.
- YIP, K., JAMES, H., LEE, V. & HARDEN, S. 2011. Hemi-thoracic Irradiation Post-cytoreductive Surgery for Mesothelioma: a Theoretical Planning Study using Tomotherapy and Volumetric Modulated Arc Therapy. *Clinical Oncology*, 23, S58.
- YOSHIDA, M., HOSOI, Y., MIYACHI, H., ISHII, N., MATSUMOTO, Y., ENOMOTO, A., NAKAGAWA, K., YAMADA, S., SUZUKI, N. & ONO, T. 2002. Roles of DNA-dependent protein kinase and ATM in cell-cycle-dependent radiation sensitivity in human cells. *Int J Radiat Biol*, 78, 503-12.
- YU, L., SHANG, Z. F., HSU, F. M., ZHANG, Z., TUMATI, V., LIN, Y. F., CHEN, B. P. & SAHA, D. 2015. NSCLC cells demonstrate differential mode of cell death in response to the combined treatment of radiation and a DNA-PKcs inhibitor. *Oncotarget*, 6, 3848-60.
- ZAIDI, S. H., HUDDART, R. A. & HARRINGTON, K. J. 2009. Novel targeted radiosensitisers in cancer treatment. *Curr Drug Discov Technol*, 6, 103-34.
- ZALCMAN, G., MAZIÈRES, J., MARGERIE, J., GREILLIER, L., AUDIGIER-VALETTE, C., MORO-SIBILOT, D., MOLINIER, O., CORRE, R., MONNET, I., GOUNANT, V., JANICOT, H., GERVAIS, R., LOCHER, C., MILLERON, B., TRAN, Q., LEBITASY, M. P., MORIN, F., CREVEUIL, C., PARIENTI, J.-J., SCHERPEREEL, A. & INTERGROUP, F. C. T. 2015. Bevacizumab 15mg/kg plus cisplatin-pemetrexed (CP) triplet versus CP doublet in Malignant Pleural Mesothelioma (MPM): Results of the IFCT-GFPC-0701 MAPS randomized phase 3 trial. *Journal of Clinical Oncology*, 33, 7500-7500.
- ZANELLA, C. L., POSADA, J., TRITTON, T. R. & MOSSMAN, B. T. 1996. Asbestos causes stimulation of the extracellular signal-regulated kinase 1 mitogen-activated protein kinase cascade after phosphorylation of the epidermal growth factor receptor. *Cancer Res*, 56, 5334-8.
- ZANONI, M., PICCININI, F., ARIENTI, C., ZAMAGNI, A., SANTI, S., POLICO, R., BEVILACQUA, A. & TESEI, A. 2016. 3D tumor spheroid models for in vitro therapeutic screening: a systematic approach to enhance the biological relevance of data obtained. *Sci Rep*, 6, 19103.
- ZAREPISHEH, M., LONG, T., LI, N., TIAN, Z., ROMEIJN, H. E., JIA, X. & JIANG, S. B. 2014. A DVH-guided IMRT optimization algorithm for automatic treatment planning and adaptive radiotherapy replanning. *Med Phys*, 41, 061711.
- ZHANG, H., NIMMER, P. M., TAHIR, S. K., CHEN, J., FRYER, R. M., HAHN, K. R., ICIEK, L. A., MORGAN, S. J., NASARRE, M. C., NELSON, R., PREUSSER, L. C., REINHART, G. A., SMITH, M. L., ROSENBERG, S. H., ELMORE, S. W. & TSE, C. 2007. Bcl-2 family proteins are essential for platelet survival. *Cell Death Differ*, 14, 943-51.
- ZHAO, Y., THOMAS, H. D., BATEY, M. A., COWELL, I. G., RICHARDSON, C. J., GRIFFIN, R. J., CALVERT, A. H., NEWELL, D. R., SMITH, G. C. & CURTIN, N. J. 2006. Preclinical evaluation of a potent novel DNA-dependent protein kinase inhibitor NU7441. *Cancer Res*, 66, 5354-62.
- ZSCHENKER, O., STREICHERT, T., HEHLGANS, S. & CORDES, N. 2012. Genome-wide gene expression analysis in cancer cells reveals 3D growth to affect ECM and processes associated with cell adhesion but not DNA repair. *PLoS One*, 7, e34279.